The University of Nottingham

UNITED KINGDOM · CHINA · MALAYSIA

Institute of Sustainable Energy Technology

Division of Infrastructure, Geomatics and Architecture

Faculty of Engineering

Investigation of Innovative Thermochemical Energy Storage Processes and Materials for Building Applications

Thesis by

Devrim Aydin, BEng, MSc

Thesis submitted to the University of Nottingham

For the degree of Doctor of Philosophy

September 2016

Table of Contents

CHAPTER 3: NUMERICAL INVESTIGATION OF SOLAR THERMAL ENERGY STORAGE POTENTIAL UNDER UK CLIMATIC CONDITIONS 60

CHAPTER 4: SALT IMPREGNATED DESICCANT MATRICES FOR ‘OPEN’ THERMOCHEMICAL ENERGY STORAGE 82

CHAPTER 6: THEORETICAL AND EXPERIMENTAL FEASIBILITY STUDIES ON THERMOCHEMICAL HEAT STORAGE UNDER MEDITERENNEAN CLIMATE CONDITIONS: NORTHERN CYPRUS CASE 185

Abstract

In this study, it is aimed to develop an innovative thermochemical energy storage system through material, reactor and process based investigations for building space heating applications. The developed system could be integrated with solar thermal collectors, photovoltaic panels or heat pumps to store any excess energy in the form of heat for later use. Thereby, it is proposed to address the problem of high operational costs and CO_2 emissions released by currently used fossil fuel based heating systems in buildings.

The aim of the study has been achieved by investigating and evaluating five of the following aspects:

- Investigation of the feasibility of building integrated solar driven THS system under cold and mild climates,
- Synthesis, characterization and physical experimentation of novel composite sorption energy storage materials
- Development and investigation of a modular laboratory scale sorption reactor that use embedded air diffusers inside the sorbent for improving the energy storage density
- Development and investigation of a full- scale modular solar driven THS system
- Development and investigation of a heat pump driven sorption storage heater using multi-layer fixed bed sorption reactor

These works have been assessed by means of computer simulation, laboratory and field experimental work and have been demonstrated adequately. The key findings from the study confirm the potential of the examined technology.

Initially, a comprehensive review on thermal energy storage, with the aim of investigating the latest advancements on THS systems was performed. A comparative analysis on applicability of different heat storage methods for short term and seasonal heat storage under climate conditions in the UK, was also carried out. Results showed that short term heat storage is not a feasible option in the UK due to the very limited solar radiation. For the case of seasonal heat storage, it was found that, each 1 m^3 of THS can provide averagely 14% of monthly (October to March) heating demand of a 106 m^2 building, whereas LHS and SHS can provide 6% and 2% respectively.

Later on, a range of candidate composite sorption materials were synthesized and characterized. Based on the applied characterization techniques, it was found that Vermicuilite-$CaCl_2$ (SIM-3a) has excellent E_d coupled with good EMC and t_{emc} with its TGA analysis also suggesting significant mass loss in the working range $30 < T < 140$ °C. Physical experimentation of the developed materials in a small scale custom test rig was also performed and in accordance with the characterization results, SIM-3a displayed the best hygrothermal and cyclic performance. These findings suggested that SIM-3a has very good potential for use in an open THS system. Upon completion of the material based studies, a 3kWh laboratory scale novel reactor using perforated pipes embedded inside the heat storage material was developed. The overall energy density of the reactor using SIM-3a was found 290 kWh/m^3. Based on the obtained encouraging results, same concept was up scaled to a modular 25 kWh sorption pipe heat storage and similar energy density was achieved.

Following the experimental work, theoretical analysis of the THS potential in Mediterranean climate conditions is conducted with a case study of the Island of Cyprus. The analysis results showed that the required heat storage volume to fully compensate heating demand of a domestic building in winter (December to February) is 5.25 m^3 whilst the time required

for charging the THS material with 8 m^2 solar air collectors is slightly more than a month. The economic and environmental analyses results showed that payback period of the solar driven THS is 6 years whilst total CO_2 emissions savings over 25 years lifetime is 47.9 tonnes. In order to validate the applicability of THS in Cyprus, a small prototype of integrated sorption pipe-solar concentrator was also developed and tested for room heating. It was found that adsorbent could be regenerated with solar energy during winter day time to be utilized at night for space heating. Study results also showed that sorption pipe with a heat storage volume of 0.017 m^3 could meet up to 87% of the daily heat demand of a 12.4 m^2 building.

In order to validate the performance of the laboratory tested THS material and concept, a real scale (1000 kWh) modular solar driven THS system was developed based on the interpretation of the obtained theoretical, numerical and experimental data in earlier stages of the study. The preliminary testing on the prototype showed that each of four reactors could discharge a total of 248 kWh of thermal energy with an average thermal power of 4.8 kW. Additionally it is found that, in direct solar heating mode, transpired solar collectors used in the system could also generate daily total of 17 kWh thermal energy for the average solar intensity of 0.3 kW/m^2.

In the final stage of the study, a heat pump driven sorption storage heater was developed and investigated. The developed system performance was assessed with 5 different adsorption materials and under different operating conditions. The study results showed that Sim-3a and Vermiculite–($LiCl$-$CaCl_2$) (Sim-3cl) has the best hygrothermal performances and hygro-cyclic efficiencies. According to study results, COP_s varies in the range of 1→2 depending on sorption materials properties and system operating conditions.

List of Publications

International Journal Papers

1. **Aydin D**, Casey SP, Riffat S. The latest advancements on thermochemical heat storage systems. *Renewable and Sustainable Energy Reviews* 41(2015): 356-367.

2. **Aydin D**, Casey SP, Riffat S. Numerical analysis of solar assisted seasonal 'open' thermochemical heat storage. *International Journal of Low Carbon Technologies* 10 (2015): 131-138.

3. Casey SP, **Aydin D**, Riffat S, Elvins J. Salt impregnated desiccant matrices for 'open' thermochemical energy storage – hygrothermal cyclic behaviour and energetic analysis by physical experimentation. *Energy and Buildings* 92 (2015): 128–139.

4. **Aydin D**, Casey SP, Riffat S . Theoretical analysis of the potential for thermochemical heat storage under Mediterranean Climate conditions: Northern Cyprus Case. *Future Cities and Environment*, Springer (2015)1:2. DOI 10.1186/s40984-015-0003-x.

5. **Aydin D**, Casey SP, Chen X, Riffat S. Novel 'open-sorption pipe' reactor for solar thermal energy storage. *Energy Conversion and Management* 121 (2016): 321–334.

6. **Aydin D**, Casey SP, Riffat S. Salt impregnated desiccant matrices for 'open' thermochemical energy storage – Improving energy density utilisation through hygrodynamic & thermodynamic reactor design. *Energy* (Under Review).

International Conference Papers

1. Casey SP, Riffat S, **Aydin D** & Elvins J. Optimisation of salt impregnated matrices for open thermochemical heat storage through material characterisation and hygrothermal cyclic analysis. 13th International Conference on Sustainable Energy Technologies, August 2014, Genava, Switzerland.

2. **Aydin D**, Casey SP, Riffat S. Numerical investigation of solar thermal heat storage potential under UK climatic conditions. 13th International Conference on Sustainable Energy Technologies, August 2014, Genava, Switzerland.

3. **Aydin D**, Casey SP, Riffat S. Numerical analysis of solar assisted seasonal 'open' thermochemical heat storage. 13th International Conference on Sustainable Energy Technologies, August 2014, Genava, Switzerland.

4. **Aydin D**, Casey SP, Riffat S. Experimental investigation of open sorption pipe heat storage under north Cyprus climate conditions. 14th International Conference on Sustainable Energy Technologies, August 2015, Nottingham, UK.

5. **Aydin D**, Casey SP, Riffat S. Nano composite “Vermiculite-CaCl2” matrix for open thermochemical heat storage: Experimental investigation of cyclic behaviour and numerical determination of “operating line”. 14th International Conference on Sustainable Energy Technologies, August 2015, Nottingham, UK.

Awards

- UK Energy Innovation Awards 2016 – Best University Technology Category - Finalist.
  Project Title: Heat pump driven sorption storage heater (StoreHeat).

Acknowledgement

I would like to express my sincere gratitude to my supervisor Professor Saffa Riffat, who encouraged me to push the boundaries in every step of my research. I am proud of being your student, and grateful for the tremendous support and guidance you provided me with.

Special thanks to Dr. Sean Casey, who generously shared all his experience, knowledge and helped me both technically and academically. Furthermore, I appreciate the efforts of the technicians of the department: Dave Oliver, Dave Taylor and Johnny Moss for their valuable technical support. I also would like to thank Zeny Amante Roberts for her sincere help.

I have utmost respect and appreciation for my family without whom I would not have been able to complete my journey. My mother, father and brothers are the light in my life that helps me find my way. Thank you for the tremendous trust, support and encouragement you have provided me with throughout my life.

I would also like to acknowledge the support of the Innovate UK (United Kingdom) for funding the presented research (101223 “Interseasonal Thermochemical Renewable Energy Storage System” and 131926 “Innovative Energy Saving Heat Pump Driven Sorption Storage Heater”).

Nomenclature

Symbol	Term	Unit
A	area	m^2
b	sorbent layer thickness	mm
c	temperature gradient	°C/min
c_p	specific heat	kJ/(kg.K)
d	diameter	mm, m
E	energy	Wh, kWh
E_d	energy density	kWh/m^3
E_{cum}	cumulative thermal energy	Wh, kWh
Ex	exergy	W, kW
Ex_{cum}	cumulative thermal exergy	Wh, kWh
f	mass uptake ratio	g_{wv}/g_{abs}
F_r	collector correction or heat removal factor	----
g	discount rate	%
h	enthalpy	kJ/kg
I	solar radiation	W/m^2
i	inflation rate	%
kn	bulk porosity	m^3/m^3
m	mass	g, kg
m_a	mass flow rate of air	kg/s
M_m	molar weight	kg/mol
n	mole number	mole
P	pressure	Pa
p_w	water vapour partial pressure	mbar
R	salt ratio in composite matrix	kg/kg
RH	relative humidity	%

Q	heat, thermal power	W, kW
Q_u	solar heat gain	kW
r	rate of interest	%
S	entropy	kJ/(kg.K)
t	time	min, h
T	temperature	°C
t_{dwell}	time interval to reach ambient temperature	hr
t_{emc}	time interval to reach equilibrium moisture content	hr
T_{reg}	regeneration temperature	°C
U	heat loss coefficient	kW/m^2 °C
V	volume	m^3
V_s	storage volume	m^3
W	power	W, kW
w	absolute humidity	kg/kg, g/kg
X	reaction advancement	----
z	sorption/desorption rate	gr/min
Δh_r	reaction enthalpy per mole of absorbent	kJ/mol
Δh_W	reaction enthalpy per mole of absorbed vapour	kJ/kg

Greek letters

ρ	density	kg/m^3
ν	reaction stoichiometry coefficient	----
λ	dry state thermal conductivity	W/(m.K)
ξ_A	moisture storage function where $\xi = f(RH_{\mathrm{ie}})$	kg/kg
ξ_B	moisture storage function where $\xi = f(RH_{\mathrm{ie}}, t_{emc})$	kg/kg
$\varnothing$	pore diameter	µm, nm
η_I	1st law efficiency	%
η_{II}	2nd law efficiency	%

Δ	difference	----
$\tau\alpha$	absorption-transmission coefficient	----
ς	conversion factor of electricity per kWh consumption	----
ξ	total yearly energy consumption	kWh
Υ	total operational cost	€

Subscripts and Superscripts

Script	Term
a	air, ambient
abs	absorbent
ads	adsorbent
ac	air – charging
ad	air – discharging
a,s	ambient – summer
ave	average
a,w	ambient – winter
b	blockwork
c	charging
$comp$	compressor
$cond$	condenser
cum	cumulative
da	dry air
d	discharging
des	desorption
e	electricity
$evap$	evaporator
f	fan
g	gain

gen	generated
h	heating
hum	humidifier
hyg-cyc	hygrocyclic
i	inlet, initial
ie	interior environment
l	lowest, loss
m	maintenance cost
max	maximum
min	minimum
N	year
o	outlet
p	peak
r	regeneration
rec	recovered
recirc	recirculation
req	required
rct	reactor
rxn	reaction
sp	set point
s	secondary
sk	skylight
t	total
tr	transferred
u	solar
v	volume, volumetric, ventilation
w	water, wet, window
wv	water vapour

Abbreviations

Abbreviation	Term
ACH	Air change per hour
BET	Brunauer– Emmett–Teller
CHP	Chemical heat pump
COP	Coefficient of performance
CSPM	Composite salt in porous matrix
DHW	Domestic hot water
DSC	Differential scanning calorimetry
EH	Electrical heater
EHL	Excess heat load
EMC	Equilibrium moisture content
EU	European Union
GH	Gas heater
GHG	Greenhouse gas
HAM	Heat & mass transfer
HEX	Heat exchanger
HP	Heat pump
HS	Heat storage
HSM	Heat storage material
HTF	Heat transfer fluid
HVAC	Heating, ventilation and air conditioning
IWT	Insipent wetness technique
LPG	Liquefied petroleum gas
LHS	Latent heat storage
MFR	Mass flow rate
MIP	Mercury intrusion porosimetry
NC	North Cyprus

nZEB	Net zero energy building
PCM	Phase change material
SC	Solar concentrator
SCH	Solid crystalline hydrates
SEM	Scanning electron microscopy
SHE	Storable excess heat
SHS	Sensible heat storage
SIM	Salt in matrix
SP	Sorption pipe
SSA	Specific surface area
STES	Sorption thermal energy storage
TES	Thermal energy storage
TGA	Thermogravimetric analysis
THS	Thermochemical heat storage
PWF	Present worth factor
V	Vermiculite
TSC	Transpired solar collector
THG	Total heat gain
THL	Total heat load
RSV	Required storage volume
WSS	Wakkanai siliceous shale

List of Figures

List of Tables

CHAPTER 1: INTRODUCTION

1.1 Introduction

Increasing population, rapid industrialization and technological developments led to a sharp rise of global energy consumption. Energy balances undertaken by International Energy Agency (IEA) accounts a global final energy use of 7209 Mtoe (Million Tonnes Oil Equivalent) in the last decade (Navarro et al., 2016). It is clear that, energy dependency is much higher than in the past while world fossil fuel reserves are diminishing. According to Shafie at al., fossil fuel reserve depletion times for oil, coal and gas are approximately 35, 107 and 37 years, respectively. This means that coal reserves are available up to 2112, and will be the only fossil fuel remaining after 2042 (Shafiee and Topal, 2009).

The increasing rate of fossil fuel consumption is a serious threat for future global energy security. It also has a major impact on ozone depletion and global warming as a result of greenhouse gas emissions. Besides, increase in fossil fuel prices and energy demand economically compelling the governments and the public. Urgent solutions are needed to reduce fossil fuel dependency and emissions also to provide energy security and global sustainability. These solutions could be achieved through effective conversion and management of energy, increasing efficiency of energy systems but more importantly by developing novel technologies for cost-effective utilization of renewable energy resources. Accordingly, EU has taken actions by putting short, medium and long term sustainability targets into force. In this context, EU's climate and energy package of binding legislation has established a set of 20-20-20 targets, with three key objectives for 2020, which includes a 20% reduction of greenhouse gases, a 20% improvement in energy efficiency and a 20% share of energy consumption from renewable resources. Objectives seek to reduce greenhouse gas emissions by up to 80-95% by 2050 (da Graça Carvalho, 2012).

In EU, building sector constitutes approximately 40% of final energy use while building sourced CO_2 emissions represent a similar proportion. Of the energy used in the building sector, HVAC (heating, ventilation and air conditioning) systems consume approximately 60% and supported by the global fact that HVAC is the major energy consuming application. Improving the efficiency of HVAC and water heating systems employed in the built environment also increasing the renewable energy share in these applications therefore has a potential to provide considerable savings (IEA, 2013).

Dependency on fossil fuels is very high in cold and severe climates where year round ambient temperature and solar intensity are low. For instance, In the UK, (DECC, 2013) in 2012, just under half (45-47%) of 206.3 mtoe total final energy consumption is used for heating purposes (See: Figure 1.1.1 a) where 80% is derived from natural gas and the rest was derived from solid or liquid fuels (See: Figure 1.1.1 d). Space and water heating account for 63% and 14% of the total UK national heat demand (See: Figure 1.1.1 c). Besides, the domestic sector is responsible for 57% of total thermal energy use where 77.5% of it is used for space heating (See: Figure 1.1.1 b). In the current situation, conventional heating systems have major impacts on environment and economy; thereby urgent solutions are seeked for achieving sustainable space heating in the built environment.

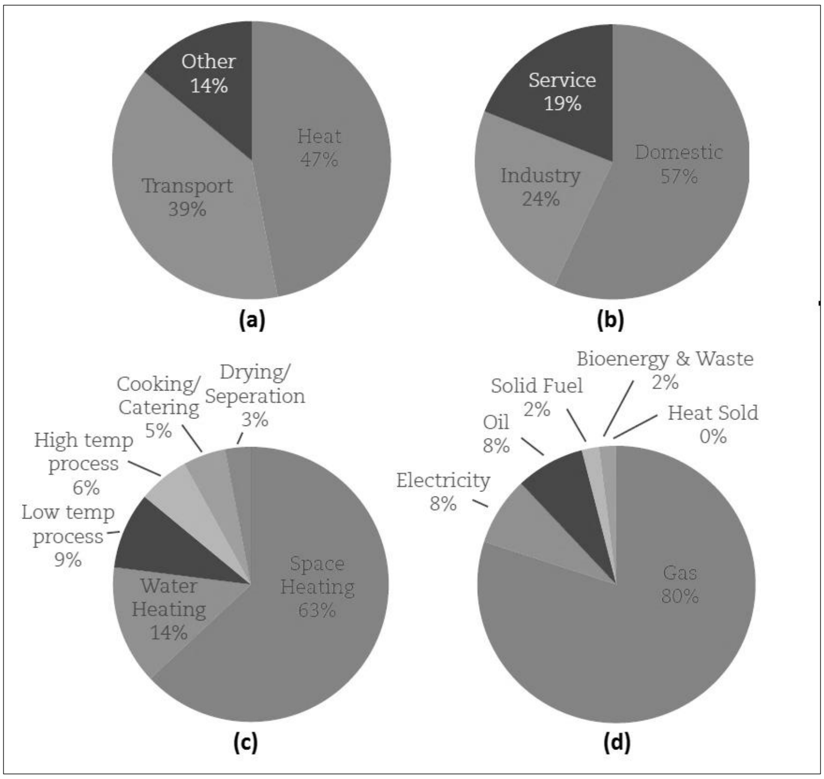

Figure 1.1.1 Energy trends in the UK; (a) energy consumption by end use, (b) heat use by sector (c) heat use by purpose, (d) breakdown by fuel of domestic heat use

In this context, parallel with the EU sustainability targets, energy efficiency requirements have been included in many building codes and energy standards. Low energy and net zero energy buildings are becoming a target in the research field, through the incorporation of solar energy systems and thermal energy storage among others. Mostly, hybrid use of multiple technologies is needed to achieve low energy rates hence engineers and architects have to deal with their integration during the building design. Building integration can be defined by the idea of a functional or constructive incorporation of the technology in the building structure (Navarro et al., 2016). Within this definition, passive systems or technologies such as seasonal shadings, blinds, thermal mass increase or thermal insulation, which are focused on reducing the energy demand, are widely incorporated in the building design process. Integrated designs are required in active systems such as renewable energy facilities (i.e. photovoltaic, solar thermal) or energy efficient HVAC systems. Many studies have been focused on improving the efficiency of these technologies by incorporating thermal energy storage systems that implies an additional storage volume (Navarro et al., 2016, Basecq et al., 2013). Building integrated thermal energy storage technologies are vital not only for increasing renewable energy share but also for efficient use of conventional systems (e.g. gas boilers) through providing supply–demand balance.

1.2 Statement of the problems

Energy supply and security is crucial, while there are arising public concerns regarding the increasing fossil fuel consumption and greenhouse gas emissions. (Asif and Muneer, 2007, Zhang et al., 2016) Global economic crisis since 2008 added additional challenges (IEA, 2013), leading worldwide governments to develop new policies and financial incentives for supporting renewable energies, enhancing their implementation and development, while simultaneously creating valuable new business opportunities for companies involved in this energy sector (Zhang et al., 2013, Zhang et al., 2014). One of the hot topics in new energy strategies is the capture and storage of thermal energy as applicable to renewable energy concepts and in waste heat recovery. These advanced energy utilization schemes call for the development and new usage of existing and/or new materials.

According to the current statistics and predictions of energy consumption, the U.S. Energy Information Administration predicated an increase in the total world energy use from 0.15 × 1012 MWh in 2008 to 0.18 × 1012 MWh in 2020, and to 0.23 × 1012 MWh in 2035 (Sieminski, 2014). Fossil fuels are important energy sources in current situation however due to the depleting reserves, a sharp increase of their prices to 120–140 US$/barrel from 60 US$/ barrel is expected from 2020 onwards. On the other hand, as a result of the intense use of fossil fuels, current global CO_2 emissions are at 30.6 × 109 tonnes per annum (tpa) against 28.2 × 109 tpa in 2005. It is however expected that world energy related emissions of CO_2 will further increase to 33.5×10^9 tpa in 2015 and 43.2×10^9 tpa in 2035 (Sieminski, 2014). The imposed reduction in CO_2 emissions will require a combination of detailed strategies and tactics, including

- A mix of energy generation technologies;
- A reduction in energy usage through the use of incentives, technologies, taxes and quotas;
- Maximizing CO_2 absorption, through carbon sequestration by both natural means and by technical developments; and
- The development of highly-efficient energy capture, storage and re-use methods (Zhang et al., 2013, Pitié et al., 2013, Zhang et al., 2016).

To achieve the legally binding targets set by several governments and organizations (e.g. UK: 80% reduction in CO_2 emissions by 2050 and EU: 20-20-20) it is essential that the gas, oil and solid fuel used for heating is substantially reduced or substituted by a sustainable energy resource. The provision of space and water heating in a low carbon way is a major challenge. New buildings can be built to have very low heat loads; however existing buildings will form a major part of the building stock in 2030 and 2050 (Eames et al., 2014). Deep retrofit of buildings to significantly improve performance and reduce heat loads is, to date, progressing at a slower pace than required. The domestic space heating load is therefore likely to remain significant for the foreseeable future. To achieve a transition to a low carbon fuel supply for space and water heating will require one or a mix of the following (Eames et al., 2014):

- A renewable substitution for gas allowing the existing gas supply network to be used

- Transition to electric driven space and water heating (assuming the electricity generation system is decarbonised)

- Generation of heat locally using a renewable energy supply source

Thermal energy storage can be used to help balance differences between heat/coolth generation and demand requirements with respect to both disparities that occur in time and magnitude. Thermal energy storage can provide several advantages:

- Increasing renewable energy share, solar thermal could be extensively used through storing the collected solar energy for use at later times either on a diurnal or interseasonal basis

- By generating and storing heat at periods of low demand and regenerating at periods of high demand, increased capacity can be realised within a given generation system allowing improved capacity factor and reducing low utilisation plant, this allows smaller plant to be used for a given peak load, plant can be operated in the most efficient way with reduced cycling and less part-load operation;

- If different tariffs are available at different times of the day, heat generation can be shifted in time to reduce peak demand and take advantage of lower tariffs
- Energy efficiency can be improved by utilising heat/coolth that would have been wasted
- Combined heat and power and district heating schemes can be operated in more effective ways to maximise income
- The effects of interruption in supply can be reduced and system reliability increased

Although thermal energy storage is a key technology for reducing energy consumption in building sector, there are a number of challenges to thermal energy storage becoming mainstream globally, including (Eames et al., 2014, Gur et al., 2012, Arteconi et al., 2012):

- Low energy density and thus large volume requirements for heat storage with current sensible heat storage approaches
- Limited time of heat storage possibility due to the heat losses
- Storage system initial costs
- Limited experience of the added benefits that storage can provide
- Difficulties in integration and subsequent optimisation when added to existing heat supply systems
- Conventional gas boiler systems can provide heat rapidly with little need of storage
- The limited time of use tariffs available to domestic customers in the current energy system mean there is little incentive to generate and store heat/coolth for later use and change from existing use patterns

In the current situation, sensible heat storage (SHS) systems are mature technologies, widely applied worldwide. In addition latent heat storage (LHS) systems are regarded as a promising alternative for heat storage due to their higher heat storage density and longer heat storage potential in comparison with SHS systems. Although these storage methods could provide some benefits to reduce energy consumption in the built environment, more radical solutions are required for achieving substantial reduction in fossil fuel use and CO_2 emissions.

The main problem with the heat storage applications is the limited availability of storable solar energy in winter while the building heat load is at its peak. Additionally, low heat storage density of the currently applied heat storage materials/systems, increases the required storage volume. This aspect makes the integration of these systems to the buildings difficult while increasing the costs simultaneously. Besides, with SHS and LHS, stored energy needs to be consumed in short period of time due to the heat losses, which limits the control and flexibility of their usage.

Thermochemical heat storage (THS) systems have gained attention in the last decade due to their higher heat storage density / lower volume requirement also long term heat storage potential without heat losses. This important aspect represents significant opportunities including inter-seasonal storage of solar energy, conversion and thermal storage of excess renewable energy sourced electricity (e.g photovoltaic panels), capturing / storing the industrial waste heat and utilizing off -peak electricity tariff with THS materials.

Despite the above given features, THS technology is relatively new in comparison with the other storage methods and there are some major challenges which should be tackled to roll out these systems commercially. Specifically; high regeneration temperature and poor cyclic ability of conventional sorbents, limitations of the heat/mass transfer in sorption reactor and complexity of the process design are major drawbacks of THS systems.

Accordingly, development of advanced sorption materials also innovative process and sorption reactor design are key fields for future progress of THS systems. These fields constitute the main area of this project and it is targeted to address the above limitations by developing novel composite sorption materials, reactor concepts and processes to realize an efficient THS system for thermal energy storage.

1.3 Research aims and objectives

The aim of this research is; developing efficient open thermochemical energy storage materials and processes suitable to integrate with solar energy and heat pump systems for improving sustainability in building space heating applications.

Therefore, the overall objectives of this research are:

- To analyse the short term and inter-seasonal solar thermal energy storage potential with sorption materials and to determine system sizes and potential energy / emission savings through application of THS under severe (e.g. UK) and mild (e.g. Cyprus) climate conditions.
- To develop advanced composite sorption materials with higher energy density, lower regeneration temperature and better cyclic ability than conventional sorbents (e.g Zeolite, silica gel)
- To develop a 3 kWh sorption reactor using embedded air diffusers inside the sorption material to enhance the heat and mass transfer thereby to obtain an improved THS process efficiency.
- To modify and scale up the 3 kWh proof-of concept to a 25 kWh modular sorption pipe reactor that provides improved energy storage density, that is easy to operate and that could be integrated with solar concentrators or transpired solar collectors to store solar energy for building space heating applications.
- To develop and demonstrate a 1000 kWh full-scale modular THS integrated with roof mounted transpired solar collectors for inter-seasonal solar thermal energy storage.

- To develop an efficient HP driven sorption storage heater that could be utilized for conversion and thermal storage of electricity generated by PV panels and/or to utilize off-peak tariff for cost-effective space heating in buildings.

The research concept of this study consists of three dimensions which are process design, reactor design and sorption material development with the purpose of developing THS systems suitable for i) *capture and storage of solar thermal energy and/or waste heat and ii) thermal conversion and storage of renewable energy sourced (e.g. PV) and/or off-peak tariff electricity* (Please see: Fig 1.3.1). Presented research covers the design, development, modelling and experimentation work with the aim of obtaining promotive outcomes that contribute the progress of THS systems.

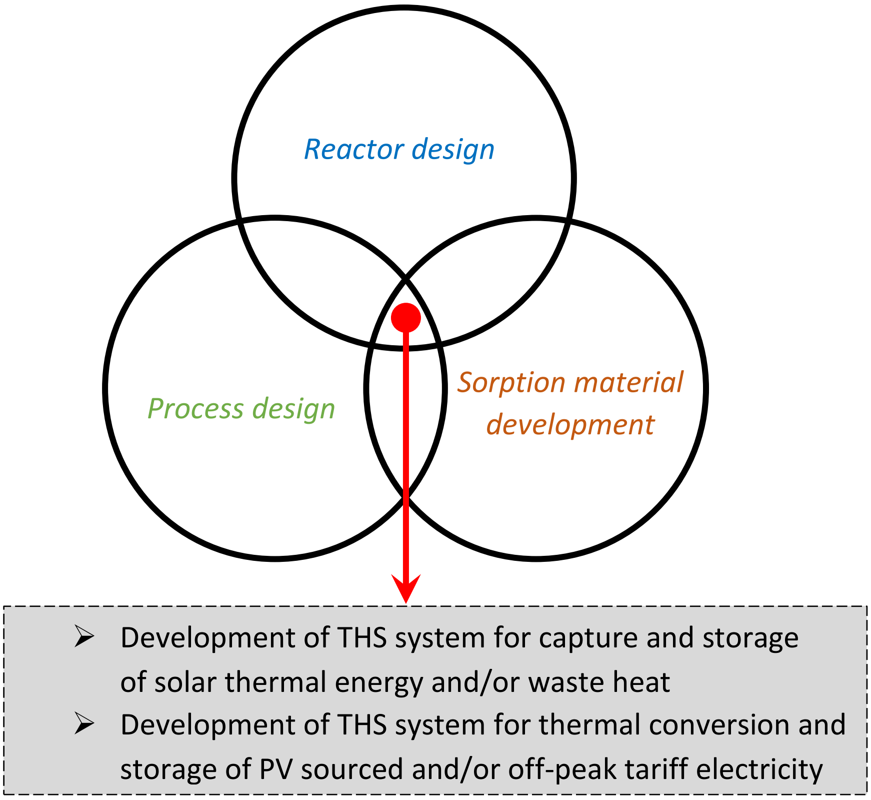

- Development of THS system for capture and storage of solar thermal energy and/or waste heat
- Development of THS system for thermal conversion and storage of PV sourced and/or off-peak tariff electricity

Figure 1.3.1 The research model

1.4 Scope of the project

The scope of this project, in order to favorably fulfill the above objectives, is categorized into following distinct stages;

- Overview of past and present work on thermal energy storage systems
- Theoretical and parametric analyses on the application of building integrated solar driven THS system in Cyprus and in the UK
- Synthesis and characterization of sorption materials
- Development and experimentation of a THS reactor under laboratory conditions
- Development of a 1000 kWh building integrated solar driven THS and carrying out field trials
- Development and experimentation of a heat pump driven sorption storage heater
- Discuss the key outcomes of the present study and interpret future directions of THS systems and other potential future applications of sorption systems/materials

1.5 Novelty

This project has the following novel aspects:

- The development of new efficient composite sorption materials that could be utilized in THS systems and in other several applications such as drying, air dehumidification, desiccant cooling, air conditioning, air purification etc.
- The design and development of a novel reactor that could be scaled up and utilized in THS applications for thermal energy storage.

- The design and development of modular sorption pipe reactor integrated with solar concentrator that eases solar charging of the sorbent, reduces heat losses and reduce space requirement for heat storage installation in buildings.
- The development of HP driven sorption storage heater for utilizing PV sourced and/or off-peak tariff electricity in buildings for efficient space heating.
- The demonstration of first of its kind, real scale solar driven THS system.

1.6 Research methods and methodology

The project work, in this thesis, is mainly based on the following stages:

- *Background work and literature review*

Comprehensive literature review covers the past and present research on heat storage technologies with the emphasis of THS and comparison of THS with other thermal energy storage (TES) systems. Within the literature review, latest advancements on adsorption/absorption cycles and sorption materials, progress in THS process and reactor design also recent THS applications were investigated to comprehend the scope of this project and retrieve the relevant data from the previously published studies.

- *Design and Modelling work*

Recognised and appropriate softwares e.g. Autocad, Microsoft Excel, Ecotect and Engineering Equation Solver (EES) was used in order to design and theoretically investigate the feasibility of solar driven THS in warm and cold climates, to perform material based comparisons also to thermodynamically analyse the proposed THS processes and evaluate their performance under different operating conditions.

- *Laboratory scale prototype development and testing*

Prototype THS systems were developed and physically experimented under laboratory conditions for assessing both material and process thermal performances.

- *Field trial*

A field trial was carried out on a remote project to detect and monitor the real-time performance characteristics of the developed full- scale THS system.

1.7 Structure of the thesis

The thesis is divided into nine chapters, following this introductory chapter, the work is presented in the following sections:

Chapter 1: Covers the introductory section to the driving forces of this work. The objectives, scopes and novelty aspects of the project are detailed. Also, the methodology approach to fulfil the objectives is provided in the present chapter.

Chapter 2: Facilitates understanding the questions prevailing in THS technology with particular emphasis of materials, sorption processes/cycles and reactor design, interpreting new research directions towards further improvement of the performance, addressing the important issues related to the, sorbent development system design, installation and operation. Also, the review work in this chapter reveals the trend of the technology, particularly the advancement in recent years and the future work required.

Chapter 3: Theoretically investigates the applicability of solar driven THS in buildings in the UK through a comparative analyse with SHS and LHS. Within the study seasonal and daily heat load of a selected real building was simulated. Based on the obtained heating demands, required heat storage volume for the case of using different heat storage materials for solar energy storage was investigated both for short term and seasonal basis.

With consideration of coupling different heat storage systems (e.g. THS, LHS, SHS) with solar collectors, potential solar energy increase in building heat supply and potential energy savings were determined.

Chapter 4: Covers selection, synthesis, characterization and small scale physical experimentation of candidate sorption materials. Wide range of adsorbents and porous host matrices selected and various composite materials were synthesized. The developed material performances were comparatively investigated through characterization (e.g. DSC, MIP, N2 physisorption, SEM etc.) techniques and later experimented in a small scale prototype testing rig. The last section of this chapter introduces a 3 kWh sorption reactor which was designed and developed with the aim of improving achievable energy density from sorption materials. Selected materials from the initial stage were tested in the developed rig and their hygrothermal performances were compared with the results obtained from initial testing rig. Accordingly, improvement of material performances through sorption reactor design was investigated.

Chapter 5: Describes the design, development, experimental set-up and testing of a modular sorption pipe heat storage system. Within the study, influence of the air moisture levels on heat storage process performance was investigated. Besides comparative hygrothermal performance analysis of two promising candidate sorption materials; vermiculite-CaCl2 (SIM-3a) and Zeolite 13X were carried out through experimentation.

Chapter 6: Covers parametric and experimental studies on solar driven THS applications under mild climate conditions. In the first section, feasibility of a seasonal THS application in a real building located in Cyprus was investigated through the consideration of technical, economic and environmental aspects. Second part introduces a novel heat storage module consisting of an integrated sorption pipe unit and a solar concentrator. Field trial of the developed module was performed under Cyprus climate conditions and obtained results were presented within this chapter.

Chapter 7: Describes the design, development, control and operational aspects of a building integrated, full-scale solar driven modular THS system. Following the introduction and system descriptions, monitoring results and thermal performance analyses of the prototype system were presented. Key outcomes of the full scale THS demonstration and potential improvements of the prototype system were also discussed.

Chapter 8: Introduces a novel heat pump driven sorption storage heater which consists of an air to air heat pump, air to air heat exchanger and a multi-layer fixed bed sorption reactor. Within the developed concept, it is aimed to recover waste heat in charging cycle thereby to improve overall efficiency of THS process. System is purposed for storing excess energy generated by PV panels and/or benefitting from off-peak electricity tariff in buildings. In order to realize the set objectives, initially, a numerical model of the process was developed and effect of several parameters on system performance was investigated. Later, new composite materials were synthesized and characterized. Finally a prototype system was designed, developed and experimented with the use of selected five different sorbents. Obtained theoretical and experimental outcomes were discussed within the chapter.

Chapter 9: Provides the general discussion and concludes the work based on the theoretical and experimental investigations performed in this project. This section also suggests further works through introduction of some potential applications and open doors to the researchers interested in this area.

CHAPTER 2: OVERVIEW OF THERMAL ENERGY STORAGE SYSTEMS

2.1 Introduction

Due to the increase in world wide human population, technological development, and industrialisation, usage of fossil fuels has been dramatically rising. Added to this, the rise in greenhouse gas emissions and fuel prices have contributed to the well-established development of various renewable energy resources such as wind, solar, tidal and geothermal etc. However there remains a mismatch between most renewable energy supplies and user demand which currently is one of the main barriers to both improving and implimentation of sucessful sustainable energy systems (Marias et al., 2014). Improving renewable energy systems and in particular energy storage systems to tackle this mismatch is arguably as important as developing new energy resources.

Solar energy is currently seen as one of the most promising alternatives to conventional energy resources. The use of solar thermal energy has been widely researched, publicly accepted and implimented for heating, ventilation and air-conditioning in both domestic and industrial buildings. (Parameshwaran et al., 2012) demonstrated that the highest energy usage takes place in the domestic sector Over half of the energy consumed in domestic sector; is for air conditioning and hot water purposes as shown in Figures 2.1.1 and 2.1.2 respectively (Parameshwaran et al., 2012).

Despite the common acceptance of solar thermal systems, the main obstacle in its application is the mismatch between the supply and demand. Development of reliable and economically feasible thermal storage systems, is of vital importance for the efficient and sustainable use of solar energy into the future.

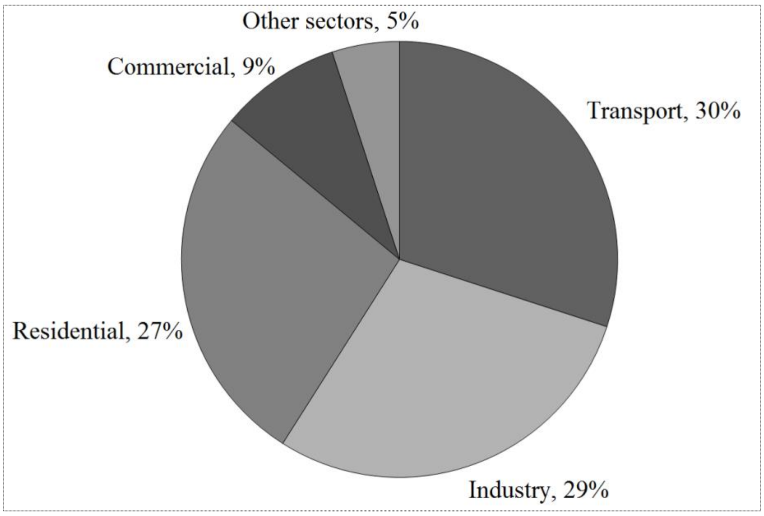

Figure 2.1.1 Energy consumption break-down by sector (adapted) (Parameshwaran et al., 2012)

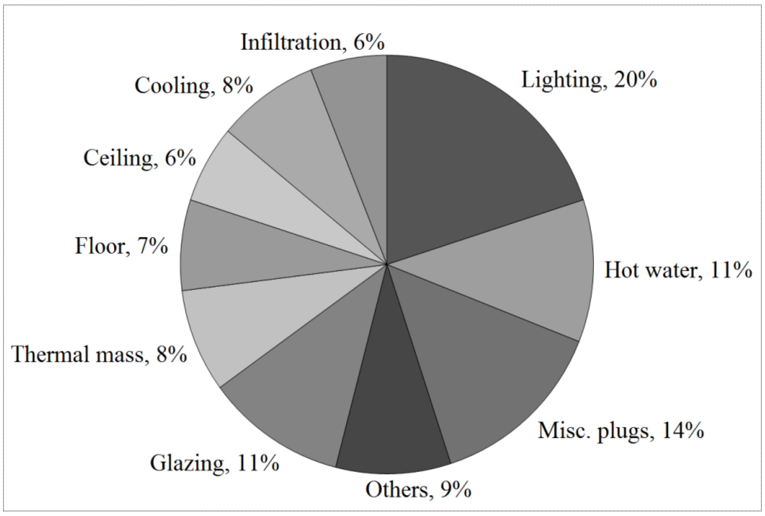

Figure 2.1.2 Average break-down of energy usage and losses in buildings (adapted) (Parameshwaran et al., 2012)

Currently, there are three main types of thermal energy storage (TES) systems known:

1. Sensible heat storage (SHS).
2. Latent heat storage (LHS). SHS and LHS are employed both on a small scale for heating purposes in buildings and on a larger scale in solar thermal power plants (Parameshwaran et al., 2012).

3. Thermochemical heat storage (THS), is a relatively new technology with much research and development on these systems ongoing.

Among the other storage techniques, THS seems to be a promising alternative to be used as a energy storage system (Pardo et al., 2014, Ervin, 1977, Garg et al., 1985). These systems can utilise both sorption and chemical reactions to generate heat and in order to achieve efficient and economically acceptable systems, the appropriate reversible reactions (suitable to the user demand needs) need to be identified (Pardo et al., 2014, Wentworth and Chen, 1976). In recent years, sorption thermal energy storage (STES) systems coupled with chemical systems are increasingly gaining credibility as they become promising options for solar heat storage (Pardo et al., 2014, Ervin, 1977, Garg et al., 1985, Wentworth and Chen, 1976). Their advantages include relatively high storage capacities and the unique function to preserve energy for longer periods with limited heat loss.

The aim of this chapter is to evaluate the current situation of THS systems research and implimentation as well as to highlight the main deficiencies of the current systems that stand in the way of proper commercialisation. A general evaluation and comparison of the current research on heat storage systems and materials has also been provided.

2.2 Thermal Energy Storage Systems

The effectiveness of TES systems are highly dependent on their dimensions, applied method and heat storage material (HSM). Heat storage can be applied as short or long term where HSM quantity and properties as well as system design are vital for TES performance. For example, if the difference between the intensity of solar energy and energy demand of building is minimal, then a ‘short term’ TES system may be suitable. A ‘long term’ TES system could be used to supply seasonal energy demand, and will increase the contribution of solar energy in the process of compensating the buildings overall energy demand. In terms of thermal energy generation prices and solar intensity, decided decision could be reached to use either a short term or long term TES system. (Sharma et al., 2009) A comparison between short and long term storage for solar heating systems is given in Table 2.1.

Table 2.1 Comparison between central solar heating systems with short term and long term storage (Schmidt et al., 2004)

	Short Term TES	**Long Term TES**
Time span	Several hours or days	3-6 months
Minimum size	More than 30 apartments	More than 100 apartments
Yearly solar fraction	10-20%	Over 50%
Costs	0.08-0.15 €/kWh	0.17-0.40 €/kWh
Collector area	0.8-1.2 kWh per person	1.4-2.4 MWh annual demand
Storage volume	0.05-0.1 m^3 water/m^2	1.4-2.1 m^3 water/m^2

2.3 Heat Storage Methods

The selection of any particular TES method primarily depends on the storage period required, economical applicability and system operating conditions (Zhou et al., 2012, Sharma et al., 2009, Aydin et al., 2015b, Kenisarin and Mahkamov, 2007, Zalba et al., 2003). For any application, the efficiency and economy of the system not only depends on the heat storage method but also the design of the system. For any TES system design, the factors shown in Figure 2.3.1 should be considered.

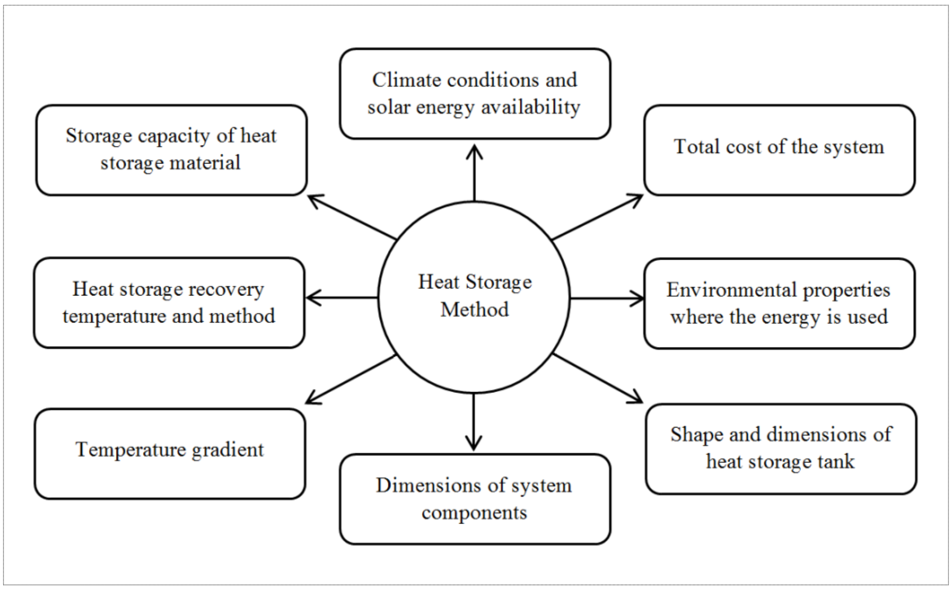

Figure 2.3.1 Factors to be considered in a heat storage system design

As mentioned in the introduction, there are three types of TES system; sensible, latent and chemical. A technical comparison of these storage systems is given in Table 2.2.

Table 2.2 Comparison of heat storage systems (Abedin and Rosen, 2011, Xu et al., 2013)

	Type of thermal energy storage		
	Sensible	*Latent*	*Thermochemical*
Temperature range	• Up to: 110°C (water tanks) • 50°C (aquifers and ground storage) • 400° (concrete)	• 20-40°C (paraffines) • 30-80°C (salt hydrates) (High temperature PCMs were not included)	• 20-200°C
Storage density	• Low (with high temperature interval): 0.2 GJ/m^3 (for typical water tanks)	• Moderate (with low temperature interval): 0.3-0.5 GJ/m^3	• Normally high: 0.5-3 GJ/m^3
Technology status	• Available commercially	• Available commercially for some temperatures and materials	• Generally not available, but undergoing research and plot project tests
Life time	• Long	• Often limited for storage material cycling	• Depends on reactant degradation and side reactions
Advantages	• Low cost • Reliable • Simple application with available materials	• Medium storage density • Relatively low volume requirement • Short distance transport possibility	• High storage density • Low heat loses (storage at ambient temperatures) • Possibility of charging in summer (high solar fraction) • Long storage period • Long distance transport possibility • Highly compact energy storage
Disadvantages	• Significant heat loss over time (depending on level of insulation) • Large volume and space needed • Charging in summer (seasonal storage) increase heat loss. • Charging in winter (short term storage) decreases solar fraction	• Low heat conductivity • Corrosivity of materials • Significant heat loses (depending of level of insulation) • Charging in summer (seasonal storage) increase heat loss. • Charging in winter (short term storage) decreases solar fraction	• High capital costs • Technically complex

There are several methods (see: Figure 2.3.2) that are commonly used for storing thermal energy. Among all, SHS is the most mature technology. It is based on increasing the temperature of a material which has a high specific heat capacity, such as rock, sandstone, water, soil or concrete among others.

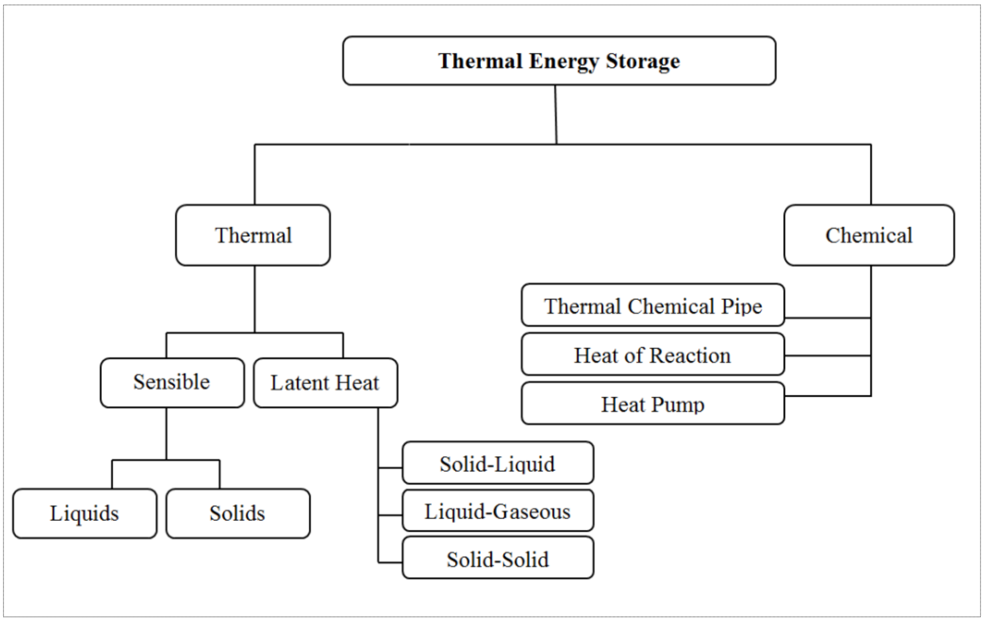

Figure 2.3.2 Heat storage methods (Sharma et al., 2009, Zhou et al., 2012, Cárdenas and León, 2013)

In this type of storage method, the storage volume must be well insulated in order to prevent heat loss to the surroundings. Underground storage using SHS is currently one of the best solutions for minimizing this heat loss. On the other hand, latent heat storage (LHS) is a relatively new TES method in which the heat is stored and released during a phase change process (Sharma et al., 2009, Kenisarin and Mahkamov, 2007, Zalba et al., 2003). LHS uses materials that are classed as phase change materials (PCMs). There are many types of both organic and inorganic PCM employed in LHS (see: Figure 2.3.3). Paraffin is the most promising organic PCM, whilst hydrated salts are highly preferred as an inorganic PCM. LHS has a higher energy storage density when compared with SHS, however, the increased complexity of design and tight control requirement of the phase change process are drawbacks.

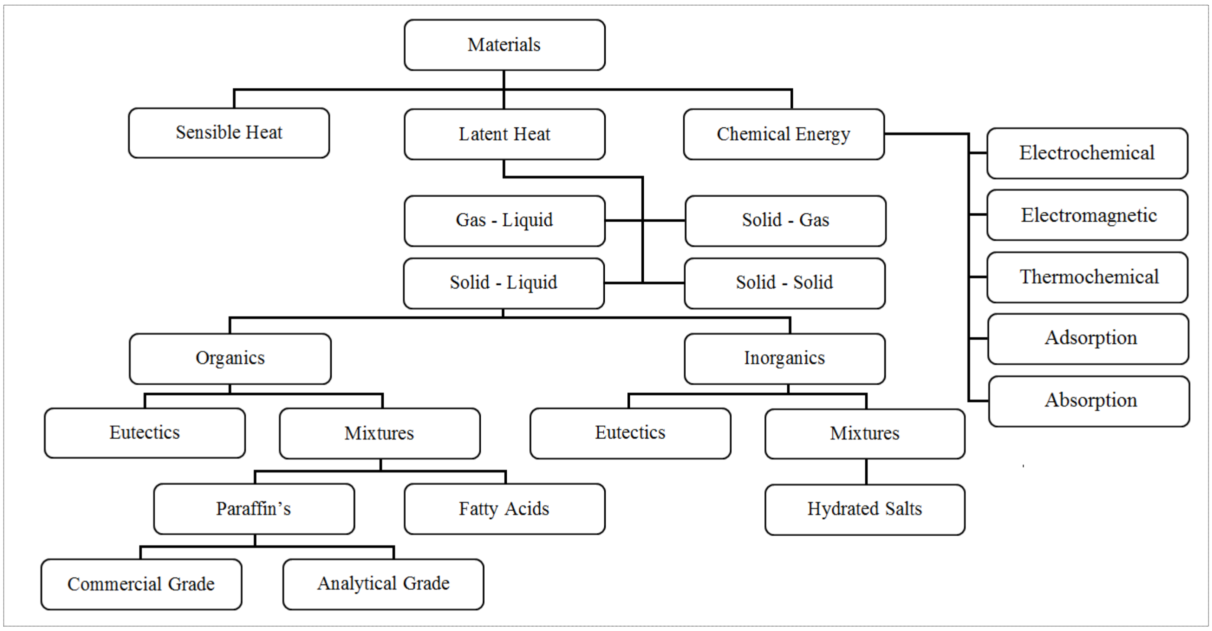

Figure 2.3.3 Classification of heat storage materials (adapted) (Xu et al., 2013)

THS materials have approximately 8 - 10 times higher storage density over SHS, and two times higher over LHS materials when compared on a like for like storage volume basis. However in THS, there are limitations in that an efficient reaction requires efficient heat and mass (HAM) transfer to and from the storage volume. This condition can severely limit the overall storage volume which is not the case in SHS and LHS systems, allowing higher volumes to be utilised. This volume limitation due to the HAM transfer characteristics is one of the key areas for current research in order to deliver effective THS or TES systems in the future. Another drawback of both THS and LHS systems is both the high costs involved and their complexity. In addition to this the implementation of large volume storage systems are both logistically and operationally hard and not feasible using the current technology. On the other hand SHS systems that require utilisation of larger storage volumes are easily achievable if there is adequate available free space. The associated heat loss and low energy density (E_d) are still large drawbacks of this storage method. The following sections look more closely at each of the discussed TES methods in greater detail.

2.3.1 Sensible Heat Storage

As stated, SHS systems store energy by changing the temperature of a heat storage material. This method converts collected energy into sensible heat in selected materials and retrieves it when that heat is required. The amount of stored energy depends on the specific heat capacity of the storage material and the temperature increase. SHS systems are considered to be a simple, low cost and relatively well developed technology. As these systems are inexpensive and very reliable, they have been used in several applications such as hot water (*e.g.* domestic, industrial) and space heating (*e.g.*domestic, greenhouse) (Zhou et al., 2012, Xu et al., 2013, Cárdenas and León, 2013, Sharma et al., 2009).

2.3.2 Latent Heat Storage

In a LHS system, the storage and absorption of heat occurs via a fusion reaction (melting / solidification) during the phase change period. Latent heat storage systems, in which PCM's are used, have higher energy density when compared to SHS materials and also have low temperature and volume changes (Zalba et al., 2003, Utlu et al., 2014). The main difference between a LHS system and a SHS one is that during absorption, heat stored with a phase change process in a constant temperature. LHS systems can have phase change processes from solid to liquid, liquid to gas or the inverse of these processes (Cárdenas and León, 2013, Dincer, 2002). There are several studies about LHS and SHS in the literature. Combining heat storage systems with solar collectors and heat pumps can bring significant advantages for decreasing energy consumption. Some of the previous studies about hybrid heating systems are listed in Table 2.3;

Table 2.3 Previous studies researching heating systems

	Type of Study	**Material**	**Heat Storage Method**	**Other Components**	**η_I**	**η_{II}**	**COP**
(Başçetinçelik et al., 1999)	Exp.	Paraffin	LHS	Solar Collectors	42%	3.3%	-
(Hussain et al., 2004)	Num.	Ethlyene glycol	SHS	HVAC	80%	0.5-14%	
(Öztürk, 2005)	Exp.	Paraffin	LHS	Flat plate solar collector	40%	4.2%	-
(Kumari et al., 2006)	Exp.	$CaCl_2.6H_2O$		-	-	-	
(Gunerhan and Hepbasli, 2007)	Exp.	Water	SHS	Solar Collectors		3.3-4.4%	-
(Han et al., 2008)	Num.	$CaCl_2.H_2O$	LHS	Solar Collectors+HP	-	-	3.3-6
(Koca et al., 2008)	Exp.	$CaCl_2.6H_2O$	LHS	Flat plate solar collector	45%	2.2%	-
(Wang et al., 2009)	Exp	Water	Underground SHS	Solar-Ground Source Heat Pump	76%		-
(Benli and Durmuş, 2009)	Exp.	$CaCl_2.6H_2O$	LHS	GSHP	-	-	2-3.5
(Wang et al., 2010b)	Exp.	Soil	LHS	Solar Collectors+HP	-	-	6.6
(Fernández-Seara et al., 2012)	Exp.	Water	SHS	Solar Collectors+HP			3.2
(Utlu et al., 2014)	Exp.	Paraffin	LHS	Solar Collectors+GSHP	62-74%	7-37%	-

2.3.3 Thermochemical Heat Storage

Thermochemical heat storage (THS) has the distinctive advantages of coupled high energy storage and low heat loses when compared to both SHS and LHS technologies and is currently regarded as the most promising alternative (Pardo et al., 2014, Abedin and Rosen, 2011, Xu et al., 2013). Another attractive property of THS is its capability of the systems to conserve the heat energy at ambient temperature as long as desired without heat loses due to the chemical reactions. Due to the advantages mentioned above, THS has become a widely researched technology for seasonal energy storage (Xu et al., 2013). Figure 2.3.4 illustrates a comparison of the energy densities of some high energy storage materials.

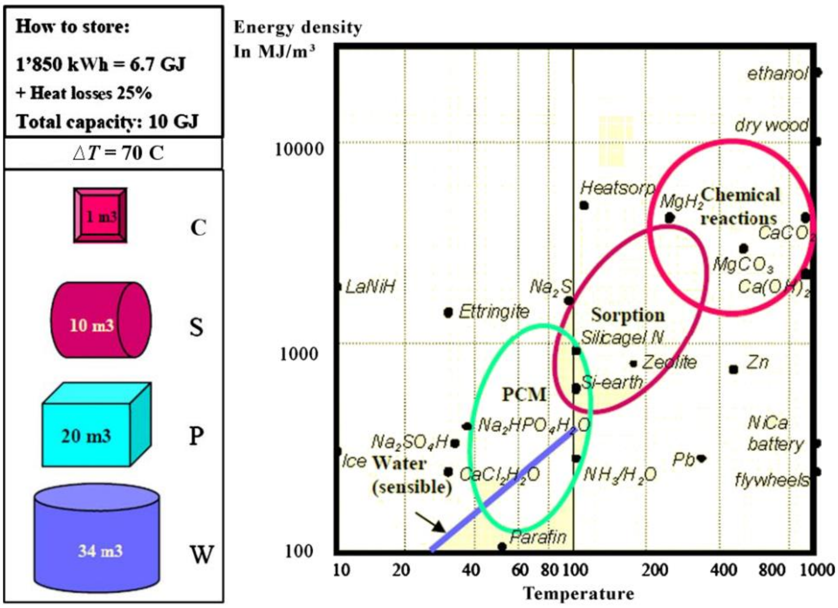

Figure 2.3.4 Comparison of energy storage densities of energy storage methods (Xu et al., 2013)

The effective performance of a THS depends on several design parameters.

- THS material
- Ambient psychrometric conditions where the storage system will be used
- Process design

- Reactor design

These are all vital parameters for achieving a high system temperature lift, Δ*T*. There are several factors to be considered when designing a thermochemical heat storage system. These factors are summarized in Figure 2.3.5.

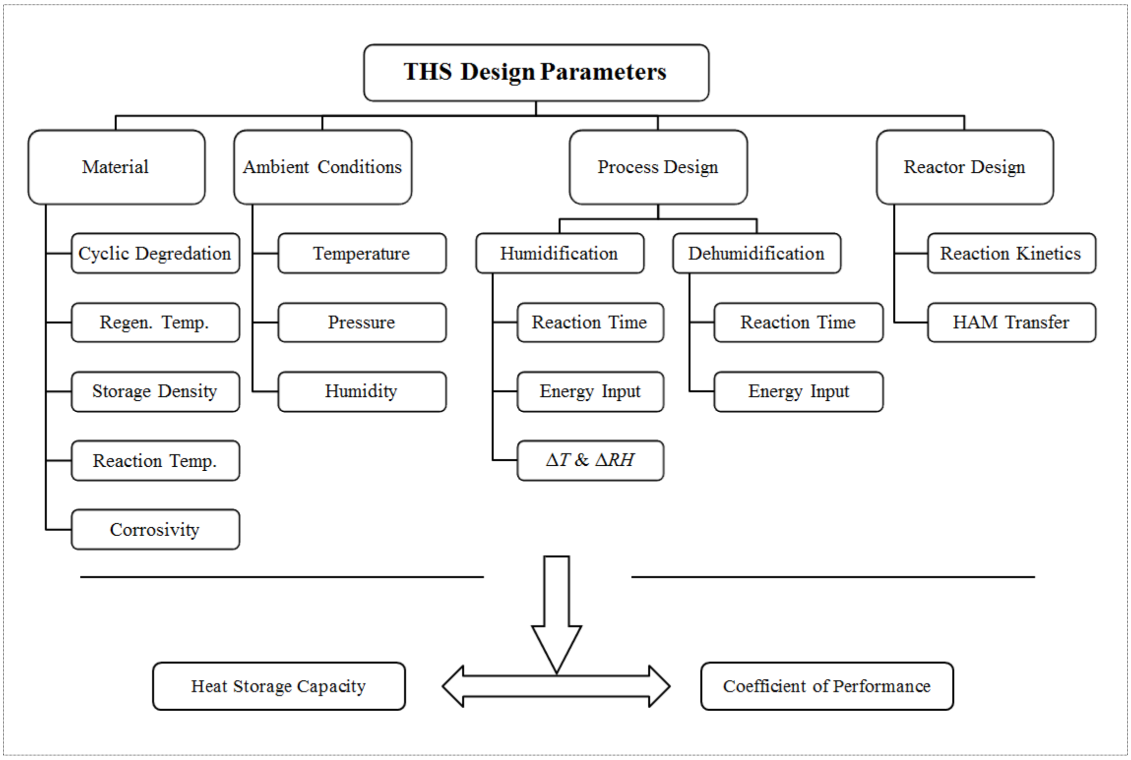

Figure 2.3.5 Design parameters of thermochemical heat storage

THS systems can be further classified as either solely chemical or thermochemical reaction storage (see: Figure 2.3.6). Chemical storage systems are based on a reversible reaction of two seperate chemical substances where a high amount of energy is generated as a result of an exothermic synthesis reaction.

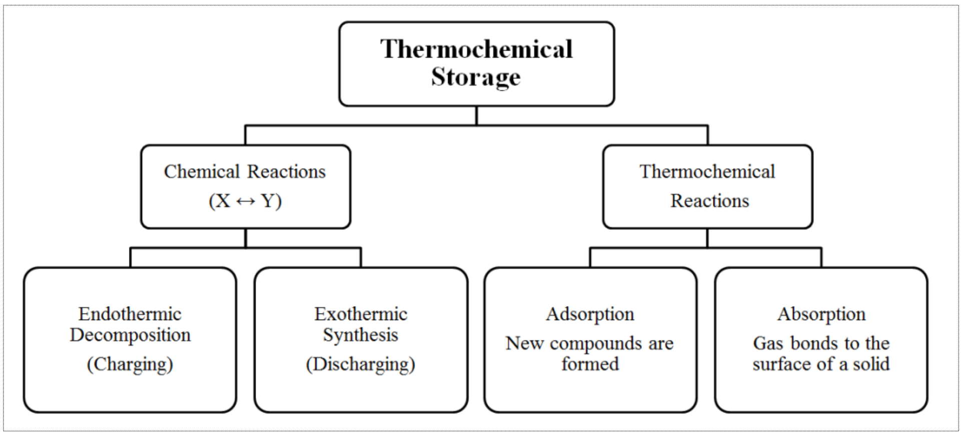

Figure 2.3.6 Classification of THS systems

Thermochemical reaction storage systems are related to sorption mechanisms. Within a sorption system a relatively small amount of energy with a lower temperature is generated, however there is a lower activation energy required to start the reaction. This provides sorption storage systems with an advantage over solely chemical systems for low temperature applications.

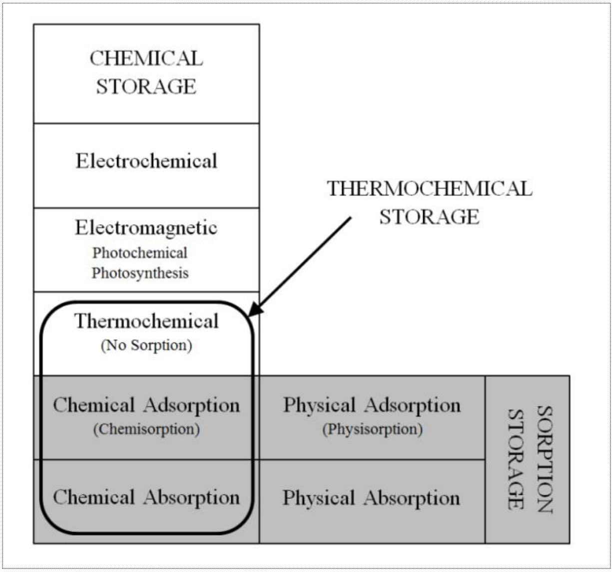

Figure 2.3.7 Sorption thermal storage types (Yu et al., 2013, N'Tsoukpoe et al., 2009)

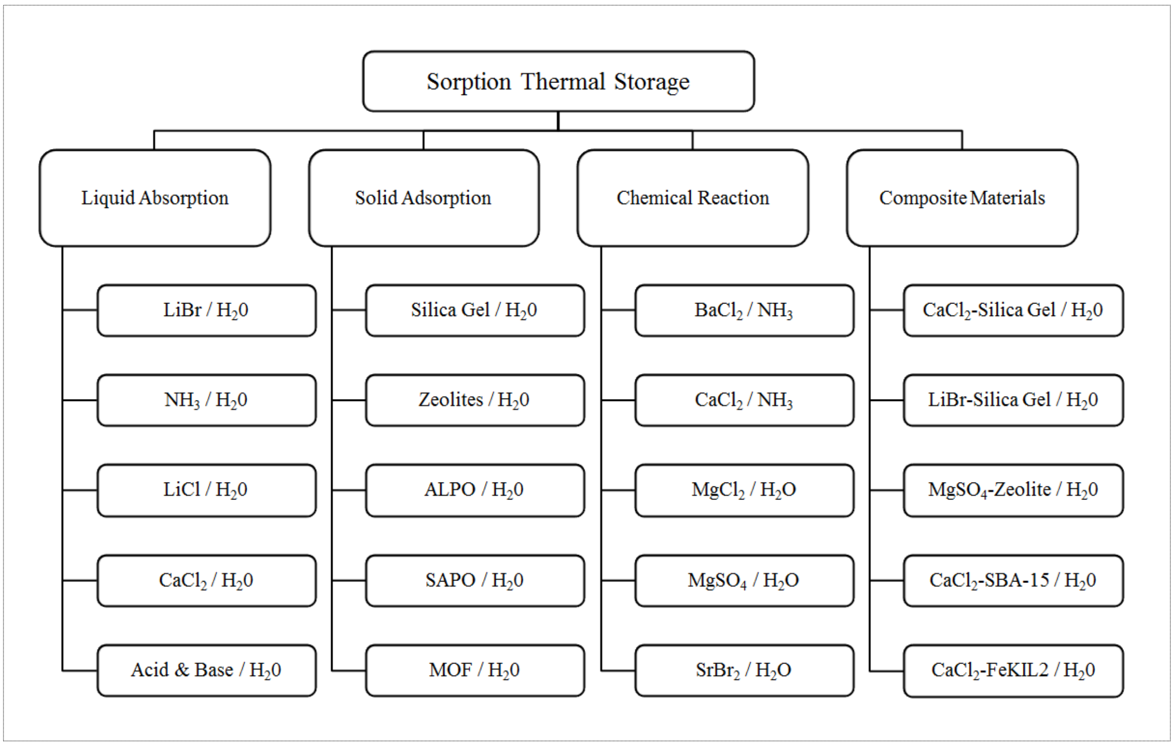

Figure 2.3.8 Sorption thermal storage mathods and materials (adapted) (Yu et al., 2013)

Figure 2.3.7 and Figure 2.3.8 illustrate sorption storage types and materials respectively. The characteristics of sorption process are (Yu et al., 2013);

- They reqire heat to expel a sorbate (gas) from the sorbent (matrix).
- No sorption process can take place until there is contact between the sorbent and sorbate. With hermetic isolation of the sorbate, thermochemical energy can be stored independent of the time.
- There is no heat or entrophy loss during storage allowing long term storage with THS.
- Solar energy can be stored during the summer (charging / desorption) to meet heating demand in winter (discharging / sorption).

- LHS can only be applied for specific temperatures ranges whereas THS has greater flexibility for determining both input and output temperatures allowing a greater range of practical applications.
- THS can also be applied either during the summer for cooling (charging) or in the winter for heating (discharging).

According to the system design, sorption thermal storage systems can be divided into either ‘open’ or ‘closed’ systems. These are discussed in the following sections.

2.3.3.1 Closed Sorption Systems

Closed sorption systems are those where the components are completely isolated from the atmospheric environment. They typically comprise a reactor in which the adsorption process takes place and a condenser for condensing water vapour into liquid form (see: Figure 2.3.9). In closed sorption systems, water vapor directly reacts with reactant.

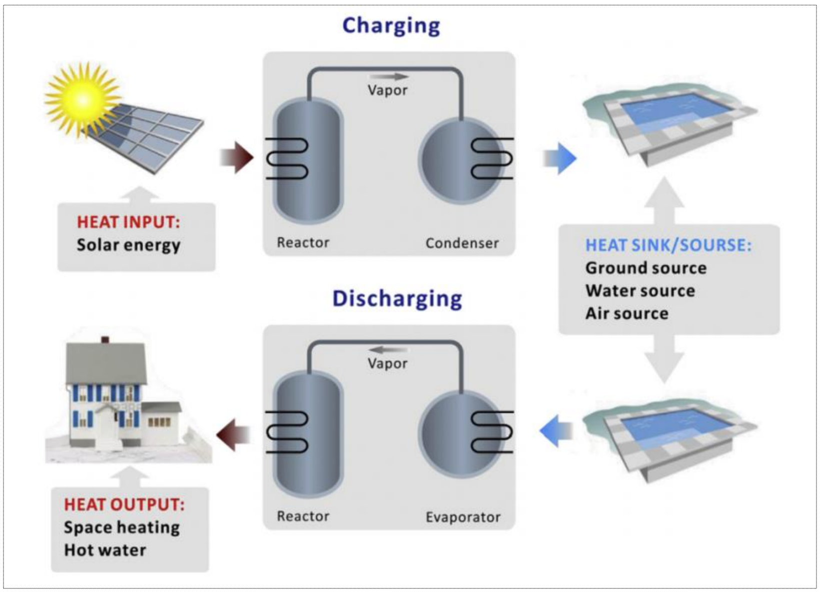

Figure 2.3.9 Schematic diagram of a closed sorption system (Yu et al., 2013)

Generated heat is extracted with an external heat transfer fluid (*e.g.* water, air). This provides a flexibility for reacting the materials and extracting the heat in different periods.

As a result of benefitting from temperature lift of the adsorbent material, a higher energy density is possible with this storage method, however this condition requires an efficient heat exchanger design. Additionally, different reaction and extraction mechanisms increase system complexity and operational conditions as well as the investment costs of closed sorption storage.

2.3.3.2 Open Sorption Systems

Open systems, as the name suggests are open to the environment. The sorbate used (typically water vapour) for the sorption process during discharging is obtained direct from the ambient air or, in some cases from a moisture source such as a humidifier (see: Figures 2.3.10 and 2.3.11).

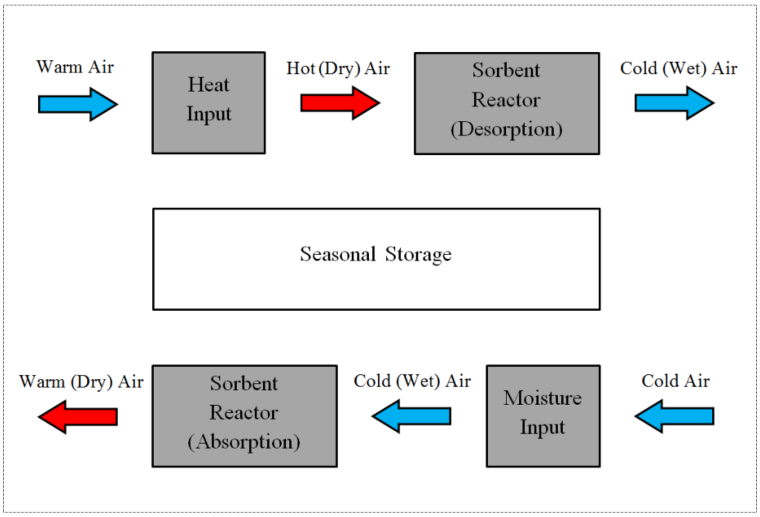

Figure 2.3.10 Schematic diagram of an open sorption system

In summer solar energy can be used to seperate the adsorbed water from the adsorbent. Comparing with closed cycles, open storage systems have an easier process design which makes operational conditions easier. However, because of the vapor adsorption-heat generation and heat transfer to air, take place at the same time, reactor design is vital for storage performance.

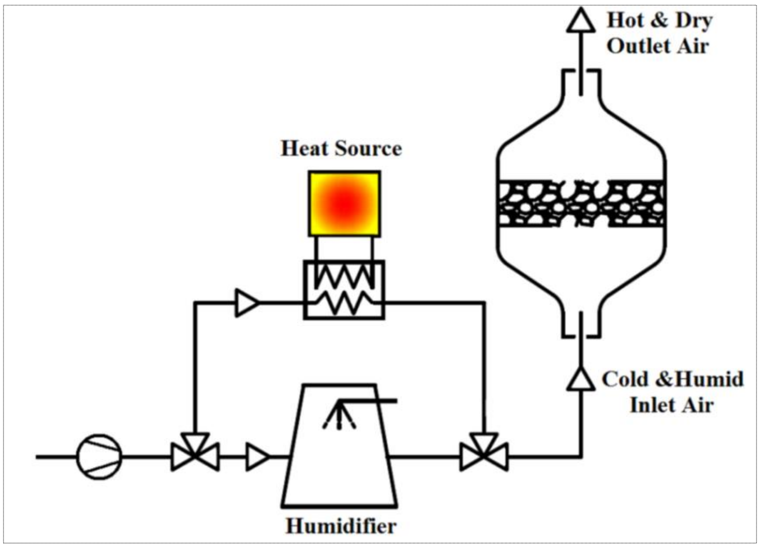

Figure 2.3.11 Operating principle of an open adsorption system

Providing a moisture adsorption for a longer time, is directly related to the temperature lifting of air. Although at the beginning of reaction, good vapor diffusion is provided in this systems, as the time passes, it shows a decreasing trend and results with a drop in temperature lifting. This causes an unstability during heat generation, contrarily to closed sorption systems. Because in closed cycles generated total heat can be stored as sensible and extracted amount can be set with changing the parameters of HTF (*e.g.* mass flow rate).

2.3.3.3 Adsorption Cycles

Adsorption is a surface based process where atoms or molecules of a gas, liquid or a solid sticks on a surface of a material as a result of adhesion forces (Yu et al., 2013, N'Tsoukpoe et al., 2009, Aristov, 2007a, Wang and Vineyard, 2011).

Adsorption cycles are based on this principal and basicly consist of four steps (see: Figure 2.3.12) described below;

A. Heating and Pressurization

B. Desorption and Condensation

C. Cooling and Depressurization

D. Adsorption and Evaporation

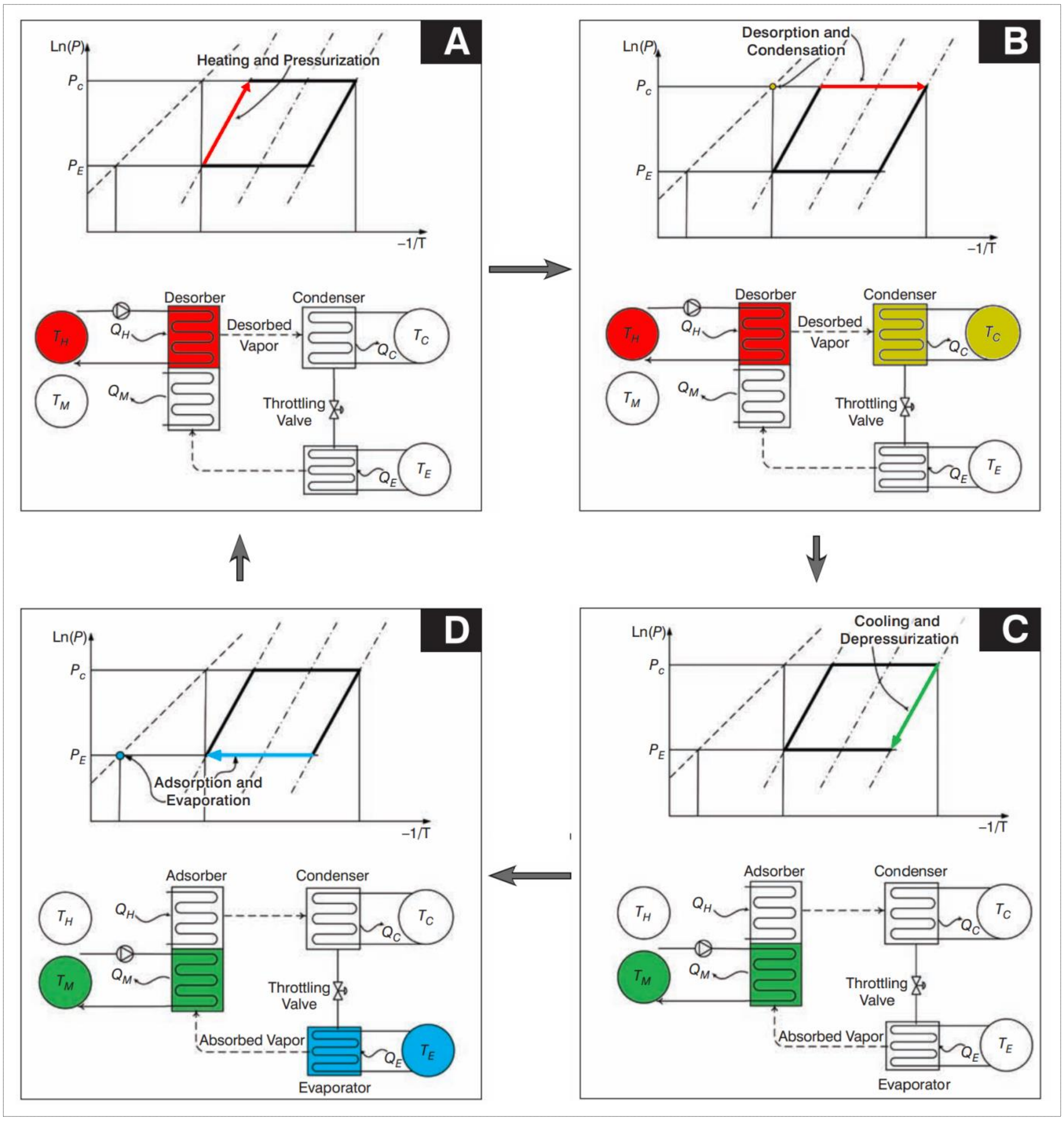

Figure 2.3.12 Basic adsorption refrigeration system (Wang and Vineyard, 2011)

There are several factors that affect the storage density of an adsorption system including density of the adsorber, porosity of the composite and properties of the additive. Hydrates and ammoniates can be used in adsorption sytems for seasonal storage. Adsorption cycles can be further divided into two groups (Chan et al., 2013):

1. Mutiple bed cycles - Combinations of two or more adsorption cycles give a more flexible heat source temperature
2. Thermal wave cycles - For low grade heat transportation

2.3.3.4 Absorption Cycles

Absorption (see: Figure 2.3.13) is the penetration of the sorbate through the surface layer of an absorbent with a change of compositon (IUPAC, 1994). Absorption heat pump (AHP) technology has been further developed when compared to adsorption heat pumps (Srikhirin et al., 2001, Fan et al., 2007). This is primarily due to the fact that the absorption cycle is more suitable for low grade heat utilization. (Aristov, 2007b, Aristov, 2009, Gordeeva and Aristov, 2012, Veselovskaya et al., 2010, Ponomarenko et al., 2010). Some of the most promising sorbent / sorbate couples for absorption cycles are water-lithium bromide (H_2O - LiBr) and ammonia - water (NH_3-H_20) (IUPAC, 1994, Srikhirin et al., 2001, Fan et al., 2007).

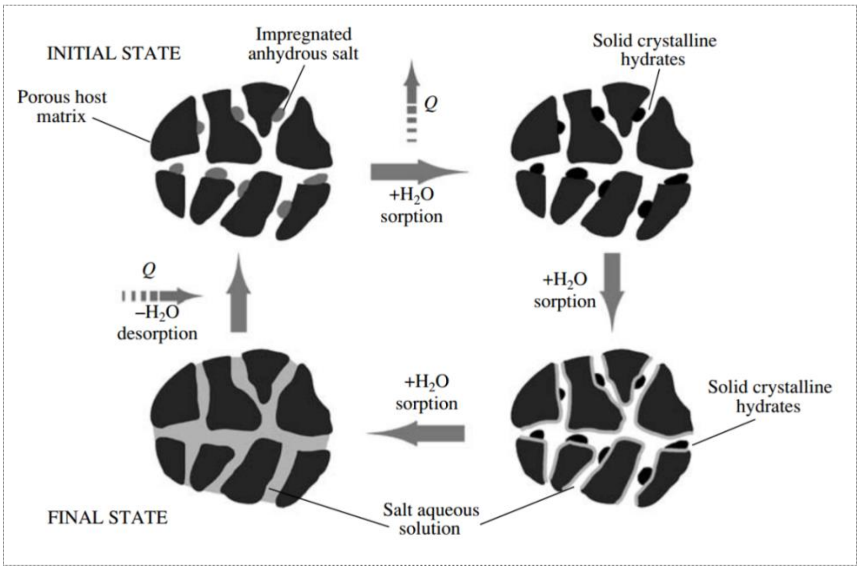

Figure 2.3.13 Water sorption mechanisms on salt (Yu et al., 2013, Aristov, 2007a)

In order to improve the sorption properties of the AHP process, a new group of composite sorbent materials have recently been developed called 'Salt In porous Matrix' (SIM) (Veselovskaya et al., 2010, Ponomarenko et al., 2010, Tanashev et al., 2013, Aristov et al., 1996b, Aristov et al., 1996a). They have been utilized for sorption cooling, heat pumps and heat storage applications. (Tanashev et al., 2013) developed a composite 'inorganic salt in a porous matrix where $CaCl_2$, $MgCl_2$ and LiBr were confined to the pores of silica gel and alumina as the porous matrix. A mathematical model was investigated for analysis of the thermal conductivity of these composites dependant on their water uptake.

If water is used as a sorbate, these materials are termed 'Selective Water Sorbents' (SWS) (Aristov et al., 1996b, Aristov et al., 1996a). There are two component parts to each SWS - one component is a host matrix (*i.e.* silica gel, alumina, expanded vermiculite, aerogel) the other is an inorganic salt (*i.e.* LiCl , $CaCl_2$, $MgCl_2$, $MgSO_4$, $Ca(NO_3)_2$, $LiNO_3$) which is placed inside the matrix pores (Aristov et al., 1996b, Aristov et al., 1996a, Aristov et al., 1997, Aristov et al., 2000b, Aristov et al., 2002, Okunev et al., 2008). The host matrix has significant importance on the overall adsorption mechanism. Where in they both hold the adsorbent and prevent dispersion of it.

Also some of the host matrices can increase HAM transfer due to the increased surface area and increase performance of the salt / sorbate reaction. The characteristic properties for some of the most promising host matrices are given in Table 2.4. The sorbate (water vapour) sorption process (see: Figure 2.3.14) contains two main mechanisms, i) a chemical reaction between the salt and sorbate and ii) liquid absorption (Aristov, 2007a, Gordeeva et al., 2009).

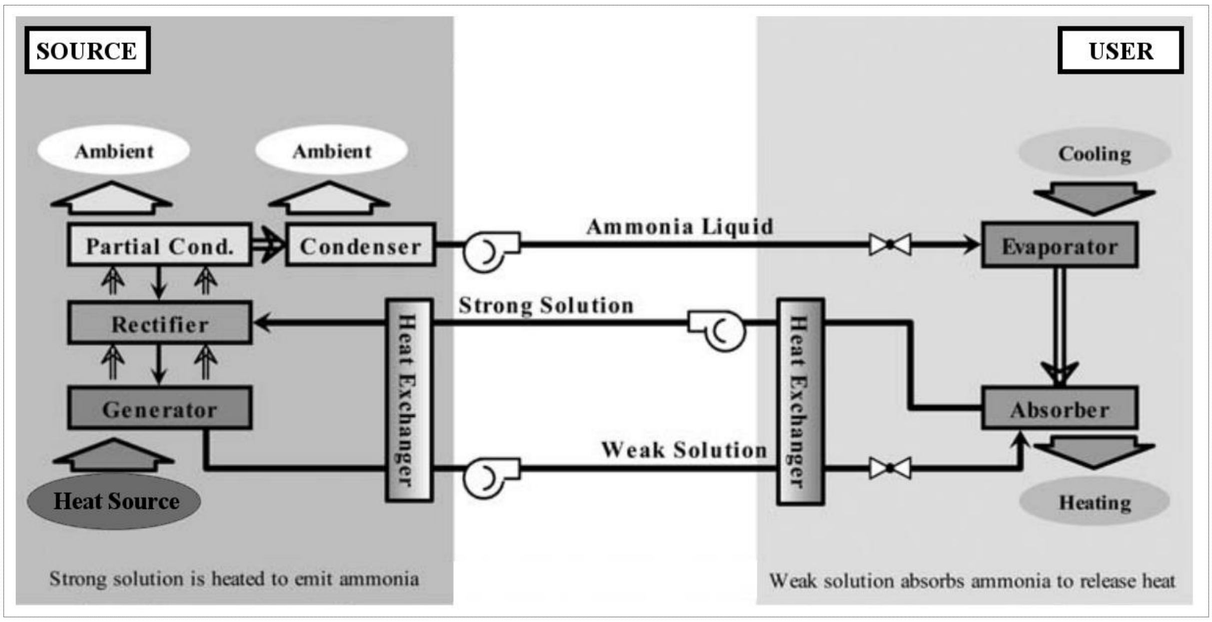

Figure 2.3.14 Schematic diagram of a low grade heat absorption cycle (adapted) (Lin et al., 2011)

Table 2.4 Comparison of the characteristic properties of the most promising host matrices

	Symbol	**SSA (m^2/g)**	**V_p (cm^3/g)**	**ρ_{bulk} (kg/m$^{3)}$**	**C_p (kJ/kgK)**	**W_{sat}**	**λ (kW/mK)**	**T_r (°C)**	**Cost ($/kg)**
Vermiculite	$(MgFeAl)_3(AlSi)_4$ $O_{10}(OH)_2.4(H_2O)$	8-10	2.8	64-160	0.84-1.08	20-50%	0.064	50-80	0.21-44
Silica Gel	SiO_2	750-850	1	480-720	1.13	30-40%	0.174	130-150	0.88-1.34
Zeolite	$Na[(AlO_2)(SiO_2)] .2(H_2O)$	550-600	0.17	1000-1120	1.08	40-75%	0.07	>200	1.65-2.2
Activated Carbon	C(AC)	1500-1700	2	2000-2100	1.06	50%	0.15-0.5	150-180	0.5-5
Expanded Natural Graphite	C(ENG)	18-22	0.073	1200-1500	0.7	40-60%	6-8	100-200	1.8-2.5
Activated Alumina	Al_2O_3	150-300	44	750-1000	1	60%	1.4-2.5	160-220	0.98-1.65

2.3.3.5 Chemical Heat Pumps

The benefit of a suitable heat pump coupled to a low-temperature heat source is that it can upgrade that heat to a higher temperature. This is however, commonly achieved by consumption of electricity in the case of vapour compression heat pumps whilst chemical heat pumps (CHP) do not require electric power since mechanical compression is not required in the system. Although conventional heat pumps are used commercially (Utlu et al., 2014), several research studies have been undertaken on chemical heat pumps because of their significant advantages in terms of energy consumption. Sharonov and Aristov (Sharonov and Aristov, 2008) developed an analysis technique to identify the ideal cycle of both chemical and adsorption heat pumps in order to compare their performance. It was shown that for chemical heat pumps it was possible to reach carnot effficiency however adsorption heat pumps have a lower efficiency due to entrophy generation. Kato et al. carried out a performance analysis of a packed bed reactor CHP (Kato et al., 2000). In this study the exhaust gas of a diesel engine was used for the desorption process. Kim et al. developed a new material to enhance the reactivity and conductivity of MgO/H_2O pair (Tae Kim et al., 2011). $CaCl_2$, expanded graphite and magnesium hydroxide were used in the mixture. Also $CaCl_2$ was introduced into the mixture to improve vapour diffusivity during the hydration process. The mixture showed improved performance when compared with pure $Mg(OH)_2$ and a $Mg(OH)_2 – CaCl_2$ mixture. (Flueckiger et al., 2012) investigated the CHP performance with reversible endothermic reactions. A mass and energy analyses of the system was undertaken and it was found that the COP and environmental impact of the system is comperable with alternative technologies such as mechanical compression heat pumps, however the exergy values were insignificant. As stated, CHPs require no electrical input for compression and for this reason they are expected to take an important role in the future utilization of solar, geothermal or waste-heats.

CHPs consist, in principle, of two different chemical reactions each run at two different temperatures. The reaction sequence functions to upgrade thermal energy, with no theoretical consumption or production of chemicals. CHP systems consist of two main units, i) an endothermic reactor (where low temperature heat is supplied) and ii) an exothermic reactor (where high temperature heat is released). Also a condenser and an evaporator will be used to condense or vapourize the adsorbate respectively (Wongsuwan et al., 2001, Karaca et al., 2002, Chua et al., 2010). A CHP can operate using either a gas-liquid absorption process or solid-gas adsorption process. Adsorption CHPs can be further classified into two groups (Wongsuwan et al., 2001, Karaca et al., 2002, Chua et al., 2010);

1. Chemisorption CHP systems – these are driven by a chemical reaction occuring at the exposed surface that can be either electronic, ionic or covalent bonding.
2. Physisorption chemical heat pump – Attraction is due to Van der Waals forces where the interaction energy is weak.

CHP systems involve endothermic desorption and exothermic adsorption/absorption processes. It is desirable to have an adsorbate/adsorbent pair or an absorbent/absorbate pair with high heat of adsorption/absorption to create a more efficient system. CHP absorption systems have been operating in industry, however the commercial applications of the adsorption cycle are much more uncommon according to Chua et al (Chua et al., 2010).

2.3.3.6 Thermochemical Heat Storage Materials

Thermochemical heat storage (THS) systems have some great advantages when compared with the other storage systems such as high energy storage density, low volume requirement and low heat loss. However there are still areas of THSs that have weaknesses which are driving the current research. Such as low heat & mass (HAM) transfer rates, low matrix permeability restricting sorbate access to and from the matrix and high pressure drops all affect THS efficiency negatively. Many studies on absorption/adsorption materials as well as reactor design are currently being carried out to enhance mass transfer during the hydration process and also to enhance heat transfer during decomposition of the absorbate/adsorbate. Table 2.5 details some of the numerous methods currently being studied to enhance HAM transfer.

Table 2.5 Methods applied in previous studies to enhance heat and mass transfer in THS

Reference	Nature	Working Pairs	Application	Method for enhance heat-mass transfer
(Willers and Groll, 1999)	Experimental-Numerical	Metal Hydride	Designing and testing a two-stage metal hydride reactor	Helical copper band, which is helically soldered into the reactor, was used as heat conduction matrix to increase thermal conductivity.
(Klein and Groll, 2002)	Experimental-Numerical	Metal Hydride	Designing hydride reactor consisted of four reaction beds.	Hydride powder was contained in Aluminium-foam cylinders to improve heat and mass transfer
(Hirata et al., 2003)	Numerical - experimental	$CaCl_2$-Expanded graphite	Adsorbent materials	Composite particles of Calcium chloride with expanded graphite and methylamine is used as reactants. Reaction and heat transfer characteristics of the composite particles was investigated experimentally in a thin packed bed reactor and confirmed with numerical solutions
(Wagner and Österreich, 2006)	Experimental	Silica gel-water	Closed thermochemical storage for solar space heating	Storage volume filled with the storage material and equipped with an internal spiral heat exchanger for enhancing heat transfer.
(Kerskes et al., 2007)	Experimental	Zeolite	Solar thermal space heating with long-term sorption heat store	Zeolite honeycomb monoliths is used for increasing sorption characteristics and decreasing pressure drop during air flow.
(Mauran et al., 2008)	Experimental	$SrBr_2$-H_2O	Thermochemical heat storage reactor	Solid/gas thermochemical heating -cooling reactor is developed

(Li et al., 2009b)	Experimental	BaCl-Ammonnia	Solar powered thermochemical cooling system	Composite block was produced by impregnating BaCl inside the graphite powder pores.
(Yang et al., 2010)	Numerical	Metal hydride	Thermochemical heat pump	Packed bed reactor design
(Kerskes et al., 2011)	Experimental	Packed bed Zeolite spheres	Thermochemical heat storage for solar thermal applications	Sorption store is divided in several segments which can be desorbed or adsorbed separately in small amounts for decreasing heat loses
(Tian et al., 2012)	Experimental	$CaCl_2$-Activated carbon-expanded graphite	Adsorbent materials	Heat and mass transfer performance of compact chemical and physical absorbents is investigated.
(Cuypers et al., 2012)	Numerical	Zeolite	Seasonal thermochemical heat storage system	Zeolite spheres are in glued contact with a copper plate to obtain high thermal conductivity with low material usage.
(Michel et al., 2012)	Experimental-Numerical	Salt powder-Vermiculite	Developing high efficiency reactive bed for thermochemical heat storage	An experimental prototype is developed in order to modelling a high density reactive bed consists of salt.
(Lass-Seyoum et al., 2012)	Experimental	Synthetic Zeolites and composites (matrix of salthydrates/porous material)	Developed a long term thermochemical heat storage	Compared 3 types of heat exchangers to achive the highest performance. %60 higher heat power rate achived with the new exchanger configuration comparing with the standart heat exchangers in the bulk.

(Kerskes et al., 2012)	Experimental	Zeolite and salt	Thermochemical heat storage	An external reactor concept has been realized where the storage material is separated from the reactor. This has the advantage that the reaction is reduced to only a small part of the total storage material amount at a time. The thermal heat capacities and heat losses especially during the regeneration process are reduced
(Sapienza et al., 2012)	Experimental	Zeolite	Thermochemical heat storage reactor	Dip coated adsorbers made of SAPO-34 Zeolite on a finned flat-tube aluminum heat exchanger was prepared
(Bao et al., 2013)	Numerical	Metal hydride	Thermochemical heat storage reactor storage reactor	Heat exchanger optimization for metal hydride thermal energy storage reactor has been made
(Schaube et al., 2013)	Numerical - experimental	Calcium Hydroxide $Ca(OH)_2$	Thermochemical heat storage reactor	Thermal behavior of a reactor with direct heat transfer between the gaseous reactant and the solid material was investigated
(Liu et al., 2013)	Experimental	$CaCl_2$	Sorption thermal energy storage	SiO_2 based mesoporous ceramic material is used. It is formed as honeycomb before $CaCl_2$ is impregnated.
(Jiang et al., 2013)	Experimental	Eight different salts and expanded natural graphite as the host matrix	Adsorbent materials	Various types of adsorbents is designed and their performances were compared in order to enhance heat and mass transfer potentials.

The reaction material or matrix is probably the key element of an entire THS system and should meet criteria such as (Xu et al., 2013, Yu et al., 2013);

- High energy storage density (Wh/kg or kWh/m^3)
- Low charging temperature
- High uptake of sorbate – compatibility of sorbent / sorbate
- Appropriate heat and mass transfer properties to ensure designed output power
- Easy to handle - nonpoisonous.
- Low cost - low price per kWh heat energy stored.
- Thermal stability - no detorioration during cycling.

Of these, the sorption properties are the foundations to find suitable THS materials for any given application, however the comprehensive evaluation of sorption properties of available sorbents is a time consuming task as it requires precise measurements of a set of sorption isobars, isosters and isotherms under a wide range of temperature of pressure. Evaluation of the materials energy density, E_d is somewhat more stright forward and reveals that metal chlorides, metal hydrides and metal oxides are considered to be promising materials for thermochemical heat storage systems (Yu et al., 2013). The energy storage densities of some of the most promising sorbents are given in Figure 2.3.15.

There are several studies in the literature about adsorbent/absorbent materials used as thermochemical storage material. (Solé et al., 2013) presented a study on characterisation of adsorption materials (solid-gas) aiming to obtain a reliable kinetic model. Different concepts when choosing a suitable material were evaluated and examplified. (Shkatulov et al., 2012) developed a new composit material Mg $(OH)_2$/ vermiculite. This material has a regeneration temperature of between 250-350 °C.

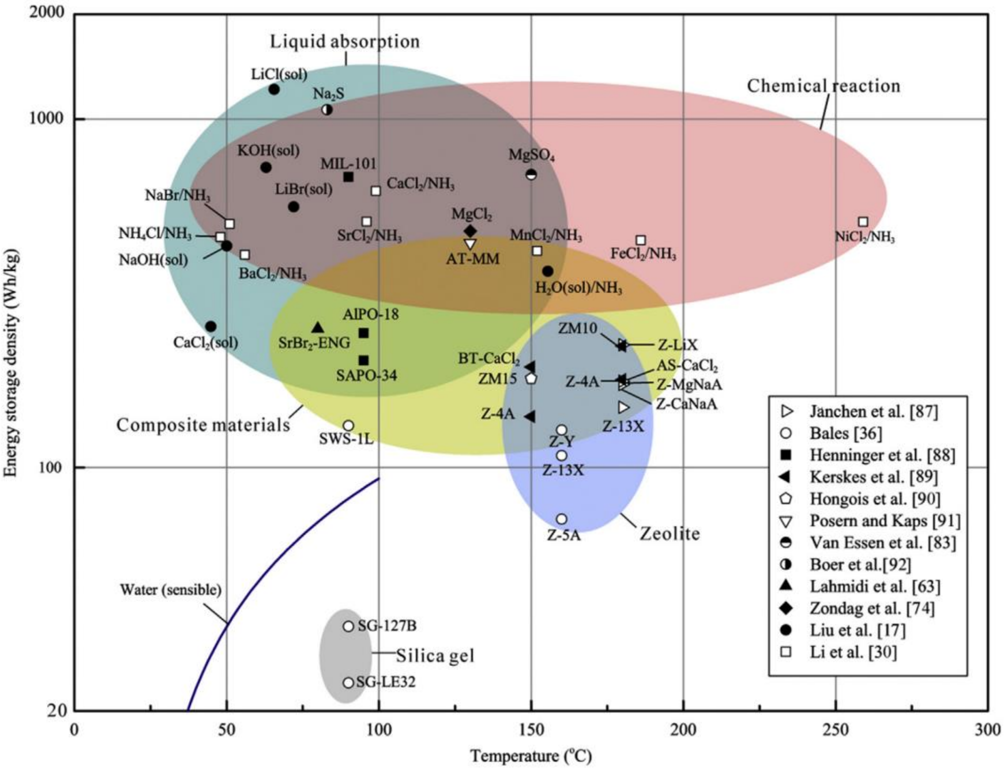

Figure 2.3.15 Energy storage densities of sorption materials (Yu et al., 2013)

Mainly it was synthesized by precipitation of magnesium hydroxide, Mg $(OH)_2$ in the pores of expanded vermiculite. This composite has a maximum heat storage capacity 540 kJ/kg with a hydroxide content of 67.4%. It was reported that this amount of heat is higher than the latent heat of most promising PCM's.

Gordeeva et al. investigated the phase composition of $(LiCl+LiBr)/SiO_2$ composities and their sorption equilibrium with both methanol and water (Gordeeva et al., 2009). It was reported that formation of a solid solution of LiCl in LiBr takes place in composites containing ≤ 25 mol % of LiCl . This condition provides a significant decrease of salt solvation from the matrix component. On the other hand increasing the LiCl percentage results in the formation of two solid phases which are the solution of LiBr in LiCl and the solution of LiCl in LiBr.

Molenda et al. investigated the hydration and dehydration behaviours of $CaCl_2$ at different partial vapour pressures (Molenda et al., 2013). The reversibility, reaction steps and stability of $CaCl_2$ was also reported. According to the experimental results the researchers showed that the hydration reaction provides good reversibility and stability for approximately 20 cycles and the results seem to be in good agreement with the literature.

Balasubramanian et al. developed a mathematical model to investigate the capability of salt hydrates to store thermochemical energy during their dissoociation into anhydrous salts and water with an external heat supply (Balasubramanian et al., 2010). They reported that the heat supplied for desorption gradually absorbed by the anhydrous salt and results in an increase of desorption duration with an associated increase of heat loss to the environment. It is indicated that the process performance may be improved with using materials that have higher thermal conductivities, higher specific heat capacities and lower thermochemical desorption rates.

Henninger et al. (Henninger et al., 2012) evaluate the current developments on materials ranging from Zeolites across aluminophosphates ($ALPO_4$) and silicoaluminophosphates (SAPO-34) to the novel class of metal organic framework materials for the use in adsorption processes for heat storage and transformation. In another study (Henninger et al., 2010), authors investigated the water adsorption characteristics and performance of these materials for the use in thermally driven adsorptive heat pumping and cooling applications with water as refrigerant. Hongois et al. (Hongois et al., 2011) developed and characterize a novel $MgSO_4$-Zeolite composite sorption material for long term seasonal solar energy storage. Through characterization of 10 mg samples, authors found that almost 80% of the total energy density can be stored at 150 °C although the material is not fully dehydrated. In a similar study, (Jänchen et al., 2004) investigated the water adsorption characteristics of Zeolites and modified mesoporous materials for seasonal solar thermal energy storage.

(Jänchen et al., 2005) also characterized the sorption properties of water in potential THS materials such as low silica X Zeolites, microporous $ALPO_4$, SAPO-34 and $CaCl_2$ accommodated in the pores of attapulgite. (Gordeeva and Aristov, 2012) studied novel two component composites 'salt in porous matrix' (CSPMs) and evaluated the current state-of-the-art and new trends in developing efficient CSPMs for various adsorption heat transformation cycles. (Aristov, 2007a) also reviewed the data concerning the new family of CSPMs for adsorptive cooling and investigated the water sorption/desorption mechanism and characteristics of these materials.

2.3.3.7 Selected Studies on THS Process Design

Zondag et al. constructed a prototype thermochemical sorption heat storage system at the Energy Research Center of the Netherlands (Zondag et al., 2013) (see: Figures 2.3.16.-2.3.17).

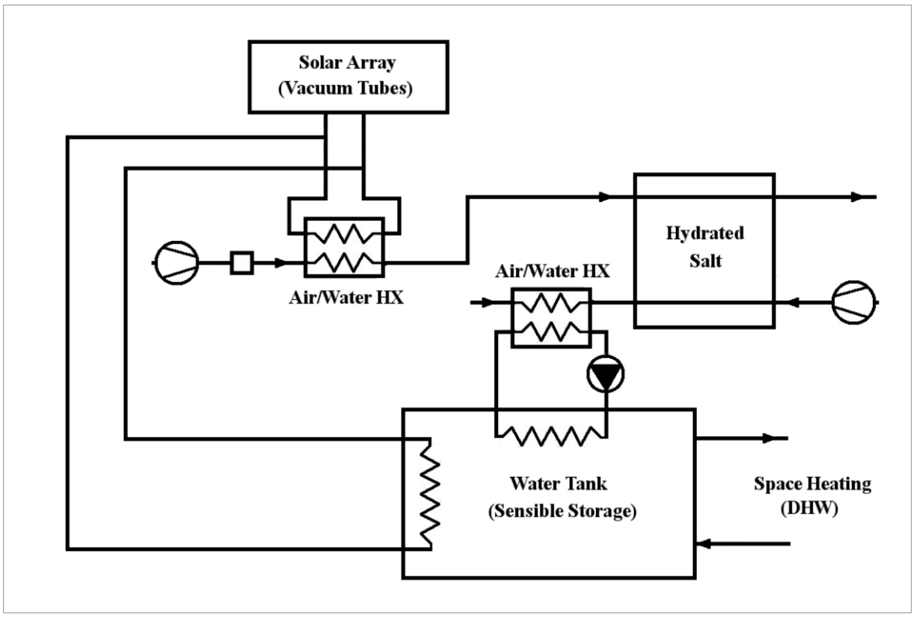

Figure 2.3.16 Open sorption thermochemical heat storage system (adapted) (Zondag et al., 2013)

It is a packed bed sorption system which contains 17 dm^3 of the sorption material ($MgCl_2.H_2O$) . They report that an effective storage density of 0.5 GJ/m^3 was obtained. It is also reported that the sorption material is capable of generating 150 W of thermal power for 40h using an airflow of 410 l/ per min. with a vapour pressure of 12 mbar. However as a result of heat loses only 50W could be transferred to the load resulting in a system COP of 12.

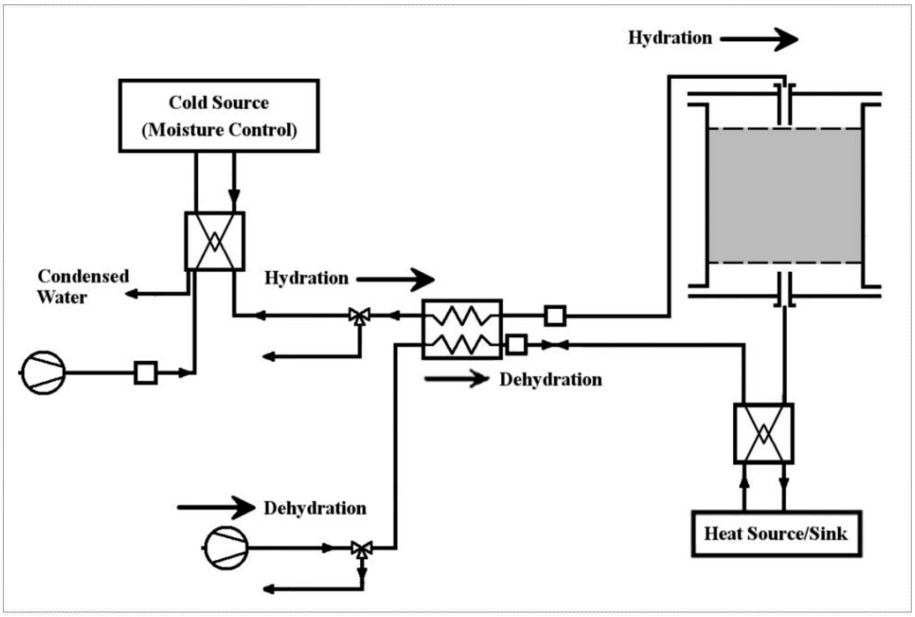

Figure 2.3.17 Schematic representation of THS system (adapted) (Zondag et al., 2013)

Tunguy et al. conducted a parametric study to evaluate the impact of both the internal (air flow rate, heat exchanger pressure drop) and external conditions (outdoor temperature) on the performance of a THS system (Tanguy et al., 2012).

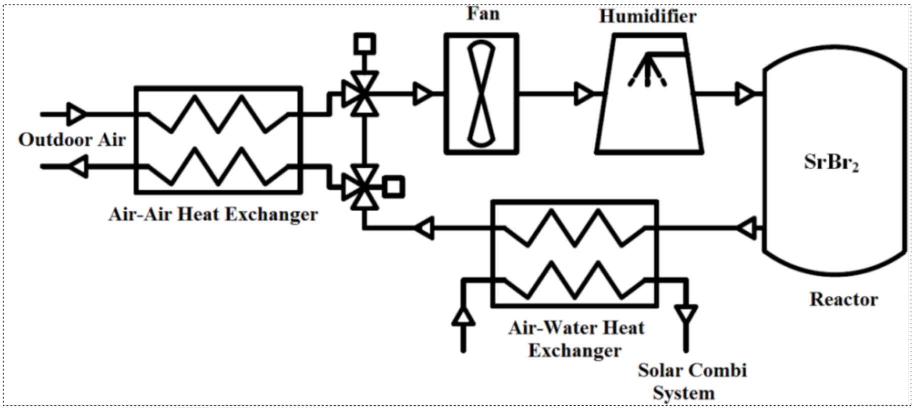

Figure 2.3.18 Thermochemical heat storage system (adapted) (Tanguy et al., 2012)

Two parameters are taken into consideration for the performance analsysis. These are the COP (useful energy/electrical energy consumption) and productivity rate (useful energy/reaction discharged energy). An integrated reactor with an external air-water heat exchanger was used in the study (see: Figure 2.13.18).

The researchers reported that the THS system had to be studied in three parts; i) material, ii) reactor and iii) process. Four experimental setups were used as part of the study: i) closed circuit, ii) open circuit, iii)open circuit with humidifier open and iv) open circuit with recirculation. These different working scenarios have been compared in terms of COP and productivity rate. The experimental results are given in Table 2.6.

Table 2.6 Performance comparison of different considerations (Tanguy et al., 2012)

	Closed circuits	**Open circuit with humidifier**	**Open circuit**	**Open circuit with recirculation**
Components (in addition to fan, reactor, air-water exchanger)	Humidifier	Air-air heat exchanger Humidifier	Air-air heat exchanger	Air-air heat exchanger Recirculation
COP	11	9.6	8.2	6.8
Productivity rate	37%	53%	80%	90%

In another experimental study, Mette et al. developed a highly efficient regeneration process for a THS system (see: Figure 2.3.19) (Mette et al., 2013). A Zeolite based composite material was used as an absorbent. It was reported that drying the air before entering the reactor significantly reduced the required regeneration temperature, T_r. Using the simulation software TRNSYS to analyse the regeneration temperature, it was found that T_r could be decreased from 180°C to 130°C, which is a suitable temperature for utilizing solar energy.

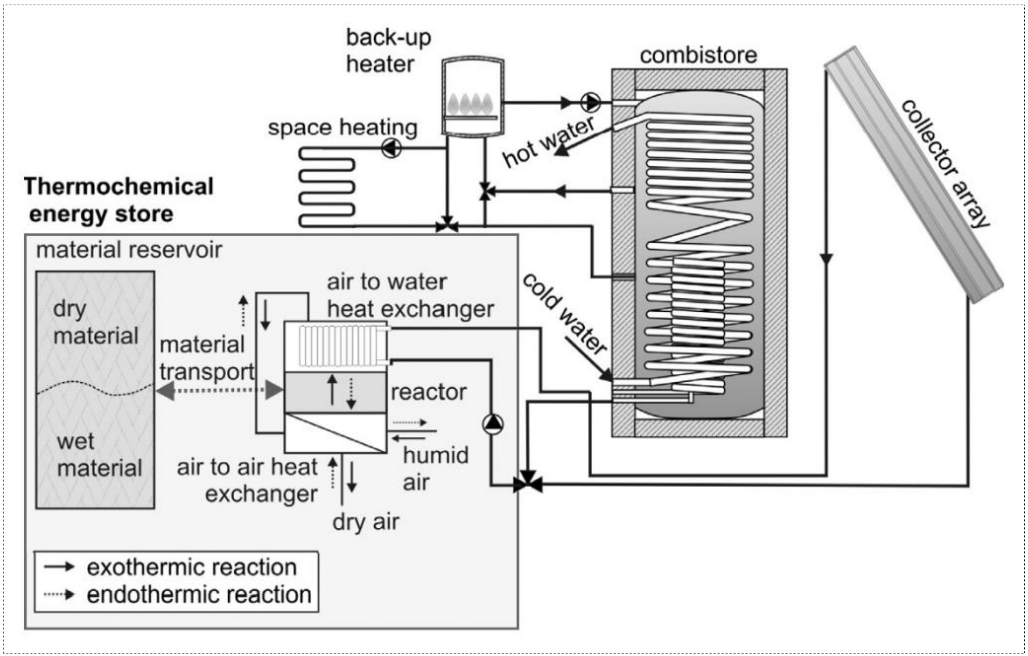

Figure 2.3.19 Shematic representation of THS (Mette et al., 2013)

Researchers developed a model for termo-economic performance of the system called fractional energy saving (f_s). Here, f_s is the comparison of auxilary energy demand of solar heating system to the energy demand of conventional heating (non-solar) system . It is found that, utilizing this system coupled with moderate collector sizes (< 20m^2) could provide a fractional energy saving f_s>60 comparing with a more conventional regeneration processes.

Abedin and Rosen investigated both closed and open THS systems using energy and exergy analysis methods to evaluate the charging behaviour and overall cycle performance of the system (see: Figure 2.3.20 a-c) (Abedin and Rosen, 2012). The energy and exergy efficiency of the systems were determined as 50% and 9% for the closed storage and 69% and 23% for the open storage respectively.

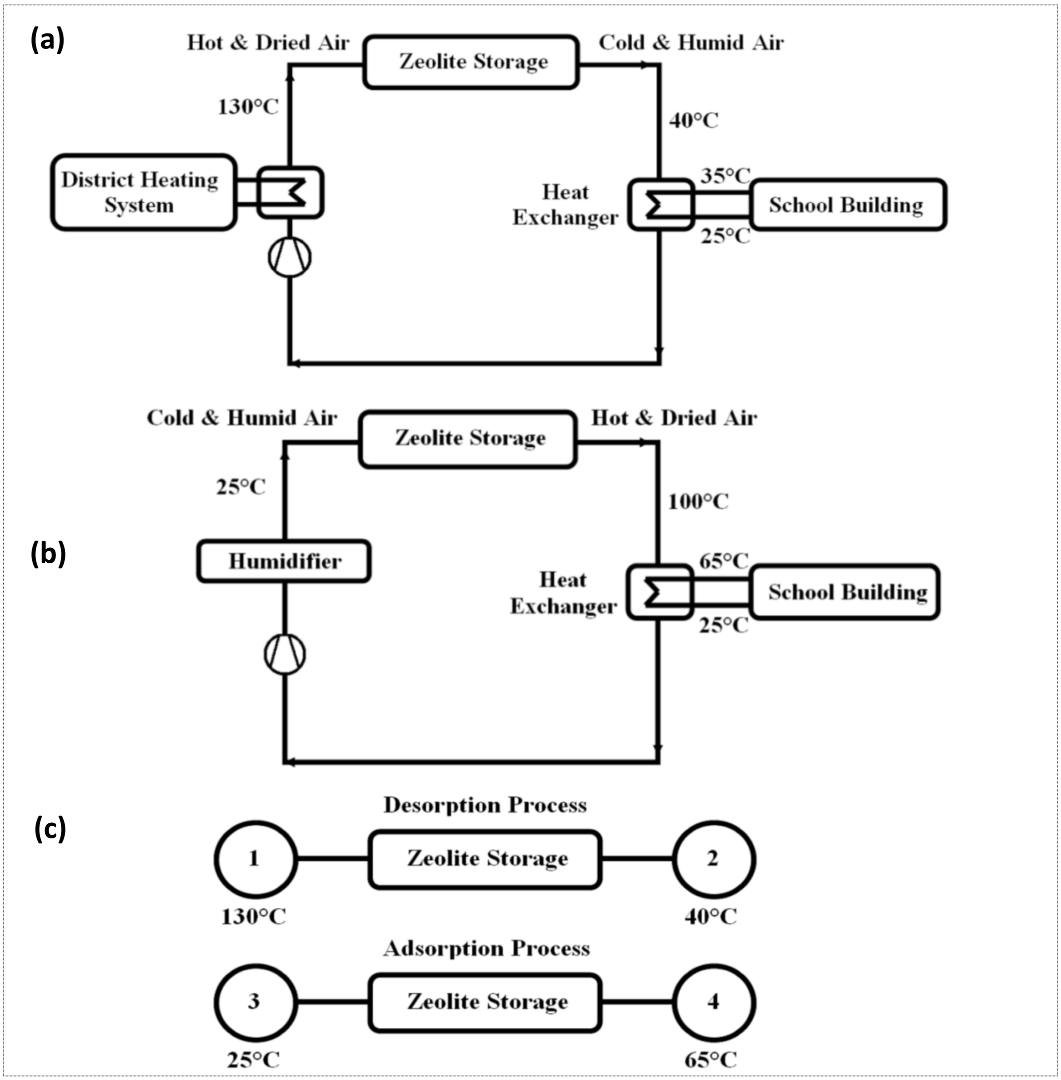

Figure 2.3.20 (a) Charging (desorption) –closed cycle, (b) discharging (adsorption)-closed cycle, (c) adsorption and desorption processes-open cycle (adapted) (Abedin and Rosen, 2012)

(Stitou et al., 2012) carried out an experimental investigation of a solar assisted THS system used for air conditioning in a pilot plant for housing in France (see Figure 2.3.21 a-b). The plant, which has a daily cooling capacity of 20 kWh, consists of a solid - gas thermochemical sorption process which is assisted at 60 - 70 °C by 20 m^2 of flat plate solar collectors. The reactive solid $BaCl_2$ and phase changed refrigerant NH_3 were used as the sorption couple. It was reported that over a period of two years the average efficiency of the solar collectors was found to be ≈ 40 - 50% whilst the process COP was ≈ 30 - 40%. It was shown that with this prototype system a 0.8-1.2 kW cooling load per m^2 of flat plate solar collector could be supplied.

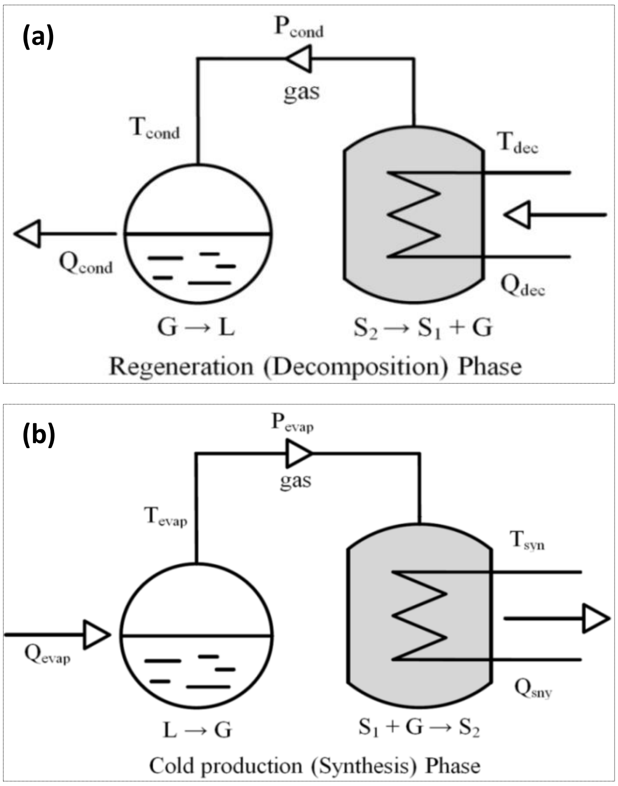

Figure 2.3.21 (a) Charging and (b) discharging of thermochemical heat storage (adapted) (Stitou et al., 2012)

Besides the process based studies, a number of theoretical and experimental researches on THS reactor design and experimentation have also been performed. In a recent study (Johannes et al., 2015) developed a fixed bed Zeolite thermal heat storage system using water as the sorbate. Average temperature lift of 38 °C during 8 h was achieved during the discharging with an airflow inlet at 20 °C, 10 g/kg of dry air of specific humidity and a flow rate of 180 m^3/h.

In another experimental study performed by (Tatsidjodoung et al., 2016), it was found that open sorption reactor loaded with 40 kg of Zeolite can supply a constant power of 2.25 kW during more than two hours corresponding to 27.5 Wkg^{-1} of material (see: Figure 2.3.22 a).

A novel “revolving drum” reactor prototype was developed and tested by (Zettl et al., 2014). Dehydrated Zeolite of the type 4A and MSX were used in form of spherical grains and it was found that, 50 kg of sorbent is able to generate an adsorption heat up to 12 kWh and temperature shifts of the process air up to 36 °C (see: Figure 2.3.22 b). The electrical COP of the system was calculated as 12. Likewise, a composite sorption reactor consisting of $CaCl_2$ impregnated mesoporous ceramic (Wakkanai siliceous shale) honeycomb filter was developed by (Liu et al., 2013) for low-temperature (< 100 °C) industrial waste heat recovery (see: Figure 2.3.22 c). Experimental results showed that; 22.4 wt% $CaCl_2$ supported with the honeycomb filter (926.2 g; 2L) can provide a temperature lift greater than 40 °C for a duration of 432 min. by supplying air at 25 °C at a flow rate of 3.0 m^3/h when the T_{reg} was 80 °C. The volumetric heat storage density obtained was 272 MJ/m^3, and the coefficient of the heat extraction performance during the heat release process was 65%.

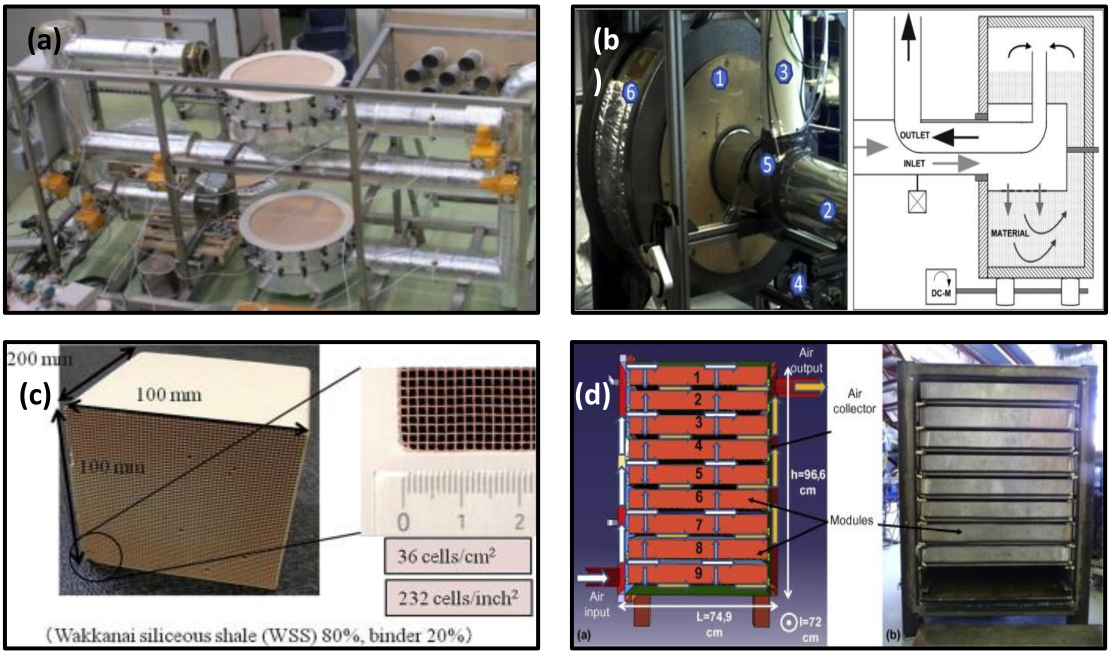

Figure 2.3.22 Different reactor concepts; (a) fixed Zeolite bed sorption reactor, (b) revolving drum reactor, (c) $CaCl_2$ impregnated mesoporous ceramic filter (d) multiple fixed bed reactor using $SrBr_2$ / H_2O reactive pair

In another study, (Michel et al., 2014) developed a large scale sorption reactor consisting of multiple sorption beds with the air flow channels in between (see: Figure 2.3.22 d). Strontium bromide/water ($SrBr_2$ / H_2O) as a reactive pair is used in the system (400 kg of hydrated salt) and hydration specific powers from 0.75 to 2 W/kg were reached for a bed salt energy density of 388 kWh/m^3.

There are several other studies into both open and closed THS systems used for various purposes with some of these are listed in Table 2.7. The materials used, storage type, method and analysis results are shown. It is clear from the comprehensive spread of usage that THS can be used in wide range of applications – heat storage, air conditioning, cold storage, deep freezing, drying and heat transformation purposes.

Table 2.7 Previous studies on THS

Reference	**Concept**	**Material**	**Type of study**	**Storage method**	**COP**	**Heat storage density**
(Ruiter, 1987)	Closed CHP	NH_3-H_2o	Experimental	Seasonal	-	119 kWh/m^3
(Cerkvenik et al., 1999)	Three stage cascade sorption refrigeration	$LiBr$-H_2O CaO-H_2O	Experimental	Seasonal	1.8	-
(Vasiliev et al., 2001)	Refrigeration	$CaCl_2$	Experimental	Seasonal	0.43	-
(De Boer et al., 2002)	Solid sorption cooling integrated THS	Na_2S	Experimental	Seasonal	0.57	2.1 kWh
(Lu et al., 2003)	Closed THS	Zeolite 13 X	Experimental	Seasonal	-	167 kWh/m^3
(Bales et al., 2005)	THS	Zeolite	Experimental	Seasonal		57.8 kWh/m^3
(Lahmidi et al., 2006)	Heating and Cooling	$Sr Br_2$	Experimental	Seasonal		26 W/kg (h)-49 W/kg (c)
(Haije et al., 2007)	Heat transformation	$LiCl$-$MgCl_2$	Experimental	Seasonal	0.11	222 W/kg
(Bales et al., 2007)	Closed CHP	$NaOH$-H_2o	Experimental	Seasonal	-	250 kWh/m^3
(Le Pierres et al., 2007)	THS for solar deepfreezing	$BaCl_2$-NH_3	Experimental	Seasonal	0.031	-
(Mauran et al., 2008)	Heating and Cooling	$SrBr_2$	Experimental	Seasonal	-	13 W/kg (h)-15 W/kg (c)
(Li et al., 2009a)	Deep freezing	$MnCl_2$	Experimental	Seasonal	0.34	350 W/kg

(Oliveira et al., 2009)	Air conditioning	NaBr	Experimental	Seasonal	0.46	129 W/kg
(Van Essen et al., 2009)	Heat storage	$AlSO_4$, $CaCl_2$	Experimental	Seasonal	-	-
(Chen et al., 2009)	Air conditioning	$BaCl_2$	Experimental	Seasonal	0.5	192W/kg
(Veselovskaya et al., 2010)	Air conditioning	$BaCl_2$	Experimental	Seasonal	0.54	370-500 W/kg
(Wang et al., 2010a)	Heat transformation	$CaCl_2$-$MnCl_2$	Experimental	Seasonal	0.25	248 W/kg
(Li et al., 2010)	Comparison of adsorption and resorption THS	$BaCl_2$-NH_3 $MnCl_2$-NH_3	Experimental	Seasonal	0.78(ads.) 0.46(res.)	-
(Fadhel et al., 2010)	Drying application	$CaCl_2$-NH_3	Experimental	Seasonal	1.2-2	-
(Basciotti and Pol, 2011)	THS for cooling application	Silica gel	Numerical	Seasonal	0.61-0.84	9.7-12.1 kW
(Hauer and Fischer, 2011)	Open THS	Zeolite 13X	Experimental	Seasonal	-	124 kWh/m^3
(Stitou et al., 2012)	Solar assisted solid/gas THS	$BaCl_2$-NH_3	Experimental	Short term	0.3-0.4	0.8-1.2 kWh
(Tanguy et al., 2012)	Optimization of THS for solar app.	$SrBr_2$	Numerical	Seasonal	6.8-11	-

(Bao et al., 2012)	THS for cold storage and refrigeration	$MnCl_2$-NH_3 NH_4Cl-NH_3	Experimental	Short term	0.3-0.31	87-125 W/kg_{salt}
(Zondag et al., 2013)	Open THS	$MgCl_2$-H_2o	Experimental	Short term	12	50W
(Li et al., 2013)	Dual mode THS	$CaCl_2$-NH_3	Numerical	Seasonal	0.6	1043 kJ/kg
(Quinnell and Davidson, 2013)	Closed CHP integrated with heat storage	$CaCl_2$	Experimental	Seasonal	-	381 kWh/m^3
(N'Tsoukpoe et al., 2013)	Long-term solar thermal storage	LiBr-H2O	Experimental	Seasonal	-	8 kWh

2.4 Conclusions

A comprehensive review of THS has been presented. Technology used for CHP, adsorption and absorption cycles, adsorbate/adsorbent, adsorbate/absorbate couples and waste heat tranport with THS materials are investigated. Some key applications of absorbent materials are also presented. It is seen that the air flow rate, ambient temperature, relative humidity and the design of the reactor are the most promising factors in obtaining significant performance from THS systems.

Recent research focus on several absorption and adsorption pairs has been presented. The most desireable properties of THS materials have been shown to be – i) high energy density, ii) low charging temperature, iii) high thermal conductivity, and iv) high sorbate uptake . Further research is needed on many aspects of THS design including i) materials, ii) reactor design factors, iii) safety, iv) size and v) efficiency and economics. In addition to this, comprehensive performance analysis of these systems, based on their energy and exergy are required in order to obtain a advanced and capable THS systems.

A primary result of this review has concluded that although many research studies are onging, THS technology is still not at a sufficiently developed stage for commercialisation. The factors outlined below should be taken into consideration in order to achieve both an efficient and economically feasible THS system:

1. Reactor Design - Effective HAM transfer is vital for THS efficiency. To achieve a high output temperature for a sufficiently long time period, a high quantity of material must be available for that reaction. Achieving full reaction is also dependant on the interaction between the reactant materials.
2. Materials Study - Developing new composite materials with higher storage density, low regeneration temperature, good cyclic ability and low price is cruical.

3. Humidification process - As the heat generation from most THS systems are relatively low, energy consumption to run them should be minimal to achive sufficient system efficiency. For this reason, in particular for large scale applications, research into development of new humidification systems with very low energy consumption is highly important.
4. Regeneration Process - Utilization of solar energy in the summer period for charging THS systems would make seasonal storage possible. However the high regeneration temperature requirement of (especially materials with high storage density) adsorbents is still the main obstacle to benefitting from solar systems. Research into hybrid processes where solar collectors coupled with THS heat pumps are integrated and optimized should be carried out together to improve the performance of THS.

CHAPTER 3: NUMERICAL INVESTIGATION OF SOLAR THERMAL ENERGY STORAGE POTENTIAL UNDER UK CLIMATIC CONDITIONS

3.1 Introduction

The UK government has identified micro generation as a key option for reducing greenhouse gas emissions from the domestic sector and for contributing towards UK's GHG reduction targets of 34% by 2020 and 80% by 2050. In the UK, micro generation is defined as the generation of electricity of up to 50 kW and or heat of up to 45 kW from a low carbon resource (Greening and Azapagic, 2014).

Solar thermal micro generation systems could help reduce UK GHG emissions arising from space and water heating in the domestic sector. Solar thermal is one of the most established micro generation technologies in the UK with more than 100 K units installed to date (Greening and Azapagic, 2014). However this is still significantly lower compared to some countries such as Germany which has over 1 million units in operation. At this point thermal energy storage (TES) systems, integrated to solar thermal systems would have significant importance for the UK to increase their solar fraction and render solar thermal systems sustainable with low cost applications.

In this context, SHS and LHS systems have been widely researched and utilized in real applications for solar thermal energy storage. On the other hand, despite its superior features, THS is an emerging technology and its heat storage and heating characteristics has not well known yet. In order to provide a better understanding of operational characteristics of THS and its superior features over other storage methods, future studies in this field should involve; comparative analyses between different HS methods based on achievable E_d and required V_s. This will enable the determination and design of optimal heat storage method (e.g. THS, LHS or SHS) and duration (short term / seasonal) for heat storage depending on the building heat load and solar availability.

Majority of the work on low temperature THS has been focused on sorption material development. Investigations on THS process design and comparative analysis between THS and other HS methods for solar thermal energy storage in the built environment is missing in the literature. To fulfil this gap, in this chapter, two different scenarios; i) short term (daily) heat storage and ii) long term (seasonal) were considered for analysing the heat storage potential in the UK. Different HS methods (SHS, LHS and THS) were investigated and compared with a materials heat storage density and volume requirement approach. The most promising materials, as identified in the literature, were employed in these storage methods and used in the numerical analysis.

3.2 Necessity of thermal storage in building heating sector

The quantity and ratios of global energy generation to consumption have a vital importance in each step of economic development, for conservation of energy and usage of it efficiently. Global energy consumption is directly related to economic and environmental improvement. For this reason, the energy consumption factor necessitates considering design of energy-saving and efficient systems as well as environmental factors. In developed countries the highest energy consumption is in the building sector with 27% where the highest share is spent for air conditioning and hot water purposes. Also 70% of consumption of electrical energy and greenhouse gas emissions originates from the building sector. Determination of energy consumption rates and energy loses are two important necessities for designing energy efficient buildings (Parameshwaran et al., 2012). Besides, benefitting from solar energy systems coupled with thermal energy storage is one of the promising methods to achieve substantial energy and cost savings in the building sector. There are several heat storage methods including SHS, LHS, and THS as extensively discussed in Chapter 1. Table 3.1 illustrates the densities, specific heats, latent heats and reaction enthalpies of different materials. (Zhou et al., 2012, Xu et al., 2013). THS materials theoretically have higher E_d over other storage methods as they utilize both chemical reaction and sorption enthalpies.

Table 3.1 Heat storage densities of various storage materials & methods

	Material	Density (kg/m^3)	Specific Heat Capacity (kJ/kg)	Latent Heat of Fusion (kJ/kg)	Reaction Enthalpy (kJ/kg)
Sensible	Water	1000	4.18	-	-
	Soil	1300	0.46	-	-
Latent	Paraffin	1802	-	174.4	-
Thermochemical	$CaCl_2.H_2O$	2100	3.06	-	433.6
	Zeolite	650	1.07	-	1107
	Silica Gel	600	1.13	-	1380

Despite the promising features of THS systems, there is no study in the literature investigating their potential for thermal energy storage in buildings with consideration of solar availability. Besides, comparative analysis between THS and other storage methods is necessary to provide a better understanding of their advantageous aspects. Accordingly, this study aims to comparatively investigate the potential increase in solar energy contribution in space heating in the UK when solar collectors are coupled with SHS, LHS or THS systems for short term or seasonal heat storage. In order to achieve the aim of the study, three objectives have been set;

- To analyse the daily and year round solar energy potential and heat load of a selected building thereby to determine; (i) mismatch between solar availability and building heat load, (ii) determine the amount of excess storable solar energy under UK climate conditions.

- To determine and compare the required storage volumes with the use of different heat storage materials to store available solar energy between September and April to meet the monthly heating demand of selected building during that period.
- To determine the contribution of per unit volume of different heat storge materials / systems to the year round heat load of the selected building for the case of seasonal heat storage.

In the following section, decription of the performed numerical work and the applied methods to meet the above given objectives were presented.

3.3 Numerical study

In the present study the solar thermal storage potential under UK climate conditions was investigated. Whilst considering the analysis results, both daily and seasonal heat storage scenarios in UK conditions were simulated. Furthermore the overall heat storage capacities of the most promising materials, employed in the model, were calculated. Regarding to analysis results promising methods and materials for heat storage application in UK conditions was discussed.

3.3.1 Introduction of the investigated building

A well-insulated, typically sized 106.6 m^2 two-floor house under UK climate conditions, built as part of a project at University of Nottingham (Nottingham H.O.U.S.E), was considered in the present numerical study. The building is proposed as a Zero Carbon House, following the codes of German Passivehous Institute Design and Code 6 of UK for sustainable homes (Zero Carbon Emission). It is a showcase of carbon and energy saving in the built environment with its innovative and sustainable design. The house consists of 8 rooms which are; two bedrooms, bathroom, toilet, living room, entrance lobby, circulation space and the plant room. The view of the building is presented in Figure 3.3.1. Ground/roof plan and the illustrations of the four elevations of the building were also given in Figures 3.3.2 and 3.3.3 respectively.

The UK government has set ambitious targets to reduce carbon emissions by 80% by 2050 and to have every new home zero carbon from 2016 onwards. In this context, The Nottingham H.O.U.S.E has designed as a starter, for evaluation of demand-side management, optimized solar energy use, energy storage and smart grid technologies. The building although has equipped with several sustainable energy saving technologies such as solar panels, skylight, air sourced heat pump and insulation materials, solar thermal energy storage has not been considered for space heating proposes. However it is obvious that space heating is the major energy consumer in domestic buildings and thermal energy storage is the key to increase solar contribution in space heating facilities. Therefore, in this case study, Nottingham H.O.U.S.E has specifically selected for evaluating the potential energy savings with the use of TES and determining the most suitable TES method/material for future's zero/low carbon buildings.

Figure 3.3.1 View of the investigated building

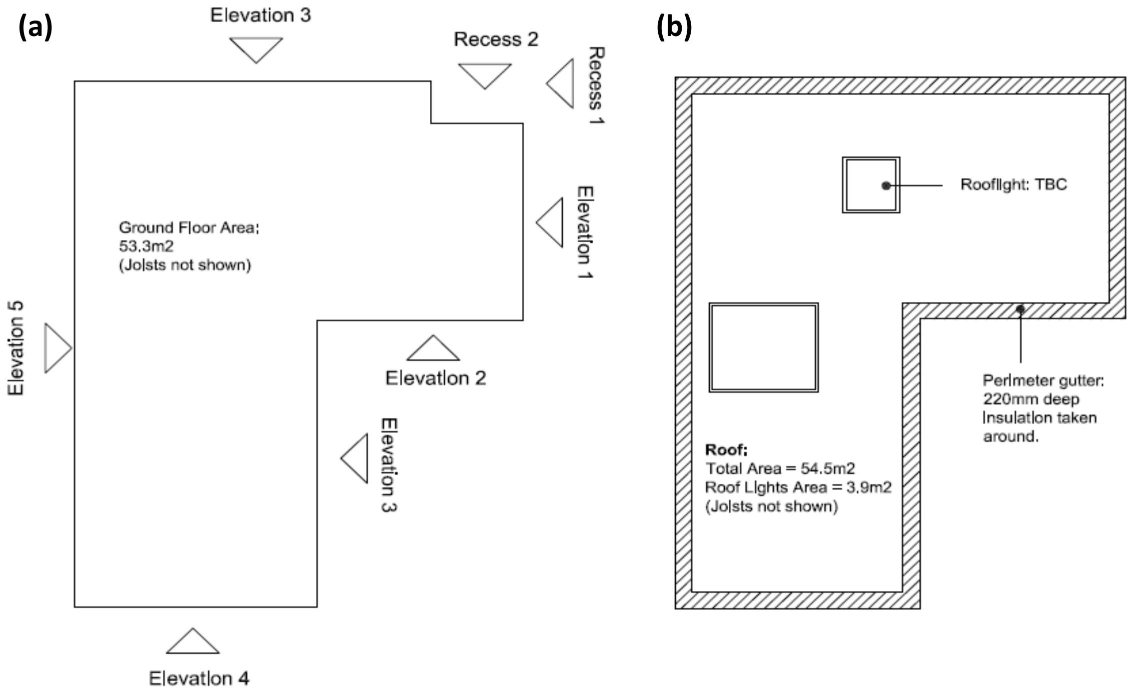

Figure 3.3.2 (a) Ground plan (b) roof plan of the Nottingham H.O.U.S.E

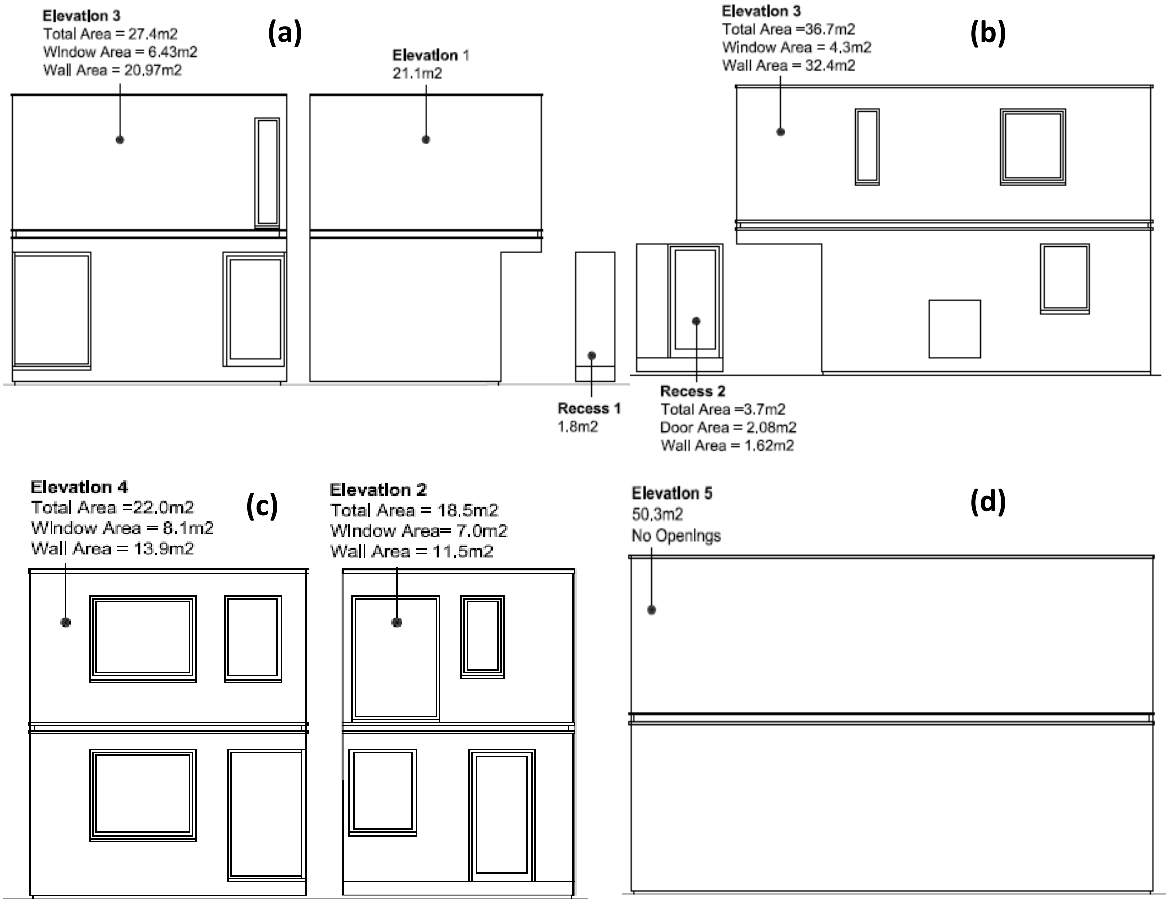

Figure 3.3.3 (a) East, (b) North, (c) South and (d) West elevations of the Nottingham H.O.U.S.E

3.3.2 Modelling of the building heat load and solar heat gain

The modelling of the building heat load is performed with Autodesk Ecotect Analysis. It is building thermal analysis software, which is capable of simulating building ventilation, conduction and convection heat losses, internal heat gains and passive solar gains simultaneously to analyse the building overall heat demand for any selected time. The software is an easy to use, powerfull and practical tool that enables performing dynamic building heat load simulation for any selected condition. Ecotect Analysis also includes year round climate data (e.g. solar intensity, ambient temperature) of any geographical region also building structural components with their physical properties. These all eliminate the need of any additional effort to access this data, save time and minimize the errors in the analysis. For these reasons Ecotect was selected to be used in the proposed study.

In order to perform the simulation with Ecotect Anlysis, it is necessary to; i)generate a 3D model of the proposed building, ii) determination/selection of the building construction materials and sizes, ii) setting the zones and iv) selection of the building geographical location. The model of the Nottingham H.O.U.S.E generated in the Ecotect is presented in Figure 3.3.4.

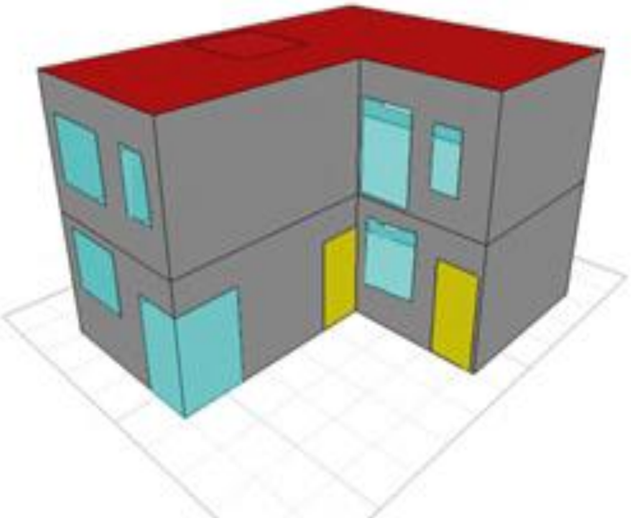

Figure 3.3.4 Model of the building created in Ecotect software

The building was set as a single zone as the aim was to simulate the heat load of the whole house. Selected building construction materials with their heat loss coefficients (U value) and dimensions used in the analysis were given in Table 3.2.

Table 3.2 Heat loss coefficients and surface areas of building components

Component	***U* value (W/m^2.°C)**	***A* (m^2)**
Window	2.8	25.83
Block work	0.1	153.59
Floor	0.1	53.30
Roof	0.13	54.50
Skylight	0.46	3.90
Door	0.16	2.08

In order to validate the Ecotect model outputs, a numerical model is also created in Microsoft Excel to determine heat load of the building and results from both softwares were found in good agreement. In the Microsoft Excel model set up Equations 3.1–3.4 were used. The general heat loss expression is given in Equation 3.1. Here the temperature difference ΔT (°C) is described as the difference between indoor temperature, T_d and outdoor temperature, T_a. Air changes per hour, N is set at $ACH = 2$ for the ventilation heat loss calculation (see: Eq. 3.2). The total heat load of the building, Q_t (W) was calculated according to Eq. 3.3. Other symbols used in the formulas are surface area, A (m^2), ventilation heat loss Q_v (W), room volume, V (m^3), specific heat capacity of air, $c_{p,a}$ (kJ/kg.K) and density of air, ρ_a. Additionally the subscripts *w, b, f, r, v, sk* represent window, blockwork, floor, roof ventilation and skylight respectively.

$$Q = U \cdot A \cdot \Delta T \tag{3.1}$$

$$Q_v = N \cdot V \cdot c_{p,a} \cdot \rho_a \cdot (T_d - T_a).(1000/3600) \tag{3.2}$$

$$Q_t = Q_w + Q_b + Q_f + Q_r + Q_v + Q_{sk} \tag{3.3}$$

Calculation of the buildings solar thermal heat gain (see: Equation 3.4) is performed in Microsoft Excel, by using data (solar radiation and ambient temperature) obtained from the EuropeanCommission's web site (www.photovoltaic-software.com). Total collector area, A_c, used in the system is considered as 10 m^2. Assumptions and constants used in the thermal analysis of solar collectors were demonstrated in Table 3.3. The instantaneous heat gain of collectors is calculated as:

$$Q_u = A_c \cdot F_r \cdot [(H_t/h_s) \cdot (\tau\alpha)_{net} - U_L \cdot (T_i - T_a)] \tag{3.4}$$

Where Q_u is the heat gain (W), A_c is the collector area (m^2), H_t is the total amount of solar radiation per m^2 (J/m^2), h_s is the radiation time (s), $\tau\alpha$ is the absorption-transmission coefficient, depends on transmissivity and absorptivity of glass cover of collectors. U_L is the heat loss coefficient of solar collectors ($W/m^2.°C$) and depends on the collector material and the temperatures, T_i is the collector fluid inlet temperature, T_a is ambient temperature and F_R is the correction factor, or collector heat removal factor. F_R can be considered as the ratio of the heat actually delivered to that delivered if the collector plate were at uniform temperature equal to that of the entering fluid. It is affected only by the solar collector characteristics, the fluid type, and the fluid flow rate through the collector (Kalogirou, 2004, Duffie and Beckman, 2013).

The first part of Equation (3.4) indicates the heat that can be gained by the collectors, and the second part indicates the heat lost to the environment. The numerical difference between these two parts gives Q_u, which is the useful net heat gain of collectors.

Table 3.3 Properties of the assumed collector (Aydin et al., 2015b)

Constant	**Symbol**	**Value**
Collector heat removal factor	F_r	0.86
Absorption-Transmission coefficient	$\tau\alpha$	0.8
Heat loss coefficient	U_L	6.9 W/m^2. °C

Two different scenarios were simulated and compared for analysis of both TES potential and the most feasible TES method to applying a UK climate. Evaluating storable excess heat in UK climate conditions for either short term (daily) or long term (seasonal) is the main purpose of this study. In the short term storage model, hourly average weather conditions and solar intensity values of each monthover an 8 month heating period (September-April) were considered. In this model excess heat gained by collectors during the day time is considered as being available for use at night time for heating purposes. In the long term storage model daily average weather conditions for the whole year round were considered to determine excess storable energy in summer months for utilization in the winter period.

3.3.3 Analysing heat storage densities of promising materials

In this section heat storage density of selected most promising SHS, LHS and THS materials were analysed and presented in Figure 3.3.5. In the analysis, physical and chemical properties of the selected candidate materials given in Table 3.1 were used to determine heat storage potential per unit volume of each material, based on either sensible temperature change, change of physical state or water sorption enthalpy.

The formulas used for analysing the TES potential of materials are outlined in Table 3.4 where Q is amount of stored heat (kJ), m is the mass of storage material (kg), C_p is the specific heat of storage material and ΔT is difference between final temperature and initial temperature of storage material (˚C), L_m is latent heat of phase change (kJ/kg), n is number of moles of adsorbent (THS material) (mole), X is the global conversion of the chemical reaction (-) and *ΔH* is the enthalpy of reaction (transformation) (kJ/mole). The first term in the Eq. 3.7 gives the total storage capacity. However a part of stored energy will be spent for sensibly heating of the reactor and adsorbent as given in second and third term. Here Cp_r and Cp_{ra} are the specific heat of the reactor and adsorbent (kJ/kg˚C), m_r and m_a are mass of the reactor and adsorbent (kg), T_{rf} and T_{af} are the final temperatures of the reactor and adsorbent (˚C), T_{ri} and T_{ai} are the initial temperatures of the reactor and adsorbent (˚C).

Table 3.4 Formulas for analysing heat storage densities

	Material	**Equation**	**Eq. No.**
SHS	Soil, Water	$Q = m \cdot Cp \cdot \Delta T$	(3.5)
LHS	Paraffin Wax	$Q = m \cdot L_m$	(3.6)
THS	$CaCl_2$, Zeolite, Silica Gel	$Q = n \cdot X \cdot \Delta H - \Big[\big[Cp_r \cdot m_r \cdot (T_{rf} - T_{ri})\big] + \big[Cp_{ra} \cdot m_a \cdot (T_{af} - T_{ai})\big]\Big]$	(3.7)

It is clear from Figure 3.3.5 that the volumetric heat storage density of the most promising THS materials far exceeds the SHS and LHS materials. As stated, SHS materials store energy by changing the temperature of the material. This method converts collected energy into sensible heat in selected materials and retrieves it when that heat is required. The amount of stored energy depends on the specific heat capacity of the storage material and the temperature increase (see: Equation 3.5). SHS systems are considered to be a simple, low cost and relatively well developed technology. As these systems are inexpensive and very reliable, they have been used in several applications such as hot water (*e.g.* domestic, industrial) and space heating (*e.g.*domestic, greenhouse) (Zhou et al., 2012, Sharma et al., 2009, Xu et al., 2013, Cárdenas and León, 2013). Although SHS is a simpler method, when compared with the other ones, SHS materials have low storage densities which mean they require larger volume. Water is the most frequently used medium and has the highest storage density among all SHS materials, which is ≈50 kWh/m^3.

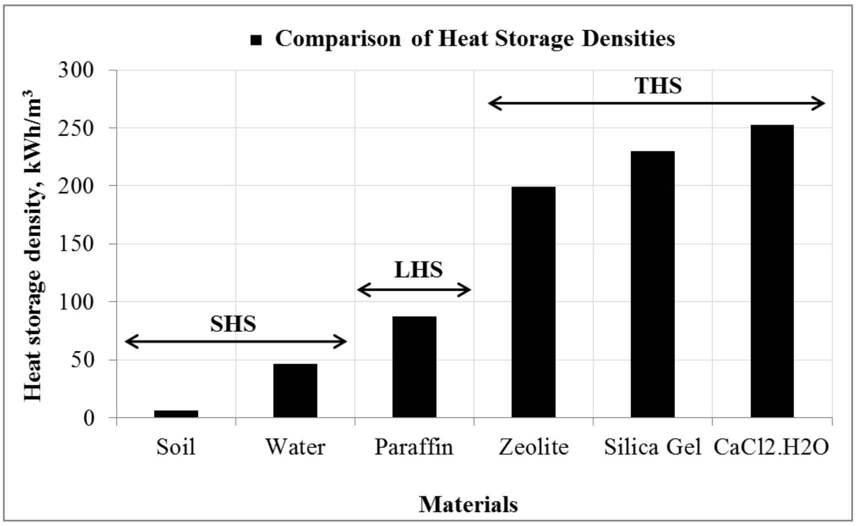

Figure 3.3.5 Heat storage densities of several materials

In a LHS material, the storage and absorption of heat occurs via a fusion reaction (melting / solidification) during the phase change period. LHS materials, in which PCMs are used, have higher energy density when compared to SHS materials and also have low temperature and volume changes (Zalba et al., 2003, Sharma et al., 2009, Zhou et al., 2012, Aydin et al., 2015b). The main difference between a LHS system and a SHS one is that during absorption, heat is stored with a phase change process at a constant temperature. LHS systems can have phase change processes from solid to liquid, liquid to gas or the inverse of these processes (Sharma et al., 2009, Cárdenas and León, 2013, Demirbas, 2006, Dincer, 2002). As a result of the phase change process, LHS has the potential of storing thermal energy using less storage volume than SHS (for storing the same amount of heat). There are several studies about LHS and SHS in the literature, however for this study, paraffin wax alone was chosen as LHS material in this evaluation.

Thermochemical heat storage (THS) has the distinctive advantages of coupled high energy storage and low heat loses when compared to both SHS and LHS technologies and is currently regarded as the most promising alternative (Pardo et al., 2014, Abedin and Rosen, 2011, Xu et al., 2013). Another attractive property of THS is its capability of the systems to conserve the heat energy at ambient temperature as long as desired without heat loses due to the reversible chemical reactions involved (*i.e.* dehydration and rehydration of salts). Due to these advantages, THS has recently become a widely researched technology for seasonal energy storage (Xu et al., 2013).

3.3.4 Results and discussion

3.3.4.1 Short term storage (daily storage)

In Figure 3.3.6, schematic diagram of a typical short term storage system is presented. In this model, daily excess stored heat is designed to supply the building at night time for heating purpose. In a solar heating application, part of the heat gain from solar collectors would be transferred to the building and any excess heat would be transferred to the TES system. Stored heat can then be used at night to provide continuity of full solar energy usage and decrease fossil fuel consumption.

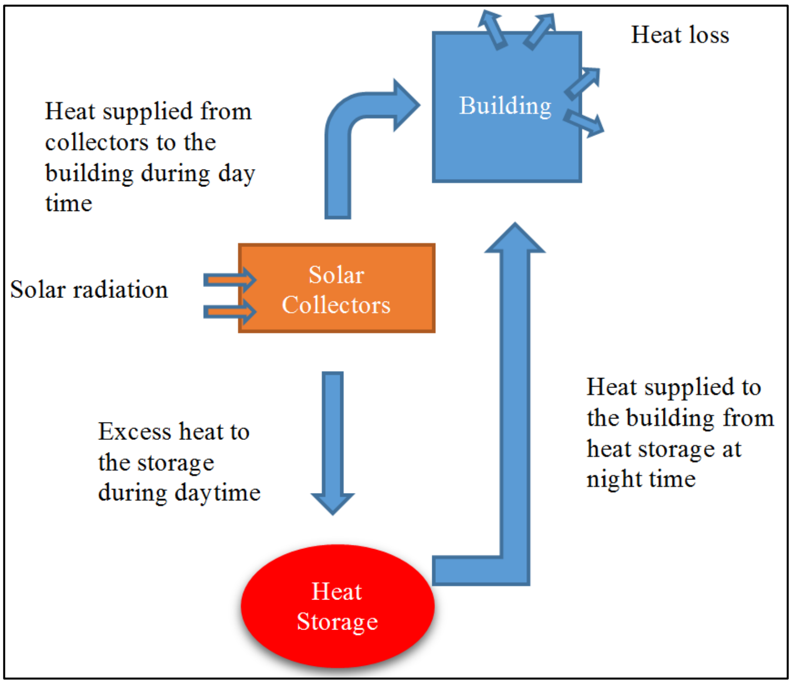

Figure 3.3.6 Schematic diagram of short term heat storage

The average hourly heat load of the building and the heat gain from a collector, for each month is graphically demonstrated in Figure 3.3.7. The black curves represent the heat gain whereas the white curves correspond to heat load of the building.

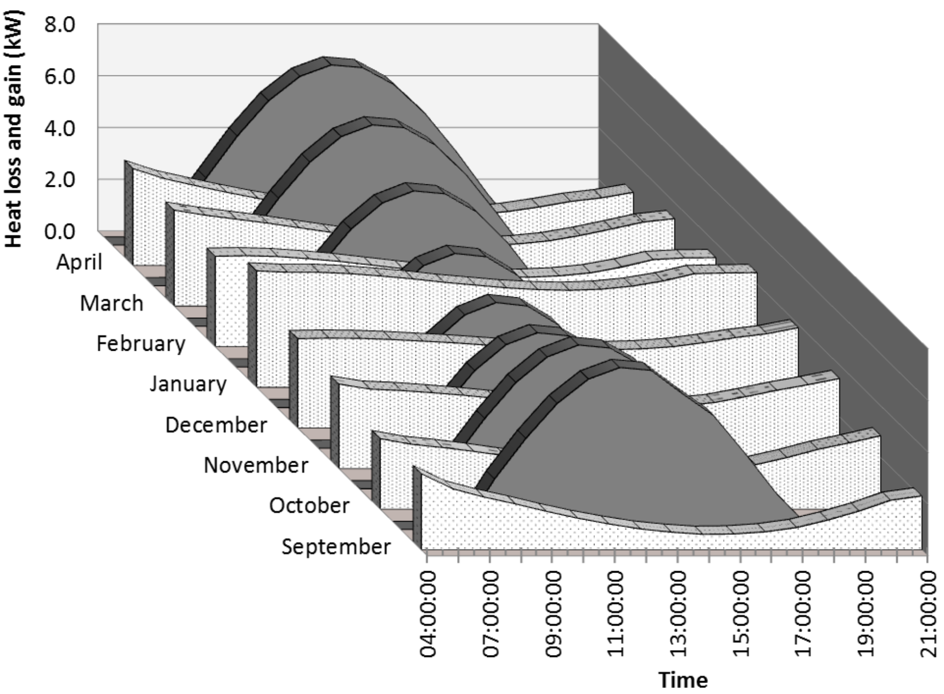

Figure 3.3.7 Average daily heat load-heat gain diagram for each month

As can be seen from the graph, during September significant amount of energy can be stored during daylight hours (09:00-17:00). Analysis for the winter months reveals that amount of storable heat in December-February period is in the range of 0.9 – 9.3 kWh whereas total heat demand of the building in these months is between 53.3-70.6 kWh. Considering the large difference between the amount of storable heat and building heat load, heat storage application in winter months in the UK seems not a feasible application.

In Table 3.5 the daily total heat load (THL) of the building, total heat gain from solar collectors (THG) as well as excess heat load (EHL) which represents the sum of the differences between heat load and heat gain during the day are given. Here, for analysis of EHL, only the periods where heat load is greater than heat gain are considered and the sum of the excess heat load in that period was calculated (See: Figure 3.3.8). On the contrary storable excess heat (SEH) is calculated as the sum of the differences between hourly heat gain from the collectors and hourly building heat demand as illustrated in Figure 3.3.8. When analysing the SEH is counted for only the periods when heat gain from collectors is higher then the building heat load. Based on the illustration in Figure 3.3.8, the relation between THL, THG, EHL and SHE could be expressed as follows;

$$\mathrm{THL} - \mathrm{EHL} = \mathrm{THG} - \mathrm{SEH} \tag{3.8}$$

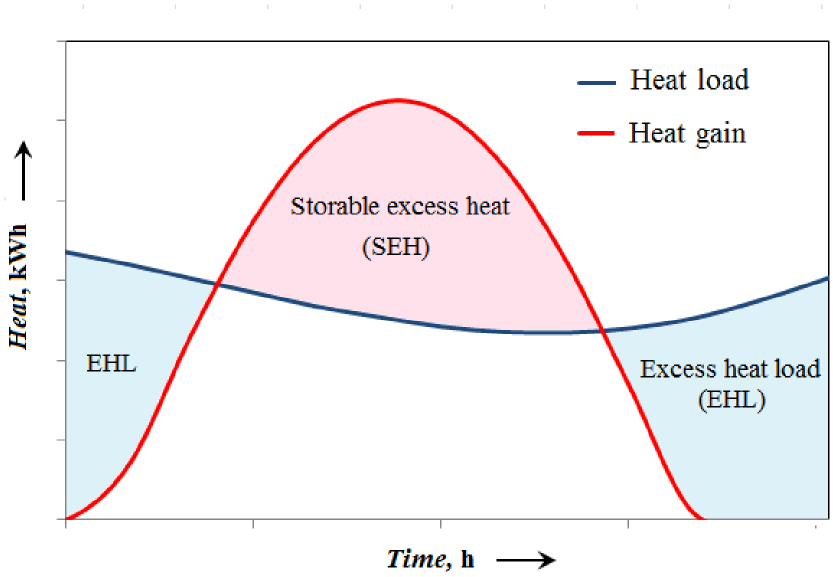

Figure 3.3.8 Schematic illustration of the methodology for determination of SHE and EHL

Table 3.5 Average daily total amount of storable excess energy in each month

Months	THL (kWh)	THG(kWh)	EHL(kWh)	SEH(kWh)
September	23.7	42.8	13.8	32.9
October	34.3	35.0	18.9	19.6
November	47.5	24.2	30.2	6.9
December	56.4	20.1	38.6	2.3
January	70.6	23	48.5	0.9
February	53.3	31.4	31.2	9.3
March	49.2	41.8	25.5	18.1
April	42.3	51.1	19.2	28.0

As seen from Table 3.5, THL is in the range 23.7-70.6 kWh, whereas THG varies between 50.1 and 20.1 kWh (see: Table 3.5). EHL in September is 13.8 kWh and rises to 48.5 kWh in January depending on the decrease in hours of sunshine, solar intensity and increase in heating demand. On the other hand there is 28 kWh and 32.9 SEH available in April and September (see: Table 3.5) as a result of the increase in solar intensity and decrease in heating demand during these months. As shown in Table 3.5, storable energy during winter months is minimal. This is because during the daytime solar heat gain does not exceed heating demand during most of the daytime, thus majority of the heat gain from the collectors is utilised in the building.

Based on the analysis results, in some periods of the day, EHL is higher than SEH, however in other periods heat gain is more than heat load which provides the possibility for heat storage. Heat storage is the best opportunity to provide a balance between supply and demand. For example, although the heat load in September is low, 13.8 kWh excess heat load appears. Without heat storage it is not possible to meet with this demand. As a result, it is clear that the use of heat storage increases solar fraction. Thence these systems render solar thermal systems more efficient and profitable.

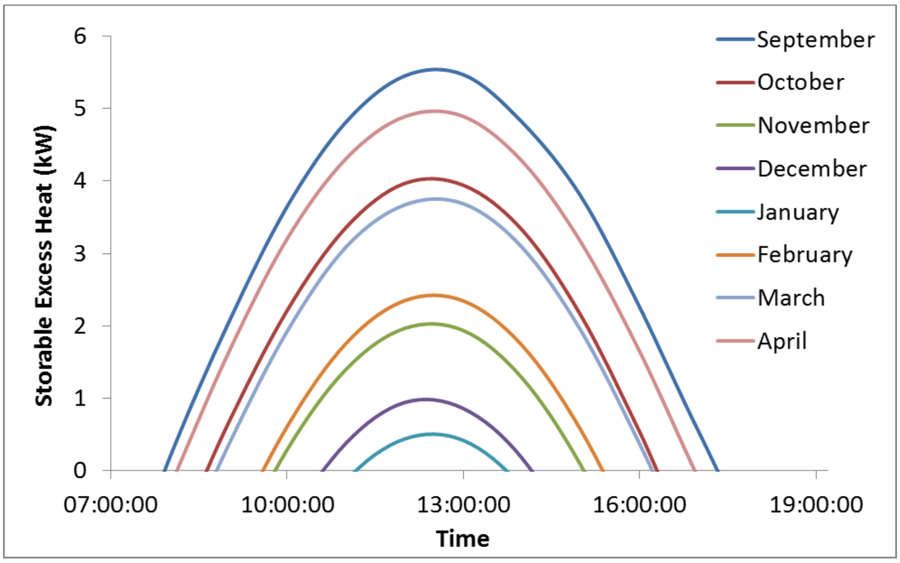

Figure 3.3.9 Average excess heat during the day for 6 months heating period

For short term storage, there are two important conditions that should be considered. These are length of the period that storable heat is available and amount of instantaneous excess heat. As can be seen from the Figure 3.3.9, both the duration and peak point of excess heat gain decrease from the spring periods to the winter. Although the excess heat gain is below 2.5 kW in November-February period, it exceeds 3 kW at midday for rest of the spring months, which provides the possibility for daily heat storage.

Determination of heat storage method and materials has significant importance on achieving an efficient heat storage system.The required storage volume (RSV) of heat is very important to the successful commercial usage of TES. As the RSV increases, applicability and operational conditionsfor TES become harder whilst the initial and maintenance costs also increase. The RSV depends primarily on;

1. energy density of the material
2. potential storable excess heat
3. collector area and properties
4. climate conditions

Table 3.6 provides the daily RSV for each material during the heating season. The percentages below the months indicate the contribution of heat storage to the average daily heating demand in each month. In terms of the amount of excess storable energy available, the average daily contribution of heat storage to the total heat load was analysed for each month. It can be seen from the table that RSV is higher in the months in which the amount of storable heat is greater; however RSV decreases as the storage density of material increases. Accordingly, thermochemical storage materials require less storage volume compared to the SHS and LHS materials. Additionally Silica gel seems to be the best candidate among the THS storage materials whilst water seems the most promising SHS material.

Table 3.6 Average daily contribution of heat storage to the total heat load with the usage of several storage materials

Heat Storage Material	Heat Storage Density (kWh/m^3)	Sep. (100%)	Oct. (58.2%)	Nov. (14.5%)	Dec. (4.0%)	Jan. (1.3%)	Feb. (17.4%)	Mar. (36.7%)	Apr. (66.1%)
		Required Storage Volume (m^3)							
Soil	6.6	4.940	3.027	1.039	0.346	0.136	1.401	2.726	4.217
Water	46.4	0.706	0.433	0.149	0.050	0.019	0.200	0.390	0.603
Paraffin	87.3	0.376	0.230	0.079	0.026	0.010	0.107	0.207	0.321
Zeolite	199.8	0.164	0.101	0.035	0.010	0.005	0.047	0.091	0.140
Silica Gel	230	0.143	0.087	0.030	0.012	0.004	0.040	0.079	0.122
$CaCl_2$	252.9	0.130	0.079	0.027	0.247	0.004	0.037	0.072	0.111

During the spring months when the quantity of storable energy is higher, more storage material should be employed. In case of thermochemical storage materials, it is possible to reduce the RSV by approximately 5-8 times when compared with SHS materials and 2 times compared to the LHS materials. Moreover in December and January there is not any short term storable heat available. This is an important point when considering the applicability of short term or daily storage to UK climatic conditions.

3.3.4.2 Long term storage (seasonal storage)

As a second storage model, long term seasonal heat storage was considered (see: Figure 3.3.10). Within this context solar energy is primarily diverted to the heat store in summer for utilization during the winter and spring periods. The stored energy supplied to the building during this period can be supported with the daily solar heat gain. In long term storage much higher storable heat is available as a result of prolonged high solar intensity. However storing heat in sensible form becomes difficult due to system heat loss. On the other hand use of the TES method has the distinct advantage in that it stores heat (hermetically) under whatever the current environmental conditions may be.

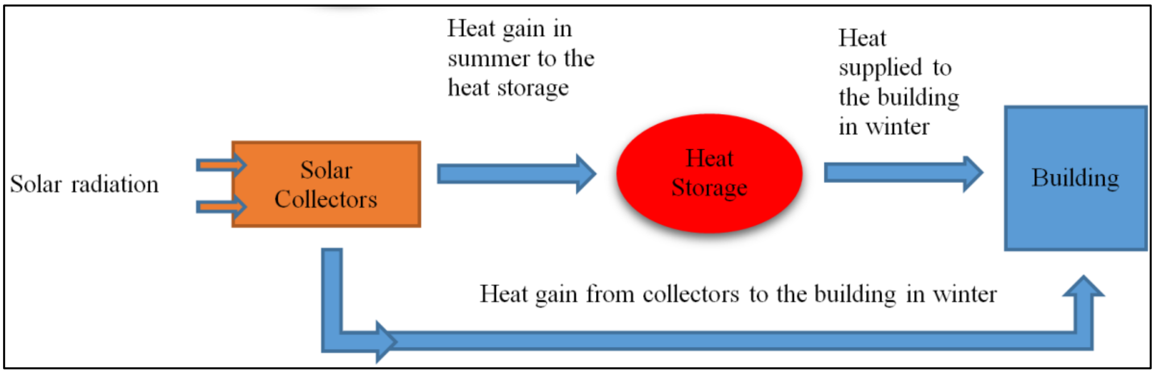

Figure 3.3.10 Schematic diagram of long term storage

Figure 3.3.11 illustrates heat load and heat gain for a twelve month period. It can be seen that during the summer period, storable heat is in the range of 1500-2000 kWh/month. Moreover, there is a significant amount of storable heat available during the spring terms. Benefitting from this excess energy will create the possibility to meet building heating demand during rest of the year, which is in the range of 500-2000 kWh per month.

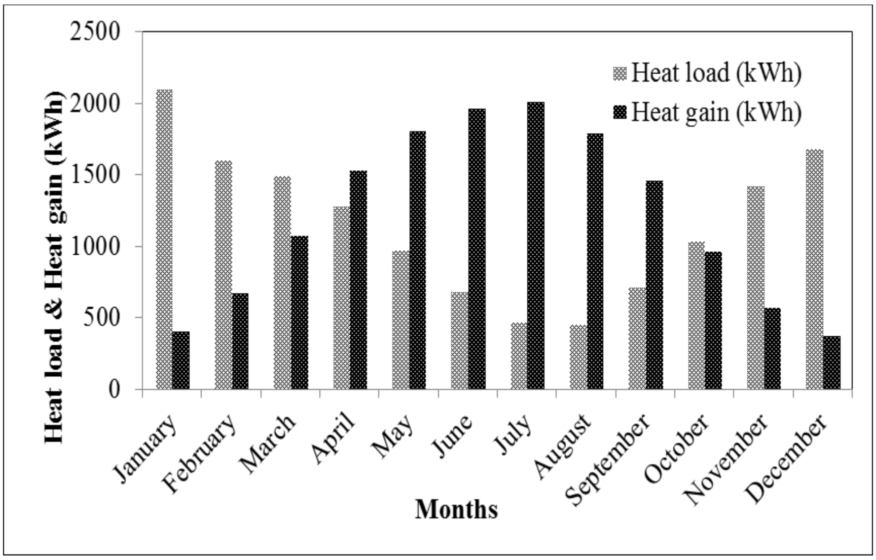

Figure 3.3.11 Monthly total heat load-heat gain

It is clear that a high amount of storable heat is available but the question remains - are there system designs, heat storage methods and material selections available to make use of it? THS materials have higher storage density and make it possible to store heat in less storage volume, however it should be considered that the storage of heat using THS is based on the decomposition of reactants (water vapour & adsorbent) where most of the THS materials require high summer regeneration temperatures (> 100 °C) which increases the complexity of design for this method.

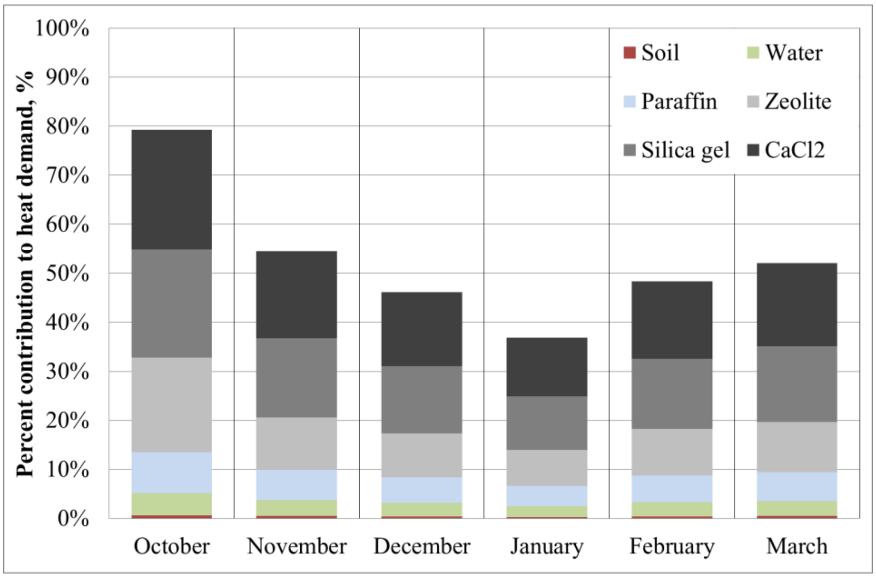

Figure 3.3.12 Contribution of heat storage to the heat load for each month with several storage materials

The average monthly heat load of a 100m^2 building in UK is in the range of 1038 kWh (October) to 2102 kWh (January). According to these values, a comparison of heat load coverage ratios (the ratio of potential storable heat to the heating demand) of different heat storage materials for each month was calculated and is presented in Figure 3.3.12. In order to compare the materials on a like for like basis, all calculations were carried out using a nominal 1 m^3 of energy storage volume. The results show that, using the same storage volume the THS materials ($CaCl_2$, silica gel, Zeolite) have the highest heat storage capacities followed by the LHS material (paraffin). With 1 m^3 THS and LHS it is possible to meet around 14% and 6% of average monthly heat load respectively, however for SHS, this ratio is less than 2% for the same storage volume. The main drawbacks of both the THS and LHS systems are high costs and complexity. In addition to this, the application of the large storage volumes in these systems is operationally difficult and not feasible with current technology. Conversely the SHS system utilizing larger storage volumes seems possible if there is adequate free space available, however heat loss and low heat storage density remain the main weaknesses of this storage method.

3.4 Conclusions

In this Chapter theoretical investigations on;

i) Design and sizing of THS for short and seasonal solar thermal storage under UK climate conditions,

ii) Comparative analyses on the heat storage capacities of different THS, SHS and LHS materials has performed

Several heat storage methods and materials were analysed and discussed to evaluate the best heat storage method under UK conditions. Within this context, a short and long term heat load of a well-insulated house in UK climate conditions was analysed. The daily and monthly average potential heat gain from solar collectors was calculated with an assumption of 10 m^2 collector area.

The main findings from the results are;

- Short term heat storage – In December and January, amount of daily storable excess heat is 4% and 1.3% of the building heat demand. Therefore, benefit of utilizing HS system in these months is minimal. In February, contribution of the HS to the building heat demand could reach to 17.4%. Therefore in February, daily heat storage application seems possible, although the benefit is low. According to study results, most favourable periods for short term HS are April, October and September. In October and April, over half of the building heat demand could be supplied by the heat storage whilst in September it is possible to fully meet the heat demand of the building. Using $CaCl_2$ as heat storage material requires 3 times less storage volume than paraffin and 6 times less storage volume than water in short term heat storage application.

- Seasonal heat storage - Building monthly heat load varies in the range of 1038 kWh (October) to 2102 kWh (January) for the six month heating period (October to March). On the other hand, during three month summer period, 6000 kWh solar energy could be gained with $8m^2$ solar collectors, which could be stored to meet the building heat demand in the heating season. Based on the performed comparative study between different heat storage methods for seasonal storage; each $1m^3$ THS can provide approximately 14% of the average monthly (October-March) heating demand of the building whereas LHS and SHS materials can provide with 6% and 2% respectively. $CaCl_2$ has been shown to have the best storage density (252 kWh/m^3) among all investigated materials.

The results showed that seasonal THS is the optimal storage method when placed in UK climate conditions. The encourageing results indicate the timeliness and importance of the development of novel THS systems. In order to fulfil this gap, composite adsorbent material synthesis and testing, as well as, open seasonal thermochemical storage reactor and process design, development and testing studies are included in the further Chapters.

CHAPTER 4: SALT IMPREGNATED DESICCANT MATRICES FOR 'OPEN' THERMOCHEMICAL ENERGY STORAGE

4.1 Introduction

The amount of solar radiation incident on a correctly orientated roof of a typical home in the UK exceeds its energy consumption over the course of a year (CIBSE, 2006). As presented in in Chapter 3, during the summer months there is an excess of solar heat energy available (see: Figure 4.1.1), however there is little or no building heat demand due to occupant comfort conditions already being met or exceeded. Conversely, peak building heat demand occurs during the winter months due to lower external temperatures when production of solar energy is at its minimum.

Research into potential inter-seasonal TES systems is still in its relative infancy however there are already many options available that have some potential to provide acceptable domestic level TES. Obtained results in Chapter 3 demonstrated that; THS offers the best opportunity in terms of inter-seasonal TES, due to low heat losses, high heat storage density and low space requirement. However there are process limitations on THS effectiveness such as the volume of material required, material cost, and the heat of reaction of the chosen material, thermodynamic design/operation of the system and applicability of the material to an 'open' THS system *i.e.* using standard operating pressures with moisture vapour as the adsorbate (gas). The aim of this research, therefore, was to narrow the selection of raw material sorbents (i.e. host matrices and desiccant salts) suitable for domestic scale 'open' THS to those that had a high affinity of each working pair to each other, were environmentally stable with low raw material costs, a low regeneration temperature, a high reaction temperature lift, high cyclic efficiency and high energy density. Additionally development of a novel reactor design for eliminating the thermal performance (e.g. heat and mass transfer) limitations in THS processes constitutes the secondary aim of the presented research.

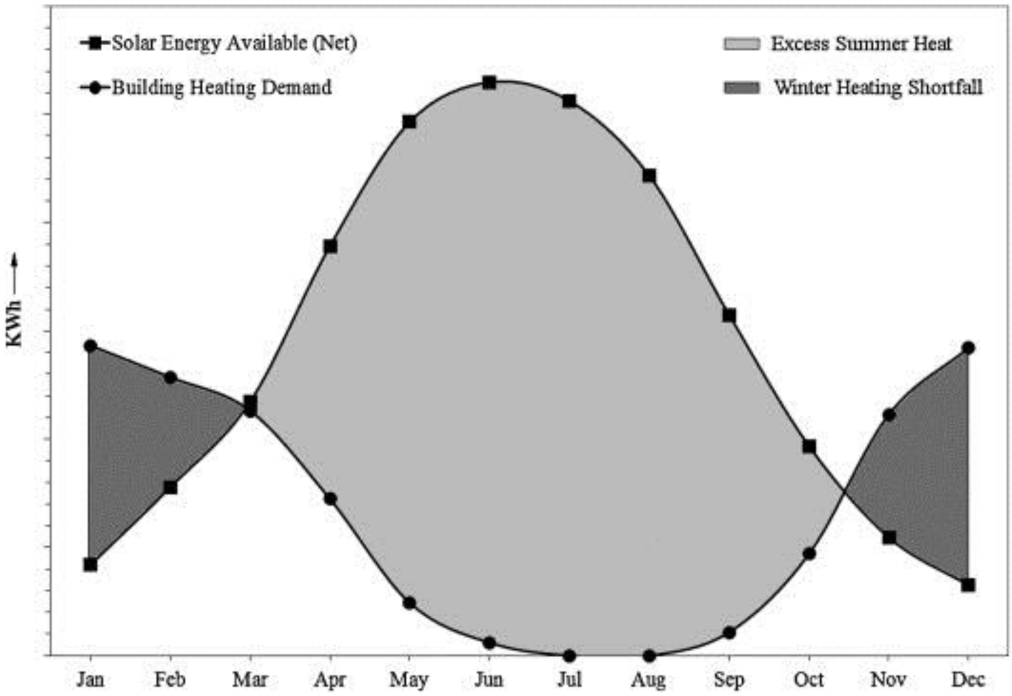

Figure 4.1.1 Graph showing the mismatch between available solar energy and building heating demand

Accordingly objectives of the study were set as follows;

i. Selection, synthesis and characterization of candidate sorption heat storage materials
ii. Hygrothermal cyclic behaviour and energetic analysis of selected sorption materials by physical experimentation in a custom testing tig
iii. Development and experimentation of a laboratory scale THS system that provides improved energy density utilisation through innovative hygrodynamic & thermodynamic reactor design

In this regard, Section 4.2, Section 4.3 and Section 4.4 present the completed work in order to meet the above given objectives. Overall outcomes of the study were discussed in Section 4.5 with the conclusions drawn.

4.2 Salt impregnated desiccant matrices for ‘open’ thermochemical energy storage - Selection, synthesis and characterization of candidate materials

There are many options available that have potential to provide acceptable inter-seasonal TES such as the thermochemical adsorption systems utilising desiccant storage materials such as Zeolites (Shigeishi et al., 1979, Hauer, 2002, Jänchen et al., 2004, Jänchen et al., 2005, Hongois et al., 2011, Jänchen and Stach, 2012, Dicaire and Tezel, 2012), silica gels (Zhu et al., 2006, Wu et al., 2007, Jänchen and Stach, 2012) and activated carbons (Dieng and Wang, 2001, Tokarev et al., 2010, Tso and Chao, 2012). There are also physical processes available based on both sensible heat *i.e.* solids and liquids (Hasnain, 1998, Cot-Gores et al., 2012, Ding and Riffat, 2012, Tatsidjodoung et al., 2013) and latent heat technologies involving materials that undergo a phase change *i.e.* solid→liquid, solid→gas (Lane, 1983, Zalba et al., 2003, Al-Abidi et al., 2012).

THS systems utilise reversible reactions (chemical or sorption) to store and release heat. For example, in the summer solar heat energy is used to remove an absorbed gas (V) from a host material (M) in an endothermic reaction. The material is then stored hermetically until the winter when the gas is allowed to react with the material creating an exothermic reaction, releasing heat as described in Figure 4.2.1. As such, no heat energy is stored inter-seasonally and therefore there are no losses due to heat degradation. The aim of this section is to select materials suitable for use as thermochemical heat storage mediums, specifically in ‘open’ systems for use under standard temperature and pressure (STP) conditions with water vapour as the adsorbate gas. Use of ‘open’ systems negates the requirement for both high vacuum setups and heat exchangers used in ‘closed’ systems. This required synthesis of sample materials and the complete characterisation of both their hygrothermal properties and pore structure in order to accurately correlate material type and behaviour.

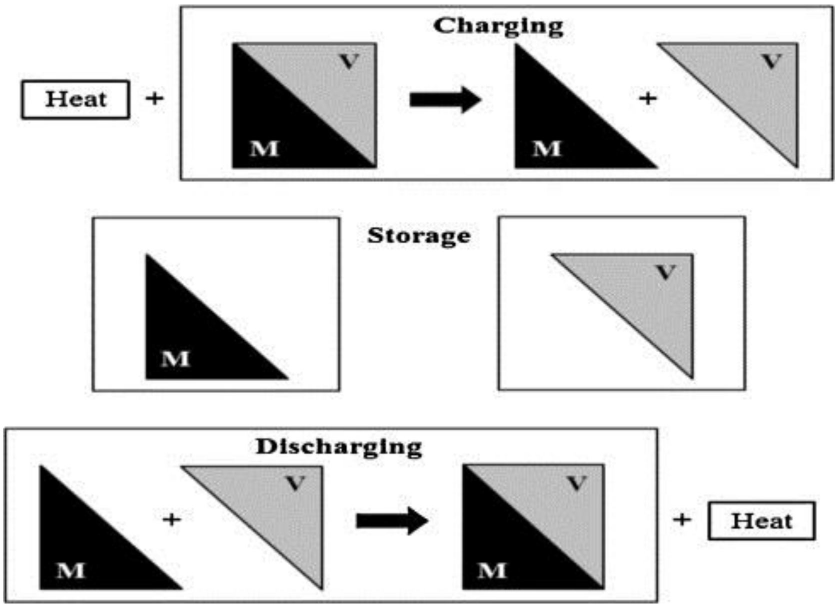

Figure 4.2.1 Charging, storage and discharging in a thermochemical storage system (adapted) (Hadorn, 2006)

4.2.1 Candidate material selection and synthesis

Similarly to the range of technologies presented in the thermal energy storage (TES) reviews presented in Chapter 2, there are many materials available for use in TES systems, dependent on system type. These can be categorised by heat storage mechanism; sensible, latent, adsorption, absorption and chemical reaction. Figure 4.2.2 maps a small range of materials suitable for TES (among other applications). Reading from left to right, the storage potential or energy density, E_d, defined as the amount of energy accumulated per unit volume or mass (Aristov et al., 2000b) increases due to the mechanism of TES. Materials such as water, rock and building materials rely on sensible storage where the TES is due to a temperature rise of the material. They have inherently low E_d which is equal to the product of the specific heat of the material by any temperature change (Çengel, 2006). PCMs have increased TES capability due to their higher E_d resulting from a change of phase within the material. As the temperature of a PCM increases above its specific melting point it melts absorbing latent energy. This latent heat is then released as the temperature drops and the PCM returns to its solid state (Zalba et al., 2003).

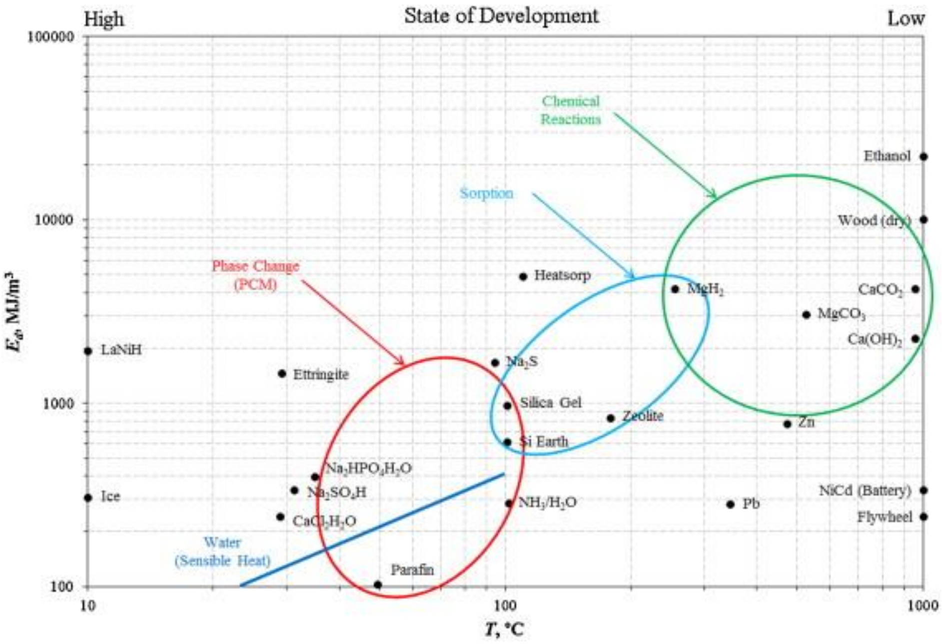

Figure 4.2.2 Energy densities of different classes of materials (adapted) (Bales et al., 2008)

The sorption group of materials (*i.e.* those that use heat of sorption reactions) offer higher E_d over the sensible and latent heat based materials. Sorption can involve both absorption of a gas into a solid or liquid and adsorption which can occur via chemisorption or physisorption. Chemisorption is rarely used in THS applications due to the high valency and ionic bonding energies involved, often being irreversible under normal working conditions (Condon, 2006). Physisorption for THS where Van der Walls forces bond the gas to the surface of pore walls has received much research and although the E_d of these desiccants is less than that for thermochemical reactions, the process can be fully reversible with little or no sorption hysteresis under the correct psychrometric conditions (Condon, 2006).

The final TES material group are the thermochemical reactions. These offer the highest E_d of all the groups, however have received the least amount of research to date (N'Tsoukpoe et al., 2009). Chemical reactions can be characterized by a change in the molecular configuration of the compound involved during the reactions *i.e.* dissociation and recombination (Tatsidjodoung et al., 2013). Any inter-seasonal TES system would greatly benefit from having materials that have a maximised E_d thus reducing storage volumes and/or mass whilst also providing adequate heat energy output.

4.2.1.1 Candidate material selection

For inter-seasonal ‘open’ THS systems the sorbent or gas used must be limited to one that is safe for human contact and is generally assumed to be water in the form of moisture vapour. A good working pair (sorbate/sorbent) would have certain desirable properties (Yu et al., 2013, N’Tsoukpoe et al., 2009, Aydin et al., 2015a):

- High affinity of the working pair to each other
- Environmentally stable
- Low raw material costs and high availability
- Low regeneration temperature for desorption *i.e.* charging the material (< 140 °C). (Higher desorption temperature is highly unlikely to obtain with building integrated solar collectors)
- High temperature lift, ΔT on absorption *i.e.* discharging
- Minimal or no hygrothermal cyclic hysteresis i.e. high cyclic efficiency
- High E_d and thermal conductivity, λ

Previous research on materials suitable for THS systems has recently migrated towards confining various types of salt within the pore structure of a desiccant (or host matrix) such as activated carbon (Tokarev et al., 2010), vermiculite (Aristov et al., 2000a), silica gel(Tokarev and Aristov, 1997), molecular sieves (Henninger et al., 2010, Jänchen et al., 2005) and synthetic Zeolites (Chan et al., 2012, Hauer, 2002, Hongois et al., 2011). In these materials, the matrix, which was typically used to provide sorption heat storage, now acts solely as a host to prevent deliquescence of the salt during hydration.

These salt and matrix combinations or Salt In Matrix (SIM) have been shown to generally meet the requirements for THS listed above and thus were included in the first pass material selection for this research (see: Table 4.1).

Table 4.1 First pass list of candidate composite matrix/salts for THS with highlighted selected materials

Host Matrix	Impregnated Salt	Reference
Silica Gel (Microporous)	Calcium Nitrate, $Ca(NO_3)_2$	(Simonova et al., 2009)
Vermiculite	Calcium Chloride, $CaCl_2$	(Aristov et al., 2000a)
Activated Carbon	Calcium Chloride, $CaCl_2$	(Gordeeva et al., 1998b)
Alumina	Calcium Chloride, $CaCl_2$	(Gordeeva et al., 1998b)
Silica Gel (Mesoporous)	Calcium Chloride, $CaCl_2$	(Aristov et al., 1996b)
Activated Carbon	Lithium Bromide, LiBr	(Gordeeva et al., 2002)
Vermiculite	Lithium Nitrate, $LiNO_3$	(Sapienza et al., 2012)
Activated Carbon / Silica Gel	Calcium Chloride, $CaCl_2$	(Tso and Chao, 2012)
Zeolite 13X	Magnesium Sulphate, $MgSO_4$	(Hongois et al., 2011)
Graphite	Strontium bromide, $SrBr_2$	(Lahmidi et al., 2006)
Silica Gel (KG5-88)	Calcium Chloride, $CaCl_2$	(Stach et al., 2005)
Silica Gel (Mesoporous)	Lithium Bromide, LiBr	(Gordeeva et al., 1998a)
Zeolite 13X	Calcium Chloride, $CaCl_2$	(Chan et al., 2012)
Xerogel	Calcium Chloride, $CaCl_2$	(Aristov et al., 2000b)
Activated Carbon	Lithium Bromide, LiBr	(Gordeeva et al., 2002)
Attapulgite	Calcium Chloride, $CaCl_2$	(Jänchen et al., 2005)

Scrutiny of the materials through investigation of published material properties, cost, regeneration temperatures suitable for open THS, and availability reduced this down to a second pass list (highlighted in Table 4.1).

To provide a representative analysis of all the composites of SIM’s under the current research time constraints, a cross-sectional sample of all the salts and matrices were chosen for characterisation (see: Table 4.2).

Table 4.2 Designation of SIM compositions with selected samples analysed highlighted

	Impregnated Salt				
	$CaCl_2$	$MgSO_4$	$Ca(NO_3)_2$	$Li(NO_3)_2$	LiBr
Silica Gel	SIM-2a	SIM-2b	SIM-2c	SIM-2d	SIM-2e
Vermiculite	SIM-3a	SIM-3b	SIM-3c	SIM-3d	SIM-3e
Activated Carbon	SIM-4a	SIM-4b	SIM-4c	SIM-4d	SIM-4e
Zeolite 13X	SIM-8a	SIM-8b	SIM-8c	SIM-8d	SIM-8e

4.2.1.2 Synthesis

For the SIM synthesis, all matrices and salts were used as supplied. The Zeolite was sourced from BASF (Faujasite type 13X Molecular Sieve) with a bead size of 2.5 - 5mm. The chemical composition of the Zeolite 13X is:

$$Na_2O \,.\, Al_2O_3 \,.\, m\ SiO_2 \,.\, n\ H_2O\ (m \leq 2.35)$$

The silica gel with a chemical composition of SiO_2 . n H_2O, was sourced from Geejay Chemicals, UK (Non-indicating white bead) with a 2 - 5mm bead size. The activated carbon (Derosex K 33 - Cylindrical) with the chemical composition of C . nH_2O was sourced from Caldic UK and had a nominal pellet size of ≈ 3mm. The vermiculite used (Micafil) was sourced from Dupre Minerals UK with a nominal particle size of 2 – 8 mm. This was sieved to narrow the distribution to 3 - 5mm in order to match that of the other matrices. The chemical composition of the vermiculite is (IMA, 2011):

$$(Na_{0.21},K_{0.39},Mg_{0.19},Ca_{0.13},6H_2O)\ (Mg_5,Fe^{+2}_{0.2},Fe^{+3}_{0.8})\ [Si_{5.5},Al_{2.5},O_{20}]\ (OH)_4$$

All salts used in the research were sourced from Sigma Aldritch, UK. The technique used to synthesise the SIM’s was that pioneered by Prof. Yuri Aristov at the Boreskov Institute of Catalysis, Novosibirsk, Russia. The Insipient Witness Technique (IWT) uses the desiccant matrix materials natural wetting or liquid absorption capacity to fill the pore structure with a selected salt solution. It was first necessary to determine the specific pore volume, V_p of the matrix material in cm^3/g using either Mercury Intrusion Porosimetry (MIP) or N_2 physisorption. A saturated salt solution to ≈ 100% of the matrix pore volume, dependant on total sample mass, m_m was then prepared as given by $m_m \times V_p$.

The saturated salt solution was slowly added to the matrix whilst stirring constantly. The matrix material should appear to remain dry as the solution will be drawn into the pore network through capillary action. Dependent on the nature of the matrix material, such as the large variance of pore volume in different vermiculite samples, additional solution was added until visual confirmation of a fully wetted transition occurs. The wetted SIM was then placed in an oven to evaporate the water and entrapping the salt within the matrix. Drying temperature, was set at a minimum of $T = 150$ °C, to achieve full dehydration of the salt. The mass of salt entrapped in the matrix (as %) was calculated as the increased mass after drying. The experimentally measured salt mass was also compared with the theoretical mass as calculated in example below:

Mass of matrix, m_m =	10 g
Specific pore volume of matrix, V_p =	1.2 cm^3/g
Maximum salt solution concentration (saturated), c_s =	20 %
Volume of solution required, $V_s = m_m \times V_p$	12 cm^3 (m_s = 12 g)
Mass of salt in solution, $m_{salt} = V_s \times c_s$	2.4 g
Mass of H_2O in solution, $m_{H2O} = m_s - m_{salt}$	9.6 g (V_{H2O} = 9.6 cm^3)
Mass of salt (%) in matrix, $m_{salt,\%}$ =	24%

In total 8 SIM's were synthesised for analysis – SIM-2a, SIM-3a, SIM-3b, SIM-3c, SIM-3d, SIM-3e, SIM-4a and SIM-8a and compared against the raw matrix materials. The raw vermiculite and vermiculite based SIM's (see: Table 4.2) were imaged using a Philips XL30 Environmental scanning electron microscope (SEM) equipped with a field emission gun to provide a visual affirmation of the presence of the salts. The SIM’s were prepared by depositing a single particle of the dried SIM onto an aluminium stub, then applying a Platinum, Pt sputter coating at a rate of 6–7 nm min^{-1} for t = 90 s. Care was taken to ensure the top facing surface of the SIM was kept level to aid clearer imaging. Micrographs were recorded using an Everhart–Thornley-type secondary electron detector. Micrographs of the six samples are presented in Figure 4.2.3, showing the (a) raw vermiculite, (b) SIM-3a, (c) SIM-3b, (d) SIM-3c, (e) SIM-3d and (f) SIM-3a.

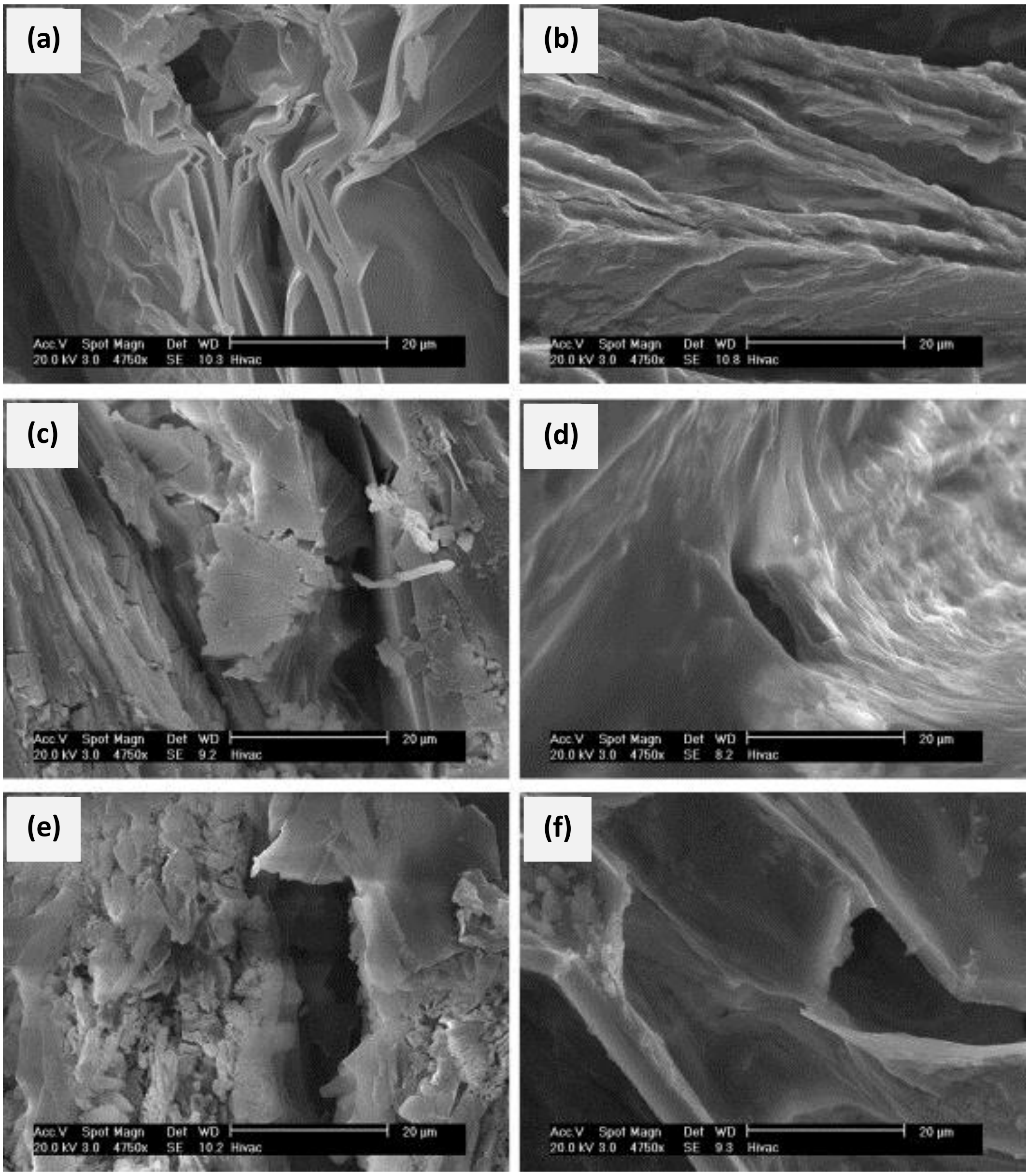

Figure 4.2.3 SEM micrographs of (a) Vermiculite, (b) SIM-3a, (c) SIM-3b, (d) SIM-3c, (e) SIM-3d, and (f) SIM-3e

The raw vermiculite displays clear definition of the lamellar structure of the material with this definition missing from all the SIM samples due to the entrapped salts. Elemental mapping was also performed using an Oxford Instruments Inca model spectrometer for energy-dispersive X-ray (EDX) spectral analysis to confirm the presence of the salts in each SIM tested.

4.2.2 Material characterisation

The performance of any material as a THS is determined by its inherent properties. The hygrothermal properties and pore geometry are interrelated and characteristic for each material. The properties measured in this research were listed below. The ideal values, which were specified based on the interpretation of the previous studies presented in Table 4.1 were also given in brackets:

- Pore volume, V_P in cm^3/g → (> 1.7)
- Specific surface area, SSA in m^2/g → (> 15 for macroporous, > 500 for mesoporous – raw matrices only)
- Apparent porosity, n in m^3/m^3 → (> 65%)
- Sorption isotherm(s) for water vapour and capillary water, where $w = f(RH)$ in kg/kg → (> 1.2 in the range 11% < RH < 94%)
- Solid and Bulk density, ρ_{solid} and ρ_{bulk} in g/cm^3 → (> 1.4 and > 0.4 respectively)
- Dry-state thermal conductivity, λ in W/(m.K) → (> 0.06)
- Specific energy density, E_d in kJ/kg → (> 200)

4.2.2.1 Characterisation of the micro-structure and pore network

Nitrogen (N_2) physisorption analysis of all 12 samples (raw & SIM's) was performed using a Micromeritics Tristar II 3020 (v1.04) analyser in accordance with BS 4359-1 (BSi, 1996). The samples ($m \approx 0.5$ g) were first oven dried to achieve the condition $w = w_0$ before being outgassed at 200 °C for $t = 6$ h prior to the analysis. N_2 gas adsorbate was used with a 5 min equilibration time at each relative pressure, P/P_o point with a constant bath temperature of -196 °C. 25 adsorption and 25 desorption P/P_o points were used for each test. The N_2 sorption isotherms for the non-vermiculite based samples are shown in Figure 4.2.4.

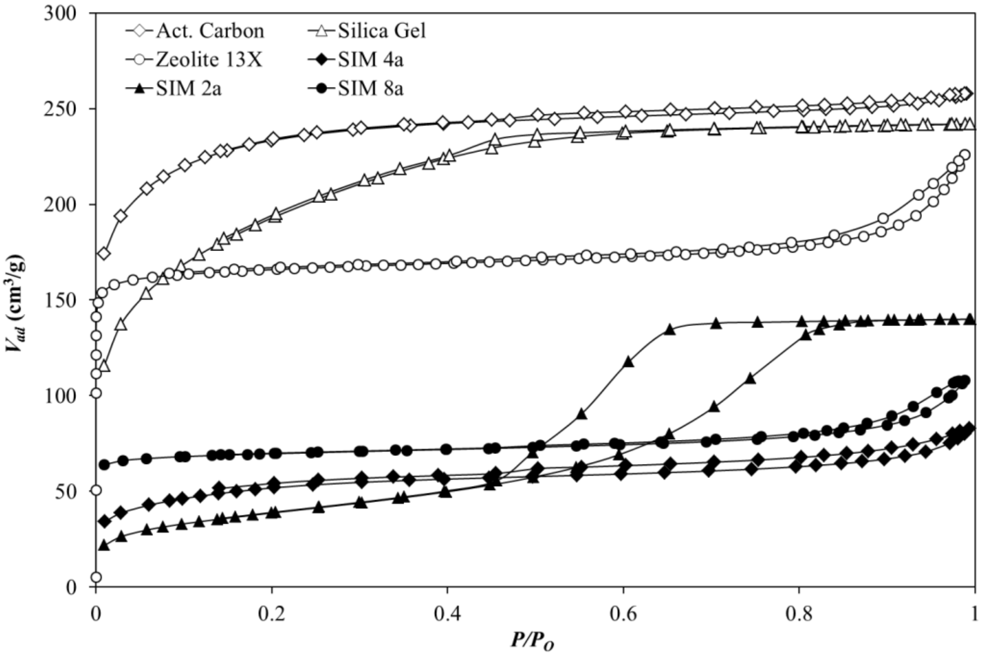

Figure 4.2.4 N_2 adsorption/desorption isotherms for the non-vermiculite based samples

As expected there was an overall reduction in the adsorbed volume for the three SIM samples when compared to the raw matrices due to the presence of the salt within the pores. In general, the IUPAC classification of isotherm type (IUPAC, 1994) from N_2 analysis can be used to provide an indication of the behaviour of a material under STP conditions (such as an ‘open’ THS system). A Type I isotherm shows that a material will take on moisture rapidly at low *RH* levels with no further absorption whereas a Type IV isotherm would absorb and desorb moisture at higher *RH*. The primary use of N_2 analysis however, is to characterise the porous solids geometry and analyse the material before and after synthesis. The raw activated carbon, silica gel and Zeolite 13X had Type I isotherms, typical of microporous materials ($Ø_{pore}$ < 2nm) although there was some macroporous filling evident in the Zeolite which was unexpected. This may be due to external filling of the inter particle voids within the powder sample. After impregnation of the salt all three SIM's displayed a change to typical Type IV isotherms with pronounced hysteresis observed in SIM-2a. This suggests that damage may have occurred within the micropore network during the wetting process with possible pore wall collapse or cracking due to the expanding forces of the advancing liquid exceeding the pore wall strength, leading to increased pore size distribution (Sakka, 2005).

The mesopore diameter distribution for the non-vermiculite based samples was determined by the Barrett– Joyner–Halenda (BJH) method from the adsorption branch of N_2 isotherm and is shown in Figure 4.2.5, with the mean mesopore diameters, $Ø_{pore}$ indicated. The raw materials all had a nominal $Ø_{pore}$ matching their manufacturer's specification, however, when impregnated with the $CaCl_2$ there was no reduction in $Ø_{pore}$ as would have been expected. The Zeolite 13X increased from 1.18nm to 42.77nm clearly suggesting that damage occurred to the pore structure as discussed previously.

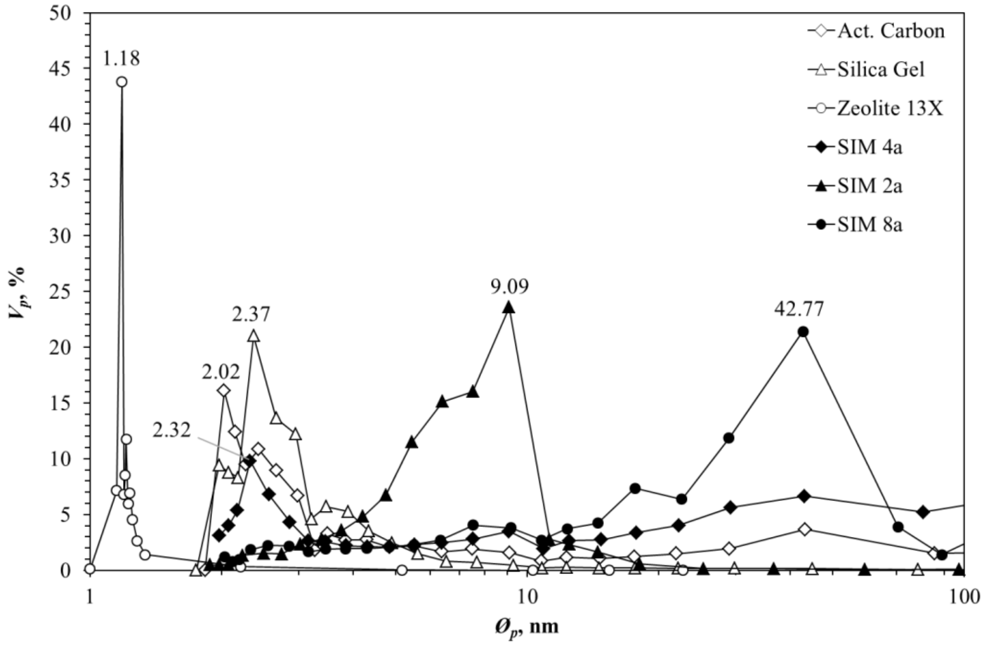

Figure 4.2.5 BJH pore size distributions for the non-vermiculite based samples

There was a smaller change in the silica gel $Ø_{pore}$ from 2.37 to 9.09nm and minimal change in the activated carbon from 2.02 to 2.32nm. This may be due to the stronger pore wall structure in the carbon material however, allowing for the presence of the salt in SIM-4a, this is still a significant increase.

The pore volume distribution for each sample was also derived from the adsorption branch of the isotherm, with the total pore volume, V_p being estimated from the adsorbed amount at the constant C for pores less than 67.38 nm, where a relative pressure of P/P_0 = 0.97 was set. Specific surface area (SSA), was determined using multipoint Brunauer– Emmett–Teller (BET) analysis with the data presented in Table 4.4. As the impregnated salt now occupies a fraction of the pore space, V_p was reduced for all the SIM samples. SIM-2a and SIM-4a showed reductions of 21% and 15% respectively but in SIM-8a (Zeolite 13X/$CaCl_2$) V_p was only reduced by 2%. This agrees with the findings on pore size where there had been substantial damage to the SIM-8a material structure.

As N_2 physisorption is not suitable for macroporous solids (>50nm), Mercury intrusion Porosimetry (MIP) analysis of the six vermiculite based samples (raw & SIM's) was performed using a Micromeritics Autopore IV 9500 analyser. Samples, $m \approx 0.5$ g were prepared by oven heating at T = 110 °C for t = 24 h and then allowed to cool to room temperature in a desiccator for t = 1 h prior to testing. The samples were first evacuated to a pressure of 9.33 Pa to remove any residual physisorbed moisture from the pores. For each sample run the pressure was increased incrementally to a maximum pressure, P_{max} = 60000 psia and then decreased incrementally back to atmospheric pressure. The MIP experiments were conducted with 53 intrusion and 30 extrusion points using an equilibration time, t = 10 s for each step. Figure 4.2.6 presents the results on the six vermiculite based samples. The raw vermiculite had a nominal $Ø_{pore}$ of 3.68 µm whilst the SIM's, in general had reduced

Ø_{pore}. SIM-3b ($MgSO_4$) showed no reduction in pore size, however as vermiculite is a natural material, there may be some discrepancy in the original sample pore distributions. Further testing with a broader range of samples will be required to investigate this further.

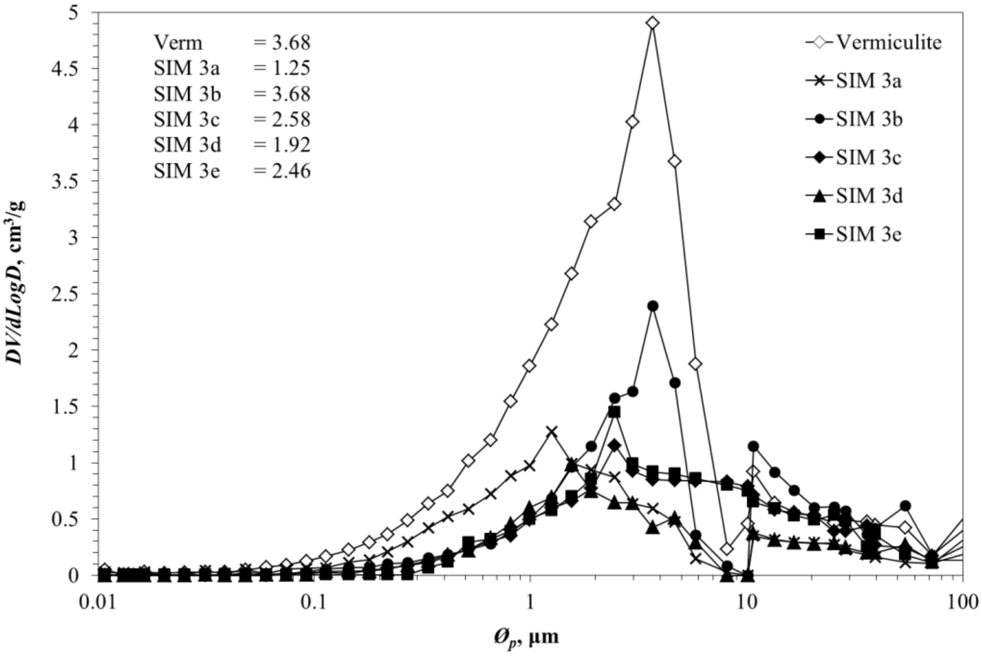

Figure 4.2.6 MIP pore size distributions for the vermiculite based samples

Total accessible pore volume, V_p for the vermiculite samples was measured at P_{max} with the data presented in Table 4.4. Unlike the non-vermiculite SIM's there was no evidence of damage to the structure of the material, due to the larger, macroporous nature of the vermiculite *i.e.* no pressure front during wetting. As expected there were reductions in V_p for all SIM's after impregnation due to the presence of the salt in the matrix.: SIM-3a = 64%, SIM-3b = 50%, SIM-3c = 69%, SIM-3d = 73% and SIM-3e = 71%. There were corresponding reductions in total pore area with an average reduction of 72% when compared to the raw vermiculite.

The relative proportion of the mesopore (N_2 physisorption) and macropore (MIP) volume to the total pore volumes are shown in Figure 4.2.7. The vermiculite and vermiculite based samples had negligible mesopore volume (< 0.5%) suggesting that without the addition of salt there would be little or no E_d through adsorption alone.

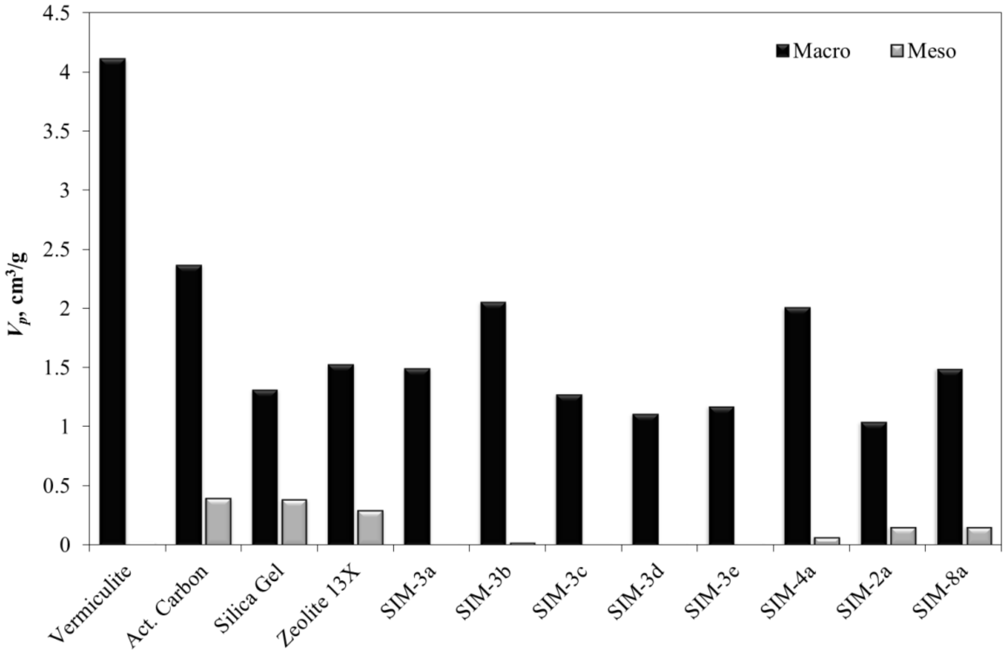

Figure 4.2.7 Relative proportions of meso/macro pore volume to total pore volume

The raw silica gel, Zeolite 13X and activated carbon had higher proportions of mesopore volume (29%, 19% and 17% respectively) with increased SSA due to the mesopore size distribution. These three materials would theoretically have higher E_d in the raw state from heat of sorption reactions, but may have pronounced hysteresis during desorption. After impregnation there was still evidence of mesopores in the SIM's however the proportion of total volume was much reduced (SIM-2a – 15%, SIM-8a – 10% and SIM 2a – 3%).

In order to determine the porosity of the materials, it was necessary to first determine the bulk, and solid densities, ρ_{solid}. Bulk density is further used to determine system volume (in later research). The loose ρ_{bulk}, of the non-vermiculite materials was measured using the gravimetric technique in accordance with BS 1097-3 (BSi, 1998). Samples, $m \approx 50$ g were prepared by oven heating at $T = 110$ °C for $t = 24$ h prior to testing. The volume V_{bulk} and mass m were recorded and ρ_{bulk} calculated. Each test was repeated 3 times allowing the mean value of ρ_{bulk} to be calculated. For the vermiculite based materials, ρ_{bulk} was obtained from the MIP testing. Solid density was determined for all materials using a Micrometrics Accupyc 1330 gas pycnometer with helium as the inert gas in accordance with BS ISO 21687 (BSi, 2007). The samples were prepared identically as for the ρ_{bulk} tests.

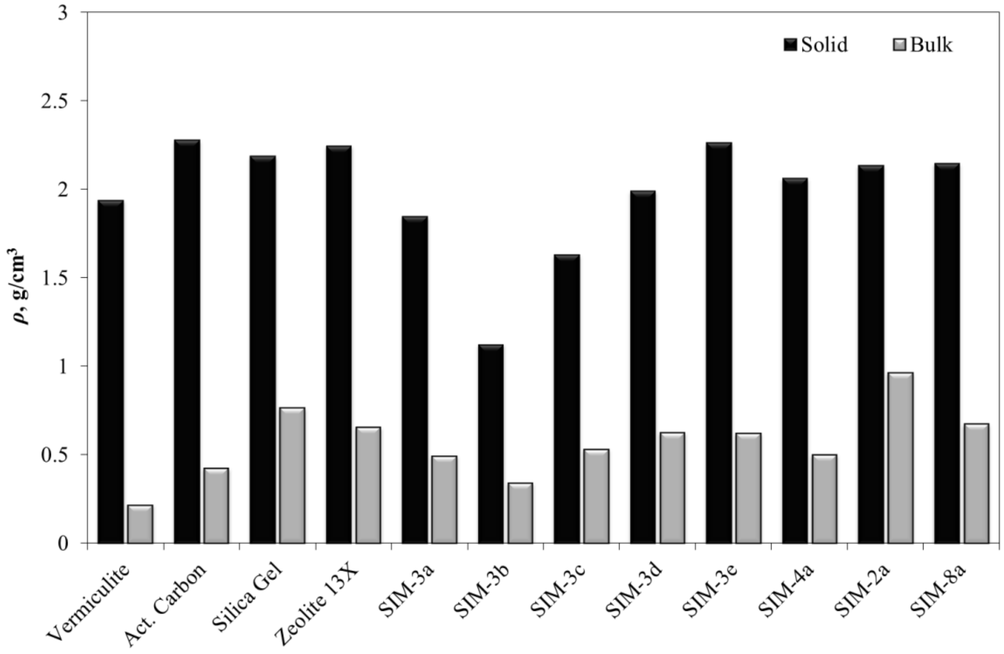

Figure 4.2.8 Comparison of bulk density to solid density

The density analysis (see: Figure 4.2.8) shows that although there was an increase in ρ_{bulk} for all SIM's after impregnation due to the addition of the salts increasing the overall mass, this was not the case for ρ_{solid}. The solid density of both the salts and raw matrices are very similar which explains this result.

4.2.2.2 Characterisation of hygrothermal functional properties

The moisture vapour adsorption isotherms for all materials were determined by gravimetric dynamic vapour sorption (DVS) in accordance with BS EN ISO 12571 (BSi, 2000). A custom built successive desiccator chamber system was used to control internal relative humidity (RH_{ie}) and T at 23 °C to an accuracy of ±1 °C. A series of 6 airtight chambers were constructed with an interchangeable low voltage circulation fan to prevent air stagnation around the sample (see: Figure 4.2.9). Each chamber contained a saturated salt solution to achieve a range of RH_{ie} at 23°C (11% < RH < 94%) and with deionised water to achieve the condition where $RH \rightarrow 100\%$. The salts used were in the sequence: Lithium Chloride (11.3% ±0.28), Magnesium Chloride (32.9% ±0.17), Magnesium Nitrate (53.5% ±0.22), Sodium Chloride (75.4% ±0.13) and Potassium Nitrate (94.0% ±0.6).

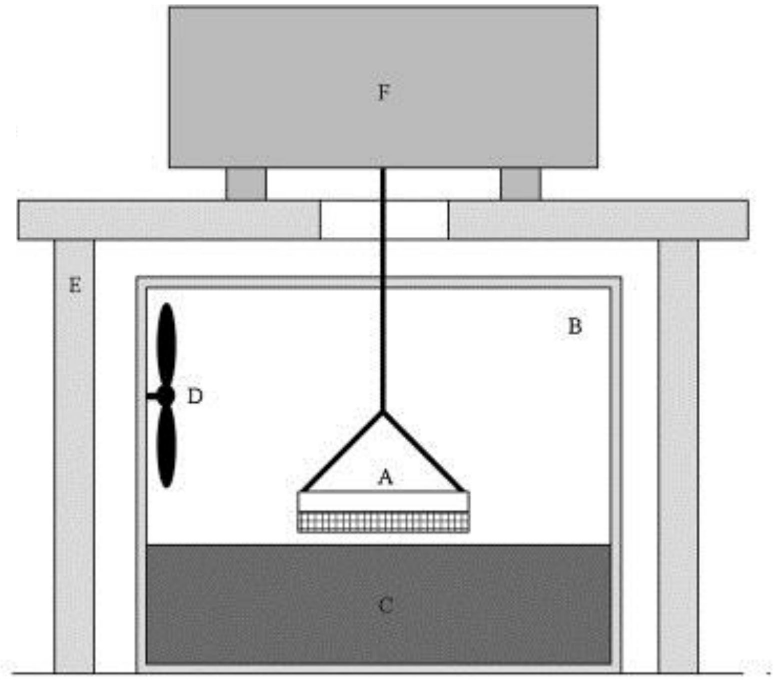

A - SIM in hanging dish
B - Sealed chamber
C - Saturated salt solution
D - Stirring fan
E - Balance support

Figure 4.2.9 Modified experimental test assembly to determine moisture vapour adsorption isotherms

Dynamic mass change, Δm of the samples was recorded at intervals of t = 30 s using an air-shielded A&D tuning fork analytical balance (±0.1 mg accuracy) via a direct USB connection to a PC. Δm was calculated as change in mass of the wetted sample, m_w per mass of the dry sample, m_{dry}; $\Delta m = m_w - m_{dry}$ (kg).

Samples, $m \approx 5$ g were prepared by oven heating at T = 110 °C for t = 24 h and then allowed to cool to room temperature in a desiccator for t = 1 h prior to testing. The samples were placed in the hanging dish suspended below the balance and Δm monitored continually. The sample was deemed to have reached equilibrium moisture content (EMC) at each $RHie$ level when $\Delta m < \pm 0.5\%$ with the sample then being transferred to the next chamber in the sequence. Figures 4.2.10 and 4.2.11 shows the compiled EMC or sorption isotherm results for all sample materials.

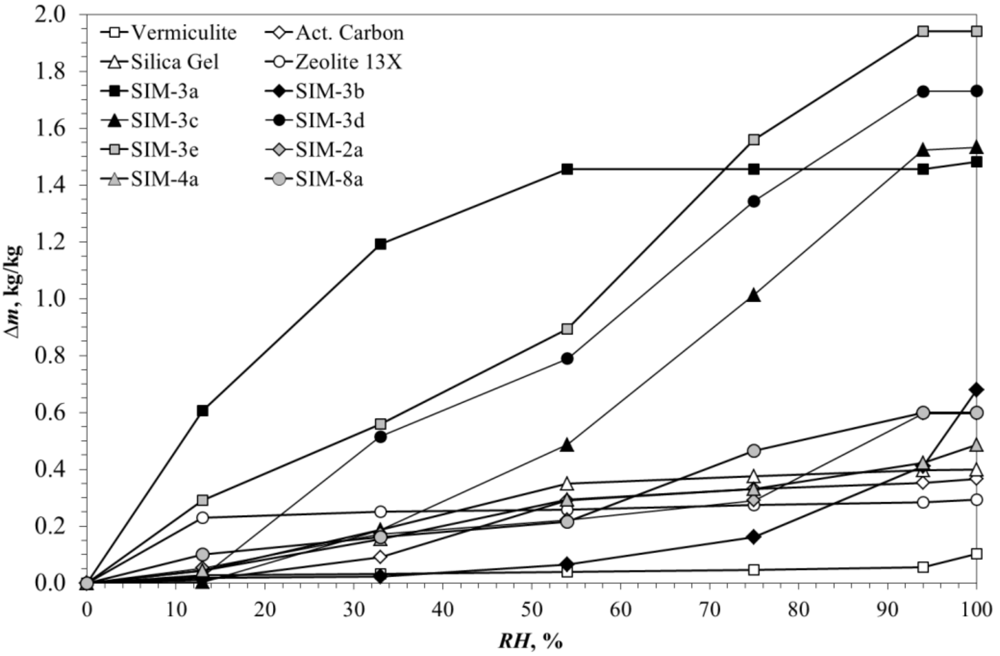

Figure 4.2.10 Moisture vapour sorption isotherms for all materials (at T = 23 °C)

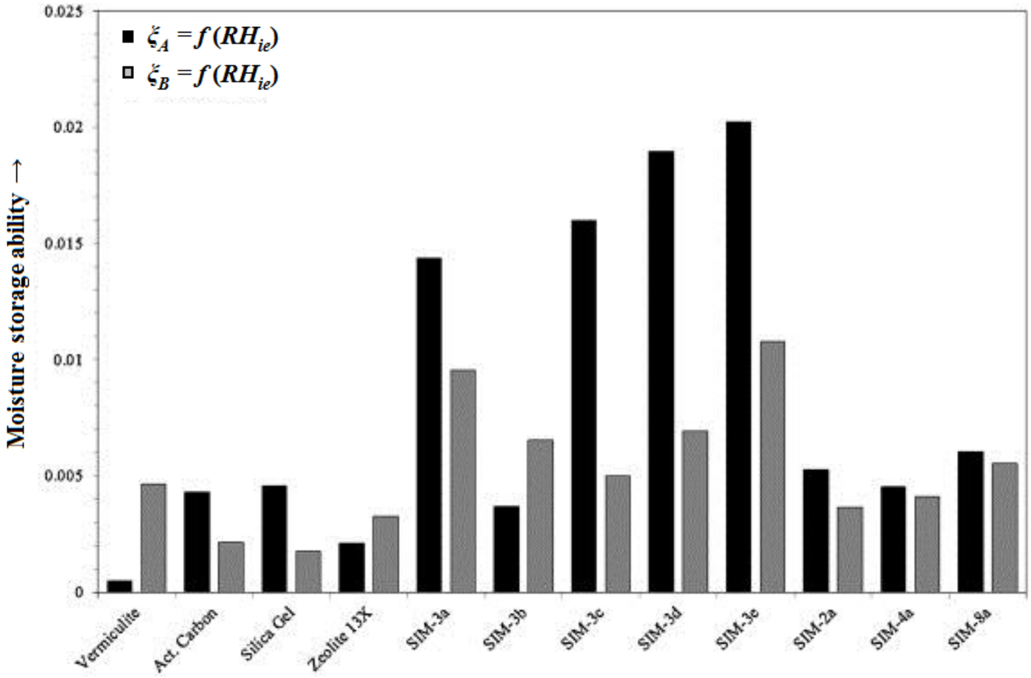

Figure 4.2.11 RH_{ie} and t_{emc} based moisture storage functions for all materials

The vermiculite based SIM-3a ($CaCl_2$), SIM-3c ($Ca(NO_3)_2$), SIM-3d ($LiNO_3$) and SIM-3e (LiBr) showed the best performance across the full RH_{ie} range with SIM-3a having good EMC (Δm >

0.6 kg/kg) in the lower range *i.e.* RH_{ie} = 11%. In the mid range (33% < RH < 54%) SIM-3a had superior perfomance over SIM-3c, SIM-3d and SIM-3e with all three displaying very similar uptake rises. SIM-3a had no further significant uptake ≈ 1.4 kg/kg in the higher RH ranges (54% < RH < 100%) whilst both SIM-3c, SIM-3d and SIM-3e had very large steps (≈ 1.1 kg/kg) between 54% and 94% and a final EMC of ≈ 1.5, 1.7 and 1.9 kg/kg respectively. This would suggest that SIM-3a may be beneficial where lower RH levels are applicable whilst SIM-3c, SIM-3d and SIM-3e would potentially suit higher humidity environments. The raw vermiculite, as expected, had very limiter EMC levels across the whole RH range due to its macro-porous nature. The other three raw desiccants had isotherms that are in-line with other published data (Hall et al., 2012). There was increased uptake for all SIM materials over their equivelant raw material host, however in the non-vermiculite SIM's, this was quite limited due to the reduction in pore volume accesible to the moisture vapour. In terms of EMC only, it is clear that SIM-3a, SIM-3c, SIM-3d and SIM-3e have much superior performance and allow good accesibility to moisture vapour transfer suggesting they may be suitable for an open THS system.

Whilst overall moisture uptake (EMC) is an important hygrothermal property of the materials, the rate of that uptake or sorption kinetics is also important, sometimes even more so. A rapid response to changing humidity environments i.e. ΔRH is necessary to also produce the required thermal reaction to enable THS. To analyse the moisture kinetics the moisture storage function, ξ (Hall et al., 2012) was used, which gives an indication of the sorption performance of the material in the hygroscopic range. Two variants of ξ were used: ξ_A which is the moisture storage as a function of RH_{ie} only and ξ_B which is the moisture storage as a function of both the RH_{ie} and the time taken to reach EMC, t_{emc} (Casey et al., 2012). In both scenarios ξ is calculated as the linear slope of the isotherm in the range 11% < RH < 94%. The data for both EMC and t_{emc} for all materials is presented in Table 4.3.

Table 4.3 Summary of mass uptake per kg with corresponding t_{emc} for all candidate materials

RH	0 → 11%		11 → 33%		33 → 55%		55 → 75%		75 → 94%		94 → 100%	
Material	Δm (kg/kg)	t_{emc} (h)	Δm (kg/kg)	t_{emc} (h)	Δm (kg/kg)	t_{emc} (h)	Δm (kg/kg)	t_{emc} (h)	Δm (kg/kg)	t_{emc} (h)	Δm (kg/kg)	t_{emc} (h)
Vermiculite	0.03	4.32	0.03	5.76	0.04	8.40	0.05	9.60	0.06	11.04	0.10	60.72
Act. Carbon	0.01	21.84	0.09	69.36	0.29	126.24	0.33	150.00	0.35	187.92	0.37	195.12
Silica Gel	0.04	21.36	0.19	112.56	0.35	151.44	0.38	170.64	0.40	250.08	0.40	269.28
Zeolite 13X	0.23	64.56	0.26	73.68	0.26	76.80	0.28	84.72	0.28	88.08	0.29	91.20
SIM 3a	0.61	22.06	1.19	93.25	1.46	118.45	1.46	134.58	1.46	145.68	1.48	153.69
SIM 3b	0.02	2.40	0.02	4.32	0.06	5.76	0.16	24.00	0.41	62.16	0.68	68.64
SIM 3c	0.04	1.28	0.19	32.53	0.49	72.08	1.01	221.14	1.52	282.36	1.52	299.36
SIM 3d	0.02	3.41	0.52	90.75	0.79	124.89	1.34	207.33	1.73	240.94	1.73	246.32
SIM 3e	0.29	26.56	0.56	49.68	0.89	82.36	1.56	129.28	1.94	186.25	1.94	190.08
SIM 2a	0.05	22.08	0.17	45.12	0.22	57.12	0.29	64.08	0.57	159.60	0.60	176.40
SIM 4a	0.05	17.52	0.15	36.72	0.29	59.76	0.33	83.28	0.42	106.80	0.49	125.04
SIM 8a	0.10	15.60	0.16	21.36	0.22	42.48	0.46	84.96	0.60	102.96	0.60	110.16

As expected from the sorption isotherms, SIM-3a and SIM-3e performed best using either method with SIM-3e having a slight advantage when t_{emc} was taken into consideration due to its lower response time. The raw vermiculite and SIM-3b (vermiculite – $MgSO_4$) had improved performances when calculated for ξ_B, also due to their more rapid t_{emc} response, however all the other materials, having high t_{emc} time showed reduced ξ_B values with a significant difference observed for SIM-3c ($Ca(NO_3)_2$) and SIM-3d ($LiNO_3$) which had very promising isotherms but also very long t_{emc} across all RH_{ie} steps.

The most important material property in terms of THS is the energy storage density, E_d (kJ/kg). Differential scanning calorimetry (DSC) was used to determine E_d using a modified experimental method based on BS EN ISO 11357-4 (BSi, 2005). A TA Instruments Q10 differential scanning calorimeter was used to first determine the specific heat capacity, c_p (J/kg.K) of the SIM’s. For each test a baseline was taken using two empty aluminium pans within the temperature range $10 < T < 150$ °C, at a ramp rate of 5 °C/min with the samples held isothermal at the lower and upper temperatures for $t = 10$ min.

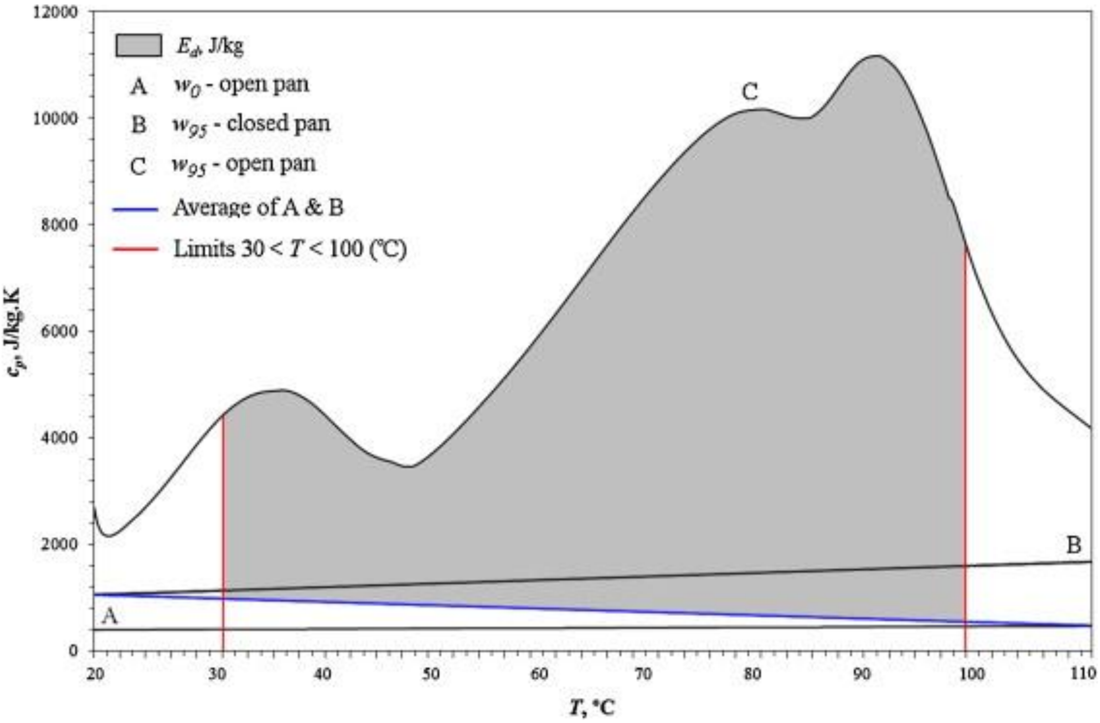

Figure 4.2.12 Methodology for determination of Ed (at $30 > T < 100$ ºC) for the SIM samples

The procedure was repeated using certified sapphire as the calibration standard. Finally the saturated SIM materials were tested in an open pan allowing moisture to desorb from the material, to determine the desorption energy. Each SIM was tested 4 times with the mean values of c_p calculated.

In principle, E_d can be calculated by integration of the area under the desorption c_p curve alone, however this does not allow for the sensible heat of the SIM in both its dry and wet states (Aristov et al., 2000b). Figure 4.2.12 outlines the methodology used to determine E_d by using the average sensible heat c_p value of the material over the selected temperature range. It is important to note that this method of determining E_d should be for comparison of materials only as it is based on the endothermic desorption reaction of the SIM equilibrated at a specific moisture level, w (kg/kg). Samples $m_{dry} \approx 25$ mg were prepared by vacuum desiccation for a period t = 24 h prior to achieve $w = w_0$ before testing in the dry state. For the wet state tests (open and closed pan) the SIM's were allowed to equilibrate in a sealed chamber at T = 23 °C and RH_{ie} = 95% for a period t = 24 h to achieve the condition $w = w_{95}$. The E_d for all SIM materials is presented in Figure 4.2.13 with the mean values highlighted. SIM-3b displayed the largest E_d of all the SIM's at 407 kJ/kg with SIM-2a performing the worst at only 123 kJ/kg. SIM-3a and SIM-3e have Ed of 364 kJ/kg and 269 kJ/kg respectively. Whilst these were not as high as SIM-3b, the sorption isotherm data discussed previously shows that SIM-3b had very limited adsorption potential and therefore is not necessarily the prime candidate. Further experimental analysis of SIM-3b will be necessary to potentially maximise adsorption which should enable access to its higher E_d.

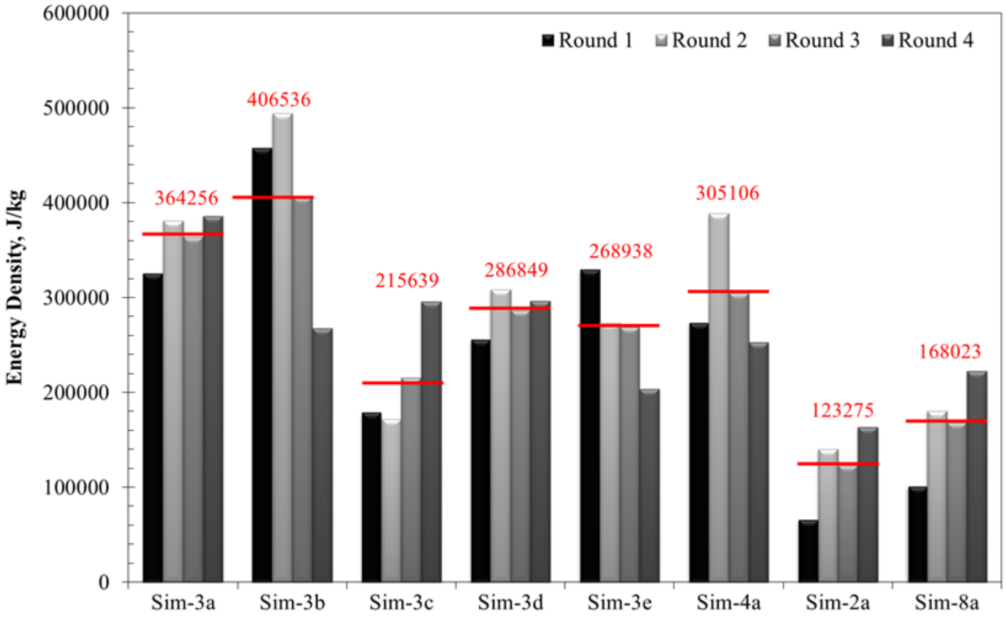

Figure 4.2.13 Energy density, E_d of the SIM samples with average values highlighted

Thermo gravimetric analysis was carried out on the SIM samples using a TA Instruments SDT Q600 V8.3 analyser in accordance with BS EN ISO 11358 (BSi, 1997). As in the DSC tests, all SIM's were allowed to equilibrate in a sealed chamber at T = 23 °C and RH_{ie} = 95% for a period t = 24 h to achieve the condition $w = w_{95}$ prior to testing. Testing was carried out using Nitrogen as the inert gas (100 ml/min) within the range 30 < T < 140 °C at a ramp rate of 5 °C/min. Mass loss, Δm was calculated as:

$$\Delta m = \frac{m_{95} - m_f}{m_{95}} \times 100\ (\%) \tag{4.1}$$

SIM-3d showed the greatest mass loss (40%) within the selected temperature range followed by SIM-3a and SIM-3e at 37% and 36% respectively (see: Figure 4.2.14). In general the results align with the sorption isotherm results on EMC's with the non-vermiculite based SIM's having less adsorbed moisture to desorb under the temperature scan. SIM-3a and SIM-3e again display good potential for their use in open THS with large mass loss within the operational temperature range.

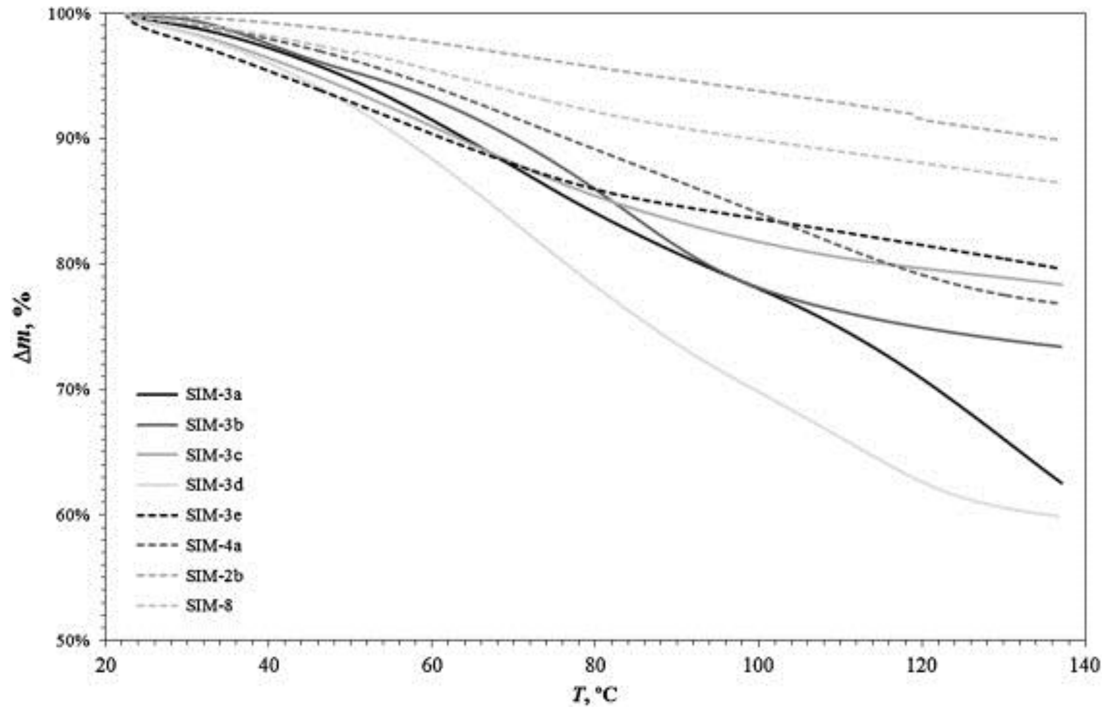

Figure 4.2.14 Thermo gravimetric plots of regeneration for the selected SIM samples

Dry state thermal conductivity, λ (W/m.K) testing of the SIM materials was carried out in accordance with BS EN ISO 22007-2 (BSi, 2012) using a Setaram TCi modified transient plane source (MTPS) device. The device applies a known, momentary current to a sensor's heating element resulting in a constant heat source at the sample/ sensor interface of $\Delta T \leq 2$ °C generating a dynamic temperature field within the sample. This induces a change in the voltage drop of the sensor element which corresponds to λ. Powder samples, $m \approx 2$ g were prepared by oven heating at $T = 110$ °C for $t = 24$ h and then allowed to cool to room temperature in a desiccator for $t = 1$ h prior to testing. There were no significant changes to λ values of the SIM samples compared to the raw materials matrices (see: Table 4.4).

Table 4.4 Combined pore characteristics and basic hygrothermal properties of all materials

Material	ρ_{bulk} g/cm^3	ρ_{solid} g/cm^3	V_{macro} cm^3/g	V_{meso} cm^3/g	$\varnothing_{pore}$ ---	SSA m^2/g	n %	E_d kJ/kg	λ W/m·K	ξ_A kg/kg	ξ_B kg/kg
Vermiculite	0.216	1.937	4.110	0.017	3.68µm	15.1	88.9	---	0.0527	0.00468	0.00048
Activated Carbon	0.423	2.275	2.365	0.395	1.98nm	678.0	81.4	---	0.0790	0.00215	0.00431
Silica Gel	0.763	2.184	1.310	0.381	2.45nm	785.0	65.0	---	0.0569	0.00177	0.00459
Zeolite 13X	0.655	2.244	1.527	0.292	1.21nm	468.0	70.8	---	0.0737	0.00329	0.00213
SIM 3a	0.492	1.844	1.491	0.003	1.25µm	10.9	73.3	364.3	0.0669	0.00955	0.01438
SIM 3b	0.340	1.122	2.054	0.022	3.68µm	3.6	69.7	406.5	0.0607	0.00653	0.00370
SIM 3c	0.529	1.627	1.274	0.001	2.58µm	2.4	67.5	215.6	0.0601	0.00501	0.01599
SIM 3d	0.625	1.989	1.109	0.002	1.92µm	2.4	68.6	286.9	0.0659	0.00693	0.01895
SIM 3e	0.620	2.261	1.172	0.009	2.46µm	1.9	72.6	268.9	0.0691	0.01079	0.02022
SIM 4a	0.498	2.059	2.007	0.066	43.1nm	121.0	75.8	305.1	0.0960	0.00364	0.00526
SIM 2a	0.962	2.134	1.039	0.151	9.09nm	224.0	54.9	123.3	0.0828	0.00410	0.00454
SIM 8a	0.671	2.145	1.489	0.153	42.8nm	233.0	68.7	168.1	0.0961	0.00554	0.00604

4.3 Salt impregnated desiccant matrices for ‘open’ thermochemical energy storage – Hygrothermal cyclic behaviour and energetic analysis by physical experimentation

Thermochemical heat storage (THS) systems utilise one of two approaches; ‘closed’ or ‘open’ systems. ‘Closed’ systems are, in general, capable of providing much greater reaction efficiencies when compared to ‘open’ systems due to the lower reaction chamber pressures (sometimes vacuum) allowing increased vapour diffusion of the sorbate (gas) to the sorbent (SIM) (Abedin and Rosen, 2012). ‘Open’ systems work under standard atmospheric pressures, negating the need for complex pressure systems however, there is much lower reaction efficiency due to a decreasing trend in diffusion causing instability during heat generation (Wu et al., 2009).

Figure 4.3.1 shows the basic operating principle of an ‘open’ adsorption heat storage system with the flow numbers used in the later numerical analysis. During the discharging process, cold air is blown into the system with a mechanical fan. If required (*i.e.* in the case where inlet relative humidity, RH_i is low), moisture is added via a humidification unit. The cold and humid air (1) enters the reactor. The moisture is absorbed and heat generated due to the exothermic nature of the reaction. This releases hot and dry outlet air (2) which can be used for either space heating or water heating applications. In the reverse, during the charging process, hot and dry air (3) is heated before entering reactor. The absorbed moisture in the material is desorbed releasing cooler, humid air. Whilst there are advantages and disadvantages evident for both systems, the ‘open’ type system was adopted for this research due their simpler process design (*i.e.* no heat exchangers or pressure vessels) which in turn should allow for more straight forward operational conditions.

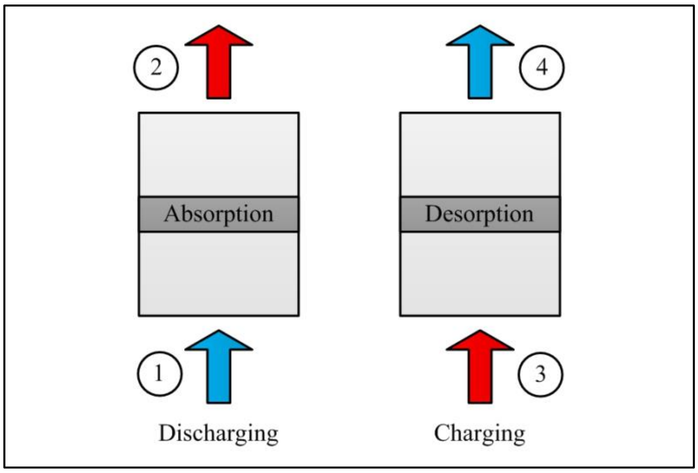

Figure 4.3.1 Basic principle of 'open' sorption heat storage

In previous section, the pore geometry and hygrothermal properties of eight SIM materials and four host matrices were analysed to provide the specific properties based solely on material characterisation. Whilst characterisation is vital in providing insight into SIM behaviour, it is also necessary to analyse a materials performance under controlled, larger scale experimental tests.

The aim of this section is to perform hygrothermal cyclic behaviour tests using physical experimentation to investigate the material behaviour of selected SIM samples, to analyse these results, carry out energy and exergy analysis.

4.3.1 Physical experimental setup

A series of experimental investigations using scaled physical models (i.e. laboratory representations of 'ideal' conditions) were undertaken to fulfil Stage 2 of the research aim. A custom rig was designed and constructed (see: Figure 4.3.2) to allow independent control of regeneration temperatures in the range 70 °C < T_r < 120 °C (± 5 °C) using a AHF Series 2 kW inline duct heater (1) and input relative humidity in the range 30% < RH_{in} < 95% (± 5%) using either a custom designed passive humidification wick chamber or a 3.78 L ultrasonic humidifier (2) from HoMedics, USA, dependant on the required RH_{in}.

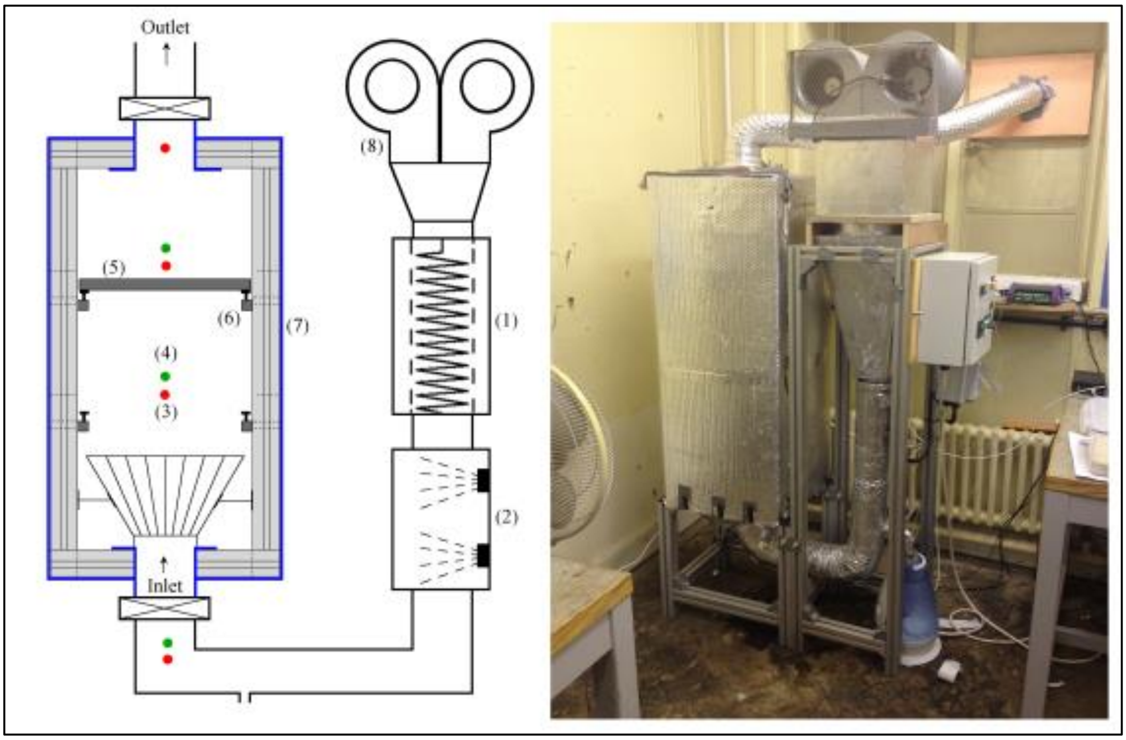

Figure 4.3.2 Schematic illlustration (left) and view (right) of the custom designed cyclic DVS test rig

Temperature was recorded using T-type thermocouples (3) connected to a Datataker DT85 data-logger with the DT-USB PC user interface software from Thermo Fisher Scientific, UK. *RH* was recorded using the EK-H4 Eval Kit for Humidity Sensors (4) from Sensiron, AG, Switzerland. Mass change, Δm of the material in the test tray (5) was monitored using the S220 - (2.7kg) single point low profile load cells (6) from Strain Measurement Devices, UK. Data output from the load cells was logged using the Datataker DT85. The test rig was internally and externally insulated and hermetically sealed (7) using 60mm Thermafloor TF70 rigid thermoset insulation (internal) from Kingspan, UK with a nominal U-value of 0.22 W/m^2 K with an aluminium foil wrap applied externally (see: Figure 4.3.2). Airflow was provided by two double inlet centrifugal blowers (8) supplied by Ebm-papst, UK operating from a variable DC power unit. The test rig was designed to provide data on the hygrothermal cyclic analysis of the characterised SIM materials, primarily:

- Temperatures – Ambient ($T_{ambient}$), Input (T_{in}), Output (T_{out}) & Regeneration (T_r)
- Relative Humidity's - Ambient ($RH_{ambient}$), Input (RH_{in}) & Output (RH_{out})
- Mass – Change in mass during adsorption / desorption (Δm)

SIM samples (≈ 1.5 l) were prepared by oven drying at $T \approx 150$ °C for a period, t >24 h to achieve the condition $m_{dry} = 0$ kg/kg. The dry SIM was then placed in a mesh tray and allowed to cool in a desiccator for $t = 2$ h prior to testing. When cooled the tray was placed onto on the load cells and the rig sealed. For the discharging cycle (adsorption), the humidifier was connected and the psychrometric state of the airflow monitored. When the desired humidity level was reached, the inlet valve was opened. In general, the discharging cycle was deemed to be complete when either of the following the conditions were achieved, depending on the experiment type;

$RH_{in} = RH_{out}$ or $\Delta m \leq 2\%$ or $T_{out} = T_{in}$ or $T_{out} = T_a$

For the charging cycle (desorption) the humidifier was disconnected and the heating unit activated and set to the desired regeneration temperature. As in the discharge cycle, the charging cycle was deemed to be complete when;

$RH_{out} = RH_{in}$ or $\Delta m \leq 2\%$ or $T_{in} = T_{out}$

Using the custom built rig, the cyclic behaviour of all twelve materials (SIM and raw) highlighted previously (see: Table 4.2) was analysed. Testing was performed across two stages:

1. To allow direct comparison of all twelve materials, a first pass set of experiments was undertaken using 1.5 l samples with four charging / discharging cycles.

2. To investigate any materials highlighted from Pass 1, a second pass was undertaken using the same material quantities.

The equations used for energetic analysis of the charging, discharging and overall performance of system are presented in Tables 4.5 – 4.7.

Table 4.5 Equations for analysis of the discharging process

Definition	Unit	Equation	Equation No.
Instantaneous heat gain	kW	$\dot{Q}_g = \dot{m}_d \times (\dot{h}_{o,d} - \dot{h}_{i,d})$	(4.2a)
		$\dot{Q}_g = \dot{m}_d \times c_p \times \left(T_{o,d} - T_{i,d}\right)$	(4.2b)
Cumulative thermal energy generation	kWh	$E_{cum} = \dot{m}_d \times c_p \times \int_0^{t_d} \left(T_{o,d} - T_{i,d}\right) dt$	(4.3)
Energy density	Wh/g	$E_{d,m} = \frac{E_{cum}}{\Delta m_d}$	(4.4a)
	kWh/m^3	$E_{d,v} = \frac{E_{cum}}{V_{ads}}$	(4.4b)
Vapour partial pressure of air	mbar	$p_w = \frac{RH \times p_{w,s}}{100\%}$	(4.5)
Air absolute humidity	g/kg$_{air}$	$w = 216.7 \times \left[\frac{\frac{RH}{100\%} \times 6.112 \times exp\left(\frac{17.62 \times T}{243.12 + T}\right)}{273.15 + T}\right]$	(4.6)
Adsorption rate	g/min	$z_{ads} = 60 \times \int_{t_{x,dr}}^{t_{x+1,dr}} \dot{m}_d \times (w_i - w_o) dt$	(4.7)
Mass increase	g	$\Delta m_d = M_{wv} = M_w - M_d$	(4.8a)
		$\Delta m_d = \int_0^{t_d} \dot{m}_d \times (w_i - w_o) dt$	(4.8b)
Mass uptake ratio	---	$f_d = \frac{M_{ads,x} - M_{ads,d}}{M_{ads,d}}$	(4.9a)

		$f_d = \left[\int_0^{t_d} \dot{m}_d \times (w_i - w_o)dt\right] \Big/ m_{ads,d}$	(4.9b)
Exergy gain	kW	$\dot{Ex}_g = (\dot{Ex}_{o,d} - \dot{Ex}_{i,d})$ $\dot{Ex}_g = \dot{m}_d \times [(h_{o,d} - h_{i,d}) - T_a \times (s_{o,d} - s_{i,d})]$ $\dot{Ex}_g = \dot{m}_d \times c_p \times [(T_{o,d} - T_{i,d}) - T_a \times \ln\left(\frac{T_{o,d}}{T_{i,d}}\right)]$	(4.10a) (4.10b) (4.10c)
Cumulative exergy gain		$\dot{Ex}_{g,cum} = \dot{m}_d \times c_p \times \int_0^{t_d} \left[(T_{o,d} - T_{i,d}) - T_a \times \ln\left(\frac{T_{o,d}}{T_{i,d}}\right)\right]$	(4.11)
COP	---	$COP_{dr} = \frac{\dot{Q}_{g,avg}}{\dot{W}_f + \dot{W}_{hum}}$	(4.12)

Table 4.6 Equations for analysis of the charging process

Definition	**Unit**	**Equation**	**Equation No.**
Instantaneous heat transfer to absorbent	kW	$\dot{Q}_{tr} = \dot{m}_c \times (\dot{h}_{i,c} - \dot{h}_{o,c})$ $\dot{Q}_{tr} = \dot{m}_c \times c_p \times (T_{i,c} - T_{o,c})$	(4.13a) (4.13b)
Cumulative energy transfer to absorbent	kWh	$E_{cum,c} = \dot{m}_c \times c_p \times \int_0^{t_c} (T_{i,c} - T_{o,c})dt$	(4.14)
Desorption specific heat transfer	Wh/g	$E_{tr,s} = \frac{E_{cum,c}}{\Delta m_c}$	(4.15)
Desorption rate	g/min	$z_{des} = 60 \times \int_{t_{x,cr}}^{t_{x+1,cr}} \dot{m}_c \times (w_o - w_i)dt$	(4.16)
Mass loss	g	$\Delta m_c = M_{wv} = M_w - M_d$ $\Delta m_c = \int_0^{t_c} \dot{m}_c \times (w_o - w_i)dt$	(4.17a) (4.17b)

Mass loss ratio	---	$f_c = \frac{M_{ads,w} - M_{ads,x}}{M_{ads,w}}$ $f_c = \left[\int_0^{t_c} \dot{m}_c \times (w_o - w_i)dt\right] \Big/ m_{ads,w}$	(4.18a) (4.18b
Exergy transfer to absorbent	kW	$\dot{E}x_{tr} = (\dot{E}x_{i,c} - \dot{E}x_{o,c})$ $\dot{E}x_{tr} = \dot{m}_c \times [(h_{i,c} - h_{o,c}) - T_a \times (s_{i,c} - s_{o,c})]$ $\dot{E}x_{tr} = \dot{m}_c \times c_p \times [(T_{i,c} - T_{o,c}) - T_a \times \ln\left(\frac{T_{i,c}}{T_{o,c}}\right)]$	(4.19a) (4.19b) (4.19c)
Cumulative exergy transfer to adsorbent	kWh	$\dot{E}x_{tr,cum} = \dot{m}_c \times c_p \times \int_0^{t_c} \left[(T_{i,c} - T_{o,c}) - T_a \times \ln\left(\frac{T_{i,c}}{T_{o,c}}\right)\right]$	(4.20)
Charging efficiency	%	$\eta_{cr} = \frac{\dot{Q}_{tr}}{\dot{W}_f + \dot{Q}_h}$	(4.21)

Table 4.7 Equations for analysis of system efficiencies

Definition	Unit	Equation	Equation No.
1st law efficiency	---	$\eta_{I,rxn} = \frac{\dot{Q}_{g,ave}}{\dot{Q}_{tr,ave}}$	(4.22)
2nd law efficiency	---	$\eta_{II,rxn} = \frac{\dot{E}x_{g,ave}}{\dot{E}x_{tr,ave}}$	(4.23)

4.3.2 Uncertainty analysis

Uncertainty analysis is necessary to prove the accuracy of the experimental results. In the present work Gauss propagation law was applied to determine the experimental uncertainties. The result w_R is calculated as a function of the independent variables x_1, x_2, x_3, …, x_n and w_1, w_2, w_3, …, w_n represents the uncertainties in the independent variables.

In the developed experimental rig, 3 sensor locations were used for determining the *T* and *RH* of the ambient, humidifier / EH outlet and reactor outlet. Air MFR (m_a) was also recorded in both charging and dicharging cycles. Then, uncertainty w_R is expressed as (Ozgen et al., 2009, Buker et al., 2014):

$$w_R = \left[\left(\frac{\partial R}{\partial x_1} w_1\right)^2 + \left(\frac{\partial R}{\partial x_2} w_2\right)^2 + \left(\frac{\partial R}{\partial x_3} w_3\right)^2 + \cdots + \left(\frac{\partial R}{\partial x_4} w_4\right)^2\right]^{1/2} \tag{4.24}$$

Experiments were conducted by using following instruments: Thermocouples with the maximum deviation of ±0.3°C for temperature and ±2% for relative humidity and air mass flow meter with the accuracy of ±2%.

It is obtained from the equations (4.2b), (4.10b) and (4.17) that the heat storage efficiency (η_I) is the function of *T* and m_a measured in charging and discharging cycles, each subject to uncertainty:

$$\eta_I = f\left(T_{i,c}, T_{o,c}, T_{i,d}, T_{o,d}, m_{a,c}, m_{a,d}\right) \tag{4.25}$$

Total uncertainty for overall system efficiency can be expressed as;

$$w_R = \left[\left(\frac{\partial \eta_I}{\partial T_{i,c}} w_{T_{i,c}}\right)^2 + \left(\frac{\partial \eta_I}{\partial T_{o,c}} w_{T_{o,c}}\right)^2 + \left(\frac{\partial \eta_I}{\partial T_{i,d}} w_{T_{i,d}}\right)^2 + \left(\frac{\partial \eta_I}{\partial T_{o,d}} w_{T_{o,d}}\right)^2 + \left(\frac{\partial \eta_I}{\partial m_{a,c}} w_{m_{a,c}}\right)^2 + \left(\frac{\partial \eta_I}{\partial m_{a,d}} w_{m_{a,d}}\right)^2\right]^{1/2} \tag{4.26}$$

Total uncertainty rate affecting the heat storage efficiency of the proposed system was computed by using Equations (4.24)-(4.26). The estimation implies that total uncertainty in calculation of the η_I is found to be 2.61%.

4.3.3 Experimental results

The results from Stage 1 are shown in Figures 4.3.3 – 4.3.5. To show the full experimental output, Figure 4.3.3 shows a full data set for SIM-3a (Vermiculite - $CaCl_2$) with plot lines for ambient, input and output temperature (T_a, T_{in} & T_{out}) and input and output relative humidity (RH_{in}, RH_{out}). The results for the remaining materials are restricted to show only output temperatures and omit results for relative humidity, input and ambient temperature in an effort to provide clarity to the comparison of material performance. It can be seen in Figure 4.3.3 that there are four clear cycles, first discharging then charging.

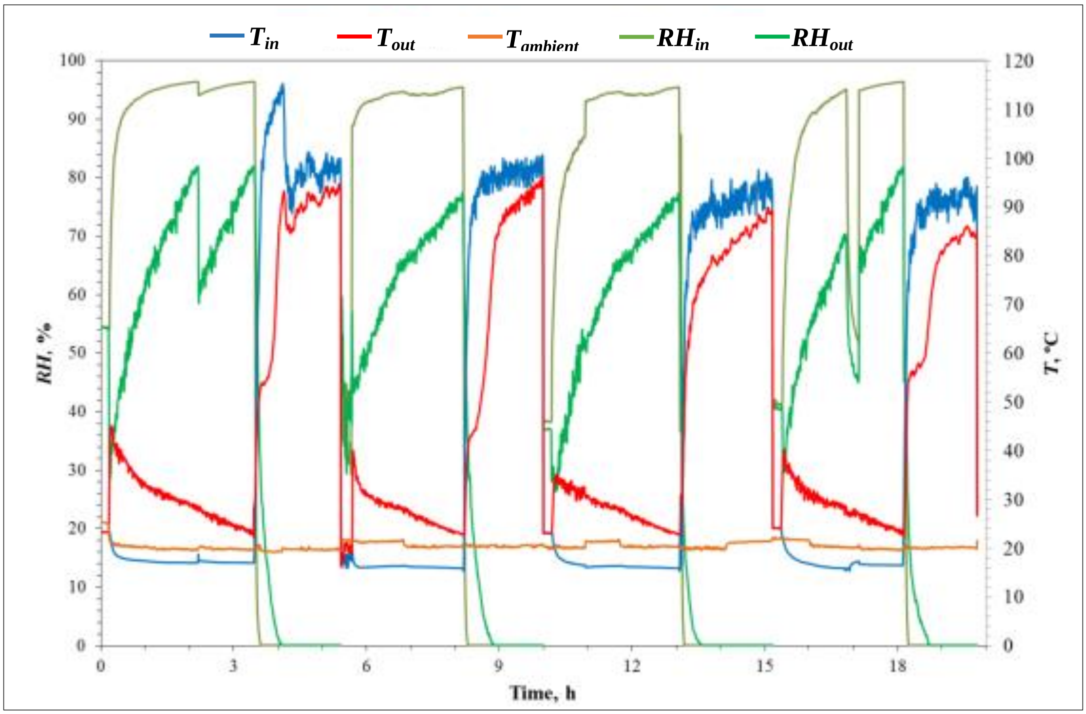

Figure 4.3.3 Full data set for SIM-3a (Vermiculite with $CaCl_2$)

Open THS is based on the temperature lifting of air due to the moisture absorption which results in a sharp temperature lifting of output air at the beginning of the reaction. As time passes, the moisture content inside the reactor increases and moisture sorption rate of THS material (*i.e.* sorption kinetics) slows down which causes drop in temperature. There is also a corresponding drop of inlet temperature due to the addiction of moisture to the air stream. It is the difference between inlet and outlet psychrometric conditions (*i.e.* pressure, temperature, humidity) that governs THS performance. As the *RH* level (RH_{in}) increases in the chamber there is an immediate increase in T_{out} due to the reaction of the moisture vapour and the SIM. RH_{in} rapidly rises to its peak level, however due to the absorption of moisture in the SIM with a corresponding removal of moisture from the air stream after the material, there is a time lag for RH_{out} to reach the same level. For thermal analysis, two measures are used here:

1. Maximum output temperature ($T_{out,\ max}$), which is the peak temperature reached in a single cycle
2. Dwell time (t_{dwell}), time from initial temperature rise until $T_{out} = T_{ambient}$

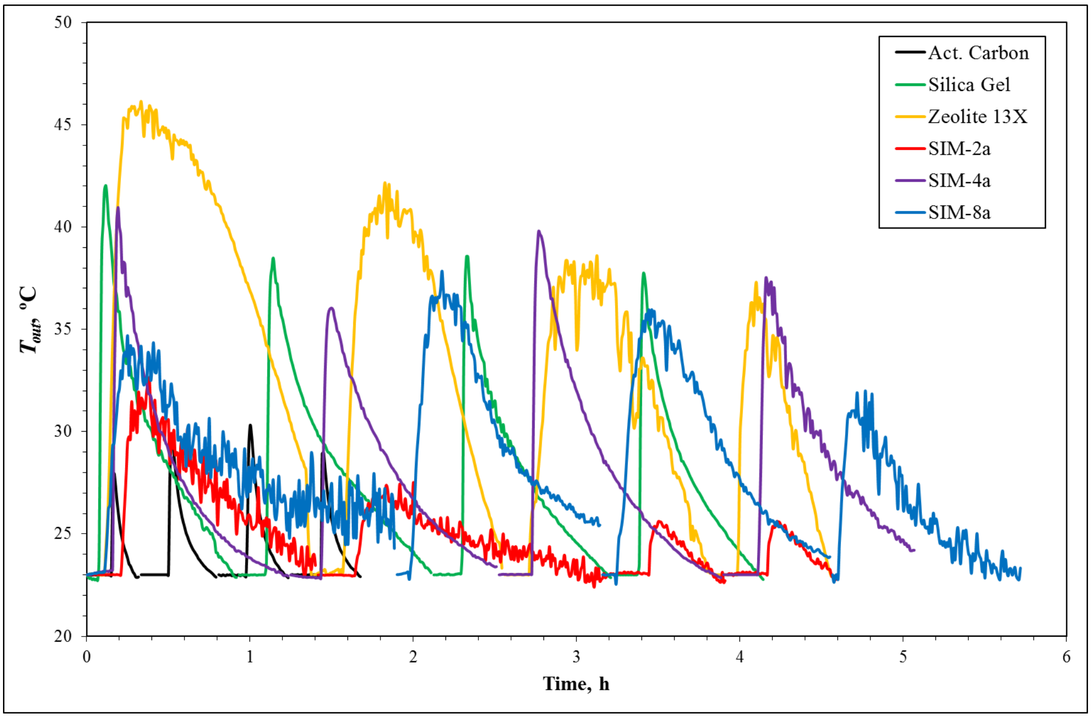

Figure 4.3.4 Full cycle T_{out} results for the non-vermiculite based materials

For SIM-3a a $T_{out,\ max}$ = 40 °C on the first cycle was observed, which reduced on the following cycles down to ≈ 30 °C. The dwell time appear to be similar (t_{dwell} = 3 h) across all four cycles.

This suggests that there is some hysteresis occurring (*i.e.* reduction in mass uptake, Δm) between cycles possibly due to the regeneration temperatures ($T_r \approx 90$ °C) being insufficient to completely remove all absorbed moisture.

The analysis of the remaining materials is subdivided into those based on a vermiculite matrix and those based on non-vermiculite matrices. In the first cycle for the non-vermiculite materials the synthetic Zeolite (13X) has the largest initial peak ($T_{out,\ max}$ = 46 ºC). Whilst the Zeolite has a lower overall sorption capacity in terms of EMC when compared to the other materials, it has a very rapid response to moisture vapour (t_{emc}) due to its high specific surface area (SSA). Thermal energy generation within the raw Zeolite, activated carbon and silica gel is based solely on the heat of sorption reactions as there is no salt present to allow thermochemical reactions. The silica gel (SC) and activated carbon (AC) had $T_{out,\ max}$ peaks of 42 °C and 28 °C respectively (see: Figure 4.3.4). The Zeolite also had a much greater dwell time, t_{dwell} achieving the condition $T_{out} = T_{ambient}$ after 1.5 h compared to the silica gel (t_{dwell} = 0.8 h) and carbon (t_{dwell} = 0.4 h).

After synthesis SIM-2a (AC-$CaCl_2$) has a higher $T_{out,\ max}$ compared to its raw state (28 °C → 33 °C). It also has a significantly longer t_{dwell} which suggests that the impregnated salt is providing additional thermochemical reactions over and above the raw AC sorption reactions. In terms of $T_{out,\ max}$ there does not appear to be any significant difference in the performance of SIM-4a (SG-$CaCl_2$) when compared to the raw silica gel. The dwell times for the impregnated SG is increased slightly (1h → 1.5h) suggesting that there is only a marginal benefit gained from addition of the salt. SIM-8a (Z - $CaCl_2$) performs somewhat worse than the raw Zeolite host in terms of $T_{out,\ max}$ with a reduction of ≈ 12 °C. As discussed previously, there was evident damage to the Zeolite after synthesis and thus the initial sorption performance may have been lost. The impregnated $CaCl_2$ is still providing some thermo-chemical output, however as there is theoretically no constraint of the salt, deliquescence may occur leading to reduced cyclic performance. As for SIM-3a previously, there is large hysteresis observed for all the non-vermiculite based samples with reductions of $T_{out,\ max}$ from cycle 1 through 4 and is particularly large for the raw Zeolite.

The results from the experiments using the vermiculite (V) based materials can be seen in Figure 4.3.5. It can be clearly seen that, in terms of $T_{out,\ max}$ and SIM-3a and SIM-3e (V-LiBr) perform markedly better than all other SIM's with $T_{out,\ max}$ levels of ≈ 45 °C. SIM-3e had a dwell time of 2.3 h whilst SIM-3a performed well with a t_{dwell} = 3.3 h. It can be seen that SIM-3a has a t_{dwell} of almost two orders of magnitude higher than it's the raw vermiculite alone.

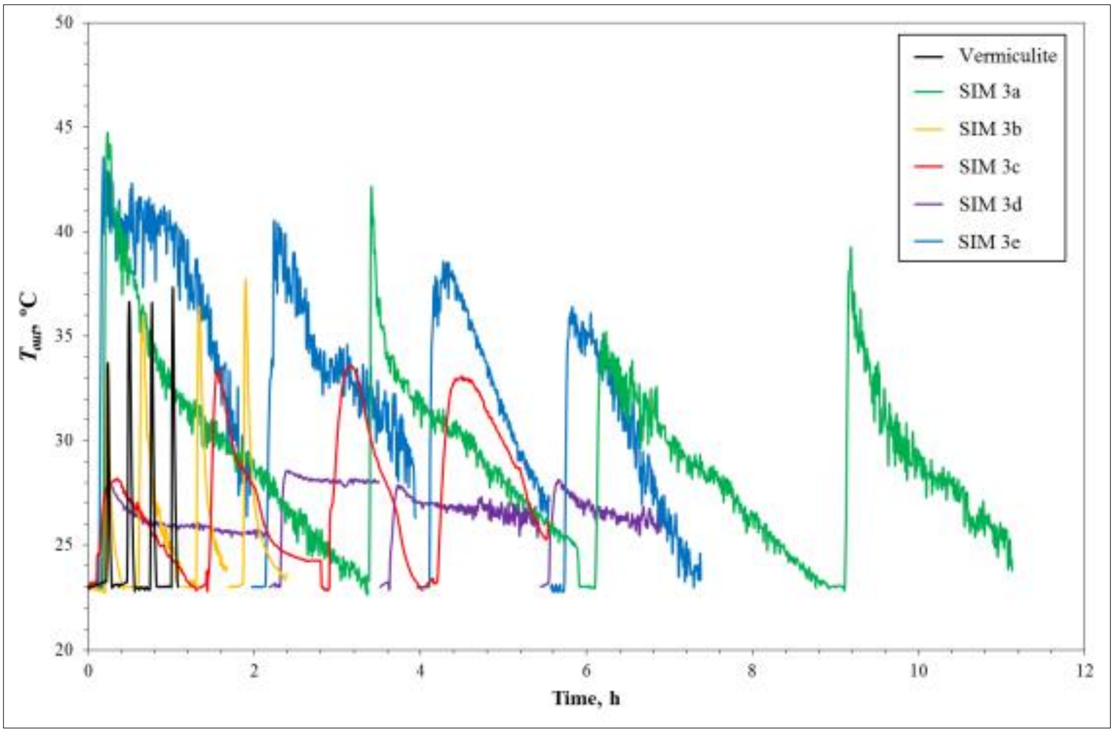

Figure 4.3.5 Full cycle T_{out} results for the non-vermiculite based materials

As expected from the characterisation, the raw vermiculite has poor performance due to its macroporous pore structure where there is minimal SSA for heat of sorption reactions. SIM-3a also has an initial $T_{out,\ max}$ that is comparative to that of the raw Zeolite in the previous results set, however its t_{dwell} is much greater.

SIM-3b (V-$MgSO_4$) appears to underperform based on its potential from the characterisation results. The material had an E_d comparable to that of SIM-3a (see: Section 4.2), however its performance is only slightly greater than the raw vermiculite in terms of both $T_{out,\ max}$ and t_{dwell}. It also had a very similar isotherm to that of SIM-3e suggesting a similar moisture capacity. Based on these two measures alone, SIM-3b would have been expected to perform somewhat similar to SIM-3a and SIM-3e. As discussed earlier however, analysis of the EMC alone without accounting for the DVS kinetics is vital for any potential open THS material. Looking at this measure, it can be seen that SIM-3b has a much lower moisture storage function for both the ξ_A and ξ_B measures when compared to SIM-3a and SIM-3b, which suggests that although it has a comparative EMC across the RH range, that potential is effectively inaccessible due to its poor t_{emc} response.

Similarly to the non-vermiculite materials, the vermiculite set showed a general reduction in performance across the four cycles with apparent hysteresis. SIM-3a shows a slight decrease for $T_{out,\ max}$ from 45 °C to ≈ 37 °C over the four cycles, however t_{dwell} does not seem to decrease and remains at ≈ 2.5 → 3 h. The raw vermiculite and SIM-3b are, as expected, the poorest performers with both decreasing $T_{out,\ max}$ and t_{dwell}. SIM-3e follows the same pattern as SIM-3a with slight decrease in $T_{out,\ max}$ but little change to t_{dwell}. SIM-3d (V-$LiNO_3$) is of interest as it performed well across all four cycles albeit with a $T_{out,\ max}$ much lower than SIM-3a and SIM-3e (≈ 12 °C) which, on its own would be too low to suit a THS system. SIM-

3d however appears to have a near horizontal slope from $T_{out,\ max}$ to $T_{ambient}$ with the experiment stopped only due to time limitations. This suggests that t_{dwell} for SIM-3d may far exceed those of the other synthesised materials and possible combinations of SIM-3d with either SIM-3a or SIM-3e may prove beneficial in future research.

4.3.3.1 Energetic analysis

For the energetic analysis two materials that have been used in other studies *i.e.* raw Zeolite 13X (Z) and silica gel (SG) were chosen from the experimental work and compared against the best performer from this research *i.e.* SIM-3a (V-$CaCl_2$). Using the test results the cyclic, hygroscopic and thermal (energetic & exergetic) performance of these materials was analysed and compared. In the selection of an adsorbent suitable for thermochemical heat storage, many factors come into question such as its cyclic ability, output temperature, average thermal power, total energy generation, mass uptake, regeneration temperature, energetic and exergetic efficiency among others.

Zeolite and SG have been shown to be promising desiccants for THS, however the high regeneration temperatures required remain as the main obstacles for implementation of these materials (≈180 → 220˚C). The experimental analysis suggests that SIM-3a has the best performance among all the tested composite adsorbents in terms of $T_{out,\ max}$ and t_{dwell} and has potential to compete with conventional desiccants. SIM-3a is a non-toxic material, has a low regeneration temperature which allows utilization of solar energy (80 → 100 ˚C), is low cost (≈0.48 $/kg) and also appears to have good cyclic ability (*i.e.* minimal hysteresis).

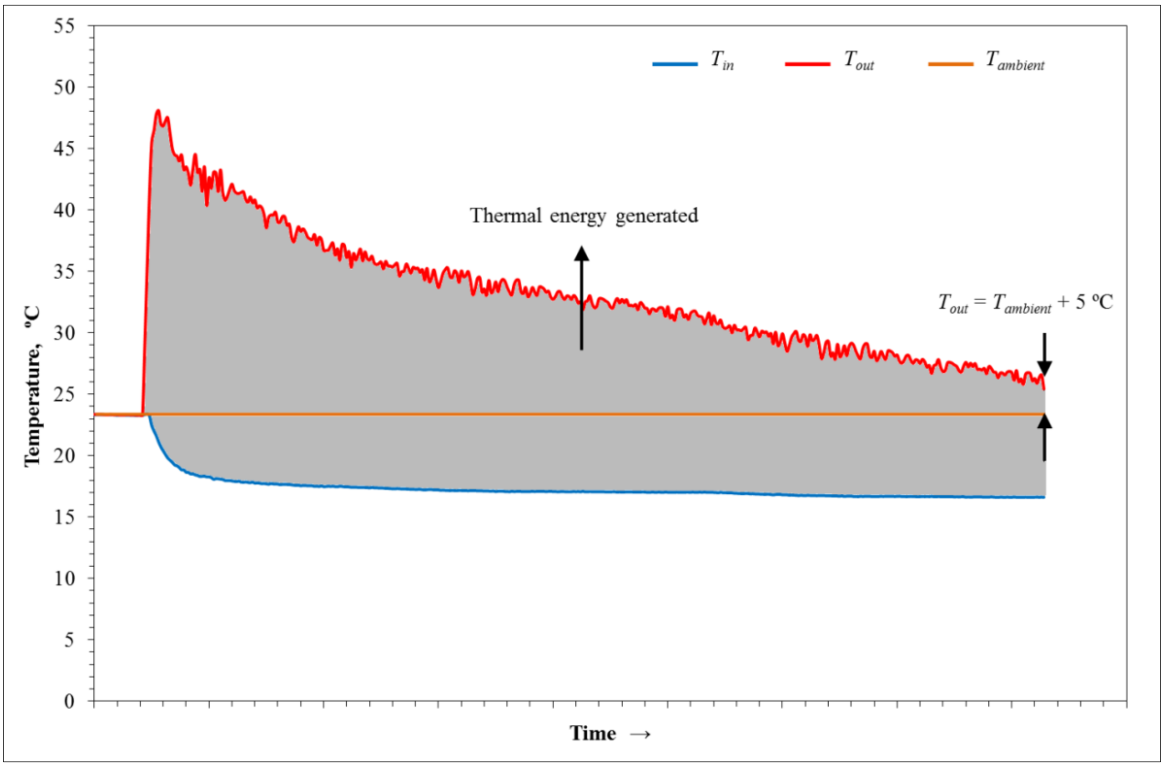

Figure 4.3.6 Discharging characteristics for open THS systems

A descriptive diagram showing the discharging characteristics of an open THS system is shown in Figure 4.3.6. For the energetic analysis, in cases where the ambient experimental temperature was higher than the inlet temperature, $T_{outlet} = T_{ambient} + 5$ °C was taken as the stop reference for the discharging period. The same volume of material was used in all tests (0.135 m^3, 1.5 l) with a corresponding initial dry mass of SIM-3a, Zeolite and silica gel recorded as 531 g, 1113 g and 943 g respectively. As stated previously, it is the difference between inlet and outlet psychrometric conditions (*i.e.* pressure, temperature, humidity) that governs THS performance, with integration of the area between the $T_{in} \rightarrow T_{out}$ curves being equal to the materials experimental energy density, E_d. During the experiments the mass flow rate of air for charging, m_{cr} and discharging, m_{dr} were set at 0.005 kg/s whilst the fan power consumption was measured as 5 W.

4.3.3.2 Heat and mass transfer

In the THS process material selection the cyclic stability is always one of the most important parameters to consider. As discussed previously, some materials show excellent performance in first cycle however, their performance reduces dramatically in following cycles due to either large hysteresis or a higher regeneration temperature, T_r requirement. In Figures 4.3.7 and 4.3.8 the thermal and hygroscopic cyclic behaviour of the tested materials is shown. Using Equations (4.5a) and (4.5b) the instantaneous heat gain (output), Q_g during the discharge and charging cycles was calculated.

Zeolite has the highest heat output in all discharging cycles at Q_g = 105 W for cycle 1, however its performance decreases to 84 W at the end of cycle 4. SIM-3a provides a relatively lower average heat output at Q_g = 64.5 W, whilst its peak at 133 W (see: Table 4.8) was achieved in cycle 1. Silica gel also has a steady cyclic performance however the Q_g is relatively low varying between 44 W and 40 W, the lowest among all the tested materials. During the charging cycles (*i.e.* regeneration), the inlet temperature was set at T_i = 100 °C and the mass flow rate of air kept constant (m_a = 0.005 kg/s). However as can be seen from Figure 4.3.7, the Zeolite absorbed the highest amount of heat (115 W) followed by SIM-3a (102 W) and silica gel (69 W). This result emphasizes the effect of the specific heat, *Cp* (*i.e.* the amount of heat required to increase 1kg of absorbent temperature by 1 °C) and density, ρ of the THS material in regeneration. Multiplication of *Cp* and ρ is highest for Zeolite, 1070 kJ/m^3.K following SIM- 3a, 970 kJ/m^3.K and Silica gel, 678 kJ/m^3.K (Aydin et al., 2015a). This condition indicates that for the same volume of material (0.135 m^3) Zeolite absorbs more heat than the other materials until it reaches equilibrium with the inlet air temperature (T_{abs} = T_i) (See: Table 4.9).

Table 4.8 Full data set for the discharging process

Material	Cycle No.		ΔRH (%)		ΔT (°C)		Total mass (g)	Δm (g)	f	E_{cum} (Wh)	Q_g (W)		E_d		Ex (W)	
			Peak	Average	Peak	Average					Peak	Average	(kWh/m^3)	(Wh/g)	Peak	Average
SIM-3a	1	**Discharging**	47	29	24	13	701	170	0.32	222	133	68	164	1.31	5.2	1.1
	2		46	29	22	11	711	159	0.29	156	120	62	116	0.98	2.8	0.6
	3		47	28	17	11	746	164	0.28	181	91	65	134	1.10	1.9	0.6
	4		40	23	19	11	761	160	0.27	162	103	63	120	1.01	2.7	0.6
Zeolite	1		52	36	29	22	1168	225	0.11	153	157	105	114	0.68	5.5	3.1
	2		54	35	24	17	1288	182	0.09	63	133	92	47	0.31	3.0	1.8
	3		54	42	22	16	1462	206	0.08	103	120	88	76	0.50	3.2	1.4
	4		46	33	20	11	1626	201	0.05	89	111	84	66	0.49	3.1	1.4
Silica Gel	1		39	30	22	10	1337	226	0.21	55	117	44	41	0.24	4.1	0.7
	2		39	31	18	9	1452	224	0.17	54	91	43	40	0.24	3.5	0.6
	3		41	35	17	8	1556	223	0.16	54	92	43	40	0.24	2.8	0.5
	4		42	31	16	8	1627	199	0.15	50	89	40	37	0.25	3.2	0.5

Table 4.9 Full data set for the charging process

Material	Cycle No.		Δ*RH* (%)		Δ*T* (°C)		Total mass (g)	Δ*m* (g)	***f***	E_{cum} (Wh)	Q_{tr} (W)		E_d		*Ex* (W)	
			Peak	Average	Peak	Average					Peak	Average	(kWh/m^3)	(Wh/g)	Peak	Average
SIM-3a	1	**Charging**	46%	23%	52	17	552	-149	0.21	168	282	107	124.44	1.13	50.1	16.2
	2		49%	25%	48	18	582	-129	0.18	151	259	100	111.85	1.17	36.3	13.1
	3		41%	22%	31	12	601	-145	0.19	163	114	101	120.74	1.12	19.4	9.3
	4		41%	20%	36	15	657	-104	0.14	139	174	100	102.96	1.34	28.1	11.6
Zeolite	1		39%	14%	36	16	1106	-62	0.04	95	185	118	71.11	1.55	26.7	13.4
	2		36%	9%	41	21	1256	-32	0.02	121	223	117	89.63	3.78	28.2	15.3
	3		41%	13%	44	22	1425	-37	0.02	146	241	123	108.15	3.95	28.9	16.4
	4		42%	13%	40	19	1575	-51	0.03	95	220	101	71.11	1.88	27.2	19.8
Silica Gel	1		25%	12%	31	12	1278	-99	0.05	41	167	68	30.37	0.69	25.5	6.5
	2		40%	13%	32	10	1333	-119	0.09	64	175	73	47.41	0.54	23.4	7.1
	3		35%	14%	33	10	1428	-128	0.09	65	181	71	48.15	0.51	24.6	7.7
	4		38%	13%	29	8	1505	-122	0.08	50	161	62	37.04	0.41	22.1	7.9

It is clear from Figure 4.3.7 that any heat absorbed by the materials during the charging process is directly related with the heat that they release during the discharging process. This relation indicates that a materials' heat requirement for regeneration increases directly proportional to its heat output for discharging.

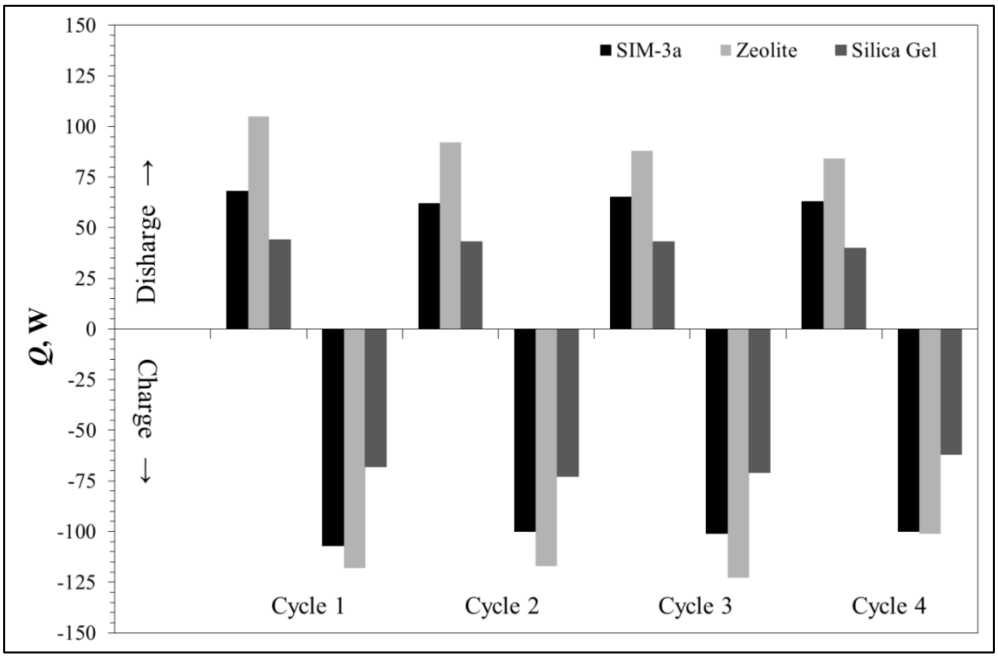

Figure 4.3.7 Instantaneous heat input/output during the charging and discharging cycles

The aim in THS system design should be achieving an equal amount of heat in discharging process to that absorbed in regeneration ($Q_{tr} \approx Q_g$). Whilst the Zeolite has the highest heat input, it has the lowest desorption rate, Δm when compared with the other two materials (see: Figure 4.3.8). This shows that Zeolite requires a much higher T_r for efficient regeneration to ensure all the water vapour is completely desorbed. Zeolite has been widely researched and according to many articles (Chan et al., 2012, Hongois et al., 2011, Jänchen et al., 2005) it promises to be a good candidate for THS, however the results from this research clearly demonstrate that very intense solar radiation would be required to enable use of solar energy for regeneration of Zeolite, which is not available under normal European climate conditions.

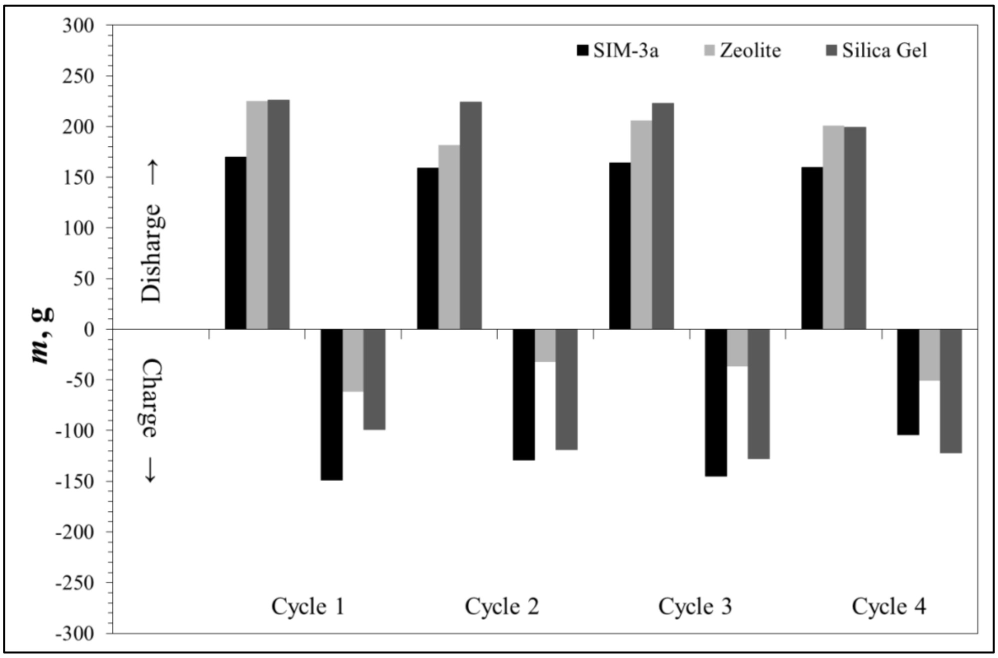

Figure 4.3.8 Instantaneous mass uptake/release during the charging and discharging cycles

The thermal performance of the tested materials in terms of COP, energy density and mass uptake ratio are presented in Figures 4.3.9 to 4.3.11. In an ‘open’ thermochemical process, COP is defined as the ratio of heat gain to power consumption (see: Equation 4.12). The electricity consumption of the fan was measured at 5 W during the experiments. There is no energy consumption for the humidifier due to the use of evaporative pads providing energy free humidification. The highest COP calculated in all cycles was for Zeolite (21 for Cycle 1) whilst silica gel was the lowest (8.5 for Cycle 4) however, as can be seen from Figure 4.3.9, the COP and thus cyclic stability of the Zeolite decreases over the subsequent cycles. SIM-3a and silica gel on the other hand have steady COP’s with averages of 14 and 8 respectively across the four cycles.

SIM-3a for Cycle 1 displays the highest experimentally measured energy storage density, E_d = 160 kWh/m^3 (see: Figure 4.3.9). Although this does decrease slightly in subsequent cycles, its storage density for Cycle 4 (120 kWh/m^3) still exceeds that for the highest calculated E_d of the Zeolite (114 kWh/m^3 in Cycle 1) or silica gel (39 kWh/m^3 in Cycle 1). As was the case for COP values, the E_d for Zeolite also shows a decreasing trend across the four cycles. Whilst

Zeolite has the ability to provide a high Δ*T* at the beginning of the first cycle, its effective reaction time is short, (<1.5 hour) as its pores (< 2 nm) are quickly blocked by the water vapour at higher humidity levels (*RH* > 80%) resulting in the reaction kinetics slowing down rapidly. SIM-a on the other hand, having pores in the macro scale (> 1µm) has a considerably longer reaction period resulting in higher cumulative energy output.

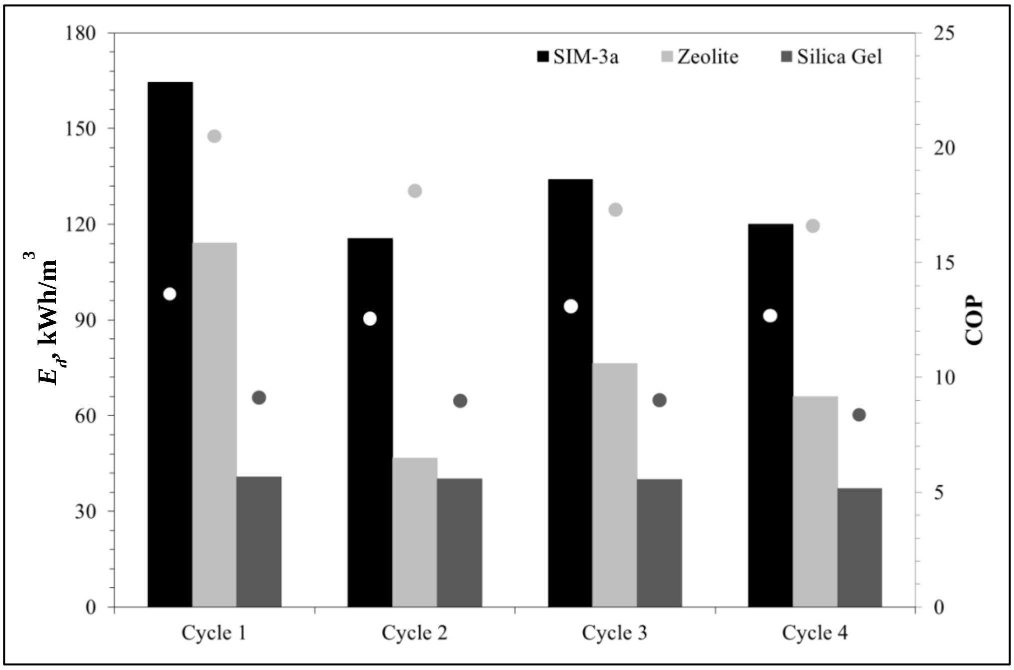

Figure 4.3.9 Discharge energy density and COP (inset) of the materials over four cycles

In Figure 4.3.10 the cyclic mass uptake ratio, *f* of materials calculated using Equation 4.9 is shown. This is the ratio of total amount of vapour adsorbed by adsorbent to the initial dry mass of adsorbent and is an important measure in the analysis of THS materials as it also accounts for the density of the material as opposed to absolute mass uptake only. Although SIM-3a absorbs the lowest mass of water vapour (*m* = 160 g) it has the highest ratio (*f* = 0.32 g/g), as its initial dry mass is the lowest (*i.e.* low density) when compared to Zeolite and silica gel. The Zeolite has a comparable mass uptake ratio (*f* = 0.27 g/g) to that of SIM-3a for the first cycle but, as in the earlier results, there is a large decrease in the subsequent cycles due to hysteresis with a total change of Δ*f* = 0.19 g/g. This is too large to be considered a viable material for THS when compared to the ratio changes for Silica Gel (Δ*f* = 0.6 g/g) and particularly SIM-3a (Δ*f* = 0.4 g/g).

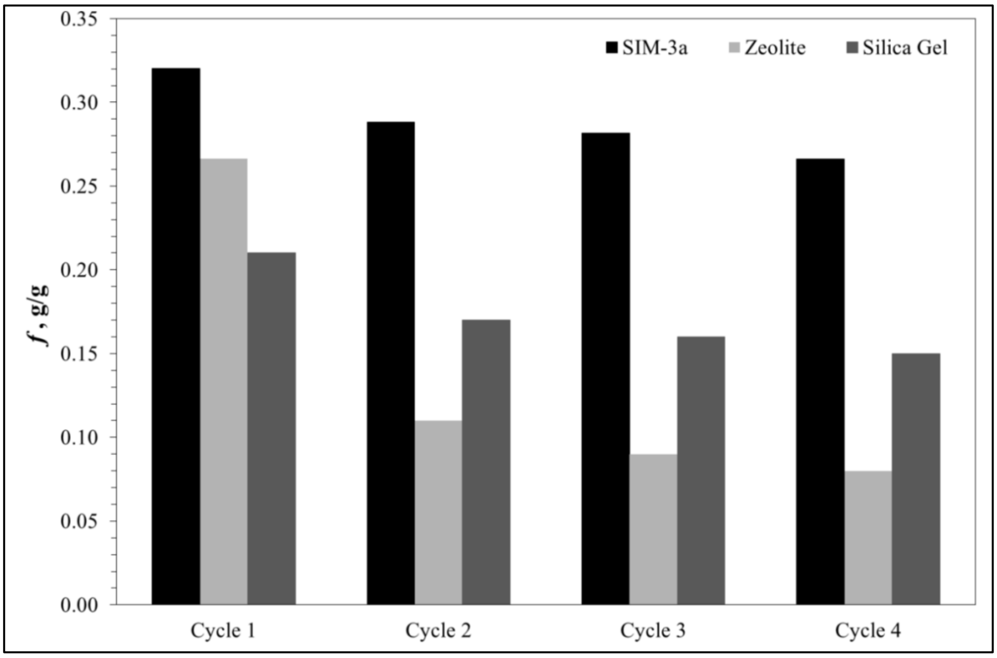

Figure 4.3.10 Mass uptake ratio of the materials over four cycles

In Figure 4.3.11 it can be seen that there is a clear correlation between cumulative energy output, E_{cum} and mass uptake ratio, *f* of materials with a decreasing trend from Cycle 1 through Cycle 4. In general, a material that shows a linear plot approaching a vertical alignment with little range on either axis (see: inset, Figure 4.3.11) is ideal for THS purposes as this indicates little hysteresis in terms of either Q_g or Δm. SIM-3a provides the best performance with the highest energy output coupled with the highest mass uptake ratio. It is also interesting to note that SIM-3a's performance drop across the four cycles was achieved via a relatively low range of adsorbed vapour where ΔE_{cum} = 66 Wh for a Δ*f* = 0.05 g/g. Zeolite's energy output difference was much larger at ΔE_{cum} = 90 Wh for a similar vapour uptake range Δ*f* = 0.06 g/g. Silica gel displays steady performance in terms of E_{cum} however it does also show degradation in its mass uptake ratio, Δ*f* = 0.06 g/g.

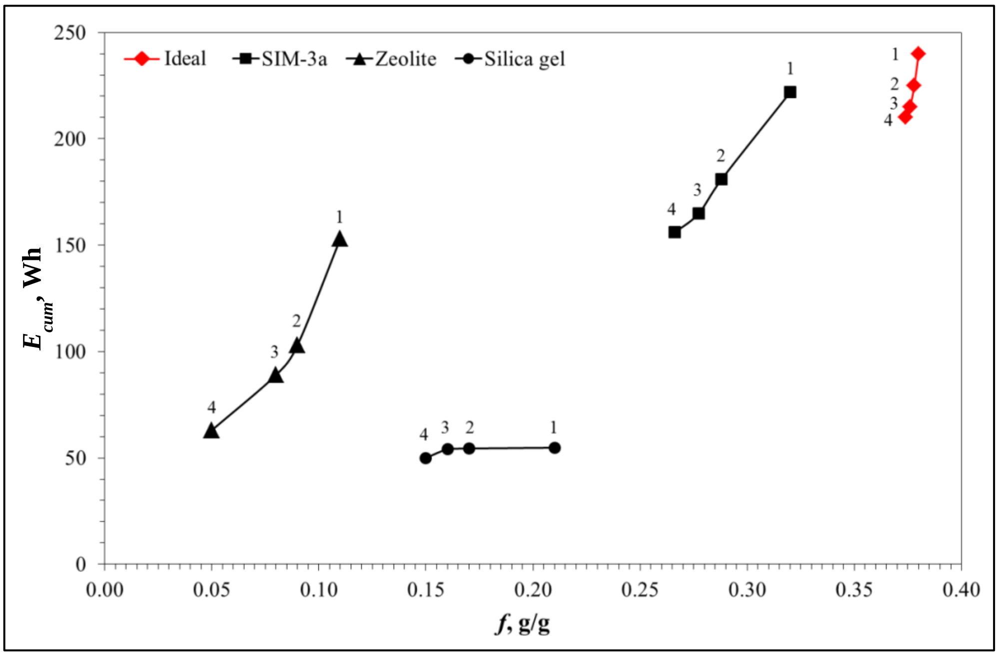

Figure 4.3.11 Graph showing the correlation between cumulative energy gain and mass uptake ratio over four cycles

4.3.3.3 System Efficiency

The cyclic efficiency behaviour of the materials over the four cycles (*i.e.* charging / discharging) was analysed with the results presented in Figure 4.3.12. The analysis is considered in terms of both the energy and exergy provided by material in the discharging cycle (see: Equations 4.2 and 4.10) and transferred to the material during the charging cycle (see: Equations 4.13 and 4.19). The 1st law (*i.e.* energetic) efficiency is calculated using Equation 4.22 whilst the 2nd law (*i.e.* exergetic) efficiency is calculated using Equation 4.23.

Zeolite has exergy efficiency above 20% in first cycle as a result of high temperature lifting. However in rest of the cycles it dropped below 12%. Zeolite also has the highest energy efficiency in the range of 70-90% which shows that it released most of the heat that it gained during charging process. On the other hand SIM-3a and Silica gel have energy efficiencies close to each other, approximately 65%. Conversely Silica Gel has higher exergy efficiency comparing with V-$CaCl_2$. Although SIM-3a cyclic exergetic performance is the worse one, in charging cycle it has a good performance.

Several criteria have been taken into consideration when evaluating the THS system efficiencies. Ambient temperature and RH, moisture content of the absorbent, amount of heat supplied in regeneration are all crucial in addition to the absorbent properties. Furthermore, discharging reaction time has a significant importance when determining heat storage density or average heat output of an absorbent. As the temperature lift during the discharging of an absorbent is not steady and drops over time, the considered reaction period is crucial. In this study the short term efficiency performance of the materials ($t_{rxn} < 3$ h) was investigated. Zeolite has the highest overall efficiencies for short term performance as it has the peak output and relatively highest temperature lift in that first 3 hours. Nevertheless it is expected that over longer periods (*i.e.* $t_{rxn} > 10$ h) SIM-3a would provide the highest average heat output and efficiencies as it has a more steady performance in terms of T_{out} than Zeolite. For commercial level usage of THS systems, the long term performance investigation of absorbents is crucial and future study will be focused on this.

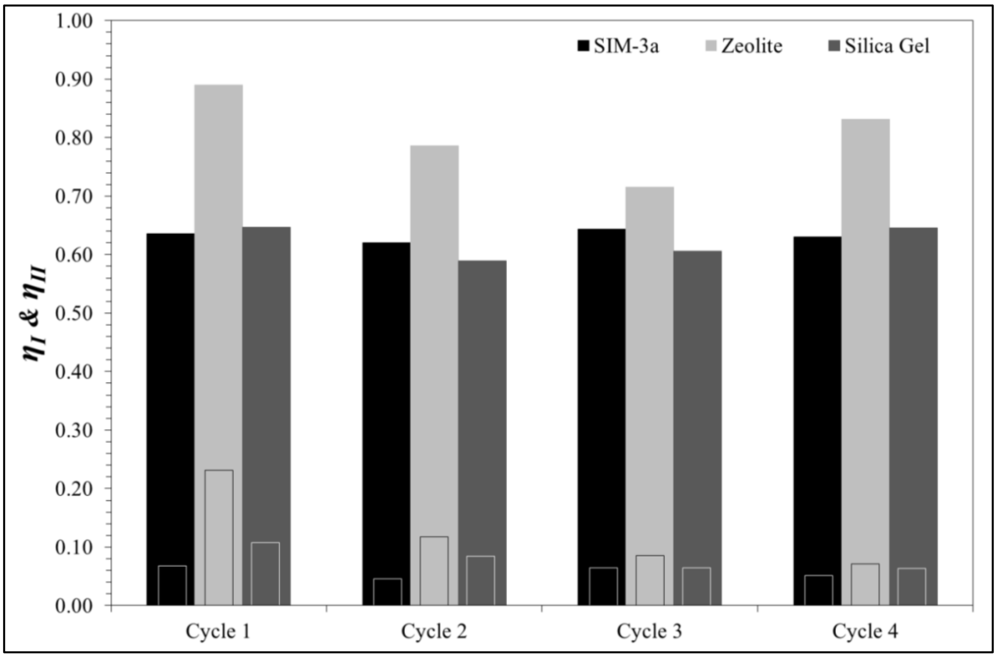

Figure 4.3.12 Graph showing the energy and exergy (inset) efficiencies for the four cycles

4.4 Salt Impragnated Desiccant Matrices - Improving energy density utilisation through hygrodynamic & thermodynamic reactor design

Uniform air flow through the sorption material is vital in THS systems for effective process performance. One of the key approaches could be enhancing the contact area of air and sorbent through the internal reactor design. This could improve the sorption kinetics, heat transfer and mass transfer. Enhanced contact area / reaction front could be achieved through using rotating reactors or conveyor systems. However moving components, increases capital and operating costs, system complexity also reduce the system lifetime. Despite the fixed bed reactors have simple embodiments, only small volume of sorbent could be utilized effectively and increasing bed size (e.g. thickness) negatively influences the system performance. In this context using corrugated bed surface, multilayer sorption bed or creating air flow channels inside the sorbent are possible solutions for this problem.

The work presented in previous section (Please see: Chapter 3.3) assesses the hygrothermal cyclic behaviour of both adsorption and thermochemical materials in a custom designed test rig (Gen1). A new design THS system (Gen2) using perforated tubes for enhancing air-sorbent contact area thereby to increase vapour diffusion to the Salt-In-Matrix (SIM) composite absorbent material was developed. The system design, experimental methodology and results of testing presented in this section. The aim of this research was to improve overall energy output using the same materials tested previously, through comparative analysis of the results achieved in both rigs and further analysis of system operating parameters and the cyclic / hysteretic performance of the Gen2 rig. There are currently a very limited number of experimental studies investigating ‘open’ THS systems suitable for domestic building thermal energy provision in the existing literature and it is envisaged that this new concept may act as a model for future short/long term development of these systems.

4.4.1 Methodology

In Section 4.2, a range of candidate porous materials and salts capable of producing adequate exothermic thermochemical reactions for ‘open’ THS when hydrated were selected from the literature. From these, a total of eight SIM composities were synthesised using the Insipient Witness Technique (IWT) method. These were SIM-2a, SIM-3a, SIM-3b, SIM-3c, SIM-3d, SIM-3e, SIM-4a and SIM-8a. SIM-3a appeared to have excellent E_d coupled with good moisture uptake and response time to moisture with TGA also suggesting significant mass loss in the working range $30 < T < 140$ °C. These findings suggested that SIM-3a appears to have very good potential for use in an ‘open’ THS system.

From hygrothermal cycling experiments carried out using the Gen1 rig, as presented in Chapter 3.3, Zeolite provided the highest temperature lift of all samples in the first cycle due to the high amount of vapour adsorption and fast reaction kinetics. Whilst the hysteretic performance of SIM-3a was minimal, the Zeolite showed a sharp drop from cycle one to cycle four. Zeolite requires a high regeneration temperature (> 180 °C) with the lower regeneration temperature prerequisite for this research unable to provide adequate dehydration, however as it is used extensively in the literature (Lass-Seyoum et al., 2012, Hauer, 2002, Henninger et al., 2012, Henninger et al., 2010, Hongois et al., 2011, Jänchen et al., 2004, Jänchen et al., 2005, Jänchen and Stach, 2012, Shigeishi et al., 1979) it was decided to use it for comparative analysis for this work.

A new composite THS material SIM-3f was developed that combined SIM-3a and SIM-3d (Vermiculite with $CaCl_2$ and $LiNO_3$). In previous findings (Casey et al., 2015) SIM-3d was considered to be of interest as it performed well across four charge/discharge cycles albeit with a maximum temperature lift, $T_{out,\ max}$ much lower than SIM-3a which, on its own, would be too low to suit an 'open' THS system. SIM-3d appeared to have a near horizontal slope during the cyclic test (*i.e.* from maximum temperature to ambient, $T_{out,\ max} \rightarrow T_{ambient}$) suggesting that the dwell time, t_{dwell} (*i.e.* time taken for $T_{out} = T_{ambient}$) for SIM-3d may far exceed those of the other synthesised materials. It was proposed that combination of SIM-3d with SIM-3a may prove beneficial and therefore is also investigated here.

SIM-3f was prepared using equal volumes of saturated solution (50% - 50%) of each salt in separate containers to prepare the final mixed $CaCl_2$-$LiNO_3$ solution before impregnation. The solubility of $CaCl_2$ and $LiNO_3$ at room temperature (20 °C) are 745 g/l and 522 gr/l with the molar weight at the same conditions being 110.98 g/mol and 68.95 g/mol respectively. Therefore the mass ratio of $CaCl_2$ / $LiNO_3$ impregnated to the host matrix (vermiculite) was calculated as 1.42 whereas molar ratio was 0.88.

The Gen1 testing rig (see: Figure 4.4.1 a) used in the previous research had a fixed flat absorbent bed where the SIM material was placed on a perforated tray and air flow was perpendicular to the perforated surface. In this system there was no additional configuration allowed for to improve diffusivity and mass transfer, as the primary aim of the testing rig was to carry out a comparative performance analysis of a large number of SIM's over a short period of time. Numerical modelling simulations of the Gen1 rig showed that high resistance occurs at the reaction front which both increases the pressure drop across the absorbent bed and reduces the diffusivity and thus moisture transfer, particularly when there is an increase in SIM layer depth. This served to limit upscaling of the THS system using the Gen1 rig design.

A new testing rig (*i.e.* Gen2), was designed and developed to demonstrate the concept/design for large scale THS applications. This system (see: Figures 4.4.1 b and 4.4.2) was designed to investigate the hygrodynamic and thermodynamic performance of the system when using perforated tubes to facilitate vapour diffusion to the SIM to reduce the effect of the reaction front. Compared to the Gen1 rig, the Gen2 reaction chamber (8) is rectangular shaped (500 mm x 250 mm x 200 mm) with a sloping roof to facilitate post absorbent airflow and is constructed of aluminium with welded seams.

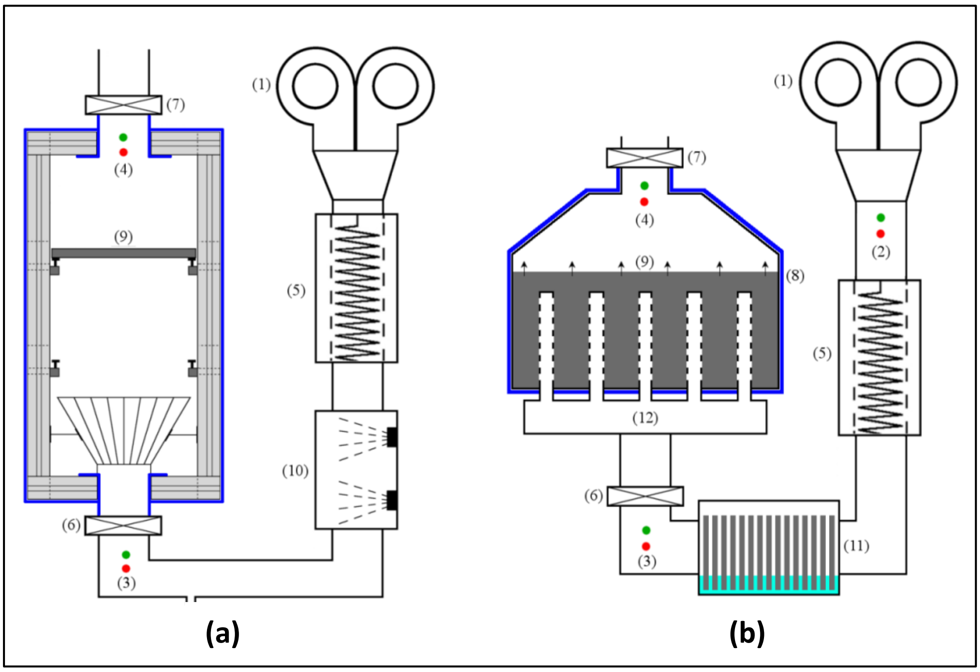

Figure 4.4.1 Schematic diagram of (a) the Gen1 and (b) the Gen2 experimental test rigs

Figure 4.4.2 View of Gen2 experimental test rig

Ten perforated tubes, *d* = 20mm, made up of 0.55 mm thick perforated aluminium sheet were placed vertically inside the reactor in two parallel rows with a horizontal distance, *d* = 100 mm between each (x and z direction) (See: Figure 4.4.3).

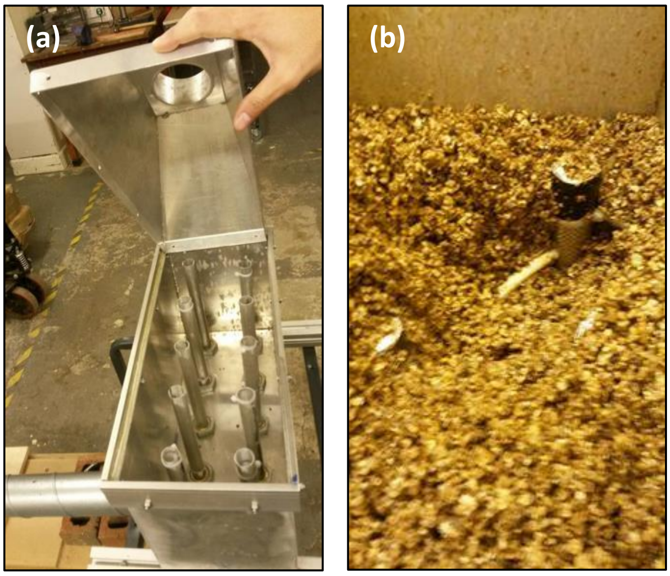

Figure 4.4.3 Internal view of reactor showing (a) perforated diffuser pipe allocation and (b) hydrated sorption material (SIM-3a)

The tubes are connected to an external manifold (12) to equalise airflow to each tube, with the top end of the tubes sealed in order to achieve sufficient internal pressure, providing air flow laterally to the absorbent (9). Humidification of the inlet air is provided using an evaporative pad matrix placed inside a rectangular shaped wick chamber (11). Air flow through the wick chamber is parallel to the evaporative pads, enabling moisture enhancement of the inlet air before entering the reaction chamber. An Xpleair (UK) XID series, inline duct fan (1) (*d* = 150 mm) is used to provide air flow and is connected to ducting (*d* = 100 mm) via a reducer. To eliminate thermal losses to the external environment, the complete system is insulated using 25 mm thick, foil lined glass wool. Temperature and relative humidity (RH) were recorded using the EK-H4 Eval Kit from Sensiron, AG, Switzerland. Thermocouples with the maximum deviation of ±0.5°C for temperature and ±2% for relative humidity and air mass flow meter with the accuracy of ±2% were used for measuring the experimental data. Three sensor locations were used – (2) ambient, (3) manifold inlet and (4) reactor outlet. Total uncertainty affecting the heat transfer rate (Q_{tr}) in the system was computed by using Equations (4.2)-(4.5). The estimation implies that total uncertainty in calculation of the efficiencies is found to be 1.54%.

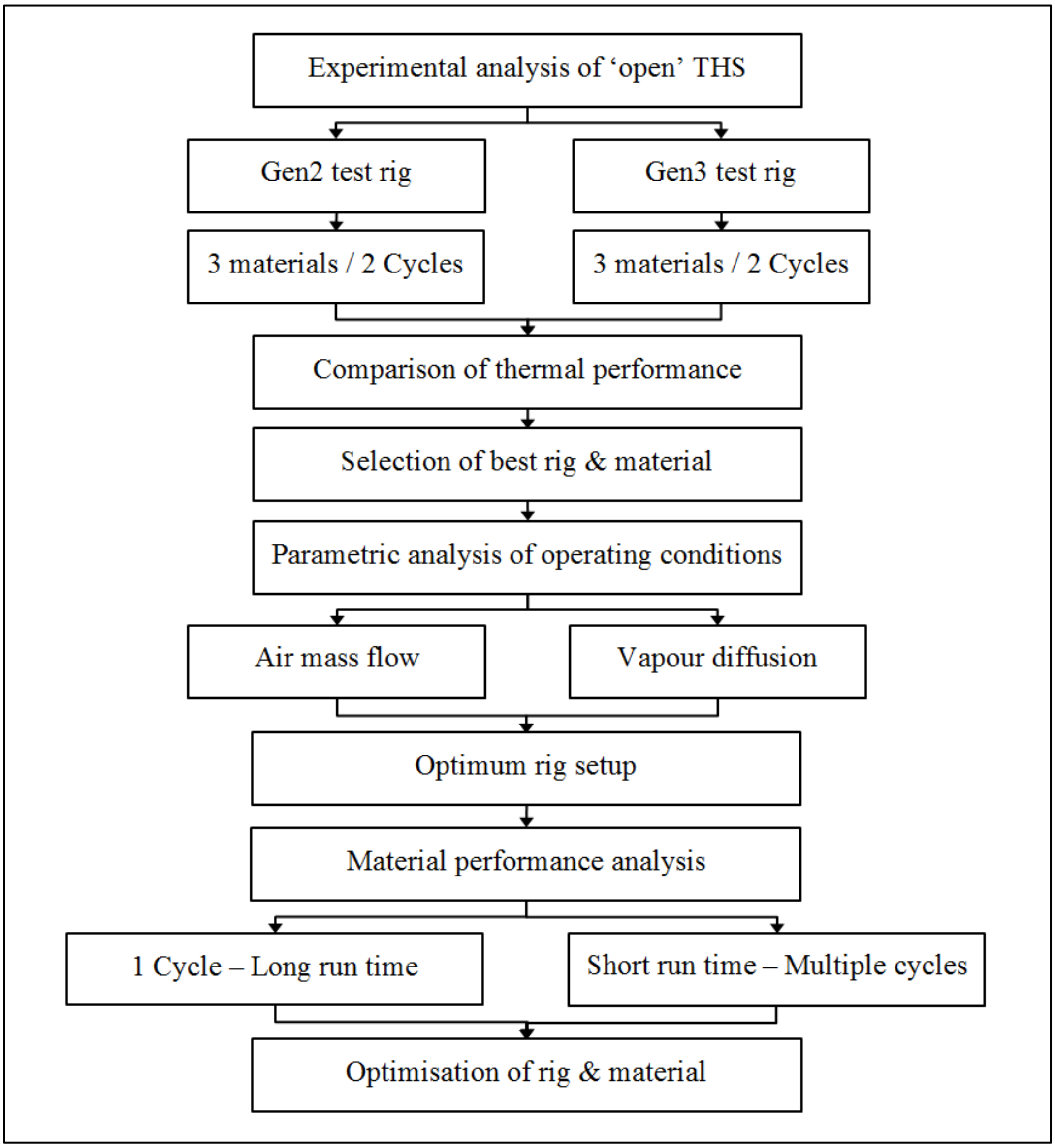

Figure 4.4.4 Graphical flow chart of the experimental methodology

The experimental methodology was divided into two phases (see: Figure 4.4.4). The first phase included a comparative energetic, exergetic and hygrothermal analysis of the three selected materials' performance in the Gen1 and newly developed Gen2 rigs. In the second phase, the best performing material from the first phase would be selected for parametric analysis using the Gen2 rig. This analysis would chart the effect on performance (*i.e.* temperature lift and moisture uptake) of i) tube hole diameter and ii) air flow rate. Additionally, both the long and short term cyclic behaviour of the SIM material with correlations between mass change, Δw and temperature change, ΔT were investigated.

4.4.2 Comparison of performance between Gen1 and Gen2

In this section an analysis of both the energetic and exergetic experimental results collected during the testing period is presented and discussed. The list of equations used in the analysis was presented in Table 4.6. All samples were prepared by oven drying at $T \approx 150$ °C for a period, $t > 24$ h to achieve the condition $m_{dry} = 0$ kg/kg. The dry SIM was then placed in a mesh tray and allowed to cool in a desiccator for $t = 2$ h prior to testing. When cooled, the material was placed into the reaction chamber and the rig sealed. For the discharging cycle (absorption), the humidifier was connected and the psychrometric state of the airflow monitored. When the desired humidity level was reached, the inlet valve was opened. Each test was carried out over two short discharging cycles of duration $t_{cycle} = 180$ min each with charging of the material occurring between each cycle. For the charging cycle (desorption) the humidifier was disconnected and the heating unit activated and set to the desired regeneration temperature ($T = 90$ °C). The charging cycle was deemed to be complete when;

$RH_{out} = RH_{in}$ or $\Delta m \leq 2\%$ or $T_{in} = T_{out}$

In Figure 4.4.5, the inlet and outlet temperatures, T_{in} and T_{out} of SIM 3a, SIM-3f and Zeolite tested in both the Gen1 and Gen2 rigs are presented with the full data set from test and subsequent analysis summarized in Table 4.10. The purpose of these tests was to compare the Gen1 and Gen2 testing rigs and demonstrate any performance improvement. In THS systems, contrarily to both SHS and LHS systems, effective mass transfer (moisture) is required, which can significantly reduce performance as the size of the THS system increases. If we assume that the heat storage capacity of all these systems is directly proportional to the amount of material employed, then novel designs which provide efficient moisture diffusion are therefore required to enable efficient sorption processes in larger storage units.

An ‘open’ THS system operation is based on the temperature lift of a building’s air due to moisture absorption. Due to the thermochemical reaction, there is a sharp temperature lift of output air at the beginning of the reaction and, as time passes, the moisture content inside the reactor increases and moisture sorption rate of THS material (*i.e.* sorption kinetics) slows down causing a drop in temperature. For thermal analysis of the tests, four measures are used here:

3. Maximum output temperature, $T_{out,\ max}$, which is the peak temperature reached in each single cycle
4. End state temperature lift, ΔT_{180}, which represents the temperature lift at the end of the cycle *i.e.* $T_{out} - T_{in}$ @ $t = 180$ min
5. Dynamic output temperature drop, *c*, which is the gradient from $T_{out,\ max}$, to $T_{out,\ 180}$, ($\mathrm{d}T/\mathrm{d}t$)
6. Average temperature lift, ΔT_{avg}, which is the average temperature differential over the full cycle i.e. $T_{out} - T_{in}$ / 180

The results show that the performance of all three materials increased across all four measures when using the Gen2 testing rig as opposed to the Gen1 rig.

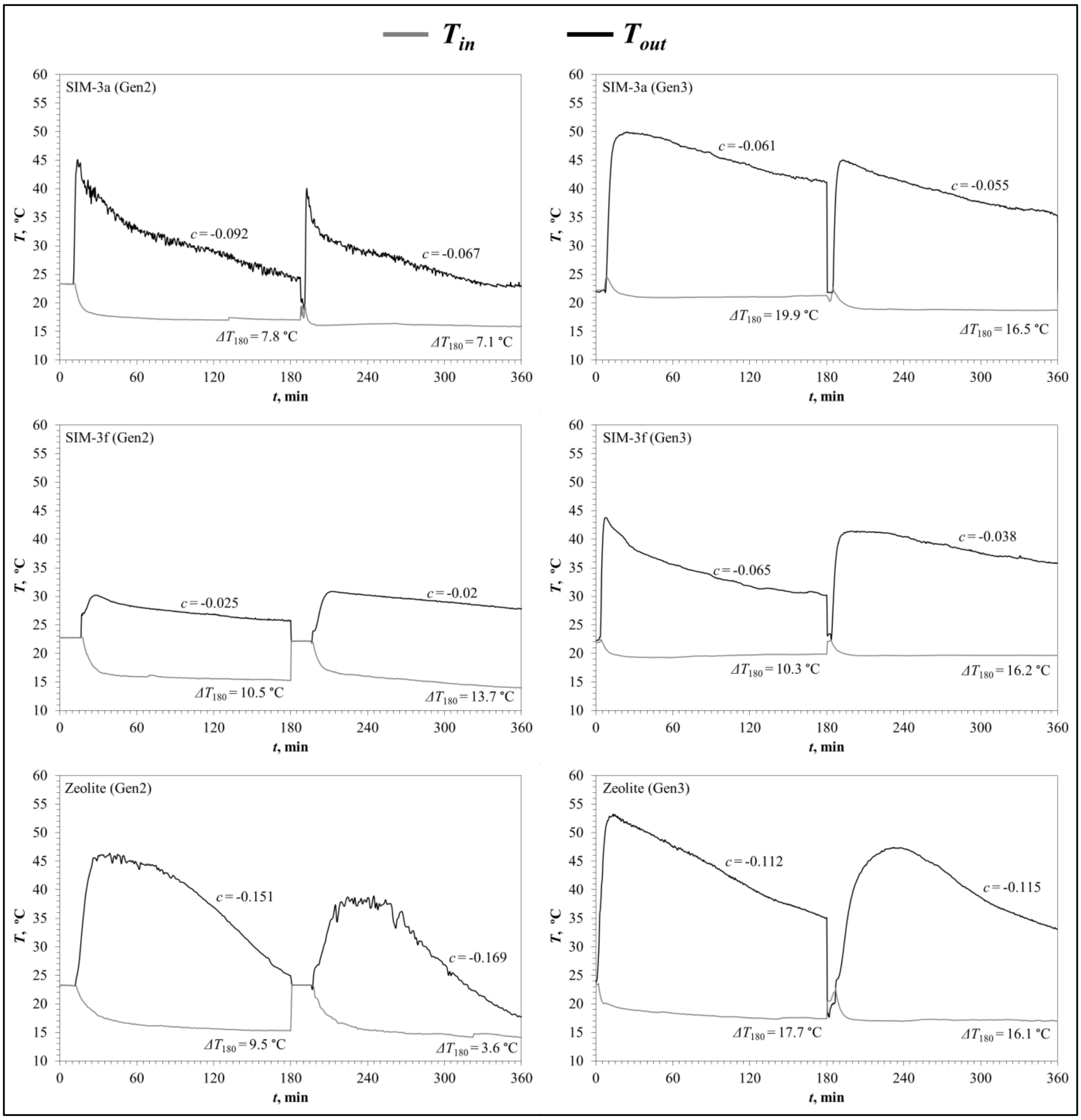

Figure 4.4.5 Three hour limited generation cycles for SIM-3a, SIM-3f and Zeolite using the Gen1 and Gen2 experimental rigs

To ease notation in the text, the first cycle of each test is denoted as $^{(1)}$ whilst the second cycle is noted as $^{(2)}$. The results for SIM-3a (Vermiculite/$CaCl_2$) clearly indicate the significant improvement in Gen2 rig with an average temperature lift ΔT_{avg} = 23 °C$^{(1)}$ and 19.9 °C$^{(2)}$ compared with 12.8 °C$^{(1)}$ and 10.7 °C$^{(2)}$ in Gen1. In both cycles of the Gen1 rig, a sharp drop in outlet temperature, T_{out} was observed with dynamic output temperature drops of, c = 0.092$^{(1)}$ and 0.067$^{(2)}$ for the Gen1 rig compared with 0.061$^{(1)}$ and 0.055$^{(2)}$ for Gen2 which are shallower and indicate better performance due to the increased diffusion and steadier vapour absorption of SIM-3a in Gen2 after the wetting of the reaction front. Initial maximum temperatures are also higher in Gen2 with, $T_{out,\ max}$ = 50 °C$^{(1)}$ and 45 °C$^{(2)}$ as opposed to 45 °C$^{(1)}$ and 40 °C$^{(2)}$. Although there was only a 5 °C difference observed in $T_{out,\ max}$, it is the end state temperature difference that indicates the superior performance of Gen2 over Gen1 with ΔT_{180} values of 7.8 °C$^{(1)}$ and 7.1 °C$^{(2)}$ in Gen1 against 19.9 °C$^{(1)}$ and 16.5 °C$^{(2)}$ in Gen2.

For SIM-3f (Vermiculite/$CaCl_2$/LiCl) both the average and peak temperature lift was higher in Gen 2. Although the temperature lifting of SIM-3f was poor in Gen1, it showed a steadier performance across both cycles with gradients c = 0.025$^{(1)}$ - 0.020$^{(2)}$ in Gen1 and 0.065$^{(1)}$ - 0.038$^{(2)}$ in Gen2. End state temperature difference, ΔT_{180} for cycle 1 was similar in Gen1 and Gen2, however, in cycle two, Gen2 was considerably higher, ΔT_{180} = 16.2 °C than 13.7 °C in Gen1. Average temperature lift was also higher for Gen 2, ΔT_{avg} = 14.3°C$^{(1)}$ and 18.5°C$^{(2)}$ as opposed to Gen 1 with ΔT_{avg} = 10.2 °C$^{(1)}$ and 12.4 °C$^{(2)}$ indicating improved performance.

Zeolites performance was also significantly enhanced using the perforated tubes (Gen2) in comparison to Gen1. A sharp drop was observed in both cycles for the Gen 1 rig with ΔT_{180} = 9.5 °C$^{(1)}$ and 3.6 °C$^{(2)}$ representing a falloff in performance of 5.9 °C between the cycles. In Gen 2 however, performance is much steadier with ΔT_{180} = 17.7 °C$^{(1)}$ and 16.1°C$^{(2)}$ representing a small drop of 1.6 °C between cycles. The improved performance in Gen 2 was due to the uniform air flow and better diffusivity through the material. This condition is evidenced with the comparison of the ΔRH_{avg} (see: Table 2) achieved in Gen 1 and Gen 2 and demonstrates three facts;

1. Reducing ΔRH_{avg} (32.5 %$^{(1)}$ → 24.4 %$^{(2)}$) between cycles led to a notable performance drop of Zeolite in the Gen1 testing rig.

2. Steady ΔRH_{avg} (75.3%$^{(1)}$ → 75.7%$^{(2)}$) provided a more stable performance without any significant drop in the Gen2 testing rig.

3. The higher ΔRH_{avg} in Gen2 enabled higher average temperatures, ΔT_{avg} = 5.2 °C$^{(1)}$ and 9.5 °C$^{(2)}$ with consequently higher energy density, E_d of 13.8$^{(1)}$ and 35.2$^{(2)}$ kWh/m^3.

The most promising results according to all chosen performance criteria (energy and exergy output, mass uptake and heat storage density) were for SIM-3a in Gen2. $CaCl_2$ is highly hygroscopic and will continue to absorb moisture until deliquescence occurs. Combination of this remarkable property with $CaCl_2$ high heat storage density (45 kJ/mole) makes it a very promising candidate for domestic THS applications. Utilising $CaCl_2$ as the thermochemical media and vermiculite as the host matrix constitutes a spectacular composite absorption material for storage of solar energy or waste heat.

Table 4.10 Full results data set for the Gen1 & Gen2 testing rigs material based performance comparison

	Test rig	**Cycle No**	**ΔRH (%)**		**ΔT (°C)**		**f (g_{wv}/g_{abs})**	**E_{cum} (Wh)**	**Ex_{cum} (Wh)**	**Q (W)**		**Ex (W)**		**E_d**	
			Peak	Avg.	Peak	Avg.				Peak	Avg.	Peak	Avg.	kWh/m^3	Wh/g
Sim-3a	Gen 1	1	47.9	27.6	24.6	12.8	0.24	209	3.4	133.3	69.5	4.7	1.1	104.5	1.61
		2	47.3	27.6	22.7	10.7	0.22	161	0.7	120.2	58.3	2.8	0.2	80.5	1.40
	Gen 2	1	76.1	66.7	28.6	23.0	0.47	1123	35.1	464.1	373.1	17.6	11.6	112.3	0.67
		2	83.5	71.7	25.3	19.9	0.46	971	24.8	410	323.6	14.2	8.2	97.1	0.59
Sim-3f	Gen 1	1	39.2	29.5	13.3	10.2	0.22	166	0.6	71	55	0.7	0.2	83.3	1.26
		2	30.8	23.9	14.3	12.4	0.21	202	0.8	77	65	0.7	0.2	101	1.64
	Gen 2	1	65.2	50.3	23.0	14.3	0.24	697	10.3	374.8	231.8	11.5	3.4	69.7	0.77
		2	65.9	61.2	21.7	18.5	0.36	901	19.1	352.6	300.5	8.7	6.3	90.1	0.66
Zeolite	Gen 1	1	52.9	32.5	29.2	20	0.22	162	4.0	157.6	108.2	5.5	2.6	81.0	0.65
		2	46.2	24.4	23.4	12.5	0.18	101	1.1	124.7	67.8	2.5	0.7	50.5	0.49
	Gen 2	1	94.8	75.3	33.4	25.2	0.18	948	25.8	435.9	327	17.6	8.5	94.8	0.69
		2	90.3	75.7	30.3	22.0	0.17	857	17.5	393.5	285	11.3	5.8	85.7	0.65

4.4.3 Parametric analysis of operating conditions

In this section experimental results of the best performing absorbent (SIM 3a), tested in the Gen2 rig using different tube configurations and different mass flow rates are presented. The aim was to investigate the effect of the perforated tube's hole diameter (acting as air diffusers) on heat and mass transfer. The thermal performance of SIM-3a using three different mass flow rates was also analysed to determine the optimum operational conditions.

4.4.3.1 Vapour diffusion - tube configuration

In 'open' THS reactor design, perforated diffuser tubes can be considered crucial components and their effectiveness can determine the performance of the entire heat storage process. As in the previous section, the measures ΔT_{180}, ΔT_{avg} and $T_{out,\ max}$ are used to determine the heat storage effectiveness. In heat storage process, the aim is to achieve steady temperature output (see: Figure 4.4.5) rather than a very high peak at the beginning followed by a sharp drop. Considering that building heat loads are dynamic, heat storage performance should be predictable to allow simple design and control for space heating applications. In this context perforated tubes with 1 mm (d_1), 2 mm (d_2) and 3 mm (d_3) hole diameters were tested to compare their performance and determine the most suitable size. The temperature and RH variation of the process air during testing is given in Figure 4.4.6 and Figure 4.4.7. It is clearly seen from Fig. 4.5.6 that d_3 provided a sharp temperature lift ($T_{out,\ max}$ > 48 °C) at the beginning of the reaction followed by d_1 and d_2 with $T_{out,\ max}$ >42 °C. In terms of overall performance, ΔT_{avg} was found to be very similar for all three hole sizes (16.1 °C, 16.4 °C and 15.9 °C for $d_{1,}$ d_2 and d_3 respectively). The cumulative energy and exergy measures, E_{cum} and Ex_{cum} confirm the greater performance of d_2 with values of 640 Wh and 12.3 Wh compared with d_1 and d_3 (630 Wh/618 Wh and 9.6 Wh/10.2 Wh respectively).

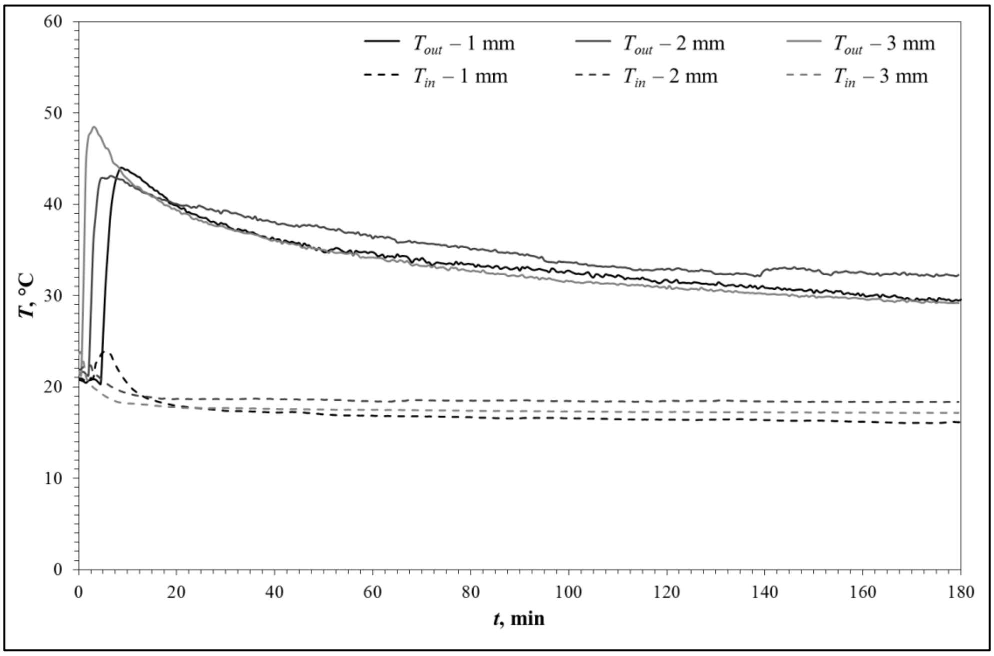

Figure 4.4.6 Temperature variation of SIM-3a with different tube configurations in the Gen2 testing rig

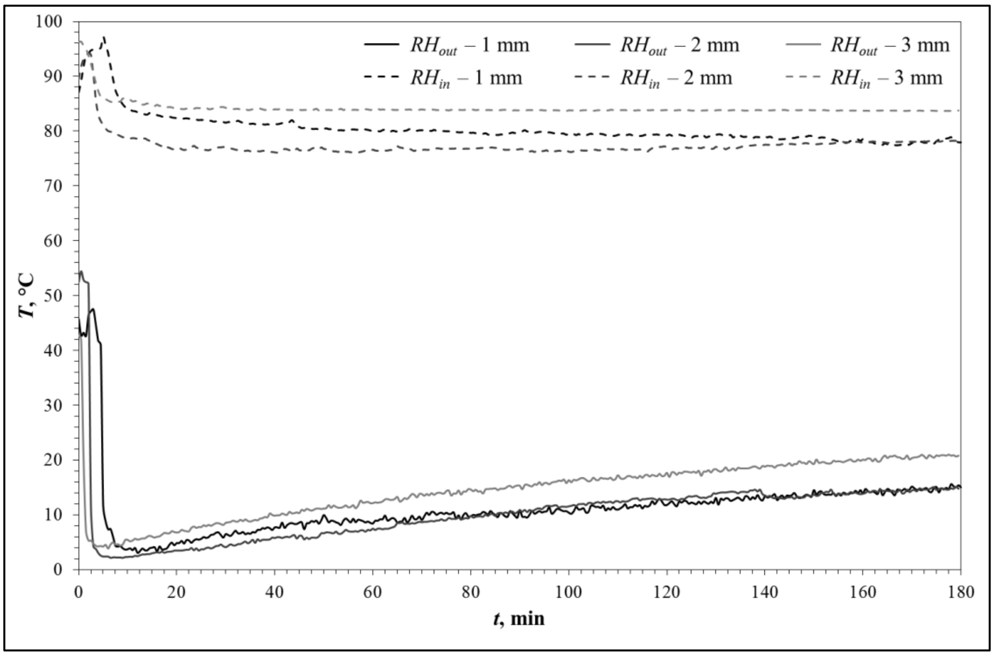

Figure 4.4.7 Relative humidity variation of SIM-3a with different tube configurations in the Gen2 testing rig

Figure 4.4.7 illustrates the RH of both inlet and outlet air for cycles with different tube configurations. As the developed evaporative humidification unit consists of evaporative pads without any additional moisture supply (e.g. water spray, atomizer, ultrasonic humidifier), a controlled amount of vapour was added to the air in each test, however there was still a slight variation to reactor inlet RH due to the varying humidity of the laboratory environment during each testing period. The higher $T_{out, max}$ observed for d_3 could be due to the slightly higher inlet RH where d_3 reached RH = 85% whereas d_1 and d_2 were lower at RH ≈ 77% at the end of 180 minutes. The moisture uptake ratio, f was found as 0.28, 0.29 and 0.31 g_{wv}/g_{abs} for d_3, d_1 and d_2 respectively. Whilst there is not any significant difference of the effectiveness of perforated tubes with different hole sizes, d_2 seems to be the best candidate for achieving steadier performance over longer periods of heat storage. Therefore d_2 was selected for the remaining tests investigating the effect of mass flow rate on thermal performance, evaluating the cyclic stability and long term behaviour of SIM 3a.

4.4.3.2 Air mass flow rate

Although 'open' THS is a relatively simple method for heat storage, it involves a complex process of absorption where mass (moisture transfer from air to the adsorbent) and heat (from adsorbent to the process air) transfer is dynamic and occurs simultaneously. Mass flow rate of the inlet air has therefore a significant effect on overall heat storage performance. This includes the influence of both moisture and air which are either directly or indirectly related with achievable temperature lift, ΔT. For instance, a higher mass flow rate can provide higher heat generation as it carries more moisture to the absorbent however a higher amount of dry air is thus also required to be heated at the same time. Simply, increasing humidity has positive influence on ΔT while increasing the dry air volume has a negative influence. A high rate of moisture absorption (from higher RH) also creates a "wetting effect" on the absorbent which can cause sensible cooling of both the absorbent and the process air. It should also be noted that heat storage capacity of any finite mass of sorption material is limited and a high rate of moisture sorption will lead to high initial thermal power release from the absorbent, but with low process time as the temperature lift drops sharply in a short period of time. On the other hand, a low mass flow rate may lead to insufficient moisture supply to the absorbent and may not provide enough pressure for uniform air and moisture diffusion through the absorbent. This condition can lead to several undesired consequences such as low temperature lift, low reaction kinetics, non-uniform moisture sorption and moisture condensation at the reaction front.

Figure 4.4.8 illustrates the inlet and outlet air temperature for three different cycles with three air mass flow rates (0.012 m^3/s, 0.015 m^3/s and 0.02 m^3/s). The results demonstrate considerably improved performance with the mid-range flow rate (0.015 m^3/s) with $T_{out,\ max}$ = 50 ºC and ΔT_{180} = 20 °C compared to the lower (0.012 m^3/s) and higher (0.02 m^3/s) flow rates.

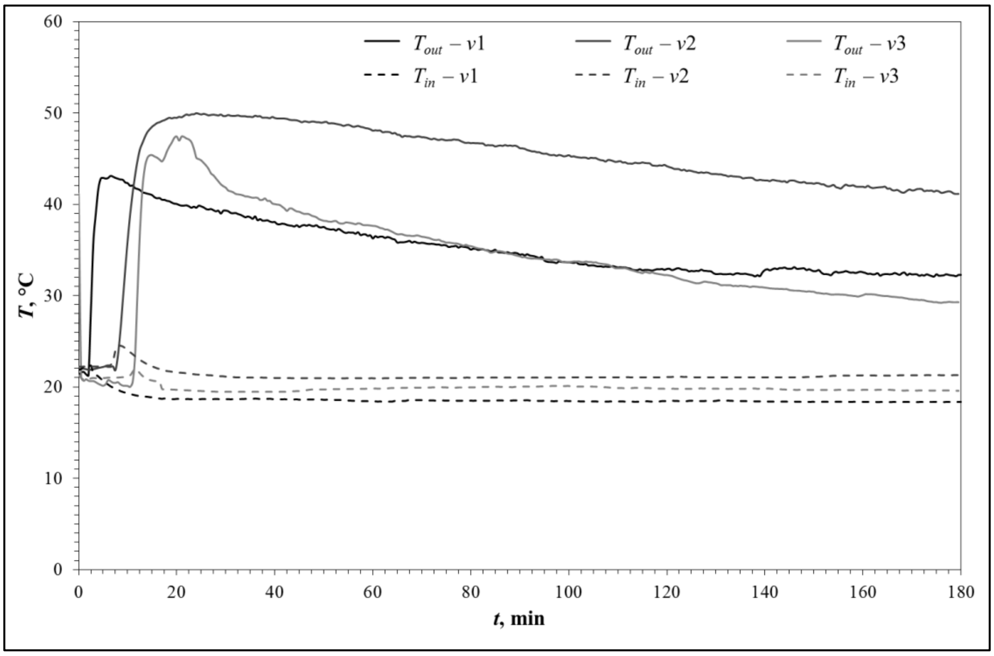

Figure 4.4.8 Temperature variation of SIM-3a with different air mass flow rates in the Gen2 testing rig

THS involves a complex process as discussed in detail above and air flow rate is one of the most important parameters determining THS performance. The results demonstrate that whilst there is not any direct correlation between THS performance and air flow rate / humidity, each reactor design will have a unique optimum flow rate which should be carefully analysed (numerically or experimentally) in order to achieve the optimum thermal output from the system.

4.4.4 Cyclic analysis of material performance

4.4.4.1 Analysis of a single long cycle

The long term performance of one cycle of SIM-3a, which provided the most promising results previously are presented in Figure 4.4.9. To investigate the maximum thermal energy that can be extracted from SIM-3a using the Gen 2 testing rig, this cycle was allowed to run until the condition $T_{out} = T_{in} + 3$ °C was achieved (at the end of 20 hours for this case).

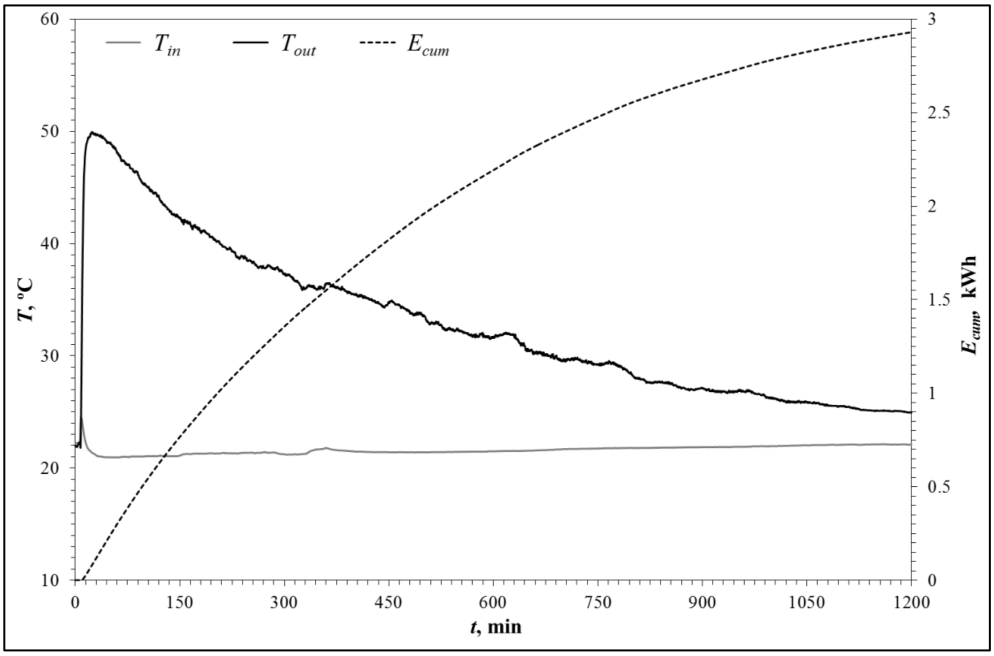

Figure 4.4.9 Thermal performance of SIM-3a over 1200 min. testing in Gen2 testing rig

During the test period the total thermal energy output reached 2.93 kWh in comparison with the 1.12 kWh at the end of first three hours in the previous tests (see: Table 4.12) with mass uptake tripling to 1.41 from 0.47 g_{wv}/g_{abs}. It is interesting 2.93 kWh that was achieved only from 0.01 m^3 of storage volume, suggesting that THS has remarkable potential for reducing the space requirement for heat storage systems in future's low/zero carbon buildings.

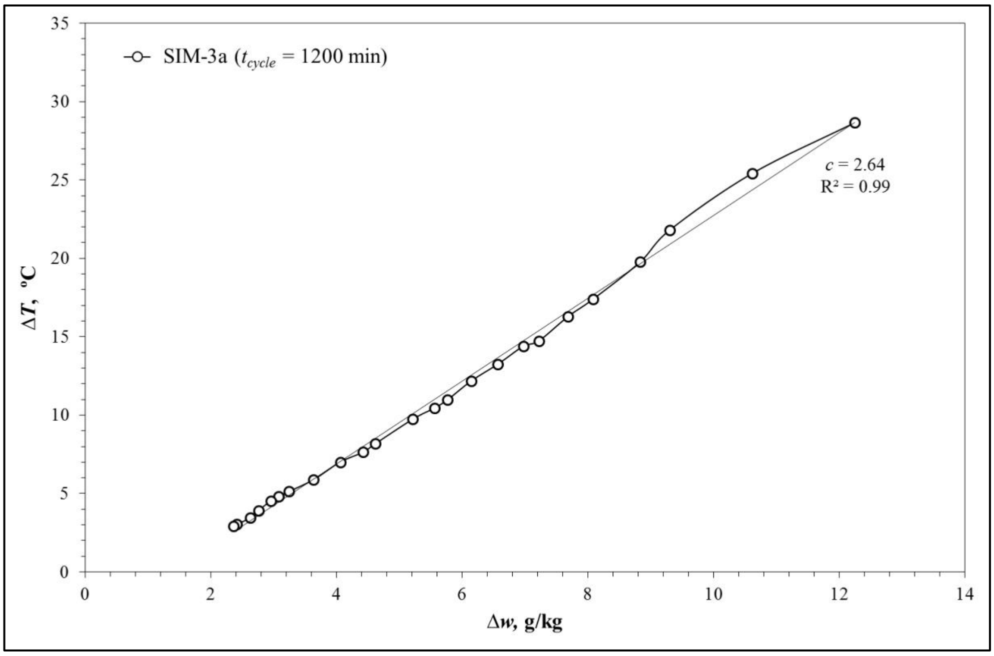

Figure 4.4.10 Correlation between air absolute humidity and temperature difference for SIM-3a in the Gen2 rig

Figure 4.4.10 illustrates the correlation of Δ*w* and Δ*T* over 20 hours testing of SIM 3a. During the test period (*t* = 20 h), it can be observed that the correlation between Δ*w* and Δ*T* is almost linear and independent of time. Recognizing and using this correlation in the future will allow easier and efficient design, control and operating conditions for THS systems.

4.4.4.2 Analysis of multiple short cycles

The last stage of testing was to analyse the cyclic behaviour of SIM-3a in order to simulate its performance for long term heat storage applications. Based on the previous results, an air flow rate of 0.015 m^3/s and perforated tubes with hole diameter of *d* = 2 mm were used during the tests. Due to technical difficulties with the rig during these cycles, SIM-3a was recharged at T = 90 °C for 24 hours following each discharging cycle in an externally located oven.

Figure 4.4.11 represents the inlet and outlet temperatures and thermal energy output in each of the four cycles. ΔT_{180} showed a decreasing trend from the 1st cycle to 4th cycle in the order of 19.5 °C → 17.2 °C → 14.8 °C → 13.2 °C which was somewhat expected. Similarly, cumulative energy outputs, E_{cum}, were 1.12 kWh → 0.96 kWh → 0.87 kWh → 0.74 kWh with cumulative exergy outputs, Ex_{cum}, calculated as 0.035 kWh → 0.024 kWh → 0.018 kWh → 0.013 kWh in the order 1st → 4th cycle respectively.

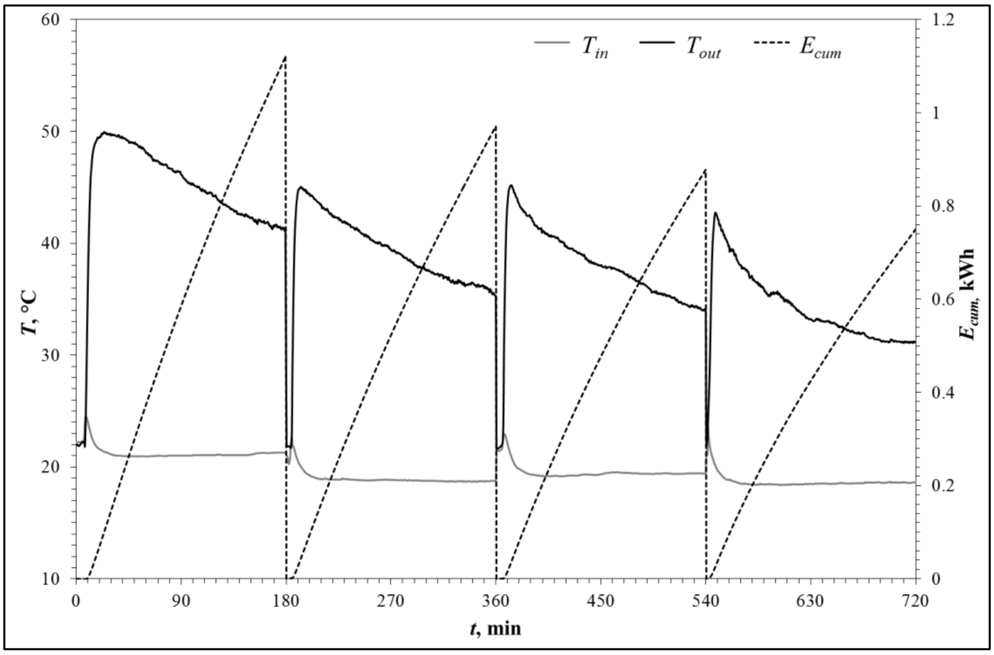

Figure 4.4.11 Cyclic performance of SIM-3a in the Gen2 testing rig

In terms of energy output this corresponds to a performance drop of 14% for the 1st → 2nd cycle, 9% for the 2nd → 3rd cycle and 14% for the 3rd → 4th cycle. One possible reason for the performance drop could be insufficient drying of the material as an electrical oven was used for recharging the material (*i.e.* static air). Usage of hot/dry air flow through the material could be more effective as air convection could significantly contribute to moisture removal from the material. Greater drying of the absorbent would undoubtedly achieve greater cyclic performance of SIM-3a as the material did not show any physical degradation over the cyclic testing. The performance drop is the result of reducing trend of mass uptake over the four repeated cycles supporting the correlation discussed earlier between moisture supplied to the material and temperature lifting.

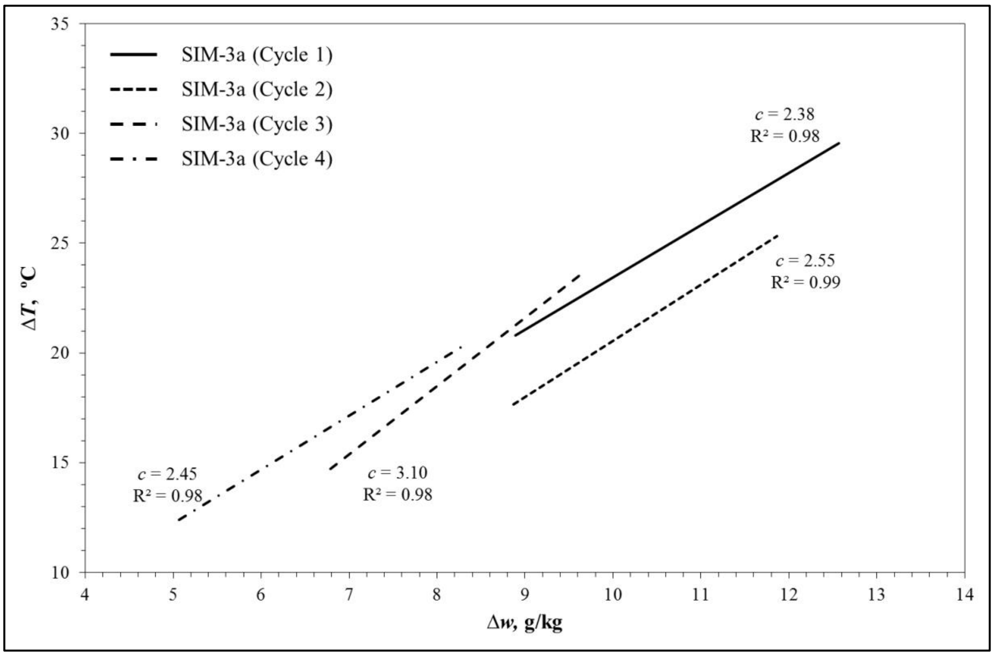

Figure 4.4.12 Correlation between air absolute humidity and temperature difference over four cycle testing of SIM-3a in Gen2 rig

As in the long cycle, Figure 4.4.12 illustrates the almost linear correlation between instantaneous Δ*w* and Δ*T* for the four repeated cycles. Although there are slight differences for each cycles line, all of them are in close approximation and can therefore be generalized to simulate THS performance according to the Δ*w* of the process air. Obviously it would be of benefit to have a considerable amount of repeated cycles (≈20 cycles) to truly assess the cyclic performance of the process and draw a more realistic operating line, unique for a certain design/absorbent, indicating the achievable temperature lift for a specific change in Δ*w*. In addition it should be noted that under real UK winter climate conditions it may not be possible to supply high moisture levels to the absorbent which could lead to a poor system performance. For instance, with an ambient temperature, T_a = 10 °C with a RH_a = 50% would correspond to a w_a = 3.77 gr/kg. In these psychrometric conditions, even if the air is saturated to 100% RH, w_a will be limited to 7.5 gr/kg. This is the maximum moisture amount that could be supplied to the absorbent and, even if all moisture is fully absorbed, the maximum temperature lift achievable is ΔT_{peak} < 20 °C (based on the operating line proposed earlier). Therefore in real applications, especially under severe winter conditions, pre-heating the air before entering the humidifier by some solar source or recycling a certain amount of the outlet air from the heat storage reactor could significantly improve heat storage performance by increasing w_a considerably. Further studies on this concept are planned as next step of this research.

4.5 Conclusions

This chapter covers the;

- Selection, synthesis, characterization of novel candidate sorption materials
- Comparative experimental analysis of the candidate sorption materials in a custom built rig and determination of the best candidates
- Design and development of a novel sorption reactor and testing the selected sorption materials with the aim of achieving improved heat storage performance

Accordingly, in Chapter 3.2, a selection of hygroscopic salts and desiccant matrices were chosen from the literature as candidate materials for TES systems. SEM analysis confirmed the presence of salt in the matrices after impregnation. The N_2 physisorption analysis suggests that damage may have occurred within the pore structure of the non-vermiculite samples based on the increase in $Ø_{pore}$, however no damage was observed in the vermiculite samples. It appears that the addition of salt to the non-vermiculite samples reduces the proportion of mesopore volume to total volume which would cause a reduction in accessibility to moisture vapour thus reducing performance under normal psychrometric conditions (STP) for an open TES system. SIM-3a, SIM-3c and SIM-3e display the most promising moisture vapour sorption isotherms with EMC values up to 1.9 kg/kg. The EMC of all SIM samples is significantly higher compared to their raw host matrices alone suggesting the addition of the salt is beneficial in terms of moisture storage. Examination of the moisture kinetics however resulted in a severe reduction in potential performance of SIM-3c due to its large t_{emc} response times. This shows the importance of proper material analysis including both characterisation of the sorption properties and thermal properties (E_d) for successful selection of open TES candidate materials. Energy density analysis suggests that SIM-3b had the highest E_d of all samples however as it has very limited adsorption potential this may not be available under standard working conditions. SIM-3a and SIM-3e appear to have excellent E_d coupled with good EMC and t_{emc} with their TGA analysis also suggesting significant mass loss in the working range $30 < T < 140$ °C. These findings suggest that both SIM-3a and SIM-3e appear to have very good potential for use in an open TES system.

Chapter 3.3 of the research focused on analysis of the hygrothermal cyclic behaviour of the SIM samples to validate these findings using a custom built experimental rig. The key findings of the study are:

- Zeolite provides the highest temperature lift at the beginning of the reaction in Cycle 1 due to the high amount of vapour adsorption and fast reaction kinetics. After the initial period (1-2 hours) however, as a result of the near surface micropores being blocked, the moisture adsorption rate and thus heat generation decrease sharply. Therefore it does not seem possible to achieve theoretical maximum output of Zeolite in long term applications.

- SIM-3a delivers a relatively lower amount of initial thermal power (68 W) compared to the Zeolite (105 W). Nevertheless it has much more steady hygrothermal cyclic behaviour and also provides the highest energy generation for the lowest vapour uptake (1.31 Wh/g). Whilst the silica gel had a similar hygrothermal stability to SIM-3a, its thermal power output (44 W) is insufficient to provide adequate TES performance.
- The 1st and 2nd law efficiencies are highest for Zeolite in first cycle. However in following cycles the ratio of energy/exergy supplied by this material and energy/exergy provided to it decreased dramatically. After the second cycle the efficiencies of all materials are almost equal.

In Chapter 3.4, the thermal performance of three different absorbents was experimentally investigated using two different testing rigs. The aim was to both compare material performance and rig performance. The main findings were;

- SIM-3a provided the best performance among the three tested absorbents in terms of thermal performance and multi-cyclic ability. It provided a temperature lift in the range of 30→3° C over a 20 hour period with an energy storage density of 290 kWh/m^3, which far exceeds conventional sensible (water, soil, concrete) or latent (paraffin) heat storage materials.
- The Gen2 test rig provided improved performance over Gen1. The results show the use of perforated tubes enhances both moisture (0.24→0.47 g_{wv}/g_{abs}) and heat transfer (69→373 W) allowing for higher and steadier temperature lift during the

discharging process. As the perforated tubes are embedded inside the absorbent in Gen2 rig, moist air is allowed to diffuse through the material uniformly, which is one of the current challenging issues in ‘open’ thermochemical heat storage systems.

- The final output achieved in this study is the evidence that there is a direct and linear correlation between the amount of water vapour supplied to the absorbent and the temperature lift. According to the experimental results, a linear correlation between ΔT - Δw with a slope of 2.64 was obtained. This outcome could be important for future THS process design and control.

Based on the obtained encouraging results with the use of perforated air diffusers in Gen 2 rig, an up scaled modular design, using the similar concept, was proposed in the next stage of the research (See: Chapter 5).

CHAPTER 5: DESIGN, DEVELOPMENT AND EXPERIMENTATION OF A MODULAR OPEN SORPTION PIPE REACTOR FOR SOLAR THERMAL ENERGY STORAGE

5.1 Introduction

Previous work presented in Chapter 3 and Chapter 4 suggests that THS has significant advantages when compared with the other heat storage methods including higher storage density, lower volume requirements and low heat loss (approaching zero). Despite the superior properties of THS system, novel reactor design, process design and sorption material development are key issues on future advancement of this method for solar thermal energy storage. In this context, within this chapter, it is aimed to experimentally investigate a modular sorption pipe (SP) reactor for solar thermal energy storage applications. Although a number of reactor and process based concepts were investigated in previous research, modular (multiple-unit) design of solid sorption heat storage systems is missing in the literature. Based on the obtained encouraging results with the Gen2 rig (Please see: Chapter 4.4), a modular scaled up version of it, using the same air diffusion mechanism has been built. Modular design of SP heat storage could ease operational control of the system and could minimize the need for advanced control equipment. Besides, heat/mass transfer could be enhanced with utilizing multiple SP units instead of a large volume of sorbent in a single storage tank.

In most cases, proving uniform air flow through the sorbent becomes difficult with the increase of the storage volume. This primarily occurs as a result of large pressure drop of air and due to the limitations of mass transfer in porous media. The proposed heat storage concept presents a solution to this problem, not only with the modular concept but also with the unique SP design using perforated air diffusers embedded inside the sorbent. This aspect enhances the contact surface area of air and sorbent, eases penetration of air through the sorbent also enables uniform air flow along the SP. Another novel feature of the proposed system is that it presents an interesting opportunity of integration with parabolic concentrators as a single module due to its cylindrical geometry. This feature of the sorption reactor could increase compactness, reduce system size and enhance solar utility with the use of a parabolic concentrator.

5.2 Selection of sorption material

Besides examining the developed reactor, presented research investigates the novel vermiculite-$CaCl_2$ (SIM-3a) composite matrix as a sorbent material. In Chapter 4, a range of candidate nano-composite materials capable of producing adequate exothermic thermochemical reactions for 'open' THS when hydrated were investigated. SIM-3a appeared to have excellent energy density, E_d coupled with good moisture uptake and response time to moisture uptake with TGA (Thermogravimetric analysis) also suggesting significant mass loss in the working range $30 < T < 140$ °C (Please see: Chapter 4.2). In addition it provided the most promising results in the developed small scale physical experimental setups in terms of average temperature lift, ΔT and total heat output, Q_t (Please see: Chapter 4.3 and 4.4). These findings suggested that SIM-3a appears to have very good potential for use in an 'open' THS system. Therefore it was selected as the sorption material to be used in the SP units. SIM-3a performance was also experimentally compared with the widely researched Zeolite 13X.

Obtained SEM images of raw vermiculite and SIM-3a were given in Figure 5.2.1. As seen in Figure 5.2.1 a, the raw vermiculite has a lamellar structure with micro-porous channels (nominal *Øpor*e = 3.68µm) in between the lamellas allowing large amount of salt to be impregnated. Figure 5.2.1 b shows the structure of SIM-3a. The structure was obtained with the impregnation of 43% wt $CaCl_2$ solution to the oven dried vermiculite, than drying the composite matrix until reaching anhydrous state. The SEM image of SIM-3a, obtained with 1000X magnification ratio shows the salt crystals loaded inside the horizontal nano-scale channels between the lamellas.

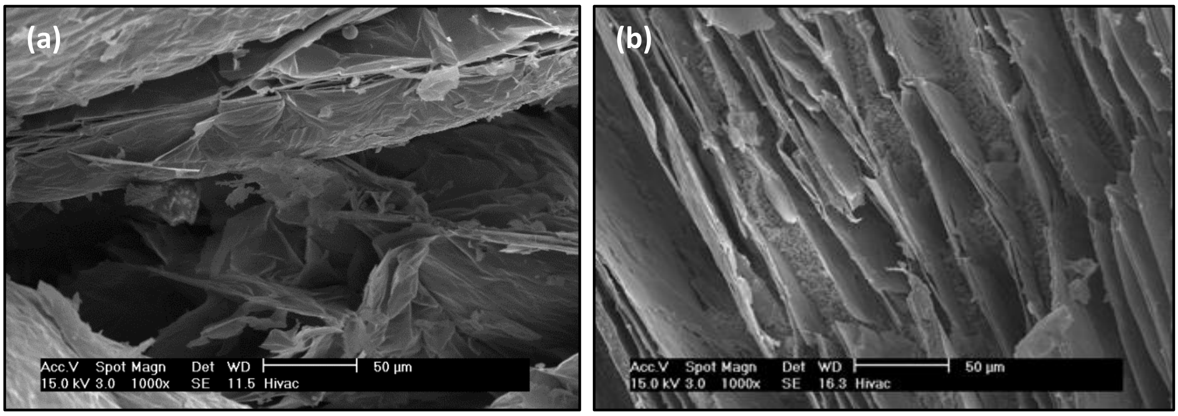

Figure 5.2.1 SEM images of (a) raw vermiculite, (b) SIM-3a

5.3 Concept and approach

The “open-sorption pipe” is a simple but a unique concept consisting of an outer and an inner (perforated) cylindrical shell and the sorption material filled in between. Its basic working principal is illustrated in Figure 5.3.1. As seen, air enters the perforated pipe from the open end at the bottom. In the discharging process, the humidity of the inlet air should be increased either by using an ultrasonic humidifier or using the evaporative method. The inlet air uniformly diffuses through the holes on the perforated pipe (See: Figure 5.3.1 a).

Moisture is adsorbed by the sorbent and sorption heat increases the air temperature. Hot air rises and leaves the SP from the top side. At the beginning of the sorption process, the salt in the matrix (SIM) is in its anhydrous form and stores energy thermo-chemically. Whilst the heat is extracted, the salt initially dissolves and turns to solid crystalline hydrates (SCH) and a high quantity of sorption heat is released. With the rising moisture level, sorption salt deliquesces and turns to an aqueous salt solution inside the porous matrix. In this stage, the extracted sorption heat is lower than the initial salt hydration (anhydrous → SCH) due to the much lower reaction kinetics and sorption rate. Once the sorbent is saturated (final state) the discharging process ends. Heat is supplied (e.g. solar, waste heat etc.) to regenerate the sorbent (charging cycle) back to anhydrous form (See: Figure 5.3.1 b).

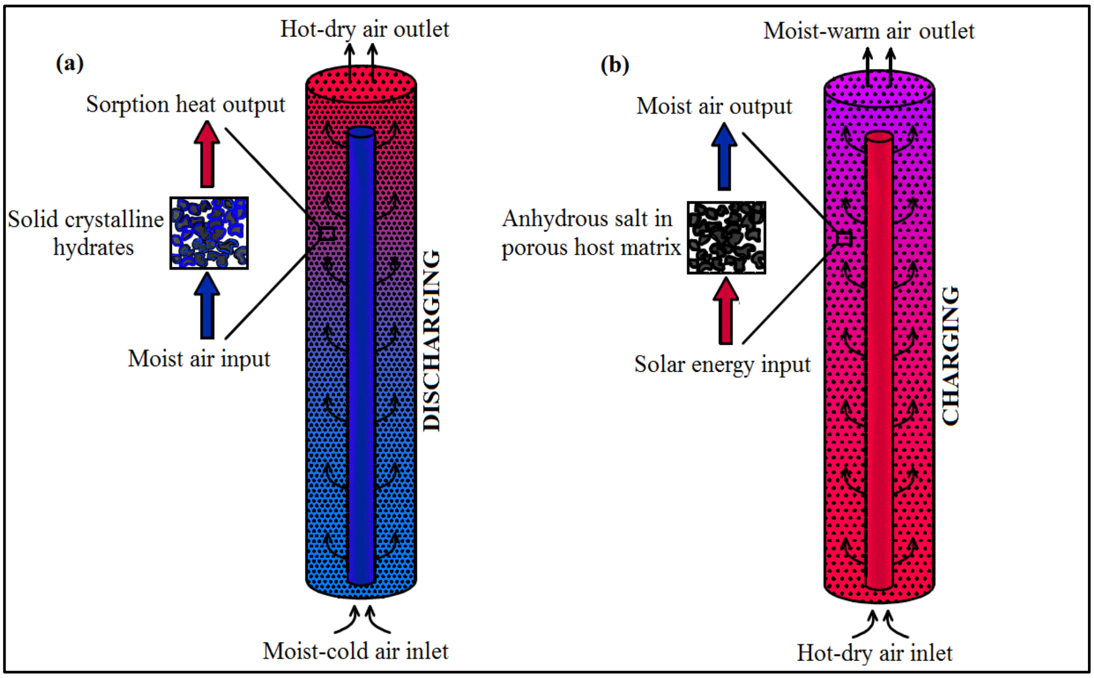

Figure 5.3.1 Operating principle of SP heat storage; (a) discharging cycle, (b) charging cycle

In present study, an electrical heating coil was used to investigate the regeneration potential of sorbent at a certain charging temperature under laboratory conditions. In real life conditions, solar air collectors could be used to heat the air for charging the sorbent either for short term (daytime: charging → night-time: discharging) or seasonal (summer: charging → winter: discharging) thermal energy storage (Yu et al., 2013).

For any particular domestic or residential space heating application with SP system; initially, heat load characteristics of the building and solar availability at the building location should be determined. Depending on the mismatch between the amount of building heat load and solar availability, either short term heat storage or seasonal heat storage should be chosen. For instance, in Northern European countries such as UK, Holland and Germany, the solar availability is minimal whilst building heat load is high in winter. Therefore seasonal design of SP heat storage system is the feasible option for utilizing the abundant solar energy during summer period. On the other hand, short term heat storage could be preferred in countries like Spain, Italy or Cyprus where solar energy is mostly available during day time in winter but there is heat load at night time. With SP system, depending on the selected storage duration, number and size of SP modules could be optimized considering the space availability of the building and the desired nominal thermal power from the heat storage.

In space heating operation, multiple SP units could be linked to each other where air flow across the units is controlled with automated valves. During discharging process, air is heated via SP, up to a certain desired temperature level (e.g. 35 °C) with optimized the moisture sorption rate and air flow rate. Hot air could be supplied to the building directly through vent holes. The moisture level of the sorbent inside the SP is measured instantaneously with humidity sensors and once the sorbent is saturated, automated valves directs the air to the next SP filled with sorbent in anhydrous form. In this way space heating with SPs will continue as long as there is heat demand in building. In charging mode (e.g. in summer), solar heated air (e.g. 70-80 °C) is supplied to the SP without moisture addiction. Hot air flow removes the moisture from the sorbent and moist air is exhausted to the environment. Optionally, waste heat of exhaust air could be extracted via a heat exchanger for utilizing in hot water applications thereby increasing the heat storage efficiency.

As an alternative concept, the purposed sorption pipe units could be integrated with compound parabolic concentrators as a compact solar-sorption module as illustrated in Figure 5.3.2. By this way solar energy could be concentrated on sorption pipes to heat the sorption material and remove the moisture. Ambient air flow supplied with a fan could also be used to increase desorption rate with the convection effect.

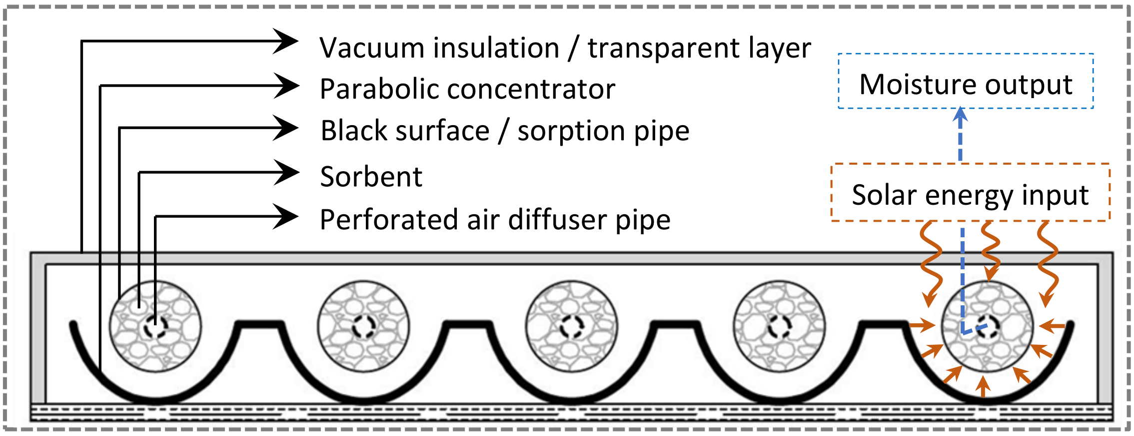

Figure 5.3.2 Integrated parabolic solar concentrator – sorption pipe heat storage unit

5.4 System description and experimental method

The schematic illustration of the charging and discharging operation of the developed testing rig is given in Figure 5.4.1 a and view of it is presented in Figure 5.4.1 b. In the system, a fan (1) at the inlet blows the air through the ducting. The flow direction of the air is controlled with butterfly valves (2) and could be either directed to the discharging line (down) where it passes through the evaporation unit (3) (discharging) or directed to the charging line where it passes through an electrical heating coil (4) (charging).

The evaporation chamber is an aluminium tank with the evaporative pads placed parallel to the air flow. A pump is used for circulating the water and a nozzle is placed inside the tank for spraying the water thus keeping the chamber humid.

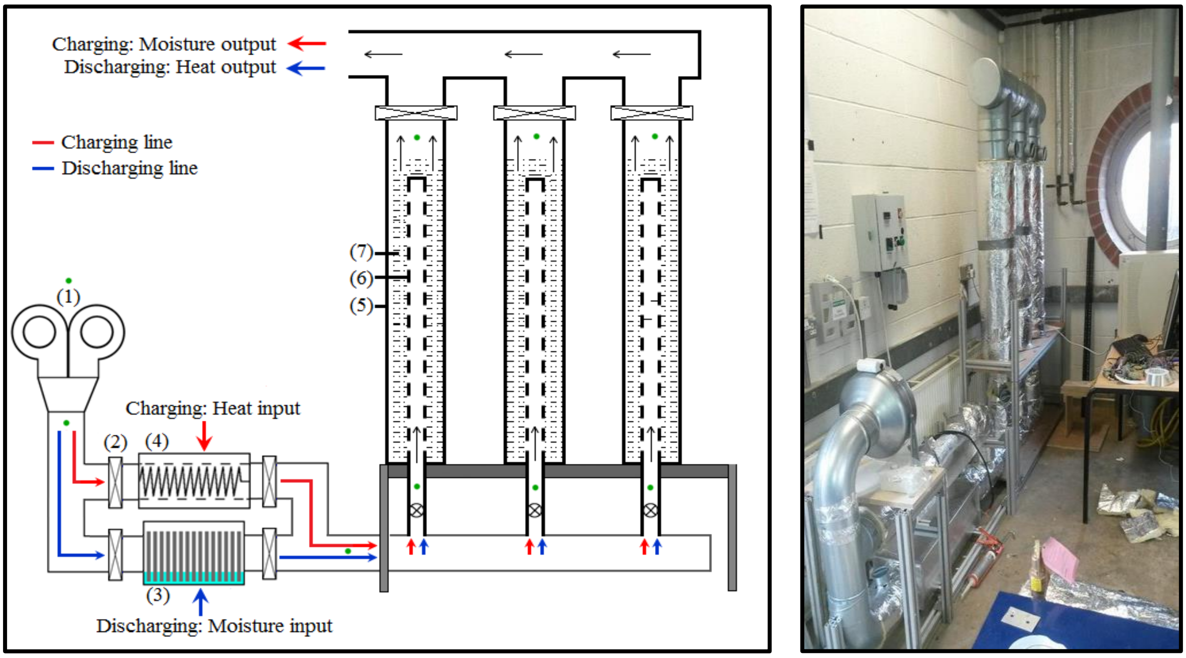

Figure 5.4.1 (a) Schematic illustration of the operation of developed testing rig in charging and discharging modes, (b) the view of the developed testing rig

The system consists of three identical SPs (5) and they could be operated either individually or together at the same time. Each pipe has a length, *l* = 1 m and diameter, *d* = 0.2 m. The perforated air diffuser pipes (6) also have the dimensions of *l*=1 m and *d*=0.05 m. The view and specifications of the perforated pipe is given in Figure 5.4.2. The space in between the sorption and air diffusion pipe gives the storage volume of sorption material (7) for each SP (29.4 litres), corresponding to a total storage volume of 88.2 litres for three pipes.

Perforated pipe specifications	
Hole diameter	3 mm
Distance between holes	3.6 mm
Hole layout	60 °
Length	1000 mm
Material	Stainless steel
Open area percentage	51%
Thickness	0.55 mm
Diameter	50 mm

Figure 5.4.2 View and specifications of the perforated pipe

To eliminate thermal losses to the external environment, the complete system is insulated using 25 mm thick, foil lined glass wool. Temperature and relative humidity (RH) were recorded using the EK-H4 Eval Kit for Temperature - Humidity Sensors from Sensiron, AG, Switzerland. Nine sensor locations were used as indicated in green in Figure 5.4.1 a namely ambient, system inlet, humidifier/heater outlet, SP1 inlet, SP2 inlet, SP3 inlet, SP1 outlet, SP2 outlet and SP3 outlet.

Aim and objectives of the study with the applied experimental procedure are presented in Figure 5.4.3. Initially the cyclic performance of SIM-3a under different inlet air moisture levels Δw was investigated. Later the thermal behaviour of the material under intermittent use was experimentally determined. Also a long cycle test was performed to analyse the maximum sorption heat that could be extracted in a continuous sorption process. Finally, the hygrothermal performance of SIM-3a was compared with Zeolite 13X.

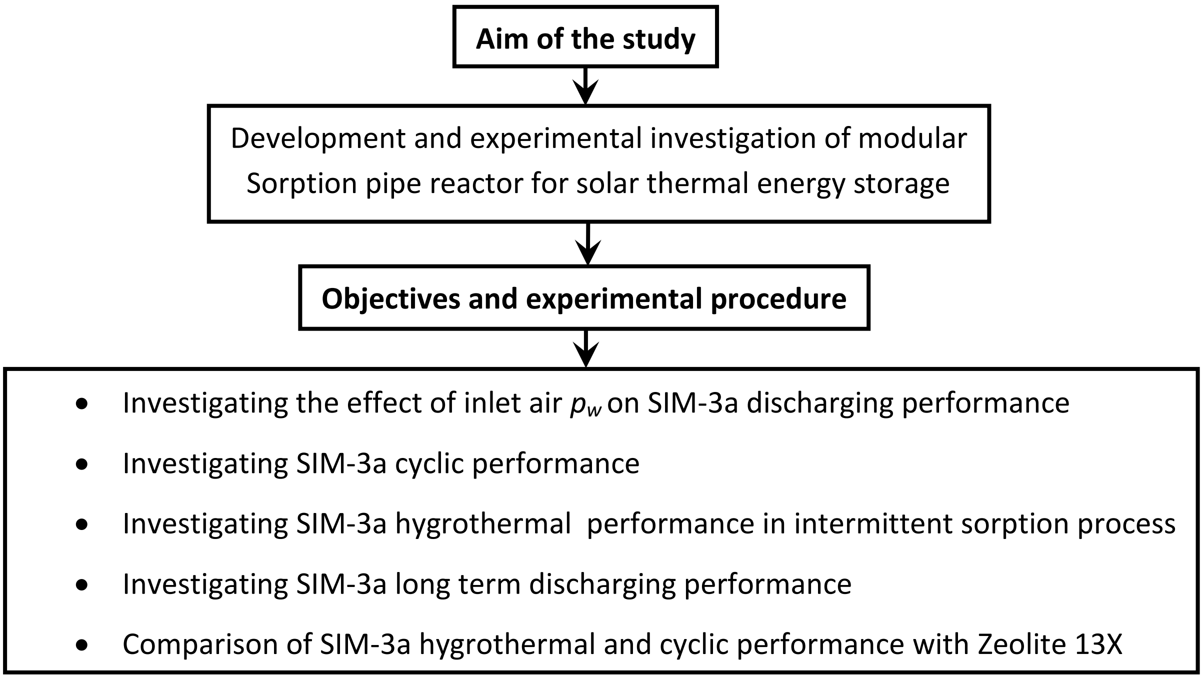

Aim of the study

Development and experimental investigation of modular Sorption pipe reactor for solar thermal energy storage

Objectives and experimental procedure

- Investigating the effect of inlet air p_w on SIM-3a discharging performance
- Investigating SIM-3a cyclic performance
- Investigating SIM-3a hygrothermal performance in intermittent sorption process
- Investigating SIM-3a long term discharging performance
- Comparison of SIM-3a hygrothermal and cyclic performance with Zeolite 13X

Figure 5.4.3 Aim, objectives and experimental procedure of the study

In the experimental research, energetic, exergetic and hygrothermal performance of the SP heat storage was investigated based on the collected experimental data (T, RH). In sorption heat storage process, instantaneous heat gain in discharging cycle is defined as the enthalpy difference of air between the SP inlet and outlet as defined in Equation 4.2. Similarly heat transferred to the sorbent during charging process could be obtained with Equation 4.13. Cumulative thermal energy output over a t_d (discharging) and energy input over a t_c (charging) period is calculated with the Equation 4.3 and 4.14 respectively. Instantaneous exergy gain in discharging process is the exergetic potential difference of the air at the sorption reactor inlet and outlet as expressed in Equations 4.10. Similarly instantaneous exergy input in charging process, which is equal to exergy transferred to the sorbent, calculates as in Equations 4.19 a-c. Integrating the Ex_g (See: Equation 4.10) and Ex_{tr} (See: Equation 4.19) terms over the t_d and t_c process durations, cumulative exergy gain (discharging cycle) and cumulative exergy transferred to the sorbent (charging cycle) are obtained as in Equations 4.11 and 4.20 respectively. The ratio of the energy/exergy gain in discharging cycle to the energy/exergy transferred to the sorbent in charging cycle defines the heat storage energetic (I. Law) and exergetic (II. Law) efficiencies, as illustrated in Equations 4.22 and 4.23.

The absolute humidity of air based on its RH and T in any particular moment, could be determined with the Equation 4.6. Vapour partial pressure of air is also calculated with the Equation 4.5. Sorption rate of moisture in any $t_{x,d}$ minute of discharging process could be determined with calculating the total amount of moisture adsorbed within that minute (See: Equation 4.7). Similar procedure is applied for determining the desorption rate in any particular $t_{x,c}$ minute of charging process (See: Equation 4.16).

The mass change of the sorbent, Δm, is the difference of its wet weight to the dry weight which is equal to the weight change material. The mass uptake of the sorbent over the discharging process is defined as the cumulative total of the moisture adsorbed over the duration of t_d (See: Equation 4.8). Similarly the mass loss due to vapour desorption, Δm_c, of the sorbent over the charging process is obtained with the Equation 4.17. The total mass uptake ratio in discharging cycle is defined as the moisture adsorbed per kg of dry adsorbent (See: Equation 4.9). Contrarily mass loss ratio is the expression of the moisture desorbed per kg of wet adsorbent as given in Equation 4.18

Based on the obtained E_{cum} (See: Equation 5.3), E_d of the sorption material could be defined in two ways. One of the definitions ($E_{d,m}$) is the E_{cum} per gr of adsorbed water vapour (See: Equation 4.4 a). The second definition of E_d gives the volumetric heat storage density ($E_{d,v}$) of the sorption material, which is the ratio of E_{cum} to V_{ads} (See: Equation 4.4 b).

5.4.1 Uncertainty analysis

The experimental uncertainties were determined by applying Gauss propagation law as explained in detail in Section 4.3.3. The independent parameters measured in each experiment are temperatures and relative humidities of; ambient (T_a, RH_a), system inlet (T_1, RH_1), humidifier/ EH outlet (T_2, RH_2), SP1 inlet ($T_{3.1}$, $RH_{3.1}$), SP2 inlet ($T_{3.2}$, $RH_{3,2}$), SP3 inlet ($T_{3.3}$, $RH_{3.3}$), SP1 outlet ($T_{4.1}$, $RH_{4.1}$), SP2 outlet ($T_{4.2}$, $RH_{4.2}$) and SP3 outlet ($T_{4.3}$, $RH_{4.3}$). MFR of air (m_a) was also measured for determining the heat transfer rates. Experiments were conducted by using following instruments: Thermocouples with the maximum deviation of ±0.3°C for temperature and ±2% for relative humidity and air mass flow meter with the accuracy of ±2%. Although temperatures and relative humidities at the inlet and outlet of three sorption pipes were recorded during the experiments, only the data relevant with the operating sorption pipe is considered in the analysis. It is obtained from the Equations (4.2), (4.3) and (4.22) that the heat storage efficiency (*η_I)* is the function of *T* and m_a measured in charging and discharging cycles, each subject to uncertainty:

$$\eta_I = f\left(T_{i,c}, T_{o,c}, T_{i,d}, T_{o,d}, m_{a,c}, m_{a,d}\right) \tag{5.1}$$

Total uncertainty for overall system efficiency can be expressed as;

$$w_R = \left[\left(\frac{\partial \eta_I}{\partial T_{i,c}} w_{T_{i,c}}\right)^2 + \left(\frac{\partial \eta_I}{\partial T_{o,c}} w_{T_{o,c}}\right)^2 + \left(\frac{\partial \eta_I}{\partial T_{i,d}} w_{T_{i,d}}\right)^2 + \left(\frac{\partial \eta_I}{\partial T_{o,d}} w_{T_{o,d}}\right)^2 + \left(\frac{\partial \eta_I}{\partial m_{a,c}} w_{m_{a,c}}\right)^2 + \left(\frac{\partial \eta_I}{\partial m_{a,d}} w_{m_{a,d}}\right)^2\right]^{1/2} \tag{5.2}$$

Total uncertainty rate affecting the heat storage efficiency of the proposed system was computed by using Equations (5.1)-(5.2). The estimation implies that total uncertainty in calculation of the η_I is found to be 2.83%.

5.5 Experimental results and discussion

5.5.1 Hygrothermal performance analysis of SIM-3a under different humidity conditions

A summary of the test results with the calculated hygrothermal performance indicators (e.g. mass uptake, heat output etc.) are presented in Table 5.1. A total of 14 cycles (t_r < 7 hours) of testing were performed with SIM-3a under varying inlet air humidity conditions. This configuration was mainly focused on analysing the relation between the moisture sorption rate (*Δm*; a function of *Δw*) and heat output (*Q;* a function of *ΔT*) of SIM-3a. This is an important aspect on determination of heat storage performance based on the vapour partial pressure, V_p, of supply air.

Table 5.1 Overall summary of the results of SIM-3a testing

	Cycle No.		t_r (min)	RH_i (%)	ΔRH (%)		T_i	ΔT (°C)		Dry mass (g)	Δm (g)	Δw (g/kg)	f_{dr}	E_{cum} (Wh)	Q(W)		E_d		Ex (W)	
				Ave.	Peak	Average	Ave	Peak	Average						Peak	Average	(kWh/m^3)	(Wh/g)	Peak	Average
Low Moisture	1	**Discharging – SIM3a**	180	76	73	56	13.7	20.2	14.4	5937	992	4.5	0.17	937	440	313	31.8	0.94	10.3	4.8
	2		322	79	78	62	16.5	28.3	16.8	5952	2442	5.8	0.41	1958	627	368	66.5	0.80	28.3	8.3
	3		180	62	68	52	20.1	30.2	15.8	5946	1489	6.8	0.25	1030	655	342	35	0.69	31.5	9.7
	4		180	90	81	71	15.7	26.5	19.0	5943	1468	6.8	0.25	1230	570	410	41.8	0.83	15.8	10.4
	5		188	53	57	42	19.5	21.8	18.1	5955	1186	5.2	0.20	1229	486	405	41.8	1.03	15.2	11.1
	6		364	67	61	49	14.4	29.9	20.5	5961	1918	4.3	0.32	2693	645	442	91.5	1.40	22.2	9.1
Medium moisture	7		307	73	73	69	18.7	31.1	25.1	5937	3859	10.4	0.65	2767	670	540	94.1	0.71	26.2	14.8
	8		351	80	80	72	17.5	26.0	18.2	5941	3890	9.2	0.66	2304	564	394	78.3	0.59	17.8	8.7
	9		340	80	80	75	18.1	29.4	22.4	5963	4434	10.8	0.74	2751	635	485	93.5	0.62	23.2	13.6
High Moisture	10		243	92	91	88	20.1	41.2	30.1	5955	4136	14.1	0.69	2628	951	666	89.3	0.63	56.3	34.2
	11		240	91	90	86	20.1	38.9	30.4	5961	4331	15.0	0.72	2638	837	657	89.7	0.61	46.7	36.7
	12		151	96	95	93	21.1	39.7	33.8	5951	2990	16.4	0.5	1844	861	730	62.7	0.62	54.2	42.3
	13		266	90	90	84	20.6	37.8	28.8	5961	3974	12.4	0.67	2752	820	622	93.6	0.69	54.4	33.7
	14		266	89	89	84	21.4	36.1	29.5	5967	3964	12.4	0.67	2957	774	637	100.5	0.74	49.0	33.9

Experimental results are divided into three groups as $\Delta w < 8$ gr/kg, $8 < \Delta w < 12$ gr/kg and $\Delta w > 12$ gr/kg. As seen in Table 5.1, for $\Delta w < 8$ gr/kg , ΔT average is in the range of 14.4 °C – 20.5 °C whereas for $8 < \Delta w < 12$ gr/kg it varies between 18.2 °C and 25.1 °C. For the condition of $\Delta w > 12$ gr/kg, the lowest and highest ΔT_{ave}*'s* are 28.8 °C and 33.8 °C across five performed cycles. These results prove an important fact on use of open THS in real applications. Considering that this system is aimed to be used for heat supply in winter conditions and air is used for transporting moisture to the material, a low ambient air temperature can limit the w_{air}, therefore substantially reduce the THS performance. Theoretically air can hold higher amounts of moisture with increasing temperature. As given in Table 5.2, for $T_a < 10$ °C conditions, air can hold less than 7.5 gr_{wv} per kg_{air} which could provide a ΔT of ≈15-20 °C, as experimentally demonstrated. On the other hand, for $T_a = 15$ °C, $\Delta T = 35$ °C could be achieved as a result of increasing water sorption rate (See: Table 5.2). This corresponds to a ≈2 times larger heat output.

Table 5.2 Water holding capacity of air at different temperatures

Air inlet temperature (°C)	Absolute humidity (Saturated, RH=100%) (gr/kg)	Achievable ΔT_p from sorption heat storage (°C)
5	5.37	≈10
10	7.57	≈15
15	10.53	≈25
20	14.47	≈35

The desired absolute humidity of the inlet air to the system is $w_i > 12$ gr/kg however this can only be provided in the case where $T_a > 18$ °C. Considering that the T_a is <15 °C in mild climates and even lower than 10 °C in severe climates in winter conditions, an external heat source such as ground or solar energy should be integrated to the system to preheat the inlet process air before entering the humidifier. Alternatively some of the hot output air could be recirculated as a solution to increase system efficiency.

The cyclic behaviour of SIM-3a for 6 cycles of low Δw (<10 gr/kg) and 5 cycles of high Δw (>15 gr/kg) are given in Figure 5.5.1 a-b. As seen from the figures, the high moisture adsorption rate of the material resulted in substantial temperature lifting where ΔT_p was higher than 36 °C and ΔT_{ave} was higher than 28 °C in all cycles (see: Figure 5.5.1 a).

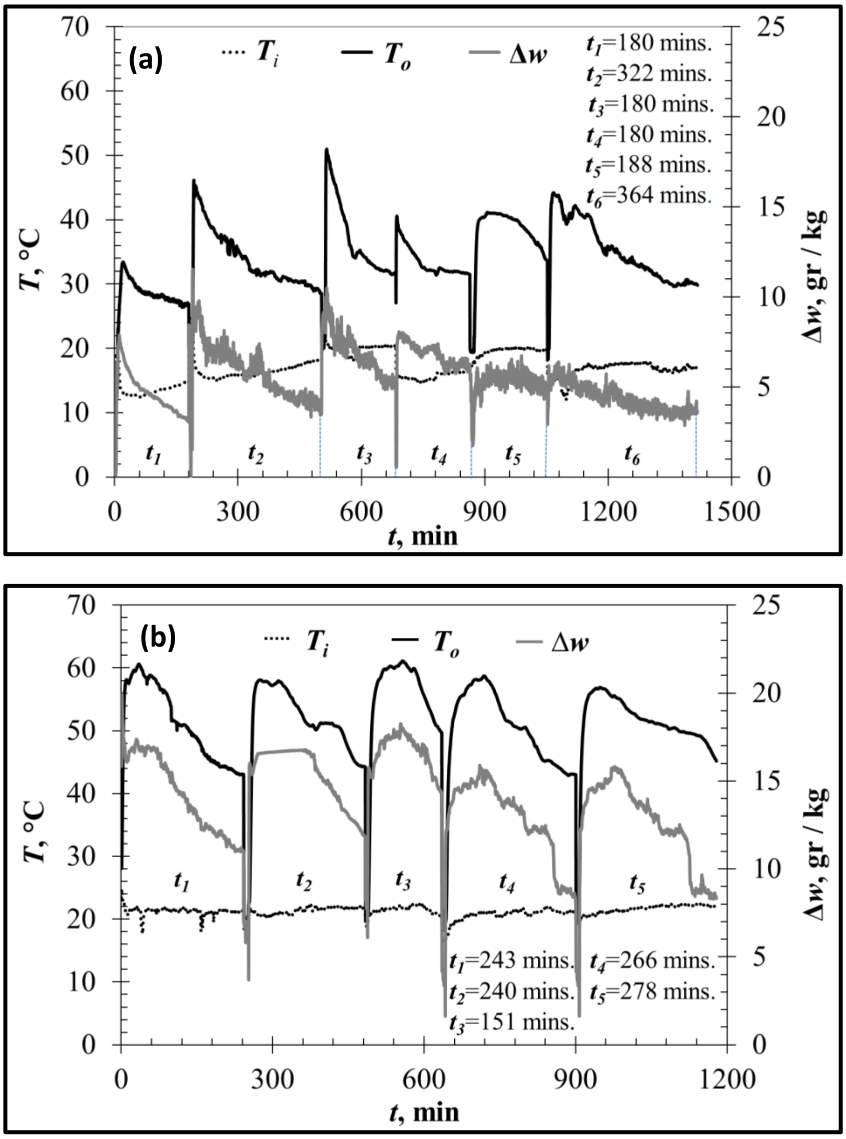

Figure 5.5.1 Cyclic behaviour of SIM-3a (a) with low moisture uptake, (b) with high moisture uptake

For the repeating cycles with lower Δw, the peak output temperature, $T_{o,p}$, was around 40 °C (See: Figure 5.5.1 b) which was 20 °C lower than the $T_{o,p}$ achieved with the high Δw cycles. In the testing with low Δw, although 2nd and 3rd cycles had higher peaks than the others, a sharp drop of ΔT was observed just after reaching the peak point in both. On the other hand, the first cycle had the poorest performance among all, due to the very low moisture uptake ratio ($f_d = 0.17$). In that cycle, as the T_i was in the range of 10-13 °C, the sorption rate remained low, therefore obtained ΔT was poor. When low and high Δw cycles are compared, it can be concluded that, a 5-10 °C increase of T_i allows for approximately a 30 °C increase in T_o as a result of higher moisture sorption rate.

Regression lines representing the relation between Δw - ΔT are given in Figure 5.5.2 for both the low and high humidity cycles respectively. The coefficients of determination (R-squared) were also represented. As seen from the Figure 5.5.2 a, in low humidity cycles, Δw varied in the range of ≈2-10 gr/kg corresponding to a temperature lift of ≈10-30 °C. In high humidity cycles (See: Figure 5.5.2 b), *highest* Δw was ≈18 gr/kg resulted with ΔT of ≈40 °C. With the reducing Δw from 18 →11 gr/kg, ΔT dropped to ≈20 °C.

During the sorption process, the target was to achieve regression lines with a low slope. However it is clear that in any kind of fixed – bed sorption reactor, moisture sorption rate cannot remain constant due to the limited sorption capacity of the material. Therefore, sorption rate will have a decreasing trend where ΔT will similarly drop over the process duration. Considering the dynamic heat load of buildings in real life conditions, it is necessary to determine the operating limits (e.g. relation of Δw-ΔT) of a particular heat storage system. This will help both to design and operate the heat storage system successfully with quick response to the fluctuating heat demand of the building. In addition, determining operating limits of the sorption heat storage system at high and low air humidity levels, allows optimization of the heat storage process. For instance, where intense and short term heat supply is needed heat storage could be operated with highly moist air. If the thermal energy is needed for longer periods but at a low intensity, air with lower moisture levels could be used.

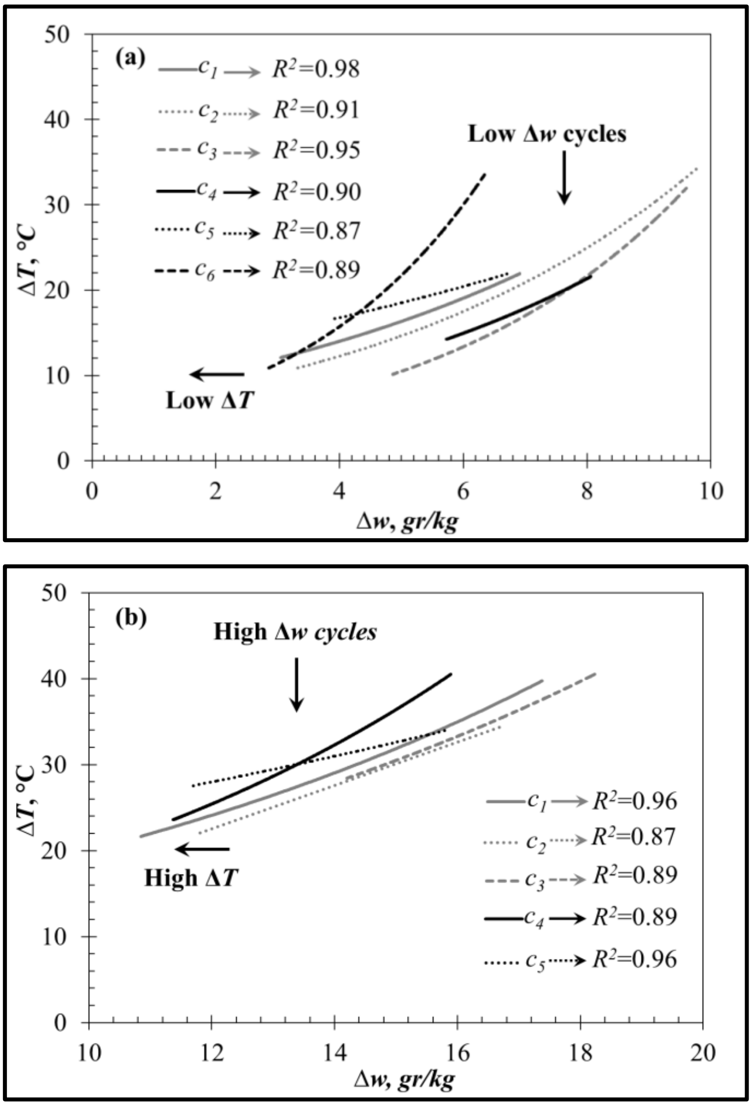

Figure 5.5.2 Fitted regression lines of air absolute humidity - temperature difference in SIM-3a testing (a) with low moisture uptake, (b) with high moisture uptake

In Figure 5.5.3 a, Q_{ave} and Ex_{ave} achieved with the cycles in the order of low → high Δ*w* were presented. Approximately a four times increase of Δ*w* (4.5gr/kg→16.4 gr/kg) led to a boost of Q_{ave} from 313W to 730W corresponding to a 2.5 times increase. Besides, with the increasing T_o, exergy of the output air, rose to 42.3 W from 4.8 W demonstrating a ≈10 times utility enhancement of the Ex_{ave}.

Although the Q_{ave} and η_{II} gradually rises with the increasing Δw, a sharp rise of Ex_{ave} *was* observed with the shift of Δw from 10.8 gr/kg to 12.4 gr/kg. The change of Δw in that range, led to a 2.5 times higher Q_{ave} and 2 times higher η_{II}.

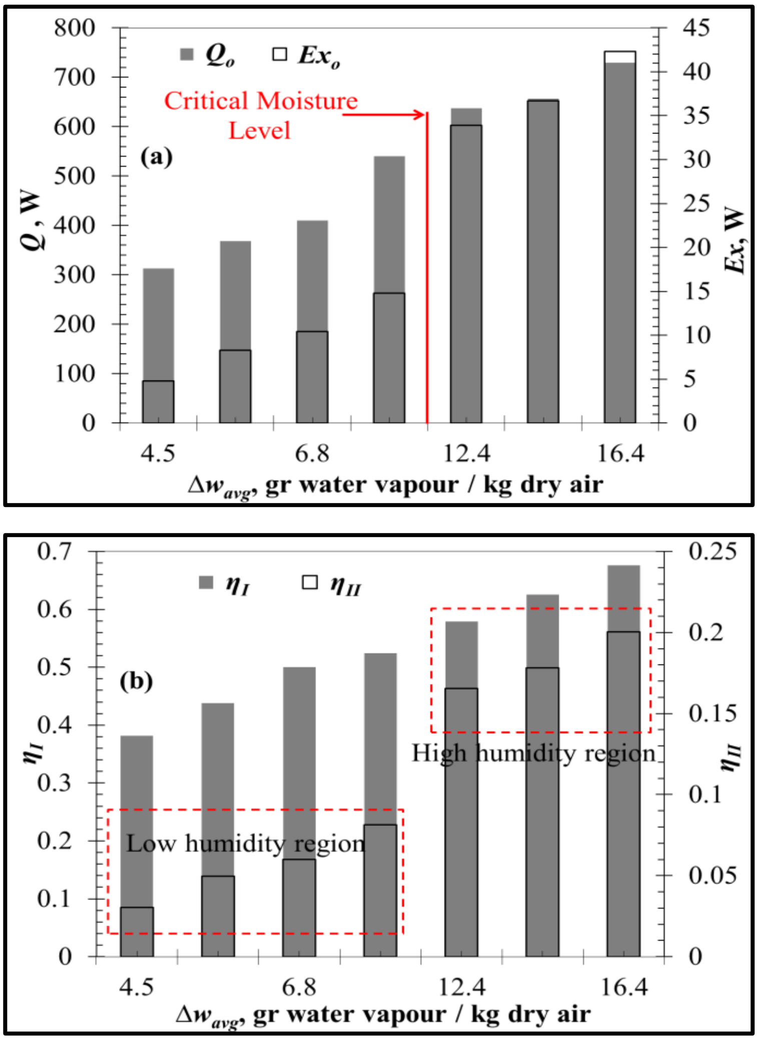

Figure 5.5.3 (a) Power and exergy output, (b) energetic and exergetic efficiency for varying absolute humidity difference levels (outlet-inlet) of air

In low Δ*w* (4.8 →10.8 gr/kg) cycles η_I and η_{II} were in the range of 39→51% and 3→8% whereas in cycles operating at high *Δw level* (10.8→16.4 gr/kg) substantial increase in both η_I (0.59→0.69) and η_{II} (0.16→ 0.20) were obtained (See: Figure 5.5.3 b). This outcome demonstrates that Δ*w*=11.2 gr/kg is the critical moisture level particularly when the exergetic efficiency, η_{II}, of the heat storage process is considered.

5.5.2 Hygrothermal performance analysis of SIM-3a under intermittent operational conditions

In real life conditions, the heat demand of a building dynamically changes as a result of the activity of occupants, internal and solar heat gains, and the varying ambient temperature. For this reason, building heating systems operates intermittently when heat supply is required. In this context, operational characteristics in intermittent use of sorption heat storage should be determined. Accordingly, this part examines the intermittent performance of SIM-3a to provide an insight on possibility of its intermittent use in real life applications. In order to realize this, a cycle of testing that consisted of four runs was performed (see: Figure 5.5.4). The cycle started with the use SIM-3a in anhydrous form and the cycle stopped at the end of the 4th, 8th, 11th and 16th hours of operation. The SP was kept hermetically insulated for 48 hours between each run. All runs were performed with the inlet air conditions of $T_i = 20$ °C and $p_{w,i}$ =21.6 mbar. The outlet air temperature over four repeating runs is presented in Figure 5.5.4. As seen, a peak of 60.9 °C was achieved in the first run following a sharp drop to 49.7 °C at the end of the 4th hour. The run was stopped and started again after 48 hours. In the second run, the outlet temperature reached to 48.2 °C, which was in a close approximation with the lowest temperature of the first run. The rate of temperature fall (gradient) in the second run was much lower than the first run. The lower rate of temperature drop indicates that the sorption material becomes more stable with the increasing moisture content. The third and fourth runs confirm this, as the gradient of T_o gets shallower in third run and is almost linear (horizontal) for the second half of the last run. The T_p in the 3rd run is only 1.5 °C lower than the T_l of 2nd run and similarly the T_p of the 4th run is 2 °C lower than the 3rd run.

The results showed that the intermittent use of sorption heat storage is possible and it does not have to be operated continuously until the sorbent is fully saturated. This fact indicates that it is possible to develop control strategies for a particular THS system to allow flexible usage of it. The only drawback of intermittent operation is the higher heat loss to the environment therefore wasting some of the sorption heat. The reason of this is, during the continuous operation certain amount of sorption heat goes to sensible heating of sorbent, absorbed moisture and the reactor material. However air flow partially recovers this sensible heat and only low amount is lost to the surroundings at the end of the discharging cycle. In intermittent operation, as the system starts/stops several times, in each cycle some of the heat is lost, which in total may represents a considerable amount.

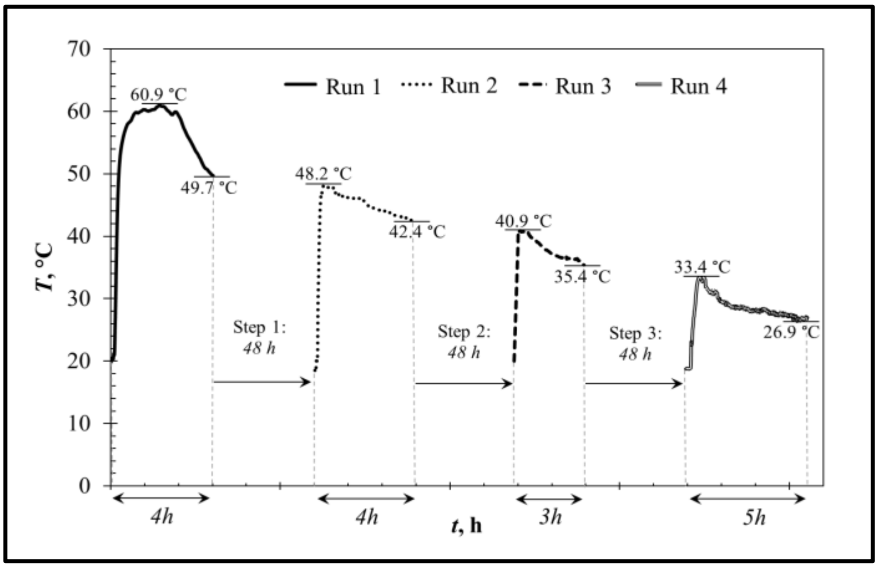

Figure 5.5.4 Intermittent operational performance of SIM-3a

5.5.3 Long cycle performance of SIM-3a

Investigating the extended performance of the sorption materials is important for determining the maximum potential thermal energy that could be extracted in a single cycle. Short repeating cycles facilitates understanding of the cyclic ability and durability of sorbents whilst allowing experimental comparison of the different sorbent performances. Short cycle testing helps to speed up the decision making process, such as quick elimination of materials with poor performance. This provides more time to undertake comprehensive experimental analyses on selected candidate sorbents. On the other hand, long cycle testing provides a better understanding of the full potential of the heat storage system. The long cycle testing results are presented in Figure 5.5.5 a-d. The cycle lasted 1300 minutes and a ΔT_p of 35 °C is achieved whilst ΔT_l was 16 °C at the end of the cycle. The *RH* and *T* variation of inlet-outlet air are given in Figure 5.5.5 a and 5.5.5 b respectively. The inlet air conditions were kept steady (T_i = 21°C and RH=75% → p_w=18.75 mbar) during the testing. Over the course of inlet moisture is fully absorbed, T_o remained steady at the peak point whilst *Q* and *Ex* also showed the same characteristics as they are a function of the ΔT. However, after the 4th hour, the descending adsorption rate led to a sharp drop of T_o from 58 °C → 48 °C. Similarly *Q* and *Ex* outputs also dropped in the range of 0.6 kW → 0.43 kW and 0.039→0.010 kW respectively (See: Figure 5.5.5 c-d). As a result, total energy and exergy gains from a single SP were calculated as ≈8.5 kWh and ≈0.41 kWh respectively. The energy storage density was determined as 290 kWh/m^3. Overall, it was found that modular use of three SPs could provide E_{tot} = 25.5 kWh with the V_s = 0.088 m^3.

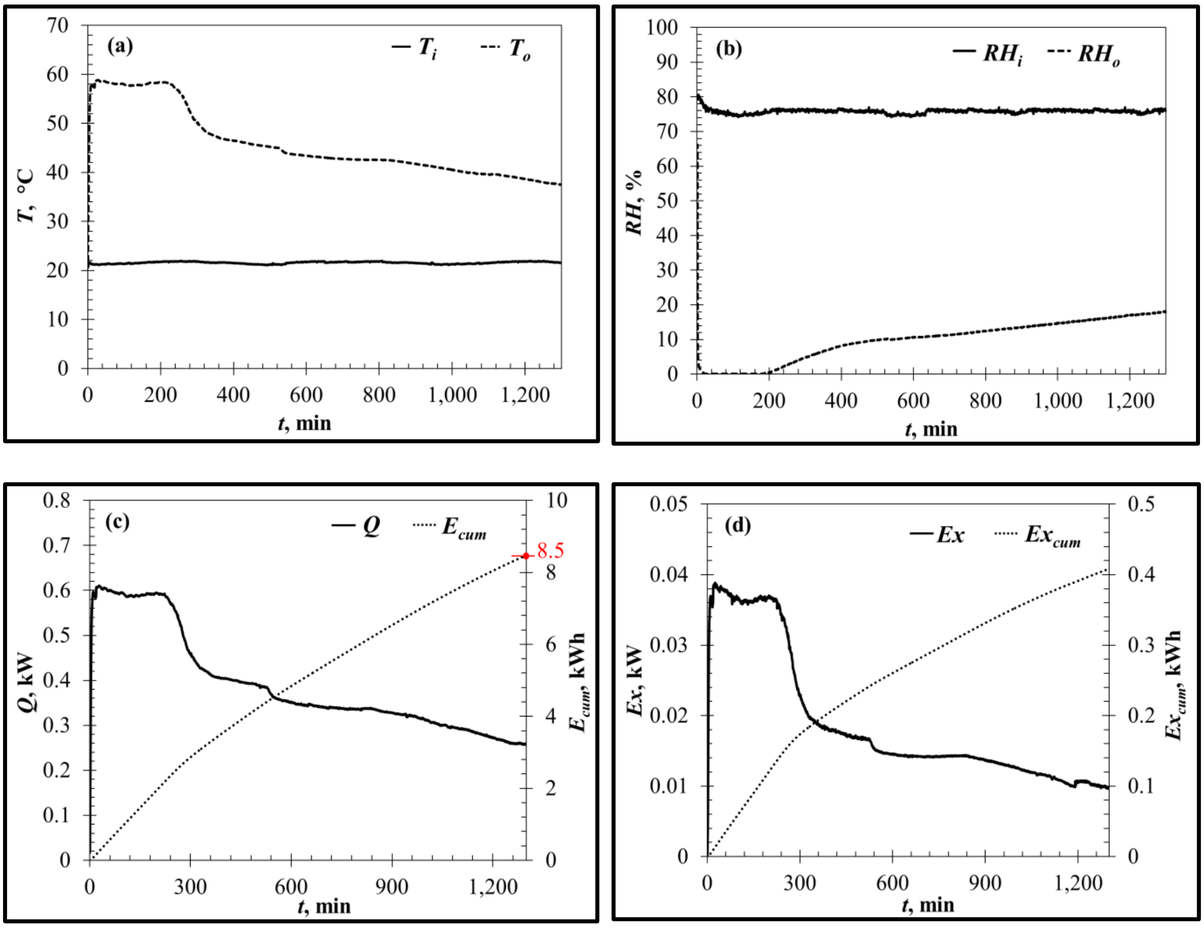

Figure 5.5.5 SIM-3a long cycle discharging performance for m_a:0.015 kg/s (a) temperature variation of inlet-outlet air, (b) relative humidity variation of inlet-outlet air, (c) thermal power and cumulative energy output, (d) instantaneous and cumulative exergy output

5.5.4 Comparative hygrothermal cyclic performance analysis of SIM 3a and Zeolite

Natural and synthetic Zeolites have been widely researched and these materials are regarded as favourable sorbents due to their advanced water sorption properties and high sorption enthalpy. Zeolites have not only been researched / employed for heat storage applications but also for air de-humidifying / drying and desiccant cooling processes. Although this material has remarkable properties such as fast sorption kinetics and high discharge temperatures, its regeneration is challenging due to the high temperature requirement. Therefore Zeolites could be useful for capturing waste heat in industrial applications where there is exhaust air or flue gas over 150 °C. However it seems highly unlikely to utilize these natural sorbents in the built environment for heat storage or air dehumidifying applications. In domestic buildings the opportunities are to store solar energy with the use of solar air collectors or to capture the waste heat from boilers. In addition where PV panels are installed, a PV driven heat pump could be used to regenerate the sorbent which could than be utilized for space heating. All these options could contribute to reduce energy consumption in domestic buildings but sorbents that regenerate at a reasonable temperature are required. In order to achieve this aim, new sorption materials which meet this target must be developed.

The four cycle discharging performance of Zeolite with T_i = ≈20 °C and $p_{w,i}$= ≈21.6 mbar is presented in Figure 5.5.6. Each cycle is performed over three hours and Zeolite is recharged at 80 °C for 6 hours to compare its performance with SIM-3a (See: Figure 5.5.1 b) for the same operational conditions.

Zeolite provided a remarkable performance in the first cycle where $\Delta T > 40$ °C *was* achieved over three hours where Δw was almost linear at 15 gr/kg until the end of the cycle. Although SIM-3a provided $\Delta T_p \approx 40$ °C*,* T_o dropped form 60→48 °C over the three hours testing in accordance with a drop of Δw*.* When only the first cycle is considered, where both the materials are fully-dry initially, it could be concluded that Zeolite has better sorption kinetics and provides a more steady thermal performance than SIM-3a. However with the applied T_{reg}= 80 °C, Zeolite performance dramatically drops in the following cycles whilst SIM-3a was much more durable. It is clearly seen from Figure 5.5.6 that, T_{180} was 59.6 °C in the 1st cycle test of Zeolite and it dropped to 31.9 °C in the 4th cycle. The T_{180} values for the 1st and 4th cycle for SIM-3a testing were 47.9 °C and 45.1 °C respectively. This could be explained with the sharp drop in the moisture sorption rate of Zeolite after the 2nd cycle due to the insufficient regeneration at T_{reg}=80 °C. Figure 5.5.6 shows that in 1st cycle, Zeolite sorption rate was high and steady. The 2nd cycle also started with a high sorption rate but after 150 minutes the sorption rate showed a descending trend causing a drop in outlet temperature. In the 3rd and 4th cycles, the period of steady sorption rate was much shorter where it sharply dropped after 120 min and 80 min respectively.

It could be concluded that; when both SIM-3a and Zeolite are fully regenerated Zeolite has better sorption kinetics and reaction enthalpy. However at the T_{reg} = 80 °C SIM-3a provides steady hygrothermal performance whilst Zeolite's sorption rate substantially drops leading to poor thermal power output.

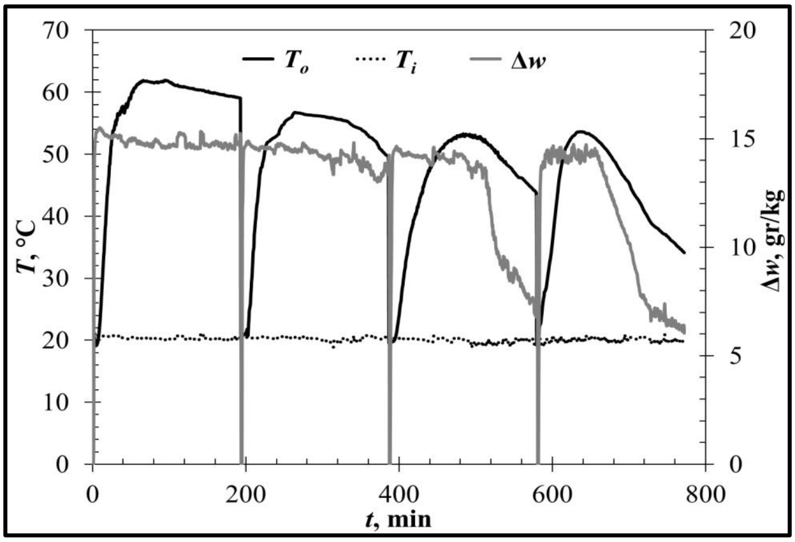

Figure 5.5.6 Cyclic hygrothermal performance of Zeolite

The thermal power and cumulative energy output obtained in four cycle testing of Zeolite and SIM-3a is presented in Figure 5.5.7 a-b respectively. In accordance with the experimental ΔT values (See: Figure 5.5.6), Q and E_{cum} of Zeolite gradually drop over the cycles. The Q > 800W obtained in the first cycle and varied in the range of 0.9 → 0.84 kW over three hours. In the 2nd, 3rd and 4th cycles, Q values were between 0.8 → 0.63 kW, 0.72 → 0.53 kW and 0.72 → 0.3 kW. On the other hand, in four cycles testing of SIM-3a $Q_{p\rightarrow l}$ values were 0.89 → 0.53 kW, 0.83 → 0.64kW, 0.82 → 0.54kW and 0.77 → 0.61kW in the order of 1st → 4th cycles respectively.

Similar to Q, the obtained E_{cum} for Zeolite dropped sharply over repeating cycles whilst SIM-3a provided much more steady energy output and E_{cum} varied in the range of 2.2 → 2.1 kWh.

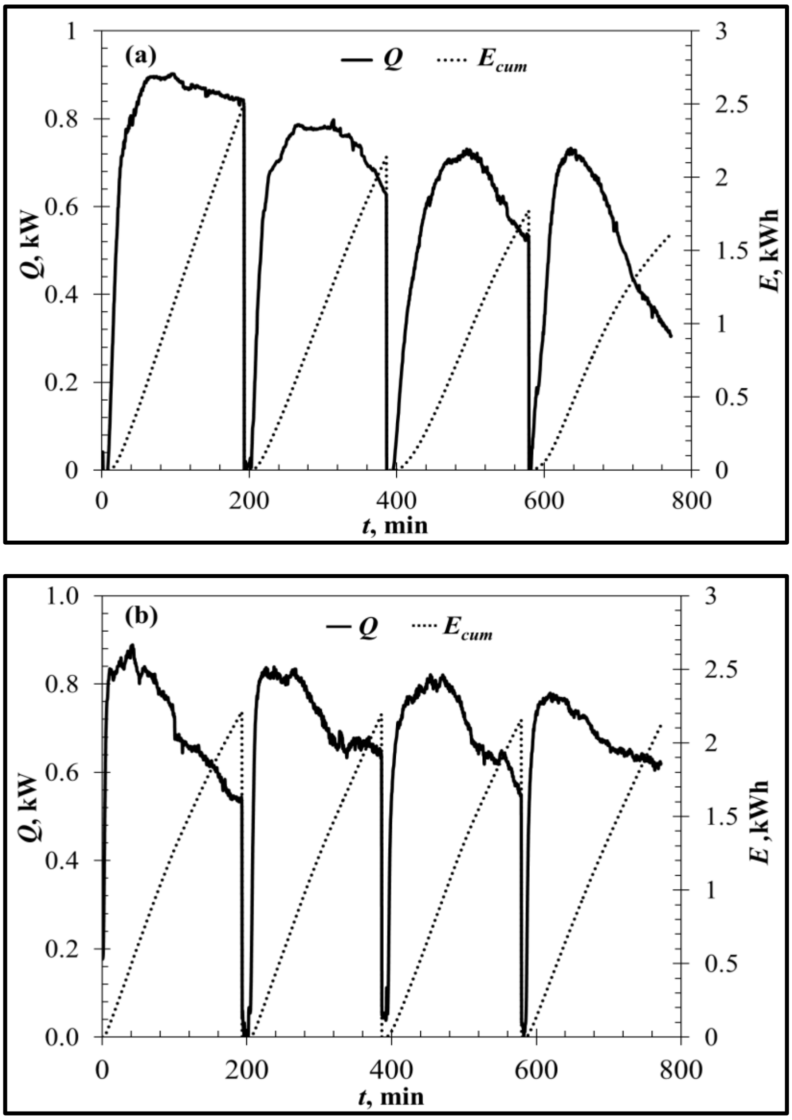

Figure 5.5.7 Thermal power and cumulative energy output in cyclic testing of (a) Zeolite, (b) SIM-3a

The overall summary of the four cycle testing results of SIM-3a and Zeolite are comparatively presented in Table 5.3. As seen from the table, the average values of performance indicators show a descending trend both for SIM-3a and Zeolite. This is most likely due to the residual moisture remained inside the materials after the charging cycles. Although thermal performance of both materials dropped with the repeating cycles, SIM-3a demonstrated a much steadier performance in comparison with Zeolite. E_{cum} and Ex_{cum} are varied in the range of 2.21 → 2.12 kWh and 0.13 → 0.11 kWh for SIM-3a whilst value of these parameters were between 2.50 → 1.62 kWh and 0.15 → 0.07 kWh for Zeolite. As presented in the table, Zeolite provided a better thermal performance than SIM-3a in the 1st cycle. However, due to poor regeneration capacity at *Treg* = 80 °C, its moisture sorption rate and sorption heat output dramatically dropped through the repeating cycles leading to lower η_I (0.48) and η_{II} (0.06). Contrarily a slight drop was observed with the SIM-3a efficiencies over repeating cycles where η_I and η_{II} were in the range of 0.69-0.64 and 0.21-0.14.

Table 5.3 Comparison of Zeolite and SIM-3a four cycle overall testing performances

	Material	**Q_{ave} (kW)**	**ΔT_{ave} (°C)**	**Δw_{ave} (g_{wv}/kg_{air})**	**E_{cum} (kWh)**	**Ex_{cum} (kWh)**	**η_I**	**η_{II}**
1st Cycle	Zeolite	0.78	36.1	14.7	2.50	0.15	0.72	0.25
	SIM-3a	0.71	32.3	15.2	2.21	0.13	0.69	0.21
2nd Cycle	Zeolite	0.66	30.8	14.1	2.12	0.13	0.66	0.20
	SIM-3a	0.68	31.5	15.0	2.19	0.12	0.66	0.18
3rd Cycle	Zeolite	0.55	25.6	12.2	1.77	0.09	0.54	0.09
	SIM-3a	0.67	30.3	14.7	2.15	0.12	0.64	0.17
4th Cycle	Zeolite	0.50	23.3	11.1	1.62	0.07	0.48	0.06
	SIM-3a	0.65	28.6	14.5	2.12	0.11	0.61	0.14

Comparsion of obtained η_I and η_{II} with different storage methods/materials in previous research is presented in Table 5.4. As seen from the table, η_I is slightly higher in SHS in comparison with the LHS and THS. In long term storage period, heat losses of SHS and LHS increase and this could significantly reduce the storage efficiency. On the other hand, THS could provide higher energetic efficiencies in longer duration (e.g. seasonal) of heat storage due to minimal heat losses in heat storage period. This aspect makes THS a promising option especially in seasonal heat storage applications to utilize abundant solar energy in summer period to be used in winter for space heating. In addition, η_{II} is generally higher in THS (See: Table 5.4) due to lower exergy losses and exergy destruction during heat storage phase.

Table 5.4 Comparsion of energetic and exergetic heat storage efficiencies obtained with different storage methods in the literature

Reference	**Type of Study**	**Material**	**Heat Storage Method**	η_I	η_{II}
(Hussain et al., 2004)	Num.	Ethlyene glycol	SHS	80%	0.5-14%
(Wang et al., 2009)	Exp	Water	SHS	76%	-
(Xu et al., 2015)	Num.	Paraffin	LHS	72%	-
(Utlu et al., 2014)	Exp.	Paraffin	LHS	62-74%	7-37%
Present study	Exp.	Vermiculite–$CaCl_2$ Zeolite 13X	THS THS	61-69% 48-72%	14-21% 25-6%
(Liu et al., 2015)	Exp.	WSS + 22.4 *wt%* $CaCl_2$ WSS + 9.6 *wt%* LiCl	THS THS	36-74% 40-66%	14-26% 16-21%
(Abedin and Rosen, 2012)	Exp	Zeolite (Open cycle) $SrBr_2$ (Closed cycle)	THS THS	69% 50%	23% 9%
(Koca et al., 2008)	Exp.	$CaCl_2.6H_2O$	LHS	45%	2.2%
(Johannes et al., 2015)	Exp	Zeolite	THS	34-54%	-
(Başçetinçelik et al., 1999)	Exp.	Paraffin	LHS	42%	3.3%
(Öztürk, 2005)	Exp.	Paraffin	LHS	40%	4.2%
(Gunerhan and Hepbasli, 2007)	Exp.	Water	SHS	-	3.3-4.4%

Besides, higher discharging temperature in sorption process is another aspect increasing η_{II} in THS applications. In addition to the characteristic properties of different storage methods, system design and size, heat storage material, storage duration and insulation material have significant impacts on heat storage efficiency and should be carefully selected and optimized in any specific application.

Figure 5.5.8 shows the cumulative mass change, Δ*m*, and sorption/desorption rate, *z,* of Zeolite and SIM-3a over equal amount of discharging and charging time. As seen Zeolite adsorbs 13 gr/min over 5 hours when it is initially in its fully dehydrated state. SIM-3a has a sorption capacity of 12.1 gr/min, however there is a linear drop and z_s was 9.1 gr/min at the end of 5th hour explaining the linear drop of SIM-3a thermal performance during discharging cycle. The total mass uptake of Zeolite was found as 3.9 kg whereas for SIM-3a it was found as 3.3 kg. On the other hand, there is a significant difference in desorption kinetics of Zeolite and SIM-3a at T_{reg} = 80 °C and $p_{w,i}$ = 0.18 mbar as seen from the figure.

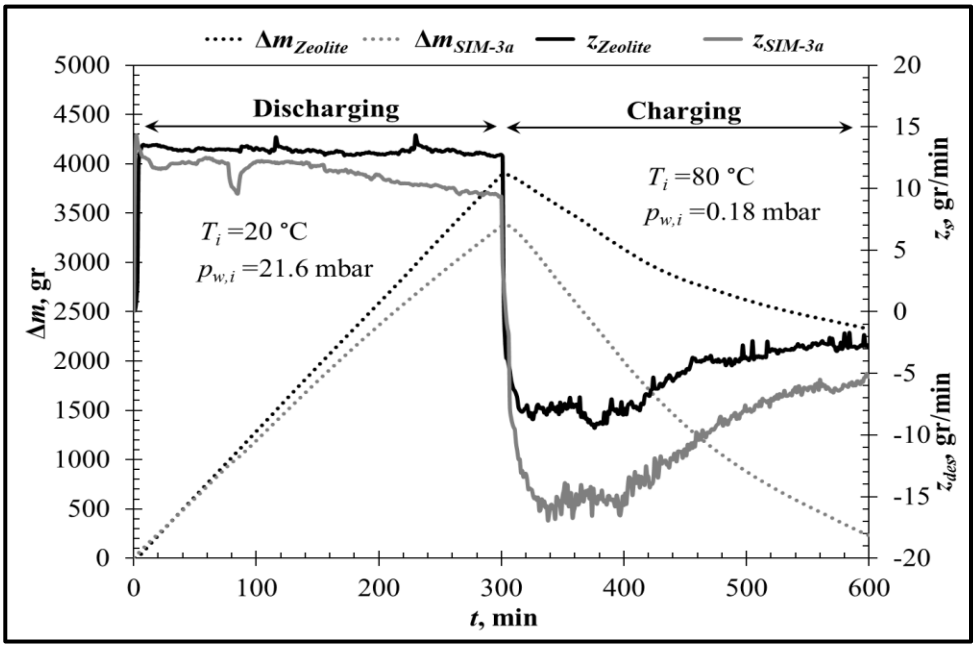

Figure 5.5.8 Mass change and sorption/desorption rates of Zeolite and SIM-3a in discharging and charging cycles

Over the course of charging, peak z_{des} of Zeolite was 9.3 gr/min whereas the desorption rate of SIM-3a was 16.2 gr/min which is almost double that of the Zeolite. Accordingly 3.13 kg of the moisture was desorbed form SIM-3a corresponding to f_{des} = 0.93. However, with the same charging procedure, only 1575gr of moisture was removed from Zeolite which represented f_{des} =0.4.

Realistically, in a domestic environment, 80 °C seems an achievable upper limit of air temperature with the current solar collector technology in warm climates. In cold/severe climate conditions it is harder to achieve this temperature range directly with solar energy. Even though it is not achieved, sorbents having T_{reg}=80 °C could still benefit from solar energy (e.g. 20 →60 C °) and the temperature could be boosted to 80 °C using a PV powered heat pump or thermoelectric module as the required additional energy is low (e.g boosting the air temperature 60→ 80 °C). However in the case of Zeolites ($T_{reg}>150$ °C), utility from solar energy remains relatively low (e.g. the ratio of auxiliary heat supply to the solar input) as an additional temperature lifting of $\Delta T > 90$ °C is required. Therefore developing sorbents that could be regenerated at low temperature is the key for benefitting from sorption heat storage in domestic buildings. The encouraging results achieved in this study push for further research into new sorption materials and new reactor designs required to obtain commercial level thermochemical heat storage systems.

5.6 Conclusions

In this chapter a novel open SP using SIM-3a was experimentally investigated for solar thermal energy storage. System examined under several operational configurations also comparative analysis between SIM-3a and Zeolite was performed.

According to the study results;

- SP reactor provided promising results in terms of high adsorption and desorption rate (*z >10 gr/min.*) and temperature lifting, ΔT > 30 °C. Modular design enables upscaling the system with increasing the number of SPs at known steady SP heat storage characteristics.
- Changes in absolute moisture levels results in a large increase of output temperature lift and power (e.g. for a 3 hour discharge: From as low as 21 °C up to 41 °C and 39 kWh/m^3 up to 123 kWh/m^3).
- Using absolute moisture levels (Δw) allows us to define a critical moisture level for each material used. For SIM-3a (Vermiculite – $CaCl_2$) the critical moisture level is ≈ 11.2 g/kg. This should not alter between different reactor designs.
- SIM-3a has good cyclic ability, durability and no degradation over repeating cycles and provides substantial temperature lifting in discharging process. η_I and η_{II} were found in the range of 0.69-0.64 and 0.21-0.14 in four cycle of testing. Additionally, Vs = 0.088 m^3 of SIM-3a provided E_{cum} = 25.5 kWh corresponding to E_d = 290 kWh/m^3 which is ≈6 times larger than $E_{d,water}$.
- In intermittent operation, each run provided a T_p equals to the T_l of the previous run. Although intermittent use could be an option for SP operation, continuous mode is more efficient due to lower heat losses.
- Zeolite provided higher thermal performance than SIM-3a in the initial testing. However due to the poor desorption kinetics, at T_{reg} = 80 °C its performance substantially dropped in cyclic testing (2.5 → 1.62 kWh). On the other hand SIM-3a provided durable performance with the same T_{reg} (2.21 → 2.12 kWh).

CHAPTER 6: THEORETICAL AND EXPERIMENTAL FEASIBILITY STUDIES ON THERMOCHEMICAL HEAT STORAGE UNDER MEDITERENNEAN CLIMATE CONDITIONS: NORTHERN CYPRUS CASE

6.1 Introduction

The Island of Cyprus has a remarkable solar potential (see: Figure 6.1.1) when compared with most of the developed EU countries such as Germany and UK. This abundance of dense solar radiation should be fully utilized, especially during the summer months when it is at its peak. Due to historically insufficient economical outlay, alongside the technical and managerial background of the country, usage of solar energy is largely limited to flat plate solar collector technology for water heating purposes (Ibrahim and Altunc, 2012). Generally, these systems can only be used from March to November as the solar availability in winter is inadequate to heat the water to a usable level (> 40 °C). There are some cases where small size water storage tanks are used to store heat sensibly however, these tanks are rarely insulated and thus provide little or no advantage in utilizing the solar resource effectively. In NC, it is traditionally direct electrical heaters that are employed for space heating purpose. Whilst water heating accounts for 45 % of end energy usage, space heating constitutes the second highest energy share (28 %) in the residential sector (Atikol and Güven, 2003, Atikol). The reason for this can be due the large total area of residential buildings which, in general, can be 150 to 200 m^2 and usually consist of many uninsulated building components (*i.e.* walls, floors and roofs) with common usage of low efficiency single glazed windows.

There are currently no residential or commercial applications for utilizing solar energy for space heating during the winter months in NC (Evcil, 2012) and, even with the abundance of energy during the summer period, it cannot be employed in winter for this purpose because of the seasonal mismatch.

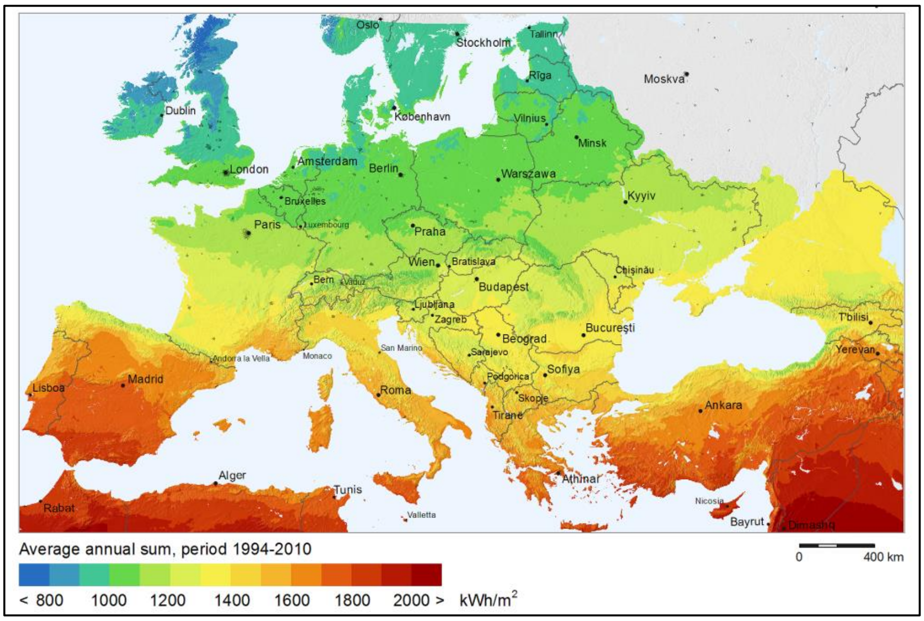

Figure 6.1.1 Global horizontal irradiation in European countries (PVGis, 2015)

Thermal heat storage (THS) systems should be the main driving force for seasonal storage of solar energy and usage of it during winter conditions. This will significantly contribute to reducing the usage of electricity and thus fossil based fuels in the residential sector for space heating applications. THS systems bring the advantage of storing summer heat, densely with very low heat loss and space requirements (Aydin et al., 2015a, Yu et al., 2013) or even storing it during sunny days of winter for utilizing at night time. Chapter 4 and 5, in which sorption material and reactor development were performed, consistute the basis of the research presented in this chapter. SIM-3a and the sorption unit using embedded air diffusers were considered as the sorption material and reactor concept in the proposed seasonal THS.

This chapter covers theoretical and experimental studies with the aim of evaluating applicability of THS systems in Cyprus. First objective of the chapter is to investigate feasibility of seasonal THS application under Cyprus climate conditions with consideration of technical, environmental and economic aspects. Another objective is to develop and examine the performance of a novel sorption pipe unit integrated with a solar concentrator under real climate conditions of Cyprus. The performed work in order to meet the above given objectives were presented Section 6.2 and 6.3 respectively.

6.2 Theoretical analysis of the potential for thermochemical heat storage under Mediterranean climate conditions: Northern Cyprus Case

6.2.1 Introduction

In this study, the suitability of THS for increasing the solar share in space heating applications for NC climate conditions is investigated. Within this context, firstly, energy trends in NC (past and future) are discussed. THS potential is evaluated through the analysis of material based experimental results (*i.e.* COP, output temperature, temperature lift and heat storage density) of the selected THS material (SIM-3a). The year round heating load of a selected building in NC with the solar heat gain of the same building from 8 m^2 solar air collectors is simulated. In the final part of the present research, an integrated solar THS system applicable to NC conditions is proposed and discussed in terms of its technical and economic feasibility.

6.2.2 Energy trends in Northern Cyprus

North Cyprus is part of a small island located in the eastern Mediterranean Sea. According to the census carried out in 2006 by the NC government the population is circa 265,000 with a total number of residential customers of ≈ 80,000 (KIBTEK, 2015). The rate of increase in demand for electricity has doubled from ≈ 7 % in 2004 to > 30 % during recent years due to population and construction growth in all geographical regions. The total energy consumption, E_c in 2009 / 2010 for NC was 913 GWh whereas for 2011 / 2012 it was 1256 GWh corresponding to a 37 % increase.

The residential sector in NC currently accounts for ≈ 35% of total national energy consumption (see: Figure 6.2.1 a) with the share of water and space heating being the two heaviest loads at 45 % and 28 % respectively (see: Figure 6.2.1 b). In total, 73 % of the energy demand of a building in NC is thermal (*i.e.* space heating and hot water). As seen in Figure 6.1.1, the remarkable solar potential of Cyprus could be utilized to reduce fossil fuel consumption for space heating and hot water purposes. Feasibility studies on thermal energy storage systems for NC should be carried out as this technology has the potential to store solar energy and increase the solar fraction for building thermal energy consumption. Furthermore thermochemical heat storage (THS) brings an advantage of storing solar energy in summer and using it in winter without any heat loss or degradation.

The high share of overall energy consumption attributed to the residential sector is primarily due to the dependency on fossil fuels for domestic activities such as space and water heating with the majority of water heating in NC provided by either electricity or Liquefied Petroleum Gas (LPG). Central or district heating systems are rarely used in NC as a high percent of buildings are detached and winter climate conditions are not extremely cold. For this reason mainly air sourced heat pumps (HP) or direct electrical heaters are used to provide heating to each room of a dwelling separately. Additionally, in some dwellings, LPG sourced single heating units are also used. Although wood burning stove or fireplaces were popular in the past, these units are currently rarely used due to health and safety issues, environmental pollution and user heavy operating conditions such as temperature control.

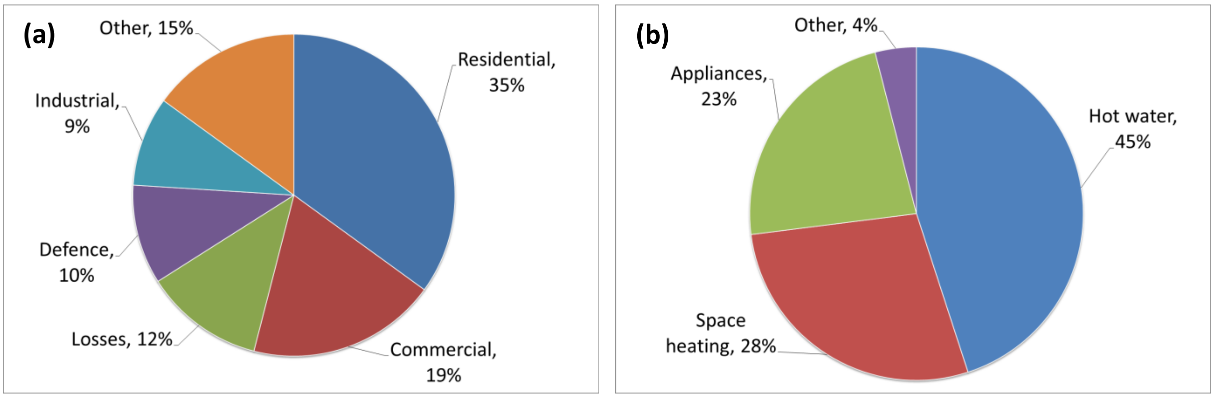

Figure 6.2.1 (a) Share of national energy consumption in NC and (b) Share of energy consumption in the residential sector in NC (adapted) (Atikol and Güven, 2003)

NC does not have any oil or natural gas based fossil sources and imports all fuels types required for electricity generation, residential and commercial needs from other countries. Increases in population and recent industrial developments have caused a significant rise in demand for electricity and fossil fuel consumption (KIBTEK, 2015). There has also been a sharp rise in electricity unit prices. In 1990 electricity was 0.08 €/kWh whereas the current unit price of electricity is 0.22 €/kWh, representing an increase of 275 %. Energy consumption in residential buildings has also increased almost 4 fold from 112 GWh to 435 GWh over the same period. NC has very good solar potential which should enable up to 100% of thermal energy demand of a building to be met. Therefore the importance of the link (and mismatch) between solar energy and the heat load of a building should be understood and innovative methods to store heat with THS materials developed. This will start a transformation in NC towards a 'green' island and a cleaner and safer environment to live.

6.2.3 Materials and methodology

To evaluate the technical, economic and environmental feasibility of 'open' THS systems under NC climate conditions, initially, the annual heat load of a real residential building was simulated. The annual solar heat gain was obtained assuming a total collector surface area, A_{coll}, = 8 m^2. The THS material was selected as SIM-3a (*i.e.* Vermiculite impregnated with $CaCl_2$) from previous research. This absorbent composite has many remarkable properties such as a high experimental heat storage density, E_d >200 kWh/m^3, good cyclic ability with little hysteresis, low regeneration temperature, T_r < 90 °C and is non-toxic. The storage density of SIM-3a is used to calculate the overall dimensions of the proposed TES system.

6.2.4 System description

A schematic diagram of the proposed THS system in charging mode is shown in Figure 6.2.2. The system is comprised of solar air collectors (1), an evaporative humidifier (2), an above or underground THS unit (3) and internal heat outlets (4) in the building (5). In the summer period (*i.e.* June to August), the system operates in charging mode, as an open cycle, where the solar collectors supply hot and dry air to the THS (T_r = 80 → 90 °C). The hot air charges the system by heating the THS material and removing any moisture. The outlet air from the THS during charging is moist and warm (T_{out} = 50 → 55 °C). Although there is not any heating demand in summer conditions, there is a requirement for hot water, particularly after sundown. Therefore any heat from the outlet air can be transferred to a hot water tank (6) via a heat exchanger before dumping waste heat to the ambient air.

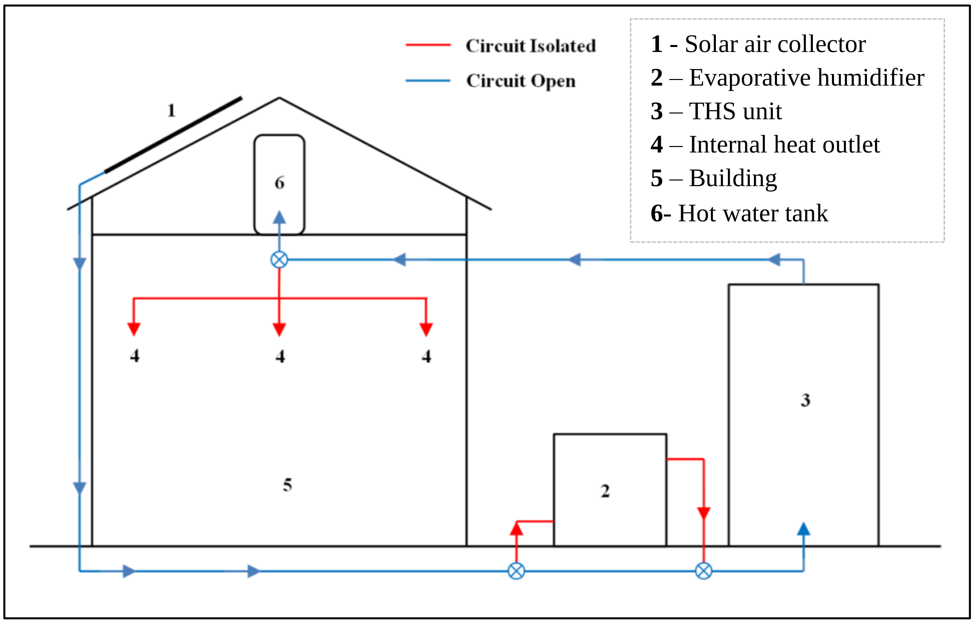

Figure 6.2.2 Schematic of the seasonal solar driven THS in charging mode

During the winter (*i.e.* December to February), the available solar energy is not sufficient to meet the total heating demand of the building during the day. In addition after sundown when heating demand peaks, solar energy is not available. In this instance (*i.e.* discharging mode) the THS is used to supplement any heat gained from the collectors providing adequate heat to the building (see: Figure 6.2.3).

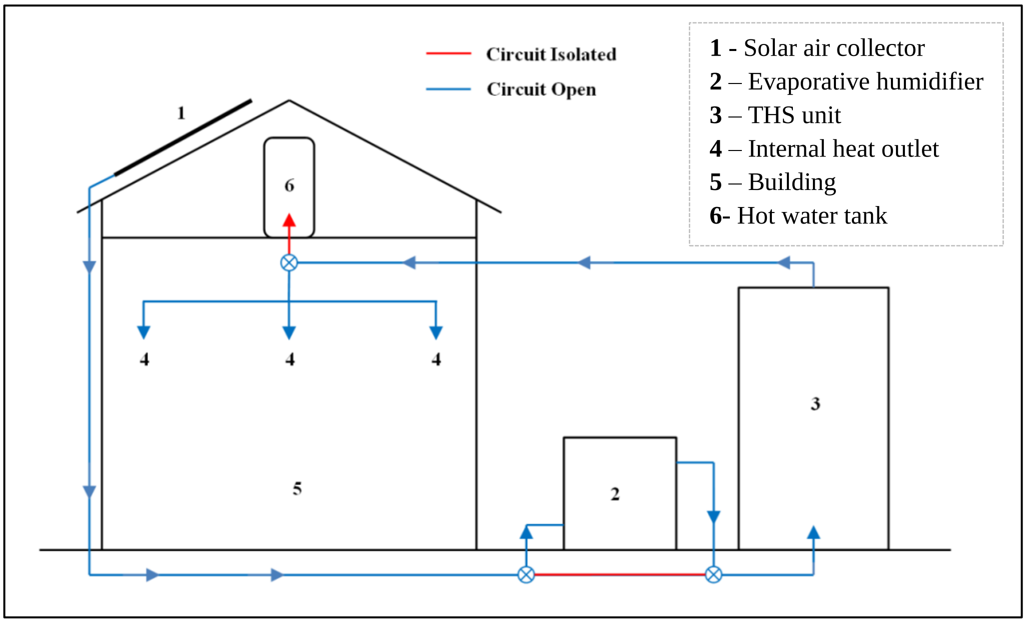

Figure 6.2.3 Schematic of the seasonal solar driven THS in discharging mode

Placing the store underground would also minimize heat loss to the surroundings enabling longer heat generation or dwell times, t_{dwell} from the THS whilst also minimizing space usage inside or around the building. A detailed illustration of system components and system operation is presented in Figure 6.2.4. In this setup, the system operates in 'closed' cycle mode where fan-coils are used to transfer the thermal energy thereby to minimize any waste heat. As an evaporative humidifier is used to introduce moisture to the input airstream, heat pipes can be used to gain some heat from the ground to ease evaporation of water in the humidifying tank (see: Figure 6.2.4). The relative humidity (*RH*) of the input air is increased to *RH* = 80 % and blown to the THS.

The THS system consists of divided units with perforated diffusion tubes in each unit as schematically described in Figure 6.2.4.

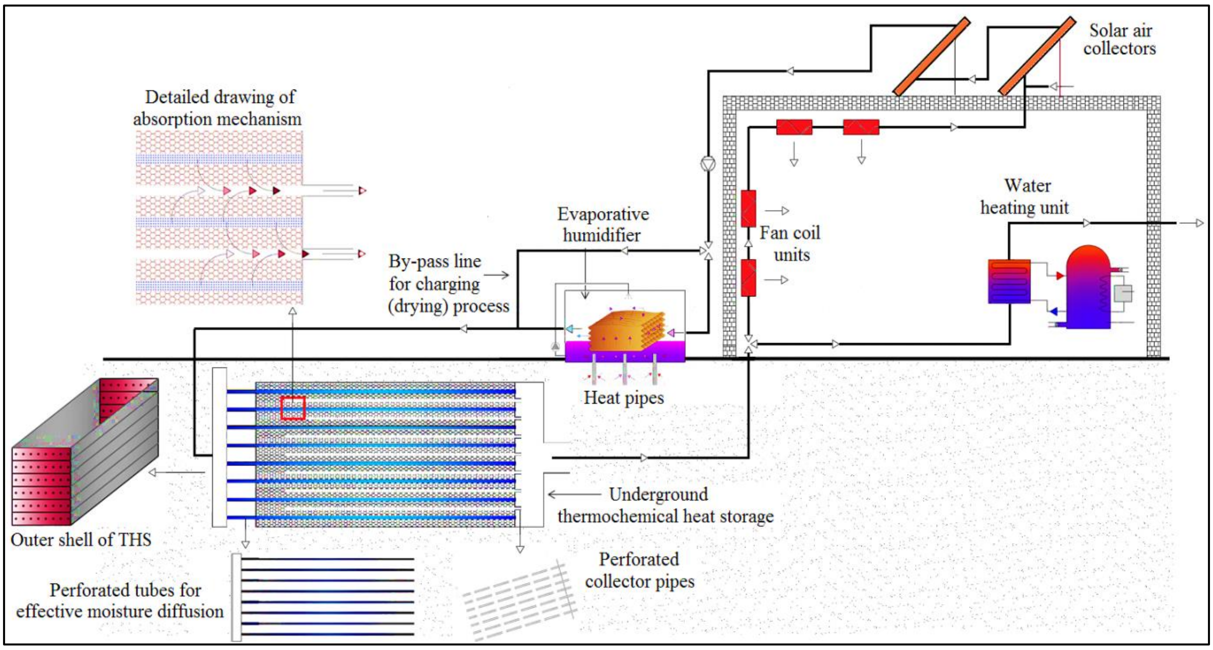

Figure 6.2.4 Detailed illustration of THS system components and process operation

The perforated tubes enable air to diffuse throughout the absorbent uniformly which is crucial for the maximising reaction performance. The tubes overcome the issue of increased air resistance at the front surface of the material due to the thickness of the absorbent bed. This resistance can slow down the reaction kinetics whilst also causing a pressure drop which results in high fan energy consumption and low temperature lift. Similarly to the diffusion tubes, perforated collector pipes are connected to the outlet side of the reactor. This allows the humid air to diffuse through the material and the hot air to be collected via outlet pipes. This concept increases the contact area of air and absorbent providing one possible solution to non-uniform HAM transfer in larger scale applications.

6.2.5 Building thermal analysis

The chosen dwelling is a 40 years old, single floor building with a floor area, A = 180 m^2 (see: Figure 6.2.5). The building is located near the west coast of the island where the weather is hot and humid in summer and mild in spring and autumn. Although Cyprus does not suffer extremely severe winter conditions, ambient temperature is below comfort conditions (18 → 20 °C) during most of the winter, and top-up heating is required. The chosen dwelling uses three types of heating systems to provide this;

1. Radiative electrical heaters are installed in the bedrooms
2. A gas heater is used in kitchen and one of the living rooms
3. Air conditioning units are used for the remaining rooms

To simulate the heat load of the building the software package Ecotect Analysis 2011 was used. The software allows user to create annual simulations using a 3D model of the building with imported building properties (*i.e.* dimensions, *U*-Values, ventilation etc.) as discussed in detail in Chapter 3. The software also provides the user with several adjustable settings. For this work the heat gain from occupants was set at 70 W (*i.e.* 4 adults living in the building), the air conditioning type was set on 24 hour heating mode whilst sensible and latent heat gains were set at 5 W/m^2 and 2 W/m^2 respectively. The 3D model created in Ecotect, using the original dimensions of the building is illustrated in Figure 6.2.6.

Figure 6.2.5 View of the investigated building

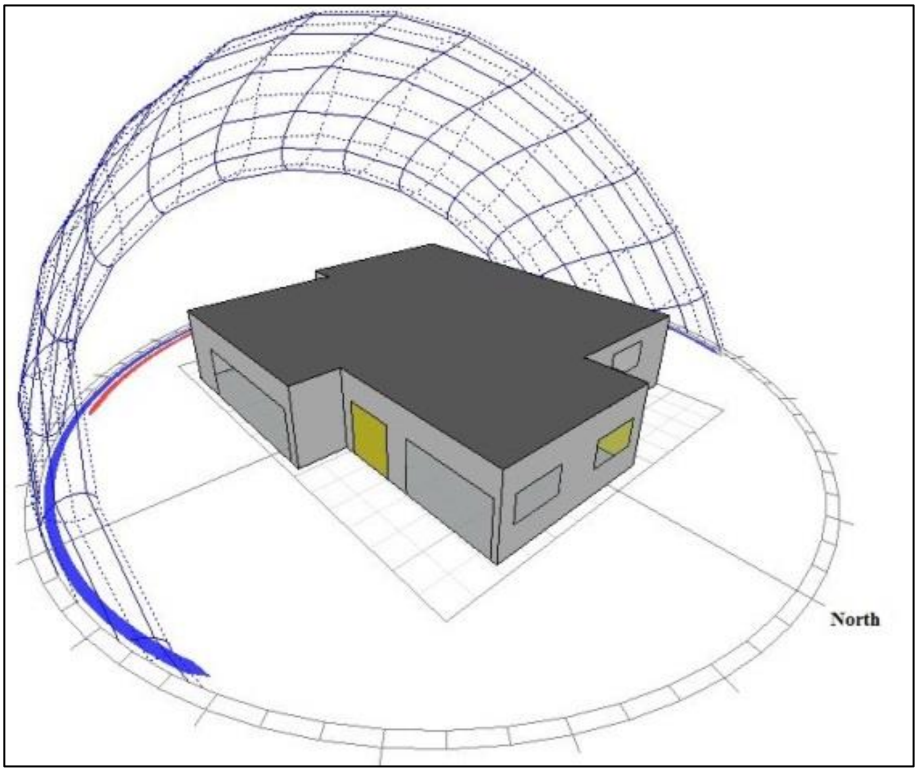

Figure 6.2.6 3D model of the building created in Ecotect

In NC, insulation of external building envelope elements is not considered important and is rarely utilised, whilst winter heat load is not as high as other northern countries such as UK, Norway or Finland, increased application of insulation could provide huge monetary and energy savings. The building case here is primarily of a concrete type construction with uninsulated brick masonry walls however, the roof is minimally insulated using an asphalt coating to the exterior. The buildings windows are of single glazed construction with an unbroken aluminium frame. The properties of the building components with their applicable surface areas are presented in Table 6.1 and the data used in Ecotect to perform the thermal analysis. Comfort conditions for the building were chosen as 18 °C for the heat load analysis.

Table 6.1 The properties of the building components with their applicable surface areas

Building component	Material	Total surface area (m^2)	Thickness (mm)	Schematic view	U-Value (W/m^2K)	Admittance (W/m^2K)	Solar absorption coefficient
Wall	Brick plaster	138.3	Brick: 110 Plaster: 20	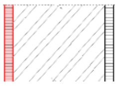	2.62	4.38	0.42
Door	Solid oak timber	7.31	40		2.26	3.19	0.46
Window	Single glazed-Aluminium frame	38.8	6		6.0	6.0	0.94
Roof	Concrete roof-Asphalt	185.5	Asphalt: 6 Concrete:150 Plaster: 20	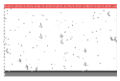	0.89	2.30	0.90
Floor	Concrete Slab-on ground	185.5	Soil:1500 Concrete:100	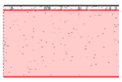	0.88	6.0	0.47

The annual total solar radiation, I_t on an optimally inclined solar collector, hours of sunshine, h_s and average ambient temperature, T_a, are presented in Figure 6.2.7. The comfort temperature, T_c used for analysing the heat load of the building, was set as 18 °C. As can be seen year round solar irradiation is in the range of 4 → 7.5 kWh, ambient temperature is 12

→ 28°C and daily sunshine is in the range of 9.5 → 14 hours. According to these data, it is clear that Cyprus has a remarkable year round solar availability to utilize in thermal applications. Data obtained from the European Commission's web site (PVGis, 2015) was used to calculate the solar thermal heat gain, Q_u (W) using Equation 3.4 (See: Chapter 3). The total collector area, A_c, used in the system was considered as 8 m^2. The properties of the solar collectors that were used in the calculation were given in Table 3.3 (See: Chapter 3).

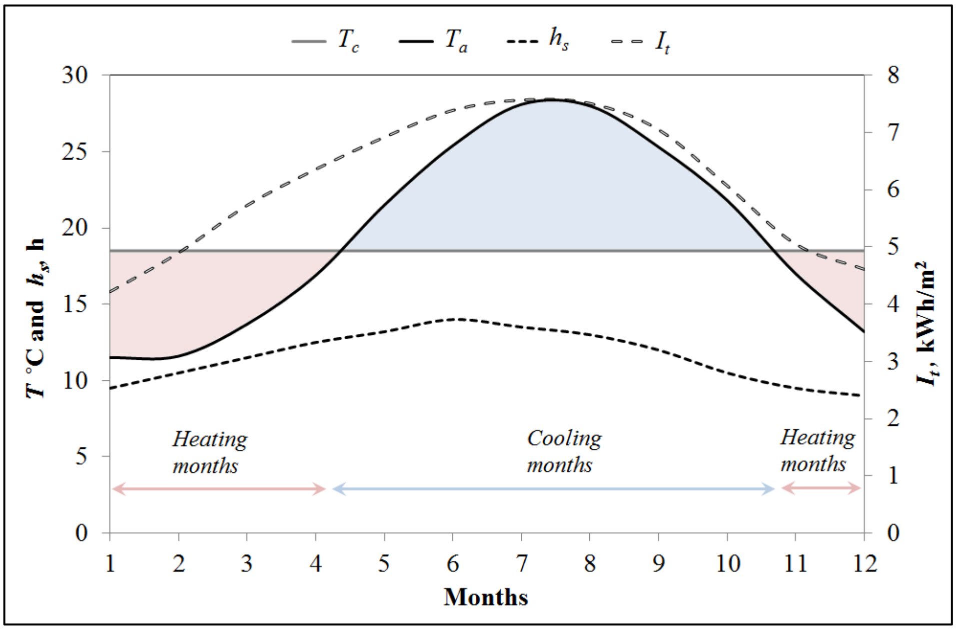

Figure 6.2.7 Year round ambient temperature, hours of sunshine and total solar irradiation in NC

A survey was conducted by (Evcil, 2012) to demonstrate the general properties of dwellings in NC with the results given in Table 6.2. The dwelling for this study was chosen as its properties are representative of the average dwelling in NC as described in the Evcil study. Therefore, outcomes of this study would be applied to the majority of the dwellings in NC, as they have the similar heat load trends. The survey consisted of multiple choice questions and results demonstrate the share of different options provided in questions. The properties of the building considered in this study are indicated with the dashed boxes in the table.

Table 6.2 General properties of dwellings in Northern Cyprus (Evcil, 2012)

	Percentage of total, %				
Type of houses	**Detached**	**Semi detached**	**Flat**	**--**	**--**
	52.6%	5.3%	42.1%	--	--
Area of houses	**<100 m^2**	**100-200 m^2**	**>200 m^2**	**--**	**--**
	10.8%	81.8%	7.4%	--	--
Insulation-external walls	**Glass wool**	**Polystyrene**	**Air gap**	**No insulation**	**--**
	1.3%	3.5%	1.7%	93.5%	--
Frames of windows	**Wood**	**Aluminium**	**PVC**	**--**	**--**
	16.9%	78.4%	4.7%	--	--
Glazing	**Single glazing**	**Double glazing**	**--**	**--**	**--**
	84.8%	15.2%	--	--	--
Type of roof	**Flat Concrete**	**Inclined concrete w tiles**	**Flat concrete, tiles on wood**	**--**	**--**
	73.6%	8.7%	17.7%	--	--
Insulation-roof	**Glass wool**	**Polystyrene**	**No insulation**	**Asphalt**	**--**
	4.4%	7.1%	88.5%	--	--
Means of heating	**Central heating**	**Heaters**	**Air-conditioners**	**--**	**--**
	2.2%	53.0%	44.8%	--	--
Energy source for heating	**Wood**	**Electricity**	**LPG**	**Kerosene**	**Diesel**
	1.3%	65.8%	27.7%	3.9%	1.3%
Number of air conditioners	**None**	**1**	**2**	**3**	**>4**
	30.7%	21.2%	23.8%	16.5%	7.8%

6.2.6 Results

The main aim of the analysis was to determine the storage volume, V_s of THS required to assist the buildings normal solar gains and fully meet building heat demand. As a 'seasonal' heat storage approach is proposed, the potential of solar energy for absorbent regeneration was also investigated. The absorbent material selected was the SIM-3a (V-$CaCl_2$) composite as discussed in previous section with the E_d used in order to determine V_s. In the dual hybrid model proposed here, integrated THS and solar air collectors are considered as the heating unit. In Figure 6.2.8 the annual heat load and solar heat gain for NC climate conditions is presented. There is no heat load from May to October as the average temperature is higher than 18 °C (*i.e.* chosen comfort limit) during this period. The heating period begins in November and lasts until April. However in November, March and April solar heat gains still exceed the building heat demand, $Q_u > Q_h$ therefore there is no necessity for any THS in these months. THS is only required in December, January and February where heat loads, Q_h are greater than heat gains are (*i.e.* Q_h = 883, 1310 and 1060 kWh whilst Q_u = 674, 582 and 683 for Dec, Jan and Feb respectively).

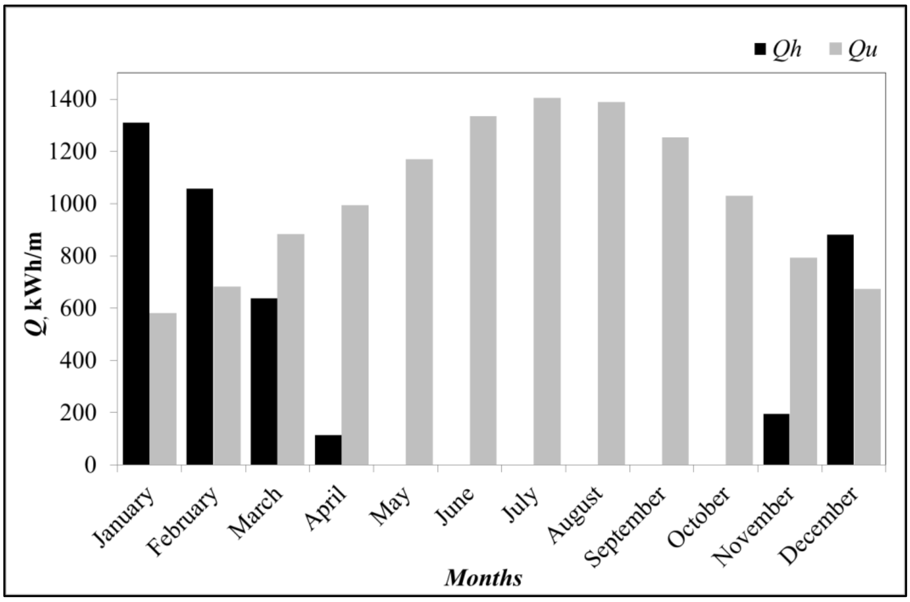

Figure 6.2.8 Monthly heat gains and heating demand for the building

These results indicate that an auxiliary heating source is required to assist solar energy for full compensation of heat load of the building. The peak difference, ΔQ between Q_u and Q_h occurs in January with 729 kWh with February and December having ΔQ of 376.2 kWh and 209.3 kWh (see: Figure 6.2.9). The total additional thermal energy required for the three heating months is 1314 kWh and, based on the assumed energy density of the absorbent (E_d = 250 kWh/m^3), the THS volume required to meet the total thermal demand was calculated as V_s = 5.25 m^3. The specific required storage volume for each month is calculated as 2.91, 1.5 and 0.84 m^3 in January, February and December respectively.

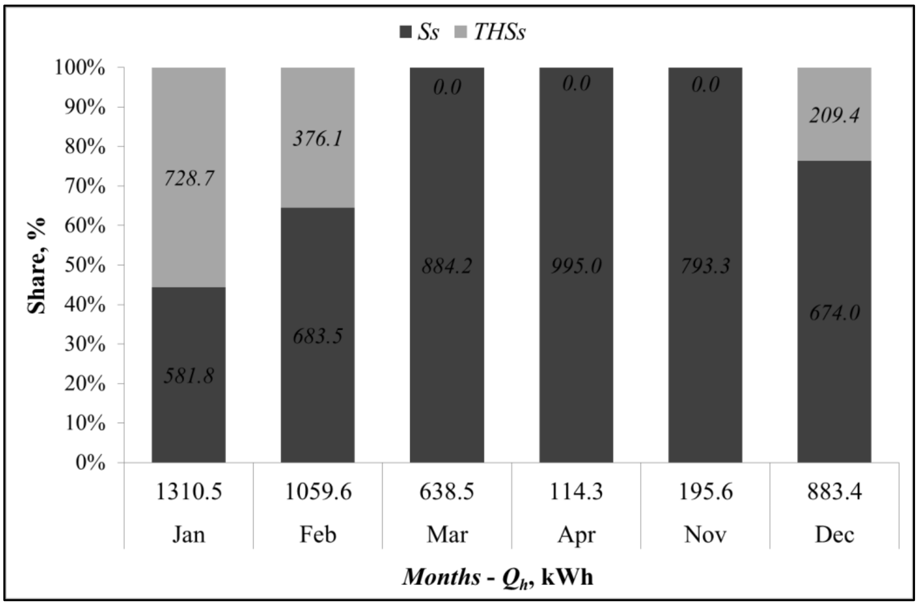

Figure 6.2.9 Share of THS required to meet heating demand during heating months

From May onwards, when there is no building heat load and the moist absorbent can be regenerated using solar energy. From the second half of spring to the first half of autumn (April - September) solar radiation is at its maximum level (> 6 kWh/m^2) and the notional 5.25 m^3 absorbent can be regenerated in a time period of slightly more than one month as presented in Figure 6.2.10. The theoretical amount of energy required for regeneration is equal to the energy supplied by the material during the discharging process (*i.e.* Q_c = 1314 kWh = Q_d) and is indicated in Figure 6.2.10. From May to October, the potential cumulative solar gain is 7582 kWh and thus only 17% of this would be sufficient for regenerating the 5.25 m^3 of SIM-3a. Any remaining heat can be used for water heating purposes, if required.

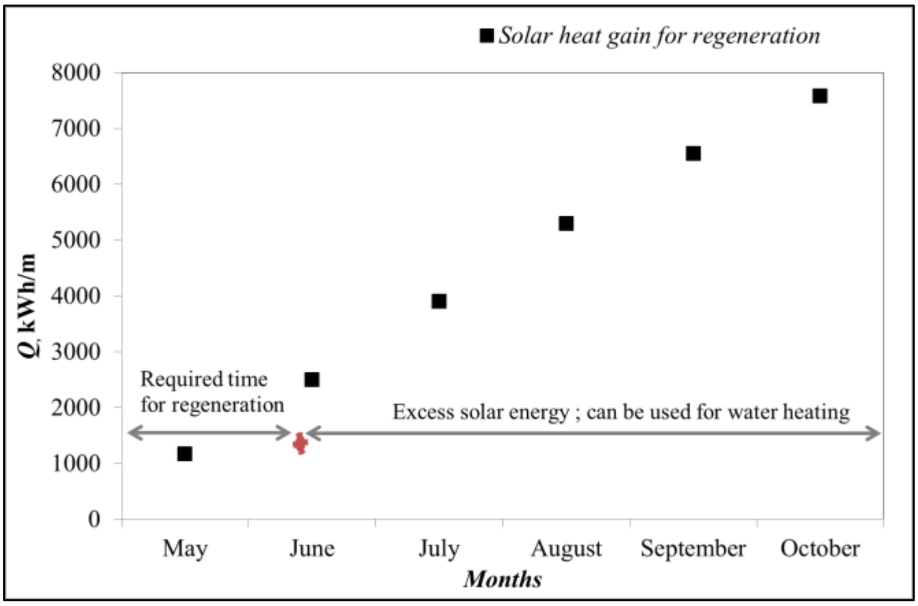

Figure 6.2.10 Regeneration time of the absorbent with solar energy in summer conditions

6.2.7 CO_2 savings and economic evaluation of the system

Control of GHG and CO_2 emissions and methods for reducing them have been gaining importance in recent years as they have been shown to have a significant effect on both Ozone depletion and global warming. Utilizing new, clean and renewable energy sources is one of the most promising solutions to this problem. In the domestic sector of NC, electricity, natural gas, fuel oil, LPG or solid fuel sourced systems are mostly preferred for space heating purposes due to their advantages for consumers such as lower prices, steady and easy operating conditions, low space requirements and long operational lifetime in comparison with renewable sourced heating systems.

Space heating applications however do not require high temperature. For example the heat pump blowing temperature is 35 → 45 °C in air conditioning applications or water circulation temperature is 35 → 40 °C for wall or ground heating methods. Using high temperature combusting fossil fuels for low temperature applications like space heating is a waste of the high quantity and quality of this energy (*i.e.* as a result of exergy destruction). In addition this is the waste of the fuel potential, which could be used for more appropriate applications such as electricity generation. The potential contribution of THS systems would facilitate this move away from high temperature fuel wastage by meeting the space heating demand with solar energy.

The conversion factor, ς is a coefficient used to determine the CO_2 emissions from energy generation or consumption processes and varies in the range of 0→1 depending on several factors (*e.g.* fuel type used etc.). The conversion factor of electricity per kWh consumption, ς_e, in Cyprus is 0.87 whilst for LPG, including residual heat or power generation ς_{LPG} = 0.21. According to a recent IEA report however, solar thermal and THS systems do not have CO_2 emissions and therefore;

$$\varsigma_{THS} = 0 \rightarrow S_{CO_2,THS} = 0. \tag{6.1}$$

According to these assumptions the CO_2 savings per year in compliance with usage of an AC heat pump (HP), electrical heater (EH) or gas heater (GH) are given in Equations 6.2 to 6.4 respectively;

$$S_{CO_2,HP} = \sum_{N=0}^{N=25} \xi_{HP} \times \varsigma_e \tag{6.2}$$

$$S_{CO_2,EH} = \sum_{N=0}^{N=25} \xi_{EH} \times \varsigma_e \tag{6.3}$$

$$S_{CO_2,GH} = \sum_{N=0}^{N=25} \xi_{GH} \times \varsigma_{LPG} \tag{6.4}$$

Based on these calculations, utilizing solar assisted THS for space heating would allow for a saving of 3.65, 1,21 and 0.88 ton CO_2 per year compared with usage of EH, GH and HP respectively (see: Figure 6.2.11). The building investigated here uses all of these systems. The living room and one of the bedrooms are heated using a HP, the kitchen and other living room are heated with GH and rest of the rooms are heated with EH. For this reason CO_2 savings for the investigated building are determined as an average of the CO_2 savings achieved for all three heating methods. Therefore yearly CO_2 savings of the investigated building with the usage of solar assisted THS, is estimated at 1.91 ton per year. As the system lifetime is assumed to be 25 years and during that period savings of 47.9 ton CO_2 are expected.

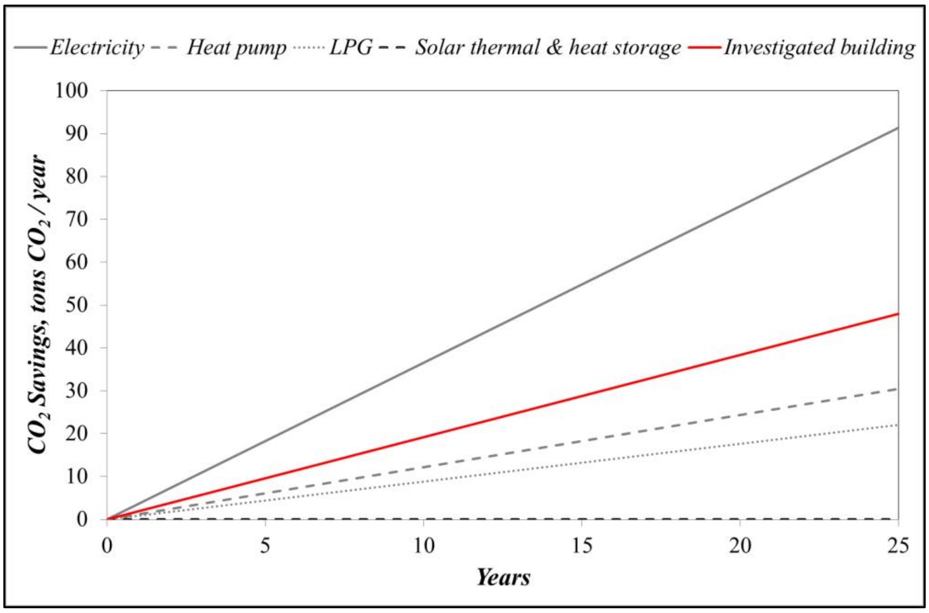

Figure 6.2.11 Total CO_2 savings using THS in comparison with traditional heating methods

In addition to the environmental effect of the proposed system, the economical evaluation of it should also be discussed in order to form a complete picture of solar assisted THS systems. Cost estimations are made based on component and material retail prices in NC at the time of printing. The heat storage material (SIM-3a) unit price was calculated as €0.15/liter and solar collector unit price was determined as €75/m^2 (Baymak, 2016).

Ducting equipment prices including pipes, fittings and vents were also determined based on the retail prices obtained from (Havalandirmacarsisi, 2016). Unit price of stainless semi flexible *d*=100 mm pipe was determined as €10/m, and prices of air damper, fitting and air diffuser were provided as €15, €2 and €6 by the supplier. Considering 6m ducting, 6 air dampers 10 duct fittings and 5 diffusers (living room, kitchen and three bedrooms) are needed in the proposed system, total cost of ducting equipment is calculated as ~€200. A BDTX type, 100 mm in line duct fan, with maximum mass flow rate of 240 m^3/h is proposed to be used in the system, which will also cost €50 (Havalandirmacarsisi, 2016). A sorption reactor with *l*: 2.5 m x *h*: 2.1m x *w*: 1m, consisting of 30 sorption pipes with the dimensions of *d*: 0.3 m and *l*: 2.5 m is proposed. The outer shell will be made up of aluminium, which has a unit price of €1.5/m^2 (Metalavm, 2016), and in total will be cost ~€17. Sorption pipes will consist of a galvanized duct pipe and an inner perforated inner air diffuser pipe which in total will cost €4.5/m. Total price of 30 sorption pipe units will be ~€338. Fittings and air valves will also required for integration of the sorption pipes to the ducting, which is expected to be cost ~€50. An avaporative humidifier will also be required for increasing air humidity in discharging process which will cost ~€100 (JohnLewis, 2016). In addition 30 m glasswool will be used to insulate the sorption pipes and ducting to minimize heat losses. The unit price of 25 mm thick glasswool is €3.3/m^2 (Hotchkiss, 2016). Thereby, total costs of insulation material will be ~€100. System built and installation costs are expected to be low as only ducting equipment and solar collectors will be used. Total built and installation costs are expected to be 15-20% of the equipment costs and considered as ~€500. The total capital cost of the proposed system is expected to be between €2500-3000 and estimated at €2750 based on the information provided above and summarized in Table 6.3.

Table 6.3 Cost of system components

System component	**Price (€)**
Ducting pipes, fittings, vents	200
Solar panels (8 m^2)	600
Heat storage tank (5.25 m^3)	400
Fan	50
Heat storage material (5.25 m^3)	800
Evaporative humidifier	100
Insulation	100
System built and installation costs	500
Total	2750

The system economic analysis has performed based on the savings/profit that could be obtained by replacing the proposed solar driven THS system with the currently used heating methods (heat pump, electrical heater and gas heater in mixed mode) in investigated building. For analysis of the total savings of the proposed system, the present worth method is used. According to this method, the rate of interest, *r*, can be found using Equation 6.5:

$$r = \frac{(i+g)}{(1-g)} \tag{6.5}$$

where *i* is inflation rate (14.5%) and *g* is discount rate (11.4%). Therefore *r* is calculated as 2.7%. The present worth factor (PWF) is expressed as in Equation 6.6 to determine the present value of the money for the N^{th} year;

$$PWF = \frac{1}{(1+r)^N} \tag{6.6}$$

The potential savings against using the HP, EH and GH over the 25 year period are analysed using Equations 6.7 to 6.9 respectively where Υ is the total operational cost, ξ the total yearly energy consumption and f_e, the unit price of electricity in NC which is currently €0.22/kWh for domestic usage.

$$\Upsilon_{HP} = \sum_{N=0}^{N=25} \xi_{HP} \times \frac{f_e}{3} \times PWF \qquad (6.7)$$

$$\Upsilon_{EH} = \sum_{N=0}^{N=25} \xi_{EH} \times f_e \times PWF \qquad (6.8)$$

$$\Upsilon_{GH} = \sum_{N=0}^{N=25} \xi_{GH} \times f_{LPG} \times PWF \qquad (6.9)$$

The total cost of the THS, Υ_{THS}, through the 25 year period including capital cost, operational and maintenance costs is calculated using Equation 6.10 where subscripts O, M and C represent operational, maintenance and capital respectively.

$$\Upsilon_{THS} = \Upsilon_C + \sum_{N=0}^{N=25} (\Upsilon_O + \Upsilon_M) \times PWF \qquad (6.10)$$

The total yearly operational and maintenance costs of the system are expected to be very low with the annual sum assumed as 2% of the total capital costs (see: Equation 6.11);

$$(\Upsilon_O + \Upsilon_M) = (2\% \times \Upsilon_C) \qquad (6.11)$$

The payback periods of HP, EH and GH are determined as follows;

$$N_{p_{HP}} \rightarrow \Upsilon_{HP} = \Upsilon_{THS} \qquad (6.12)$$

$$N_{p_{EH}} \rightarrow \Upsilon_{EH} = \Upsilon_{THS} \qquad (6.13)$$

$$N_{p_{GH}} \rightarrow \Upsilon_{GH} = \Upsilon_{THS} \qquad (6.14)$$

The summary of economic analysis results are presented in Table 6.4 and system payback period is illustrated in Figure 6.2.12. Similar to the environmental analysis, the analysis has conducted based on the savings of solar assisted THS compared with the operating costs of usage of the current systems/methods (HP, EH and GH) and the average. It was found that the solar assisted THS system could provide a saving of €550 / year whilst cumulative savings exceed the sum of total (capital, maintenance and operating) cost of system, (3081> €3050) at the end of year 6 years. Over the full 25 years the cumulative total saving would be €10,077 whereas the total cumulative cost of the system would be €3731 over the same period corresponding to a €6346 profit with the usage of THS compared to HP, GH and EH.

Table 6.4 Summary of the system economic analysis results

Year ***N***	***PWF***	Υ_C	Υ_{THS} **(C+O+M)**	$\Upsilon_{HP,cum}$	$\Upsilon_{EH,cum}$	$\Upsilon_{GH,cum}$	**Investigated building cost savings** $(\Upsilon_{HP}+\Upsilon_{EH}+\Upsilon_{GH})/3$
0	1.00	2750	2750.0	0.0	0.0	0	0
1	0.97	0	2803.5	299.7	899.2	449.6	549.5
2	0.95	0	2855.5	591.3	1774.0	887.0	1084.1
3	0.92	0	2906.2	875.1	2625.2	1312.6	1604.3
4	0.90	0	2955.5	1151.1	3453.3	1726.6	2110.3
5	0.87	0	3003.4	1419.7	4259.0	2129.5	2602.7
6	0.85	0	***3050.1***	1681.0	5042.9	2521.4	***3081.7***
7	0.83	0	3095.4	1935.2	5805.6	2902.8	3547.8
8	0.80	0	3139.6	2182.5	6547.6	3273.8	4001.3
9	0.78	0	3182.6	2423.2	7269.5	3634.7	4442.4
10	0.76	0	3224.4	2657.3	7971.9	3985.9	4871.7
11	0.74	0	3265.0	2885.1	8655.3	4327.6	5289.3
12	0.72	0	3304.6	3106.7	9320.1	4660.0	5695.6
13	0.70	0	3343.1	3322.3	9967.0	4983.5	6090.9
14	0.68	0	3380.5	3532.1	10596.3	5298.1	6475.5
15	0.66	0	3417.0	3736.2	11208.7	5604.3	6849.7
16	0.64	0	3452.4	3934.8	11804.4	5902.2	7213.7
17	0.63	0	3486.9	4128.0	12384.0	6192.0	7568.0
18	0.61	0	3520.5	4316.0	12947.9	6473.9	7912.6
19	0.59	0	3553.1	4498.8	13496.5	6748.2	8247.8
20	0.58	0	3584.9	4676.8	14030.3	7015.1	8574.0
21	0.56	0	3615.8	4849.9	14549.7	7274.8	8891.4
22	0.55	0	3645.9	5018.3	15054.9	7527.4	9200.2
23	0.53	0	3675.1	5182.2	15546.5	7773.2	9500.6
24	0.52	0	3703.6	5341.6	16024.8	8012.4	9792.9
25	0.50	0	3731.3	5496.7	16490.2	8245.0	10077.3

The average annual energy consumption (e.g. appliances, heating cooling, hot water) of the investigated building is ≈5600 kWh whilst the energy (electricity, gas) consumed for space heating is ≈1900kWh. Therefore the average annual energy saving rate is found to be 34%. The floor area of the building investigated is 180 m^2 whereas the floor area of dwellings in

NC is generally 100-150 m^2 and therefore, in NC conditions the average annual energy saving rate and payback period is expected to be somewhat less than the investigated building *i.e.* 25-30% and 5-7 years respectively.

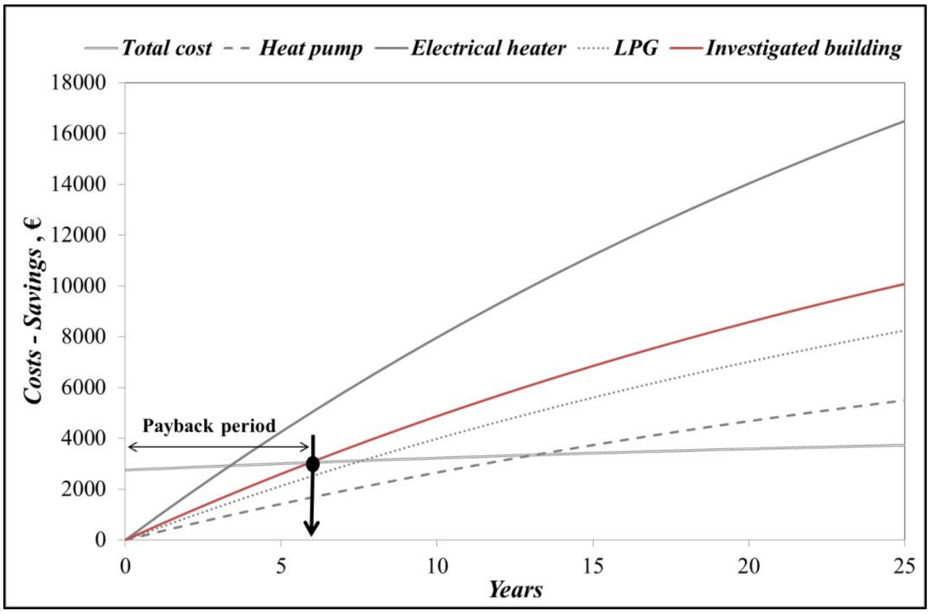

Figure 6.2.12 Payback period of the integrated solar assisted THS

6.3 Development and testing of integrated sorption pipe - solar concentrator thermal system under Cyprus climatic conditions

6.3.1 Introduction

Previous section focuses on the evaluation of the applicability and technical feasibility of solar driven THS systems through technical, economical and environmental assesments. Analyses results showed that Cyprus has a good potential for utilizing THS systems in solar heating applications. Based on the promising theoretical results, a small scale prototype experiemental unit was proposed for investigating THS operational performance with a real application. Accordingly, with consideration of the successful development and investigation of the SP concept under laboratory conditions as presented in Chapter 5, it was intended to integrate it with the solar concentrator and examine the prototype performance under

Cyprus climate conditions where solar energy in abundant. The aim was to present an alternative solution to fossil fuel based inefficient and expensive heating methods applied in the country, which could also promote sustainable space heating in other Mediterranean countries having similar climate conditions such as Greece, Lebanon, Turkey, Italy and Spain . The Island of Cyprus has a remarkable solar potential when compared with most of the developed EU countries. This abundance of dense solar radiation should be fully utilized, especially during the days when it is at its peak.

Despite THS systems have many promising advantages; the main problem within the development of this method is high temperature requirement for regenerating (charging) the sorbent. Indeed, it is highly unlikely to achieve required temperature in built environment with the current transpired solar air collector technology, especially in cold climate regions, due to the low solar intensity.

In order to benefit from THS materials in buildings, research should focus on novel solar collector design, efficient regeneration process and reactor design suitable for THS applications. Although there are a number of studies on experimentation of THS systems, there is no research in the literature experimenting integrated solar concentrator and reactor for sorbent regeneration. Solar concentrators (SCs) were initially proposed for solar thermal power plants. Recently new version of this technology was introduced for domestic space/water heating. It is obvious that concentrating technologies are more efficient to achieve higher temperatures. In this context, a new concept based on direct integration of solar concentrators with SPs is proposed. In this method, instead of heating the inlet air, the sorbent is heated with the concentrated solar radiation on the SP. Air flow through the sorbent provides convection effect and extracts the evaporated water from the SP. The proposed module has the similar concept with the conventional SCs. The difference is replacing the water flow pipe with a larger diameter duct filled with sorbent. The SP also has a central cylindrical perforated air diffuser to provide uniform air flow through the sorbent.

Integrated sorption pipe / solar concentrator technology could enhance the utility of solar energy therefore presents a unique method/solution for overcoming the barriers of sorbent regeneration with solar energy. It will reduce the required space, minimize the heat losses, in charging process, ease operational control of heat storage and allow long term storage of solar energy in high storage density sorption materials. The integrated SP-SC (sorption pipe-solar concentrator) module could be designed as single or multiple units depending on the specific requirements and conditions of an application. A multiple unit design illustrating the working principle of the described system in charging and discharging modes is presented in Figure 6.3.1. The compact nature of the purposed unit allows to be fitted in limited roof /wall area of existing / new buildings which is the main barrier in majority of solar thermal applications.

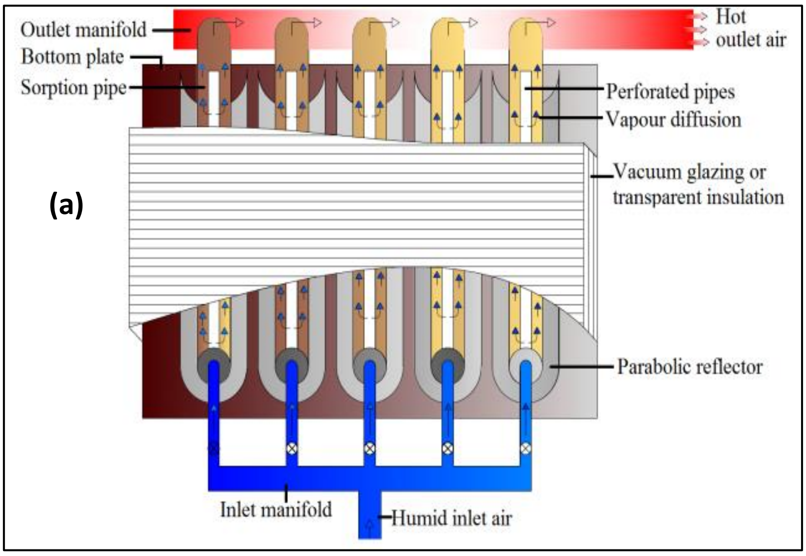

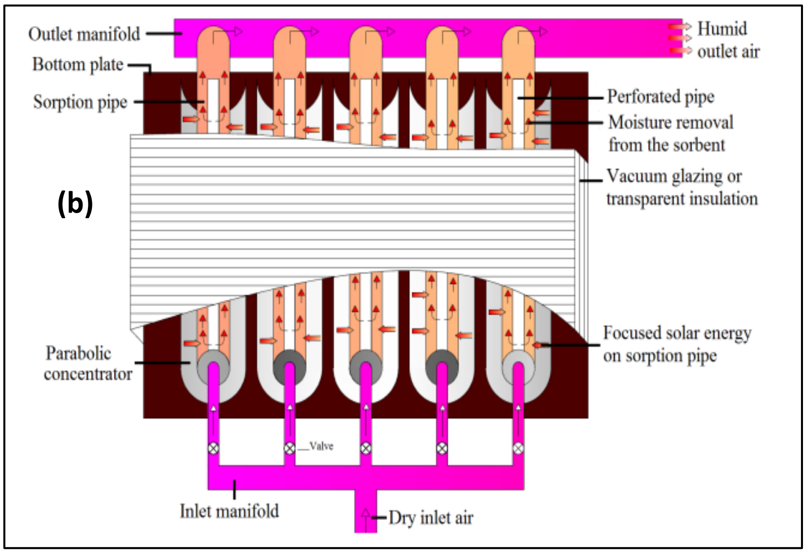

Figure 6.3.1 Schematic illustration of multiple unit SP - SC heat storage module; (a) discharging cycle, (b) charging cycle

Even with the year round abundance of solar energy in the Cyprus Island, it cannot be employed in winter for space heating purpose because of the mismatch. THS systems should be the main driving force for storage of solar energy and usage of it during winter conditions. Achieving adequate storage of solar energy with absorption materials will allow fulfilling the gap between heat load of the buildings and solar availability. This will significantly contribute to reducing the usage of electricity and thus fossil based fuels in the residential sector for space heating applications. THS systems bring the advantage of storing solar energy, densely with very low heat loss and space requirements.

Accordingly, a single unit SP-SC is developed and tested. It is proposed to investigate the compact SP-SC unit performance for short term storage of solar energy. A test room, located near west cost of Cyprus and act as a farmhouse is used for examining the SP performance under real climate conditions of Cyprus. Initially, the experimental procedure, methods and materials used for realizing the proposed study is introduced. Later, experimental results are presented and further improvements discussed.

6.3.2 System description and experimental method

In this section, a novel SP-SC unit is developed and tested for solar thermal energy storage under Cyprus climate conditions. Although providing uniform moisture diffusion to extract the stored energy in THS is important, an effective design allowing efficient drying of THS material with solar energy is crucial. Therefore designs/concepts of THS should ease solar heat input to sorption media for removing the moisture without increasing the costs and complexity. In this context, based on the promoting results achieved in first phase lab testing of SP, as presented in previous section, a solar concentrator consisting of two mirrors for focusing the solar energy onto the SP is proposed for drying the sorbent (See: Figure 6.3.2 a-b). The SP is made up of 0.7 mm thick stainless steel and has a diameter and length of d = 0.15 m and l = 0.8 m respectively. It is painted black in order to maximize solar absorptivity. A perforated pipe (d_p = 0.04 m), consisting of holes with a diameter of d_h = 3mm is placed at the centre of the SP.

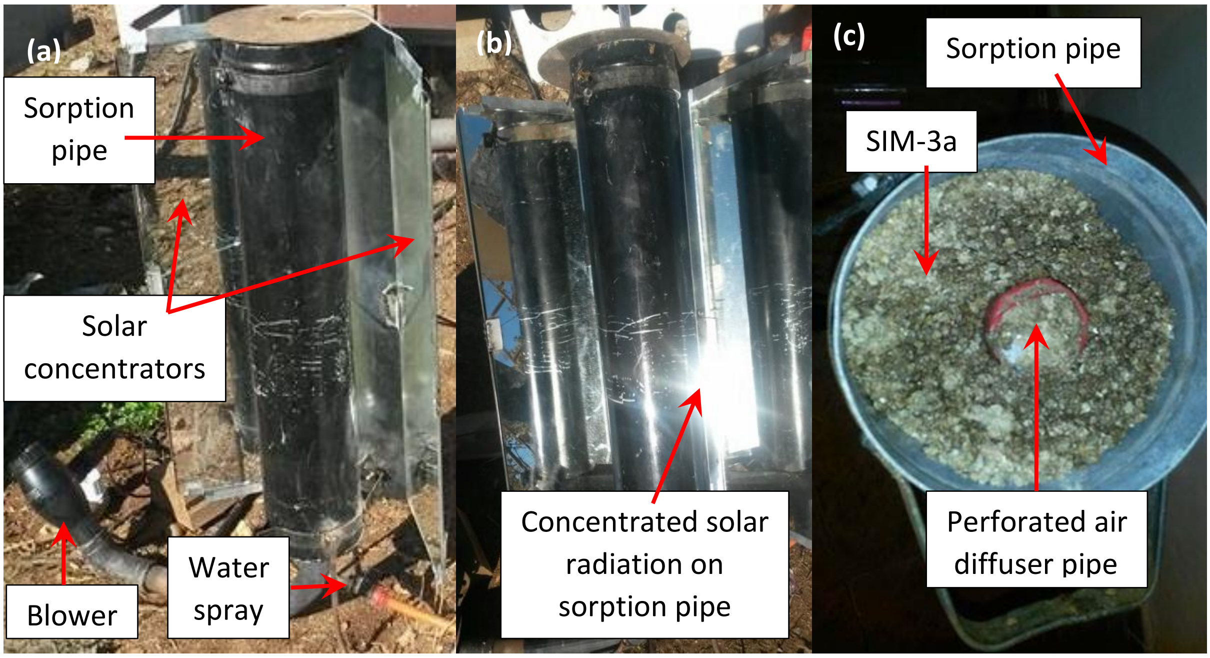

Figure 6.3.2 (a) View of the SP-SC unit (b) concentrated solar energy on SP (c) top view of the SP showing wetted SIM 3a after discharging cycle

During the process, air enters from the bottom of the perforated pipe and rises vertically inside the pipe. As the top of the perforated pipe is sealed, compressed air diffuses in horizontal direction and flows through the absorbent which is placed in between the SP and perforated pipe. SIM-3a (Vermiculite-$CaCl_2$) was used as the sorption material (See: Figure 6.3.2 c). Basic operating principle and technical illustration of the SP-SC unit are presented in Figures 6.3.3 and 6.3.4 respectively. More detailed information on SP design and and operational aspects can be found in Section 5.3.

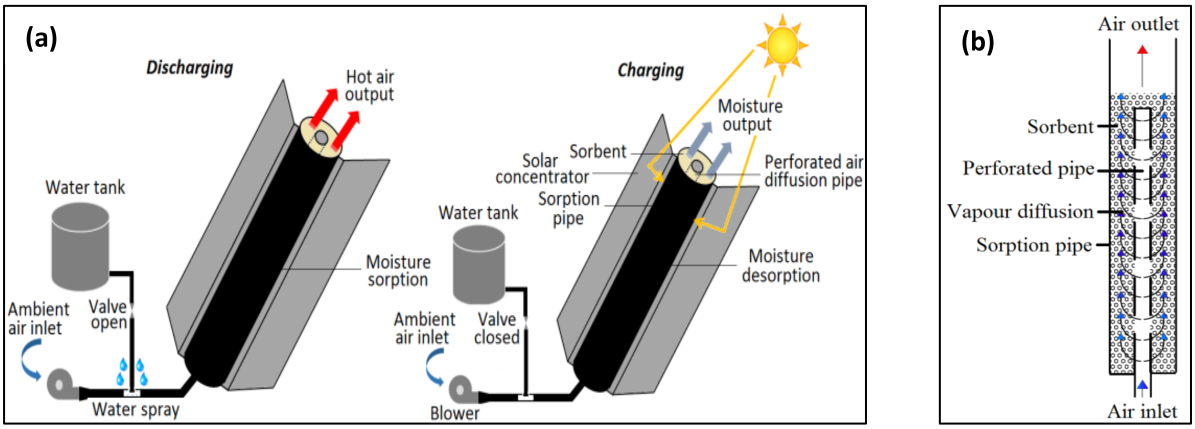

Figure 6.3.3 (a) Schematic illustration of charging and discharging operation of integrated sorption pipe solar concentrator unit, (b) schematic illustration of heat extraction from the sorption pipe

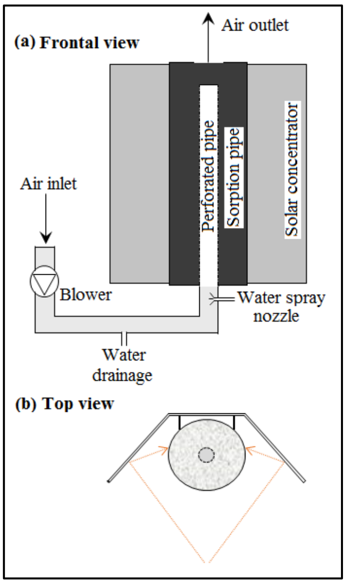

Figure 6.3.4 (a) Frontal, (b) top view of the integrated sorption pipe solar concentrator unit

Experimental investigation of the developed test rig consisted of two stages; discharging (humidification) in the test room (12.4 m^2 floor area) (see: Figure 6.3.5 a) following charging (drying) in open environment with utilizing solar energy. The discharging process lasted 9 hours and due to the sufficient ambient relative humidity (RH ≈ 70%) during the testing period, no additional moisture was added to the inlet air. In this way, while the SP was providing heat, at the same time it allowed to maintain the humidity level inside the room. A small blower with the diameter of d_f = 40mm was used for providing air flow. The discharging process was conducted on 28th December 2014 in the time range of 13:00-22:00. The charging process was carried out on 29th December 2014 between 10:00-16:00. The measurement time interval was 15 minutes both for the discharging and charging processes. The volume of SIM-3a used in the testing was 0.013 m^3. It was dried for 48 hours at 150° in an electrical oven before the discharging process to ensure the removal of all residual moisture. The initial dry weight of the material was measured as 5.9 kg.

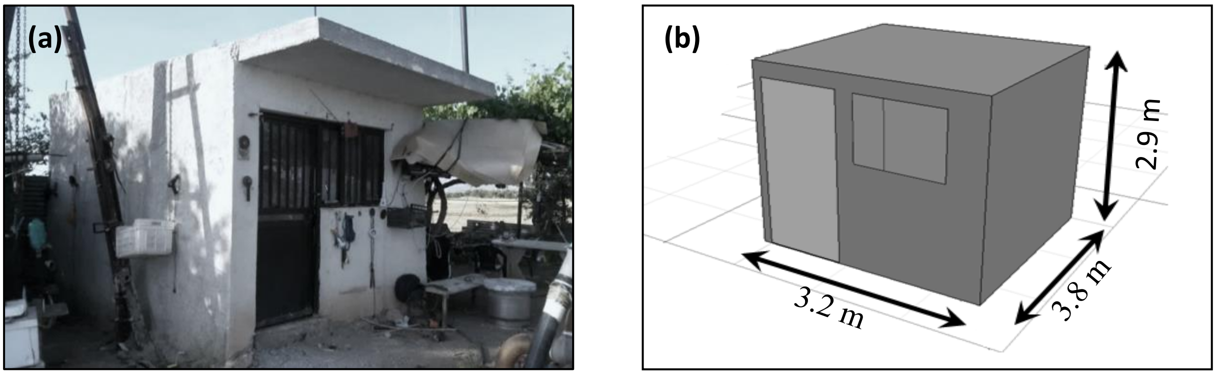

Figure 6.3.5 (a) View of the test room, (b) 3D model of the test room created in Ecotect

According to the experimental results, the energetic performance of the tested SP was evaluated both for charging and discharging processes. A model (See: Figure 6.3.5 b) was created in Ecotect software to simulate the heat load of the investigated building during the experimental period. By this way, heat output of the SP was evaluated in comparison with the building heat load. Additionally, solar charging efficiency (charging) and sorption/desorption kinetics were also investigated. The equations listed in Table 4.5-4.6 (See: Chapter 4) were used for analysing the experimental results.

In the developed experimental rig, 3 sensor locations were used for determining the *T* and *RH* of the ambient also at the sorption pipe inlet and outlet. Air MFR was also measured in both charging and dicharging cycles. Data is recorded using the EK-H4 Eval Kit for Temperature - Humidity Sensors from Sensiron, AG, Switzerland. The experimental uncertainties were determined by applying Gauss propagation law (See: Section 4.3.3).

Experiments were conducted by using following instruments: Thermocouples with the maximum deviation of ±0.3°C for temperature and ±2% for relative humidity and air mass flow meter with the accuracy of ±2%. Total uncertainty rate affecting the calculated heat gain (Q_g) from the system is found to be 1.72%.

6.3.3 Experimental results and discussion

6.3.3.1 Thermal analysis of discharging process

Experimental results of discharging process are presented in Figure 6.3.6 and 6.3.7. Figure 6.3.6 represents the temperature (see: Figure 6.3.6 a) and relative humidity (see: Figure 6.3.6 b) variation of air during the experimental period. Inlet humidity varied in the range of 73%-63% whereas outlet relative humidity increased to 22% from 3%. In open THS systems temperature lifting is dependent to the instantaneous moisture absorption of the absorbent as demonstrated in previous section. Therefore both the reactor design to provide uniform air diffusion as well as properties of the THS material have vital importance on temperature lifting. High moisture sorption rate, high thermal energy generation per unit mass of absorbed moisture (kWh/gr_{wv}) and low regeneration temperature are desired outputs/properties of an effective heat storage system. In Figure 6.3.6 a temperature variation of inlet outlet and ambient temperature during the discharging process is given. Initially, resulting with the high absorption rate, the outlet temperature reached 40.1° C at the beginning of the experiment. At that time room temperature was 16° C while ambient/inlet temperature was 15.8° C. The mass flow rate of air was 0.021 kg/s during the experiment. Thermal power output varied in the range of 0.53 kW - 0.37 kW.

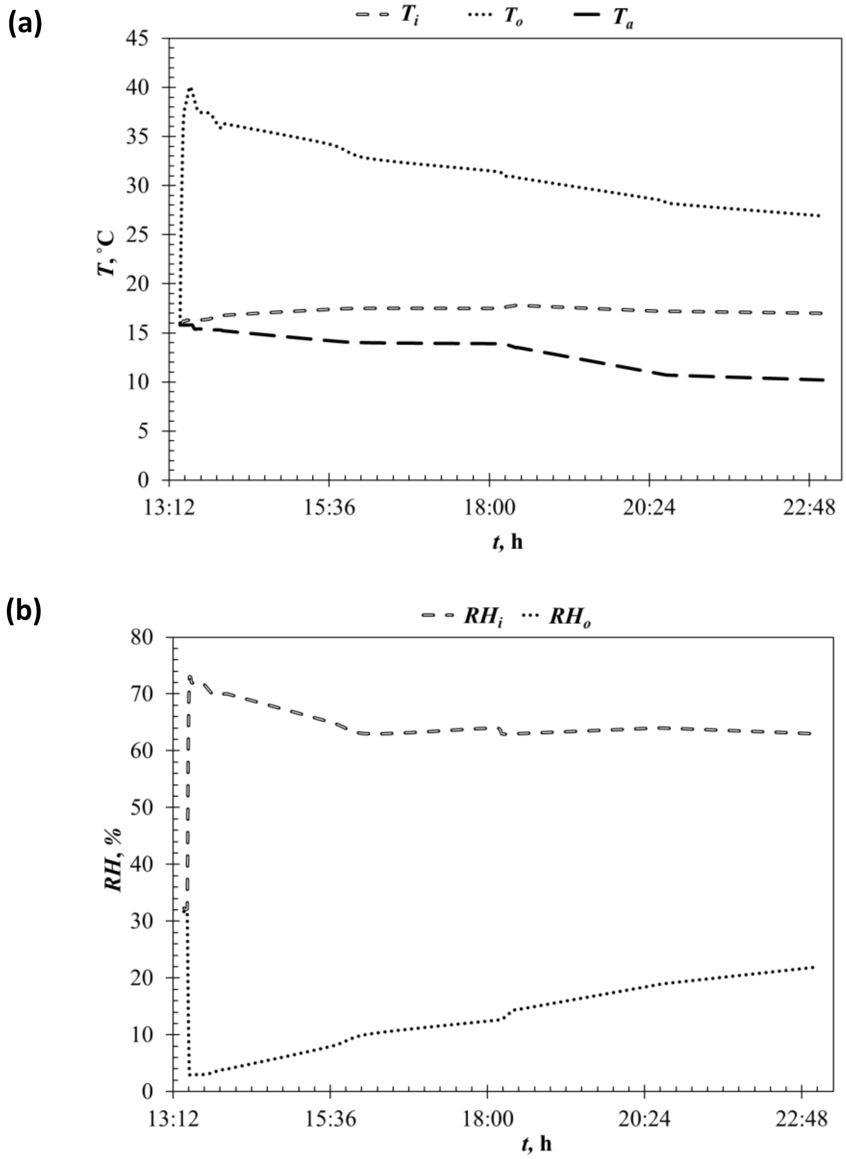

Figure 6.3.6 (a) Temperature and (b) relative humidity variation of air in discharging process

Figure 6.3.7 a illustrates the increase of mass uptake, *Δm* and the mass uptake ratio, *f*. In total, 2.15 kg moisture is adsorbed in 9 hours discharging duration where the initial dry mass of V-$CaCl_2$ was 5.9 kg. This result corresponds to *f* = 0.37 at the end of the testing while total energy output was 2.85 kWh at that time. Accordingly heat storage density is calculated as 1.32 kWh / kg wv while volumetric energy storage density was 219.2 kWh. Fig 6.3.7 b shows the analysed heat load of the room and total thermal energy output during the experiment and as seen from the graph they are in close approximation. Thereby, although the ambient temperature dropped sharply after 18:00 pm the supplied heat by the heat storage was still sufficient to keep room temperature at a comfortable level.

Room temperature was 17.1 °C at the end of the experiment while ambient temperature was measured as 10.2° C. Applying insulatation to the building would allow to achieve higher room temperature as the heat losses would be minimized in that case.

On the other hand a mismatch between supplied heat and the room heat load is observed after 9 pm as a result of increasing heat loss of the room (due to the reducing ambient temperature) and decrease in heat generation. This was an expected situation as wetting of the absorbent leads to a performance drop naturally. An effective method for drying the absorbent during daytime (9am - 4pm) would allow reusage of the SP over the following days. Therefore, a sustainable, low cost heating method was examined and presented in the following section, which will lead to minimize carbon emissions for space heating applications.

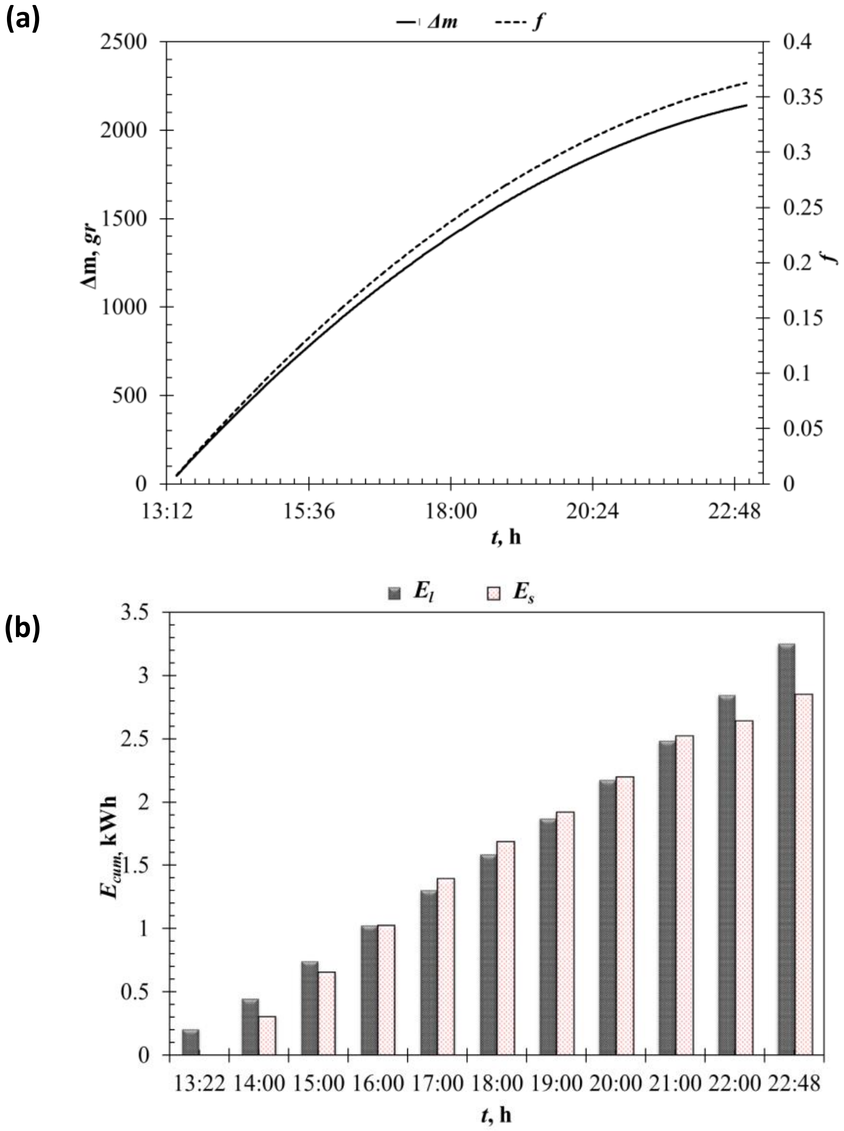

Figure 6.3.7 (a) Moisture absorption and mass uptake ratio during discharging process, (b) heat load of test room and supplied thermal energy to the room with SP in discharging process

6.3.3.2 Thermal analysis of charging process

In the charging process, a solar concentrator consisting of two mirrors is attached to the SP and the system is placed facing east with a tilt angle of 43 °C. It was aimed to heat the absorbent while ambient air is blown through it to enhance moisture removal via convection effect. The charging experiment lasted 6 hours between 10:00 - 16:00. Measured inlet and outlet temperatures of air in charging process is given in Figure 6.3.8 a. During the testing, ambient temperature reached to a peak of 27 °C while it was 20° C at the beginning and 18 °C at the end of experiment. At the same time, the highest outlet air temperature from the SP was measured as 41 °C at 13:00 while it was 30 °C at 16:00 as a result of descending solar radiation. Additionally the highest sorbent temperature was recorded as 67 °C during the experiment. Figure 6.3.8 b shows the relative and specific humidity of air at the inlet and outlet of the SP during the experiment. The main challenge of drying the absorbent in Cyprus' climate conditions is the high ambient relative humidity. This phenomenon reduces the drying efficiency as the inlet air already holds significant amount of moisture and it can remove limited amount of moisture from the absorbent. It is seen from Figure 6.3.8 b that ambient RH, which was assumed equal to the inlet air humidity, was in the range of 56-63%. As the absorbent was heated with the solar concentrators, it increases the temperature of air passing through the SP. Thereby moisture holding capacity of air increases with its increasing temperature. Air leaves from the SP with lower RH but higher temperature than the inlet resulting with higher moisture output than the input. Figure 6.3.8 b also presents the inlet and outlet humidity content of air. As seen, at the beginning and at the end of charging, inlet air humidity content was higher than the outlet, indicating that no moisture removal is provided in these short periods. Conversely it caused more moisture to be loaded to the sorbent. This was most probably happened as a result of the insufficient temperature of absorbent at the beginning for water evaporation. Additionally after 3 pm, again, inlet specific humidity exceeds the outlet as a result of descending solar irradiation. Finally it is calculated that the total amount of desorbed moisture was 1294 gr in charging cycle (See: Figure 6.3.8 c) whereas the total amount of absorbed moisture was 2150 gr in discharging cycle. These results correspond to a drying ratio of 60% which is achieved only with solar energy.

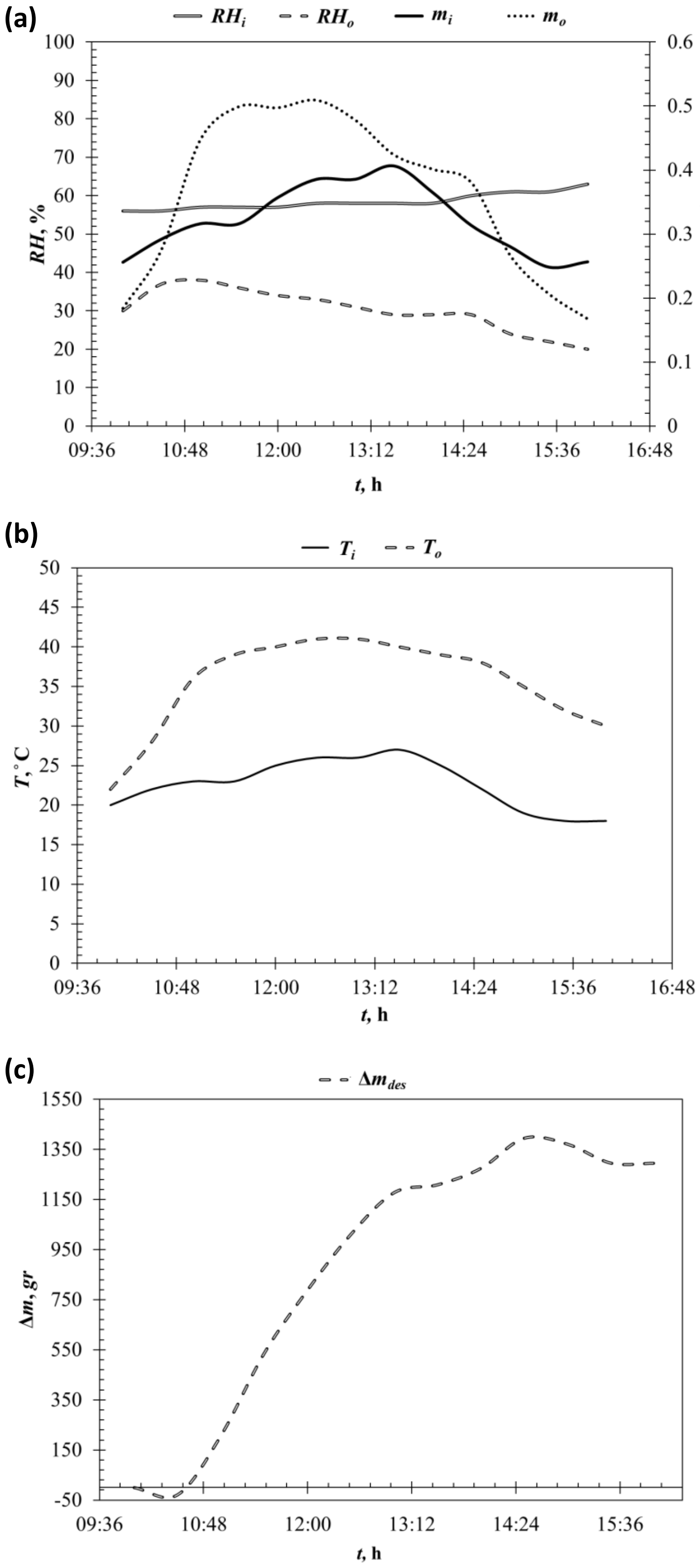

Figure 6.3.8 (a) Temperature variation of air in charging process, (b) relative humidity and vapour content of inlet-outlet air in charging process, (c) moisture desorption rate in charging process

It is obvious that further improvement is required to achieve full dehydration of the absorbent with solar energy to achieve efficient cyclic usage of the SP heat storage. However the results demonstrate a future potential for the designed system.

6.4 Conclusions

This chapter covers theoretical and experimental studies investigating feasibility and thermal performance of THS system for solar heating applications in Cyprus.

In Chapter 6.2, applicability of thermochemical heat storage (THS) under Cyprus climate conditions is theoretically investigated. An underground THS system, integrated with 8 m^2 solar air collectors placed on the roof of a flat roof, detached building is considered. In addition, an evaporative humidification unit for humidifying the air during the discharging process is assumed. It was found that 5.25 m^3 of absorbent was required to meet the mismatch between solar energy supply and building heat load during winter period (December, January, February) where the total solar heat gain and heat load are 1939 kWh and 3253 kWh respectively. The heat storage could be a moduler design consisting of 30 sorption pipes, with the dimensions of d=30 cm and l=2.5 m, placed in a reactangular vessel. In that case, each sorption pipe will have 0.175 m^3 storage volume, corresponding to heat storage capacity of 42.5 kWh. For the operating conditions of m_a=0.1 m^3/s and ΔT_{ave}=20 °C, each sorption pipe could provide 2 kW heat over three days (assuming daily 7 hours operational time) and with the use of all sorption pipes, continuous heat supply (30 sorption pipes x 3 days each) to the building could be obtained over 3 months winter period. On the other hand with 8 m^2 of solar air collectors, 35 days in the summer period (May / June) where the solar irradiation is in the range of 6 → 7 kWh/m^2 are required to regenerate the absorbent.

Gas heaters, electrical heaters and heat pumps are widely used in North Cyprus for space heating. The results of an economic and environmental comparison in respect to use THS instead of these systems showed that payback time would be 6 years based on the capital and operational costs of THS compared to the average operational costs of GH, EH and HP. Similarly, CO_2 savings would be 47.9 tonnes.

According to the theoretical analysis, THS was found to be a feasible method to utilize for space heating purposes in Northern Cyprus. It has very good potential to replace electrical and gas sourced heating systems which have negative effects on the environment and economy. The remarkable solar potential in Northern Cyprus, which is > 6 kWh/m^2 in summer, should be harvested to meet the heating demand in winter by utilizing THS.

It should be noted that; obtained results are based on a non-insulated concrete building, which is most common type of dwelling in NC. Using insulation materials in buildings could provide a substantial reduction in yearly heat load, thereby required THS storage volume and collector size will be smaller. This condition will also reduce the system installation costs and payback period thus brings the THS application in Cyprus to more feasible level. In this respect, the Northern Cyprus government should raise the public awareness and promote a transformation away from traditional space heating systems for a sustainable future.

In the second part of Chapter 6 (Please see: Chapter 6.3), a novel open THS concept is experimentally investigated. It is aimed to present an alternative design / method for reactor design and efficient solar harvesting concept for open THS systems. Discharging performance of the purposed system was tested in a real building and charging performance was examined with the integrated solar collectors in an open environment under Cyprus climate conditions.

According to the testing results 2.85 kWh thermal energy is generated using 0.013 m^3 of absorbent corresponding to a 219.2 kWh energy storage density. Additionally thermal power output and discharging COP varied in the range of 0.53 kW-0.37 kW and 13-9 for a 9 hour discharging period respectively. During that time, provided heat was sufficient to meet the heat load of the test room having floor area of 12.4 m^2. On the other hand, 60% drying ratio is achieved during the charging process utilizing solar energy. It is concluded that high ambient humidity is the main challenge for drying the absorbent in Cyprus climate conditions. However further improvement (e.g. optimization of SP and SC dimensions, materials etc.) of the designed unit could allow to achieve higher sorbent temperatures. Thereby full dehydration could be achieved. Realizing this condition will lead to multi-cylic usage of the absorbent as solar-rechargable thermal battery.

Due to the compact nature of the presented system (SP-SC), space requirement can be significantly reduced therefore wider usage of THS could be realized. Additionally the unit could be made up of light structural materials and could even be used as a portable heater. Thus an alternative low cost and sustainable method could be achieved for space heating applications.

CHAPTER 7: DESIGN DEVELOPMENT AND FIELD TESTING OF A FULL SCALE SOLAR DRIVEN THERMOCHEMICAL HEAT STORAGE

7.1 Introduction

Transpired solar collector (TSC) technology is a building integrated solar air heating system, combining design, renewable energy generation and control to provide space heating. It can easily meet the thermal demands of a typical building in summer, however, due to seasonal changes and increase in heat demand, it can only deliver limited amount of thermal demands in winter. The challenge is therefore the efficient storage and release of this generated solar thermal energy. Thermochemical storage can be used to store the excess solar thermal energy generated by TSC in summer, to be recovered in winter months. The solar driven THS concept has been proven with the theoretical (See: Chapter 3) and laboratory scale experimentation (Chapters 4-6) as presented in previous chapters and this part of the study looks development of a full scale prototype and its thermal performance analysis.

Within the study, it is aimed to upscale the reactor concept (using embedded air diffuser pipes) which has provided high E_d in lab. scale experimentation (See: Chapters 4.4 and 5) and construct a building scale demonstrator to evaluate the THS performance integrated with TSCs in a typical industrial building under UK climatic conditions. Based on the obtained promising results in Chapters 3-6, SIM-3a was chosen as the sorption material to be used in the system.

The objectives of the study were:

- To construct a building scale demonstration system as proof of concept on large scale solar driven THS
- To perform testings and investigate the system thermal performance in THS discharging and TSC space heating modes
- To analyse the E_d of the THS system and compare with the E_d obtained in lab-scale unit to evaluate the effectivity of the reactor concept with the increased system size.

7.2 Concept and system design

The 3D front and back side views of the developed heat storage prototype were given in Figure 7.2.1. System consists of roof mounted TSCs, an auxiliary gas sourced heater, an ultrasonic humidifier, computer and datalogging equipment, system control tools, air handling unit, heat storage container and ducting. The system operation is fully automated and system operating modes, operating parameters and air flow is controlled and monitored with a computer connected control system.

The heat storage system consists of 4 sorbent vessels placed inside the heat storage container. There are air dampers at the bottom of each vessel. The position (open/closed) of the dampers are controlled with actuators. The applied contol is based on the air pressure difference. Air flows inside the fully sealed container and once the air pressure reaches to the set level, the chosen vessel damper opens and allows air flow through the sorbent vessel. As seen from the Figure 7.2.1, each vessel is connected to the outlet port where air flows either to the building (discharging) or exhausted to the environment (charging). Sorbent vessels are made up of steel and has the dimensions of 998 mm x 996 mm x 1396 mm and V_s of 0.8 m^3 .

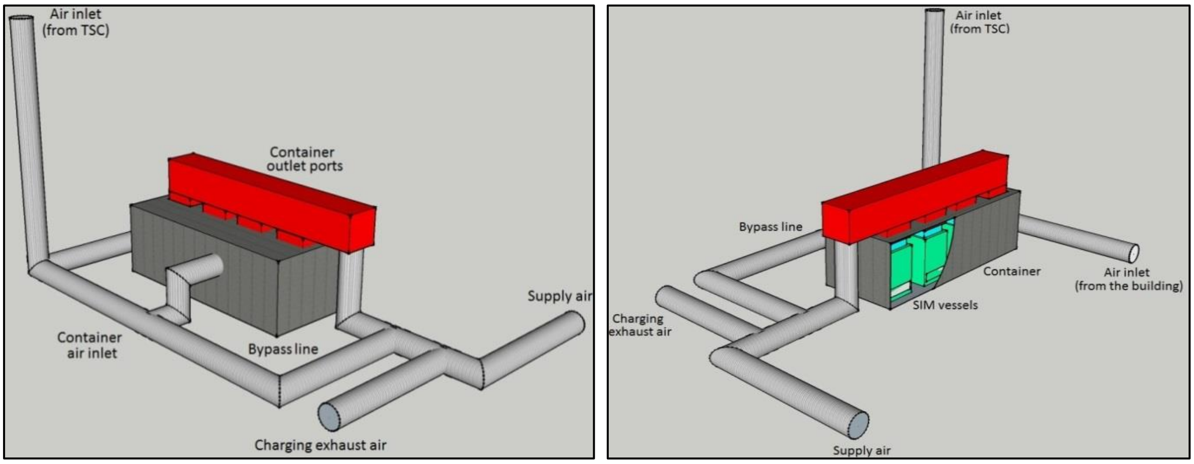

Figure 7.2.1 3D views of the front (left) and back (right) side of developed prototype

Perforated air diffusers used inside the sorption vessels to provide effective heat and mass transfer. The concept has tested under laboratory conditions as presented in Chapter 4 and Chapter 5 and based on the obtained promising results decided to be applied in the full scale prototype. Views of the sorbent vessels were given in Figure 7.2.2. As seen there are 36 perforated pipes with the hole diameter, *d*=4 mm placed vertically inside the vessel with a distance of *l*=100 mm between each other.

Figure 7.2.2 Views of the sorbent vessel

In discharging process, adequate amount of water vapour needs to be continuously added to the air in order to provide an effective sorption process and extracting the stored heat. An ultrasonic humidifier (see: Figure 7.2.3) is employed in the system with the vapour generation capacity of 30 kg/h. The ultrasonic humidifier uses a piezoelectric transducer to create a high frequency mechanical oscillation in a film of water. This forms an extremely fine mist of droplets about one micron in diameter that is quickly evaporated into the air flow. In the system, the humidifier is connected to the air channel with a pipeline and where generated vapour mixes with the air.

Figure 7.2.3 Internal and external view of the ultrasonic humidifier

The schematic of the system design is given in the Figure 7.2.4 below. There are two inlets where ambient air can pass through the TSCs and enter the system or air inside the building could be blown into ducting. If needed system could be used in mixed mode. The inlet air then could be either directed to the container or could be used directly via bypass line. In discharging or TSC direct heating mode, process air is supplied to the building. In charging mode, moist air is exhausted to the ambient. More detailed description of system operational modes will be given in section 7.5.

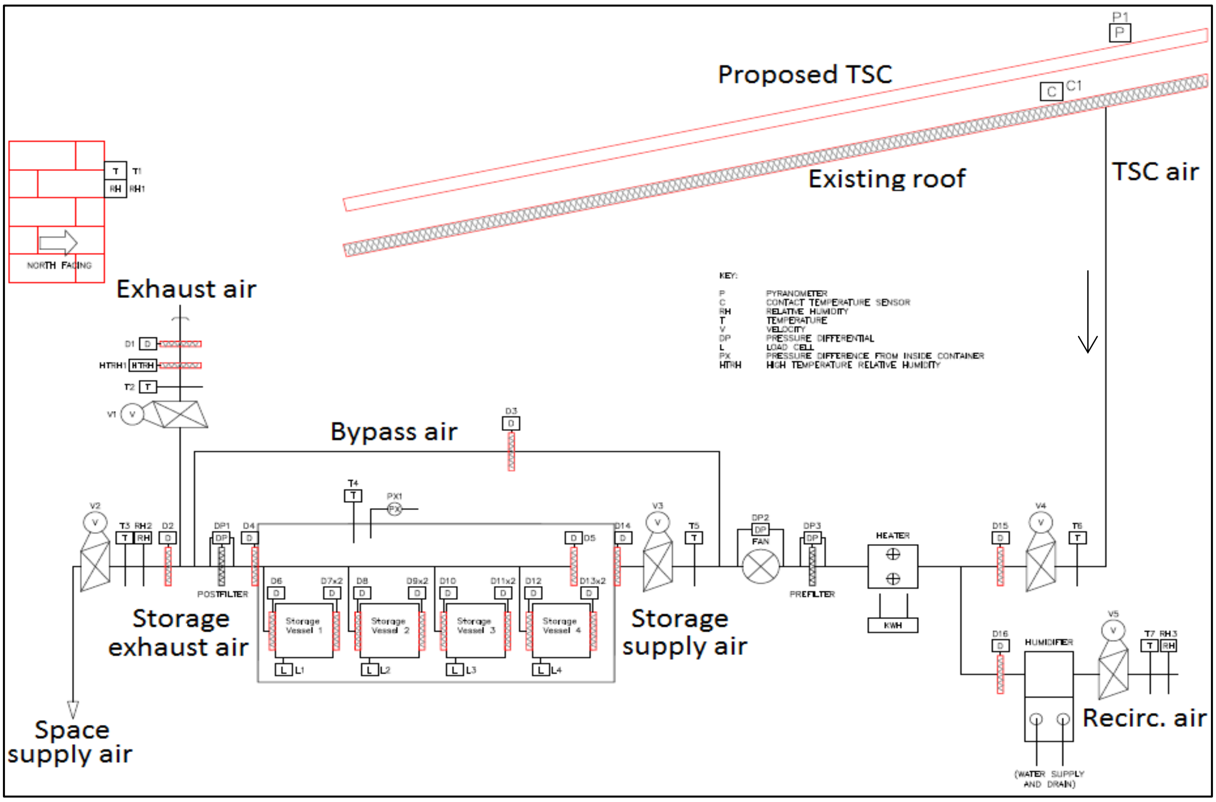

Figure 7.2.4 System technical drawing and illustration of system components

Developed prototype uses mainly conventional equipment that is available in the market and easy to access. The novelties of the system are;

- The design of the sorbent vessels that provides uniform air flow and enhanced heat/mass transfer in the sorption system.
- Roof mounted/retrofitted TSCs that absorbs solar energy while creating an aesthetic appearance on the building roof,
- Composite sorption material that has high E_d, low T_{reg} and low cost also which is environmentally friendly and durable,
- Process design enabling five different operational modes therby providing operational flexibility and effective system operation,
- The advanced control system that maximizes utility of both solar energy and stored heat also eases system operation.

All system components/materials were specifically selected/manufactured and sized, based on the results obtained from developed numerical models and laboratory scale experimental prototypes. The sorption material SIM-3a was synthesized by applying the same procedure described in Chapter 4.1. The design of the developed sorption reactor is the up-scaled version of the Gen2 rig which has introduced in Chapter 4.3. The modularity aspect and process design of the system is based on the modular sorption pipe unit experimented in Chapter 5. The integrated THS and TSC design and operation is also adapted from the theoretically investigated system for Cyprus as presented in Chapter 6.1. The equipments used in the system were given with their specification in the Table 7.1 below ;

Table 7.1 System component specifications

Equipment	**Specification**
Ductwork Insulated	Galvanized spiral
Fan	Variable speed (sized to meet given flows and static drops defined by contractor's design). Unless stated otherwise static pressure drops are assumed of 100 and 200 Pa for TSC collector and storage container respectively.
Humidifier	Ultrasonic humidifier with the capacity to add 30kg/h of water to the air. 
Heating Element	Indirect gas fired burner fed from local bottle supply (no mains gas in this area). Burner capacity is 50kW. 

Filter	G4 filters as drawn pre and post storage container. All SIM should stay in its vessel but the post storage filter is a failsafe to ensure none is discharged to internal space or outside. It should be noted that the SIM is corrosive.
Attenuator	Contractors specification
Damper (normal)	Contractors specification 
Damper (100%)	Dampers D4, 5 & 14 are specified to be 100% close. These 3 dampers will also have position feedback to the controller. 
Container	Typical sea ISO container
SIM Vessels	See sketch below; shows a steel structure lined with stainless where in contact with SIM. Vessels provided by others to exclude dampers. Mechanical contractor to allow for 8 off SIM inlet dampers (2 off per vessel) nominally 300 x 1000 mm. Mechanical contractors also to provide bellows connection to ductwork as drawn that can be disconnected to allow for vessel removal. 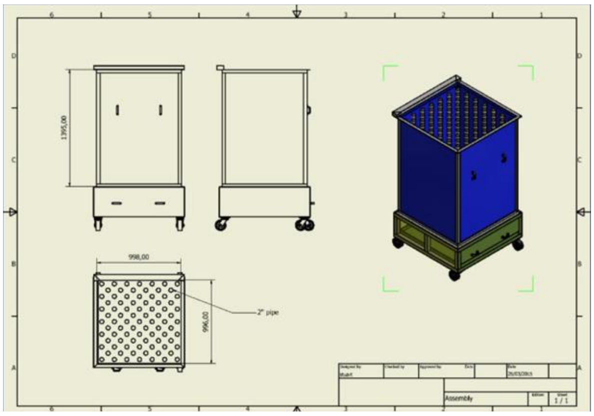
Load cells	These instruments are critical to the system control. There are 4 SIM vessels each circa 1.5 tonnes. The SIM can gain / loose up to 50% of its weight in water during discharge / charge. The container environment could be up to 80 °C during charging and 75% relative humidity during discharge.

TSC	150 m^2 corrugated absorptive cover with air flow channels - installed to the roof. 

7.3 Description of TWI building and system integration

The TWI is a research building located in Port Talbot, UK and it is used for demonstration of novel energy systems/technologies. Beside the proposed solar powered THS system, there is a solar assisted heat pump system which has been already installed in the building as part of another project. In that system, building's corrugated wall is retrofitted with TSC (See: Figure 7.3.1) and solar heated air transfers its energy to an air to water heat pump via a heat exchanger for hot water generation. A 10 m^3 insulated tank is used in the system for store the hot water thereby to balance the mismatch between solar energy availability and building heating demand.

The proposed seasonal solar driven thermochemical heat storage system was integrated in the first floor of the building as a showcase of solar heating which promotes the use of renewables in building space heating applications.

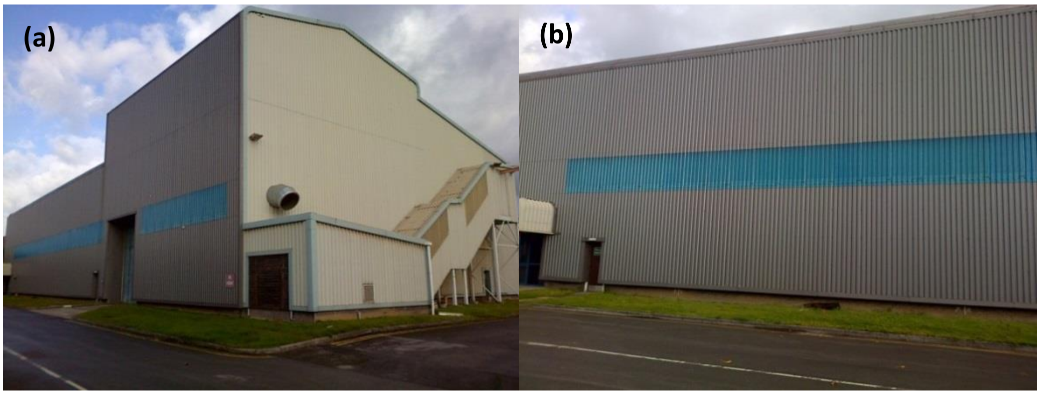

Figure 7.3.1 (a) Frontal view, (b) side view of the demonstration building

Within the project, the building roof is retrofitted with 150 m^2 TSC. The heated air is proposed to be used for charging the sorbent, thereby storing solar energy in summer. In sunny days of winter, solar heated air could be used directly for space heating. For the days when solar energy is not available or insufficient, air could be heated via stored solar energy in sorption materials to meet the building heating demand. The view of building roof before and after TSC installation is presented in Figure 7.3.2. Basically TSC is a corrugated absorptive black layer placed on the building roof creating an air channel where the air flows in between. The aim of using the TSCs in the developed system is to heat the air with solar energy for charging the sorbent (e.g. desorbing the moisture) over the summer period when solar energy is abundant. Additionally TSCs were also purposed to be used for direct solar space heating in sunny winter days. This will reduce the load on THS and enable using it in more effective manner (e.g. using TSCs during daytime and THS at night time).

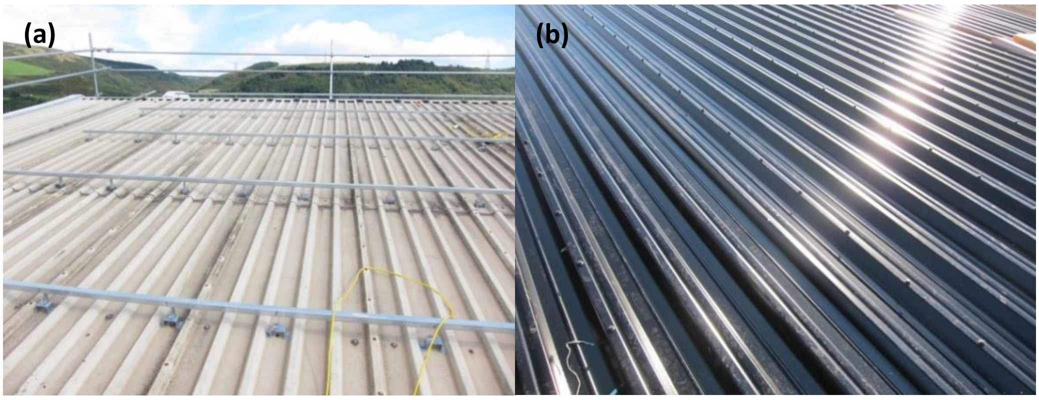

Figure 7.3.2 View of building roof (a) before and (b) after TSC installation

In Figure 7.3.3 installation steps of the heat storage container is illustrated. The fabricated container made up of galvanized steel placed to the specially designed area in the first floor of the TWI building.

Figure 7.3.3 (a) Location, (b) external, (c) internal view of the THS container, (d) view of sorption vessels installed inside the container

The container sits on a frame and it has inlets on the right side and four outlets at the top which are connected to the sorbent vessels. The internal view of the container before and after locating the sorbent vessels can be seen at the bottom part of Figure 7.3.3. As the sorbent vessel dampers controlled with the air pressure created inside, the container is fully insulated to prevent any air leakage during the system operation.

7.4 System operational modes and demand control

Schematic illustration of the sytem is presented in Figure 7.4.1. In order to use the system in most effective way and meet the varying heat demand of the building, designed process includes 5 modes of operation as explained below. The component numbers seen in Figure

7.4.1 is also given in the brackets in description of the system operational modes (see: Sections 7.4.1-7.4.5) to provide clarity.

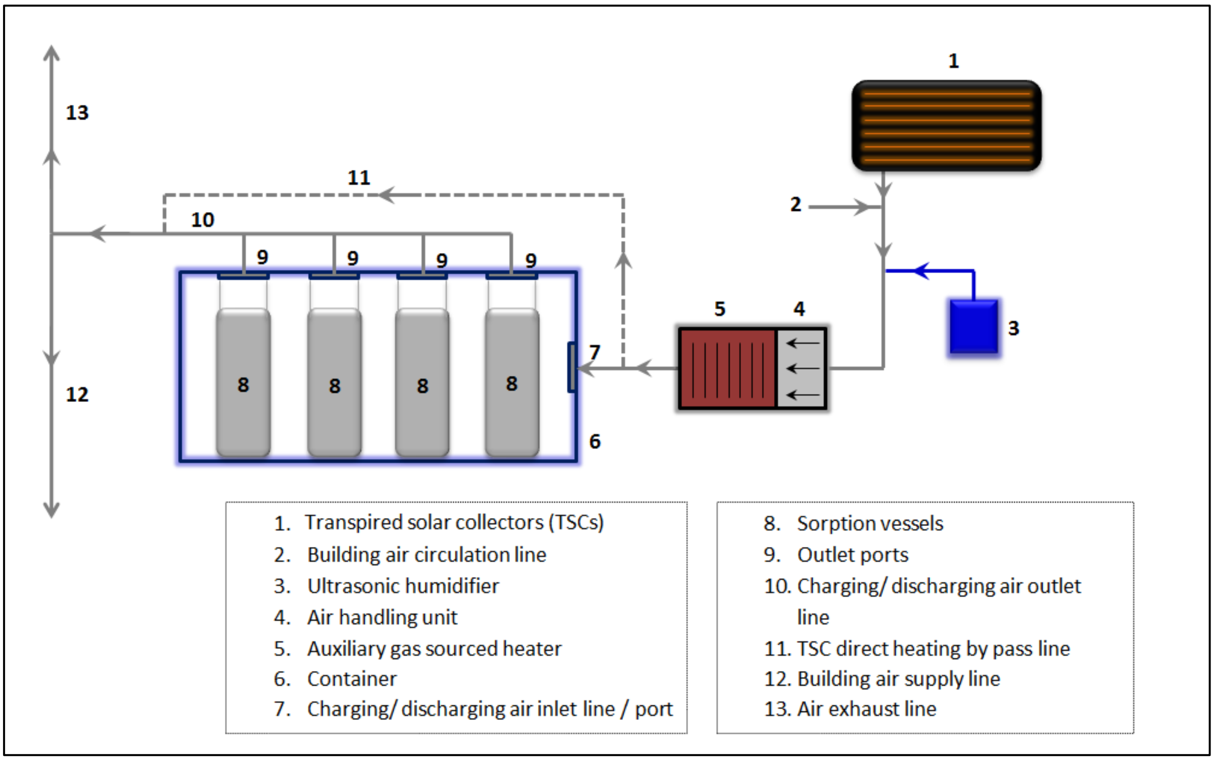

Figure 7.4.1 Schematic illustration of the solar powered THS system

7.4.1 Heat storage charge only

Warm air from the TSC (1), possibly boosted by the conventional heater (4), passes through 1 or more of the storage vessels (7) to drive the water off the Salt in Matrix (SIM). Air is discharged to atmosphere (12). Thermal storage charge rate and capacity will be measured by the weight of the individual storage vessels within the container.

7.4.2 Heat storage discharge only

Recirculation air (2) from the internal space is humidified (3) to add the water to the Salt in Matrix (SIM) (1 or multiple vessels simultaneously). This heated air is delivered direct back to the internal space (12). The humidity levels of the air stream before and after the storage container will be key control parameters as well as temperature. Thermal storage discharge rate and capacity is measured by the weight of the individual storage vessels within the container.

7.4.3 TSC space heating only

a. Variable speed fan (4) draws air from the TSC plenum (1), by-passes the storage container (11) and delivers space heating and ventilation air direct to the internal space (12).

b. At times when TSC air temperature is too high internal recirculation air (2) can be blended with TSC air (1) to maintain a maximum supply temperature.

7.4.4 Auto mode selection

In auto mode system switches automatically between the TSC space heating (1-11-12) and heat storage discharging (2-7-10-12) modes depending on the air temperature obtained with the TSC. This mode maximizes utility of solar energy and unnecessary usage of heat storage while eliminating the need for system operator.

7.4.5 Off / shutdown

a. In a controlled standby condition it is important that the heat storage vessels (8) and their container (6) are sealed so that moist air does not ingress in and discharge the SIM.

b. In an emergency shutdown or when preparing for maintenance requiring access to the container the SIM vessels will still be isolated but the container supply (7) and exhaust

dampers (9) would be open to allow the container to cool and depressurise.

7.5 System settings and operating parameters

The key system settings / operating parameter ranges are detailed within this section for the different modes of operation and presented in Tables 7.2-7.4 for heat storage charge, heat storage discharge and TSC space heating modes respectively.

Table 7.2 System settings and operating parameters in heat storage charging mode

No	*Parameter*	Value	Unit	Description
1	V_{min} *TSC*	0.1	m^3/s	TSC minimum air flow rate
2	V_{max} *TSC*	1.8	m^3/s	TSC maximum air flow rate
3	V_{sp} *TSC*	1.2	m^3/s	Set point of container air flow rate
4	T_{min} *TSC*	12	°C	TSC minimum outlet air temperature
5	T_{max} *TSC*	80	°C	TSC maximum outlet air temperature
6	T_{sp} *TSC*	70	°C	Set point of TSC outlet air temperature – depends on solar gain
7	V_{min} *SIM*	TBD	m^3/s	Minimum air flow rate through SIM 1 or more vessels simultaneously
8	V_{max} *SIM*	1.5	m^3/s	Maximum air flow rate through SIM 1 or more vessels simultaneously.
9	V_{sp} *SIM*	TBD	m^3/s	Set point of air flow rate through SIM 1 or more vessels simultaneously.
10	P_{max}	400	Pa	Container max pressurisation
11	P_{min}	20	Pa	Container minimum pressurisation to prevent ingress of moist air when system is in standby.
12	P_{sp}	TBD	Pa	Set point of container pressure
13	T_{min} exhaust	40	°C	Mimimum air temperature exiting the container/exhausted to outside during charging
14	T_{max} exhaust	70	°C	Minimum air temperature exiting the container/exhausted to outside during charging
15	TSC charge rate	20 - 50	kW	TSC heat generation at design flow rate of $1.2m^3/s$.
16	Gas heater rate	20 - 50	kW	Gas heater heat generation at design flow rate of $1.2m^3/s$.
17	Heat in during charge rate	70	kW	Combined TSC & gas heat generation - assuming a 60 ^oC lift over ambient is required
18	Heat transfer to SIM during charge	10 - 20	kW	At $1.2m^3/s$ air speed supplied to SIM at 70 ^oC and exit SIM at 57 ^oC leads to 17.5kW
19	Charge capacity	3500	kWh	Thermal storage capacity of SIM as drawn.
20	Charge duration	200	hours	Time to charge SIM at 17.5kW.
21	SIM water desorption rate	5 - 15	kg/h	SIM mass will decrease by up to 50% during charge. This as measured by the vessel load cells is the critical control parameter.

Table 7.3 System settings and operating parameters in heat storage discharging mode

No	*Parameter*	Value	Unit	Description
1	*V TSC*	0	m^3/s	TSC supply damper closed – no air flow
2	V_{min} recirc	0.1	m^3/s	Recirculation minimum air flow rate
3	V_{max} recirc	1.2	m^3/s	Recirculation maximum air flow rate
4	V_{sp} recirc	1.0	m^3/s	Set point of recirculation air flow rate
5	T_{min} recirc	12	°C	Minimum building internal space/recirculation air temperature in recirculation duct
6	T_{max} recirc	30	°C	Maximum building internal space/recirculation air temperature in recirculation duct
7	*RH* recirc	30 - 50	%	Relative humidity of recirculation air - Depends on time of day, internal space and seasonal conditions
8	*RH* storage	>75	%	Relative humidity of air supplied to the SIM vessel -

	supply air			Humidifier will add water according to RH set point
9	V_{min} SIM	TBD	m^3/s	Minimum air flow rate through SIM 1 or more vessels simultaneously.
10	V_{max} SIM	1.5	m^3/s	Maximum air flow rate through SIM 1 or more vessels simultaneously.
11	V_{sp} SIM	TBD	m^3/s	Set point of air flow rate through SIM 1 or more vessels simultaneously.
12	P_{max}	400	Pa	Container max pressurisation
13	P_{min}	20	Pa	Container minimum pressurisation to prevent ingress of moist air when system is in standby.
14	P_{sp}	TBD	Pa	Set point of container pressurisation
15	T_{min} space supply air	16	°C	Minimum air temperature exiting the container during discharging and returning to the internal space
16	T_{max} space supply air	40	°C	Maximum air temperature exiting the container during discharging and returning to the internal space.
17	SIM heat discharge rate	<35	kW	This heating capacity is directly dependent on the rate of water adsorption onto the SIM and by definition the rate of change of SIM vessel mass
18	SIM water adsorption rate	5 -25	kg/h	SIM mass will increase by up to 50% during discharge. This is measured by the vessel load cells is the critical control parameter.

Table 7.4 System settings and operating parameters in TSC Space Heating mode

No	*Parameter*	Value	Unit	Description
1	V_{min} TSC	0.1	m^3/s	TSC minimum air flow rate
2	V_{max} TSC	1.8	m^3/s	TSC maximum air flow rate
3	V_{sp} TSC	1.2	m^3/s	Set point of TSC air flow rate - will turn down if solar gain insufficient to maintain set point temperature at design flow rate.
4	T_{min} TSC	12	°C	TSC air in duct temperature
5	T_{max} TSC	60	°C	TSC air in duct temperature
6	V storage supply	0	m^3/s	Flow rate bypasses storage container and discharges to the internal space.
7	V_{min} recirc	0	m^3/s	Recirculation minimum air flow rate
8	V_{max} recirc	1.0	m^3/s	Recirculation maximum air flow rate
9	V_{sp} recirc	controlled	m^3/s	If T_{TSC} is greater than upper limit (e.g. 40 °C) then some internal recirculation air will blend to ensure the space supply air does not exceed 40 °C.
10	T_{min} space supply air	12	°C	Minimum Space supply air temperature
11	T_{max} space supply air	40	°C	Maximum Space supply air temperature

7.6 System control and operation

7.6.1 Heat storage charge

So long as the duty vessel has heat charge capacity left (see below) then the system will run with the flow rate being determined as follows:

1. Flow rate at design so long as TSC + conventional heat achieve set point for storage feed air.
2. If gas has modulated to 100% and gas + TSC cannot achieve set point for storage feed air then fan modulates flow rate down to achieve set point for storage feed air.

The duty vessel will be deemed to have charge capacity left if both the following criteria are met:

1. Vessel weight, which is the total of the SIM and empty vessel weight, is above the initial weight (SIM in dry state) measured at the start of the previous discharging cycle. (Provides a general indication that sorbent is still moist)
2. Vessel rate of mass decrease due to water desorption is above a certain minimum level (e.g. >10 kg). (Provides a more accurate indication that desorption rate is still higher than the set level. This is a sign that the sorbent is highly moist and charging cycle should continue)

7.6.2 Heat storage discharge

So long as the duty vessel has heat discharge capacity left (see below) then the system will run with the flow rate being determined as follows:

1. Fan to deliver flow at design rate.

2. Container supply, extract and by-pass dampers (100089-007 D4, 5 &14) modulate to maintain storage exhaust air at space heating set-point (e.g. 40 ^{o}C).

The duty vessel will be deemed to have discharge capacity left if both the following criteria are met:

1. Vessel weight is which is the total of the SIM and empty vessel weight, is above the initial weight (SIM in wet/saturated state) measured at the start of the previous charging cycle. (Provides a general indication that sorbent is still not saturated with moisture)
2. Vessel rate of mass increase due to water adsorption is above a certain minimum level (e.g. >10 kg/h). (Provides a more accurate indication that adsorption rate is still higher than the set level. This is a sign that sorbent is not highly moist yet and discharging cycle should continue)

7.6.3 TSC space heating

So long at the space presents a heating demand and the TSC can deliver useful renewable heat the fan will operate as follows:

1. If TSC air temperature > space set point, then fan will run at full design flow rate.
2. If T_{min} < TSC air temperature < space set point, then fan will modulate down to V_{min}.

7.7 Measurement, datalogging interface and sensor locations

During system operation, all measured parameters are monitored and recorded via a computer integrated datalogging software (see: Figure 7.7.1) specially designed by the Building Services Ltd. for the developed heat storage prototype. The software has two interfaces as presented in Figures 7.7.2 where one of the interfaces illustrates the air *T* and

RH variation between TSC and container inlet and the second one between the container and building supply /exhaust.

Figure 7.7.1 Datalogging and monitoring hardware

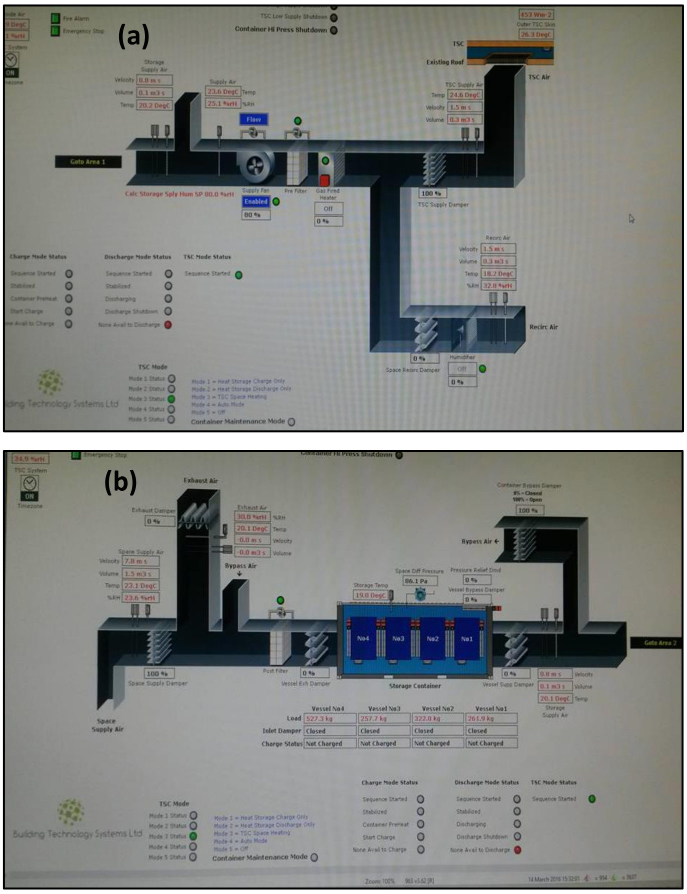

(a)

453 Wm-2

Outer TSC Skin 26.3 DegC

Storage Supply Air: Velocity 0.8 m s; Volume 0.1 m3 s; Temp 20.2 DegC

Supply Air: 23.6 DegC Temp; 25.1 %rH %RH

TSC Supply Air: Temp 24.6 DegC; Velocity 1.5 m s; Volume 0.3 m3 s

Calc Storage Sply Hum SP 80.0 %rH

Supply Fan: Enabled ●; 80 %

Gas Fired Heater: Off; 0 %

TSC Supply Damper: 100 %

Recirc Air: Velocity 1.5 m s; Volume 0.3 m3 s; Temp 18.2 DegC; %RH 32.8 %rH

Space Recirc Damper: 0 %

Humidifier: Off ●; 0 %

Charge Mode Status: Sequence Started ○; Stabilized ○; Container Preheat ○; Start Charge ○; None Avail to Charge ○

Discharge Mode Status: Sequence Started ○; Stabilized ○; Discharging ○; Discharge Shutdown ○; None Avail to Discharge ●

TSC Mode Status: Sequence Started ●

TSC Mode: Mode 1 Status ○; Mode 2 Status ○; Mode 3 Status ●; Mode 4 Status ○; Mode 5 Status ○

Mode 1 = Heat Storage Charge Only
Mode 2 = Heat Storage Discharge Only
Mode 3 = TSC Space Heating
Mode 4 = Auto Mode
Mode 5 = Off

Container Maintenance Mode ○

(b)

34.9 %rH

Exhaust Damper: 0 %

Exhaust Air: 30.8 %rH %RH; 20.1 DegC Temp; -0.0 m s Velocity; -0.0 m3 s Volume

Space Supply Air: Velocity 7.8 m s; Volume 1.5 m3 s; Temp 23.1 DegC; %RH 23.6 %rH

Space Supply Damper: 100 %

Container Bypass Damper: 0% = Closed, 100% = Open; 100 %

Space Diff Pressure: 86.1 Pa

Pressure Relief Dmd: 0 %

Vessel Bypass Damper: 0 %

Storage Temp: 19.0 DegC

Vessel Exh Damper: 0 %

Vessel Supp Damper: 0 %

Storage Supply Air: 0.8 m s Velocity; 0.1 m3 s Volume; 20.1 DegC Temp

	Vessel No4	Vessel No3	Vessel No2	Vessel No1
Load	527.3 kg	257.7 kg	322.0 kg	261.9 kg
Inlet Damper	Closed	Closed	Closed	Closed
Charge Status	Not Charged	Not Charged	Not Charged	Not Charged

Charge Mode Status: Sequence Started ○; Stabilized ○; Container PreHeat ○; Start Charge ○; None Avail to Charge ○

Discharge Mode Status: Sequence Started ○; Stabilized ○; Discharging ○; Discharge Shutdown ○; None Avail to Discharge ●

TSC Mode Status: Sequence Started ●

TSC Mode: Mode 1 Status ○; Mode 2 Status ○; Mode 3 Status ●; Mode 4 Status ○; Mode 5 Status ○

Mode 1 = Heat Storage Charge Only
Mode 2 = Heat Storage Discharge Only
Mode 3 = TSC Space Heating
Mode 4 = Auto Mode
Mode 5 = Off

Container Maintenance Mode ○

Figure 7.7.2 Datalogger interfaces illustrating measurement points between (a) TSC inlet and THS inlet, (b) THS inlet and space supply/exhaust vents

The first interface displays the temperature and relative humidity measurements of the ambient air, TSC skin (surface), air drawn from TSC and from the building also outlet of air handling unit. The second interface displays the measurements of the container inlet air, container internal conditions, container outlet air, bypass line, supply air and exhaust air.

7.8 Field trial and experimental results

In order to investigate the performance of the developed solar driven THS prototype, preliminary experimental investigations have been performed. System performance was examined in TSC space heating and heat storage discharging modes. Obtained experimental results were presented and discussed in the following sections.

7.8.1 TSC Space heating

TSC space heating testings were performed between the dates of 23rd February – 28th February 2016. Measured TSC skin (surface) temperature, TSC supply temperature, ambient temperature and solar intensity for each testing day were presented in Figures 7.8.1 – 7.8.6. On 23th February, peak solar radiation of 0.58 kW was achieved during midday, whereas highest TSC skin and supply temperatures were 28 °C and 26 °C. During the day, ambient temperature varied in the range of 5 →13 °C. ΔT_{ave} of air across the TSC is calculated as ≈5.1 for 10 hours testing period whilst the ΔT_p was 14 °C. In the testing on 24th February, peak solar intensity was slightly lower (≈0.49 kW) but was much steadier than the solar radiation on 23rd February. As a result solar heat gain was considerably higher in that day. TSC skin and supply air temperatures reached to 30 °C and 27 °C, whilst the ambient temperature was in the range of 3 → 10 °C. Accordingly ΔT_p and ΔT_{ave} were found 14 °C and ≈8 °C for 10 hours testing period respectively.

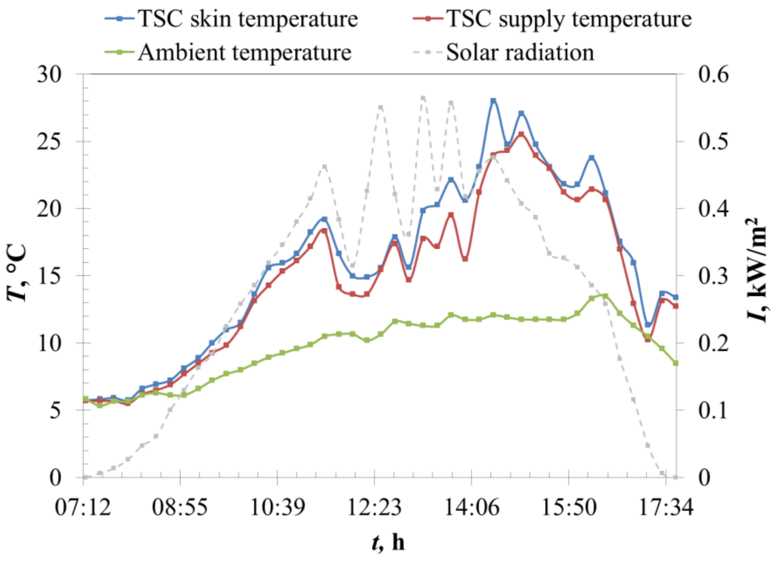

Figure 7.8.1 Measured temperatures and solar intensity on 23rd February 2016

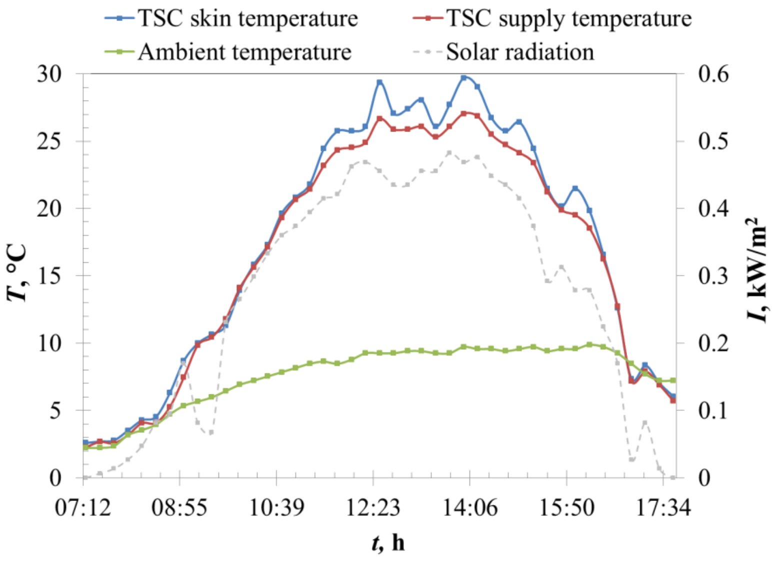

Figure 7.8.2 Measured temperatures and solar intensity on 24th February 2016

On 25th and 26th February, solar heat gain remained low due to the limited solar availability. Average solar radiation was found ≈0.17 kW for these days wheras it was in the range of 0.25-0.27 kW in first two days of testing, which led to higher heat gain. Peak supply air temperatures were obtained as 18 and 20 °C on 25th and 26th February respectively, and the ambient temperature was between 6 and 12 °C in both days.

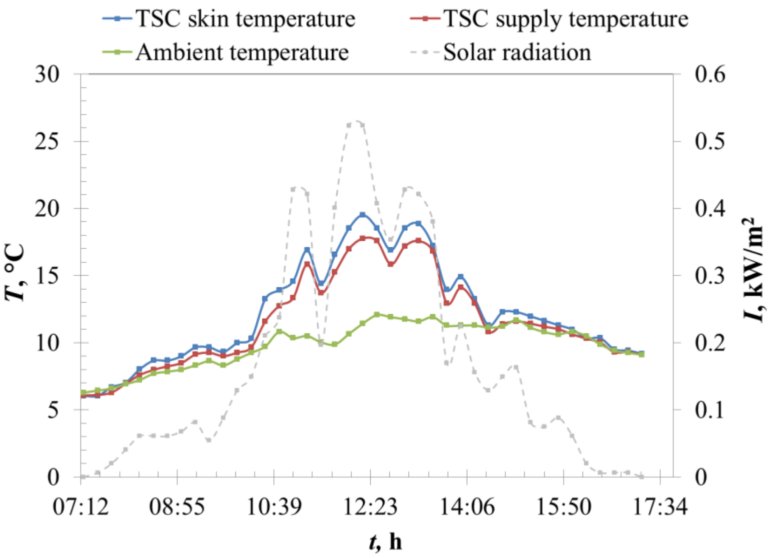

Figure 7.8.3 Measured temperatures and solar intensity on 25th February 2016

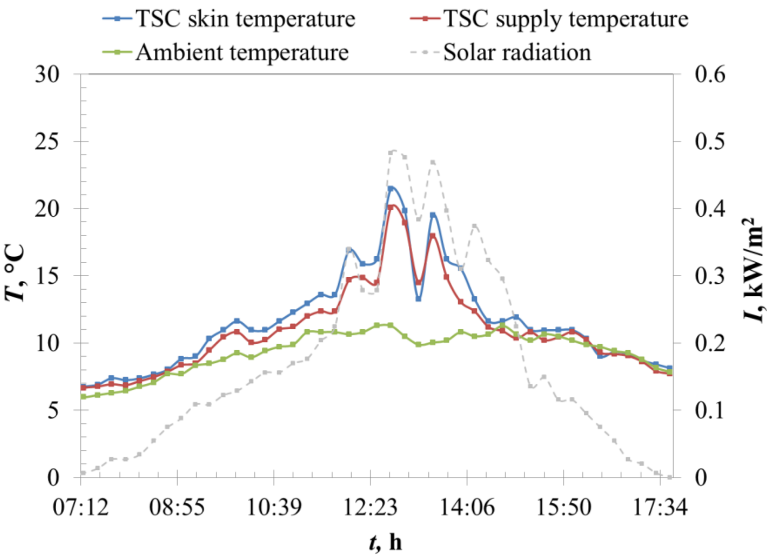

Figure 7.8.4 Measured temperatures and solar intensity on 26th February 2016

On 27th February, supply air temperature exceed 20 °C between 11 am – 1 pm, however due to reducing solar intensity, it sharply dropped to ambient level just after 2 pm. A Peak TSC skin temperature of 29 °C was also obtained for a short period of time. The ambient temperature was in the range of 5 →13 °C as represented in Figure 7.8.5.

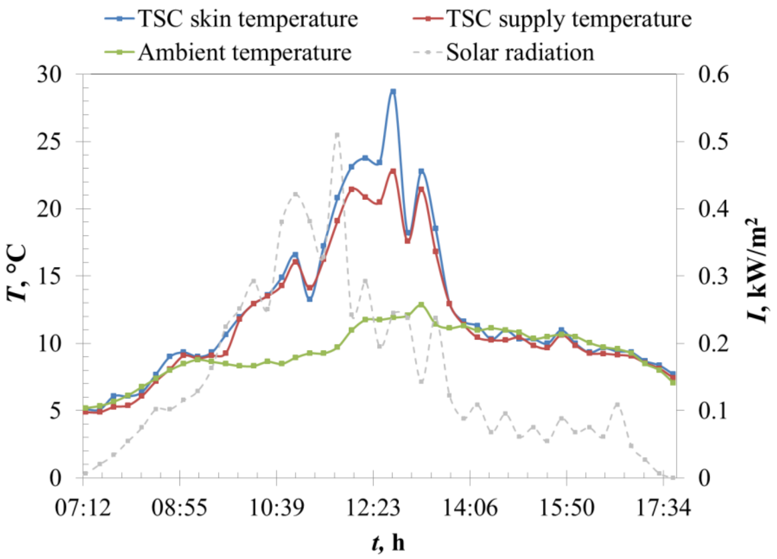

Figure 7.8.5 Measured temperatures and solar intensity on 27th February 2016

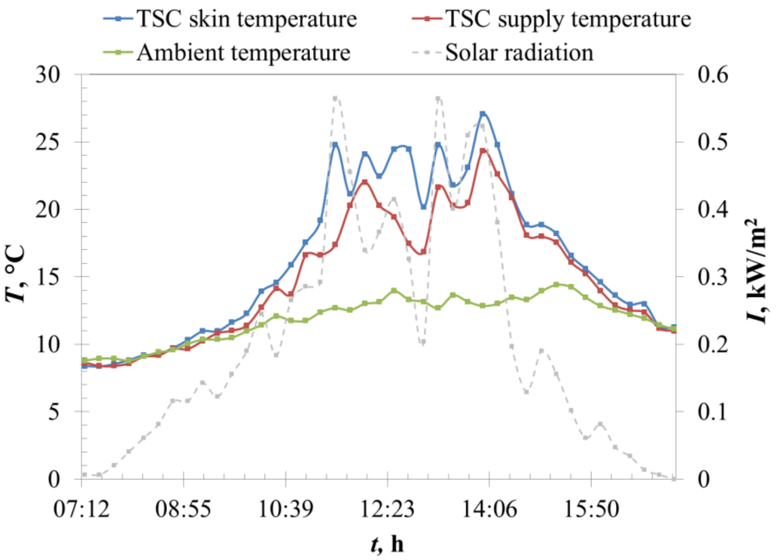

Figure 7.8.6 Measured temperatures and solar intensity on 28th February 2016

In the last day of testing, solar intensity was higher when compared with the previous three days of testing. However due to the shading effect by clouds, it dropped form 0.55 kW to 0.22 kW during midday, which considerably reduced the TSC skin and supply temperature. Average ΔT of 4 °C was obtained in the testing whilst the ΔT_p was 11 °C. Figure 7.8.7 illustrates the daily average solar intensity, average solar heat gain and daily total solar energy gain that is supplied to the building over the testing period. As seen from the Figure, highest solar energy gain (17.2 kWh) and highest average solar heat gain (1.6 kW) were obtained on 24th February. Second highest solar gain was achieved on 23rd Fubruary where Q_{ave} *and* E_{cum} were 1.2 kW and 12.2 kWh respectively. As seen from the Figure, on 23rd and 24th of February, I_s was in close approximation, however due to lower ambient temperature on 24th of February, solar gains were higher. Despite the high utility of solar energy in the first two days of the testing, in the remaining testing days, energy gain from TSCs was considerably less due to the low solar intensity. The lowest solar gains were obtained on 25th, 26th, 27th of February where obtained E_t was 4.02, 3.83and 4.53 kWh in these three days respectively. In the last day of testing (28th of February), with the increase of $I_{s,ave}$ to 0.25 kW/m^2, Q_{ave} rose to 0.83 kW and E_{cum} was reached to 7.3 kWh at the end of the day.

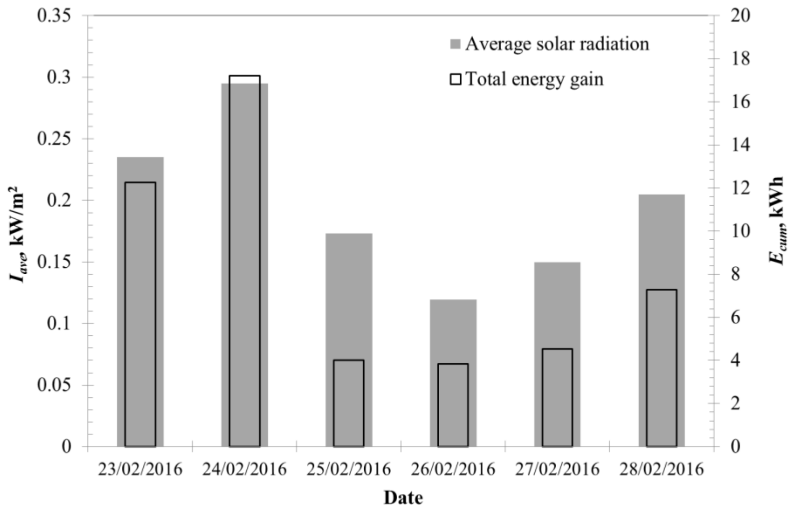

Figure 7.8.7 Daily average solar heat gain, solar radiation and daily total solar energy gain

Average ambient, TSC skin and TSC supply temperatures obtained over the testing period were presented in Figure 7.8.8. Temperature difference between TSC supply and ambient are the highest in first two days of testing, where the third highest ΔT was obtained on 28th of February.

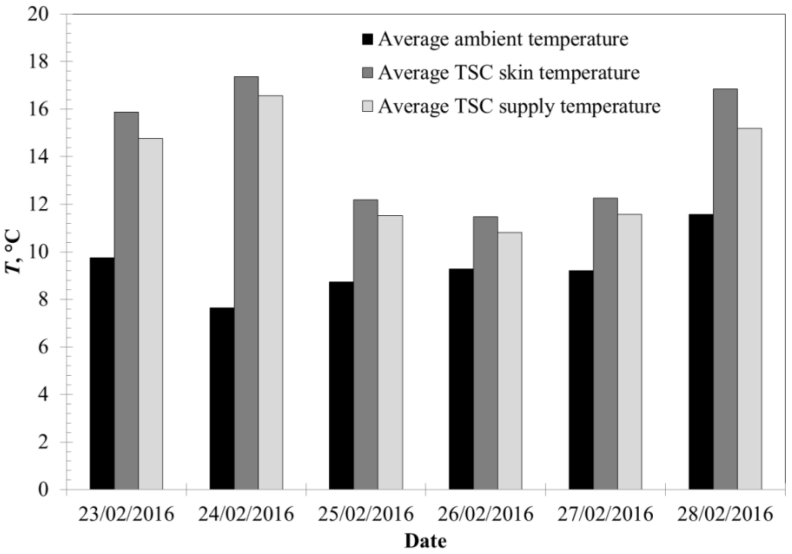

Figure 7.8.8 Daily average ambient, TSC skin and TSC supply temperature

As seen from Figure 7.8.8, average ambient temperature was lowest (7.6 °C) on 24th of February whilst the obtained ΔT was the highest (8.9 °C) among all testing days. TSC skin and supply temperatures remained low in the days of 25th – 27th February due to the low $I_{s,ave}$ as demonstrated above. In those testing days average TSC supply temperature was ≈8 °C and ΔT_{ave} was < 3°C.

The correlation between the average air temperature lift, ΔT_{ave}, across the TSCs and average solar radiation, I_{ave}, for six days testing period are presented in the Figure 7.8.9. As seen from the figure, there is a polynomial correlation between the I_{ave} and ΔT_{ave} indicating that increasing solar intensity has a major impact on solar heat gain of TSCs, particularly at higher I_{ave} levels due to the increasing rate of dT_{ave} / dI_{ave}. Variation of I_{ave} in the range of 0.12 kW →0.29 kW provided a substanatial increase of ΔT_{ave} from 1.5 °C to 8.9 °C.

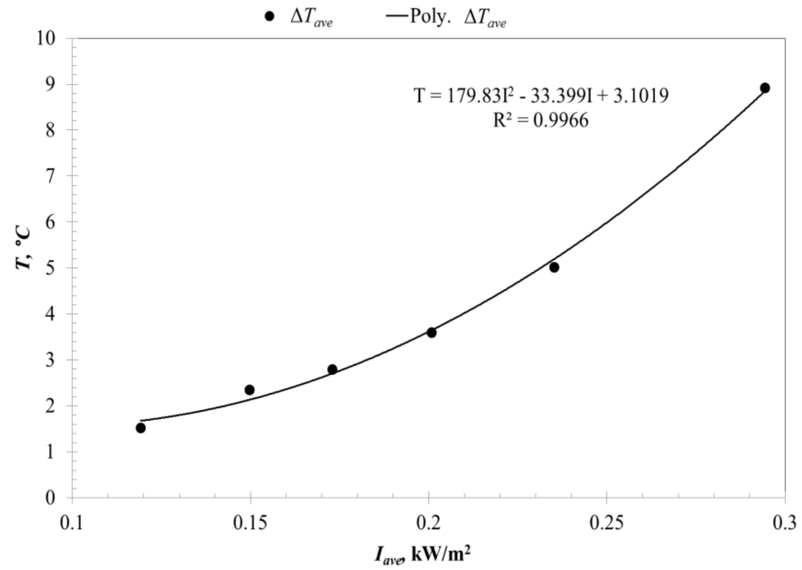

Figure 7.8.9 Correlation between daily average solar intensity and air temperature lift across the TSCs

According to the obtained correlation, I = 0.7 kW/m^2 would be sufficient to achieve ΔT = 67 °C during summer period for charging the sorbent. However, in that condition, due to higher TSC surface temperature, heat losses are also expected to be higher. Therefore I > 0.7 kW/m^2 should be met for solar charging of adsorbent without a need of an auxiliary heater.

Despite the low solar intensity under UK climate conditions, results showed that it is possible to utilize solar energy in some days of winter/spring for space heating with the use of building integrated TSCs. However there is a mismatch between building heat demand and available solar energy in most of the days and at nightime. Coupling THS with TSCs could provide a solution to this problem, which is proposed within this project. THS could be discharged when solar energy is not available to meet the building heat demand and balance the mismatch. Performance of the THS operation is investigated in the next section.

7.8.2 THS discharging

Preliminary testings performed on the prototype system in THS discharging mode were presented in this section. System performance was investigated with three different air

MFRs. Figure 7.10.10 shows a single sorption vessel performance (V_s = 0.8 m^3) over 50 hours discharging cycle for air MFR of 0.4, 0.6 and 0.8 kg/s. During the testings, recirculation air from the building was used as heat storage supply air (inlet air) and it was measured as 17±1 °C in all testings. Inlet air *RHs* varied in the range of 55-60% and boosted to 80% with the ultrasonic humidifier before entering the sorption vessel. Experimental results showed that, ΔT_a drops with the increasing m_a. For m_a= 0.4 kg/s T_o reached to 29 °C and it was steady over t = 20 hours. After that time a gradual drop started and at the end of 50 hours T_o was measured as 18.9 °C while T_i was 16.1 °C. As seen from the Figure 7.8.10, for m_a= 0.6 kg/s and m_a= 0.8 kg/s, $T_{o,p}$ was 26.3 °C and 24.5 °C respectively. $T_{o,ave}$ is calculated as 25.6, 23.9 and 22.5 °C and ΔT_{ave} was calculated as 9.5, 7.7 and 6.1 °C for m_a = 0.4, 0.6 and 0.8 kg/s respectively. Indeed, drop of ΔT at higher m_a level was something expected, as larger quantity of air needs to be heated per unit time with the same amount of generated sorption heat.

With the laboratory scale experimental units, as presented in Chapters 4 and 5, the obtained ΔT values were > 20 °C whilst in the real scale prortotype system ΔT_p was <10 °C in all testings as seen in Figure 7.8.10. Two reasons mainly influenced on the reduced ΔT. First, due to the increase in system size, large quantity of heat is spent for sensible heating the reactor, ducting material and adsorbent. Despite the system is externally insulated, heat loss to the surroundings is also unavoidable due to the large system dimensions. Second factor affecting the ΔT is the humidity content of inlet air. As demonstrated in Chapter 5, moisture sorption rate has a pivotal role on the achievable ΔT. In the performed testings, the inlet conditions were T_i =17 °C *and* RH_i= 80% corresponding to w_i =9.5 g/kg and p_v= 15.3 mbar which may not be sufficient for adequate sorption heat generation. With the increase of T_i, for the same *RH* level, supplied moisture content considerably increases and that could enhance the ΔT. However it should be noted that higher rate of moisture supply could reduce the reaction time while enabling a rise in ΔT. Morover energy consumption of the humidifier increases when system is operating at high moisture level. This is also an important aspect that should be considered. Figure 7.8.11 illustrates the thermal power (Q_g) and cumulative energy (E_{cum}) gained form the system in discharging process. Results showed that both the Q_g and E_{cum} have an increasing trend with the increasing m_a. This could be explained with the higher moisture sorption rate (e.g. higher moisture supply at higher m_a) also better diffusion of air through the sorbent as a result of increasing air pressure. $Q_{g,ave}$ were determined as 3.8, 4.6 and 4.8 kW for the m_a in the order of 0.4, 0.6 and 0.8 kg/s. Accordingly, E_{cum} over 50 hours discharging duration was calculated as 195, 236 and 248 kWh for the same order of MFRs.

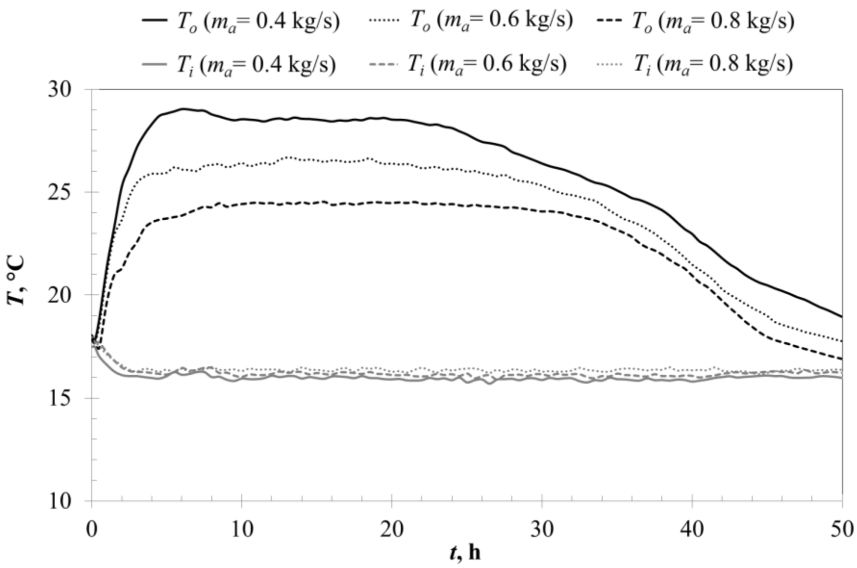

Figure 7.8.10 Variation of air inlet and outlet temperature for three different air mass flow rates in discharging cycle

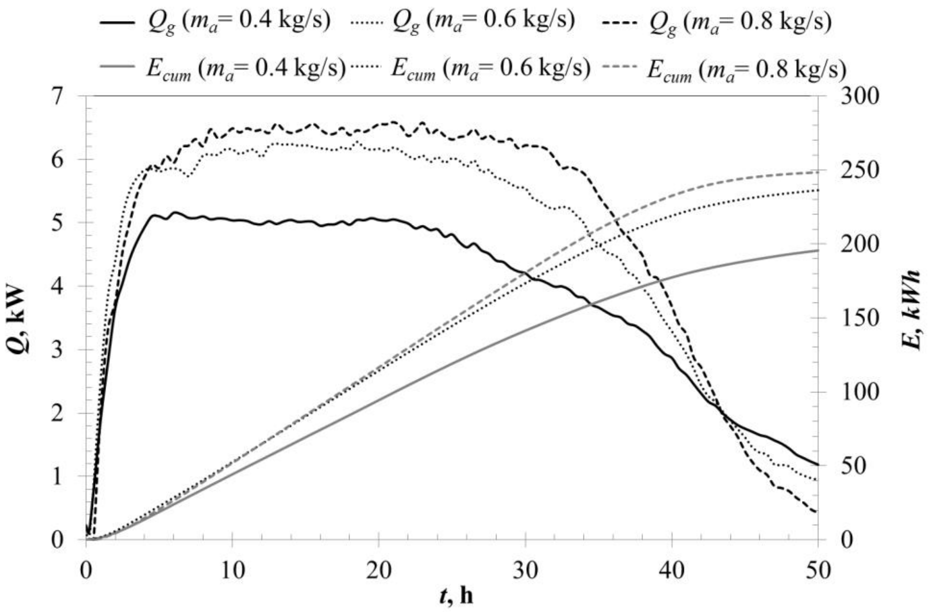

Figure 7.8.11 Variation of heat gain and cumulative thermal energy gain for three different air mass flow rates in discharging cycle

7.9 Conclusion

This chapter covers the development of a building integrated solar driven THS system and primary experimental investigations on its thermal performance. It was aimed to realize a thermal energy storage system capable of storing low grade solar energy, releasing on demand and recharging to acceptable levels.

Heat storage density in the range of 244→310 kWh has been achieved in the testings with different m_a values. Results are in good agreement with the previously obtained E_d with small scale laboratory prototypes (See: Chapter 4.4 and Chapter 5).

During THS discharging operation, 29 °C peak temperature output from the SIM material has been achieved, with output continuing for (up to) 25 hours after initiation. ΔT_{ave} of 11.4 °C over 25 hours and ΔT_{ave} of 9.5 °C over 50 hours were obtained (m_a =0.4 kg/s). The investigations on the effect of m_a on system discharging performance showed that reducing m_a increases the ΔT, whilst increasing m_a positively influences the achievable Q_g and E_{cum} in discharging cycle. According to the testing results, COP_d (see: Equation 4.2) was found 5.11, 6.18 and 6.49 for the m_a of 0.4, 0.6 and 0.8 respectively, indicating the improvement of the THS discharging performance with the increasing m_a. In the performed testings, m_a was kept high (> 0.4 kg/s) in order to observe the system full performance and to find out the achievable peak thermal power, Q_g, from the THS system. For the selected operating conditions, discharging duration of each vessel was found ~50 hours which in total corresponds to 200 hours total discharging period. Assuming a 6 hours daily operation of the system for three months winter period, 540 hours operating time is required. This could be obtained by maintaining air mass flow rate and air absolute humidity levels as both of these factors influence on the heat extracting rate thereby on the process duration. By consideration of the obtained experimental results, reducing m_a to 0.15 kg/s (for the same humidity levels), would reduce the Q_g to ~1.5 kW but increase the discharging duration up to ~600 hours which could be sufficient to provide continuous heating over the winter period.

Peak ΔT_a > 15 °C was obtained on 28th February with the ΔT_{ave} > 10 °C over 4 hours corresponding to cumulative solar energy gain, $E_{cum,s}$ = 17.2 kWh. According to testing results, useful heat gain from TSC has been obtained in 3 days (23rd, 24th and 28th of February) of the 6 days testing. This was mainly due to the insufficient solar radiation during the testing period. It was expected that during April and May, contribution of the TSC will be higher. Further testing is required to analyse TSC performance in these months.

Study results showed that there is a correlation between solar intensity and achievable temperature lift with the TSCs. Over the testing period, variation of daily average solar intensity in the range of 0.12 kW →0.29 kW led to an increase of ΔT_{ave} between 1.5 °C and

8.9 °C. Based on the obtained correlation it was found that for solar intensity levels > 0.7 kW/m^2 would enable to obtain temperature lift of air > 65 °C with the TSCs. Assuming summer ambient temperature of ~20 °C, THS charging supply temperature of 85 °C could be achieved, which is sufficient for desorbing the moisture from SIM-3a without the need for an auxiliary heater.

CHAPTER 8: DESIGN, DEVELOMENT AND PERFORMANCE EVALUATION OF A NOVEL HEAT PUMP DRIVEN SORPTION STORAGE HEATER (HEAT-STORE)

8.1 Introduction

THS should not be only rely on solar thermal technologies but also should be able to incooperate with electric heating systems. This will provide multiple benefit both for increasing efficiency of fossil based systems as well as increasing utility of renewable energy sources. Although using electricity is an expensive and inefficient way of heat production, there is a transition to solar and wind sourced on site domestic electricity generation. Especially with the increasing trend of PV applications, storage of electricity is questioned. Current electrical energy storage technologies are expensive and research is ongoing. At today's battery prices, we're not at the point where the financial returns obviously justify the investment (Carboncommentary, 2014). However, without electrical batteries, utility of PV panels is very low as electricity could only be generated during daytime whereas the majority of domestic energy demand is at night time. Besides, high percent of that demand is for space and water heating. Thermal batteries using sorption materials could be an option to balance the mismatch with their high and long term energy storage potential. PV powered buildings could use sorption storage heaters to charge the sorption material during day time. The main advantage of solid sorption storage heater system over conventional storage heater systems is that there is no heat loss over the heat storage period. This allows householders to benefit from the stored thermal energy any time they need.

In addition to PV sourced electricity, another promising option to benefit from storage heater technologies is charging the sorbent with off-peak electricity. This helps both to provide supply-demand balance in electricity grid also represents a cost-effective heating method to be used in domestic heating. In the UK, Economy 7 and Economy 10 are variable rate electricity tariffs that householders pay a different price for electricity used at different times of day. With Economy 7, the electricity used at night costs about a third of the price of the electricity used during the day which is a considerable difference. The hours of cheap electricity are normally from 12 midnight until 07.00 in winter, and from 01.00 to 08.00 in summer, although this can vary between suppliers (UKPower, 2016a). Economy 7 tariff use a different kind of electricity meter, which, unlike a standard meter, can track the electricity used in buildings during the day and at night separately. Similar to the Economy 7, Economy 10 tariff consists of 10 hours of off-peak electricity, which suppliers charge at a discounted rate. Different than the Economy 7 which provides off-peak electricity only night-time, Economy 10 consists of off-peak rate for 3 hours in the afternoon, 2 hours in the evening and 5 hours over night (UKPower, 2016b).

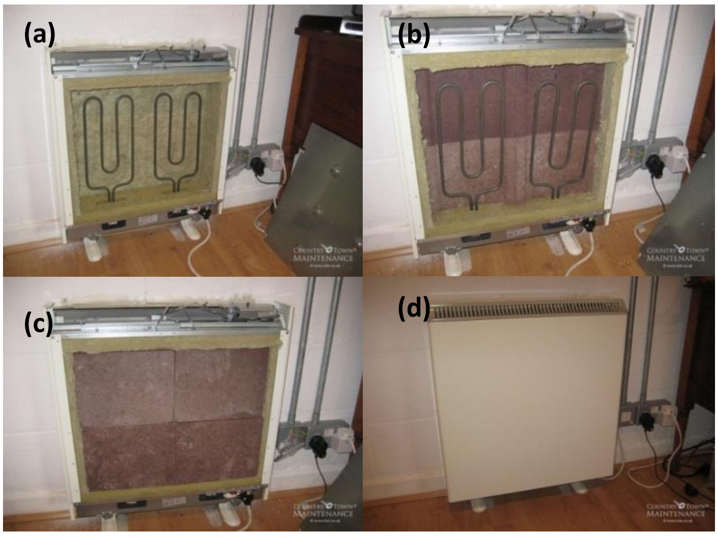

Figure 8.1.1 Instalation steps of an electric storage heater; (a) view of internal insulation, (b) – (c) installation of bricks, (d) completed installation (CTM, 2016)

Electrical storage heaters are very popular in several countries where variable tariffs like Economy 7 and 10 exist. Especially in buildings which do not have gas connection, electricity is the only option and storage heaters using off peak tariff are considered as a cost effective heating method. Conventional storage heaters use brick as shown in Figure 8.1.1. Bricks are sensibly heated at night time with electrical resistance coils. Stored heat is slowly released to the room while bricks are cool down. However, in these systems, due to the large amount of heat loss during heat storage period, the efficiency is low and stored heat should be consumed in a short time frame.

Within this study a novel heat pump driven sorption storage heater (Heat-Store) that could be powered with both PV sourced electricity and off-peak electricity was proposed. Optionally, solar air collectors could also be incorporated with the system to increase solar share. High heat storage density and low heat losses of the proposed system could provide significant benefits such as;

- Larger amount of heat storage for the same volume of heat storage material in comparsion with the SHS and LHS
- Higher utility of off-peak tariff and solar energy (solar thermal and PV)
- Flexibility in use of storage heater (e.g long term heat storage)
- Higher overall heat storage efficiency (caharging + discharging)

A schematic illustration of the building integrated operation of proposed Heat-Store system is given in Figure 8.1.2. A HP could be installed to the loft. Solar air collectors could also be used to preheat the air before entering the HP. A commercially available PEC (physiometric energy core) unit is used in the system. The PEC could be multipropose, where in winter it adds water vapour to the air needed for sorption reaction whilst in summer it could act as evaporative cooler.

In the system, HP is used for charging the sorbent and where needed an auxiliary heater could be installed to boost the charging air temperature before entering the sorption reactor. Current domestic attic HPs can increase air temperature up to 60 °C. According to the obtained data in pevious work (See: Chapters 4-5), SIMs could be charged around 80°C Therefore using a small duct installed resistance heater at the HP outlet could be beneficial to efficiently regenerate the sorbent. HP and electrical heater are powered with electricity generated via PV panels. Alternatively they could be powered with off-peak tariff at night time. In charging cycle, as seen from the Figure, air is pre-heated by solar collectors then further heated in HP condenser. Hot air passes through the sorption reactor and desorbs moisture from the sorbent. The moist exhaust air initially passes through a wall mounted air-to-air heat recovery unit to and heat the incoming ventilation air. Pre-cooled process air then enters the HP evaporator and transfers the rest of the waste heat to the refrigerant. This significantly increases the HP COP (COP_{HP}) as the compressor work is minimal as a result of the heat input in evaporator. In discharging cycle, ambient air is humidified in PEC and passes through the sorption reactor where moisture is adsorbed and sorption heat is generated. Generated hot air is supplied to the building via ducting for space heating.

The charging and discharging cycles were described below with the assigned flow numbers given in the Figure 8.1.2;

Sorption heat storage charging :

1-2-3-10-4-5-6 (Charging primary air stream),

7-8-12 (Charging secondary/product air stream)

Sorption heat storage discharging

9-10-3-11-8-12 (Discharging air stream)

Indirect evaporative cooling line

9-4-5-6 (Indirect evaporative cooling primary/working air stream)

7-8-12 (Indirect evaporative cooling secondary/product air stream)

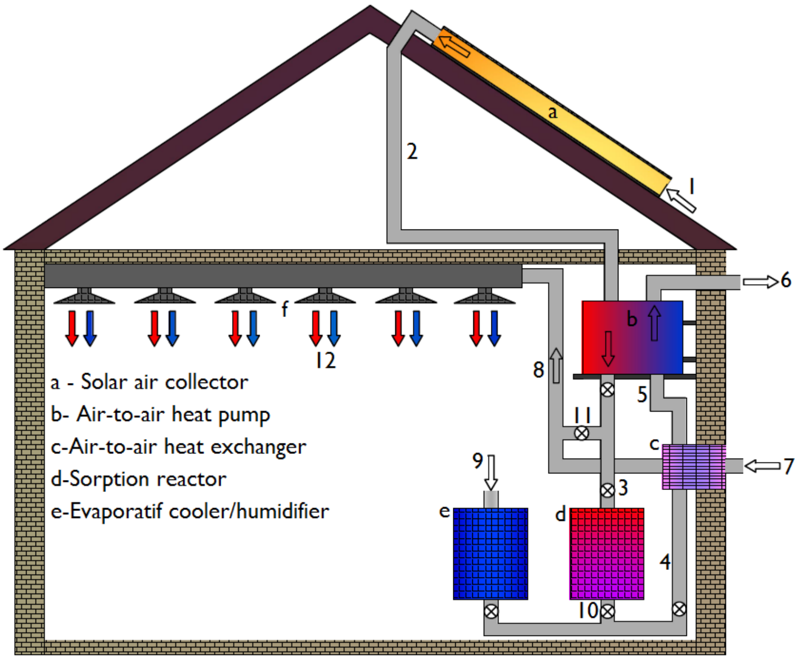

Figure 8.1.2 schematic illustration of the building integrated operation of Heat-Store system

HP technology is one of the most sustainable and efficient ways of household space or water heating. However their performance is strongly dependent on the ambient energy level. COP value of the HP dramatically drops with the reducing ambient temperature. Several methods have been investigated to improve HP performance such as benefitting from ground energy or solar energy (Utlu et al., 2014). In addition there are several studies coupling SHS or LHS with HPs (Utlu et al., 2014). Benefitting from HS is vital because it can store the solar energy until the heat demand increases. With recovering the stored solar energy, HP can operate efficiently even in extremely low ambient temperatures. However, the main difficulty within the use of LHS is; controlling the phase change process and within the use of SHS is; the relatively low heat storage density therefore the high space requirement. Additionally in both HS methods, heat loss is a big problem and in most cases stored heat is required to be consumed in a short period of time. THS materials have several promising aspects as discussed in Chapter 2 extensively. The main disadvantage of this HS method is the high temperature requirement for desorbing the moisture in charging cycle. The conventional sorbents Zeolite and Silica gel have widely researched however high regeneration temperature (>150 °C) requirement is the main drawback of these materials to be used in the built environment. As presented in Chapter 4 and 5, salt based composite sorbents (e.g. SIMs) can provide competitive heat output with Zeolite and higher than Silica gel whilst being able to regenerate at lower temperatures. Particularly, SIM-3a provided high performance with E_d >250 kWh/m^3 and T_{reg} of 80-85 °C.

The key that differs the THS is the fact that mass (moisture) transfer occurs during the charging-discharging processes whilst this is not an issue in other HS methods. In discharging process, ambient moisture is used, and if needed, the humidity of air could be boosted with evaporative or ultrasonic method with a little energy input.

In charging process, although the heated dry input air (e.g 80 °C) spends its energy for desorbing/evaporating the water from the sorbent, the evaporated warm water (water vapour) leaves the system with the input air. Therefore in charging process, input thermal power with the hot-dry air and the output thermal power with the moist-warm air are in close approximation. According to the experimental data obtained with Gen1 testing rig (see: Chapter 8.3), the average inlet conditions of the air to the reactor was T = 80.2 °C and RH = 3.1%, corresponding to 105 kJ/kg$_{air}$ and the outlet conditions of the air was T = 51.7 °C and RH = 17.4%, corresponding to 90 kJ/kg$_{air.}$ This condition indicates the high heat recovery potential of moist-warm exhaust air with the use of HP system. Accordingly, in this chapter it is aimed to demonstrate a novel concept that integrates HP and sorption heat storage for effective conversion and storage of renewable sourced or low cost electricity. In order to achieve this aim four objectives have set;

- To numerically investigate the effect of several operating parameters on Heat-Store,
- To design and develop a 6 kWh multilayer fixed bed sorption reactor,
- To install the Heat-Store system and experimentally investigate its thermal performance under different operational conditions
- To validate the numerical model with the experimental results

In the following section performed numerical studies on Heat-Store system are presented.

8.2 Numerical analysis of the Heat-Store system

8.2.1 System description

The schematic diagram illustrating the charging and discharging system operation is given with the assigned flow numbers in Figure 8.2.1 a and 8.2.1 b respectively. The description of the flow numbers were also illustrated in Table 8.1. System basically consists of a fan, ultrasonic humidifier, sorption reactor, attic HP, auxiliary electrical heater and an air-to-air heat exchanger. Solar air collectors could also be optionally used at the system inlet to preheat the air before entering the HP.

The full cycle of the system consists of charging (1→6) and discharging (9→11) cycles.

In charging process, the primary aim is to achieve an energy efficient drying cycle of sorbent with benefitting from ambient energy and system exhaust waste heat. This cycle includes two stage heat recovery where the moist air leaving the sorption reactor (4) transfers some of the energy to an external air flow (7→8) via an air to air heat exchanger and rest of its energy is recovered with HP. This condition allows both increasing heat pump COP at the same time gaining useful heat for space heating while the waste heat of charging is fully recovered. In charging cycle, ambient air is pre-heated with the transpired solar collectors. Than inlet air (1) enters the condenser and heated up to 50°- 60°C (2). Later temperature of the air is boosted with an electrical heater (3). Hot air passes through the sorbent and leaves the sorption reactor with increased moisture content (4). Moist warm air transfers sensible heat to an external line with a heat exchanger (5). The output air from the heat exchanger is close to saturation. Finally it passes through the evaporator where it reaches to the saturation point and some of the moisture condenses. As a result condensation energy is transferred to the refrigerant which considerably reduces the compressor energy consumption. Air leaving the evaporator is exhausted to the ambient (6). In discharging cycle, inlet air (9) passes through the humidifier and moisture content of the air increases. Moist inlet air (10) than enters the sorption reactor where it is heated as a result of moisture sorption by the sorbent. Hot output air (11) finally leaves the system.

Table 8.1 Description of the flow numbers

Charging			**Discharging**
1	System inlet	**9**	System inlet
2	HP condenser outlet	**10**	Humidifier outlet
3	EH outlet – reactor inlet	**11**	Reactor outlet
4	Reactor outlet – HEX inlet		
5	HEX outlet – HP evaporator inlet		
6	HP evaporator outlet- exhaust		
7	HEX inlet (secondary air flow)		
8	HEX outlet (secondary air flow)		

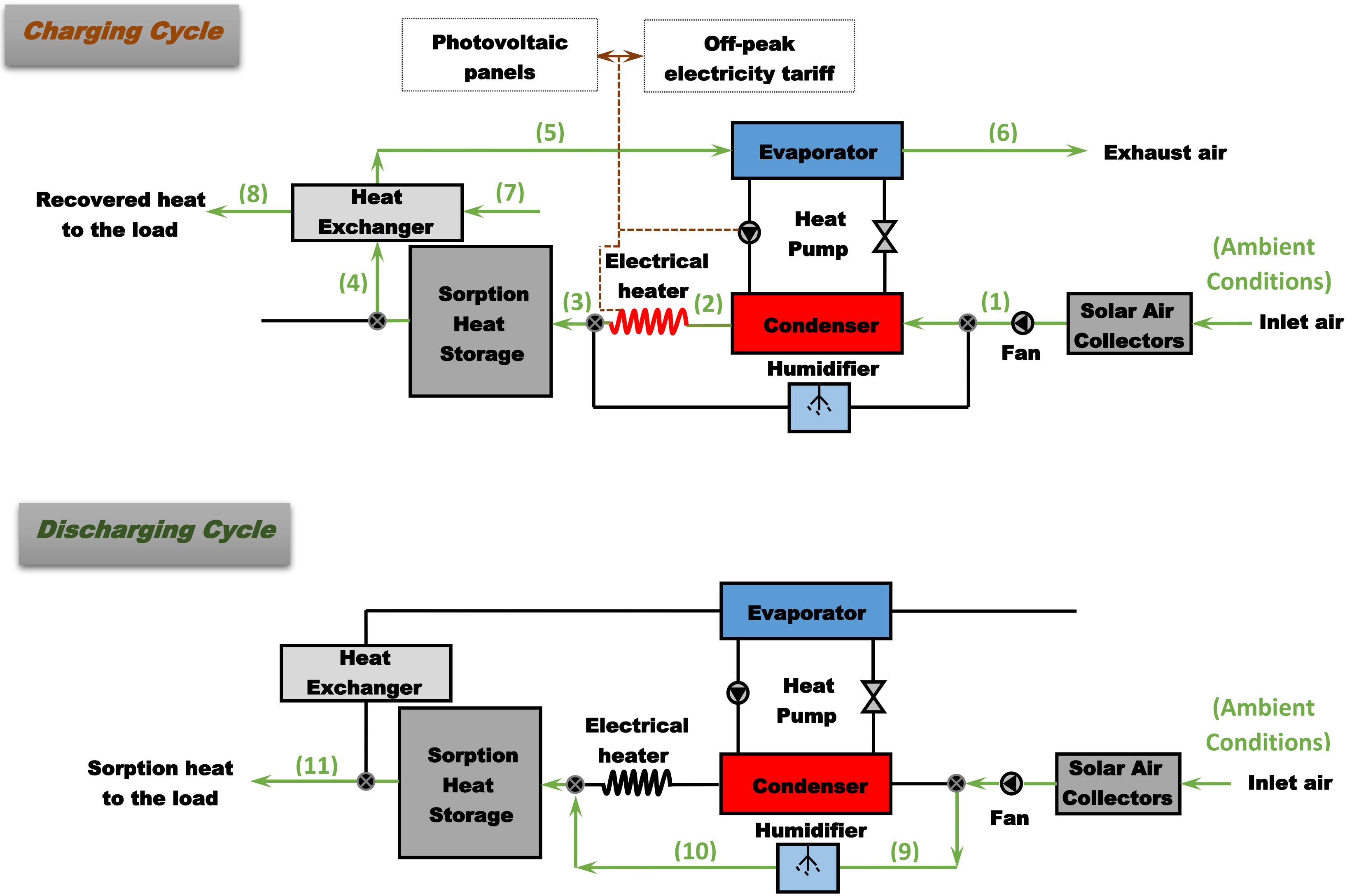

Charging Cycle

Discharging Cycle

Figure 8.2.1 Schematic illustration of heat pump driven sorption storage heater (a) charging cycle, (b) discharging cycle *Active flow lines are represented in green

8.2.2 Numerical model

The initial psychrometric conditions set for the numerical analyses are presented in Figure 8.2.2 a (charging) and Figure 8.2.2 b (discharging). In the analyses, the effect of different parameters including the air temperature, humidity, mass flow rate and solar energy input on system performance was investigated. While simulating the effect of any parameter, the rest of the conditions, which were not a function of the simulated parameter, was kept as constant (See: Figure 8.2.2).

SIM-3a was selected as the sorption material to be used in the analyses. The physical properties of SIM-3a and other constants used in the model are presented in Table 8.2.

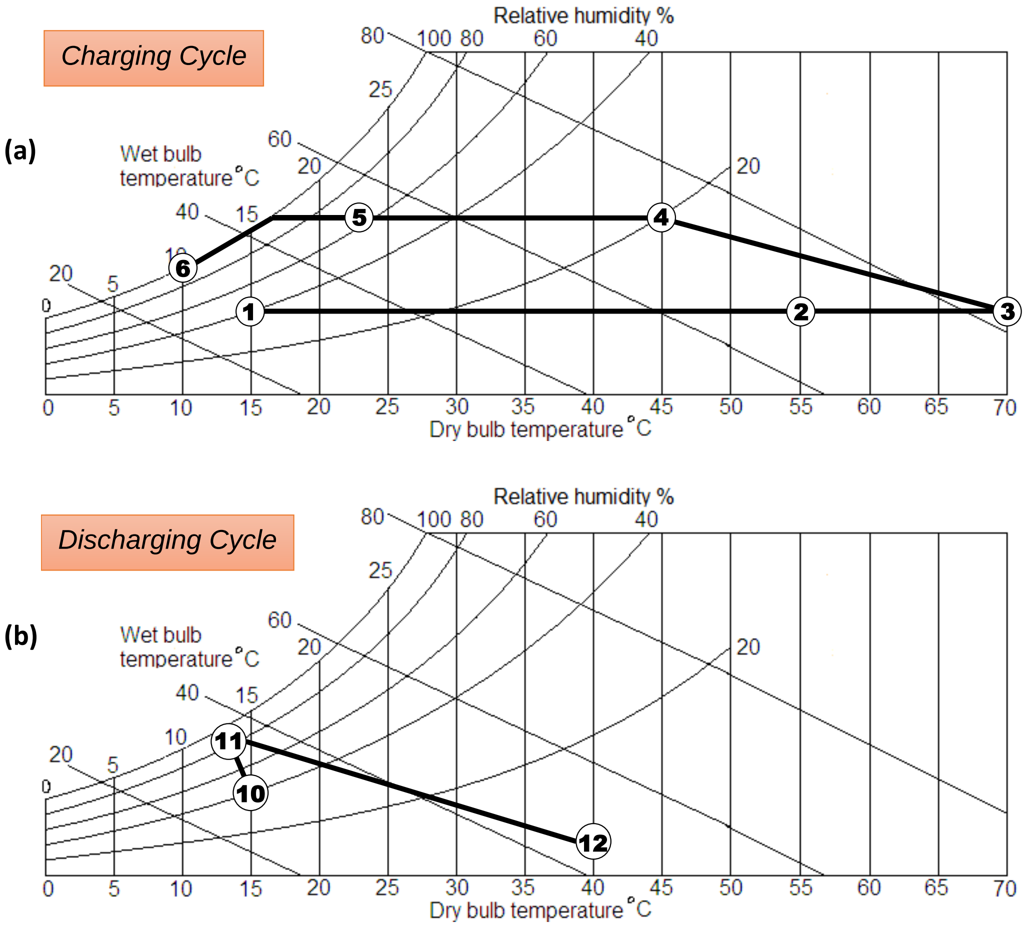

Figure 8.2.2 Illustration of the initial physiometric conditions of process air set in the numerical model; (a) charging cycle, (b) discharging cycle

Table 8.2 Constants and assumptions used in the analysis

Parameter	**Value**	**Unit**
V_{abs} (V-$CaCl_2$)	0.05	m^3
ρ_{abs}	175	kg/m3
m_{abs}	8.75	kg
Porosity	65	%
t_d	600	minutes
W_{fan}	0.05	kW
W_{hum}	0.03	kW
$T_{i,c}$ (T_1)	15	°C
$RH_{i,c}$ (RH_1)	30	%
m_a	0.02	kg/s
$m_{a,\ HEX}$	0.005	kg/s
$T_{i,d}$ (T_9)	15	°C
T_c (T_3)	70	°C
$RH_{i,d}$ (RH_9)	30	%
Δh_w	435.1	kJ/kg$_{water}$
Cp_w	4.18	kJ/kg K
Cp_a	1.008	kJ/kg K
$M_{m,w}$	0.018	kg/mol
F_r	0.93	-
$\tau\alpha$	0.75	-
U	4 x 10^{-3}	kW/ m^2 °C

In order to perform the simulations Engineering Equation Solver (EES) V9.933-3D was used which is powerful software to solve a series of mathematical equations simultaneously. Thereby, with EES, it is possible to simulate timewise variation of several parameters during sorption storage heater charging and discharging processes. Moreover EES software enables investigating the effect of the multiple variables on any target function (e.g. system COP). The investigated parameters with the developed model were given in the flowchart below (See: Figure 8.2.3). As seen from the figure, collector area (A_{coll}), solar intensity (I), charging temperature (T_3), air mass flow rate (m_a) and discharging air inlet temperature (T_{10}) were used as variables. Based on the temporal variation of each of these variables, the change of the system performance indicators such as system total energy input-output in charging and discharging processes, COP_{HP} and overall system COP (COP_S) were investigated.

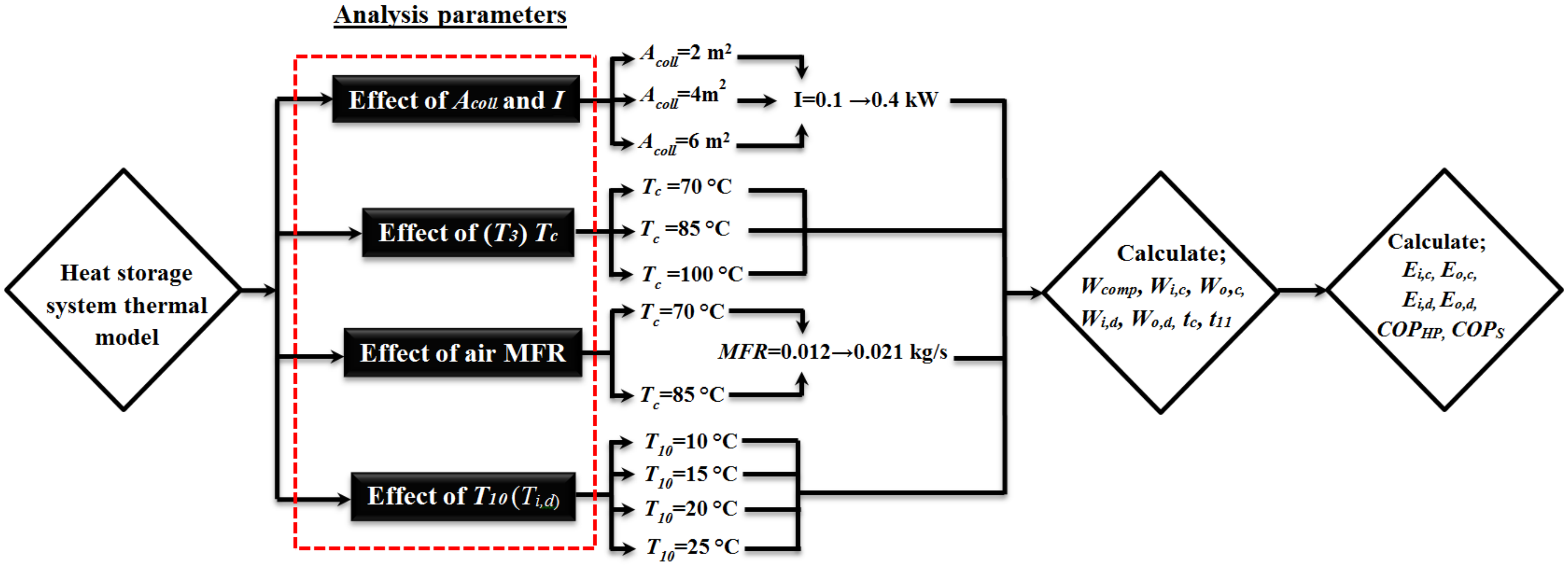

Figure 8.2.3 Flow chart of numerical model illustrating the investigated parameters

The formulations used in the developed model were presented with their definitions below;

The heat gain with the solar collectors is expressed in Equation 3.4. Based on the heat gained with the solar collectors, the air temperature at the collector outlet could be obtained with the Equation 8.1. Here air absolute humidity, w_a, is assumed equal at the collector inlet and outlet,

$$Q_u = m_{a,p} \times c_{p,a} \times (T_1 - T_a) \tag{8.1}$$

Similarly at the HP condenser inlet-outlet and electrical heater inlet-outlet, w_a is assumed constant;

$$w_1 = w_2 \tag{8.2}$$

$$w_2 = w_3 \tag{8.3}$$

Neglecting the heat loss in heat exchanger, heat transferred from the charging exhaust air to the secondary air stream is equal to recovered useful heat, Q_{rec}. The energy balance between process air and secondary air stream is given in Equation 8.4;

$$m_{a,p} \times (h_4 - h_5) = m_{a,s} \times (h_8 - h_7) = Q_{rec} \tag{8.4}$$

Here, it is assumed that, there is no condensation in the heat exchanger and moisture content/absolute humidity, w, of both process and secondary air streams are constant as illustrated below;

$$w_4 = w_5 \tag{8.5}$$

$$w_7 = w_8 \tag{8.6}$$

The specific enthalpy of the air for any certain w_x and T_x conditions, is calculated with the Equation 8.7 (Cengel and Boles, 2006). Here, first and second part of the equation represents the specific enthalpy of the dry air and water vapour respectively.

$$h_x = 1.006 \times T_x + [w_x \times (1.84 \times T_x + 2501)] \tag{8.7}$$

The absolute humidity of air at any specific RH_x and T_x condition is defined as in Eq. 4.6 (See: Chapter 4);

RH is the ratio of the moisture content of the air to the saturation moisture content at any specific condition (*P*, *T*). *RH* could also be expressed as the ratio of vapour partial pressure to the saturation vapour partial pressure at actual dry bulb temperature of air as given in the Equation 4.5.

The sum of the compressor work and the heat gain in the HP evaporator is equal to the heat output at the HP condenser. Based on the energy balance of the HP, enthalpy change of the air could be calculated with the Eq. 8.8 (Cengel and Boles, 2006) and Eq. 8.9;

$$Q_{evap} + W_{comp} = Q_{cond} \tag{8.8}$$

$$m_{a,p} \times (h_5 - h_6) + W_{comp} = m_{a,p} \times (h_2 - h_1) \tag{8.9}$$

Based on the product-fuel principle, heat pump *COP* is equal to the ratio of heat output at the condenser to the electrical power input to the compressor as given Eq. 8.10 (Cengel and Boles, 2006) below ;

$$COP_{HP} = \frac{Q_{cond}}{W_{comp}} \tag{8.10}$$

Here Q_{cond} is defined as the enthalpy difference of the air between the condenser outlet and inlet and W_{comp} is equal to the difference between Q_{cond} and $Q_{evap.}$ Inserting Equation 8.8 and 8.9 in the Equation 8.110, COP_{HP} could be expressed as in Equation 8.11 below;

$$COP_{HP} = \frac{m_{a,p} \times (h_2 - h_1)}{m_{a,p} \times [(h_2 - h_1) - (h_5 - h_6)]} \tag{8.11}$$

Electrical resistance heater is used to boost the air temperature before it enters the sorption reactor. Here, thermal power transferred to the air is equal to the electrical power input to the electrical heater. Assuming that the air duct is well insulated $Q_l=0$, the energy balance is written as follows;

$$m_{a,p} \times (h_3 - h_2) = W_{EH} \tag{8.12}$$

In charging process, the difference of the specific enthalpy of air at the sorption reactor inlet and outlet is equal to the multiplication of specific desorption enthalpy of the sorbent (kJ/kg$_{wv}$) and the amount of desorbed water vapour. The energy equilibrium of the sorption reactor is written as follows (Michel et al., 2014) ;

$$m_{a,p} \times \left[\left(T_3 \times C_{p,a} + w_3 \times T_3 \times C_{p,w}\right) - \left(T_4 \times C_{p,a} + w_3 \times T_4 \times C_{p,w}\right)\right]_{t_c} = \Delta h_w \times m_{a,p} \times (w_4 - w_3) \tag{8.13}$$

By simplifying the above formulation, Eq. 8.14 is obtained as below (Marias et al., 2014);

$$\left[\frac{T_3 - T_4}{w_4 - w_3}\right]_{t_c} = \frac{\Delta h_w}{C_{p,a} + \left(w_3 \times C_{p,w}\right)} \tag{8.14}$$

The state of the sorbent during charging process is defined with reaction advancement, X (Marias et al., 2014). Reaction advancement (see: Equation 8.15) varies in the range of 0→1 where 0, stands for dehydrated (anhydrous) state while 1 represents the equilibrium (saturated) state of the sorbent.

$$X_c = \frac{m_{a,p} \times \int_{t_0}^{t_c}(w_4 - w_3)dt}{v \times n \times M_{m,w}} \tag{8.15}$$

Here, time dependant variation of w_4 is calculated with the Eq 8.16 given below;

$$W_4(t_c) = w_{4,i} - \frac{dw_4}{dt} \times t_c \tag{8.16}$$

The initial moisture content of the charging outlet air absolute humidity, $w_{4,I}$, was obtained experimentally (see: Equation 8.17). The time dependant variation of the w_4 was also determined with the experimentally obtained correlation between t_c and w_4 as in Equation 8.18 (See: Appendix VI);

$$w_{4,i} = 0.025 \ \text{g/kg} \tag{8.17}$$

$$\frac{dw_4}{dt} = 1.6 \ \times 10^{-4} \ \text{g/kg.s} \tag{8.18}$$

The total desorbed moisture in a t_c time frame during charging process is calculated with the Equation 8.19,

$$M_{t,c} = 60 \times m_{a,p} \ \times \left(\int_0^{t_c}(w_4 - w_3)\, dt\right) \tag{8.19}$$

Inserting the Eq. 8.16 in the Eq. 8.19, Equation 8.20 is obtained;

$$M_{t,c} = 60 \times m_{a,p} \times \int_0^{t_c}((w_{4,i} - \frac{dw_4}{dt} \times t_c) - w_3))dt \tag{8.20}$$

By inserting Eq. 8.17 and Eq. 8.18 in the Eq. 8.20, and integrating the terms on the right hand side, the relation with $M_{t,c}$ (kg) and t_c is defined as follows;

$$M_{t,c} = 60 \times m_{a,p} \times \left(0.025 \times t_c - 1.6 \ \times 10^{-4} \times \frac{{t_c}^2}{2} - w_3 \times t_c\right) \tag{8.21}$$

Simplifying the Eq. 8.21, Eq.8.22 writes as follows;

$$M_{t,c} = 60 \times m_{a,p} \times t_c \times \left(0.025 - 1.6 \times 10^{-4} \times \frac{t_c}{2} - w_3\right) \tag{8.22}$$

Considering that in discharging cycle, ambient air temperature and solar intensity is low/zero, heat gain from solar collector could be neglected. Therefore system inlet temperature could be considered as equal to the ambient;

$$T_1 = T_a \tag{8.23}$$

In discharging process; the general energy balance of the humidification process is defined as follows,

$$m_{a,p} \times h_9 = m_{a,p} \times h_{10} \tag{8.24}$$

Substituting h_9 and h_{10} with their expression given in Eq 8.7, the following equality is obtained (Cengel and Boles, 2006),

$$1.006 \times T_9 + [w_9 \times (1.84 \times T_9 + 2501)] = 1.006 \times T_{10} + [w_{10} \times (1.84 \times T_{10} + 2501)] \tag{8.25}$$

The simplified version of the energy balance, based on the air physiometric conditions (*T* and *w*) at the humidifier inlet and outlet, is written as follows;

$$1.006 \times (T_9 - T_{10}) + 1.84 \times (w_9 \times T_9 - w_{10} \times T_{10}) - 2501 \times (w_9 - w_{10}) = 0 \tag{8.26}$$

The sorption heat gained by the air, Q_g, during adsorption process is defined with Equation 8.27;

$$Q_g = m_{a,p} \times (h_{11} - h_{10}) \tag{8.27}$$

Assuming that there is no heat loss in the sorption reactor, the relation between the sorption specific enthalpy (kJ/kg_{wv}) of adsorbent and enthalpy change of air is calculated with the Equation 8.28 (Marias et al., 2014);

$$\left[\frac{T_{11}-T_{10}}{w_{10}-w_{11}}\right]_{t_c} = \frac{\Delta h_w}{C_{p,a}+(w_{11}\times C_{p,w})} \tag{8.28}$$

The reaction advancement during discharging process is defined as follows (Marias et al., 2014);

$$X_d = \frac{m_{a,p}\times\int_{t_0}^{t_d}(w_{10}-w_{11})dt}{v\times n\ x M_{m,w}} \tag{8.29}$$

In contrast to the X_c, given in Eq.8.15, X_d represents the vapour pressure level of the sorbent and defines how close the sorbent is to the saturation point. As the material moisture content increases, its state changes from anhydrous to hydrate which is represented with the scale of 0→1. Therefore, in any t_d moment, the sum of X_c and X_d should be equal to 1;

$$X_c + X_d = 1 \tag{8.30}$$

Here w_{11} is calculated with the Equation 8.31 as below;

$$W_{11}(t_d) = w_{11,i} + \frac{dw_{11}}{dt}\times t_d \tag{8.31}$$

At the beginning of the discharging cycle, as the sorbent is in dry state, moisture is fully adsorbed. Thefore air leaving the system is considered as dry;

$$w_{11,i} = 0 \text{ g/kg} \tag{8.32}$$

The time dependant variation of the discharging outlet air absolute humidity, $w_{11,}$ was determined with the experimentally obtained correlation between t_d and w_{11} (See: Appendix VI);

$$\frac{dw_{11}}{dt} = 1\times10^{-4}\ \text{ g/kg.s} \tag{8.33}$$

The total moisture uptake of the sobent in a t_d discharging period is calculated with the Equation 8.34;

$$M_{t,d} = 60 \times m_{a,p} \times \left(\int_0^{t_d} (w_{10} - w_{11})\, dt\right) \tag{8.34}$$

By replacing the term w_{11} with the formulation given on the right hand side of the the Eq. 8.31;

$$M_{t,d} = 60 \times m_{a,p} \times \int_0^{t_d} (w_{10} - (w_{11,i} + \frac{dw_{11}}{dt} \times t_d))dt \tag{8.35}$$

Inserting Equations 8.32 and 8.33 in the Equation 8.35 and integrating the terms, time dependant variation of $M_{t.d}$ is obtained as follows;

$$M_{t,d} = 60 \times m_{a,p} \times \left(w_{10} \times t_d - 10^{-4} \times \frac{{t_d}^2}{2}\right) \tag{8.36}$$

By simplifying the Equation 8.37,

$$M_{t,d} = 60 \times m_{a,p} \times t_d \times \left(w_{10} - 10^{-4} \times \frac{t_d}{2}\right) \tag{8.37}$$

Assuming the moisture adsorbed in a t_d period should be equal to the moisture desorbed in duration of t_c, Equation 8.38 writes as follows;

$$M_{t,d} = -M_{t,c} \tag{8.38}$$

Here the required t_c after the discharging process with a length of t_d is calculated with solving Equalities 8.22 and 8.37. The ratio of t_c to t_d for any particular operational condition is defined with t_x;

$$\frac{t_c}{t_d} = t_x \tag{8.39}$$

During discharging process, in any t_d moment, the total heat output is equal to the sorption heat gained by air;

$$W_{o,d} = Q_g \tag{8.40}$$

Fan and humidifier are the only energy consuming components during discharging process. The total electric power input to the system is defined as follows;

$$W_{i,d} = W_{hum} + W_f \tag{8.41}$$

In charging process, HP compressor and depending on the regeneration temperature electrical heater constitute the highest share of electrical power input. Besides low amount of electrical power is used for running the fan;

$$W_{i,c} = W_{comp} + W_{EH} + W_f \tag{8.42}$$

The waste heat from the charging exhaust air is partially recovered in air-to air heat exchanger and it is considered as the useful heat gain during charging process;

$$W_{o,c} = Q_{rec} \tag{8.43}$$

The total energy output and input for full cycle (charging+discharging) heat storage process is calculated with Equations 8.44 and 8.45 respectively;

$$E_{o,t} = \int_0^{t_d} W_{o,d}\, dt + \int_0^{t_c} W_{o,c}\, dt \tag{8.44}$$

$$E_{i,t} = \int_0^{t_d} W_{i,d}\, dt + \int_0^{t_c} W_{i,c}\, dt \tag{8.45}$$

Accordingly the total system COP is defined as the ratio of total energy output to the total energy input as given below;

$$COP_S = \frac{E_{o,t}}{E_{i,t}} \tag{8.46}$$

8.2.3 Results and discussion

8.2.3.1 Effect of solar collector area and solar intensity

In this section effect of solar collector area (A_{coll}) on system performance was investigated for different solar intensity levels (I). The aim was to analyse the reduction of HP energy consumption with the increasing solar energy input during adsorbent regeneration process. The drop of compressor power requirement boosts COP_{HP} thereby increases overall system COP (COP_S). The simulations were performed for 2, 4 and 6 m^2 total solar collector area and solar radiation in the range of 0.1→0.4 kW were used for each simulation. In the simulations, discharging time was assumed steady (600 minutes) and charging time was considered as the time required for removing the adsorbed moisture during discharging process. As seen from the Figure 8.2.4, 280 mins is required for regenerating the adsorbent for 600 minutes discharging time. The charging temperature was set to 70 °C, therefore the higher I does not affect the t_c, but it significantly reduces W_{comp} resulting with an enhanced process COP. The variation of T_1 with the depending on the A_{coll} and I levels is given in Figure 8.2.5. As seen T_1 linearly rises with the increasing A_{coll} and I. The impact of the A_{coll} is low at low I levels however it gets more significant with the increasing I. The effect of A_{coll} and I on system performance is investigated in detail in the following sections.

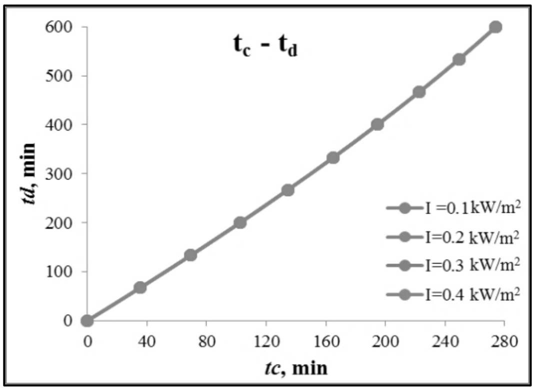

Figure 8.2.4 Graph showing the relation between charging and discharging time

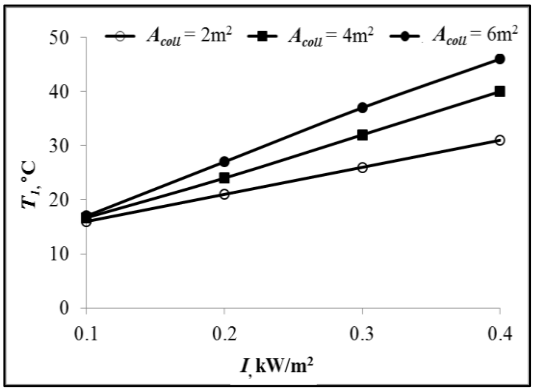

Figure 8.2.5 Variation of charging inlet temperature for different collector area and solar radiation levels

i. ***A_{coll} = 2 m^2***

Based on the analysis results, for A_{coll}=2 m^2, each 0.1 kW input of solar energy provides approximately same amount of reduction of W_{comp}. Four fold increase of I (0.1 kW →0.4 kW), allows a drop of average W_{comp} from 0.65 kW to 0.32 kW for the solar collector area of 2 m^2 (see: Figure 8.2.6). Accordingly, COP_{HP} was found in the range of 3.5 → 2.6 for I=0.4 kW whereas it varies between 2.1→ 1.8 for the$I$=0.1 kW (see: Figure 8.2.7 a). With the increase of the COP_{HP}, COP_S significantly increases as seen in Figure 8.2.7 b.

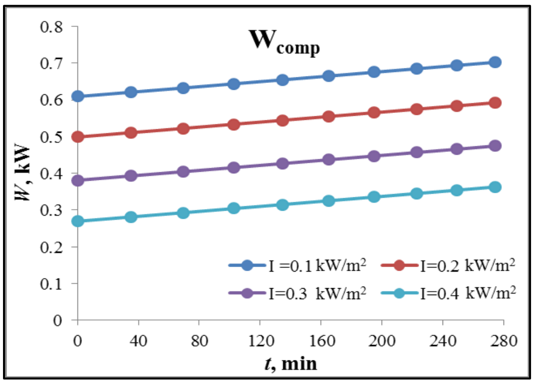

Figure 8.2.6 Effect of solar radiation on compressor power consumption for solar collector area of 2m^2

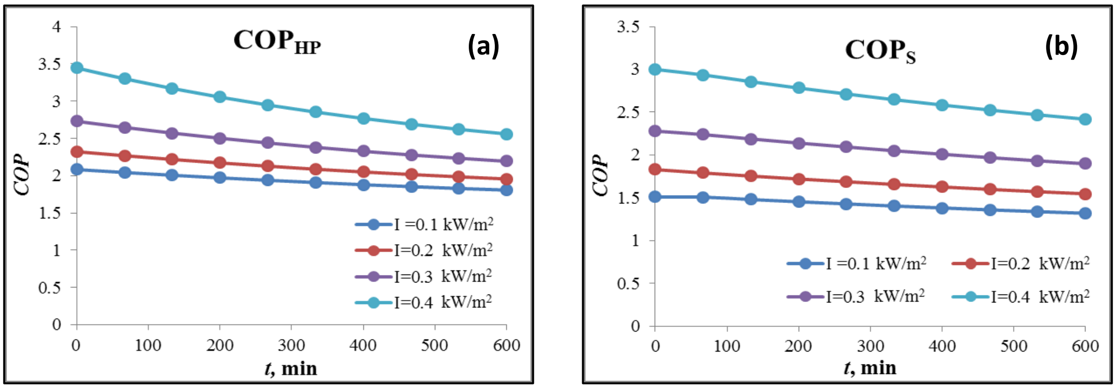

Figure 8.2.7 Effect of solar radiation on (a) COP_{HP} and (b) COP_S for solar collector area of 2m^2

Based on the varying I, the average COP_s is 2.7 for I=0.4 whilst it is 1.4 for I=0.1. The reason of the sharp decrease in COP_S could be explained with the increase in total $E_{i,c}$ from 1.6 kWh to 3.1 kWh for the reducing I in the range of 0.4 → 0.1 kW (see: Figure 8.2.8 a). As the $E_{o,d}$, $E_{o,c}$, $E_{i,d}$ are steady (3.1, 1.4 and 0.3 kWh respectively) for the varying I levels (See: Figure 8.2.8 b), the increase of $E_{i,c}$ reduces the COP_S.

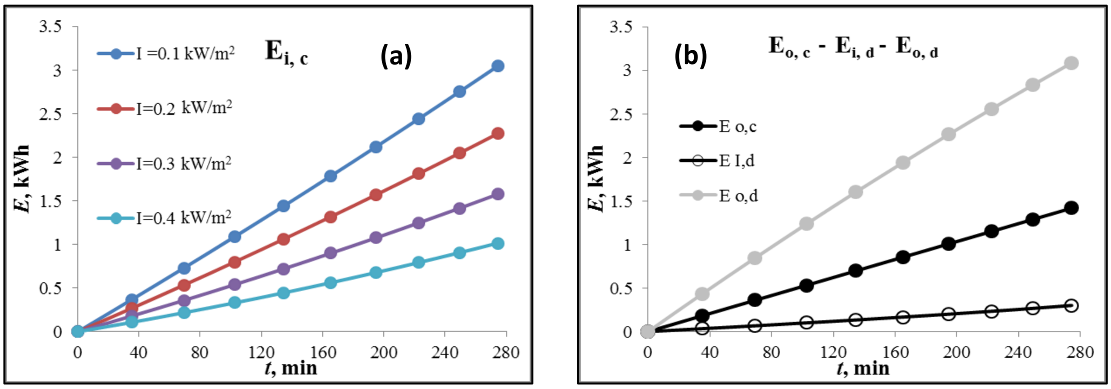

Figure 8.2.8 (a) Effect of solar radiation on charging cycle input energy and (b) variation of charging outlet, discharging inlet and discharging outlet energy

ii. A_{coll} = 4 m^2

The increase in solar collector area from 2 m^2 to 4 m^2 enables a further decrease in HP power consumption as expected. For I =0.1 kW, the reduction in W_{comp} with the increase of solar collector area is low and it varies in the range of 0.59→0.68 kW. However with the increase of I, the effect of solar collector area becomes more considerable (see: Figure

8.2.9). For I =0.4, Wcomp is in the range of 0.15 → 0.24 kW, whereas it varies between 0.26 → 0.36 kW for A_{coll}=0.2 m^2. The significant reduction of W_{comp}, boosts COP_{HP} and COP_S. Results showed that COP_{HP} and COP_s varies in the range of 5.3 →3.3 and 4.5 →3.4 respectively for *I=0.4 kW* and A_{coll}=0.4 m^2 conditions (See: Figure 8.2.10).

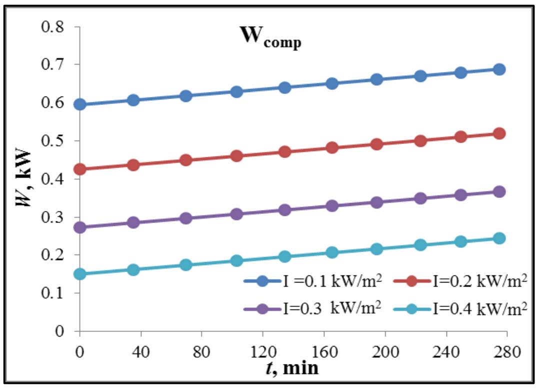

Figure 8.2.9 Effect of solar radiation on compressor power consumption for solar collector area of 4m^2

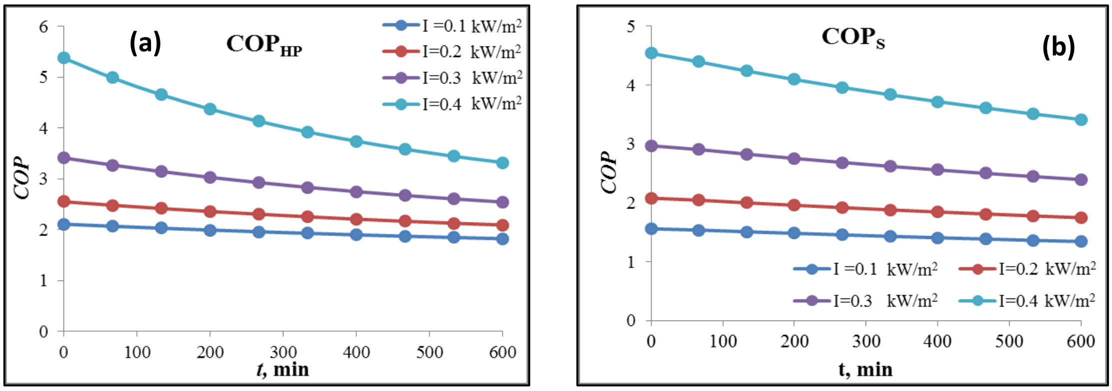

Figure 8.2.10 Effect of solar radiation on (a) COP_{HP} and (b) COP_S for solar collector area of 4m^2

iii. A_{coll} = 6 m^2

With the increase on A_{coll} to 6 m^2, $W_{comp,ave}$ drops to 0.16 kW, for I=0.4 kW conditions. On the other hand, for I=0.1 kW, W_{comp} varies between 0.58 – 0.67 kW which is slightly lower than the achieved W_{comp} for the A_{coll} =2 m^2 and 4 m^2 under the same I levels (see: Figure 8.2.11). It could be concluded that the increasing solar collector area enables a considerable reduction in W_{comp} when I in the range of 0.3 - 0.4 kW, whereas it does not have much impact at lower *I* levels (0.1-0.2 kW). Accordingly COP_{HP} and COP_S are in the range of 6.2→3.5 and 5.1→ 3.7 for *I*=0.4, whilst they vary between 2.1→1.8 and 1.6→1.3 for *I*=0.1 kW respectively. For *I*=0.2 and 0.3 kW the values are in between the given ranges as seen in Figures 8.2.12 a-b.

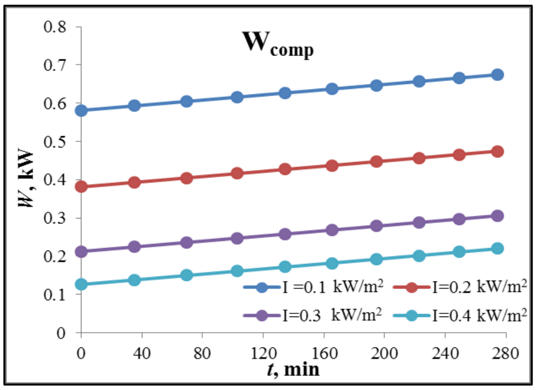

Figure 8.2.11 Effect of solar radiation on compressor power consumption for solar collector area of 6 m^2

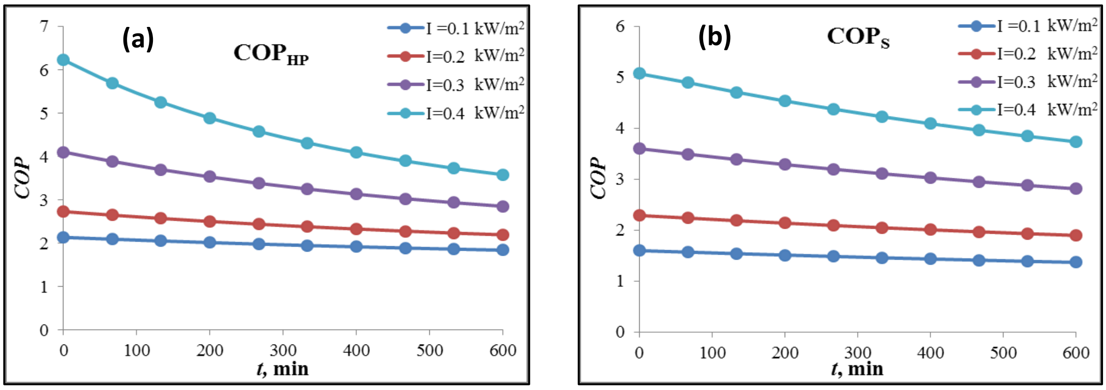

Figure 8.2.12 Effect of solar radiation on (a) COP_{HP} and (b) COP_S for solar collector area of 6m^2

Based on the simulations performed for different A_{coll} and *I*, it could be concluded that using air sourced HP at low T_a levels for adsorbent regeneration does not provide a considerable benefit, unless the electricity used to power the HP is not PV sourced or off peak tariff. On the other hand, integrating solar air collectors to HP and regenerating the material when solar energy is available seems as a suitable and energy efficient option. As a result of the solar input to the system, lower W_{comp} is required to achieve the desired air temperature for regeneration. This condition increases the HP_{COP} thereby the overall heat storage performance. The conditions of A_{coll}>4 m^2 and I>0.3 kW was found as the lowest limit values to achieve competititive performance with the conventional air sourced HP which generally has an average COP of ≈3. For climate conditions where winter solar intensity is above 0.3 kW, COP_s>3 could be achieved. This condition makes the use of integrated sorption heat storage and solar assisted heat pump an attractive solution for space heating purposes.

8.2.3.2 Effect of reactor inlet air temperature in discharging cycle

The temperature of reactor inlet T_{10} ($T_{i,d}$) air discharging process has a vital importance on overall heat storage performance. The change in discharging inlet air temperature does not only affect the discharging heat output but also it affects the charging process heat input and output. For the same RH level, moisture content of the inlet air increases with the increasing temperature. As a result, with the increasing T_{10} (e.g. 10° C →25 ° C) for steady RH_{10} (e.g. 80%), amount of the moisture loaded to the sorbent increases during adsorption process. Although this leads to higher sorption heat output, it also increases the t_{reg}, therefore the required energy for regenerating the material. As seen in Figure 8.2.13 a, t_{reg} increases from 132 min. to 482 min. with the rise of the $T_{i,d}$ in the range of 10 →25 °C for RH = 80% conditions. On the other hand peak temperature lifting ΔT is 12 °C for $T_{i,d}$ =10 °C, whilst ΔT= 31 °C could be achieved for $T_{i,d}$ =25 °C (see: Figure 8.2.13 b).

Increase of $T_{i,d}$ in the range of 10→25 °C increases $E_{i,c}$, $E_{o,c}$ and $E_{o,d}$ in the range of 1.01→4.24 kWh, 0.68→2.48 kWh and 1.51→5.10 kWh respectively (See: Figure 8.2.14 a-b and 8.2.15 a). As a result, COP_s, which takes into account both the input and output energy in charging and discharging process, does not show a considerable change with the varying $T_{i,d}$ (See: Figure

8.2.15 b). Time-dependent variation of COP_S's were in close approximation for each considered $T_{i,d}$ condition and average COP_s were ≈1.85 for all cases.

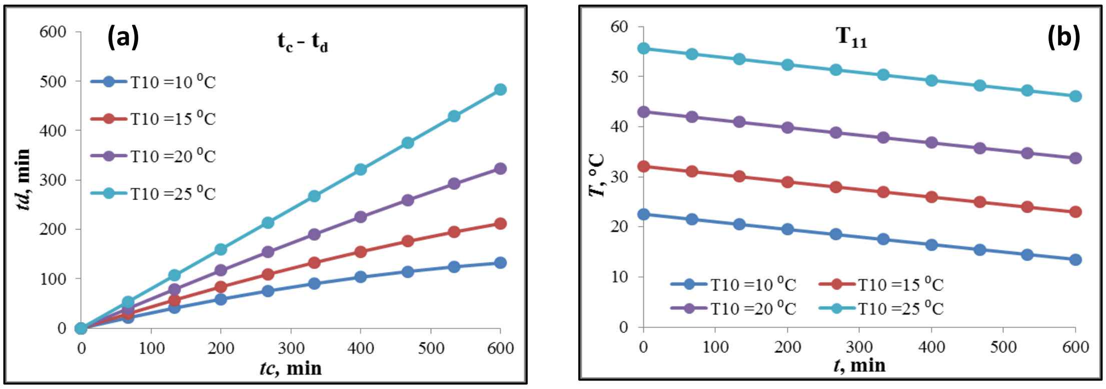

Figure 8.2.13 (a) Relation between charging and discharging time for different discharging inlet temperatures (b) effect of discharging inlet temperature on discharging outlet temperature

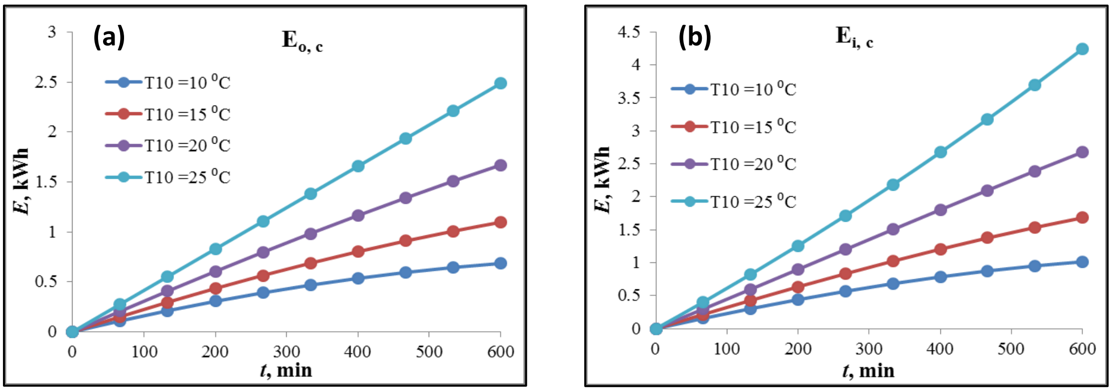

Figure 8.2.14 Effect of discharging inlet temperature on (a) charging inlet energy and (b) charging outlet energy

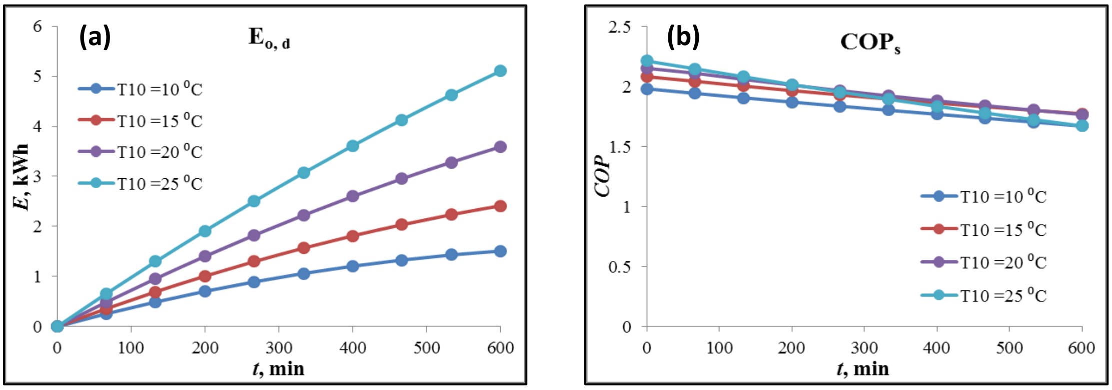

Figure 8.2.15 Effect of charging inlet temperature on (a) discharging outlet energy and (b) COP_S

8.2.3.3 Effect of charging temperature

The effect of T_c (T_3) on system performance was simulated in this section. In the model, $T_{i,c}$ is considered as 15 °C and T_{HP} assumed steady at 55 °C. Three cases were investigated where T_c (T_{EH}) is 70, 85 and 100 °C. Although t_c drops considerably (274 →228 min) with the increasing T_c (see: Figure 8.2.16 a), energy consumption of HP and EH are contrarily higher. This condition results with an increase of overall energy input to the system (see: Figure 8.2.16 b). For the increase of T_c in the range of 70→100 °C, total $E_{i,c}$ varies between 2.3 and 4.2. As a result of the increasing $E_{i,c}$, COP_{HP} and COP_S drop in the range of 4.8 →2 and 1.9→1 respectively (see: Figure 8.2.17 a-b). With the current available domestic HP technologies, it is highly unlikely to achieve air temperature >60 °C. Therefore temperatures an auxiliary EH is required to boost the air temperature to the required regeneration temperature. Use of EH significantly increases the energy consumption. Also at high T_c levels, both the energy losses and exergy destruction are high. Moreover HP evaporator inlet temperature is higher with the increasing T_c, thus waste heat could only partially be recovered. As a result of the combined effect of these factors, heat storage performance drops at higher T_c. It could be concluded that efficient regeneration of the sorbent at low T_c is crucial for THS process. Sorption materials that could be regenerate at T_c < 70 °C needs to be sought.

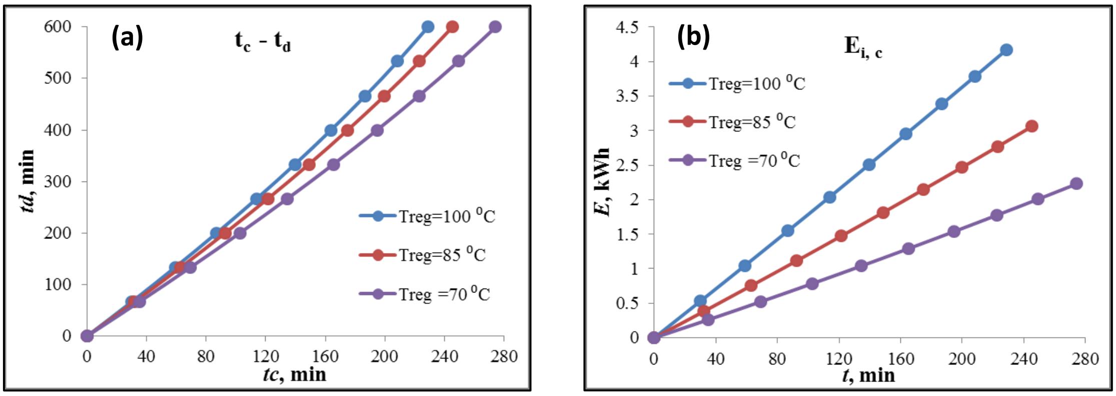

Figure 8.2.16 Effect of charging temperature on (a) charging time and (b) charging inlet temperature

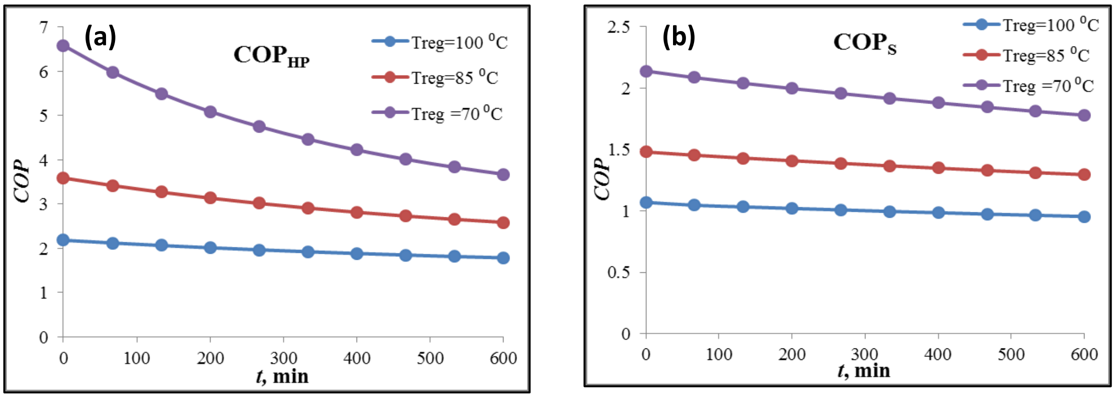

Figure 8.2.17 Effect of charging temperature on (a) COP_{HP} and (b) COP_S

8.2.3.4 Effect of mass flow rate

In this section effect of air MFR on sorption storage heater performance is analysed. T_c has a critical importance on sytem performance as demonstrated in previous section. Therefore, two different cases were considered in the analyses in which the effect of MFR on system performance at T_c=70 °C and T_c=85 °C were seperately investigated. In the simulations HP outlet temperature was set to 55 °C and kept steady for both cases. The EH outlet (T_3), which is equal to T_c, was considered as 70 and 85 °C in first and second cases respectively. Air MFR is varied in the range of 0.012→0.21 kg/s in both cases.

i. T_c = 70 (55+15 °C)

With the increasing MFR (0.012→0.21 kg/s), HP operates more efficiently (lower W_{comp}), as the amount of heat recovered at the evaporator side is larger as a result of the increasing condensation rate. However EH requires larger energy input to heat the air to 70 °C with the increasing flow rate. As a result, both the $W_{i,c}$ and $W_{o,c}$ (see: Figure 8.2.18 a-b) increases with the higher MFR of air. On the other hand ΔT_{ave} drops in the range of 37→ 26 °C for the change of air MFR between 0.012→0.021 kg/s in discharging cycle (see: Figure 8.2.19). However, total heat output remains steady and varies in the range of 0.42→0.25 kW over the 600 minutes discharging cycle. At higher MFR, there is a considerable increase in COP_{HP}

whilst the enhancement of COP_s is relatively small as seen in Figures 8.2.20 a-b. $COP_{S,ave}$ is 1.85 for MFR= 0.012 and a little improvement is achieved when MFR= 0.021. In that condition $COP_{S,ave}$ is equal to 1.95.

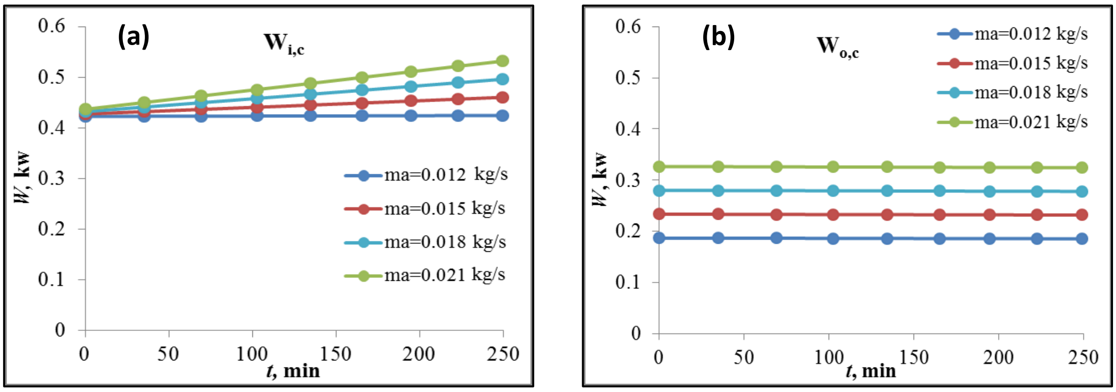

Figure 8.2.18 Effect of air mass flow rate on (a) charging power input and (b) charging power output for charging temperature of 70 °C

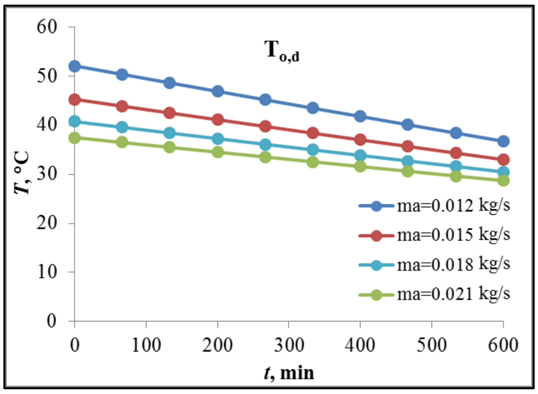

Figure 8.2.19 Effect of air mass flow rate on discharging outlet temperature

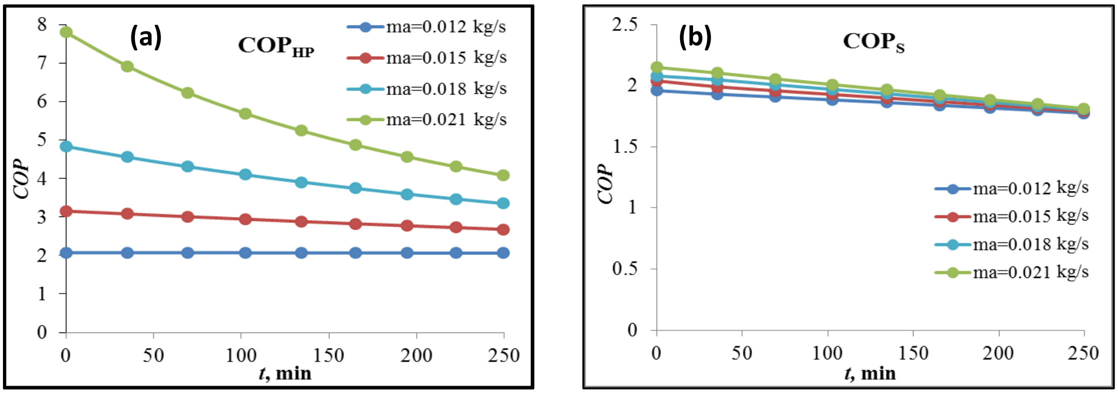

Figure 8.2.20 Effect of air mass flow rate on (a) COP_{HP} and (b) COP_S for T_c =70 °C

ii. T_c = 85 (55+30 °C)

In this section simulations were performed for T_c = 85 °C where HP output temperature was assumed as 55 °C and air temperature boost of ΔT=30 °C (55 → 85 °C) with the auxiliary EH was considered. The increasing MFR results with a rise of both $W_{o,c,ave}$ and $W_{i,c,ave}$ in the range of 0.44→0.78 kW and 1.02→1.16 kW respectively (see: Figures: 8.2.21 a-b). On the other hand $W_{o,d,ave}$ and $W_{i,d,ave}$ were found as 1.68 and 0.15 kW for all MFRs. The increase of T_c in the range of 70 →85 °C results with a considerable drop of both COP_{HP} and COP_S (see: Figures 8.2.22 a-b). COP_{HP} varies between 4→2.7 for MFR=0.021 kg/s. For the lowest MFR, COP_{HP} is 1.4 and steady; indicating that at low MFR levels COP_{HP} becomes time-independent. According to the analysis results, required charging time was found 245 mins. at T_c =85 °C for T_d=600 mins., whereas it is 275 mins. at T_c=70 °C. COP_s, which represents the ratio of $E_{o,t}$ to $E_{i,t}$ was found in close approximation for all MFR values and was in the range of 1.5 →1.3. On the other hand, at T_c = 70 °C, COP_s was between 2.2→1.8 demonstrating the inversely proportional relation between the T_c and COP_s.

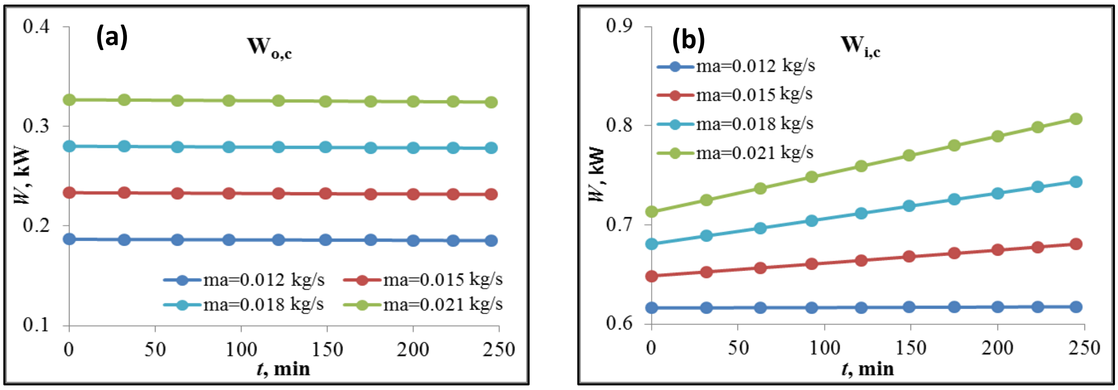

Figure 8.2.21 Effect of air mass flow rate on (a) charging power input and (b) charging power output for charging temperature of 85 °C

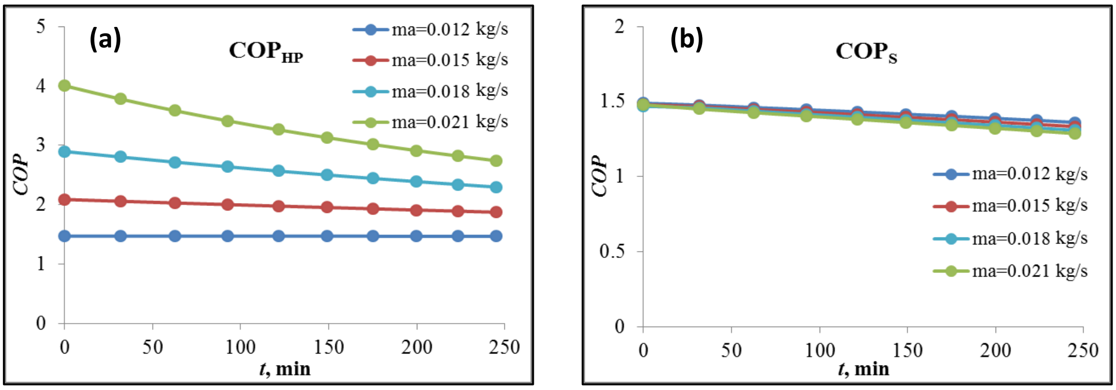

Figure 8.2.22 Effect of air mass flow rate on (a) COP_{HP} and (b) COP_S for T_c =80 °C

8.3 Design, development and experimental investigation of Heat-Store system

This section covers the design and development of the proposed Heat-Store system. The aim was to experimentally investigate the system performance;

i) With the use of different sorption materials

ii) Under different operational parameters

In order to realize this aim, 5 different composite sorbents were selected where 4 of these were SIM based materials and the last one was Zeolite 13X. The SIM composites were;

a. SIM-3a (Vermiculite + 43 wt% $CaCl_2$)

b. SIM-3m (Vermiculite + 35 wt% $MgCl_2$)

c. SIM-3cl (Vermiculite + 22 wt% CaCl2 +17%wt LiCl)

d. SIM3ml (Vermiculite +18 wt%$MgCl_2$ + 17%wt LiCl)

Among the selected 5 sorption materials, SIM-3a and Zeolite have been investigated in previous stages of the research and comparatively analysed in different experimental test configurations (See: Chapters 4 and 5). In addition to these materials, $MgCl_2$ is selected from the literature (Zondag et al., 2013) due to its high E_d and LiCl is selected due to its steady hygrothermal performance (e.g. sorption rate, heat supply) in discharging cycle. LiCl was used only as a support material in modified SIM-3a and Sim-3m composites as it is not suitable for single use due to its high cost and highly corrosive nature. It was aimed to stabilize the performance of modified Sim-3a and Sim-3m materials with the contribution of LiCl to obtain steadier discharging performances. SIM-3a and SIM-3m composites were also examined without any modification to evaluate the influence of LiCl on their performances.

Prior to preparation of large quantity of composite sorbents for experimental testing, small quantities of base materials; V-CaCl2 (SIM-3a), V-LiCl (SIM-3k), V-MgCl2 (SIM-3m), raw vermiculite and Zeolite 13X were synthesized and prepared. The samples were used to determine the physical properties of each salt with the characterization techniques including Mercury Intrusion Porosimetry (MIP), Helium (He) Pycnometer, Differential scanning calorimetry (DSC) and Nitrogen (N_2) physisorption. Moreover, in order to visualise physical structure and pore distribution of the materials, Scanning Electron Microscopy (SEM) was used. Characterization is a highly sensitive process and several factors may influence on the characterized material properties (e.g. humidity level, impregnated salt content, impregnation conditions, percentage of salt in prepared solution etc.). For this reason, SIM-3a and Zeolite were characterized again with the new selected candidates although they were characterized previously as presented in Chapter 4.2. By this way, it is proposed to provide a more realistic comparison between all selected candidate materials. Performed studies on material characterization with the achieved results were presented in the following section (See: Section 8.3.1).

8.3.1 Synthesis and characterisation of sorption materials

8.3.1.1 Determination and comparison of solid and bulk densities of the sorption materials

Bulk densities of vermiculite based samples were determined using MIP and bulk density of Zeolite was determined using the N_2 Physisorption testing. In addition, solid densities were determined for all materials using a Micrometrics Accupyc 1330 gas pycnometer with helium as the inert gas in accordance with BS ISO 21687. The samples were prepared identically as for the bulk tests. The density analysis of the samples was presented in Figure 8.3.1. The increase in bulk density for all SIM's in comparison with raw vermiculite is seen form the Figure 8.3.1. This is due to the addition of the salts which increase the overall mass of the material. Zeolite has the highest solid and bulk densities whereas the SIM-3k has the lowest among all materials.

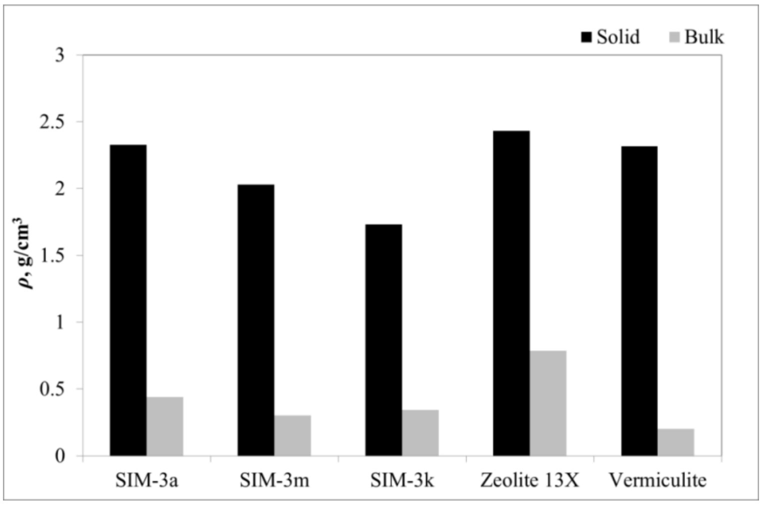

Figure 8.3.1 Comparison of bulk density to solid density

8.3.1.2 Scanning Electron Microscope (SEM) imaging of the selected sorption materials

SEM images of three salt impregnated vermiculite samples, a raw vermiculite sample and the Zeolite sample were presented in Figures 8.3.2 a-f. Raw vermiculite surface consists of thin lamellas that significantly increase surface area for salt impregnation (See: Figure 8.3.2

f). As presented in Figures 8.3.2 a-d, each salt creates a unique structure on vermiculite surface. While $CaCl_2$ settles between the layers of lamellar structure of vermiculite (See: Figure 8.3.2 a) LiCl is absorbed by the layers creating damage on the lamellar surface structure (See: Figure 8.3.2 b). In contrast, $MgCl_2$ sticks on the lamellas of vermiculite as a coating (See: Figure 8.3.2 c) and crystallizes in various sizes as seen in Figure 8.3.2 d. In Figure 8.3.23 e, highly porous structure of Zeolite 13X is seen with relatively much smaller pores than SIM's, mainly consisting of holes rather than a lamellar structure.

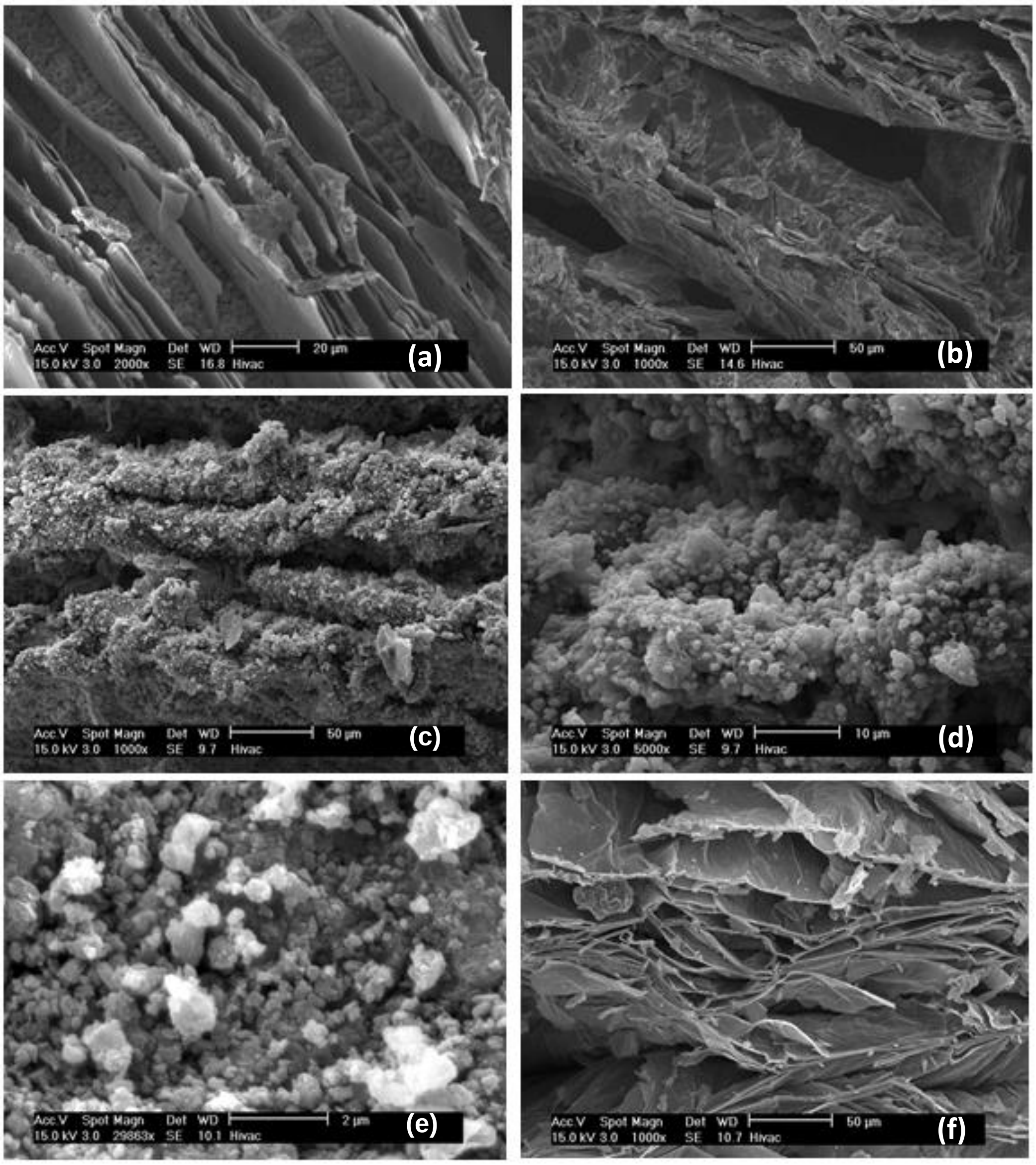

Figure 8.3.2 SEM images of candidate materials; (a) SIM-3a, (b) SIM-3k, (c-d) SIM-3m, (e) Zeolite, (f) Raw vermiculite

8.3.1.3 Determination of the pore size distribution of the sorption materials

Mercury intrusion porosimetry (MIP) analyses of the raw vermiculite and SIM's were performed using a Micromeritics Autopore IV 9500 analyser. Figure 8.3.3 presents the pore size distribution of the three vermiculite based samples and the raw varmiculite. The raw vermiculite has a nominal Φ_{pore} of 4.06 µm whilst the SIM-3a and SIM-3m has smaller pore diameter (see: Figure 8.3.3). Contrarily SIM-3k has larger pore size, however, there may be some discrepancies in the original sample pore distributions of vermiculite as it is a natural material. Total accessible pore volume V_p, for the vermiculite samples was measured at P_{max} illustrated in Figure 8.3.4 with the black columns. As expected, V_p *is* smaller for all SIM samples after impragnation due to the existence of the salt in the matrix. The reduction ratios relative to the raw vermiculite were calculated as 46%, 60%, 42% for SIM-3a, SIM-3k and SIM-3m respectively. Contrarily, the bulk densities of all composite samples increased with the impragnation of the salt to the raw varmiculite. Due to the presence of the salt, bulk densities of SIM-3a, SIM-3k and SIM-3m showed 116%, 68% and 48% increase in comparison with raw vermiculite (ρ_v=0.2 g/mL) respectively (See: Figure 8.3.5). The porosity of the samples also presented in Figure 8.3.5. Porosity of SIM-3k and SIM-3m were found as 38% and 49% respectively where raw vermiculite had a porosity of 57%. Surprisingly, the porosity of SIM-3a (65%) was found higher than raw vermiculite. As the porosity is defined as the fraction of the volume of voids over total volume of a material, vermiculite was expected to have the highest porosity, as there is no salt presence to fill the void volume. However, as heat is applied to dry the material after impragnation of salt solution, volume reduction of material is possible due to heat effect. This condition could increase the ratio of voids over volume of material resulting with an enhanced porosity. As an overview, this data demonstrates an important advantage of SIM-3a as a thermochemical heat storage (THS) material. A uniform air diffusion through the sorption material with minimal pressure drop and maximum vapour absorption rate is vital in THS systems. Higher porosity provides larger channels for air flow, enhances contact surface area between the sorbent and air also enables higher moisture uptake. Therefore THS materials with higher porosity can significantly improve the performance of THS systems.

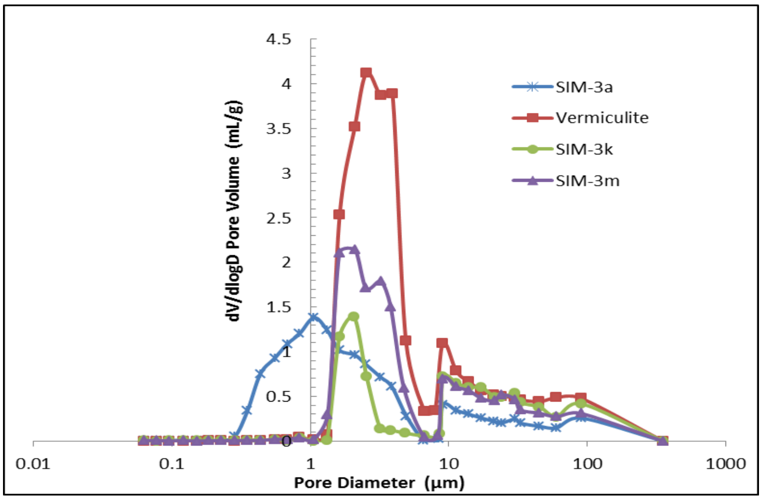

Figure 8.3.3 BJH pore size distributions for SIM samples and raw vermiculite

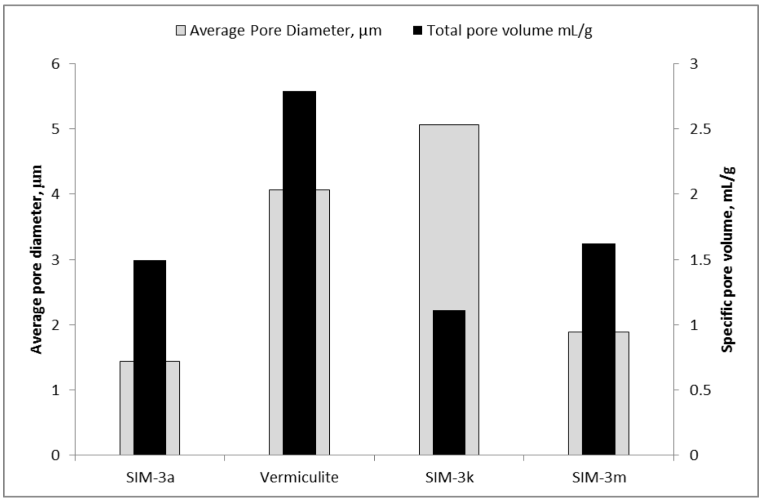

Figure 8.3.4 Average pore diameter and specific pore volume of the tested samples

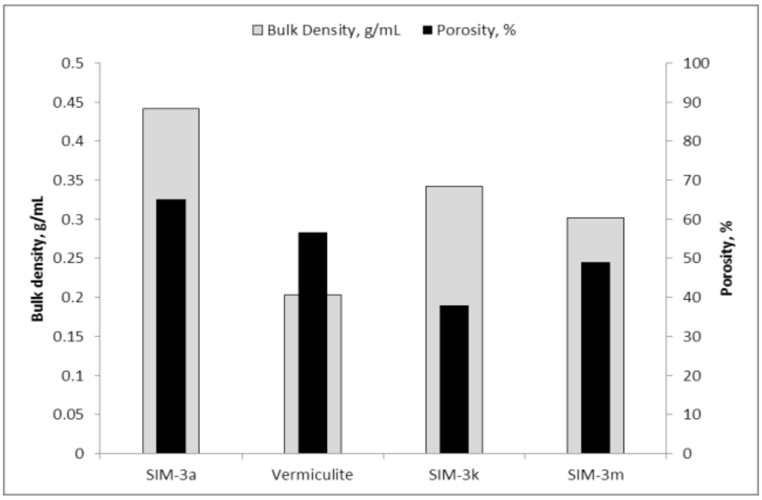

Figure 8.3.5 Bulk density and porosity of the tested samples

As Zeolite is not suitable for MIP testing due to the small pore size, Nitrogen (N_2) physisorption analysis was performed to determine pore size distribution and sorption isotherms of Zeolite 13X. Micrometrics Tristar II 3020 (v1.04) analyser in accordance with BS 4359-1 was used to conduct the analysis. The sample ($m_{\approx}$0.5 g) was first oven dried to achieve the condition $w=w_0$ before being outgassed at 200 °C for 3 hour prior to the analysis. N_2 gas adsorbate was used with a 5 min equilibration time at each relative pressure, P/P_0 points were used for each test. The pore diameter distribution for the sample was determined by the Barrett-Joyner-Halenda (BJH) method from the adsorption branch of N_2 isotherm and the results were presented in Figure 8.3.6. The Zeolite sample has a nominal Φ_{pore}=9 nm. High percent of pores have Φ_{pore} in the range of 1nm →10 nm suggesting that majority of pores were micro and meso. In Figure 8.3.7 the total pore volume of Zeolite sample which is 0.143 cm^3/g was illustrated, also the volume share of micropores, mesopores and macropores were indicated. Accordingly share of micro,meso and macropores were calculated as 17%, 78% and 5% respectively. In Figure 8.3.8 adsorption / desorption isotherms of Zeolite is presented. It can be seen that Zeolite can take on moisture rapidly at low RH levels with little further absorption.

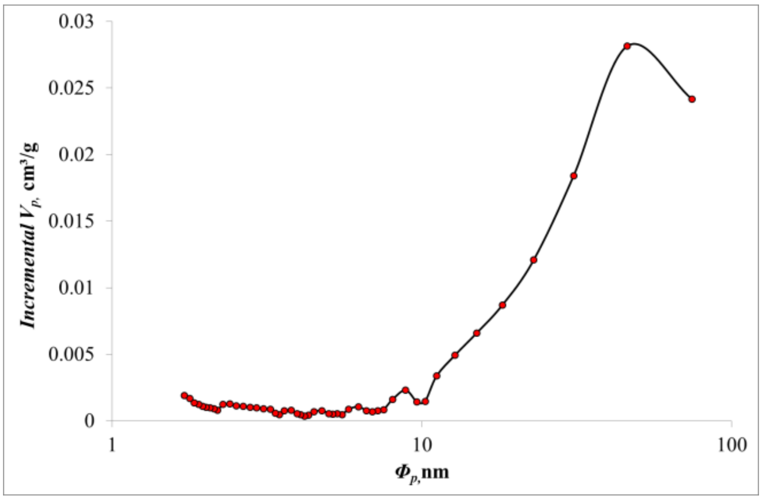

Figure 8.3.6 BJH pore size distribution for Zeolite 13X sample

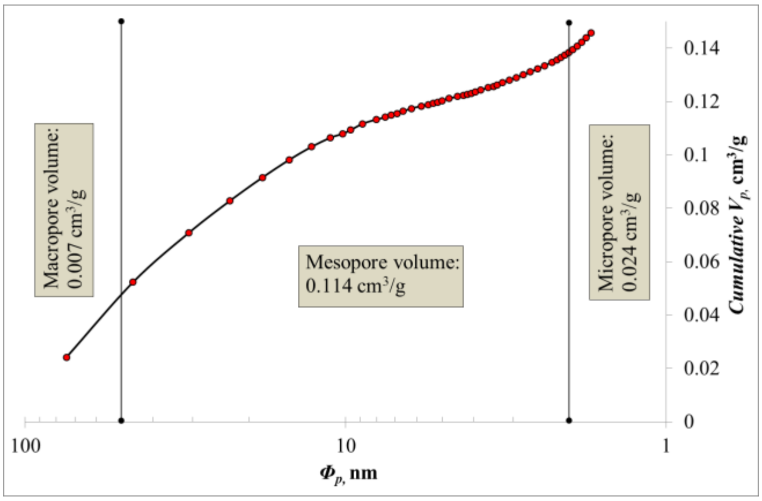

Figure 8.3.7 Proportions of micro/meso/macro pore volume and the total pore volume of Zeolite 13X sample

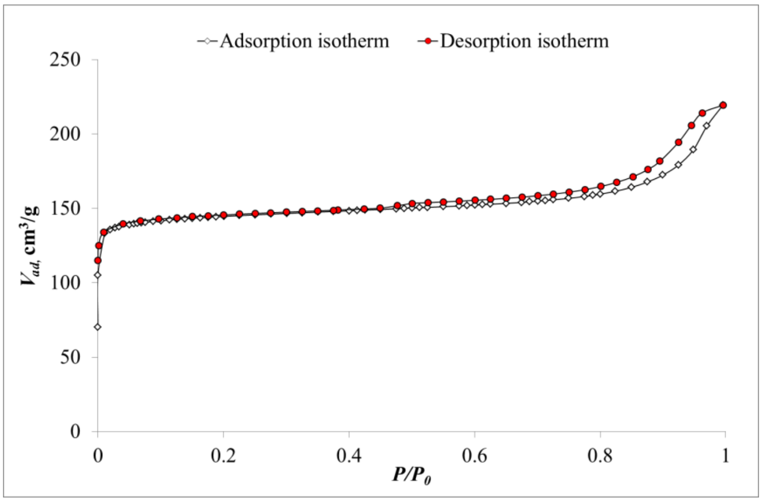

Figure 8.3.8 N_2 adsorption/desorption isotherms for the Zeolite 13X sample

8.3.1.4 Determination of the energy storage density of the sorption materials

The most important material property in terms of thermal energy storage is the energy storage density, E_d (kj/kg). Differential scanning calorimetry (DSC) was used to determine E_d using a modified experimental method based on BS EN ISO 11357-4. A TA Instruments Q10 differential scanning calorimeter was used to first determine the specific heat capacity, c_p (J/kg/K) of the samples. Each sample was tested 3 times with the mean values of c_p calculated. Principally the area under c_p–T curve gives the heat applied to desorb the moisture which is theoretically equal to absorption energy that could be achieved (Please see Chapter 4.2 for more detail). The calculated E_d of SIM samples, raw vermiculite and Zeolite are presented with the mean values highlighted in Figure 8.3.9. SIM-3a and SIM-3k displayed the largest E_d equal to 388 kJ/kg and 393 kJ/kg respectively. It is found that SIM-3m has relatively low E_d of 324 kJ/kg whereas Zeolite provided the lowest E_d (271 kJ/kg) among all samples except raw vermiculite. Here it should be noted that Zeolite and SIM-3m have desorption temperatures in the range of 150-200 °C. This indicates that; to completely desorb the moisture and achieve the full energy density of these materials, higher temperatures should be applied in DSC testing. However as prior aim in THS is to use low temperature clean energies such as solar energy, peak temperature was set to 120 °C for DSC testing. This is because achieving temperature higher than 120 °C with domestic solar collectors seems highly unlikely under real world conditions. Therefore, the results indicate the energy density of the selected materials for regeneration temperature of T_{reg}<120 °C. Finally, the raw vermiculite has a very low E_d of 57 kJ/kg, indicating that this material is not suitable to be utilized in THS in row state. However, as demonstrated in previous analysis, it has a good potential to be used as host matrix for salt impregnation. It has a light and highly porous structure preventing salt leakage, also high surface area allowing impregnation of large quantities of salt. Besides, it allows uniform air flow through its pores which minimizes the pressure drop also increases the absorption capacity of the salt.

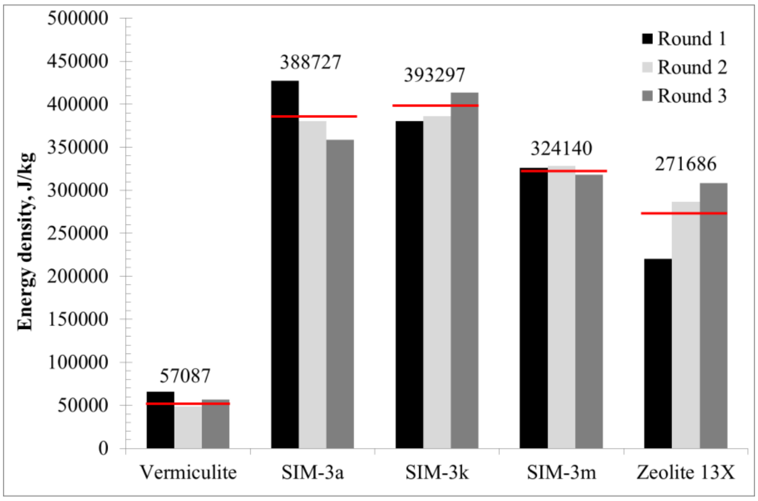

Figure 8.3.9 E_d of the samples with average values highlighted

Work on the characterization of several candidate materials showed that SIMs have numereous advantages when compared with Zeolite such as larger pore diameter enabling large quantity of salt impregnation without a major damage to the pore structure also higher E_d at low regeneration temperatures. Among the SIMs; SIM-3a has the optimal properties including uniform pore distribution, high porosity and bulk density also high E_d at moderate T_{reg}. Beside SIM-3a and SIM-3k provided the highest E_d at same T_{reg} which is promising. Although E_d of SIM-3m remained lower than SIM-3a and SIM-3k, it is known that at T_{reg}>150 °C SIM-3m has higher theoretical E_d. Therefore this material deserves attention for THS applications as well. Despite the possibility of creating and investigating several composites with the use of various compositions of the selected salts $CaCl_2$, $MgCl_2$ and LiCl, time is the main limitation. Therefore, based on the characterization results, cost of materials and chemical properties of salts (e.g. corrosiveness, toxicity) SIM-3a, SIM-3cl, SIM-3m and SIM-3ml were selected as target composites to be experimentally investigated. Accordingly, following the characterization work, these materials were prepared in larger quantities and experimented in the developed Heat-Store system as presented in the following section.

8.3.2 Development and physical experimentation of sorption storage heater

Following the thermal performance modelling of the proposed system and characterisation of the synthesized heat storage materials, an experimental prototype was developed an investigated under various operational conditions also with the use of different sorbents. The applied experimental procedure and methodology, system description and operational modes and the obtained experimental results with the conclusions were presented within this chapter.

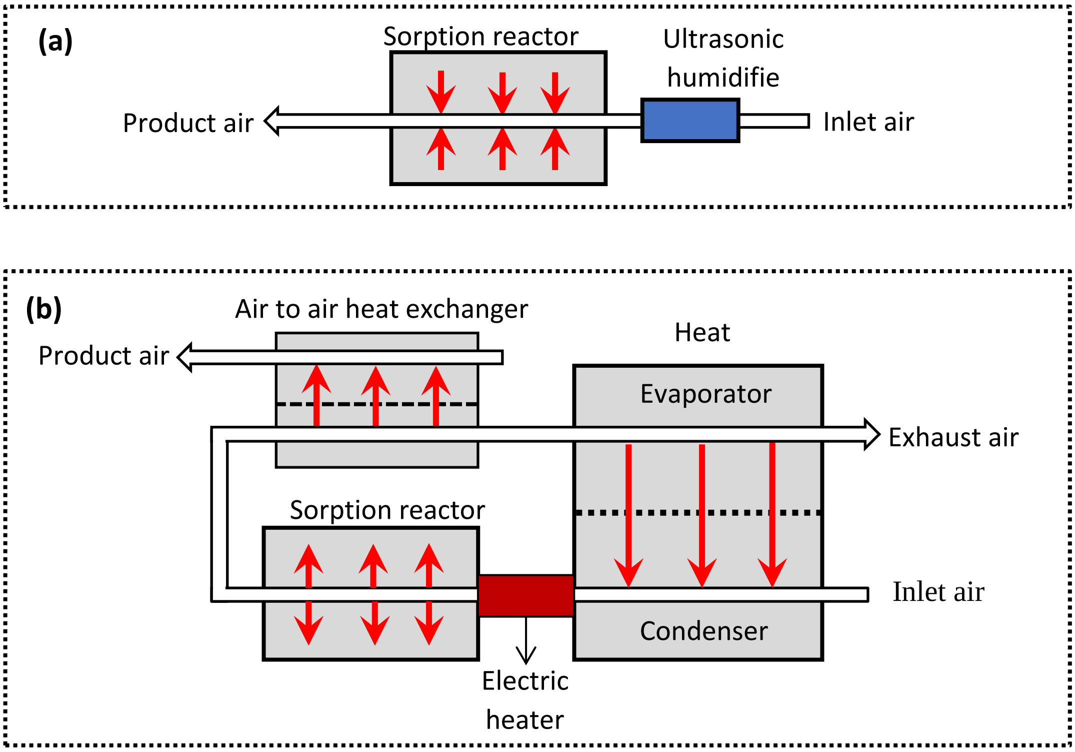

Figure 8.3.10 Schematic illustration of heat flow in (a) discharging and (b) charging cycles

The simplified schematic illustrations of the heat flow in charging and discharging operations of the proposed system are presented in Figures 8.3.10 a-b. As seen from the Figure 8.3.10 a, in discharging cycle generated sorption heat is transferred to the air. In charging cycle, an energy efficient process is used for desorbing the water from the sorbent. Here, initially air is heated at the heat pump (HP) condenser then electrical heater (EH) boosts air temperature. Later heat is partially transferred to the sorbent for endothermic dehydration process. Part of the waste heat of air leaving the reactor is utilized for heating the secondary air stream via a heat exchanger. In the final stage, rest of the waste heat is transferred to the refrigerant and air is exhausted to the ambient.

The view and the schematic illustration of the developed testing rig are given in Figures 8.3.11 and 8.3.12 respectively. In charging process an air to air attic heat pump is used. Two reasons primarily influenced the decision on usage of a heat pump.

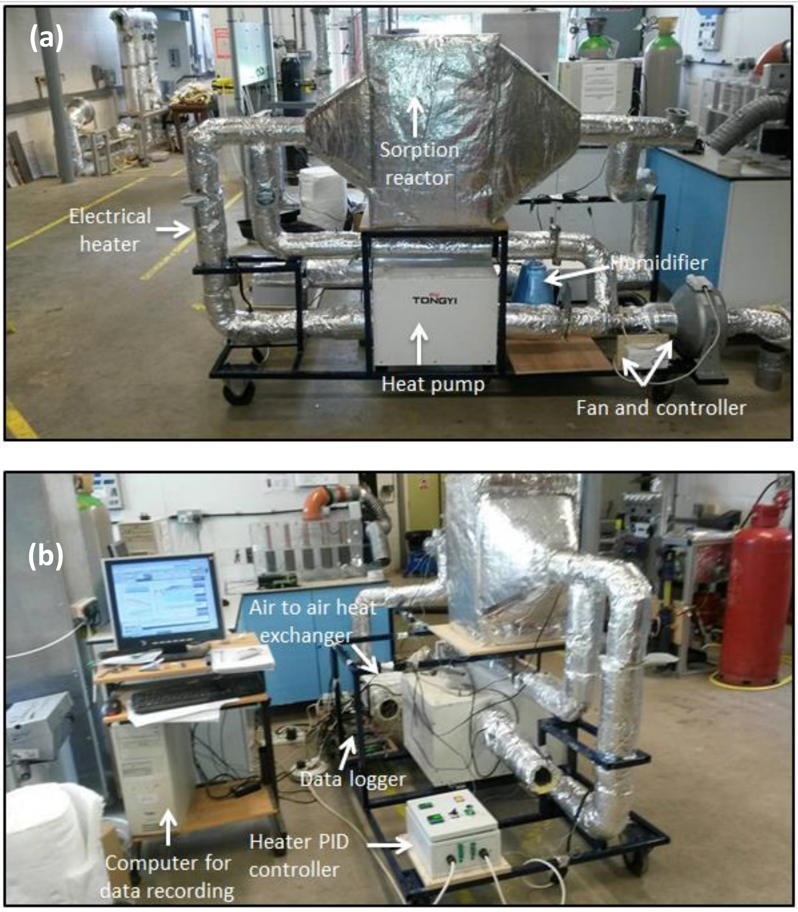

Figure 8.3.11 (a) Frontal view of the experimental rig, (b) side view of the experimental rig and computer used for data acquisition

Firstly, benefitting from vapour compression cycle allows achieving the desired air temperature with less energy consumption in comparison with single usage of direct electrical heater. Secondly, as the refrigerant temperature is very low in evaporator, waste heat in reactor exhaust air could be recovered effectively with condensing the moisture. Using only a heat exchanger limits the amount of recovered heat as it is highly unlike to cool the air to dew point with the heat exchanger. Combined use of heat recovery and heat pump enables effective recovery of the waste heat.

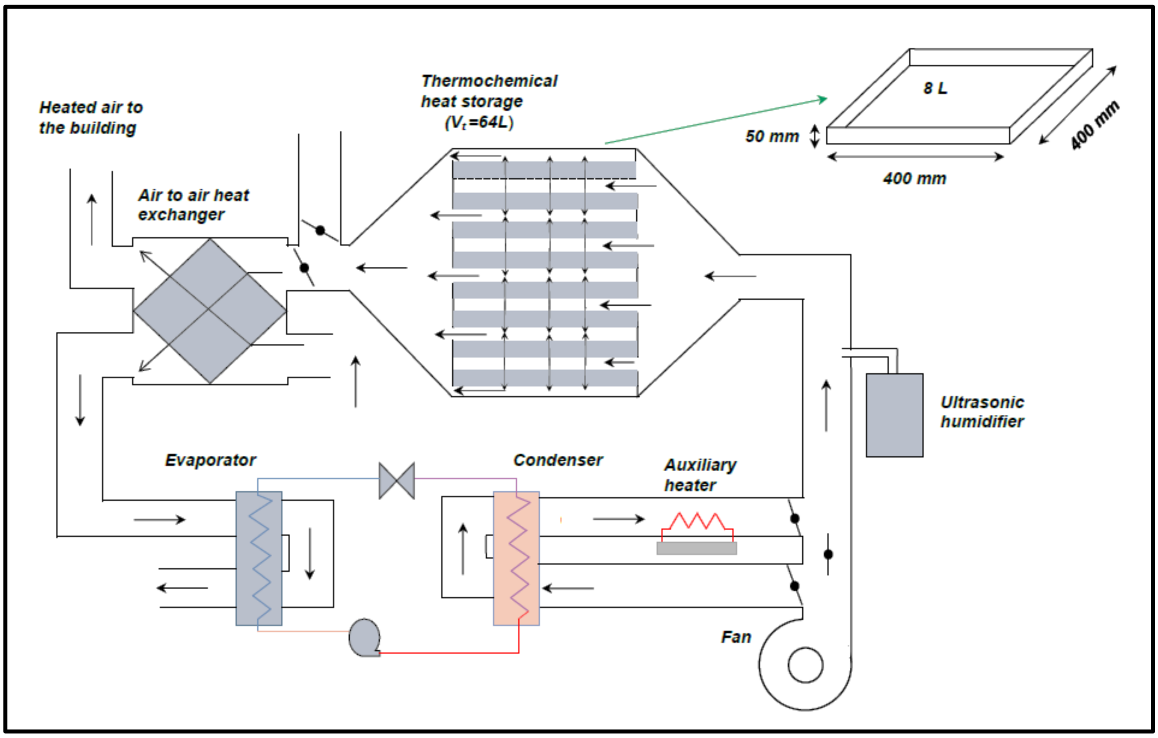

Figure 8.3.12 Schematic illustration of the experimental rig

In the proposed system, a novel multilayer fixed bed sorption reactor was used. As the system is charged with electricity sourced HP and EH, moisture desorption should be effective both for higher rate of heat recovery (e.g high rate of vapor condensation) also for reducing the operational time of HP and EH. Therefore uniform air flow through the sorption bed is crucial. In any particular reactor design, with the increasing bed thickness, resistance to air flow increases which could lead to insufficient heat transfer to the sorbent thereby longer charging time. By considering that, it was decided to use multiple sorption beds with low bed thickness also to use air channels between each bed for uniform air flow.

In the developed system, there are four air inlet channels between the sorption beds where the channel ends are sealed. Air entering the channels is forced to flow through sorption beds (up and down) and by following the outlet channels leaves the reactor. 8 trays, made up of 1.2 mm thick aluminium mesh, were used in the reactor where each tray has the dimensions of *h*: 50 mm, *l*: 400 mm and *w*: 400 mm. The maximum V_s of each tray is 8 *l* corresponding to V_s reactor of *64 l.* The distance between the trays, constituting the air flow channels was designed as 20 mm. The 3D schematic illustration and view of the sorption reactor in construction stage showing the inlet and outlet air channels was presented in Figures 8.3.13 a-b. The final version of the constructed sorption reactor was also presented in Figure 8.3.14 below.

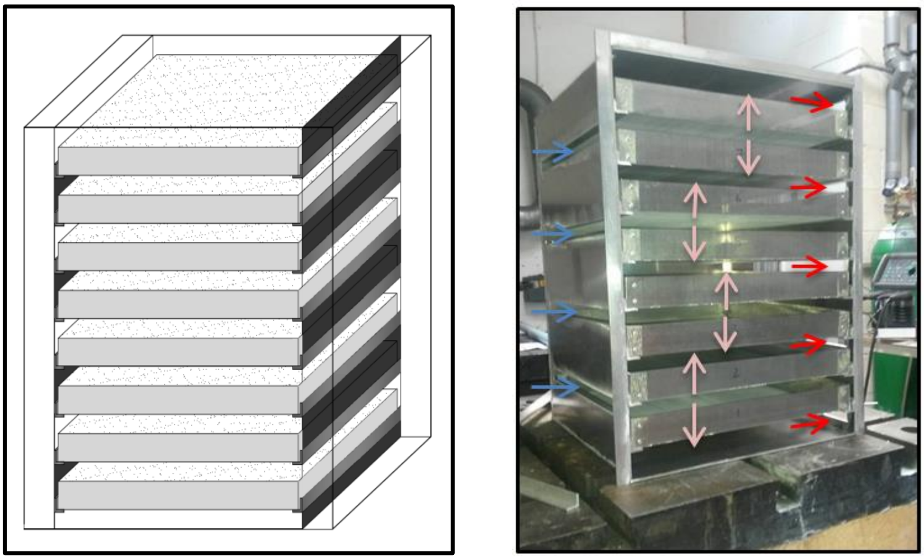

Figure 8.3.13 (a) Schematic illustration and (b) view of the sorption reactor in construction stage showing the inlet and outlet air flow channels

Figure 8.3.14 View of the constructed multi-layer fixed bed sorption reactor

The schematic diagram representing the charging and discharging cycles and description of system operational modes were previously presented in 8.2.1. It is proposed to provide continuous space heating with the use of the developed sorption storage heater. In discharging cycle free sorption heat is utilized for heat supply where only energy consuming components are fan and humidifier. In charging cycle, while off peak or PV sourced electricity could be used for charging the heat storage material, waste heat is also recovered for heat supply to the building.

8.3.2.1 Uncertainty Analysis

In the developed experimental rig, 8 sensor locations were used for determining the *T* and *RH* at the inlet and outlet of HP, HEX, sorption reactor and EH. System inlet / ambient conditions were also recorded in both charging and discharging cycles. Data is recorded using the EK-H4 Eval Kit for Temperature - Humidity Sensors from Sensiron, AG, Switzerland. The experimental uncertainties were determined by applying Gauss propagation law (See: Section 4.3.3).

The independent parameters measured in the experiments are temperatures and relative humidities of; system inlet (T_1, RH_1), humidifier outlet (T_2, RH_2), HP condenser outlet (T_3, RH_3), EH outlet (T_4, RH_4), reactor outlet (T_5, RH_5), HEX inlet (T_6, RH_6), HEX outlet (T_7, RH_7) and HP evaporator outlet (exhaust) (T_8, RH_8). MFR of air (m_a) was also measured for determining the heat transfer rates. Experiments were conducted by using following instruments: Thermocouples with the maximum deviation of ±0.3°C for temperature and ±2% for relative humidity and air mass flow meter with the accuracy of ±2%.

It is obtained from the equations (8.1) – (8.46) that the COP_s is the function of measured 8 *T* and *RH* values in charging cycle, measured 2 *T* and *RH* (system inlet, , reactor inlet and reactor outlet) values during discharging cycle also measured m_a ($m_{a,c}$, $m_{a,d}$) in both cycles, each subject to uncertainty:

$$COP_S = f\left(T_{1\rightarrow 8}, RH_{1\rightarrow 8},\ T_{9\rightarrow 11},\ RH_{9\rightarrow 11}\ ,\ m_{a,c},\ m_{a,d}\ \right) \tag{8.47}$$

Where subscripts 1→8 stands for eight measurements points in the system during charging cycle and 9→11 stands for three measurement points during discharging cycle as described above.

Total uncertainty for overall system efficiency can be expressed as;

$$w_R = \left[\sum_1^8\left[\left(\frac{\partial COP_S}{\partial T_{1\rightarrow 8}} w_{T_{1\rightarrow 8}}\right)^2\right] + \sum_1^8\left[\left(\frac{\partial COP_S}{\partial RH_{1\rightarrow 8}} w_{RH_{1\rightarrow 8}}\right)^2\right] + \left(\frac{\partial COP_S}{\partial m_{a,c}} w_{m_{a,c}}\right)^2 + \sum_9^{11}\left[\left(\frac{\partial COP_S}{\partial T_{9\rightarrow 11}} w_{T_{9\rightarrow 11}}\right)^2\right] + \sum_1^8\left[\left(\frac{\partial COP_S}{\partial RH_{9\rightarrow 11}} w_{RH_{9\rightarrow 11}}\right)^2\right] + \left(\frac{\partial COP_S}{\partial m_{a,d}} w_{m_{a,d}}\right)^2\right]^{1/2} \tag{8.48}$$

Total uncertainty rate affecting the efficiency of the proposed system was computed by using Eqs. 8.47-8.48. The estimation implies that total uncertainty in calculation of the efficiency is found to be 3.36%.

8.3.2.2 Experimental Methodology

Three main objectives have set within the experimental investigation of the developed prototype system. These include;

- Investigating the system thermal performance with the use of different sorption materials
- Investigating the system thermal performance under different operational conditions (e.g. at different humidity levels, regeneration temperature, sorption bed thickness and air MFR)

In order to meet the given objectives of the study, methodology of the experimental work is designed as presented in Figure 8.3.15. Experimental work started with the testing of the selected five sorption materials at low and high inlet air humidity. High humidity tests were performed under RH_{air} =80% and low humidity test were performed under RH_{air} =60% conditions where T_a was kept constant at ≈17 °C. Low humidity cycles were targeting investigation of the thermal energy output of sorbents at low sorption rate. A single cycle testing at low RH_{air} has performed for each sorption material. Within the high humidity testing, two repeating cycles were performed. In first round of cycles, increase of sorption rate and heat output of each material with the increase of humidity levels were investigated. In the following round, cyclic stability of the sorbents at T_c=80 °C was investigated. Upon completion of the testing of different materials at low and high humidity conditions, material hygrothermal performances and overall system performances were comparatively analysed. Based on the analysis results, best sorption material was selected.

In second part of experimental work only selected sorbent was used and effect of air MFR and sorption bed thickness on sorption storage heater performance was investigated. Based on the experimental results, system is optimized by determining the optimum MFR and sorption bed thickness.

In the final step of experimental work, 2 long cycles of testing with the optimized system and selected sorption material was performed. It was aimed to investigate the system overall performance within these cycles.

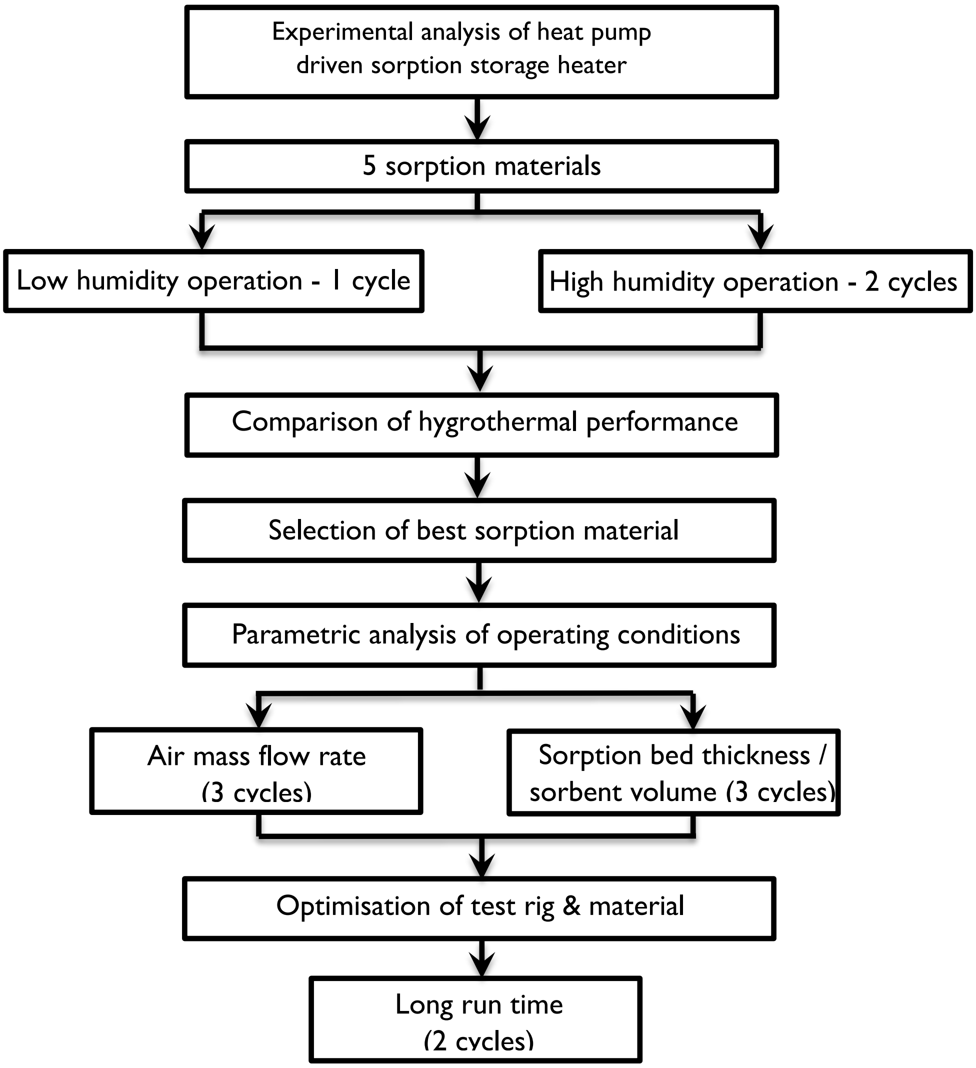

Figure 8.3.15 Flowchart illustrating the experimental methodology

8.3.2.3 Results and discussion

In this section, full set of the experimental results were presented and discussed. In the first and second parts, performance of sorbents under high and low air humidity levels were illustrated. In third part, a general overview of material and system performances at high and low humidity operational conditions were presented. In the fourth part, effect of MFR and sorption bed thickness on system thermal performance was investigated with the use of best performing sorbent. Finally long cycle performance of the system was investigated.

8.3.2.3.1 Material hygrothermal performances under high air humidity operating conditions

i. Zeolite testing

Zeolite provided an avarage temperature lift, $\Delta T_{ave,}$ of 23 °C for the average relative humidity difference of reactor inlet and outlet, ΔRH_{ave}, of 70% in the first discharging cycle (See Figure 8.3.16 a-b). In charging cycle, it was observed that the moisture was partially removed, indicating a low hygro-cyclic effectivity. Hygro-cyclic effectivity ($\eta_{hyg\text{-}cyc}$), defines the ratio of the $m_{w,abs}$ in dicharging process to the $m_{w,des}$ in charging process. $\eta_{hyg\text{-}cyc}$ was calculated as 50% for Zeolite 13X. Due to the low $\eta_{hyg\text{-}cyc}$, ΔRH_{ave} and ΔT_{ave} were dropped to 55% and 20.3 °C respectively in the second discharging cycle (See Figure 8.3.17 a-b). Results clearly showed that Zeolite requires higher regeneration temperature to be fully charged. In the applied testing procedure, 41% of the absorbed moisture could not be desorbed at the end of 180 min. of charging cycle. Accordingly, Q_{ave} dropped in the range of 0.5 →0.43 kW with the reduction of moisture sorption rate.

During the charging of all materials, electrical heater outlet temperature has set to 85°C where the heater was controlled with a PID controller. An air-to-air HP, using refrigerant R410a was employed in the system. During the charging process inlet air was heated at the condenser side whilst the exhaust air from the reactor was transferring the waste heat to refrigerant in the evaporator side. As seen from Figure 8.3.18 a, the HP outlet (condenser side) temperature is flactuating in the range of 40 – 70 °C. This is because large amount of heat was transferred to the refrigerant in evaporator side and once the refrigerant was reached to critical temperature the heat pump was cutting off. It was not operating until the refrigerant transferred some heat to the air and cooled down.

The average temperature and relative humidity values were presented in Figure 8.3.18 b and 8.3.19 b. The values have calculated based on the original data given in Figure 8.3.18 a and 8.3.19 a. A seen from Figure 8.3.18 b, HP increases the inlet air temperature from ≈22 °C to ≈55 °C and from that level air temperature was boosted to 85 °C with the help of electrical heater. The reactor outlet temperature increased gradually and reached to 60 °C at the end of 180 minutes charging cycle. There was a slight temperature difference (2-3 °C) between the measurements of reactor outlet and heat exchanger (HEX) inlet due to the heat losses through the ducting. The heat transffered to the secondary line in HEX was calculated by considering the temperature difference of the process air at the HEX. In the last stage, air leaving the HEX enters the evaporator and transfers the rest of its heat to the refrigerant.

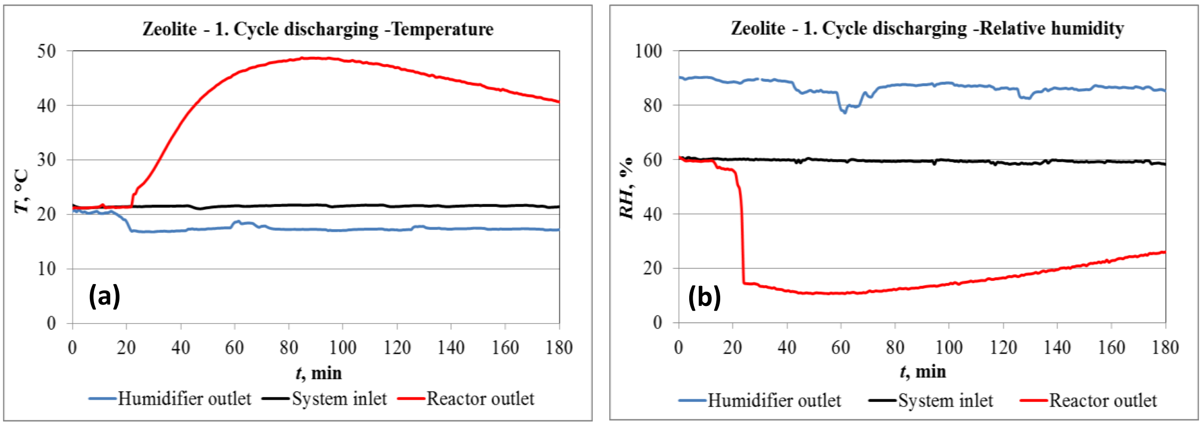

Figure 8.3.16 Measured (a) temperatures, (b) relative humidities in 1st discharging cycle of Zeolite

As represented in Figure 8.3.18 b, the temperature difference between the evaporator inlet and outlet was averagely 21.5 °C and the exhaust air temperature gradually rose from 10 °C to 20°C over the charging process and slightly exceed the ambient level (≈23°) at the end of the cycle.

Results showed that average heat input to the air in condenser and electrical heater were 0.58 kW and 0.57 kW respectively corresponding to a total heat input of 1.15 kW. It was also found that 0.39 kW of input heat was recovered in HEX and the 0.41 kW of it was recovered in the evaporator. Considering the total heat input and total heat recovered , the heat recovery ratio was obtained as 70%.

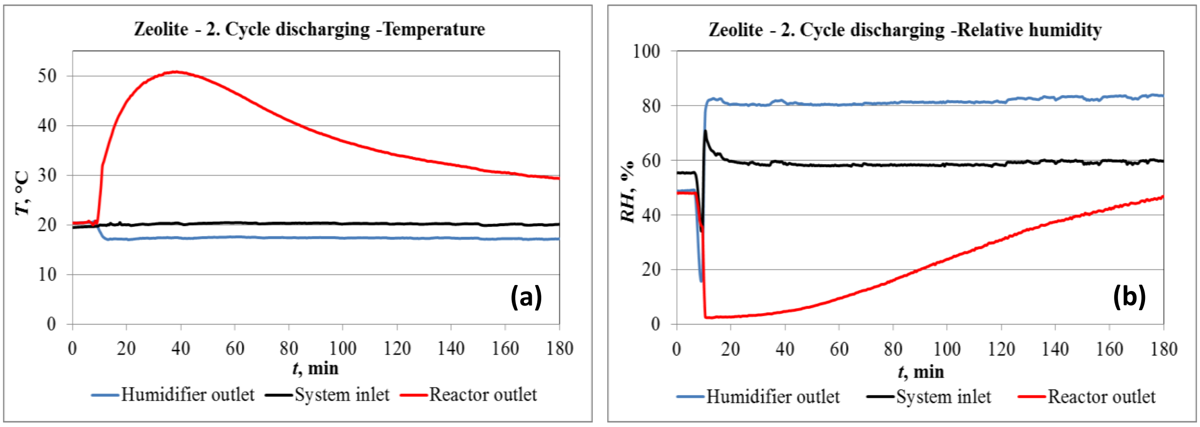

Figure 8.3.17 Measured (a) temperatures, (b) relative humidities in 2nd discharging cycle of Zeolite

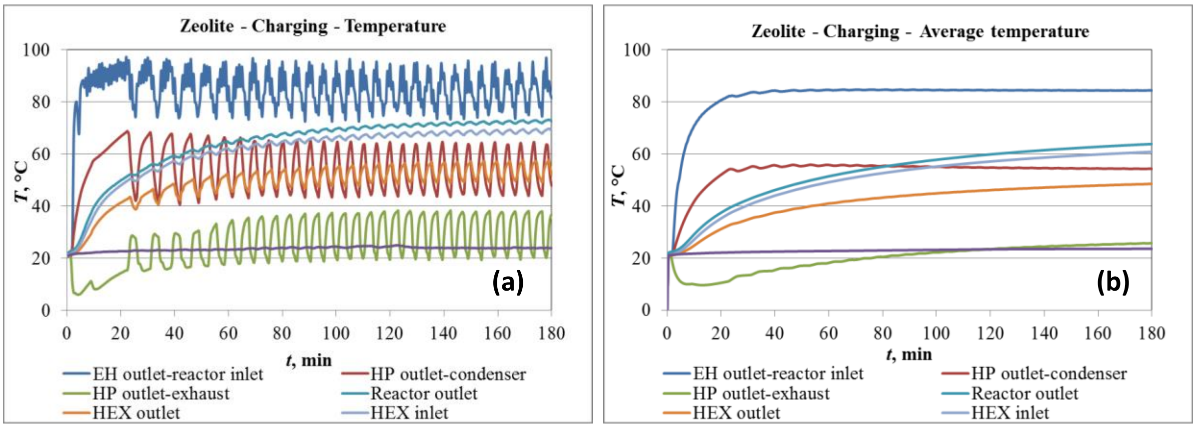

Figure 8.3.18 (a) Measured, (b) average temperatures in charging cycle of Zeolite

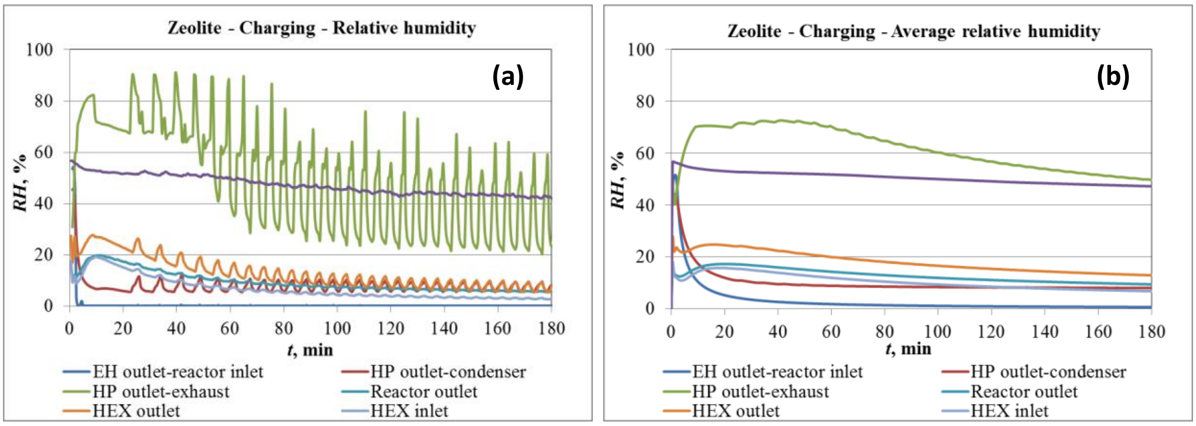

Figure 8.3.19 (a) Measured, b) average relative humidities in charging cycle of Zeolite

ii. V-MgCl$_2$ (SIM-3m) testing

ΔT_{ave} and ΔRH_{ave} were found 25.5 °C and 70.4% respectively in the first cycle testing of SIM-3m (See Figure 8.3.20 a-b). As a result of poor $\eta_{hyg\text{-}cyc}$ (67.7%), 33% of the moisture remained inside the material and could not be desorbed . This aspect negatively influenced the second discharging cycle and ΔT_{ave} and ΔRH_{ave} dropped to 16.7 °C and 55% respectively (See Figure 8.3.21 a-b). Similarly, lower moisture sorption rate resulted with much lower Q and E_{cum} in the second cycle. Q varied in the range of 0.54 kW$\rightarrow$0.36 kW in the 1st and 2nd cycle, corresponding to 33% drop of E_{cum} between the cycles.

Similar drying procedure with Zeolite is applied to SIM-3m. Although in the 1st discharging cycle, SIM-3m has provided the highest heat output, its performance was the worst in the 2nd cycle among 5 tested sorbents. The results obtained in charging cycle indicates that SIM-3m requires much higher desorption temperatures than 85°C.

The average temperature and relative humidity values of charging cycle were presented In Figure 8.3.22 b and 8.3.23 b. The values have calculated based on the original data given in Figure 8.3.22 a and 8.3.23 a. As seen from Figure 8.3.22 b, HP increased the inlet air temperature from ≈20 °C to an average of ≈57 °C and from that level air temperature was boosted to ≈83 °C with the help of EH. The reactor outlet temperature increased gradually and reached to 66 °C at the end of 180 minutes charging cycle. Air leaving the reactor is cooled ≈10 °C at the HEX via transferring heat to the secondary air flow. The HP provided the majority of heat recovery with a large ΔT_{air} at the evaporator. As represented in Figure 8.3.22 b, ΔT_{air} between the evaporator inlet and outlet was averagely 23.4 °C and the exhaust air temperature gradually rose from 10 °C to 22°C over the charging process and slightly exceed the ambient level (≈22°) at the end of the cycle. According to the experimental results, average heat transferred to the air in condenser and electrical heater was 0.66 kW and 0.56 kW corresponding to a total of 0.96 kW heat input. The total recovered heat in HEX and evaporator was 0.42 kW and 0.55 kW respectively. Considering the total heat input and total recovered heat, the heat recovery ratio was obtained as 80%.

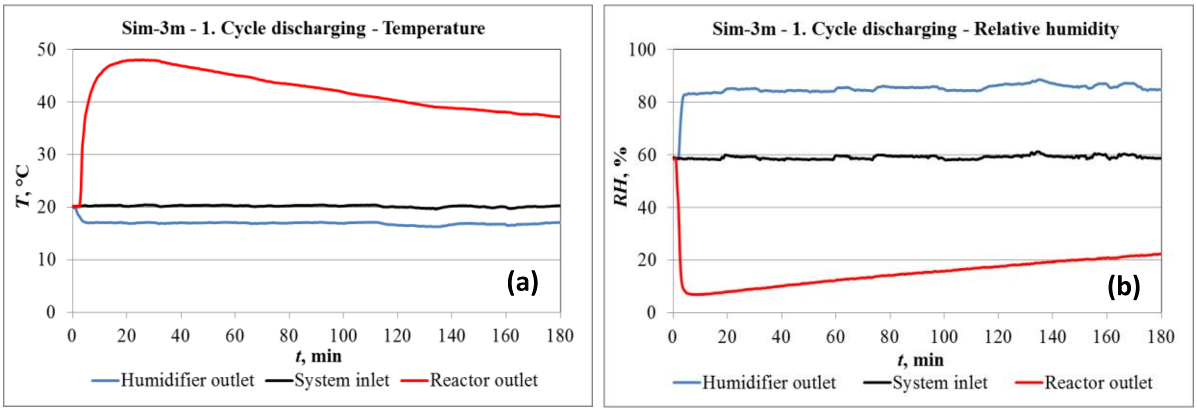

Figure 8.3.20 Measured (a) temperatures, (b) relative humidities in 1st discharging cycle of Sim-3m

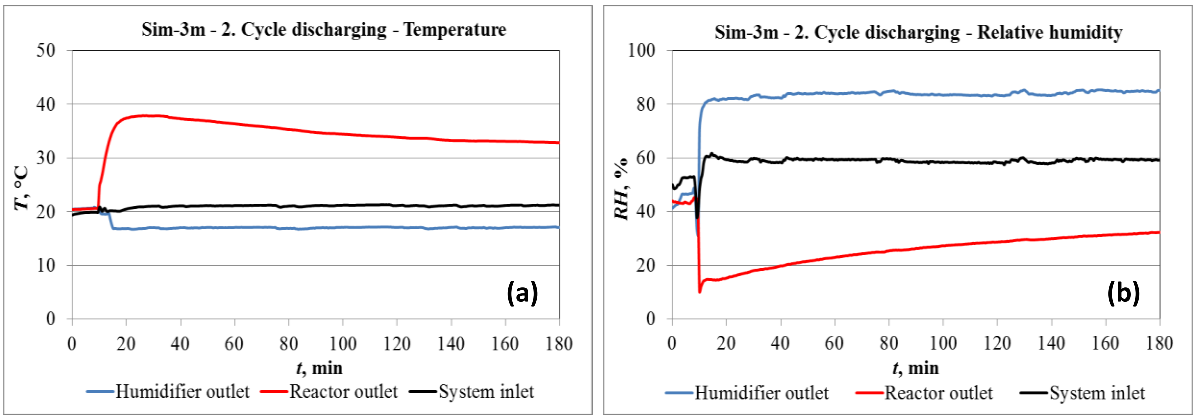

Figure 8.3.21 Measured (a) temperatures, (b) relative humidities in 2nd discharging cycle of Sim-3m

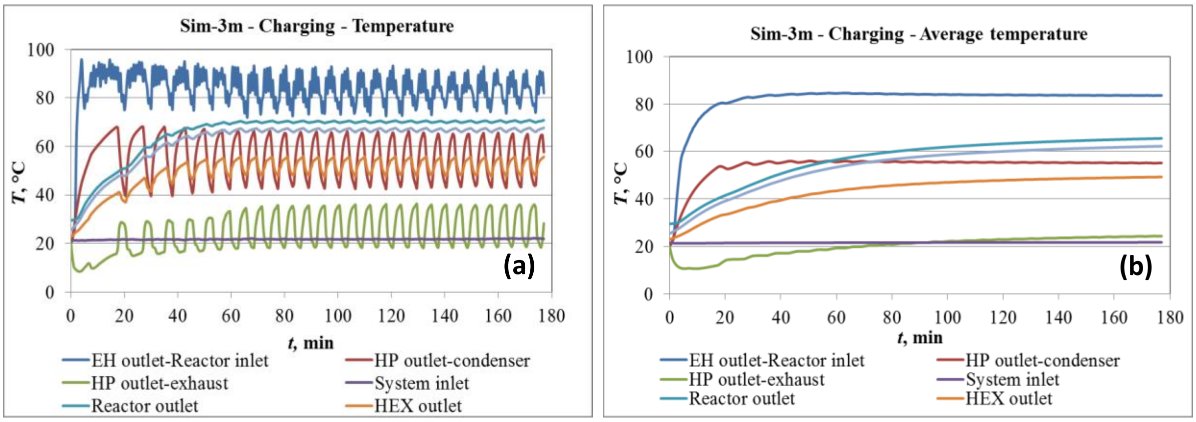

Figure 8.3.22 (a) Measured, (b) average temperatures in charging cycle of Sim-3m

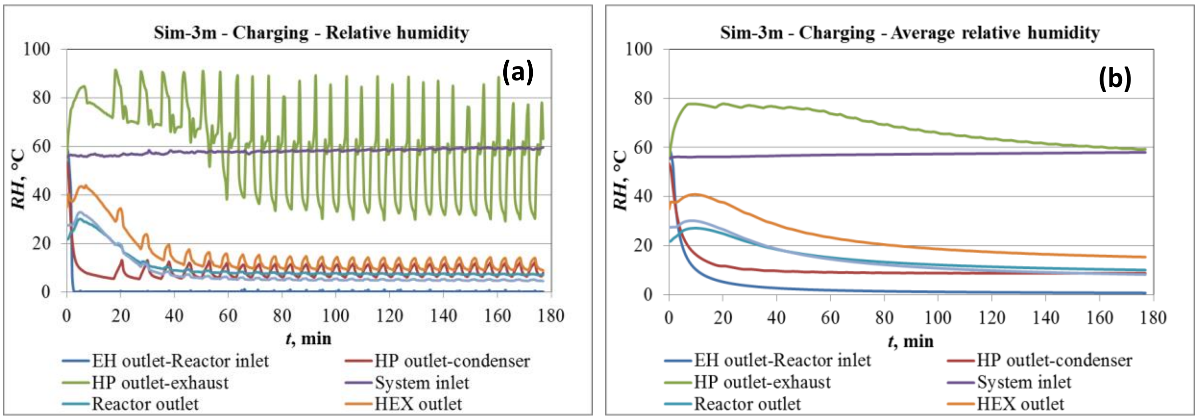

Figure 8.3.23 (a) Measured, (b) average relative humidities in charging cycle of Sim-3m

iii. V-CaCl$_2$ (Sim-3a) testing

V-CaCl$_2$ provided an avarage temperature lift, ΔT_{ave} = 23.1 °C, for the ΔRH_{ave} = 57.8% in the 1st cycle (See Figure 8.3.24 a-b). After regenerating the material at $T_{c,ave}$ = 82 °C for 180 mins, ΔT_{ave} and ΔRH_{ave} were found as 22.9 °C and 64.9 % in the 2nd discharging cycle (See Figure 8.3.25 a-b). As seen, there is a very slight change of ΔT_{ave} between two discharging cycles. This fact demonstrates that the SIM-3a has a regeneration potential at 80-85°C temperature range, which was not the case in Zeolite and SIM-3m. The high $\eta_{hyg\text{-}cyc}$ (88%) proves this aspect, as only 12% of the moisture remained inside the material corresponding to only 0.26 kg of the 2.17 kg moisture absorbed in the first discharging cycle. A further increase of $\eta_{hyg\text{-}cyc}$ could be achieved with applying heat/mass enhancement techniques and improving the reactor design.

Similar drying procedure applied to SIM-3a with the SIM-3m and Zeolite 13X. Achieved full cycle-results indicated that SIM-3a is a promising candidate to be used in the developed sorption storage heater. It has not only high and steady heat output in discharging process, but also has the potential to be regenerated at 80-85 °C which is vital for multi-cyclic use of the sorbent. The measured ΔT and ΔRH values were illustrated in Figures 8.3.26 a and 8.3.27 a and ΔT_{ave} and ΔRH_{ave} values of SIM-3a charging cycle were presented in Figures 8.3.26 b and 8.3.27 b. As seen from Figure 8.3.26 b, the temperature rise of air in heat pump was ≈37 °C and a further ΔT_{ave} of 35 °C was obtained with the EH. The reactor outlet temperature increased gradually and reached to 60 °C at the end of 180 minutes charging cycle. It should be noted that comparing with Zeolite and V-$MgCl_2$, reactor outlet temperature of V-$CaCl_2$ remained lower. This condition indicates that higher amount of vapour is extracted from the sorbent, resulting with lower reactor outlet temperature but more effective drying process. Similar to the charging of other materials, a slight temperature difference (2-3 °C) between the reactor outlet and heat exchanger (HEX) inlet temperature was observed due to the heat losses through the ducting. Average heat transferred to the secondary line in HEX was calculated as 0.29 kW, which was lower than the transferred heat in Zeolite (0.39 kW) and V-$MgCl_2$ (0.42 kW) charging cycles. Indeed, lower heat recovery via HEX demonstrates that higher percent of inlet energy to the reactor was spent for desorbing the moisture in SIM-3a charging cycle. Contrarily, in Zeolite and SIM-3m charging cycles, lower percent of energy input was used for desorption of moisture. This situation resulted in higher reactor outlet temperature in Zeolite and SIM-3m charging in comparison with SIM-3a, which explains the higher rate of heat recovery potential of these materials.

As represented in Figure 8,3,26 b, the temperature difference between the evaporator inlet and outlet was averagely 21.3 °C and the exhaust air temperature varied in the range of 12 °C →22°C over the charging process. The results showed that average heat gain of air in condenser and electrical heater were 0.65 kW and 0.53 kW respectively corresponding to a total heat input of 1.18 kW. On the other hand total heat recovered in HEX and evaporator was 0.82 kW corresponding to a heat recovery ratio of 79%.

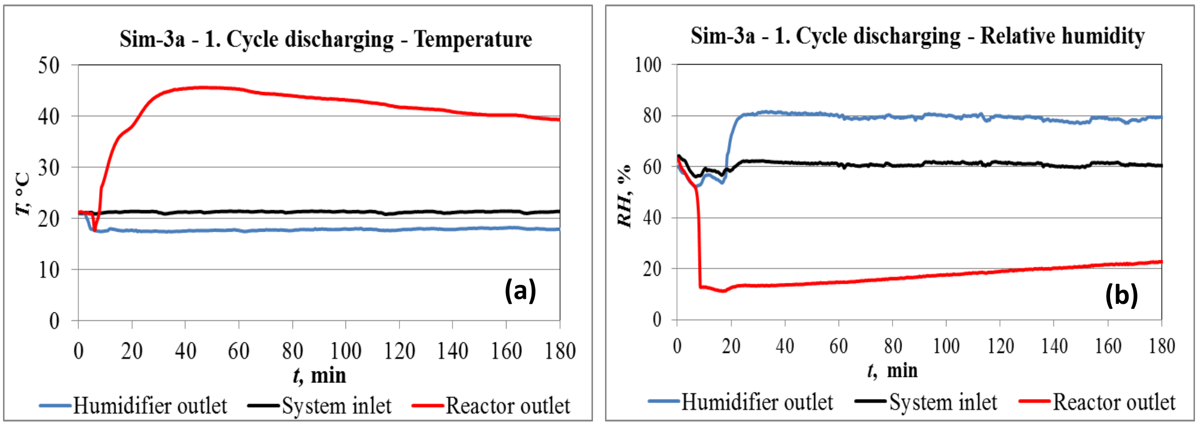

Figure 8.3.24 Measured (a) temperatures, (b) relative humidities in 1st discharging cycle of Sim-3a

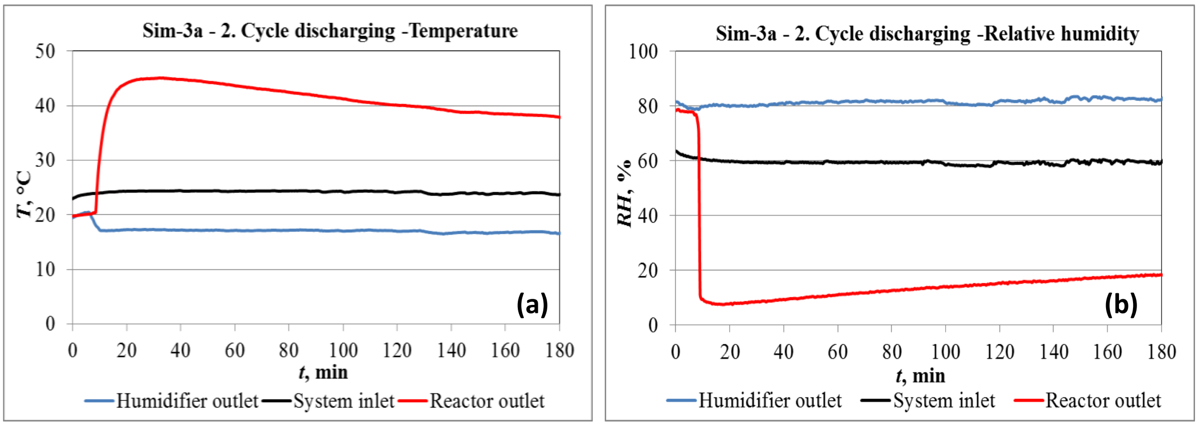

Figure 8.3.25 Measured (a) temperatures, (b) relative humidities in 2nd discharging cycle of Sim-3a

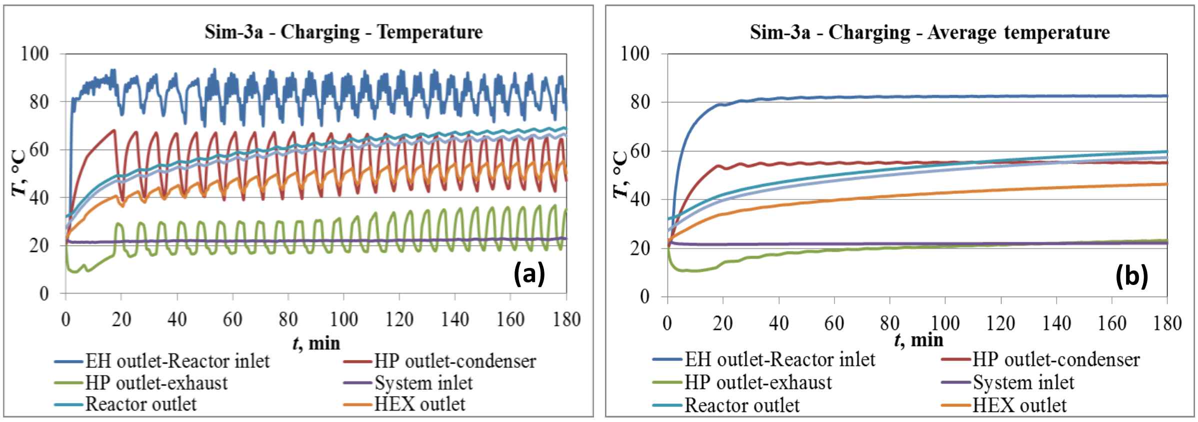

Figure 8.3.26 (a) Measured, (b) average temperatures in charging cycle of Sim-3a

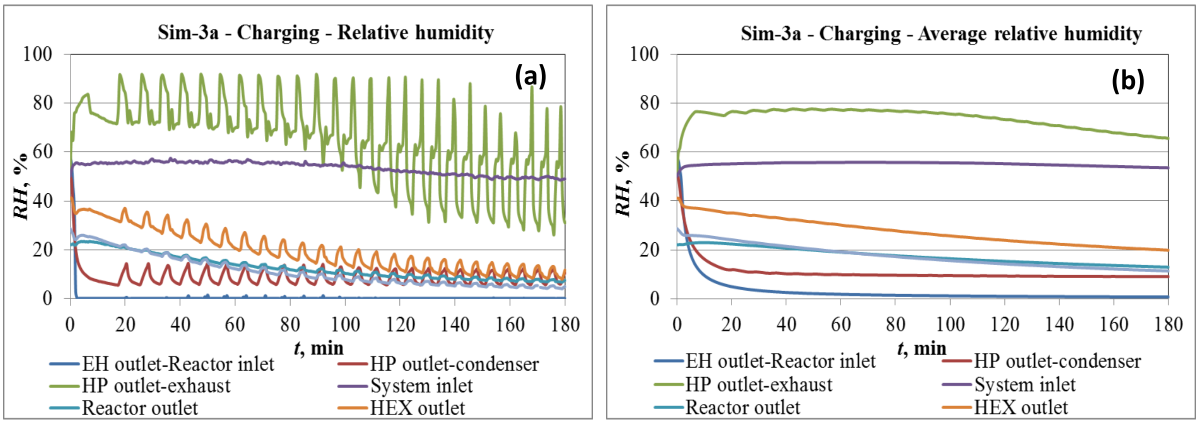

Figure 8.3.27 (a) Measured, (b) average relative humidities in charging cycle of Sim-3a

iv. (V-$MgCl_2$ – LiCl) (SIM-3ml) testing

V-(LiCl-$MgCl_2$), was synthesised by mixing equal volume of salt solution of 18 wt% $MgCl_2$ and 17 wt% LiCl and impragnating the mixture solution to the vermiculite. The main target within the development and testing of this composite material was to improve the performance of $MgCl_2$ by lowering its charging temperature and increasing the stability of its discharging temperature.

When the discharging cycles of SIM-3m (See: Figure 8.3.20 a - 8.3.21 a) and SIM-3ml (See: Figure 8.3.28 a – 8.3.29 a) are compared, ΔT_{ave} of V-$MgCl_2$ in the 1st and 2nd cycles were 25.5 °C and 16.7 °C respectively. In SIM-3ml testing, ΔT_{ave} was 22.8 °C and lower than SIM-3m in the 1st cycle. However ΔT_{ave} was 19.2 °C and ≈2.5°C higher than SIM-3m in the 2nd cycle. This can be explained with the improved $\eta_{hyg\text{-}cyc}$ of SIM-3ml in the charging cycle which was 79% and higher than $\eta_{hyg\text{-}cyc}$ of SIM-3m. Although at the end of 2 cycles the difference of ΔT_{ave} was not large between the materials, it could become larger over repeating cycles due to the low $\eta_{hyg\text{-}cyc}$ of SIM-3m. Besides $\eta_{hyg\text{-}cyc}$, ΔT_{180} (ΔT at the end of 180 minutes during the discharging process) is a useful measure to compare the steadiness of these materials. Accordingly, ΔT_{180} for the 1st and 2nd cycles of SIM-3m were ≈20 °C and ≈15 °C whilst for SIM-3ml, these values were 22 °C and 18.5 °C respectively.

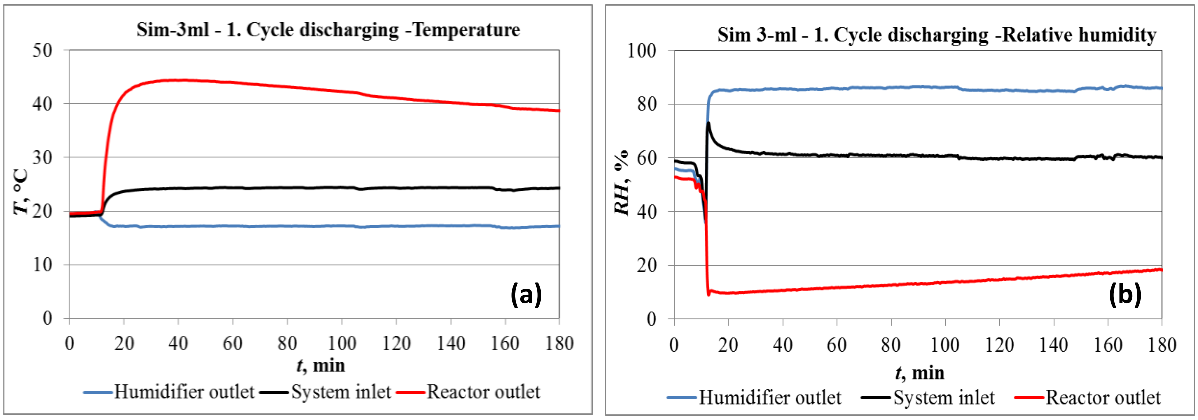

Figure 8.3.28 Measured (a) temperatures, (b) relative humidities in 1st discharging cycle of Sim-3ml

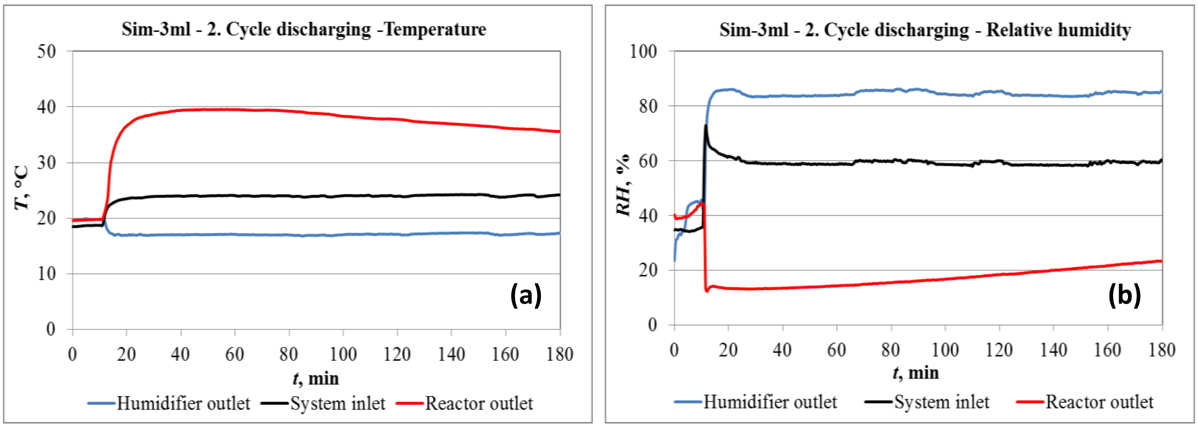

Figure 8.3.29 Measured (a) temperatures, (b) relative humidities in 2nd discharging cycle of Sim-3ml

Although SIM-3m had a higher peak temperature, in longer period, SIM-3ml showed a steadier behaviour and exceed the ΔT achieved with SIM-3m at the end of the cycle. This is an important parameter to be considered as in THS applications durability and stability of sorption material is vital for effective operation of the system.

Measured *T* and *RH* of charging cycle of SIM-3ml were illustrated in Figures 8.3.30 a - 8.3.31 a whilst T_{ave} and RH_{ave} values were presented In Figures 8.3.30 b and 8.3.31 b. A seen from Figure 8.3.30 b, air temperature was increased to ≈57 °C at the HP outlet and it was boosted to ≈80 °C with the electrical coil. The reactor outlet temperature increased gradually and reached to 60 °C at the end of 180 minutes. Recovered average thermal power in HEX was calculated as 0.30 kW, which was slightly higher than the value achieved in SIM-3a charging cycle and lower than the recovered heat in Zeolite (0.39 kW) and SIM-3m (0.42 kW) charging cycles.

Temperature difference of air at the evaporator was averagely 21.3 °C (Please see: Figure 8.3.30 b) where exhaust air temperature varied between 12 °C and 21°C over the charging process. Experimental results showed that, average heat input to the air in condenser and electrical heater were 0.66 kW and 0.44 kW respectively corresponding to a total heat input of 1.11 kW. The total of recovered heat was calculated as 0.80 kW where 0.50 kW of it was recovered in HP and the rest in HEX. Accordingly heat recovery ratio was obtained as 72%.

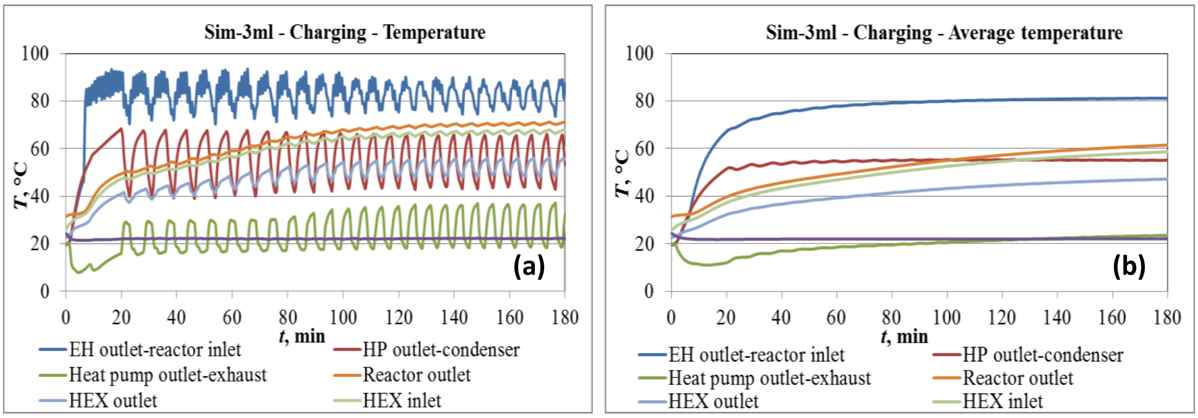

Figure 8.3.30 (a) Measured, (b) average temperatures in charging cycle of Sim-3ml

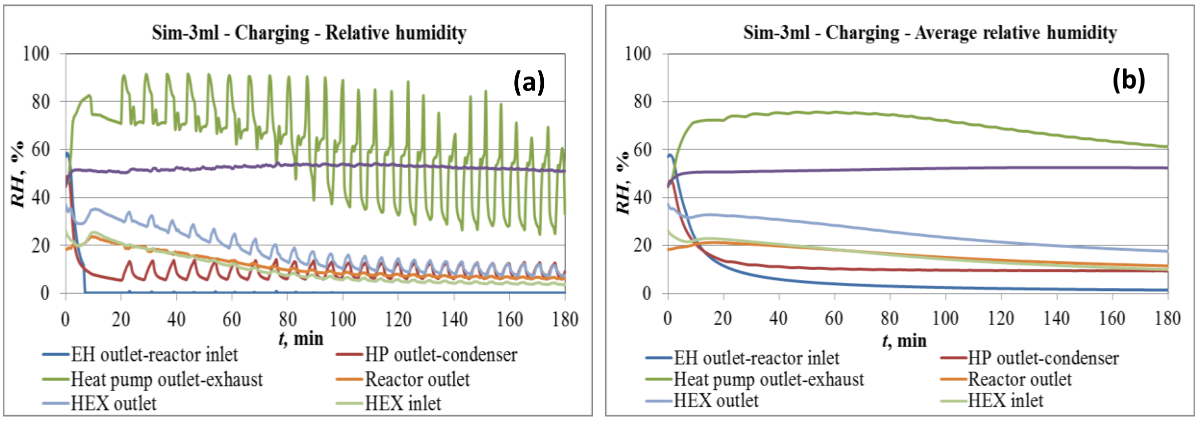

Figure 8.3.31 (a) Measured, (b) average relative humidities in charging cycle of Sim-3ml

v. (V-$CaCl_2$ – LiCl) (Sim-3cl) testing

The last investigated material, SIM-3cl, was synthesised with mixing equal volume of salt solution of 22 wt% $CaCl_2$ and 17 wt% LiCl and impragnating the mixture solution to the vermiculite. It was proposed to improve the discharging thermal performance and cyclic stability of $CaCl_2$ with developing the composite SIM-3cl.

SIM-3a provided (See: Figure 8.3.24 a - 8.3.25 a) ΔT_{ave} of 23.1 and 22.9 °C in the 1^{st} and 2^{nd} cycles respectively. A considerable improvement was achieved with SIM-3cl as the ΔT_{ave} rose to 24.2 ° C and 24.5 °C in the 1^{st} and 2^{nd} cycles. Both materials were also compared with using the measure of ΔT_{180}, which is the key indicator of hygrothermal steadiness of materials. Accordingly, ΔT_{180} for the $1^{st} \rightarrow 2^{nd}$ cycles of SIM-3a were 21.5 °C and 21.2 °C whilst for SIM-3cl, these values were 23.3 °C and 23.6 °C respectively. Results showed that mixing LiCl with $CaCl_2$ positively incluences the thermal performance in terms of both temperature lifting, ΔT, and stability of T_o.

ΔT_{ave} and $\Delta RH_{ave\ values}$ of charging cycle of SIM-3cl were given in Figures 8.3.32 b – 8.3.33 b with the original data presented in Figures 8.3.32 a – 8.3.33 a. During charging process air is heated from 20 °C to 57 °C at the condenser and its temperature was boosted to 82 °C with the electrical coil (see: Figures 8.3.34 a-b). The hot and dry air was blown through the reactor, removing the moisture from the sorbent. The reactor outlet air temperature increased gradually and reached to 68 °C at the end of 180 minutes whereas RH of air varied in the range of 28.3% → 5.1% over the same period (see: Figures 8.3.35 a-b). Waste heat of the moist warm air partially recovered at the HEX (0.19 kW).

Air is cooled averagely 23.2 °C by the refrigerant in the HP where evaporator outlet air temperatere varied between 5→25°C over the charging process.

According to the experimental results, total of supplied heat to the air in charging cycle was 1.06 kW and the total heat recovered at the HEX and evaporator was 0.6 kW. The ratio of heat recovery was calculated as 56% for SIM-3cl charging cycle which was the lowest among all tested materials. This result demostrates that higher proportion of heat input was utilized for moisture desorption and regeneration of Sim-3cl in comparsion with other sorbents. Despite the low heat recovery ratio, it was found that SIM-3cl could be effectively regenerated at 80-85 °C temperature level. The high $\eta_{hyg\text{-}cyc}$ (88%) of SIM-3cl proves this and makes SIM-3cl a promising candidate.

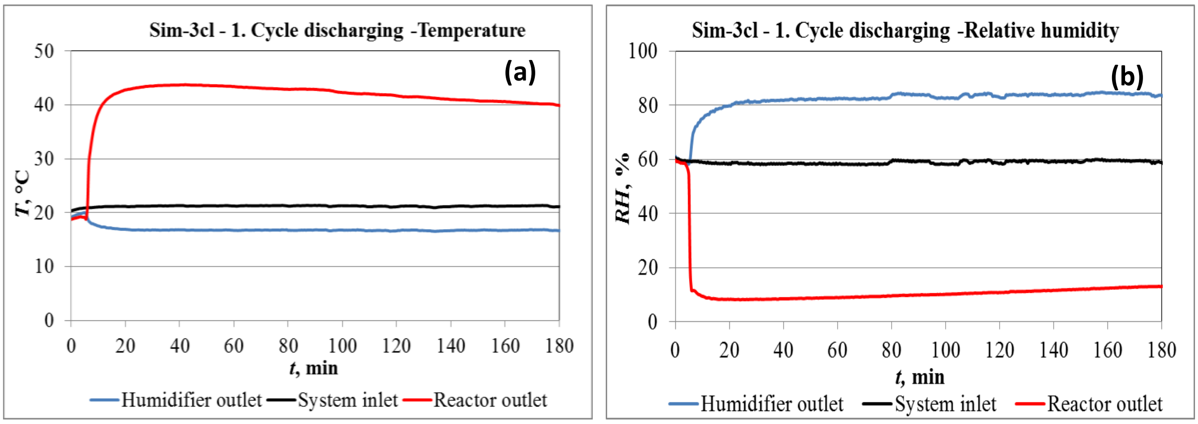

Figure 8.3.32 Measured (a) temperatures, (b) relative humidities in 1st discharging cycle of Sim-3cl

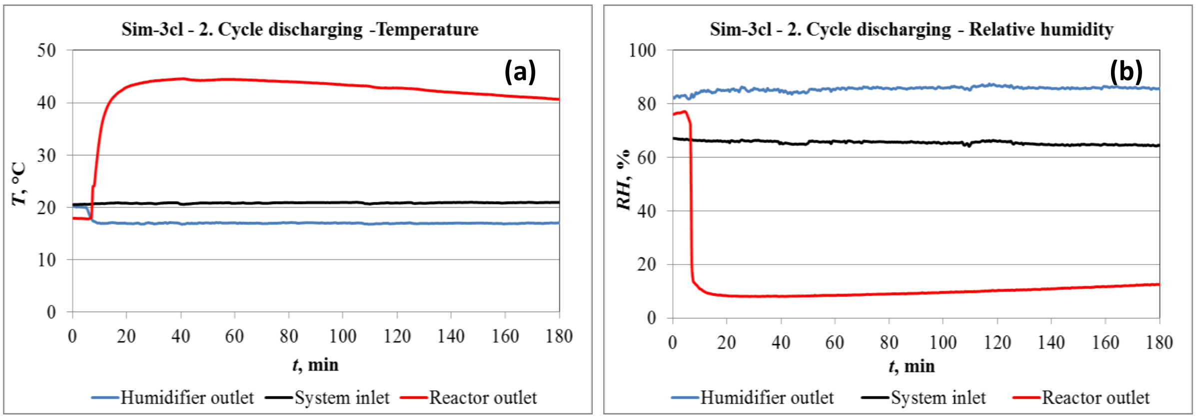

Figure 8.3.33 Measured (a) temperatures, (b) relative humidities in 2nd discharging cycle of Sim-3cl

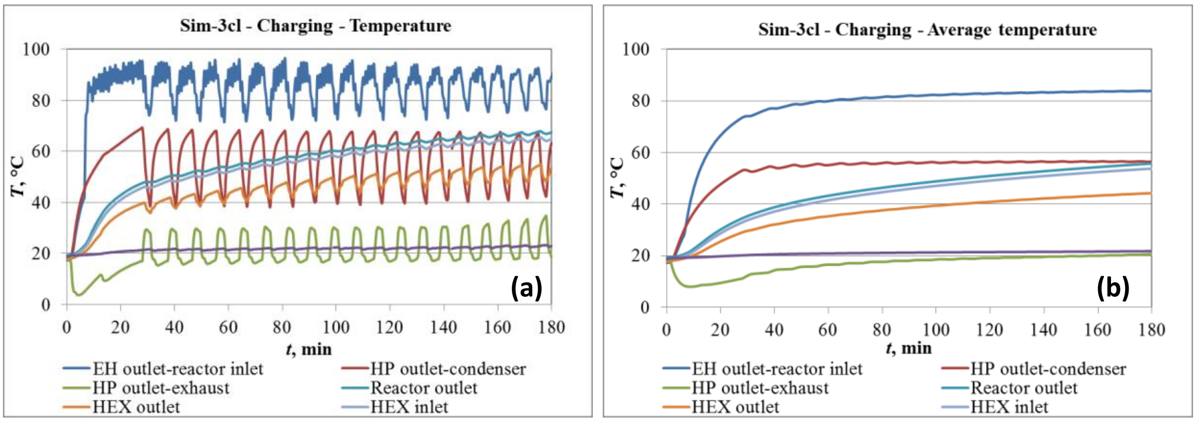

Figure 8.3.34 (a) Measured, b) average temperatures in charging cycle of Sim-3cl

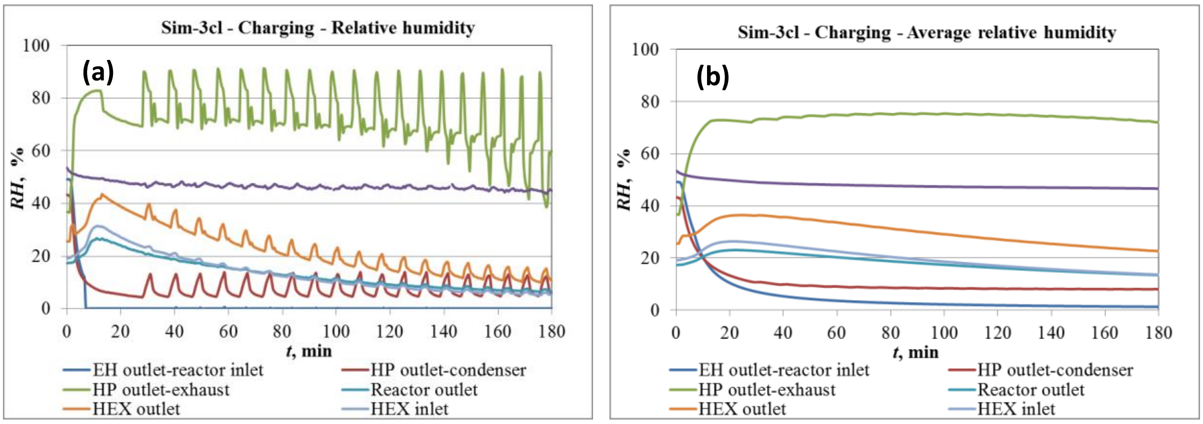

Figure 8.3.35 (a) Measured, (b) average relative humidities in charging cycle of Sim-3cl

8.3.2.3.2 Material Hygrothermal performances under low air humidity operating conditions

In order to assess the hygrothermal performance of the materials at low (inlet air) humidty conditions, a single cycle testing at RH_i = 60% and T_i = 17 °C corresponding to P_v = 11.6 mbar was performed. Obtained results were compared with the material/system experimental performances at high (inlet air) humidty (RH_i = 80% and T_i = 17 °C, P_v =16.4 mbar) conditions which presented in previous section. Due to the lower rate of moisture supply to the sorbent, in low humidtiy testings discharging duration was increased to 240 mins which was 180 mins in high humidity cycles to keep the moisture uptake of materials same in both testing conditions. The charging temperature was also reduced from 82 °C→72 °C to investigate the material charging potential at lower temperature range. All materials dried in the oven at 150° for 48 hours prior to perform low humidity testings to ensure that any residual moisture is removed. One cycle (discharging →charging) experimental performance of Zeolite 13x, SIM-3m, SIM-3a, SIM-3ml and SIM-3cl performed in the prototype Heat-Store system at low humidity conditions (P_V = 11.6 mbar) were presented and discussed below;

i. Zeolite testing

Initially, Zeolite 13X performance was assessed at low air humidity conditions. During the testing it was seen that Zeolite discharging performance substantially dropped with the reducing w_i and P_V (see: Figures 8.3.36 a-b). ΔT_p found as 27.7 °C for V_p =11.6 mbar, whilst it was 31.5 °C at P_V = 16.4 mbar. Similarly a large drop was observed in ΔT_{ave} in the range of 23.0 →16.4 °C. $Z_{abs,ave}$ also reduced nearly half (0.23→0.13). The substantial decrease of $Z_{abs,ave}$ highly influenced the Zeolite hygrothermal performance. Accordingly, Q_{ave} decreased by 28% in comparison with high humidity operation. This was the largest drop of Q_{ave} among all tested materials. Testing results demonstrate that air moisture level significantly affects

Zeolite 13X performance and similar to SIM-3a and SIM-3m, released heat substantially drops with the reducing air moisture content and sorption rate (Z_{abs}). According to the testing results, reduction of Z_{abs} of 0.015 gr/s, results in a decrease of ΔT_{ave} = 1 °C. Although the discharging time was longer in low humidity cycle, m_{abs} remained 23% lower than the high humidity cycle due to the lower moisture content of inlet air which resulted with lower Z_{abs}. On the other hand, mass uptake was measured as 1.92 kg whereas it was 2.49 kg in high humidity cycle. Accordingly Q_{ave} and E_{cum} were found 0.36 kW and 1.42 kWh respectively.

In charging process, $T_{reg,\ ave}$ was set to 72 °C. The T and RH data obtained during the charging process was presented in Figures 8.3.37 a-b. The average condenser outlet temperature was measured as 58 °C and reactor outlet temperature varied in the range of 20→66 ° C. It was found that 1.13 kg of the 1.92 kg absorbed moisture was removed over the charging period corresponding to $\eta_{hyg\text{-}cyc}$ of 0.59, whilst $\eta_{hyg\text{-}cyc}$ was 0.50 in high humidity testing. However, it should be noted that the primary reason of higher $\eta_{hyg\text{-}cyc}$ in low humidity testing was not because of the more effective charging of material, but as a result of lower Z_{abs} and Δm during discharging process.

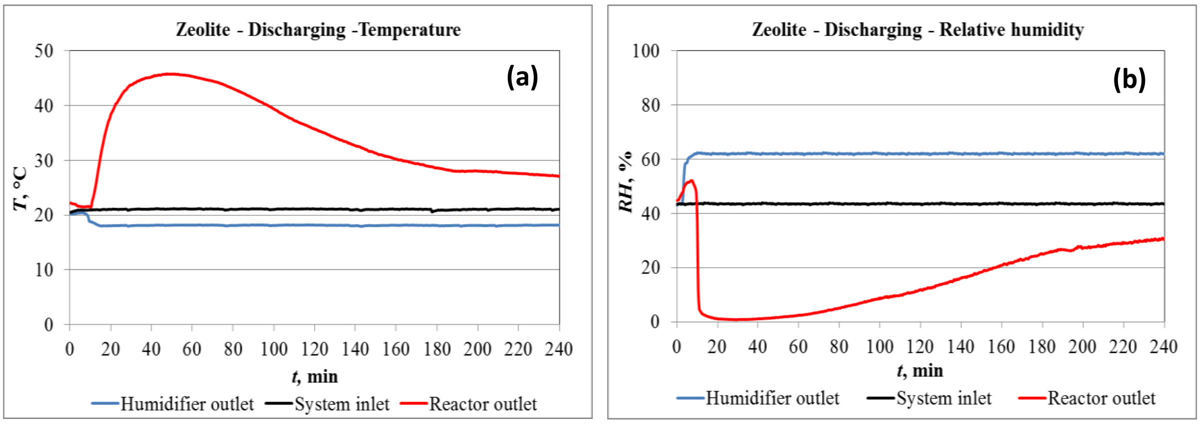

Figure 8.3.36 Measured (a) temperatures, (b) relative humidites in low humidity discharging cycle of Zeolite

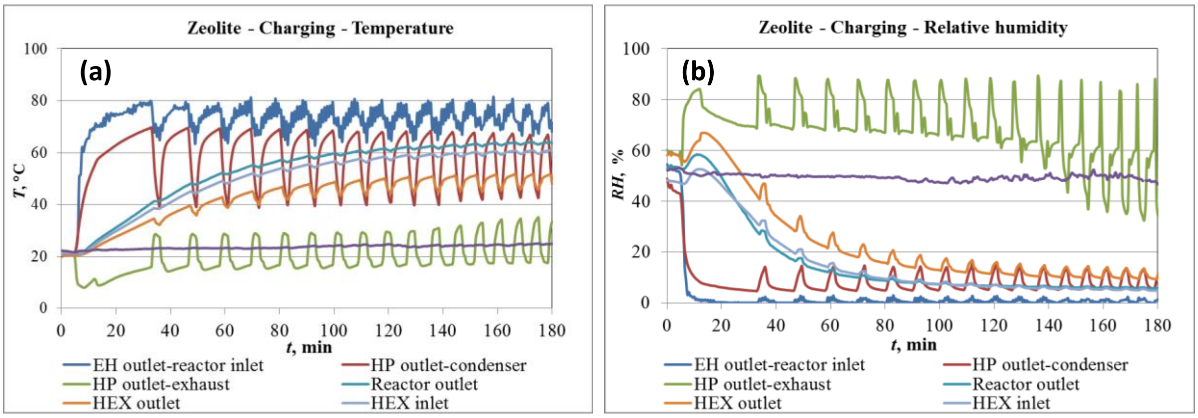

Figure 8.3.37 Measured (a) temperatures, (b) relative humidities in low temperature charging cycle of Zeolite

ii. V-$MgCl_2$ (SIM-3m) testing

Similar to the Zeolite, SIM-3m discharging performance dropped with the reducing inlet air humidity. ΔT_p was found 25.6 °C, whilst it was 31 °C at high humidity operating conditions. In accordance with the ΔT_p, ΔT_{ave} dramatically dropped from 25.5 to 18.9 °C (See: Figures 8.3.38 a-b). Morover, $Z_{abs,ave}$ showed a decreasing trend in the range of 0.20→0.11 with the reduced humidity. The substantial decrease of $Z_{abs,ave}$ highly influenced the SIM-3m hygrothermal performance and Q_{ave} dropped 24% in comparison with high humidity operation.

According to the experimental results, air moisture level significantly affects SIM-3m performance and similar to Zeolite, released heat substantially drops with the reducing Z_{abs}. It is found that, reduction of Z_{abs}= 0.014 gr/s results in a decrease of ΔT_{ave} = 1 °C. On the other hand, mass uptake was measured as 1.87 kg whereas it was 2.12 kg in high humidity cycle representing a 12% drop of mass increase of sorbent. Accordingly Q_{ave} and E_{cum} were calculated as 0.41 kW and 1.63 kWh respectively.

In charging cycle, SIM-3m was regenerated at $T_{reg,ave}$ = 71 °C. Figures 8.3.39 a-b illustrate the T and RH variation of air over the process duration. Reactor outlet temperature varied in the range of 20→66 ° C and average air temperature leaving the condenser was measured as 58

°C. Amount of desorbed moisture over the charging cycle was 1.16 kg whereas the total of absorbed moisture in discharging cycle was 1.87 kg. Accordingly $\eta_{hyg\text{-}cyc}$ is found 0.62, indicating a slight decrease in comparison with the high humidity cycles ($\eta_{hyg\text{-}cyc}$ = 0.67).

Low humidity testing demonstrated that SIM-3m performance dramatically drops with the reducing inlet air moisture content. In order to achieve ΔT_p >25 °C, w_i should be > 0.01 gr/kg. In low inlet humidity operating conditions ΔT varied in the range of 22.9→ 18.3 °C showing that ineffective vapour sorption rate leads to reduced heat output over the discharging process.

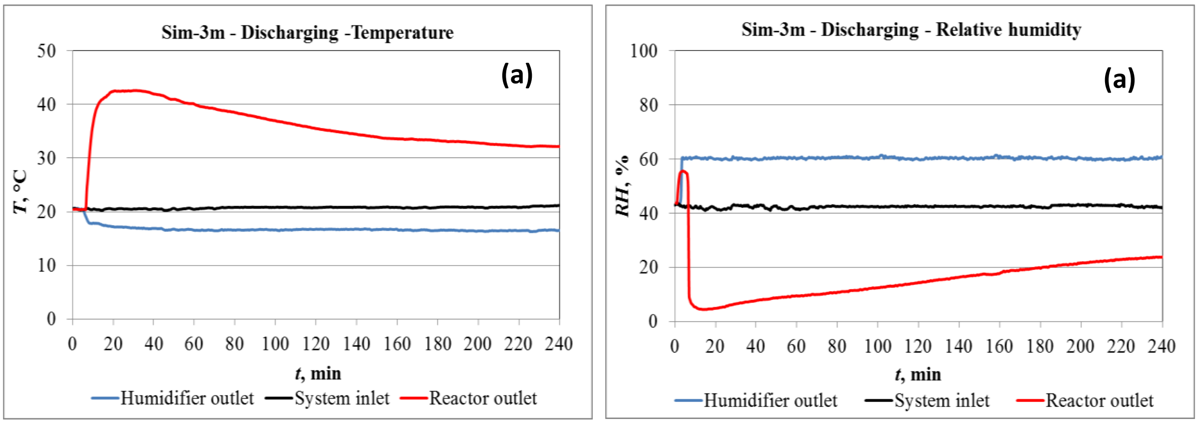

Figure 8.3.38 Measured (a) temperatures, (b) relative humidites in low humidity discharging cycle of Sim-3m

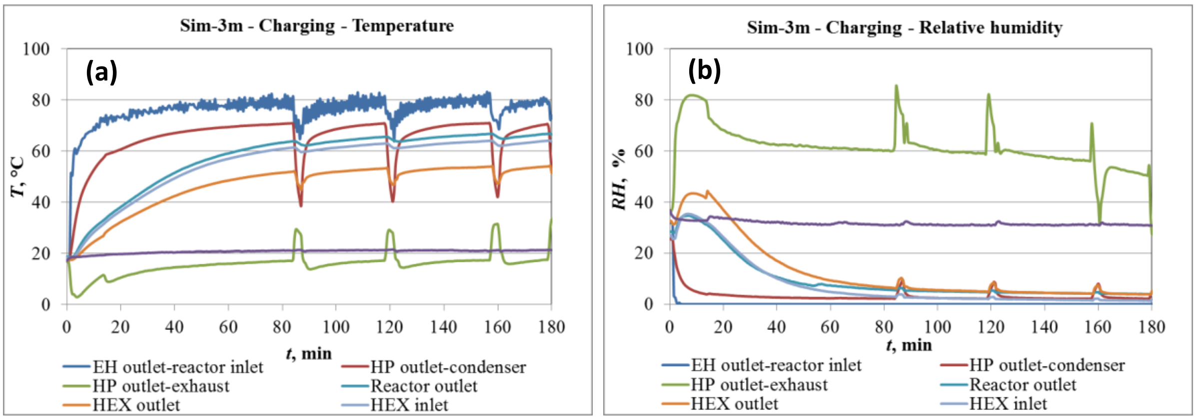

Figure 8.3.39 Measured (a) temperatures, (b) relative humidities in low temperature charging cycle of Sim-3m

It could be concluded that in discharging process, humidity of inlet air siginificantly influences SIM-3m discharging performance and air humidity level should be carefully optimized. Besides SIM-3ml's low desorption rate at 70-80 °C temperature range is an important drawback on utilizing solar energy for charging this material.

iii. V-$CaCl_2$ (Sim-3a) testing

Similar with the SIM-3m and Zeolite 13X, thermal performance of SIM-3a showed a decreasing trend with the reducing inlet air humidity (see: Figures 8.3.40 a-b). ΔT_p and ΔT_{ave} dropped from 28 °C to 21.6 °C and 23.1 to 19.2 °C respectively. Testing results demonstrated that air moisture level is critical for SIM-3a performance and released heat substantially drops with the lowering Z_{abs}. Experimental results showed that, reduction of Z_{abs} of 0.015 gr/s results in a drop of ΔT_{ave} = 1 °C. The reduction in mass uptake of SIM-3a at low humidity level found much lower when compared with Zeolite 13X and SIM-3m. Mass uptake of the material was measured as 2.04 kg whereas it was 2.17 kg in high humidity cycle. This condition led to a steady performance of SIM-3a, with a smaller drop of ΔT_{ave} than the other sorbents at low humidity operation. Q_{ave} and E_{cum} were found 0.42 kW and 1.65 kWh over 180 minutes discharging duration.

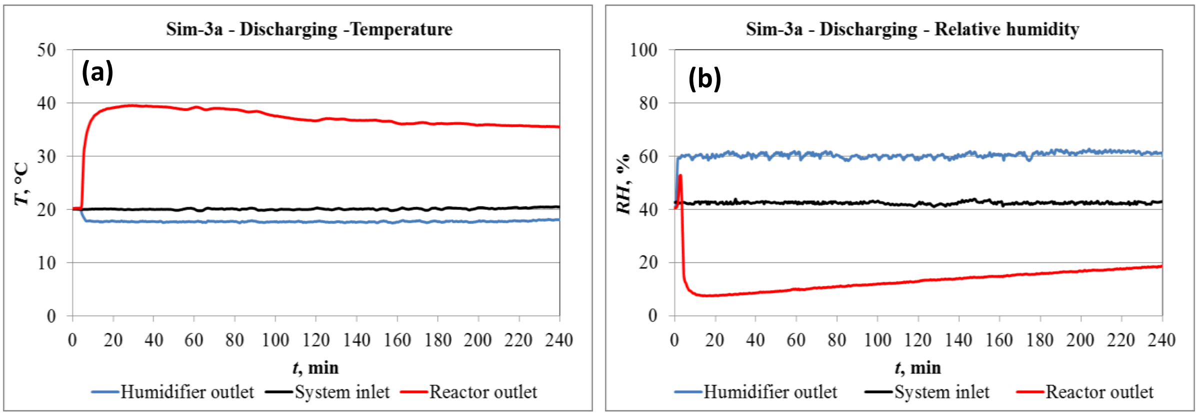

Figure 8.3.40 Measured (a) temperatures, (b) relative humidites in low humidity discharging cycle of Sim-3a

Following the discharging cycle, SIM-3a was regenerated at $T_{reg,ave}$=70 °C (See: Figures 8.4.41 a-b). Reactor outlet temperature varied in the range of 22→62 ° C and average condenser outlet temperature of air was 56 °C. Amount of desorbed water was found 1.91 kg over the

180 minutes charging cycle. Accordingly, $\eta_{hyg\text{-}cyc}$ calculated as 0.88, which was slightly higher than the $\eta_{hyg\text{-}cyc}$ obtained in high humidity testing.

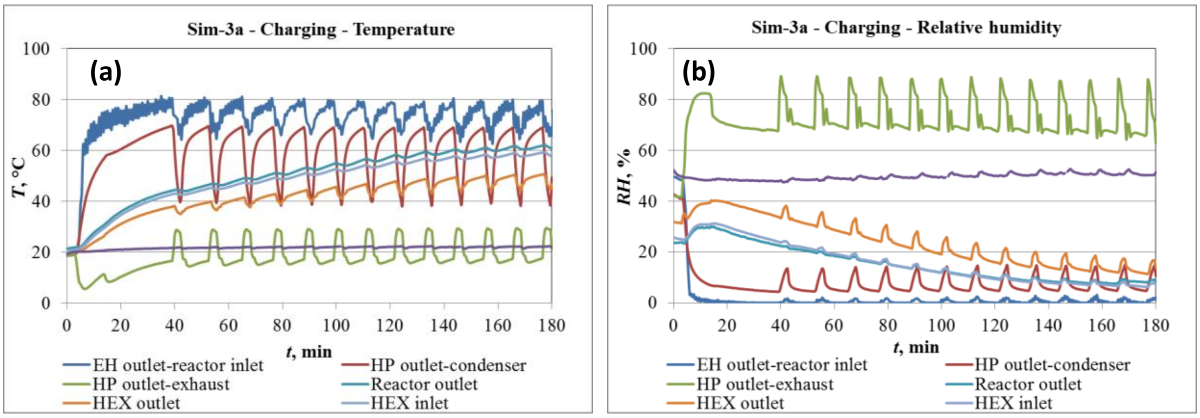

Figure 8.3.41 Measured (a) temperatures, (b) relative humidities in low temperature charging cycle of Sim-3a

iv. V-MgCl2-LiCl (SIM-3ml) testing

Testing results of SIM -3ml discharging cycle under low humidity conditions were presented in Figures 8.3.42 a-b. ΔT_p and ΔT_{ave} were found 24.1 °C and 19.3 °C whereas ΔT_p and ΔT_{ave} were 27.3 and 22.8 °C for high humidity operation respectively. Although Q_{ave} was dropped (0.49→0.42 kW) in low humidity cycle, E_{cum} increased from 1.48 to 1.66 kWh due to the longer discharging duration. However m_{abs} was found 1.69 kg in low humidity testing which was 17% lower than the m_{abs} in high humidity cycle which explains the drop in Q_{ave}.

In charging cycle, SIM-3ml was regenerated at $T_{reg,ave}$ = 71 °C . T and RH variation of air over the process was presented in Figures 8.3.43 a-b. The average HP and condenser outlet temperatures were 56 °C and reactor outlet temperature varied in the range of 19→63 °C over 180 mins charging period. 1.29 kg of the 1.69 kg absorbed moisture was removed over the charging cycle corresponding to $\eta_{hyg\text{-}cyc}$ of 0.76, which was 0.03 lower than the $\eta_{hyg\text{-}cyc}$ obtained in SIM-3ml high humidity testing and 0.12 higher than the $\eta_{hyg\text{-}cyc}$ obtained in SIM-

3m low humidity testing. Results indicated that modifiying $MgCl_2$ with LiCl, considerably improves steadiness, cyclic ability, sorption rate also reduces the T_{reg} of SIM-3m.

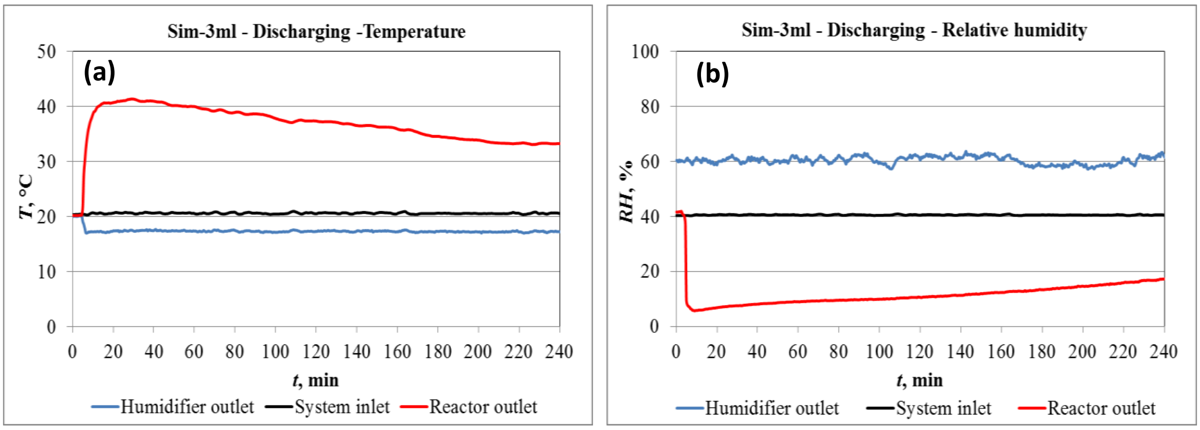

Figure 8.3.42 Measured (a) temperatures, (b) relative humidites in low humidity discharging cycle of Sim-3ml

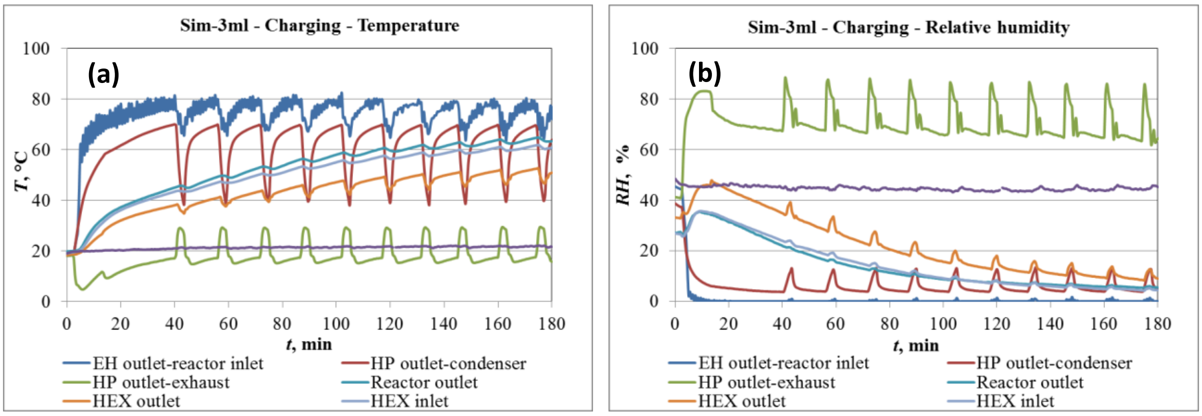

Figure 8.3.43 Measured (a) temperatures, (b) relative humidities in low temperature charging cycle of Sim-3ml

v. V- CaCl2-LiCl (SIM-3cl) testing

SIM-3cl discharging performance under low humidity conditions were presented in Figures 8.3.44 a-b. It provided high thermal performance at low humidity operating conditions, indicating that sorption kinetics of this material is very effective and its sorption rate is high even the moisture content of inlet air is low. This is an important fact showing that air does not have to be fully moisturized to achieve high ΔT. LiCl has low critical humidity therefore it readily absorbs the moisture from the air even at low RH levels. Although achieved ΔT_p was slightly higher in high humidity testing of SIM-3cl, obtained ΔT_{ave} was same in both high and low humidity conditions (19.2 °C). However considering that the low humidity testing was 60 mins longer, it could be concluded that SIM-3cl performance at low humidity level is more stable. On the other hand m_{abs} was found 2.12 kg in low humidity testing which was 14% higher than the m_{abs} in high humidity cycle. E_{cum} was also calculated as 1.57 kWh and 2.08 kWh for high and low humidity cycles respectively. This outcome indicates that lower moisture content of inlet air enables longer duration of discharging process thereby higher thermal energy output supplied by the SIM-3cl.

T and *RH* variation of air in Sim-3cl charging cycle were presented in Figures 8.3.45 a-b. Average HP and EH outlet temperatures were 59 °C and 72 °C respectively while reactor outlet temperature varied in the range of 20→60 °C over 180 mins charging period. As seen in Figure 8.3.45 b, reactor outlet humidity approached to 0% at the end of charging cycle demonstrating that high percent of the moisture was desorbed. Accordingly it was measured that 1.86 kg of the 2.12 kg absorbed moisture was removed over the charging cycle corresponding to $\eta_{hyg\text{-}cyc}$ of 0.88, which was equal to the $\eta_{hyg\text{-}cyc}$ obtained in high humidity testing.

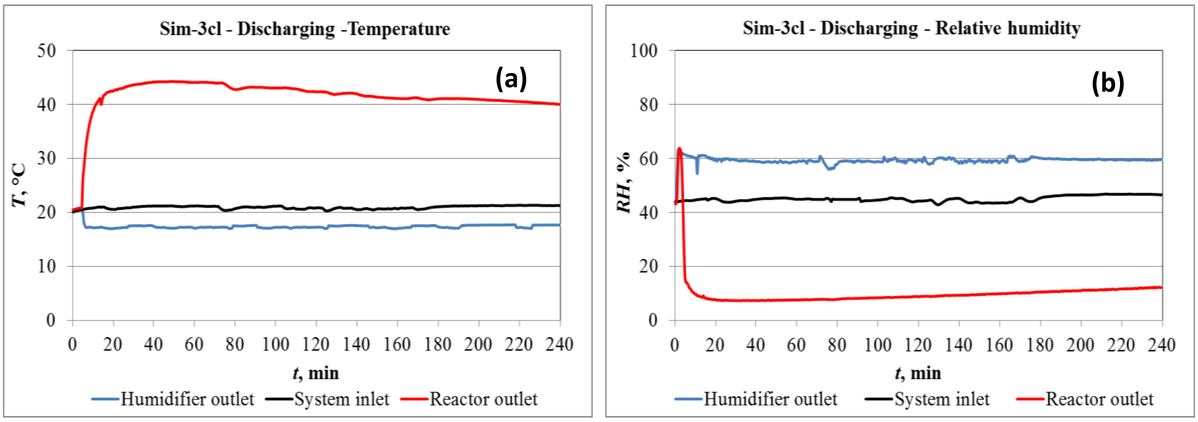

Figure 8.3.44 Measured (a) temperatures, (b) relative humidites in low humidity discharging cycle of Sim-3cl

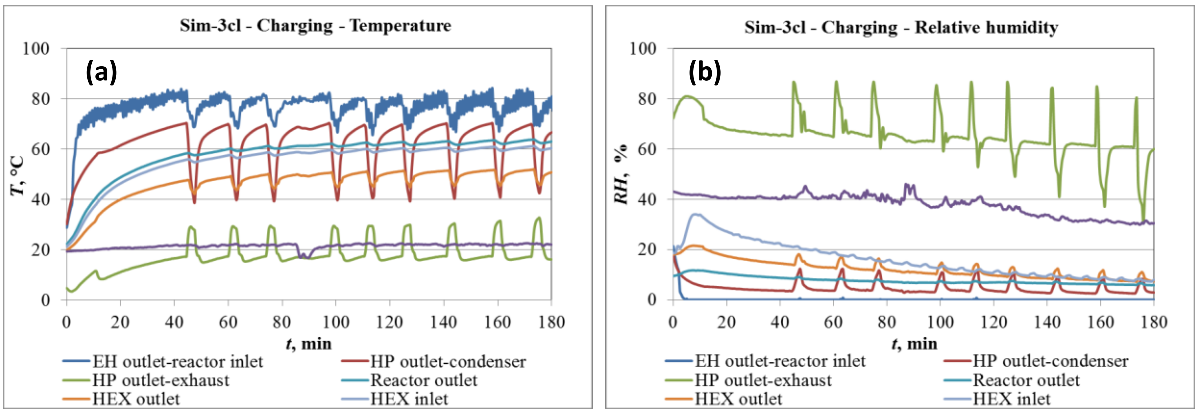

Figure 8.3.45 Measured (a) temperatures, (b) relative humidities in low temperature charging cycle of Sim-3cl

8.3.2.3.3 Evaluation of the overall experimental results

In this section, analysed discharging and charging average performance parameters and overall cycle effectivities related with sorption/desorption kinetics for full cycle testing of each material are presented. The summary of discharging, charging and full cycle results of high and low humidity testing were given in Tables 8.3 a-c and 8.4 a-c respectively. The key results were also comparatively presented in Figures 8.3.46-8.3.48. Here $m_{d,i}$; measured initial dry mass of sorbent before discharging, $m_{w;}$ measured wet mass of sorbent after discharging, $m_{d,f;}$ measured final mass of sorbent after charging. $f_{ads;}$ ratio of mass uptake $(m_{w}\text{-}m_{i,d})$ to initial dry mass ($m_{i,d}$) of sorbent *whilst* f_{des} is the ratio of the amount of moisture desorbed $(m_{w}\text{-} m_{f,d})$ to the wet mass (m_w) of sorbent. Finally the $\eta_{hyg\text{-}cyc}$ is the key parameter defined as the ratio of total moisture desorbed in charging to the total moisture loaded to the sorbent in discharging. The condition of $\eta_{hyg\text{-}cyc}$ =1 indicates that the final mass of sorbent is equal to the initial mass of it, which is a prior target in THS systems for effective cyclic use of the sorbents.

SIM-3a and SIM-3cl provided the most promising results among the five tested sorbents. As seen from the Table 8.3 c, $\eta_{hyg\text{-}cyc}$ was found 0.88 in high humidity cycles of these sorbents for $t_c = t_d$ condition. Although the target was to achieve $\eta_{hyg\text{-}cyc}$ =1, there are several factors negatively influencing the desorption rate which results with lower $\eta_{hyg\text{-}cyc}$ than the desired. These include the limitation of heat mass transfer due to the wetting which reduces permeability and thermal conductivity of sorbent during discharging process. Moreover, the experiments were performed in a closed environment (laboratory conditions), therefore moist air from the system is exhausted to the room. This resulted with the increasing moisture level of the surroundings thereby higher absolute humidity of charging inlet air. This aspect reduced the desorption rate due to the limitation of air moisture uptake capacity.

On the other hand, $\eta_{hyg\text{-}cyc}$ was found 0.67 for SIM-3m and 0.79 for SIM-3ml in high humidity cycles (see: Table 8.3 c). This outcome clearly indicates that LiCl enhances the moisture desorption capacity of $MgCl_2$. $\eta_{hyg\text{-}cyc}$ Zeolite 13X was found 0.5 which indicates the high T_{reg} requirement for charging this sorbent.

In Figures 8.3.46 a-b, $E_{i,t}$ and $E_{o,t}$ in full cycle testing of materials under low and high humidity conditions were comparatively presented. $E_{o,t}$ is the total of sorption energy gained in discharging process (E_d), and heat recovered with HEX in charging process (E_{HEX}). As seen from Figure 8.3.46 a, Sim-3m provided $E_{o,t}$ =2.88 kWh, which was the highest among all tested materials in high humidity testing conditions. $E_{o,t}$ varied in the range of 2.15→2.60 kWh for other sorbents. In same tests, highest $m_{ads,w}$ was achieved with Zeolite (2.49 kg) and $m_{ads,w}$ for other materials were in the range of 1.86→2.17 kg (See Figure 8.3.47 b). SIM-3cl provided the the lowest sorption capacity (1.86 kg) resulting with the lowest $E_{o,t}$. Contrarily, in low humidity testing conditions, total mass uptake and average moisture adsorption rate $(Z_{ads,ave})$ were found the highest in SIM-3cl testing which were 0.37 g_{wv}/g_{ads} and 0.15gr/s respectively. Whilst $Z_{ads,ave}$ of SIM-3a, SIM-3m, SIM-3ml and Zeolite dropped 30%, 35%, 37%

and 44% respectively with the reduced humidity level, $Z_{ads,ave}$ of SIM-3cl reduced only 12%, making it favourable under low humidity operating conditions. Accordingly $E_{o,t}$ of SIM-3cl increased from 2.15 kWh to 2.61 kWh at higher humidity. $E_{o,t}$ of all other materials showed decreasing trend with the reduced humidity level. Similarly $m_{abs,w}$ increased from 1.86 kg to 2.12 kg in Sim-3cl testing, while the rest of the sorbents showed lower sorption capacities that led to poor hygrothermal performances of these materials.

Total energy input in full cycle testing was calculated as the sum of compressor, electrical heater, fan and humidifier energy consumptions based on the obtained experimental data. It was found that highest $E_{i,t}$ was supplied in Zeolite (2.30 kWh) high humidity cycle (T_c= 82°C) . This mainly occurred as a result of the Zeolite's high desorption enthalpy and high specific heat that increases the required amount of energy for extracting the moisture. In charging cycle of Zeolite at T_{reg}= 72°C, $E_{i,t}$ considerably dropped from 2.30 kWh to 1.18 kWh. SIM-3cl provided highest f_{ads} in low humidity cycles. Due its high moisture content, it adsorbed large amount of input heat thereby lower amount of waste heat recovered in evaporator leading higher energy consumption of compressor and electrical heater. $E_{i,t}$ was the highest in SIM-3cl charging at T_{reg}= 72°C while $E_{i,t}$ for the other tested materials were 1.38 kWh (SIM-3ml), 1.36 kWh (SIM-3a), 1.22 kWh (SIM-3m), and 1.18 kWh (Zeolite) at the same $T_{reg.}$

Based on the obtained data in full cycle testing of materials the overall system COP was calculated with the equation below;

$$COP_s = \frac{\int_0^{t_d} Q_{dchr} dt + \int_0^{t_c} Q_{HEX} dt}{\int_0^{t_c} (W_{comp} + W_{EH} + W_{fan}) dt + \int_0^{t_d} (W_{hum} + W_{fan}) dt} \tag{8.49}$$

By integrating the terms in Equation 8.49 for the charging *(t_c)* and discharging *(t_d)* durations, Equation 8.50 is obtained as follows;

$$COP_s = \frac{E_{dchr}+E_{HEX}}{E_{comp}+E_{EH}+E_{fan}+E_{hum}} \tag{8.50}$$

Here; E_{dchr} is the total energy output in discharging process, E_{HEX} is the total energy recovered in heat exchanger during charging process, E_{comp} is the energy consumption of heat pump compressor, E_{EH} is the energy consumption of electrical heater, E_{fan} is the energy consumption of the fan and the E_{hum} is the energy consumption of ultrasonic humidifier. The overall system COP's are presented in Figures 8.3.48 a-b. COP_S of the heat storage processes using SIM-3m and SIM-3ml found to be the two highest with 1.37 and 1.25 respectively, where COP_S of SIM-3a, Zeolite and SIM-3m were in the order of 1.18, 1.13 and 1.06 for the 1st high humidity discharging cycle. In the second phase testing under low humidity discharging and low T_{reg} (72 °C), COP_S of the heat storage process with all materials substantially increased due to the lower electrical heater energy consumption. SIM-3m again found to be the sorbent providing the highest COP with 1.83. Zeolite and SIM-3cl were in close approximation with the COP values of 1.61 and 1.60 respectively. Due to their poor hygrothermal performance under low humidity discharging conditions, obtained COP_S values were lower with SIM-3ml (1.46) and SIM-3a (1.41) testing.

Table 8.3 Summary of the testing results of different sorbents at high humidity levels; (a) charging cycle, (b) discharging cycle (c) full cycle

(a)	**Cycle No**	**t_d (min)**	**Δ*RH* (%)**		**Δ*T* (°C)**		**$m_{d,i}$ (kg)**	**m_w (kg)**	**f_{ads} (g_{wv}/g_{ads})**	**E_{cum} (kWh)**	**$Z_{ads,ave}$ (gr/s)**	***Q* (kW)**		**E_d** (Wh/g)
			Peak	Avg.	Peak	Avg.						Peak	Avg.	
Sim-3a	1	180	68.2	57.8	28.0	23.1	6.97	9.14	0.31	1.50	0.20	0.60	0.50	0.69
	2	180	72.6	64.9	27.8	22.9	7.23	9.35	0.29	1.49	0.20	0.60	0.50	0.70
Sim-3m	1	180	77.2	70.4	31.0	25.5	7.22	9.34	0.29	1.61	0.20	0.67	0.54	0.75
	2	180	67.9	55.0	21.1	16.7	7.91	9.55	0.21	1.08	0.15	0.45	0.36	0.66
Sim-3ml	1	180	75.1	67.2	27.3	22.8	5.89	7.92	0.34	1.48	0.19	0.59	0.49	0.73
	2	180	72.8	62.9	22.5	19.2	6.31	8.02	0.27	1.24	0.16	0.49	0.42	0.72
Sim-3cl	1	180	74.7	70.0	26.9	24.2	5.72	7.58	0.33	1.57	0.17	0.58	0.52	0.84
	2	180	77.8	73.1	27.7	24.5	5.94	7.85	0.32	1.59	0.18	0.60	0.53	0.83
Zeolite	1	180	75.2	65.0	31.5	23.0	18.09	20.58	0.14	1.50	0.23	0.68	0.50	0.60
	2	180	80.1	55.7	33.4	20.2	19.34	21.51	0.11	1.29	0.20	0.72	0.43	0.59

(b)	**Cycle No**	**t_c (min)**	**E_{comp} (kWh)**	**COP_{HP}**	**E_{EH} (kWh)**	**W_{HEX} (kWh)**	**$m_{d,f}$ (kg)**	**f_{ads} (g_{wv}/g_{ads})**	**$Z_{des,ave}$ (gr/s)**	**E_{in} (kWh)**	**E_{rec} (kWh)**
Sim-3a	1	180	0.36	5.70	1.59	0.87	7.23	0.27	0.18	2.01	0.87
Sim-3m	1	180	0.33	5.71	1.68	1.26	7.91	0.20	0.13	2.10	1.27
Sim-3ml	1	180	0.48	3.97	1.32	0.90	6.31	0.27	0.15	1.89	0.89
Sim-3cl	1	180	0.51	3.98	1.41	0.57	5.94	0.29	0.15	2.03	0.58
Zeolite	1	180	0.48	3.15	1.74	1.17	20.31	0.07	0.11	2.30	1.10

(c)	**Cycle No**	**$E_{i,t}$ (kWh)**	**$E_{o,t}$ (kWh)**	**COP_S**	**$m_{abs,w}$ (kg)**	**$m_{des,w}$ (kg)**	**$\eta_{hyg\text{-}cyc}$**
Sim-3a	1	2.01	2.37	1.18	2.17	1.91	0.88
Sim-3m	1	2.10	2.88	1.37	2.12	1.43	0.67
Sim-3ml	1	1.89	2.37	1.25	2.03	1.61	0.79
Sim-3cl	1	2.03	2.15	1.06	1.86	1.64	0.88
Zeolite	1	2.30	2.60	1.13	2.49	1.24	0.50

Table 8.4 Summary of the testing results of different sorbents at low humidity levels; (a) charging cycle, (b) discharging cycle (c) full cycle

(a)	**Cycle No**	**t_d (min)**	**ΔRH (%)**		**ΔT (°C)**		**$m_{d,i}$ (kg)**	**m_w (kg)**	**f (g_{wv}/g_{abs})**	**E_{cum} (kWh)**	**$Z_{abs,ave}$ (gr/s)**	**Q (kW)**		**E_d (Wh/g)**
			Peak	Avg.	Peak	Avg.						Peak	Avg.	
Sim-3a	1	240	52.2	46.7	21.6	19.2	6.98	9.02	0.29	1.65	0.14	0.47	0.42	1.20
Sim-3m	1	240	56.1	44.3	25.6	18.9	7.24	9.11	0.26	1.63	0.13	0.55	0.41	1.30
Sim-3ml	1	240	55.2	48.6	24.1	19.3	5.88	7.57	0.29	1.66	0.12	0.51	0.42	1.47
Sim-3cl	1	240	52.7	49.2	27.2	24.1	5.71	7.83	0.37	2.08	0.15	0.59	0.52	1.98
Zeolite	1	240	61.3	45.9	27.7	16.4	18.1	20.02	0.11	1.42	0.13	0.59	0.36	1.10

(b)	**Cycle No**	**t_c (min)**	**E_{comp} (kWh)**	**COP_{HP}**	**E_{EH} (kWh)**	**E_{HEX} (kWh)**	**$m_{d,f}$ (kg)**	**f (g_{wv}/g_{abs})**	**$Z_{des,ave}$ (gr/s)**	**E_{in} (kWh)**	**E_{rec} (kWh)**
Sim-3a	1	180	0.63	3.11	0.66	0.27	7.2	0.26	0.17	1.36	0.27
Sim-3m	1	180	0.45	4.32	0.66	0.57	7.95	0.16	0.11	1.22	0.57
Sim-3ml	1	180	0.57	3.8	0.72	0.36	6.28	0.22	0.12	1.38	0.36
Sim-3cl	1	180	0.72	3.20	0.81	0.54	5.97	0.33	0.17	1.63	0.53
Zeolite	1	180	0.45	4.76	0.66	0.54	18.89	0.06	0.10	1.18	0.48

(c)	**Cycle No**	**$E_{i,t}$ (kWh)**	**$E_{o,t}$ (kWh)**	**COP_S**	**$m_{abs,w}$ (kg)**	**$m_{des,w}$ (kg)**	**$\eta_{hyg\text{-}cyc}$**
Sim-3a	1	1.36	1.92	1.41	2.04	1.82	0.89
Sim-3m	1	1.22	2.20	1.83	1.87	1.16	0.62
Sim-3ml	1	1.38	2.02	1.46	1.69	1.29	0.76
Sim-3cl	1	1.63	2.61	1.60	2.12	1.86	0.88
Zeolite	1	1.18	1.90	1.61	1.92	1.13	0.59

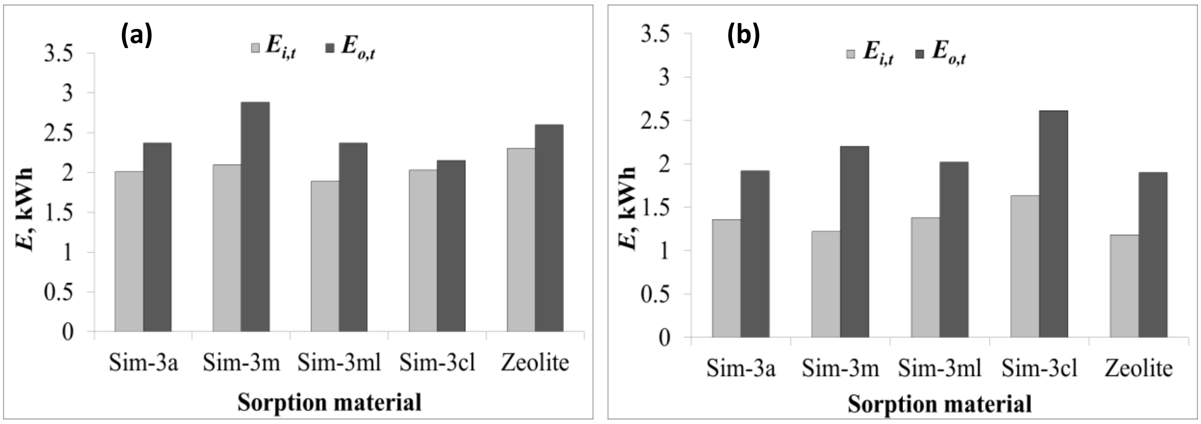

Figure 8.3.46 (a) Total energy input-output in testing of different sorbents at (a) high (b) low humidity conditions

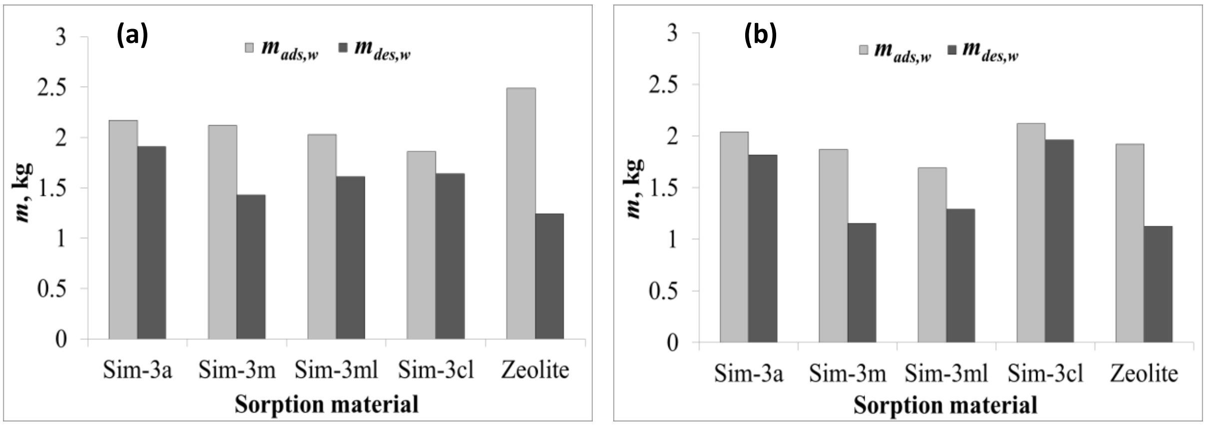

Figure 8.3.47 (a) Amount of absorbed-desorbed moisture in testing of different sorbents at (a) high (b) low humidity conditions

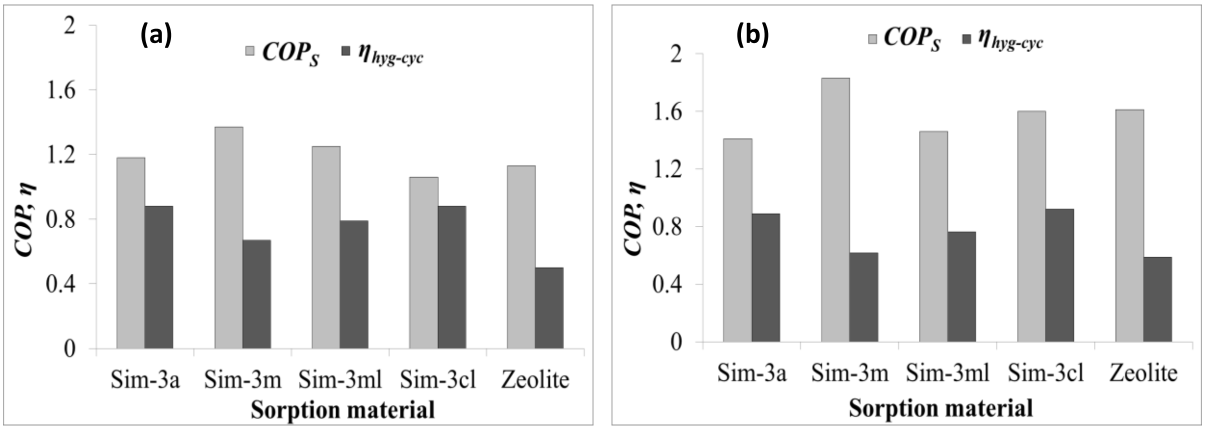

Figure 8.3.48 (a) COP_S and $\eta_{hyg\text{-}cyc}$ in testing of different sorbents at (a) high (b) low humidity conditions

8.3.2.3.4 Experimental parametric investigations on the system performance

In this section parametric experimental studies were performed to investigate the effect of sorption bed thickness (*b*) and MFR on system perfomance. Long cycle performance of the system was also investigated. SIM-3a was selected as the sorption material based on the promising results obtained with this material in previous section. Although SIM-3cl was also provided improved performance, SIM-3a was preferred due to its better known characteristics, low cost and less corrosive nature.

i. Effect of sorption bed thickness

Developed sorption reactor that consists of multiple sorption beds was tested with three different bed thicknesses. Trays were initially filled with *b*=15 mm thick sorbent layer corresponding to V_s =0.003 m^3 sorbent in each tray and totally 0.024 m3 sorption material in total(8 trays). After performing a cycle, the material was regenerated and the discharging cycle was repeted with increasing the bed thicknesses first to *b*=25 mm (V_s=0.005 m^3 per tray and V_s =0.04 m^3 total) and later to *b*=35 mm (V_s=0.007 m^3 per tray and V_s=0.056 m^3 total). The discharging testing results were given in Figures 8.3.49 a-b. Peak output temperature ($T_{p,o}$) in the range of 40→45 °C was achieved with three different bed thicknesses where *b*=25 mm was the highest. Increasing thickness of the bed, enabled high sorption rate for longer duration therefore provided a steadier thermal performance. The inlet *RH* in all testings was in the range of 81-83% (see: Figgure 8.3.49 b). Although the inlet RHs were almost same, the *RH* outlet was found 31% ,25% ,and 21% at the end of cycles for the *b*= 15, 25, 35mm respectively. For the same order of bed thickness, ΔT_{300} (ΔT at the end of 300 minutes) was also calculated as 16°C, 19 °C , 21 °C demonstrating the directly proportional correlation between *b* and ΔT.

After each cycle of testing, material is initially charged with the heat pump-electrical heater for 300 mins (See: Figure 8.3.50 a-b) to analyse the material charging performance. However to ensure that all residual moisture is removed, later material is dried in the oven at T_{reg} =120 °C for 24 hours. This allowed to use the material with the same thermal potential in each cycle thereby enabled a more realistic evaluation of the effect of bed thickness on system discharging performance.

The weight of the material was measured after discharging and charging cycles. Results showed that 2.68, 2.92 3.15 kg moisture was adsorbed and 2.56, 2.58, 2.51 kg of it was desorbed in equal time of discharging-charging process for the order of *b*= 15,25,35 mm. This corresponds to $\eta_{hyg\text{-}cyc}$ of 96% (*b*= 15mm), 88% (*b*= 25mm) and 80% (*b*= 35mm). It is concluded that increasing bed thickness enhances the discharging cycle performance however substantially reduces the moisture removal rate in charging cycle which leads to lower $\eta_{hyg\text{-}cyc.}$ Therefore the optimal bed thickness was determined as *b*= 25 mm which provided satisfactory outcome both in discharging and charging cycles.

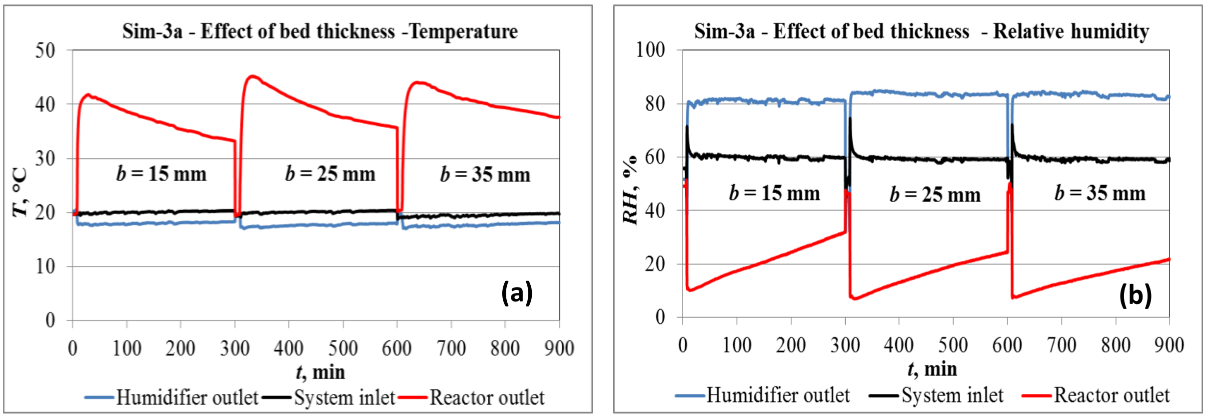

Figure 8.3.49 Measured (a) temperatures and (b) relative humidites in discharging cycles with different bed thicknesses

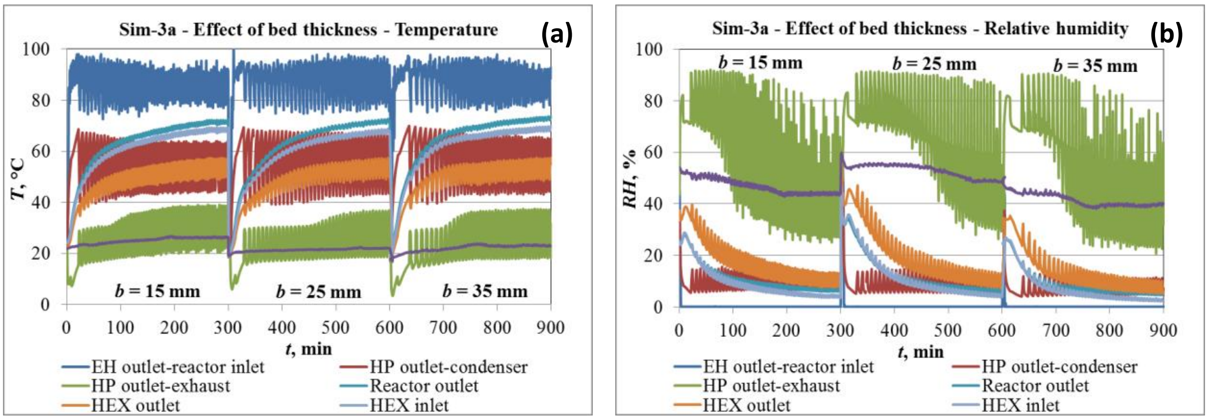

Figure 8.3.50 Measured (a) temperatures and (b) relative humidites in charging cycles with different bed thicknesses

ii. Effect of Mass flow rate

Air mass flow rate (MFR) has a significant importance on heat storage performance as it determines the amount of supplied/extracted moisture to or from the material also the extracted/supplied sorption heat during discharging/charging cycles. In order to determine optimal MFR in the designed sorption reactor, three MFRs of 0.015 kg/s, 0.02 kg/s and 0.025 kg/s were selected and one cycle (discharging +charging) of testing was performed with each flow rate (see: Figures 8.3.51 - 8.3.52). Although previous experiments were performed with MFR= 0.02 kg/s, it was aimed to investigate the effect of lower and higher MFR on system performance. Testing results of discharging cycle were presented in Figures 8.3.51 a-b. Δ*T* at *MFR*= 0.015 kg/s varied in the range of 24→16 °C whilst Δ*T* for MFR = 0.02 and 0.025 kg/s was between 26→19 °C and 24→17 °C respectively. The most promising result was achieved with MFR=0.02 kg/s wheras the lower and higher MFR provided almost similar performances. This is most likely due to the varying *RH* (88→72%) of air (for the same amont of moisture supplied to air) with changing MFR as RH_a may effect the sorption rate and thereby the heat output.

The weight of the material was measured after discharging and charging cycles. Results showed that 2.45, 2.56, 2.48 kg moisture was adsorbed and 2.11, 2.28, 2.39 kg of it was desorbed in equal time of discharging and charging process for the MFR= 0.015, 0.02, 0.025 kg/s. This corresponds to $\eta_{hyg\text{-}cyc}$ of 86% (MFR=0.015kg/s), 89%(*b*=0.02 kg/s) and 96% (*b*= 0.025 kg/s). It is concluded that medium MFR (0.02 kg/s) provides best discharging performance however increasing MFR substantially increases moisture removal rate in charging cycle where MFR= 0.025 kg/s was far higher in terms of $\eta_{hyg\text{-}cyc}$. Therefore using different MFR in discharging and charging cycles could led to a higher performance output.

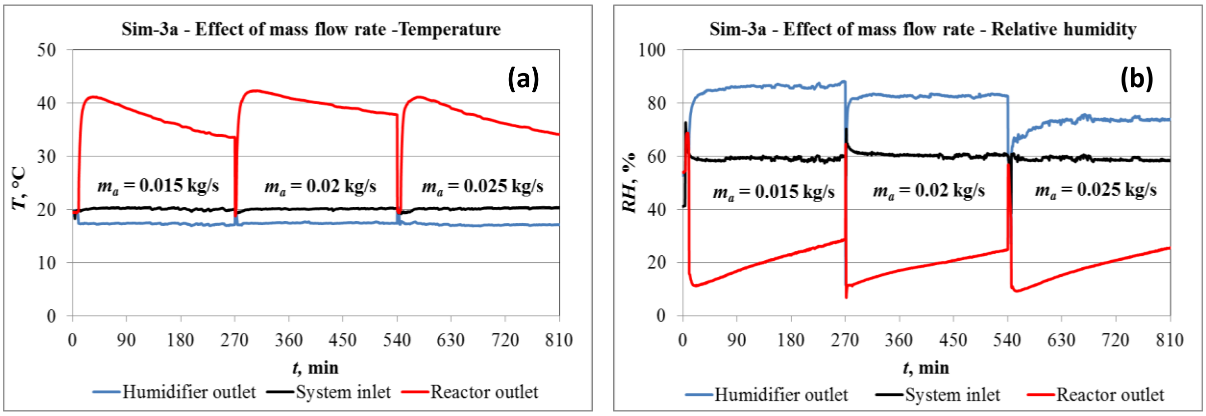

Figure 8.3.51 Measured (a) temperatures and (b) relative humidites in discharging cycles with different MFRs

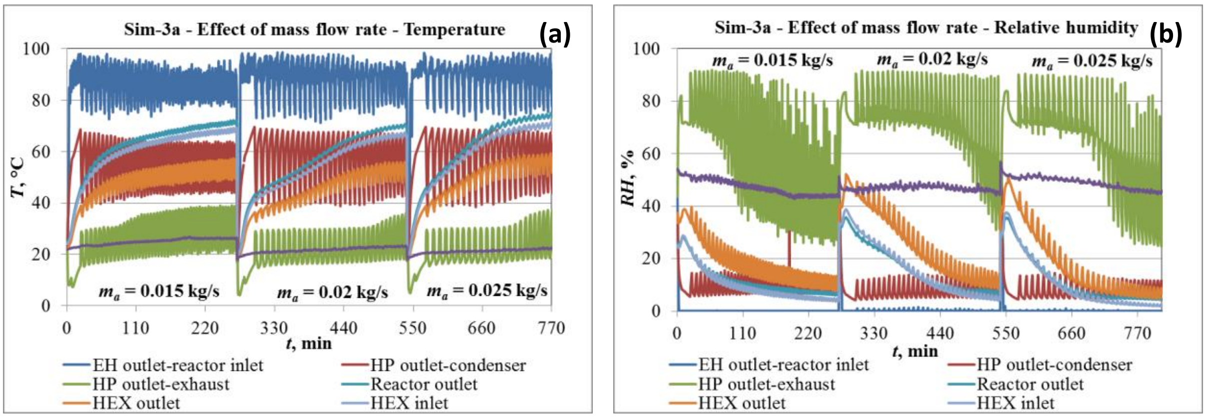

Figure 8.3.52 Measured (a) temperatures and (b) relative humidites in charging cycles with different MFRs

However it should be noticed that with the increasing MFR required energy input is higher to heat the air to the desired T_{reg}. Therefore the conditions and availability of energy sources (e.g solar energy) should be considered in any specific application for determining the optimal MFR used in charging-dsicharging cycles.

iii. Long cycle performance

Two long cycle testings were performed with SIM-3a consisting of a 1200 min discharging following a 360 min charging and 900 min. discharging cycle. As the previous section investigates multiple materials in the developed system, short cycles were performed to compare their performances for the operation of equal time frames. In this part, overall performance of SIM-3a was investigated. In the first discharging cycle, T_o, reached to 45 °C (See: Figure 8.3.53 a) and $\Delta T/\Delta t$ was found 0.0125 °C/min. showing the steady performance of SIM-3a. At the same time RH_o was varied in range of 11→50% while RH_i was flactuating between 70-80% (see: Figure 8.3.53 b). Thermal power output, Q_t, varied in the range of 0.6-0.22 kW while E_o reached to 6.77 kWh at the end of 1200 min discharging period. Following the discharging period, material was regenerated at $T_{reg,\ ave}$= 82 °C (see: Figure 8.3.54 a-b). In charging process, total electric energy input to the system was calculated as 2.83 kWh where 0.96 kWh of it was thermally recovered with HEX.

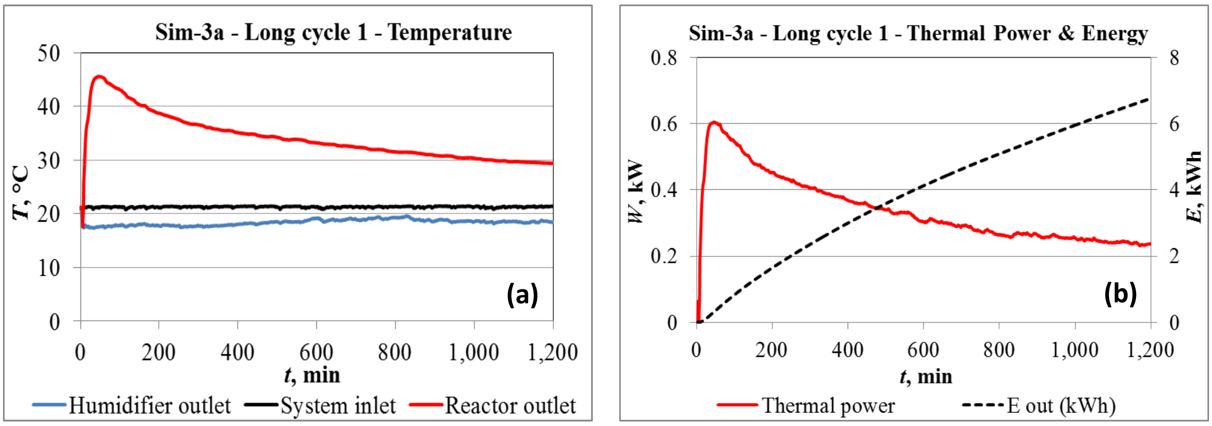

Figure 8.3.53 Measured (a) temperatures and (b) relative humidites in 1st long discharging cycle of Sim-3a

Based on the total energy input–output in charging and discharging processes, COP_S was calculated as 2.39. The COP_S was substantially higher than short term testing. The lower operating time limits the extracted heat output from the material, which is a factor significanly reducing the COP_S.

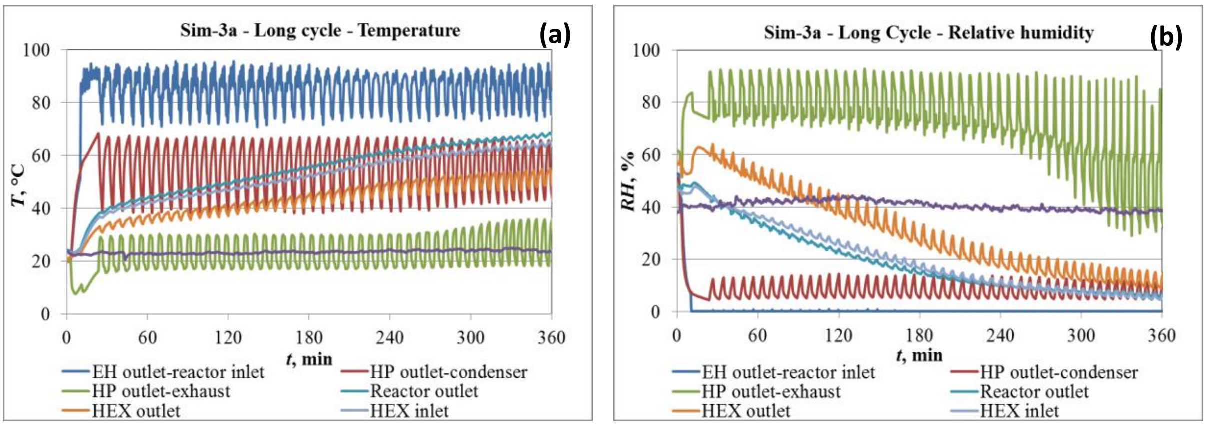

Figure 8.3.54 Measured (a) temperatures and (b) relative humidites in long charging cycle of Sim-3a

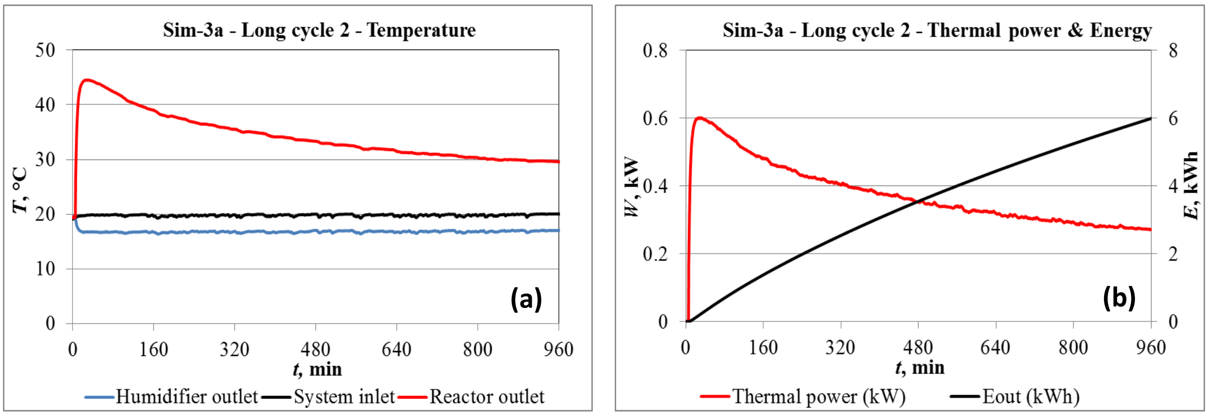

Figure 8.3.55 Measured (a) temperatures and (b) relative humidites in 2nd long discharging cycle of Sim-3a

Upon charging the material, 2nd discharging cycle performed (See: Figure 8.3.55 a-b) . In 960 min discharging period T_o varied in the range of 45→30 °C, corresponding to $\Delta T/\Delta t$ = 0.0156 °C/min. which was higher than the initial cycle. Higher $\Delta T/\Delta t$ indicates the faster drop of temperature lift, ΔT, which is undesirable. This is most likely occurred as a result of the residual moisture remained inside the material. Measurement results showed that only 0.61 kg of the loaded 6.54 kg moisture was remained inside the material after charging. This corresponds to *ηhyg-cyc* = 91% showing that the regeneration of the material was very efficient. Further development could be on improving reactor design for enhancing the heat and mass transfer.

8.4 Validation of numerical results

The numerical results presented in Section 8.2 were validated with the experimental data obtained from the prototype testing rig (see: Section 8.3) as presented in Figures 8.4.1-8.4.2.

The numerical and experimental temperature variations of air at the reactor outlet in discharging cycle were given in Figure 8.4.1. Based on the simulation results, air temperature varies in the range of 39.4→ 29.2 °C. The numerical data compared with 5 different experimental cycles having process durations in the range of 300→600 °C. Despite the small differences in obtained peak temperatures, all cycles have similar profiles and they are in close approximation with the numerical data.

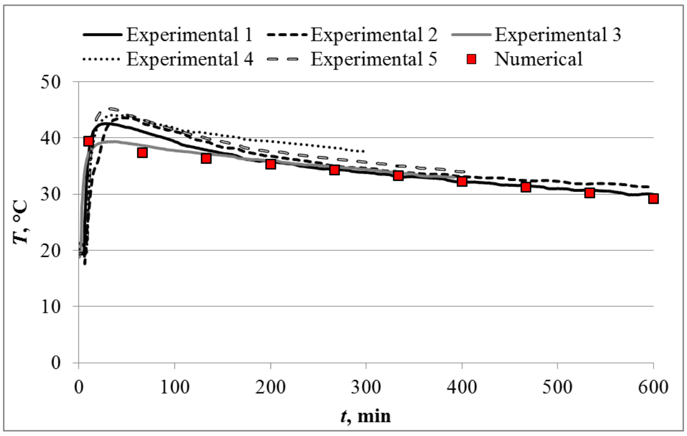

Figure 8.4.1 Numerical and experimental air temperature variation during discharging cycle

Numerically and experimentally obtained COP_{HP} and COP_S values are comparatively presented in Figures 8.4.2 a-b respectively. In order to realize this, numerically obtained variation range of average process *COPs* were compared with average COPs of 10 different experimental cycles. As seen from Figure 8.4.2 a, COP_{HP} varies in the range of 3.01→4.81 while experimentally obtained $COP_{HP,ave}$ values were between 3.11→5.71. Although experimental results were slightly higher than the numerical data, it was found that in general they are in close approximation. A similar approach is applied to compare numerical and experimental COP_s (See: Figure 8.4.2 b). Based on the simulation results, $COP_{s,ave}$ varies in the range of 1.18→1.74 and experimentally obtained COP_s values were between 1.06→1.83. Accordingly it could be concluded that numerical and experimental results are in good agreement.

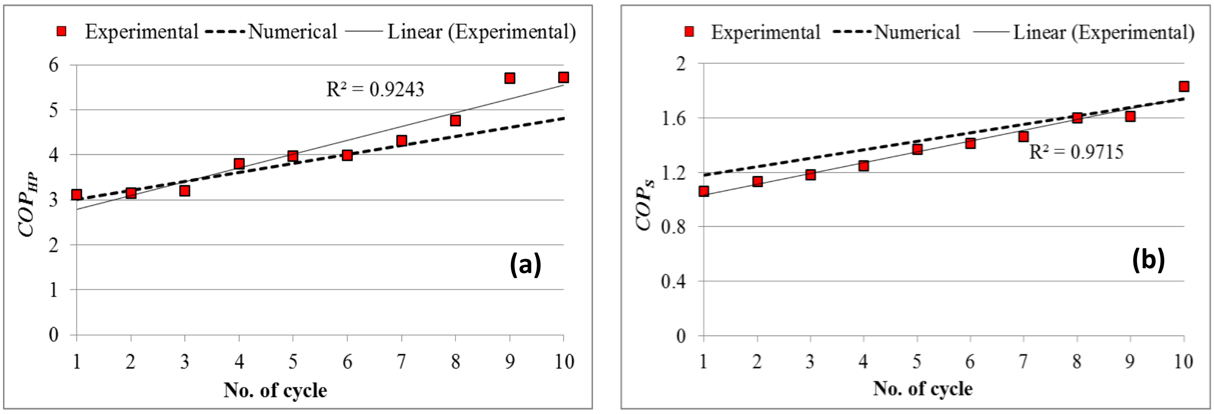

Figure 8.4.2 Numerical and experimental (a) COP_{HP} and (b) COP_s values in different cycles

8.5 Conclusions

In this Chapter a novel heat pump driven sorption storage system (Store-Heat) was numerically and experimentally investigated. In addition, new composite sorption materials were developed, characterized and experimented in the developed sorption reactor.

According to the performed numerical analysis; $T_{i,c}$ (T_1) is one of the key parameters determining system performance. Utilizing solar energy to increase T_1 in charging process, substantially reduces the W_{comp} thereby improves the COP_{HP} and COP_S. For the conditions of $A_{coll} > 4$ m^2 and $I > 0.3$ kW, $COPs > 3$ could be achieved. On the other hand increase of $T_{i,d}$ (T_{10}) in the range of 10→25 °C (for the same RH level) enables obtaining higher $E_{o,d.}$ However it also increases the quantity of loaded moisture to the sorbent during the discharging process which results with higher $E_{i,c}$. As a result, it is found that overall effect of $T_{i,d}$ on *COPs* is negligible. On the other hand, $T_{i,d}$ is important on achieving higher temperature lifting in discharging cycle. Low $T_{i,d}$ may result in low temperature lift of air, which limits the benefit from the system. Therefore it should be optimized depending on the operating conditions in any application. Analysis results also showed that increasing air MFR improves COP_{HP}. However as it also increases W_{EH}. It is concluded that varying MFR has a minimal effect on *COPs.*

According to testing results, COP_s varies in the range of 1-2 depending on sorption material properties and system operating conditions. Both the numerical and experimental results showed that, increasing T_{reg} significantly reduces COP_S. Therefore further development of sorption materials that could be regenerated at 60-70 °C is crucial. That condition will enable individual use of HP without the need of electrical heater and could substantially increase COP_S. Studies on material characterization showed that Zeolite and SIM-3m has low E_d at T_{reg} of *80* °C which is also validated with experimental testing. LiCl demonstrated a potential benefit for improving energy density and sorption kinetics. It is found that modifying $CaCl_2$ and $MgCl_2$ with LiCl enhances the heat output in discharging cycle while enhancing the moisture removal rate in charging cycle. According to experimental results SIM-3a and SIM-3cl were found to be the two promising candidates among the five tested materials. Due to its better known hygrothermal and cyclic characteristics, SIM-3a was used in parametric investigations on system experimental thermal performance. Within these testings, it was obtained that *b*=25 mm and MFR=0.02 kg/s are optimal operating parameters. Performed long cycle testing under these operating conditions showed that

0.04 m^3 material could provide ≈6.8 kWh $E_{o,d}$ for ΔT *in the range of* 28→10 *°C* over 1200 minutes.

The outcomes obtained with the laboratory scale prototype system are promising, especially for the conditions that the system is driven by PV panels (e.g. during day time) to be charged. The main benefit of the developed process is to significantly reduce the peak power required for charging the material thereby being suitable to be coupled with PV panels. For instance, considering a single electrical heater used for charging the material, the required power exceeds 1 kW for the same air flow rate (0.02 kg/s). In that case assuming η_{PV}=10% and I=1000 W/m^2, required PV area is ≈10 m^2. Whilst in the developed system, the total required power was lower than 0.45 kW for charging the material as majority of the wasted heat was recovered. In that case required PV area is 4.5 m^2.

Considering the highest energy consumption in UK building sector goes to space heating, storing the electricity generated with PV panels as thermal energy could be a promising option. That will enhance the utility of PV technology whilst reducing the costs for energy storage.

The purposed system uses the technologies such as HP and heat recovery units which are available in the market and integrates them with a novel sorption reactor in a state of the art design. Results showed that the composite sorbent SIM-3a and SIM-3cl has a promising potential to be regenerated at the temperature level of 70-80°C in the developed system. This is important because that temperature range is feasible to benefit from off-peak tariff (at night time) or PV panels (during daytime). At higher regeneration temperature (e.g. 150°C) low amount of waste heat can be recovered reducing the system performance.

Besides, processes working at high temperature level seem unlikely to be effectively benefited from HP which plays a vital role on system efficiency.

A low temperature HP was employed in the developed system which uses R410a as refrigerant. During the testing, the HP was intermittently operating as the refrigerant was reaching the critical temperature due to high heat gain in evaporator side. Average HP outlet temperature of air at the condenser side was ≈55 °C (40→70 °C), whereas the required T_{reg} was 70-80 °C creating a need for an auxiliary EH. As an option, benefitting from high temperature HP working up to temperature levels 80 °C could eliminate the need of electrical heater to boost the temperature, therefore higher COP_s could be achieved.

As a future work, developed system could be developed in a compact way with optimizing the size of system components. The compact sorption heat storage module could have a high market potential especially in countries with high heat demand like UK. It can be a promising way of using PV technology and off peak tariff in an efficient way. However further development of sorption materials and process optimization is required. Besides long term performance monitoring with real time applications is necessary to understand the technical, economic and environmental benefits of the Store-Heat system.

Chapter 9: Discussion, Conclusions, Recommendation and Future Work

9.1 Discussion and conclusions

Present research has investigated THS system, which is a relatively new, but a novel concept enabling storage of thermal energy for long term with high E_d and without heat loss. According to the performed comparative analysis for UK climate conditions (see: Chapter 3), with 1m^3 storage volume, ≈14% of the average monthly heat demand of a building could be met with THS whereas this ratio is 6% and 2% for LHS and SHS respectively. This is important as reduced volume of heat storage could fit in limited space in buildings.

Sorption material has a vital importance in THS systems. Research in this field relied on the natural conventional materials including Zeolites, Silica Gels and Activated carbon. Despite their high sorption heat, high regeneration temperature requirement of these materials remains as the main obstacle for their use in THS systems. Development of advanced materials, those satisfy the requirements of THS process are required. Accordingly, Chapter 4 of the presented research covered selection, synthesis and experimental testing of a selected group of candidate sorption materials. Based on the Part I (See: Chapter 4.2) of material based studies, SIM-3a and SIM-3e demonstrated excellent E_d coupled with good EMC and t_{emc} with their TGA analysis also suggesting significant mass loss in the working range $30 < T < 140$ °C. These findings suggest that both SIM-3a and SIM-3e are promising candidates to be used in an open TES system. Part II (See: Section 4.3) of this Chapter, focused on analysis of the hygrothermal cyclic behaviour of the SIM samples to validate these findings using a custom built experimental rig. SIM-3a showed steadier performance over repeating cycles when compared with Silica gel, Zeolite and other tested SIMs. Its excellent hygrothermal performance and high sorption heat output per gr of adsorbed moisture suggested that this material is the most promising candidate among all tested materials. In last part (Section 4.4) of Chapter 4, a new sorption reactor (Gen2) consisting of perforated pipes embedded inside the sorbent was developed and experimented. Testing results also compared with the performance of the same materials in previously developed testing rig (Gen1). The Gen2 test rig provided improved performance over Gen1. According to study results, use of perforated tubes enhances both moisture and heat transfer allowing for higher and steadier temperature lift during the discharging process. It is found that Gen2 prototype reactor using SIM-3a provides E_d= 290 kWh/m^3 which is much higher than achievable E_d with SHS and LHS systems.

In real applications, large volume of sorbent requirement for seasonal heat storage, brings complexity in THS process and with the increasing volume of sorbent material, extracting the full yield of stored heat becomes challenging due to the heat/mass transfer limitations. In order to address this problem, a modular concept consisting of three identical sorption pipe reactors was developed (Chapter 5). According to study results, it was found that modular use of three SPs could provide E_{cum} = 25.5 kWh with the V_s = 0.088 m^3 corresponding to ≈290 kWh/m^3, which was similar with the E_d obtained in Gen2 rig. The modular concept, with the previously proved design using perforated pipes for air diffusion, could be a favourable direction for advancing THS systems to commercial level.

In order to understand the potential benefits of THS, a theoretical feasibility study for the Cyprus Case was performed. According to the study results, 5.25 m^3 THS system coupled with 8 m^2 solar air collectors, could regenerate in ≈35 days over summer period and the amount of stored heat together with the available solar energy in winter will be sufficient to meet the full heat demand of the studied building. With the use of proposed solar powered THS for space heating in Cyprus, 1900 kWh/year energy and 1.91 tons/year emission savings could be obtained. Accordingly, ROI period was found as 6 years and CO_2 savings for the same time frame was computed as ≈11.5 tons.

A novel concept based on the integration of sorption pipe with a solar concentrator was also experimented under Cyprus climate conditions. Sorption pipe provided 2.85 kWh heat output in discharging cycle, which was sufficient to meet the heat demand of investigated building. In charging cycle, high percent of the moisture (~60%) was desorbed with the use of solar concentrator. Results indicated that, integration of solar concentrators with the sorption pipe is an effective method for charging the sorbent.

Following the work on sorbent development and characterization, process optimization, reactor design and laboratory scale investigation of THS system, a full scale prototype was developed and tested in a real building. According to the testing results, it was found that TSCs could provide thermal energy >15kWh/day for an average solar intensity of 0.3 kW/m^2. On the other hand testing on THS showed that each sorption vessel could generate E_{cum} in the range of 195→248 kWh. Based on the obtained results, total heat storage capacity of the system was found between 780→990 kWh depending on the air mass flow rate. The results obtained with the commercial level prototype demonstrate that THS could provide significant energy and cost savings for space heating in buildings in close future. UK has low winter ambient temperature, and in such a severe climate, inter-seasonal THS represents one of the promising solutions for increasing the solar share in space heating applications.

In Chapter 8, a sorption storage heater system driven by a HP, with the purpose of utilizing off-peak or PV sourced electricity, was investigated. Study results indicated that, with the developed system, thermal energy could be stored 2-3 times more efficient and 4-6 times more densely (*i.e*. higher E_d) than the conventional storage heaters. System performance could be further improved with the development of sorbents that have low regeneration temperature also by utilizing solar energy in charging process.

9.2 Recommendation and future work

THS has many promising advantages as extensively discussed in this communication. Simple concept of open cycle THS system, such as operating at atmospheric pressure without a need of heat exchange mechanism, being suitable to be integrated with any kind of heat source and using low cost material and equipment makes it even more attractive for various applications.

New sorption materials were examined within this research for heat storage purposes. Despite the encouraging results obtained within the study, further work on sorption materials is vital. Development of novel sorbents that could be regenerate at low temperatures (e.g. 30-50 °C) could provide a promising opportunity to benefit from THS in the built environment. This could not only enhance the utility of solar thermal energy, but also enables using solar, ground or air sourced heat pumps in more effective manner. In this regard the field of nano-materials will serve as a basis for developing advanced composite sorbents.

An interesting field could be utilizing electro-osmosis process for regenerating sorption material. The process requires electricity with very low intensity for moving water through a porous matrix. It was exploited for the applications such as moving the damp on the building walls to the soil, or removing the water from desiccant materials in desiccant cooling or dehumidification applications (Li et al., 2012). Electro-osmotic regeneration method could be used individually or could be integrated with PV thermal collectors, where solar heated air flow and PV driven electro-osmosis process operates simultaneously for regenerating the sorbent.

Sorption materials also present a promising opportunity for industrial waste heat recovery. This field is gaining attention with its high potential for improving energy efficiency and reducing emissions in energy intensive industrial sectors. Sorption materials could enable storage of industrial waste heat which could be re-used in any heat generation process, transported between industries or even supplied to the buildings. In this regard, development of heat exchanger type sorption reactors made up of adsorbent coated plates could be a promising solution. Besides the industrial heat recovery, sorbent coating technology could be utilized in building ventilation heat recovery units or in HPs for preventing defrosting. Preliminary work has performed on sorbent coating under laboratory conditions to examine the performance of such concept.

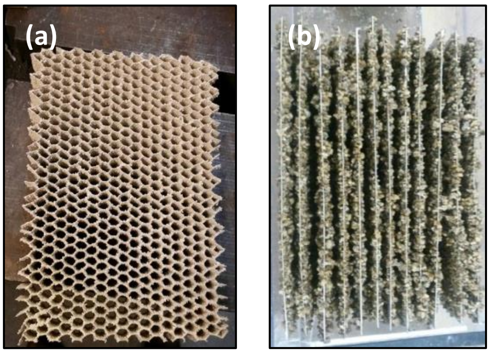

Figure 9.2.1 (a) Zeolite-$CaCl_2$ coated honeycomb filter, (b) SIM-3a coated aluminium plates

As seen in Figure 9.2.1, Zeolite powder-$CaCl_2$ composite was coated on aluminium honeycombs and Vermiculite-$CaCl_2$ (Sim-3a) was coated on aluminium plates. Despite the use of small amount of sorbent, sorption and thermal performance of the coatings found effective. SIM-3a coated plates adsorbed 152 gr moisture over 3 hours and provided ΔT_{ave} = 13 °C. $CaCl_2$ –Zeolite powder coated honeycomb performance was lower than SIM-3a coated plates due to low sorbent layer thickness. Zeolite-$CaCl_2$ coated honeycombs adsorbed 93 gr moisture whilst ΔT_{ave} was found 8.8 °C.

Besides the heating purposes, thermochemical materials that provide adequate endothermic reactions for cooling could be investigated as a future direction. That kind of technology could store/utilize the abundant solar energy in coolth form during summer, for space cooling in the built environment. Potential candidate materials could be $NaNO_3$, CH_4N_2O, KNO_3 and $Ca(NO_3)_2$ and their mixtures. Some preliminary investigations performed on the selected candidate CH_4N_2O (urea), which is safe, harmless, and environmentally friendly material with a high cooling enthalpy. The view of the urea impregnated vermiculite composite in anhydrous form was illustrated in Figure 9.2.2 below. According to the performed tests, total volumetric cooling capacity of the urea-vermiculite was found in the range of 60-70 kWh/m^3 for average ΔT_{air} of 15°C. Additionally, it was observed that material could be effectively regenerate with solar energy at 40-50 °C temperature range.

Figure 9.2.2 View of the developed vermiculite-urea composite material

References

ABEDIN, A. H. & ROSEN, M. A. 2011. A Critical Review of Thermochemical Energy Storage Systems. *Open Renewable Energy Journal,* 4.

ABEDIN, A. H. & ROSEN, M. A. 2012. Closed and open thermochemical energy storage: energy-and exergy-based comparisons. *Energy,* 41**,** 83-92.

AL-ABIDI, A. A., BIN MAT, S., SOPIAN, K., SULAIMAN, M. Y., LIM, C. H. & TH, A. 2012. Review of thermal energy storage for air conditioning systems. *Renewable and Sustainable Energy Reviews,* 16**,** 5802-5819.

ARISTOV, Y. I. 2007a. New family of solid sorbents for adsorptive cooling: Material scientist approach. *Journal of Engineering Thermophysics,* 16**,** 63-72.

ARISTOV, Y. I. 2007b. Novel materials for adsorptive heat pumping and storage: screening and nanotailoring of sorption properties. *Journal of Chemical Engineering of Japan,* 40**,** 1242-1251.

ARISTOV, Y. I. 2009. Optimal adsorbent for adsorptive heat transformers: Dynamic considerations. *International Journal of Refrigeration,* 32**,** 675-686.

ARISTOV, Y. I., DI MARCO, G., TOKAREV, M. & PARMON, V. 1997. Selective water sorbents for multiple applications, 3. $CaCl_2$ solution confined in micro-and mesoporous Silica Gels: Pore size effect on the “solidification-melting” diagram. *Reaction Kinetics and Catalysis Letters,* 61**,** 147-154.

ARISTOV, Y. I., RESTUCCIA, G., CACCIOLA, G. & PARMON, V. 2002. A family of new working materials for solid sorption air conditioning systems. *Applied Thermal Engineering,* 22**,** 191-204.

ARISTOV, Y. I., RESTUCCIA, G., TOKAREV, M., BUERGER, H. D. & FRENI, A. 2000a. Selective water sorbents for multiple applications. 11. $CaCl_2$ confined to expanded vermiculite. *Reaction Kinetics and Catalysis Letters,* 71**,** 377-384.

ARISTOV, Y. I., RESTUCCIA, G., TOKAREV, M. & CACCIOLA, G. 2000b. Selective water sorbents for multiple applications, 10. Energy storage ability. *Reaction Kinetics and Catalysis Letters,* 69**,** 345-353.

ARISTOV, Y. I., TOKAREV, M., RESTUCCIA, G. & CACCIOLA, G. 1996a. Selective water sorbents for multiple applications, 2. $CaCl_2$ confined in micropores of Silica Gel: Sorption properties. *Reaction Kinetics and Catalysis Letters,* 59**,** 335-342.

ARISTOV, Y. I., TOKAREV, M. M., CACCIOLA, G. & RESTUCCIA, G. 1996b. Selective water sorbents for multiple applications, 1. $CaCl_2$ confined in mesopores of silica gel: Sorption properties. *Reaction Kinetics and Catalysis Letters,* 59**,** 325-333.

ARTECONI, A., HEWITT, N. J. & POLONARA, F. 2012. State of the art of thermal storage for demand-side management. *Applied Energy,* 93**,** 371-389.

ASIF, M. & MUNEER, T. 2007. Energy supply, its demand and security issues for developed and emerging economies. *Renewable and Sustainable Energy Reviews,* 11**,** 1388-1413.

ATIKOL, U. Residential energy consumption survey. *Eastern Mediterranean University Energy Research Centre Report ERC-96/001,* Famagusta, N. Cyprus.

ATIKOL, U. & GÜVEN, H. 2003. Feasibility of DSM-technology transfer to developing countries. *Applied energy,* 76**,** 197-210.

AYDIN, D., CASEY, S. P. & RIFFAT, S. 2015a. The latest advancements on thermochemical heat storage systems. *Renewable and Sustainable Energy Reviews,* 41**,** 356-367.

AYDIN, D., UTLU, Z. & KINCAY, O. 2015b. Thermal performance analysis of a solar energy sourced latent heat storage. *Renewable and Sustainable Energy Reviews,* 50**,** 1213-1225.

BALASUBRAMANIAN, G., GHOMMEM, M., HAJJ, M. R., WONG, W. P., TOMLIN, J. A. & PURI, I. K. 2010. Modeling of thermochemical energy storage by salt hydrates. *International Journal of Heat and Mass Transfer,* 53**,** 5700-5706.

BALES, C., GANTENBEIN, P., HAUER, A., HENNING, H. M., JAENIG, D., KERSKES, H., NÚÑEZ, T. & VISSCHER, K. 2005. Thermal Properties of Materials for Thermo-chemical storage of solar heat. *A Report of IEA Solar Heating and Cooling programme–Task,* 32.

BALES, C., GANTENBEIN, P., JAEHNIG, D., KERSKES, H., VAN ESSEN, M., WEBER, R. & ZONDAG, H. 2008. Chemical and sorption storage–Results from IEA-SHC Task 32. *Eurosun 2008*.

BALES, C., GANTENBEIN, P., JAENIG, D. & WEBER, R. 2007. Laboratory prototypes of thermo-chemical and sorption storage units. *Report B3—IEA SHC Task,* 32.

BAO, H., WANG, R., OLIVEIRA, R. & LI, T. 2012. Resorption system for cold storage and long-distance refrigeration. *Applied Energy,* 93**,** 479-487.

BAO, Z., YANG, F., WU, Z., NYALLANG NYAMSI, S. & ZHANG, Z. 2013. Optimal design of metal hydride reactors based on CFD–Taguchi combined method. *Energy Conversion and Management,* 65**,** 322-330.

BAŞÇETINÇELIK, A., PAKSOY, H. & DEMIREL, Y. 1999. Energetic and exergetic efficiency of latent heat storage system for greenhouse heating. *Renewable Energy,* 16**,** 691-694.

BASCIOTTI, D. & POL, O. A theoretical study of the impact of using small scale thermo chemical storage units in district heating networks. Proceedings of the International Sustainable Energy Conference 2011, Belfast, Ireland, 2011.

BASECQ, V., MICHAUX, G., INARD, C. & BLONDEAU, P. 2013. Short-term storage systems of thermal energy for buildings: A review. *Advances in Building Energy Research,* 7**,** 66-119.

BAYMAK 2016. *www.baymak.com.tr* [Online]. Available:
http://www.eyuboglukombi.com/baymak-gunes-kollektoru-kat85.html [Accessed 19.08.2016].

BENLI, H. & DURMUŞ, A. 2009. Performance analysis of a latent heat storage system with phase change material for new designed solar collectors in greenhouse heating. *Solar Energy,* 83**,** 2109-2119.

BSI 1996. BS 4359-1: 1996: Determination of the specific surface area of powders. BET method of gas adsorption for solids (including porous materials) London: BSI Group.

BSI 1997. BS EN ISO 11358: 1997: Plastics. Thermogravimetry (TG) of polymers. General principles. London: BSi Group.

BSI 1998. BS EN 1097-3: 1998: Tests for mechanical and physical properties of aggregates. Determination of loose bulk density and voids. London: BSI Group.

BSI 2000. BS EN ISO 12571: 2000: Hygrothermal performance of building materials and products. Determination of hygroscopic sorption properties. London: BSI Group.

BSI 2005. BS EN ISO 11357-4: 2005: Differential scanning calorimetry (DSC). Determination of specific heat capacity. London: BSI Group.

BSI 2007. BS ISO 21687: 2007: Carbonaceous materials used in the production of aluminium. Determination of density by gas pyknometry (volumetric) using helium as the analysis gas. Solid materials. London: BSi Group.

BSI 2012. BS EN ISO 22007-2: 2012: Plastics. Determination of thermal conductivity and thermal diffusivity. Transient plane heat source (hot disc) method. London: BSi Group.

BUKER, M. S., MEMPOUO, B. & RIFFAT, S. B. 2014. Performance evaluation and techno-economic analysis of a novel building integrated PV/T roof collector: An experimental validation. *Energy and Buildings,* 76**,** 164-175.

CARBONCOMMENTARY 2014. *www.carboncommentary.com. Domestic batteries to store excess PV and reduce peak demand loads* [Online]. Available: www.carboncommentary.com/blog/2014/10/17/domestic-batteries-to-store-excess-pv-and-reduce-peak-demand-loads [Accessed 15.05.2016.

CÁRDENAS, B. & LEÓN, N. 2013. High temperature latent heat thermal energy storage: Phase change materials, design considerations and performance enhancement techniques. *Renewable and Sustainable Energy Reviews,* 27**,** 724-737.

CASEY, S. P., AYDIN, D., RIFFAT, S. & ELVINS, J. 2015. Salt impregnated desiccant matrices for 'open' thermochemical energy storage—Hygrothermal cyclic behaviour and energetic analysis by physical experimentation. *Energy and Buildings,* 92**,** 128-139.

CASEY, S. P., HALL, M. R., TSANG, S. C. E. & KHAN, M. A. 2012. Nanocomposite materials for rapid-response interior air humidity buffering in closed environments. *Journal of Building Performance Simulation***,** 1-13.

CENGEL, Y., A & BOLES, M., A 2006. *Thermodynamics: An engineering approach*. McGraw-Hill, 5th Edition. ISBN: 0072884959.

ÇENGEL, Y. A. 2007. *Heat and mass transfer: A practical approach.* Maidenhead, Mcgraw-Hill, 3rd Edition. ISBN: 0073129305.

CERKVENIK, B., SATZGER, P., ZIEGLER, F. & POREDOŠ, A. 1999. High efficient sorption cycles using CaO/H_2O and LiBr/H_2O for gas cooling. 3rd ASME/RAES Renewable and Advanced Energy Systems for the 21st Century Conference, 11-14 April 1999, Lahaina, Maui, Hawaii.

CHAN, C., LING-CHIN, J. & ROSKILLY, A. 2013. A review of chemical heat pumps, thermodynamic cycles and thermal energy storage technologies for low grade heat utilisation. *Applied Thermal Engineering,* 50**,** 1257-1273.

CHAN, K. C., CHAO, C. Y. H., SZE-TO, G. N. & HUI, K. S. 2012. Performance predictions for a new Zeolite 13X/$CaCl_2$ composite adsorbent for adsorption cooling systems. *International Journal of Heat and Mass Transfer,* 55**,** 3214-3224.

CHEN, H., LI, T., WANG, L., WU, J., WANG, R. & RG, O. 2009. Sorption performance of consolidated composite sorbent used in solar-powered sorption air-conditioning system. *Journal of the Chemical Industry and Engineering Society of China,* 5**,** 008.

CHUA, K., CHOU, S. & YANG, W. 2010. Advances in heat pump systems: A review. *Applied Energy,* 87**,** 3611-3624.

CIBSE 2006. *Guide A - Environmental Design, 7th edn,* London, Chartered Institute of Building Service Engineers.

CONDON, J. B. 2006. Chapter 1 - An Overview of Physisorption. *In:* CONDON, J. B. (ed.) *Surface Area and Porosity Determinations by Physisorption.* Amsterdam: Elsevier Science.

COT-GORES, J., CASTELL, A. & CABEZA, L. F. 2012. Thermochemical energy storage and conversion: A-state-of-the-art review of the experimental research under practical conditions. *Renewable and Sustainable Energy Reviews,* 16**,** 5207-5224.

CTM 2016. www.ctm.co.uk [Online]. [Accessed 03.05.2016].

CUYPERS, R., MARAZ, N., EVERSDIJK, J., FINCK, C., HENQUET, E., OVERSLOOT, H., SPIJKER, H. V. T. & DE GEUS, A. 2012. Development of a seasonal thermochemical storage system. *Energy Procedia,* 30**,** 207-214.

DA GRAÇA CARVALHO, M. 2012. EU energy and climate change strategy. *Energy,* 40**,** 19-22.

DE BOER, R., HAIJE, W. & VELDHUIS, J. 2002. Determination of structural, thermodynamic and phase properties in the Na_2S–H_2O system for application in a chemical heat pump. *Thermochimica acta,* 395**,** 3-19.

DECC 2013. *Department of Energy & Climate Change - Energy Consumption in the UK. Overall energy consumption factsheet* [Online].
Available: www.gov.uk/government/publications/energy-consumption-in-the-uk [Accessed 22.01.14].

DEMIRBAS, M. F. 2006. Thermal energy storage and phase change materials: An overview. *Energy Sources, Part B: Economics, Planning, and Policy,* 1**,** 85-95.

DICAIRE, D. & TEZEL, F. H. 2012. Use of adsorbents for thermal energy storage of solar or excess heat: Improvement of energy density. *International Journal of Energy Research*, 37**,** 1059-68.

DIENG, A. O. & WANG, R. Z. 2001. Literature review on solar adsorption technologies for ice-making and air-conditioning purposes and recent developments in solar technology. *Renewable and Sustainable Energy Reviews,* 5**,** 313-342.

DINCER, I. 2002. Thermal energy storage systems as a key technology in energy conservation. *International Journal of Energy Research,* 26**,** 567-588.

DING, Y. & RIFFAT, S. 2012. Thermochemical energy storage technologies for building applications: A state-of-the-art review. *International Journal of Low-Carbon Technologies***,** 8, 106-116.

DUFFIE, J. A. & BECKMAN, W. A. 2013. *Solar engineering of thermal processes*. JohnWiley & Sons, New York, 4th Edition. ISBN: 1118415418.

EAMES, P., LOVEDAY, D., HAINES, V. & ROMANOS, P. 2014. The future role of thermal energy storage in the UK energy system: An assessment of the technical feasibility and factors influencing adoption. *UKERC: London*.

ERVIN, G. 1977. Solar heat storage using chemical reactions. *Journal of Solid State Chemistry,* 22**,** 51-61.

EVCIL, A. 2012. An estimation of the residential space heating energy requirement in Cyprus using the regional average specific heat loss coefficient. *Energy and Buildings,* 55**,** 164-173.

FADHEL, M., SOPIAN, K. & DAUD, W. 2010. Performance analysis of solar-assisted chemical heat-pump dryer. *Solar Energy,* 84**,** 1920-1928.

FAN, Y., LUO, L. & SOUYRI, B. 2007. Review of solar sorption refrigeration technologies: development and applications. *Renewable and Sustainable Energy Reviews,* 11**,** 1758-1775.

FERNÁNDEZ-SEARA, J., PIÑEIRO, C., ALBERTO DOPAZO, J., FERNANDES, F. & SOUSA, P. X. 2012. Experimental analysis of a direct expansion solar assisted heat pump with integral storage tank for domestic water heating under zero solar radiation conditions. *Energy Conversion and Management,* 59**,** 1-8.

FLUECKIGER, S. M., VOLLE, F., GARIMELLA, S. V. & MONGIA, R. K. 2012. Thermodynamic and kinetic investigation of a chemical reaction-based miniature heat pump. *Energy Conversion and Management,* 64**,** 222-231.

GARG, H., MULLICK, S. & BHARGAVA, A. 1985. *Solar thermal energy storage,* Dordrecht, Holland, D. Reidel Publishing Company, Springer.

GORDEEVA, L. & ARISTOV, Y. I. 2012. Composites 'salt inside porous matrix'for adsorption heat transformation: a current state-of-the-art and new trends. *International Journal of Low-Carbon Technologies,* 7**,** 288-302.

GORDEEVA, L. G., GREKOVA, A. D., KRIEGER, T. A. & ARISTOV, Y. I. 2009. Adsorption properties of composite materials (LiCl+LiBr)/Silica. *Microporous and Mesoporous Materials,* 126**,** 262-267.

GORDEEVA, L. G., RESTUCCIA, G., CACCIOLA, G. & ARISTOV, Y. I. 1998a. Selective water sorbents for multiple applications, 5. LiBr confined in mesopores of Silica Gel: Sorption properties. *Reaction Kinetics and Catalysis Letters,* 63**,** 81-88.

GORDEEVA, L. G., RESTUCCIA, G., FRENI, A. & ARISTOV, Y. I. 2002. Water sorption on composites "LiBr in a porous carbon". *Fuel Processing Technology,* 79**,** 225-231.

GORDEEVA, L. G., TOKAREV, M. M., PARMON, V. N. & ARISTOV, Y. I. 1998b. Selective water sorbents for multiple applications, 6. Freshwater production from the atmosphere. *Reaction Kinetics and Catalysis Letters,* 65**,** 153-159.

GREENING, B. & AZAPAGIC, A. 2014. Domestic solar thermal water heating: A sustainable option for the UK? *Renewable Energy,* 63**,** 23-36.

GUNERHAN, H. & HEPBASLI, A. 2007. Exergetic modeling and performance evaluation of solar water heating systems for building applications. *Energy and Buildings,* 39**,** 509-516.

GUR, I., SAWYER, K. & PRASHER, R. 2012. Searching for a better thermal battery. *Science,* 335**,** 1454-1455.

HADORN, J.-C. IEA solar heating and cooling programme Task 32: Advanced storage concepts for solar and low energy buildings. Ecostock 2006 - The 10th International Conference on Thermal Energy Storage, 2006.

HAIJE, W. G., VELDHUIS, J. B., SMEDING, S. F. & GRISEL, R. J. 2007. Solid/vapour sorption heat transformer: Design and performance. *Applied Thermal Engineering,* 27**,** 1371-1376.

HALL, M. R., TSANG, S. C. E., CASEY, S. P., KHAN, M. A. & YANG, H. 2012. Synthesis, characterization and hygrothermal behaviour of mesoporous Silica high-performance desiccants for relative humidity buffering in closed environments. *Acta Materialia,* 60**,** 89-101.

HAN, Z., ZHENG, M., KONG, F., WANG, F., LI, Z. & BAI, T. 2008. Numerical simulation of solar assisted ground-source heat pump heating system with latent heat energy storage in severely cold area. *Applied Thermal Engineering,* 28**,** 1427-1436.

HASNAIN, S. M. 1998. Review on sustainable thermal energy storage technologies, Part I: heat storage materials and techniques. *Energy Conversion and Management,* 39**,** 1127-1138.

HAUER, A. Thermal energy storage with zeolite for heating and cooling applications. Proceedings of the International Sorption Heat Pump Conference, Shanghai, 2002. p. 24-27.

HAUER, A. & FISCHER, F. 2011. Open adsorption system for an energy efficient dishwasher. *Chemie Ingenieur Technik,* 83**,** 61-66.

HAVALANDIRMACARSISI. 2016. [Online]. Available: havalandirmacarsisi.com.
[Accessed 19.08.2016].

HENNINGER, S. K., JEREMIAS, F., KUMMER, H., SCHOSSIG, P. & HENNING, H.-M. 2012. Novel Sorption Materials for Solar Heating and Cooling. *Energy Procedia,* 30**,** 279-288.

HENNINGER, S. K., SCHMIDT, F. P. & HENNING, H. M. 2010. Water adsorption characteristics of novel materials for heat transformation applications. *Applied Thermal Engineering,* 30**,** 1692-1702.

HIRATA, Y., FUJIOKA, K. & FUJIKI, S. 2003. Preparation of fine particles of calcium chloride with expanded graphite for enhancement of the driving reaction for chemical heat pumps. *Journal of Chemical Engineering of Japan,* 36**,** 827-832.

HONGOIS, S., KUZNIK, F., STEVENS, P. & ROUX, J.-J. 2011. Development and characterisation of a new MgSO4–zeolite composite for long-term thermal energy storage. *Solar Energy Materials and Solar Cells,* 95**,** 1831-1837.

HOTCHKISS. 2016. [Online]. Available: www.hotchkissairsupply.co.uk/pdf/tech/HVAC-Ductwrap.pdf. [Accessed 19.08.2016].

HUSSAIN, M., DINCER, I. & ZUBAIR, S. 2004. A feasibility study of using thermal energy storage in a conventional air-conditioning system. *International Journal of Energy Research,* 28**,** 955-967.

IBRAHIM, D. & ALTUNC, M. 2012. Using Solar Energy in the Cleaning of Swimming Pools in North Cyprus. *Journal of Sustainable Energy & Environment,* 3**,** 31-34.

IEA 2013. World Energy Outlook 2013. IEA Publications Paris.

IMA. 2011. *Vermiculite* [Online]. Available:
www.ima-europe.eu/sites/ima-europe.eu/files/minerals/Vermiculite_WEB-2011.pdf
[Accessed 22.01.14].

IUPAC 1994. Recommendations for the characterization of porous solids. *Pure and Applied Chemistry,* 66**,** 1739-1758.

JÄNCHEN, J., ACKERMANN, D., STACH, H. & BRÖSICKE, W. 2004. Studies of the water adsorption on Zeolites and modified mesoporous materials for seasonal storage of solar heat. *Solar Energy,* 76**,** 339-344.

JÄNCHEN, J., ACKERMANN, D., WEILER, E., STACH, H. & BRÖSICKE, W. 2005. Calorimetric investigation on Zeolites, AlPO4's and $CaCl_2$ impregnated attapulgite for thermochemical storage of heat. *Thermochimica Acta,* 434**,** 37-41.

JÄNCHEN, J. & STACH, H. 2012. Adsorption properties of porous materials for solar thermal energy storage and heat pump applications. *Energy Procedia,* 30**,** 289-293.

JIANG, L., WANG, L., JIN, Z., WANG, R. & DAI, Y. 2013. Effective thermal conductivity and permeability of compact compound ammoniated salts in the adsorption/desorption process. *International Journal of Thermal Sciences,* 71**,** 103-110.

JOHANNES, K., KUZNIK, F., HUBERT, J.-L., DURIER, F. & OBRECHT, C. 2015. Design and characterisation of a high powered energy dense Zeolite thermal energy storage system for buildings. *Applied Energy,* 159**,** 80-86.

JOHNLEWIS. 2016. [Online] Available:
www.johnlewis.com/browse/electricals/heaters-fans-dehumidifers/humidifiers/_/N-ah7
[Accessed 19.08.2016].

KALOGIROU, S. A. 2004. Solar thermal collectors and applications. *Progress in Energy and Combustion Science,* 30**,** 231-295.

KARACA, F., KINCAY, O. & BOLAT, E. 2002. Economic analysis and comparison of chemical heat pump systems. *Applied thermal engineering,* 22**,** 1789-1799.

KATO, Y., TAKAHASHI, F., WATANABE, A. & YOSHIZAWA, Y. 2000. Thermal performance of a packed bed reactor of a chemical heat pump for cogeneration. *Chemical Engineering Research and Design,* 78**,** 745-748.

KENISARIN, M. & MAHKAMOV, K. 2007. Solar energy storage using phase change materials. *Renewable and Sustainable Energy Reviews,* 11**,** 1913-1965.

KERSKES, H., METTE, B., BERTSCH, F., ASENBECK, S. & DRÜCK, H. Development of a thermo-chemical energy storage for solar thermal applications. Proceedings. ISES, Solar World Congress Proceedings, 2011.

KERSKES, H., METTE, B., BERTSCH, F., ASENBECK, S. & DRÜCK, H. 2012. Chemical energy storage using reversible solid/gas-reactions (CWS)–results of the research project. *Energy Procedia,* 30**,** 294-304.

KERSKES, H., SOMMER, K. & MÜLLER-STEINHAGEN, H. 2007. Integrales Konzept zur solarthermischen Gebäudeheizung mit Sorptionswärmespeicher. *Forschungsbericht FZKA-BWPLUS*.

KIBTEK. 2015. *www.kibtek.com. Official Website of Electricity Authority of Northern Cyprus* [Online]. Available: https://www.kibtek.com/uretim/ [Accessed 10.01.2015].

KLEIN, H.-P. & GROLL, M. 2002. Development of a two-stage metal hydride system as topping cycle in cascading sorption systems for cold generation. *Applied Thermal Engineering,* 22**,** 631-639.

KOCA, A., OZTOP, H. F., KOYUN, T. & VAROL, Y. 2008. Energy and exergy analysis of a latent heat storage system with phase change material for a solar collector. *Renewable Energy,* 33**,** 567-574.

KUMARI, N., TIWARI, G. & SODHA, M. 2006. Effect of phase change material on passive thermal heating of a greenhouse. *International Journal of Energy Research,* 30**,** 221-236.

LAHMIDI, H., MAURAN, S. & GOETZ, V. 2006. Definition, test and simulation of a thermochemical storage process adapted to solar thermal systems. *Solar Energy,* 80**,** 883-893.

LANE, G. A. 1983. *Solar heat storage: Latent heat materials,* Boco Raton, FL, CRC Press.

LASS-SEYOUM, A., BLICKER, M., BOROZDENKO, D., FRIEDRICH, T. & LANGHOF, T. 2012. Transfer of laboratory results on closed sorption thermo-chemical energy storage to a large-scale technical system. *Energy Procedia,* 30**,** 310-320.

LE PIERRES, N., MAZET, N. & STITOU, D. 2007. Experimental results of a solar powered cooling system at low temperature. *International Journal of Refrigeration,* 30**,** 1050-1058.

LI, B., LIN, Q. Y. & YAN, Y. Y. 2012. Development of solid desiccant dehumidification using electro-osmosis regeneration method for HVAC application. *Building and Environment,* 48**,** 128-134.

LI, T., WANG, R., KIPLAGAT, J. & CHEN, H. 2010. Experimental study and comparison of thermochemical resorption refrigeration cycle and adsorption refrigeration cycle. *Chemical Engineering Science,* 65**,** 4222-4230.

LI, T., WANG, R., KIPLAGAT, J. & WANG, L. 2009a. Performance study of a consolidated manganese chloride–expanded graphite compound for sorption deep-freezing processes. *Applied Energy,* 86**,** 1201-1209.

LI, T., WANG, R., KIPLAGAT, J. K. & KANG, Y. 2013. Performance analysis of an integrated energy storage and energy upgrade thermochemical solid–gas sorption system for seasonal storage of solar thermal energy. *Energy,* 50**,** 454-467.

LI, T., WANG, R., WANG, L. & KIPLAGAT, J. 2009b. Study on the heat transfer and sorption characteristics of a consolidated composite sorbent for solar-powered thermochemical cooling systems. *Solar Energy,* 83**,** 1742-1755.

LIN, P., WANG, R., XIA, Z. & MA, Q. 2011. Ammonia–water absorption cycle: a prospective way to transport low-grade heat energy over long distance. *International Journal of Low-Carbon Technologies,* 6**,** 125-133.

LIU, H., NAGANO, K., SUGIYAMA, D., TOGAWA, J. & NAKAMURA, M. 2013. Honeycomb filters made from mesoporous composite material for an open sorption thermal energy storage system to store low-temperature industrial waste heat. *International Journal of Heat and Mass Transfer,* 65**,** 471-480.

LIU, H., NAGANO, K. & TOGAWA, J. 2015. A composite material made of mesoporous siliceous shale impregnated with lithium chloride for an open sorption thermal energy storage system. *Solar Energy,* 111**,** 186-200.

LU, Y., WANG, R., ZHANG, M. & JIANGZHOU, S. 2003. Adsorption cold storage system with zeolite–water working pair used for locomotive air conditioning. *Energy Conversion and Management,* 44**,** 1733-1743.

MARIAS, F., NEVEU, P., TANGUY, G. & PAPILLON, P. 2014. Thermodynamic analysis and experimental study of solid/gas reactor operating in open mode. *Energy,* 66**,** 757-765.

MAURAN, S., LAHMIDI, H. & GOETZ, V. 2008. Solar heating and cooling by a thermochemical process. First experiments of a prototype storing 60kWh by a solid/gas reaction. *Solar Energy,* 82**,** 623-636.

METALAVM. 2016. [Online]. Available: metalavm.com/aluminyum-sac-duz-yuzey [Accessed 19/08/2016.

METTE, B., KERSKES, H., DRÜCK, H. & MÜLLER-STEINHAGEN, H. 2013. New highly efficient regeneration process for thermochemical energy storage. *Applied Energy,* 109**,** 352-359.

MICHEL, B., MAZET, N., MAURAN, S., STITOU, D. & XU, J. 2012. Thermochemical process for seasonal storage of solar energy: Characterization and modeling of a high density reactive bed. *Energy,* 47**,** 553-563.

MICHEL, B., MAZET, N. & NEVEU, P. 2014. Experimental investigation of an innovative thermochemical process operating with a hydrate salt and moist air for thermal storage of solar energy: Global performance. *Applied Energy,* 129**,** 177-186.

MOLENDA, M., STENGLER, J., LINDER, M. & WÖRNER, A. 2013. Reversible hydration behavior of CaCl2 at high H_2O partial pressures for thermochemical energy storage. *Thermochimica Acta,* 560**,** 76-81.

N'TSOUKPOE, K. E., LE PIERRÈS, N. & LUO, L. 2013. Experimentation of a LiBr–H2O absorption process for long-term solar thermal storage: Prototype design and first results. *Energy,* 53**,** 179-198.

N'TSOUKPOE, K. E., LIU, H., LE PIERRÈS, N. & LUO, L. 2009. A review on long-term sorption solar energy storage. *Renewable and Sustainable Energy Reviews,* 13**,** 2385-2396.

NAVARRO, L., DE GRACIA, A., COLCLOUGH, S., BROWNE, M., MCCORMACK, S. J., GRIFFITHS, P. & CABEZA, L. F. 2016. Thermal energy storage in building integrated thermal systems: A review. Part 1. active storage systems. *Renewable Energy,* 88**,** 526-547.

OKUNEV, B., GROMOV, A., HEIFETS, L. & ARISTOV, Y. I. 2008. A new methodology of studying the dynamics of water sorption/desorption under real operating conditions of adsorption heat pumps: Modelling of coupled heat and mass transfer in a single adsorbent grain. *International Journal of Heat and Mass Transfer,* 51**,** 246-252.

OLIVEIRA, R., WANG, R., KIPLAGAT, J. & WANG, C. 2009. Novel composite sorbent for resorption systems and for chemisorption air conditioners driven by low generation temperature. *Renewable Energy,* 34**,** 2757-2764.

OZGEN, F., ESEN, M. & ESEN, H. 2009. Experimental investigation of thermal performance of a double-flow solar air heater having aluminium cans. *Renewable Energy,* 34**,** 2391-2398.

ÖZTÜRK, H. H. 2005. Experimental evaluation of energy and exergy efficiency of a seasonal latent heat storage system for greenhouse heating. *Energy Conversion and Management,* 46**,** 1523-1542.

PARAMESHWARAN, R., KALAISELVAM, S., HARIKRISHNAN, S. & ELAYAPERUMAL, A. 2012. Sustainable thermal energy storage technologies for buildings: A review. *Renewable and Sustainable Energy Reviews,* 16**,** 2394-2433.

PARDO, P., DEYDIER, A., ANXIONNAZ-MINVIELLE, Z., ROUGÉ, S., CABASSUD, M. & COGNET, P. 2014. A review on high temperature thermochemical heat energy storage. *Renewable and Sustainable Energy Reviews,* 32**,** 591-610.

PITIÉ, F., ZHAO, C. Y., BAEYENS, J., DEGRÈVE, J. & ZHANG, H. L. 2013. Circulating fluidized bed heat recovery/storage and its potential to use coated phase-change-material (PCM) particles. *Applied Energy,* 109**,** 505-513.

PONOMARENKO, I., GLAZNEV, I., GUBAR, A., ARISTOV, Y. I. & KIRIK, S. 2010. Synthesis and water sorption properties of a new composite "$CaCl_2$ confined into SBA-15 pores". *Microporous and Mesoporous Materials,* 129**,** 243-250.

PVGIS 2015. *photovoltaic-software.com/pvgis.php. EU Official Photovoltaic Software* [Online]. Available: re.jrc.ec.europa.eu/pvgis/apps4/pvest.php?lang=en&map=europe [Accessed 10.01.2015].

QUINNELL, J. & DAVIDSON, J. 2013. Heat and mass transfer during heating of a hybrid absorption/sensible storage tank. *Solar Energy*.

RUITER, J. 1987. Storage of thermal energy by means of an absorption cycle. *NASA STI/Recon Technical Report N,* 88**,** 27619.

SAKKA, S. 2005. *Handbook of sol-gel science and technology processing, characterization, and applications* [Online]. Boston: Kluwer Academic Publishers.

SAPIENZA, A., GLAZNEV, I. S., SANTAMARIA, S., FRENI, A. & ARISTOV, Y. I. 2012. Adsorption chilling driven by low temperature heat: New adsorbent and cycle optimization. *Applied Thermal Engineering,* 32**,** 141-146.

SCHAUBE, F., KOHZER, A., SCHÜTZ, J., WÖRNER, A. & MÜLLER-STEINHAGEN, H. 2013. De-and rehydration of $Ca(OH)_2$ in a reactor with direct heat transfer for thermo-chemical heat storage. Part A: Experimental results. *Chemical Engineering Research and Design,* 91**,** 856-864.

SCHMIDT, T., MANGOLD, D. & MÜLLER-STEINHAGEN, H. 2004. Central solar heating plants with seasonal storage in Germany. *Solar energy,* 76**,** 165-174.

SHAFIEE, S. & TOPAL, E. 2009. When will fossil fuel reserves be diminished? *Energy Policy,* 37**,** 181-189.

SHARMA, A., TYAGI, V., CHEN, C. & BUDDHI, D. 2009. Review on thermal energy storage with phase change materials and applications. *Renewable and Sustainable energy reviews,* 13**,** 318-345.

SHARONOV, V. & ARISTOV, Y. I. 2008. Chemical and adsorption heat pumps: comments on the second law efficiency. *Chemical Engineering Journal,* 136**,** 419-424.

SHIGEISHI, R. A., LANGFORD, C. H. & HOLLEBONE, B. R. 1979. Solar energy storage using chemical potential changes associated with drying of Zeolites. *Solar Energy,* 23**,** 489-495.

SHKATULOV, A., RYU, J., KATO, Y. & ARISTOV, Y. 2012. Composite material “$Mg(OH)_2$ / Vermiculite”: A promising new candidate for storage of middle temperature heat. *Energy,* 44**,** 1028-1034.

SIEMINSKI, A. 2014. International Energy Outlook. *Energy Information Administration (EIA)*.

SIMONOVA, I. A., FRENI, A., RESTUCCIA, G. & ARISTOV, Y. I. 2009. Water sorption on composite “silica modified by calcium nitrate”. *Microporous and Mesoporous Materials,* 122**,** 223-228.

SOLÉ, A., FONTANET, X., BARRENECHE, C., FERNÁNDEZ, A. I., MARTORELL, I. & CABEZA, L. F. 2013. Requirements to consider when choosing a thermochemical material for solar energy storage. *Solar Energy,* 97**,** 398-404.

SRIKHIRIN, P., APHORNRATANA, S. & CHUNGPAIBULPATANA, S. 2001. A review of absorption refrigeration technologies. *Renewable and Sustainable Energy Reviews,* 5**,** 343-372.

STACH, H., MUGELE, J., JÄNCHEN, J. & WEILER, E. 2005. Influence of cycle temperatures on the thermochemical heat storage densities in the systems water/microporous and water/mesoporous adsorbents. *Adsorption,* 11**,** 393-404.

STITOU, D., MAZET, N. & MAURAN, S. 2012. Experimental investigation of a solid/gas thermochemical storage process for solar air-conditioning. *Energy,* 41**,** 261-270.

TAE KIM, S., RYU, J. & KATO, Y. 2011. Reactivity enhancement of chemical materials used in packed bed reactor of chemical heat pump. *Progress in Nuclear Energy,* 53**,** 1027-1033.

TANASHEV, Y. Y., KRAINOV, A. V. & ARISTOV, Y. I. 2013. Thermal conductivity of composite sorbents “salt in porous matrix” for heat storage and transformation. *Applied Thermal Engineering,* 61**,** 401-407.

TANGUY, G., MARIAS, F., ROUGE, S., WYTTENBACH, J. & PAPILLON, P. 2012. Parametric studies of thermochemical processes for seasonal storage. *Energy Procedia,* 30**,** 388-394.

TATSIDJODOUNG, P., LE PIERRÈS, N., HEINTZ, J., LAGRE, D., LUO, L. & DURIER, F. 2016. Experimental and numerical investigations of a Zeolite 13X/water reactor for solar heat storage in buildings. *Energy Conversion and Management,* 108**,** 488-500.

TATSIDJODOUNG, P., LE PIERRÈS, N. & LUO, L. 2013. A review of potential materials for thermal energy storage in building applications. *Renewable and Sustainable Energy Reviews,* 18**,** 327-349.

TIAN, B., JIN, Z., WANG, L. & WANG, R. 2012. Permeability and thermal conductivity of compact chemical and physical adsorbents with expanded natural graphite as host matrix. *International Journal of Heat and Mass Transfer,* 55**,** 4453-4459.

TOKAREV, M. M. & ARISTOV, Y. I. 1997. Selective water sorbents for multiple applications, 4. CaCl2 confined in silica gel pores: Sorption/desorption kinetics. *Reaction Kinetics and Catalysis Letters,* 62**,** 143-150.

TOKAREV, M. M., VESELOVSKAYA, J. V., YANAGI, H. & ARISTOV, Y. I. 2010. Novel ammonia sorbents “porous matrix modified by active salt” for adsorptive heat transformation: 2. Calcium chloride in ACF felt. *Applied Thermal Engineering,* 30**,** 845-849.

TSO, C. Y. & CHAO, C. Y. H. 2012. Activated carbon, silica-gel and calcium chloride composite adsorbents for energy efficient solar adsorption cooling and dehumidification systems. *International Journal of Refrigeration,* 35**,** 1626-1638.

UKPOWER. 2016a. *Economy 7 Tariffs* [Online].
Available: www.ukpower.co.uk/home_energy/economy-7 [Accessed 10.03.2016].

UKPOWER. 2016b. *Economy 10 electricity heating tariff* [Online].
Available: www.ukpower.co.uk/home_energy/economy_10 [Accessed 10.03.2016].

UTLU, Z., AYDıN, D. & KINCAY, O. 2014. Comprehensive thermodynamic analysis of a renewable energy sourced hybrid heating system combined with latent heat storage. *Energy Conversion and Management,* 84**,** 311-325.

VAN ESSEN, V., HE, Z., RINDT, C., ZONDAG, H., GORES, J. C., BLEIJENDAAL, L., BAKKER, M., SCHUITEMA, R. & VAN HELDEN, W. 2009. Characterization of $MgSO_4$ hydrate for thermochemical seasonal heat storage. *Journal of Solar Energy Engineering,* 131**,** 041014.

VASILIEV, L., MISHKINIS, D., ANTUKH, A. & VASILIEV JR, L. 2001. Solar-gas solid sorption refrigerator. *Adsorption,* 7**,** 149-161.

VESELOVSKAYA, J., CRITOPH, R. E., THORPE, R., METCALF, S., TOKAREV, M. & ARISTOV, Y. I. 2010. Novel ammonia sorbents “porous matrix modified by active salt” for adsorptive heat transformation: 3. Testing of “$BaCl_2$ / vermiculite” composite in a lab-scale adsorption chiller. *Applied Thermal Engineering,* 30**,** 1188-1192.

WAGNER, W. & ÖSTERREICH, B. F. V. 2006. Modularer Energiespeicher nach dem Sorptionsprinzip mit hoher Energiedichte: (MODESTORE); ein Projektbericht im Rahmen der Programmlinie" Haus der Zukunft"; Impulsprogramm Nachhaltig Wirtschaften, *Bundesministerium für Verkehr, Innovation und Technologie*.

WANG, C., ZHANG, P. & WANG, R. 2010a. Performance of solid–gas reaction heat transformer system with gas valve control. *Chemical Engineering Science,* 65**,** 2910-2920.

WANG, H., QI, C., WANG, E. & ZHAO, J. 2009. A case study of underground thermal storage in a solar-ground coupled heat pump system for residential buildings. *Renewable energy,* 34**,** 307-314.

WANG, K. & VINEYARD, E. A. 2011. Adsorption refrigeration: New opportunities for solar. *ASHRAE Journal,* 53**,** 14-22.

WANG, X., ZHENG, M., ZHANG, W., ZHANG, S. & YANG, T. 2010b. Experimental study of a solar-assisted ground-coupled heat pump system with solar seasonal thermal storage in severe cold areas. *Energy and Buildings,* 42**,** 2104-2110.

WENTWORTH, W. & CHEN, E. 1976. Simple thermal decomposition reactions for storage of solar thermal energy. *Solar Energy,* 18**,** 205-214.

WILLERS, E. & GROLL, M. 1999. The two-stage metal hydride heat transformer. *International Journal of Hydrogen Energy,* 24**,** 269-276.

WONGSUWAN, W., KUMAR, S., NEVEU, P. & MEUNIER, F. 2001. A review of chemical heat pump technology and applications. *Applied Thermal Engineering,* 21**,** 1489-1519.

WU, H., WANG, S. & ZHU, D. 2007. Effects of impregnating variables on dynamic sorption characteristics and storage properties of composite sorbent for solar heat storage. *Solar Energy,* 81**,** 864-871.

WU, H., WANG, S., ZHU, D. & DING, Y. 2009. Numerical analysis and evaluation of an open-type thermal storage system using composite sorbents. *International Journal of Heat and Mass Transfer,* 52**,** 5262-5265.

XU, B., LI, P. & LIK CHAN, C. 2015. Energy storage start-up strategies for concentrated solar power plants with a dual-media thermal storage system. *Journal of Solar Energy Engineering,* 137**,** 051002-051002.

XU, J., WANG, R. & LI, Y. 2013. A review of available technologies for seasonal thermal energy storage. *Solar Energy*.

YANG, F., WANG, G., ZHANG, Z. & RUDOLPH, V. 2010. Investigation on the influences of heat transfer enhancement measures in a thermally driven metal hydride heat pump. *International Journal of Hydrogen Energy,* 35**,** 9725-9735.

YU, N., WANG, R. & WANG, L. 2013. Sorption thermal storage for solar energy. *Progress in Energy and Combustion Science,* 39**,** 489-514.

ZALBA, B., MARÍN, J. M., CABEZA, L. F. & MEHLING, H. 2003. Review on thermal energy storage with phase change: materials, heat transfer analysis and applications. *Applied Thermal Engineering,* 23**,** 251-283.

ZETTL, B., ENGLMAIR, G. & STEINMAURER, G. 2014. Development of a revolving drum reactor for open-sorption heat storage processes. *Applied Thermal Engineering,* 70**,** 42-49.

ZHANG, H., BAEYENS, J., CÁCERES, G., DEGRÈVE, J. & LV, Y. 2016. Thermal energy storage: Recent developments and practical aspects. *Progress in Energy and Combustion Science,* 53**,** 1-40.

ZHANG, H., VAN GERVEN, T., BAEYENS, J. & DEGRÈVE, J. 2014. Photovoltaics: reviewing the European feed-in-tariffs and changing PV efficiencies and costs. *The Scientific World Journal,* 2014.

ZHANG, H. L., BAEYENS, J., DEGRÈVE, J. & CACÈRES, G. 2013. Concentrated solar power plants: Review and design methodology. *Renewable and Sustainable Energy Reviews,* 22**,** 466-481.

ZHOU, D., ZHAO, C.-Y. & TIAN, Y. 2012. Review on thermal energy storage with phase change materials (PCMs) in building applications. *Applied energy,* 92**,** 593-605.

ZHU, D., WU, H. & WANG, S. 2006. Experimental study on composite silica gel supported CaCl2 sorbent for low grade heat storage. *International Journal of Thermal Sciences,* 45**,** 804-813.

ZONDAG, H., KIKKERT, B., SMEDING, S., BOER, R. D. & BAKKER, M. 2013. Prototype thermochemical heat storage with open reactor system. *Applied Energy,* 109**,** 360-365.

Appendixes

Appendix I – Gen1 rig specifications

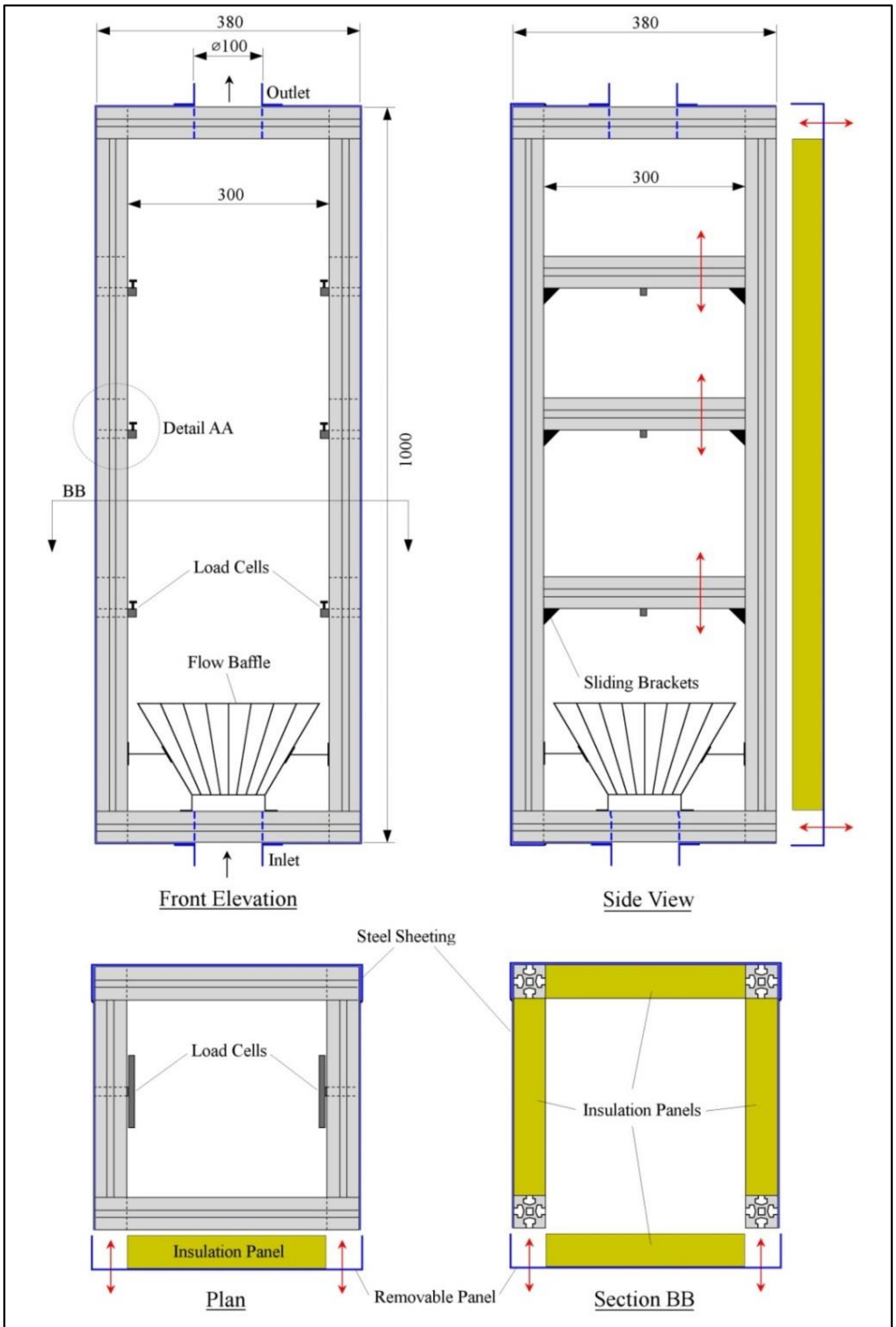

Flow Baffle detail shown separatley
Inlet/Outlet and Top/Bottom Steel Sheeting not shown in Plan
Side Steel Sheeting not shown in Side Elevation
Removeable Panel not shown in Front Elevation

Figure 1 Gen1 rig detailed drawing

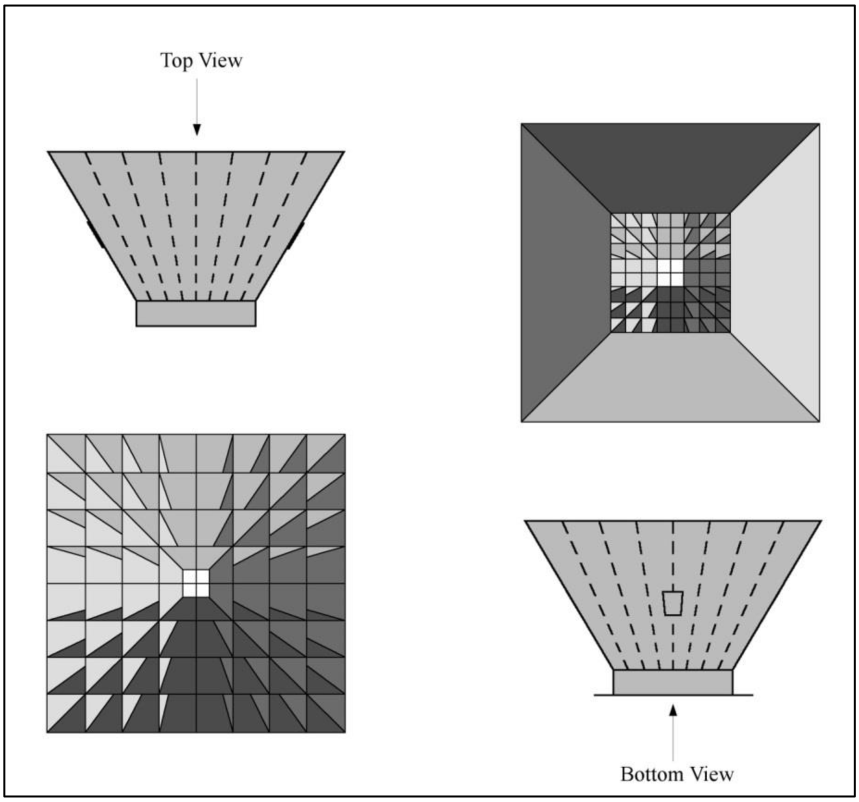

Figure 2 Gen1 rig baffle details

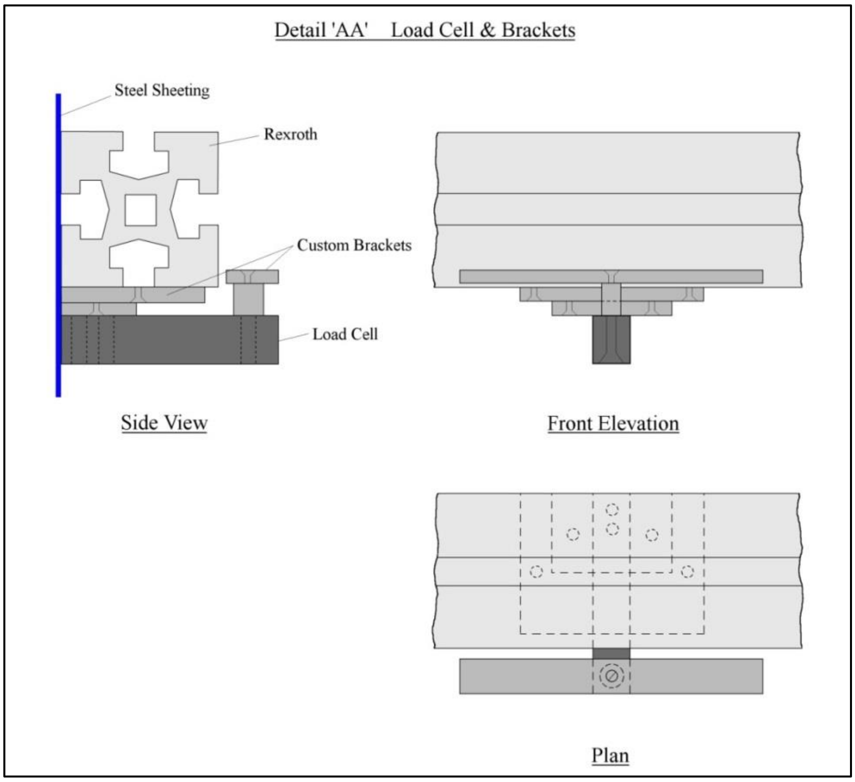

Figure 3 Gen1 rig Load cell and bracket details

Legend

1	Blower Fan
2	Anemometer
3	Electric Heater
4	Thermocouple # 1
5	Steam Generator
6	Bypass Valve
7	Thermocouple # 2 & RH Sensor #1
8	Inlet Valve
9	Thermoouple # 3
10	2.5 kg Load Cell # 1a
11	2.5 kg Load Cell # 1b
12	Thermocouple # 4 & RH Sensor #2
13	2.5 kg Load Cell # 2a
14	2.5 kg Load Cell # 2b
15	Thermocouple # 5 & RH Sensor #3
16	2.5 kg Load Cell # 3a
17	2.5 kg Load Cell # 3b
18	Thermocouple # 6 & RH Sensor #4
18	Outlet Valve

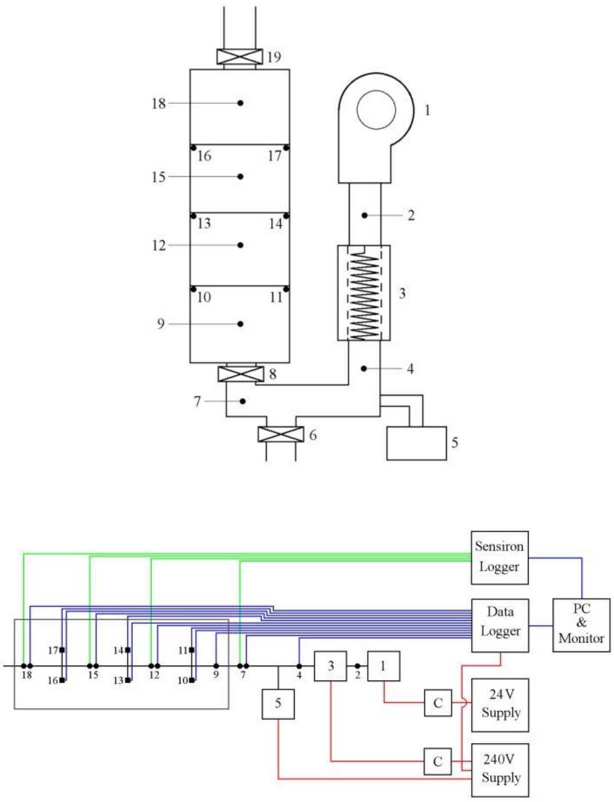

Part Costs

1	Blower Fan x 1	N/A	
2	Anemometer x 1	£128.40	
3	Electric Heater x 1	N/A	
4	Steam Generator x 1	N/A	
5	Valves x 3	N/A	
6	Thermocouple x 6	N/A	
7	RH Sensor Kit x 1 (4 Sensors / kit)	N/A	
8	2.5 kg Load Cell x 8	£440.67	
9	Data Logger (DT85) x 1	N/A	
10	Ducting (ø100mm)2m length, 2 x 90°, 1 x T	£142.86	
11	Sundries	N/A	£711.93

Figure 4 Gen1 rig components

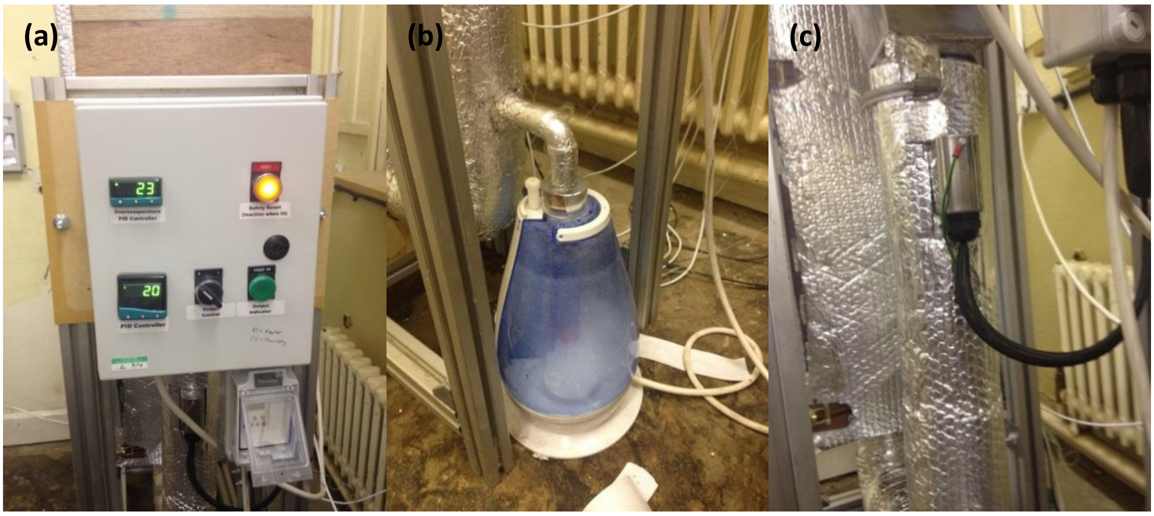

Figure 5 Views of (a) PID controller, (b) ultrasonic humidifier and (c) electrical heater used in the experiments

Appendix II – Experimental Procedure

a. Sample Preparation

1. Prepare the selected desiccant by oven drying at temperature, T > 125 °C for a period, t >24 h to achieve the condition m_{dry} = 0 kg/kg.
2. When ready for experimental cycle, remove the material from the oven, place in the cooling mesh and allow it to cool in the desiccator unit for t > 2h.
3. Wait for the temperature and the relative humidity, *RH* of the chamber to be stable at ambient conditions before proceeding further.
4. Clear data from the Datalogger and restart it. Clear data from the Sensirion and restart it.
5. Wait ≈ 5 minutes then remove the material from the desiccator (only if cooled to ambient temperature) and place onto a mesh tray. Place the tray on the load cells in the Thermal Matrix Chamber (TMC) – ensure the tray does not touch the sides of the chamber.
6. Carefully but quickly seal the chamber.

b. Experimental Cycle

1. Switch on the fan (if off), but do not adjust the dial (10VDC).
2. Ensure there is adequate water in the humidifier. Insert the humidifier pipe into the duct.
3. Turn on the humidifier – C1 on the timer unit.
4. When the outlet temperature (*T4*) has returned to the Input T (*T2*) switch off the humidifier and remove the pipe from the duct.

5. Turn on the duct heater – C2 on the timer unit.
6. When the outlet temperature (*T4*) and inlet T (*T2*) are stable and have levelled off, switch off the heater and remove the mesh tray from the chamber.
7. Place the material in the cooling mesh and allow it to cool in the desiccator unit until the next cycle is due to start.
8. Stop both the datalogger and the Sensiron. SAVE the data from both as a NEW file. Be sure to use sequential file names for further material cycles.

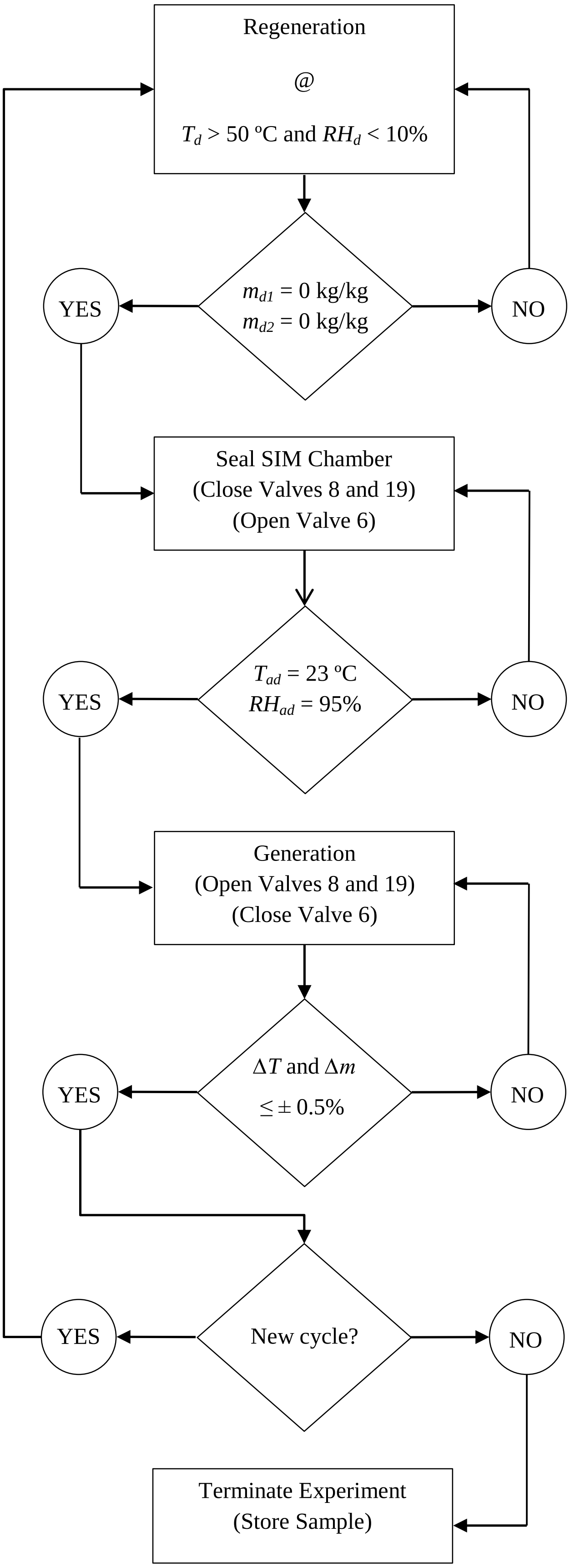

Figure 6 Experimental flow chart

Appendix III - Method for preparation of SIMs using the 'Insipient Witness' technique

1. Oven dry the material at 200 °C for t = 2 h to remove any remaining residual moisture.
2. Record the dry mass of the matrix, m_0.
3. Determine the specific pore volume, V_p of the matrix material in cm^3/g
    a. Can be determined using water (saturated v dry mass) or N_2 physisorption
4. Prepare a saturated salt solution to ≈ 100% of the matrix pore volume
    b. Calculate volume required as matrix mass, m_m x V_p.
    c. Different salts will have a maximum saturated %
5. Slowly add the saturated salt solution to the matrix whilst constantly stirring
6. The matrix should appear to remain dry as the solution will be drawn into the pore network
7. Additional solution may be added until 'visual' confirmation of a 'wetted' transition occurs
8. Place the composite in the oven to evaporate the water
    d. Drying temperature, T_d should be above 110 °C, but may be higher depending on the salt used – full dehydration of hydrates is necessary
9. Record the dry mass of the SIM, m_{SIM}. The mass of salt in. the matrix (as %) can be calculated as the increased mass after drying
10. Calculate the wt.% of the impregnated salt, m_s using;

$$m_s = \frac{m_{SIM} - m_0}{m_0/100} \quad (wt.\%) \tag{1}$$

11. Theoretical salt mass can also be calculated as per example below:

Mass of matrix, m_m =	10 g
Specific pore volume of matrix, V_p =	1.2 cm^3/g

Maximum salt solution concentration (saturated), c_s =	20 %
Volume of solution required, $V_s = m_m \times V_p$	12 cm^3 (m_s = 12 g)
Mass of salt in solution, $m_{salt} = V_s \times c_s$	2.4 g
Mass of H_2O in solution, $m_{H2O} = m_s - m_{salt}$	9.6 g (V_{H2O} = 9.6 cm^3)
Mass of salt (%) in matrix, $m_{salt, \%}$ =	24%

12. If m_s does not match the target wt.% for the SIM, there are two options;
    a. Repeat procedure with altered wt.% salt solution
    b. Repeat procedure with altered mixing time
13. Store SIM in airtight container.

Appendix IV - Standard operating procedures for material characterization

a. Standard Operating Procedure for N_2 Physisorption Analysis

1. Vacuum desiccate samples of mass $m \approx 0.25$ g for a period t = 24 h.
2. Select a suitable sample vial and record its dry mass, m_v.
3. Place the sample in the vial and locate it on the test rig.
4. Outgas under elevated temperature ($T \geq 120$ °C, dependent on sample type) and vacuum conditions for a period of time $t \geq 6$ h to ensure the pores are adequately evacuated of moisture and volatiles prior to testing.
5. Record the combined vial and sample mass, m_c.
6. Calculate the DRY sample mass, m_s (g) using;

$$m_s = m_c - m_v \tag{2}$$

7. Using the volumetric measurement method, perform sample analysis using a minimum of 25 increments for both adsorption and desorption branches of the isotherm.
8. Perform post-processing analysis (dependant on test rig type) to determine Isotherm Type, Specific Surface Area (SSA) using BET, Pore Volume (V_p) and Pore Diameter ($Ø_p$) using BJH.
9. Samples of both the virgin matrix and impregnated SIM should be tested to provide quantitative data on pore filling of the matrix by the salt.
10. Store tested SIM in airtight container.

b. Standard Operating Procedure for Differential Scanning Calorimetry (DSC) Analysis

Two specific tests should be carried out using the DSC;

1. Analysis of the SIM in the dry state
2. Analysis of the SIM in the wetted state

The following procedure should be followed in both cases

1. Prepare samples mass $m \approx 10 - 50$ mg either using vacuum desiccation (dry) or conditioning at 95% Relative Humidity (RH) (wetted) for a period $t = 24$ h.
2. Record the mass of an empty test pan and lid, m_p.
3. Perform a baseline test run on the DSC using the empty pan and lid as follows;
    a. Reduce DSC temperature to 258 K and hold isothermal for $t = 5$ min.
    b. Ramp temperature through the range $258 < T < 393$ K at a ramp rate of 5 K min^{-1}.
    c. Hold isothermally for $t = 5$ min.

4. Place a calibration reference sample with recorded mass, m_{ref} (i.e. sapphire) in the sample pan.
5. Perform a calibration test run on the DSC using identical conditions as in Step 3.
6. Place the sample in the same test pan and secure the lid.
7. Record the combined pan, lid and sample mass, m_c
8. Calculate the DRY/WETTED sample mass, m_s (g) using;

$$m_s = m_c - m_p \tag{3}$$

9. Perform the sample test run on the DSC using identical conditions as in Step 3.
10. Calculate the specific heat capacity, c_p of the sample using the heat flow rates form the baseline (Q_{base}), sample (Q_s), and reference (Q_{ref}) runs along with the mass of the sample (m_s) and reference (m_{ref}) using;

$$c_{p,sp} = c_{p,ref} \cdot \frac{m_{ref}(F_{sp} - F_{base})}{m_{sp}(F_{ref} - F_{base})} \qquad \text{(J/(kg K)} \tag{4}$$

c. Standard Operating Procedure for Thermo Gravimetric (TGA) Analysis

1. Record the mass of the pan to be used, m_p.
2. Place the sample of mass $m_s \approx 10 - 50$ mg in the pan.
3. Prepare samples by conditioning at 95%RH (WETTED) for a period $t = 24$ h in desiccator jars with a Potassium Nitrate saturated salt solution.
4. Quickly place the conditioned sample in the TGA chamber.
5. Ramp TGA temperature through the range $\approx 303 < T > 523$ K at a ramp rate of 5 K min^{-1}.
6. Record dynamic sample mass loss (Δm_s) using;

$$\Delta m_s = \Delta m - m_p \tag{5}$$

7. Analyse mass loss (Δm_s) against desorption temperature (T_d).

d. Standard Operating Procedure for Dynamic Vapour Sorption (DVS) Analysis

1. Record the mass of the dish to be used, m_p.
2. Place the sample of mass $m_s \approx 5$ g in the dish.
3. Vacuum desiccate the samples for a period $t = 24$ h.
4. Prepare the first saturated salt solution using deionised water to achieve the state $RH = 11.3\%$ at 23 ºC.
5. Place the solution in the conditioning chamber and monitor RH level.
6. When $\Delta RH < \pm 2\%$ over $t = 1$ h, place the DRY samples in the conditioning chamber on the balance.
7. Record dynamic sample mass loss (Δm) and Equilibrium moisture contents (EMC) by logging from the balance.
8. EMC for the set internal RH is achieved when change in mass uptake was below 0.5% for a period $t = 4$ h *i.e.* $\Delta m < \pm 0.5\%$.
9. Repeat steps 5 to 8 using the remaining four saturated salt solutions (see: Table 1) to achieve a range of relative humidities at 23°C ($11\% < RH < 94\%$) and with deionised water to achieve the condition where $RH \rightarrow 100\%$.
10. Collate and plot the individual EMC for the sample at each set point of RH to obtain the adsorption branch of the isotherm.
11. If required, the desorption branch of the isotherm may be plotted using a reverse of this process.

Table 1 Critical *RH*s of various salt solutions used for DVS analysis

Saturated Salt Solution	***RH* (%) at 23°C**
Lithium chloride	11.30 ± 0.28
Magnesium chloride	32.90 ± 0.17
Sodium bromide	58.20 ± 0.42
Sodium chloride	75.36 ± 0.13
Potassium nitrate	94.00 ± 0.60

Appendix V - Cyclic testing results of the full set of materials

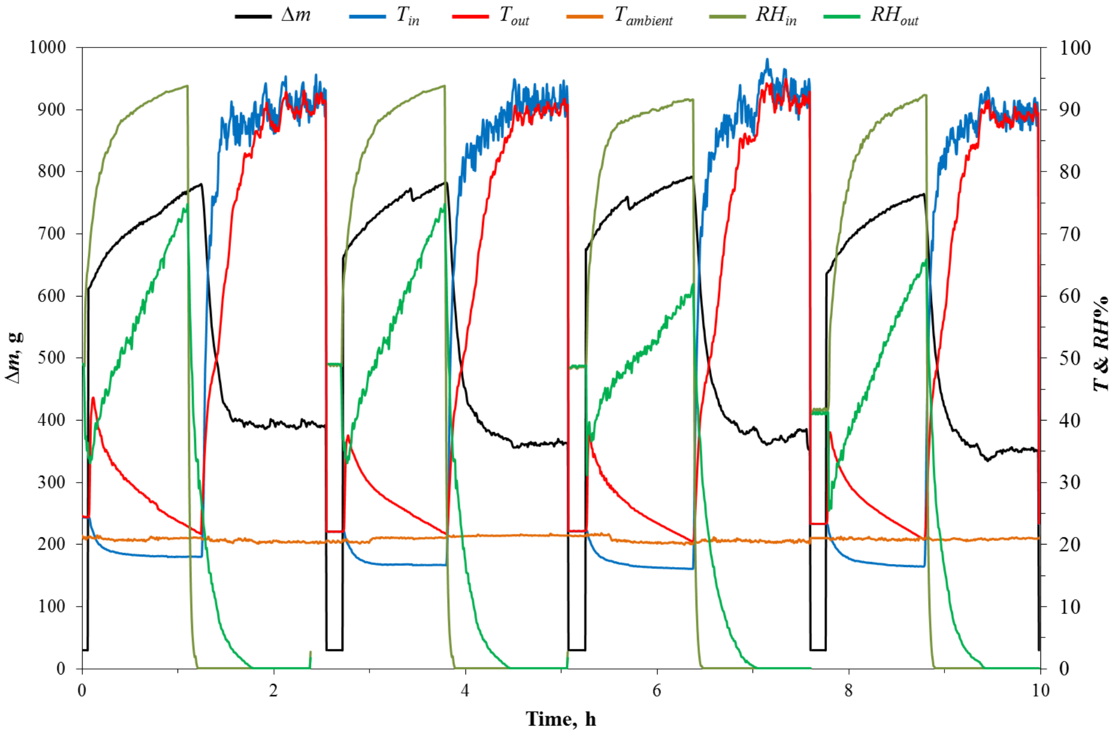

Figure 7 Silica gel cyclic testing results

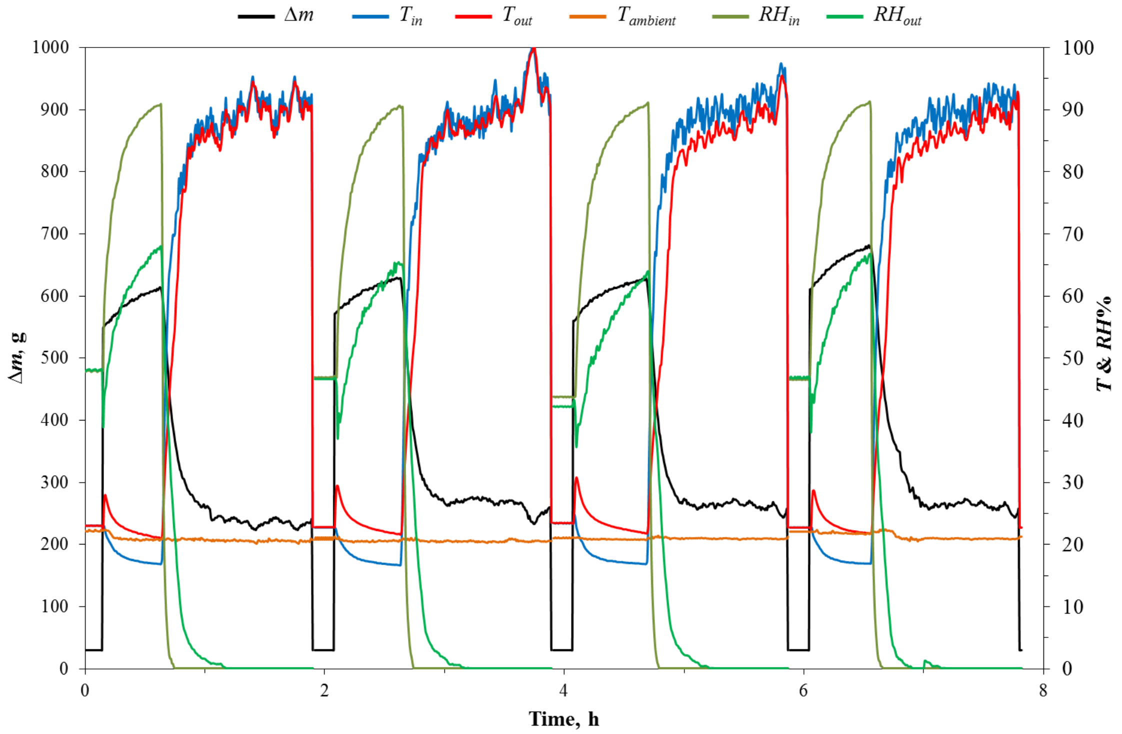

Figure 8 Activated carbon cyclic testing results

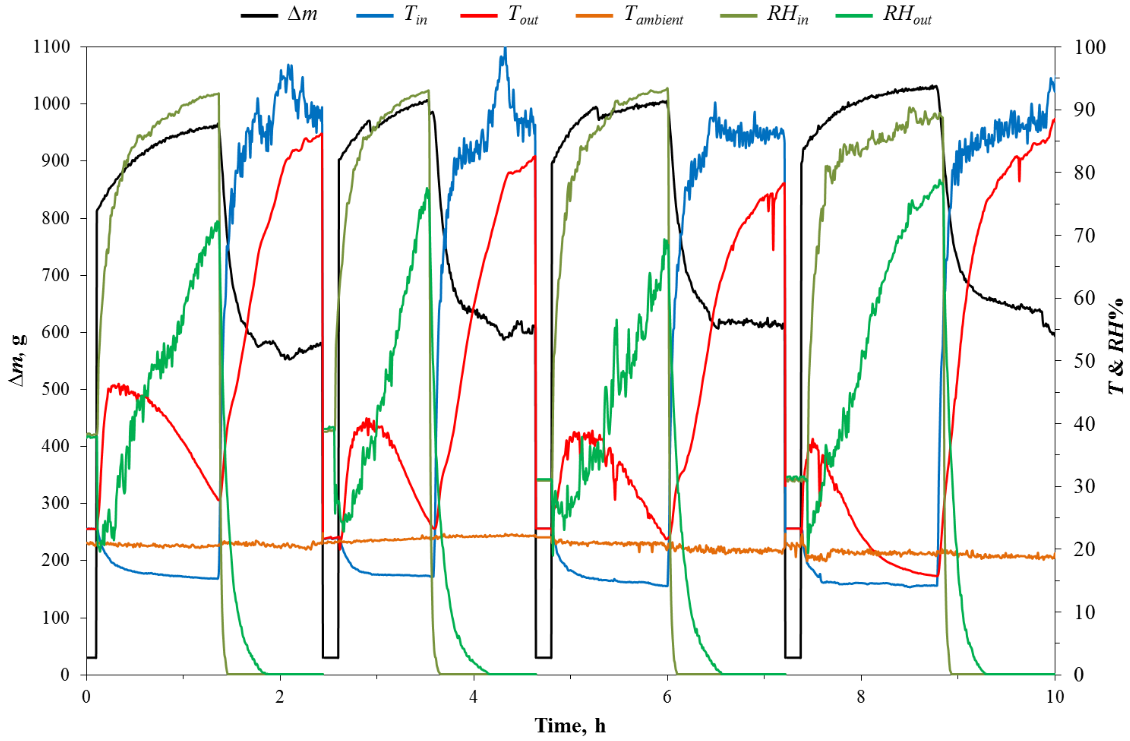

Figure 9 Zeolite cyclic testing results

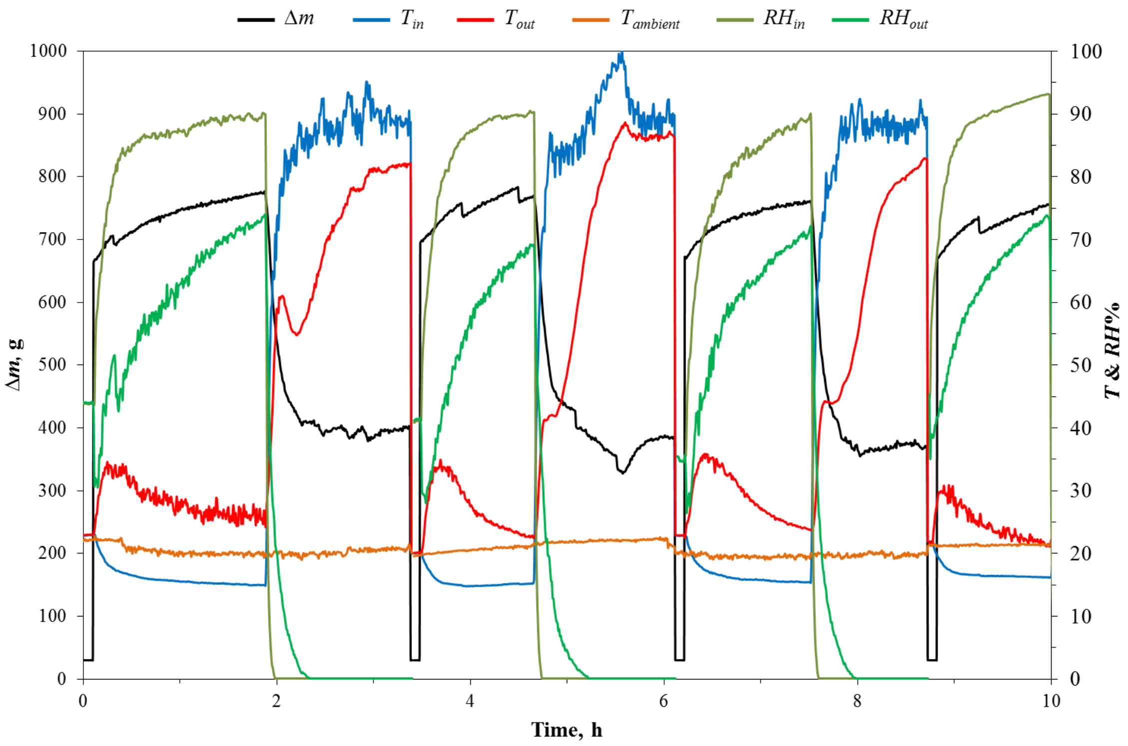

Figure 10 Zeolite-$CaCl_2$ cyclic testing results

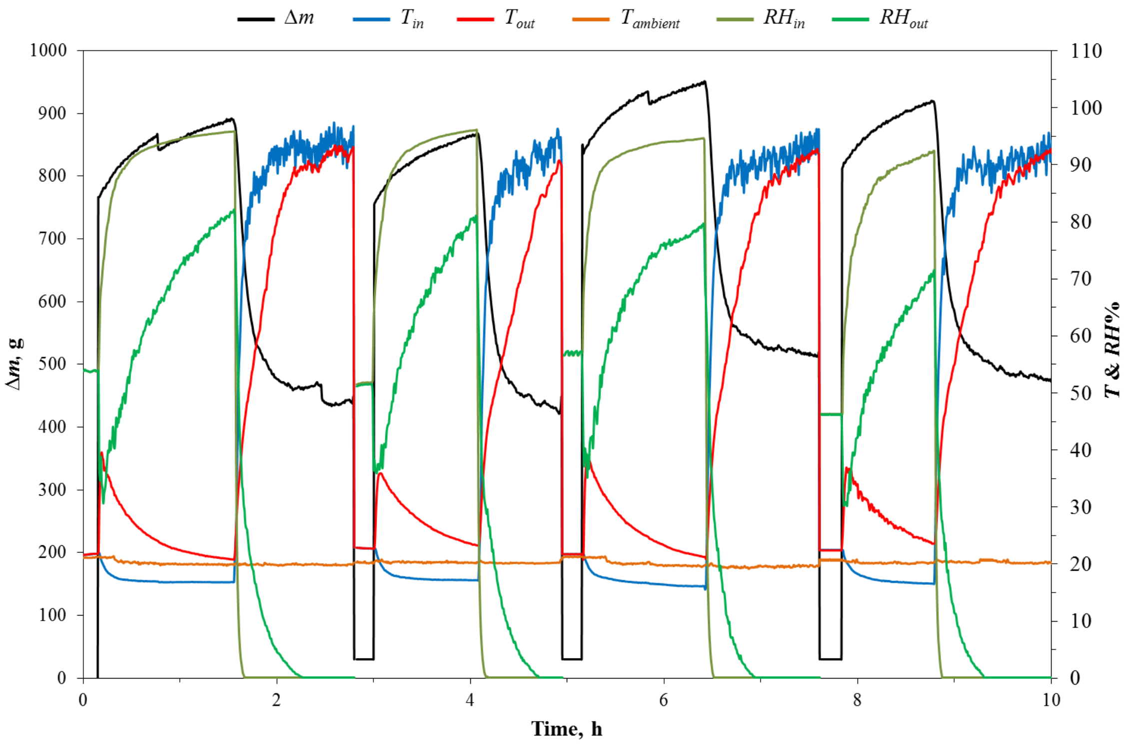

Figure 11 Activated carbon - $CaCl_2$ cyclic testing results

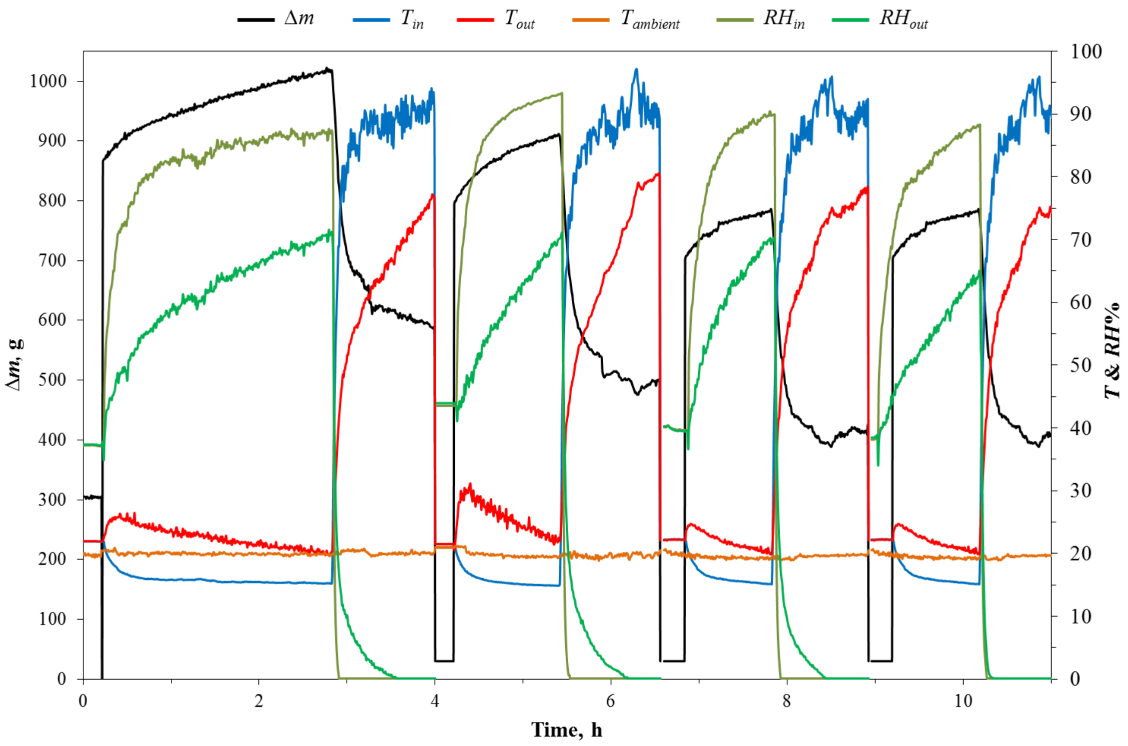

Figure 12 Silica gel - $CaCl_2$ cyclic testing results

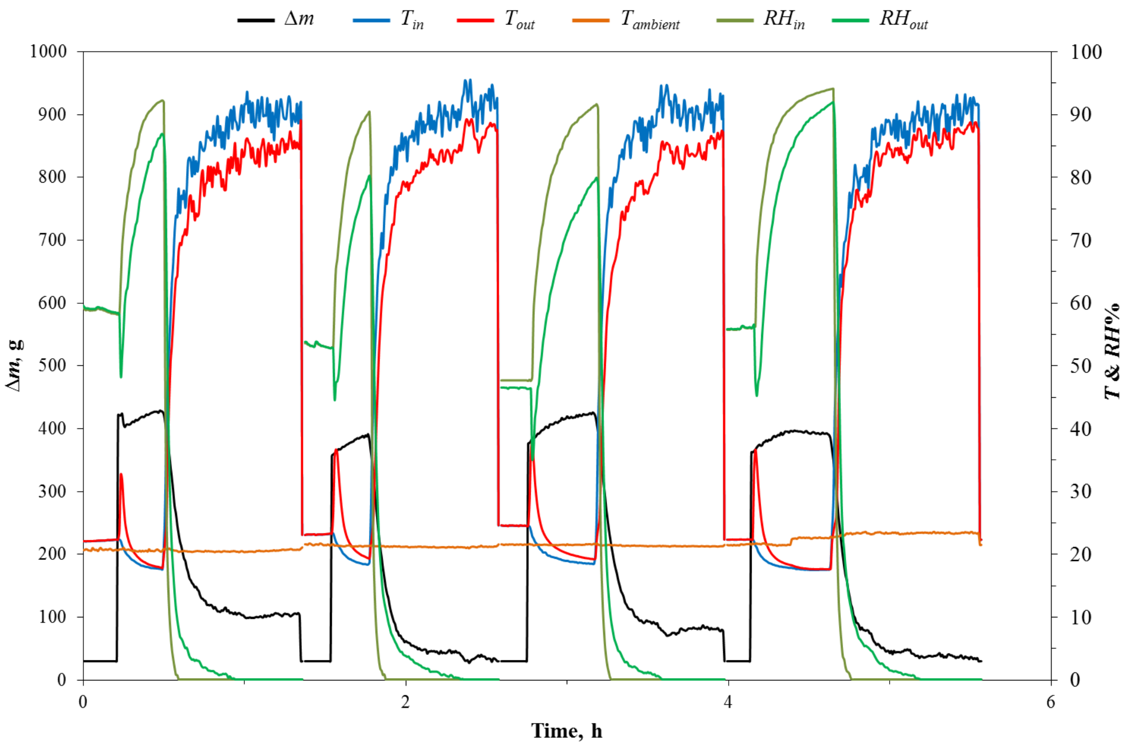

Figure 13 Raw vermiculite cyclic testing results

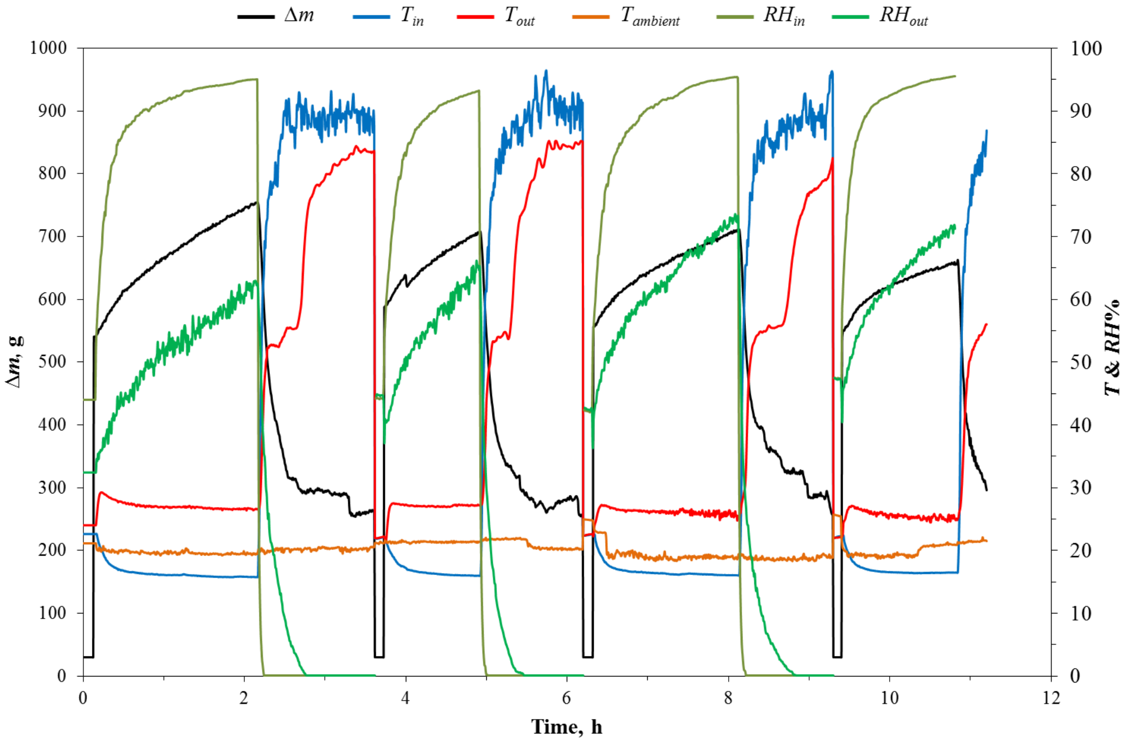

Figure 14 Vermiculite-LiNO$_3$ cyclic testing results

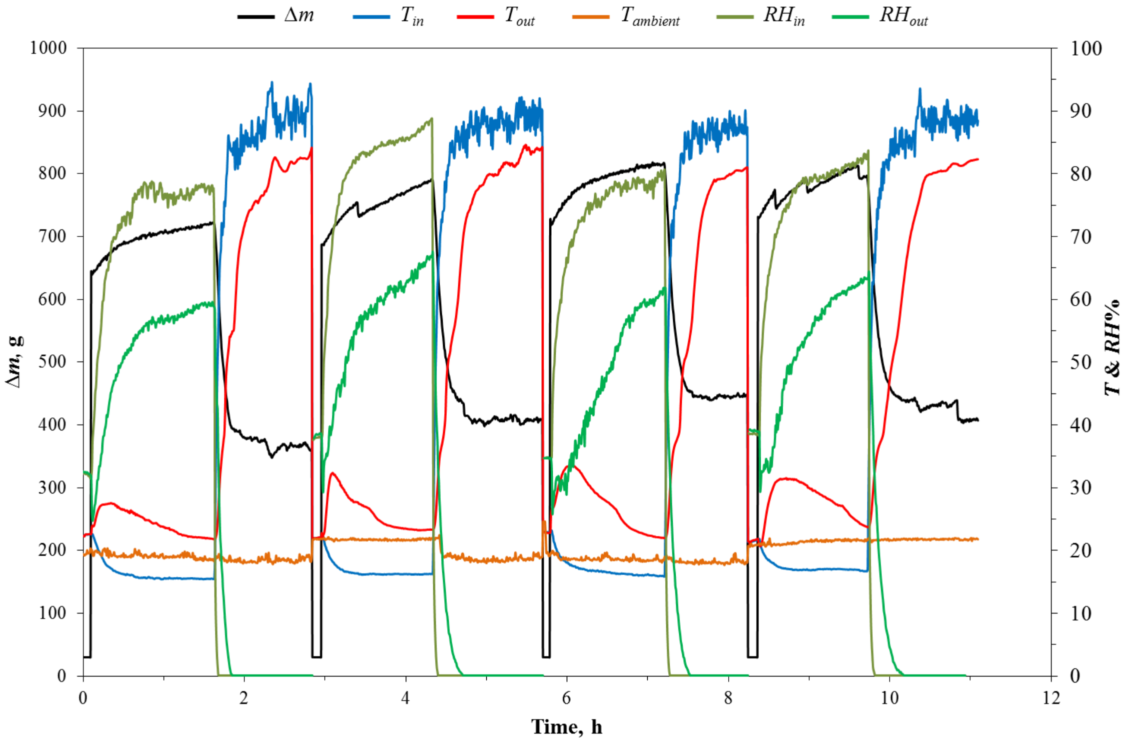

Figure 15 Vermiculite-CaNO$_3$ cyclic testing results

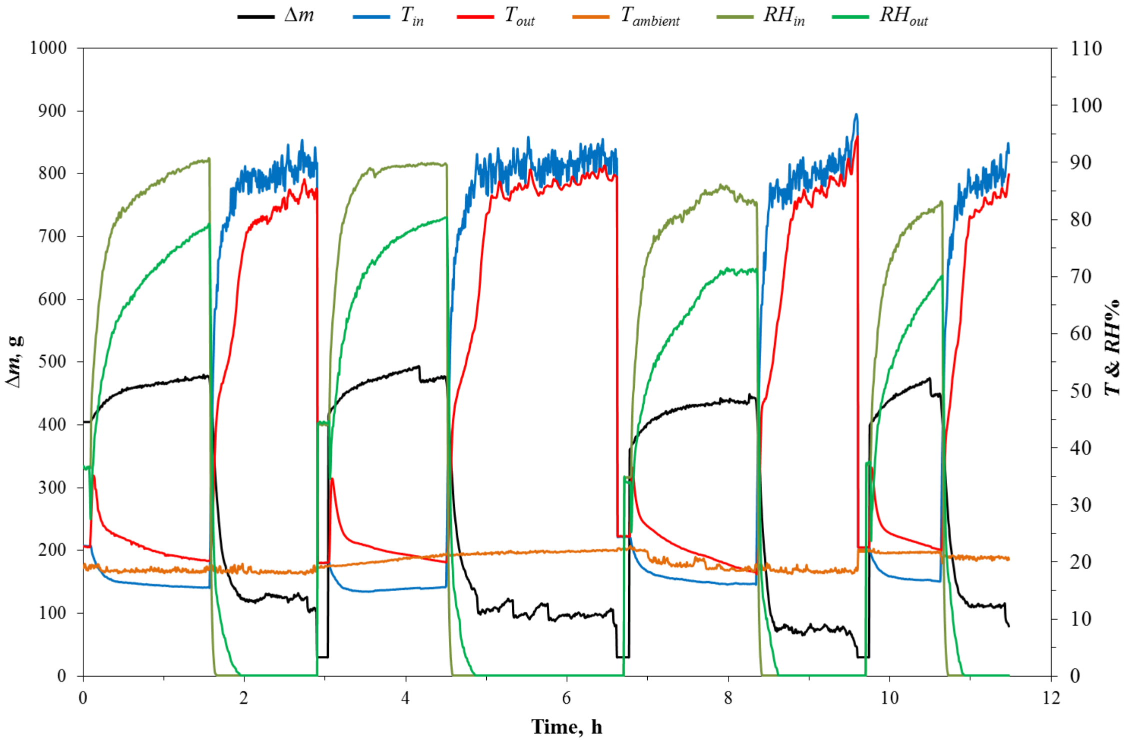

Figure 16 Vermiculite-$MgSO_4$ cyclic testing results

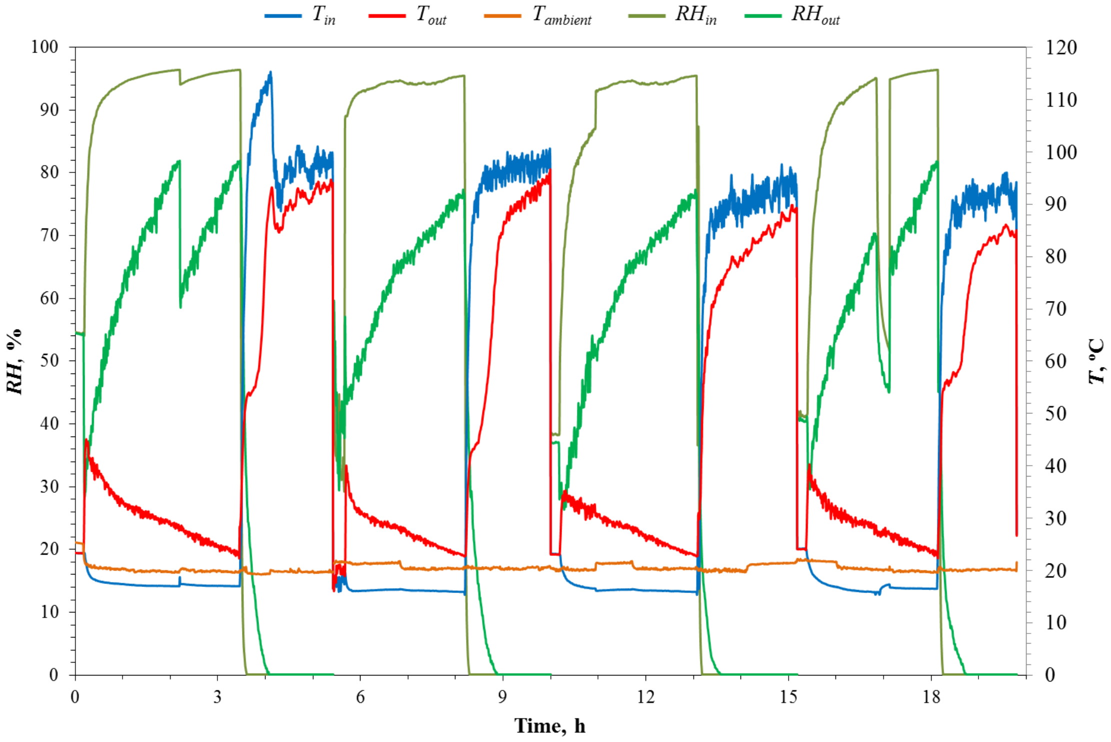

Figure 17 Vermiculite-$CaCl_2$ cyclic testing results

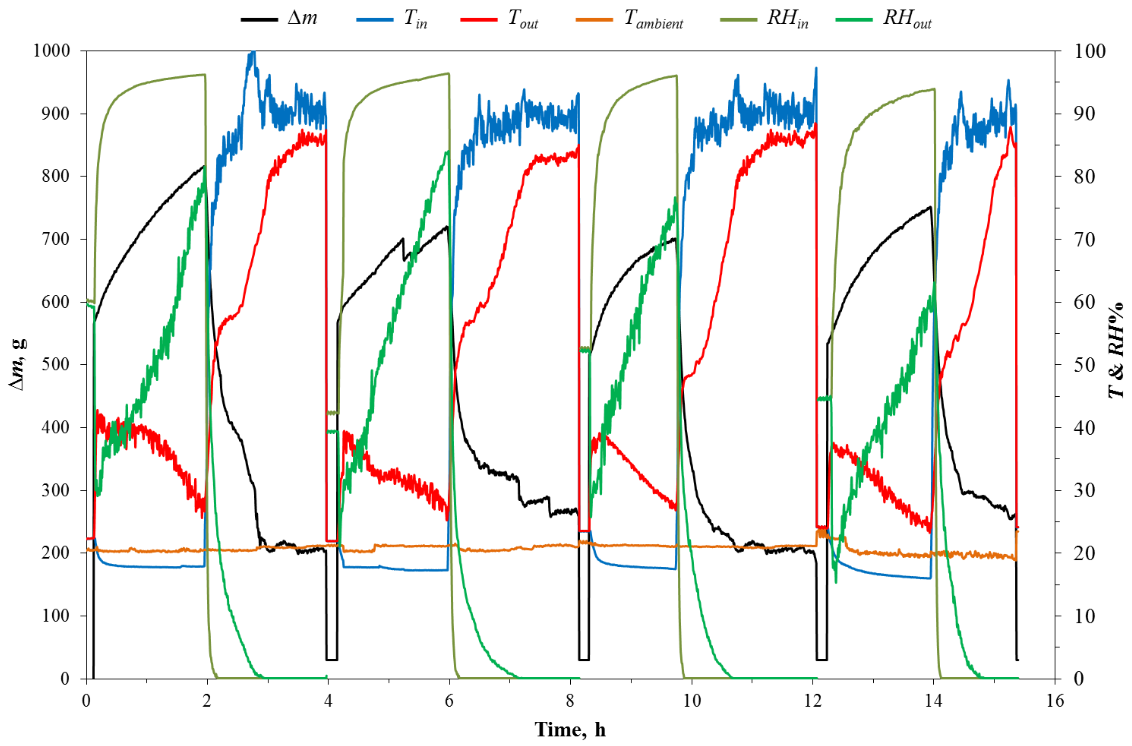

Figure 18 Vermiculite-LiBr cyclic testing results

Appendix VI – Correlation between air absolute humidity and time in charging and discharging processes

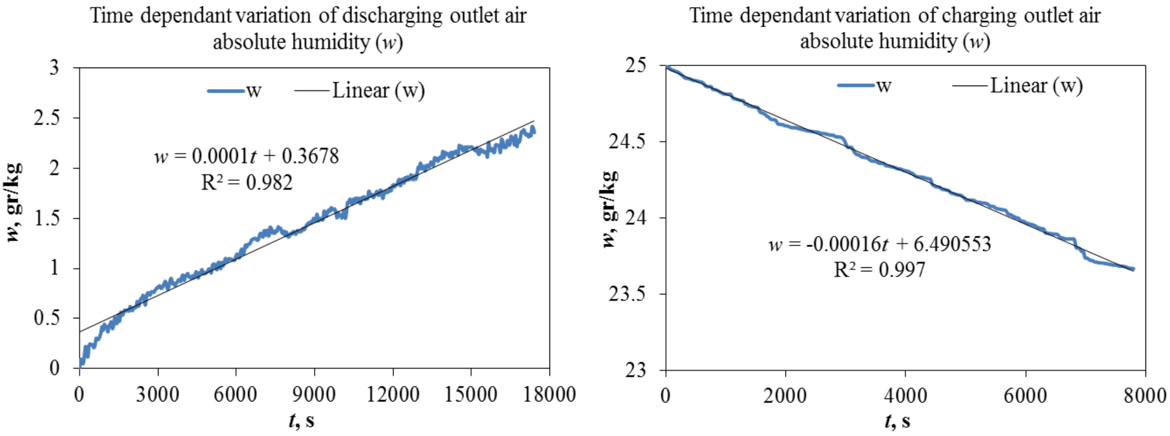

Figure 19 Correlation between outlet air absolute humidity and time during (a) discharging process, (b) charging process